Probabilistische Erdbeben-Gefährdungs-Analyse für KKW-StandOrte in der Schweiz (PEGASOS)

Probabilistic Seismic Hazard Analysis for Swiss Nuclear Power Plant Sites (PEGASOS Project)

Final Report
Volume 5
Elicitation Summaries
Ground Motion Characterisation (SP2)

prepared for the
Unterausschuss Kernenergie (UAK) der Ueberlandwerke (UeW)

by the
Nationale Genossenschaft für die Lagerung radioaktiver Abfälle (Nagra)

Wettingen, 31 July 2004

nagra

PEGASOS

TABLE OF CONTENTS

Part I: Ground Motion Characterisation, Elicitation Summary

Dr. Julian Bommer

Imperial College of Science,
Technology and Medicine,
London - UK

Probabilistische Erdbeben-Gefährdungs-Analyse für die KKW-Stand Orte in der Schweiz (PEGASOS)

SP2 Ground Motion Characterisation

Elicitation Summary

Julian Bommer

Imperial College of Science,
Technology and Medicine,
London – UK

nagra

PEGASOS

TABLE OF CONTENTS

LIST OF TABLES

LIST OF FIGURES

1 INTRODUCTION

This Elicitation Summary forms part of the PEGASOS Project (Abrahamson et al. 2002), a comprehensive probabilistic assessment of seismic hazard at nuclear power plant (NPP) sites in Switzerland. The locations of the four power plant sites are shown in Figure 1.1.

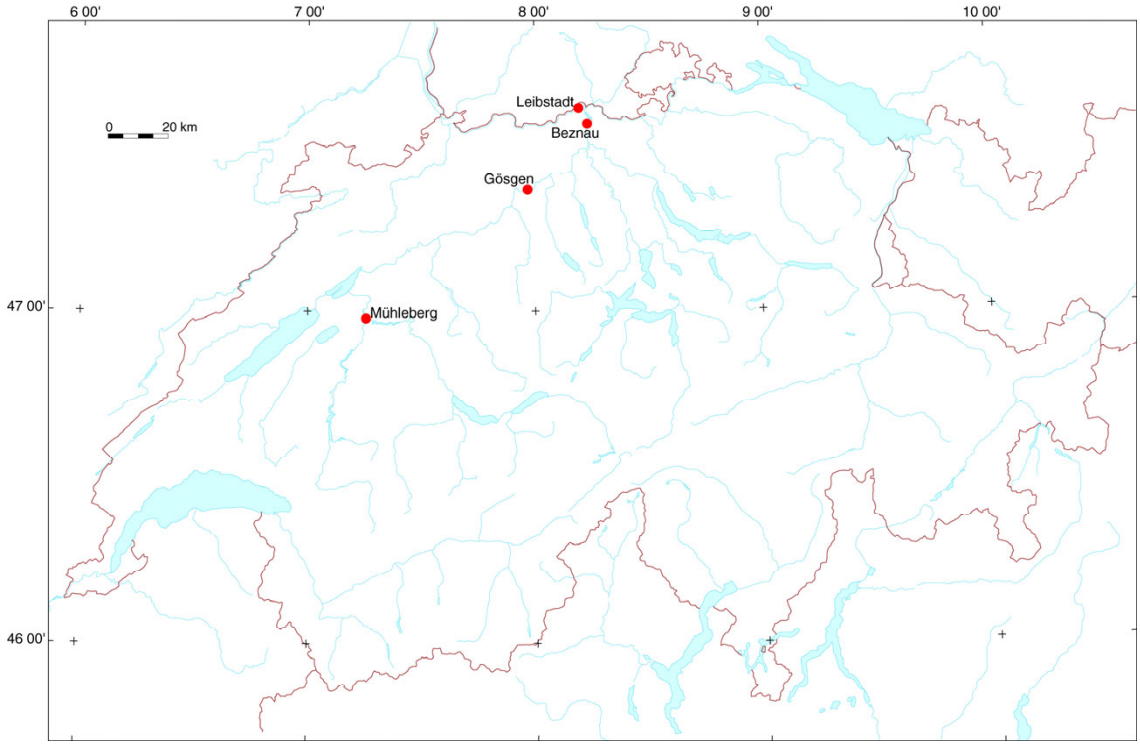

Fig. 1.1: Locations of NPP sites in Switzerland (courtesy of Philippe Roth, Proseis)

The report presents a complete ground-motion model for the prediction of horizontal and vertical ordinates of 5 % damped spectral acceleration at 9 response periods from 0.01 to 2.0 seconds. The predictions are made through logic-trees in order to capture and to rate the epistemic uncertainty in all of the elements of the predictive model. The predictions are calibrated to be applicable for earthquakes with moment magnitude M_w between 5.0 and 7.5 and for sites at distances of up to 200 km from the source of an earthquake. In addition to magnitude and distance, the predictions are also made in terms of site classification and style-of-faulting.

The ground-motion prediction model presented herein is one of five developed in Sub-Project 2 (SP2) of the PEGASOS Project, which are intended to form five equally weighted branches of the logic-tree used for the probabilistic seismic hazard analyses (PSHA) to be carried out at each of the four sites. The report describes not only the structure and weights of this part of the logic-tree, but also the background to the design of the logic-tree and the rationale behind the assignation of the branch weights. The model presented herein has been altered appreciably from its first conception through feedback obtained in an elicitation meeting in July 2002 and the workshops held in October 2002 (WS-3/SP2) and February 2003 (WS-4/SP2). Developments and improvements have also been investigated by the provision of new studies and additional data during the course of the project.

A key issue in the development of the ground-motion models is the question of their applicability to Switzerland, and specifically the north west of Switzerland where the NPP sites are located. In common with all regions of relatively low seismicity, as well as several with elevated levels of earthquake activity, a problem is immediately encountered in that strong-motion data from Switzerland is very limited. A similar study in Japan or California would be far more straightforward, since in both regions there are large bodies of strong-motion data and several attenuation equations have been derived using that data. Therefore, for Japan or California, it would be quite straightforward to select some or all of the published attenuation equations derived from the regional database in order to construct the logic-tree with a high degree of confidence of applicability. In a very low seismicity area such as the United Kingdom, where data is very sparse and there are currently no published attenuation relationships (empirical or stochastic) derived for local conditions, the problem becomes much more complicated. Equations need to be adopted or adapted from other regions, calibrated to whatever reliable local data is available and structured in a logic-tree in such a way as to capture the epistemic uncertainty in the pattern of ground motion radiation in the UK. This specifically means that the bounds specified in the logic-tree should encompass the space in which the attenuation model would be expected to fall at such time as data becomes sufficient to define a local attenuation equation.

The situation is Switzerland is different from that of California and the UK, although perhaps much closer to the latter than the former. There is now a single published response spectral ordinate attenuation for Switzerland and therefore this would be expected to be of great significance in setting up the logic-tree. However, this Swiss attenuation model has not been incorporated into the logic-tree presented in this report, for reasons that are expounded at length, particularly in Section 2.2. The author is of the opinion that the doubts regarding the applicability of this model to the range of magnitudes of interest in these projects are strong enough to support the conscious decision of not including this equation in the ground motion model. This decision may appear counter intuitive to some observers, since the model in question is the only one derived exclusively from Swiss data. However, it should be noted that the only alternatives permitted by the applicability issue mentioned above, namely including the model as it is but assigning it a low weight, or modifying the model to fit results from the other equations, do not represent a guarantee for introducing any genuinely Swiss characteristics into the ground-motion logic tree either (and, in the latter case, may even be unphysical).

The PSHA will be Swiss specific, using seismic source zones that reflect seismicity and tectonics in Switzerland and surrounding areas, and incorporating the effect of the known geological profiles at the NPP sites. The ground-motion models will capture the range of expected strong-motion amplitudes, as well as having several merits in terms of compatibility in terms of explanatory and response variables (through appropriate conversions), adjustments for style-of-faulting and site classifications, and the definition of upper limits on the ground motion that are possibly of great importance at the very low annual frequencies of exceedance (10^{-7}) of interest in the PEGASOS Project. In the ground-motion model presented in this report, many factors have been considered in selecting and weighting the various candidate attenuation models, including the tectonic regions from which they have been derived. At longer distances from the source, the logic-tree gives greatest weight to the equations from ENA, an intraplate region of low-to-moderate seismicity. At short distances from the source, where regional differences in ground motions may not be so large, the logic-tree gives greatest influence to those equations that are well constrained by near-field recordings and that include explanatory variables to explicitly account for factors that may affect the strongest motions such as rupture mechanism and the hanging wall effect. Preliminary analyses and disaggregations have shown that even at annual frequencies of exceedance of 10^{-4}, the hazard will be dominated by events within 20 km of the sites, hence the calibration of the logic-tree to produce the most robust estimates of motion possible in the near-source of moderate and large magnitude earthquakes is of vital importance.

2 EVALUATION OF PROPONENTS MODELS FOR APPLICABILITY

This chapter describes the candidate attenuation relationships for the ground motion model and their characteristics, as well as their potential for applicability to Switzerland.

2.1 Summary of Candidate Equations

As a consequence of discussions between WS-1/SP2 and WS-2/SP2, a list of candidate equations was drawn up, which are listed in Table 2.1. The table presents an outline summary of the equations in terms of the magnitude and distance definitions that they employ, the number of earthquakes and accelerograms in their data sets, and the ranges of magnitude and distance covered. In the sections that then follow, each equation is briefly described in terms of the data set on which it is based and the explanatory variables included in the attenuation model.

Tab. 2.1: Candidate equations for prediction of horizontal median motions

Study	Magnitude			Distance[1]			Data	
	Scale	M_{min}	M_{max}	Scale	R_{min}	R_{max}	EQs	Recs
Abrahamson & Silva (1997)	M_w	4.4	7.4	R_{rup}	0.1	220	58	655
Ambraseys et al. (1996)	M_s	4.0	7.9	R_{jb}	0.0	260	157	422
Ambraseys & Douglas (2000)	M_s	5.8	7.8	R_{jb}	0.0	15	44	186
Atkinson & Boore (1997)	M_w	4.0	7.25	R_{hyp}	10	500	-	-
Berge-Thierry et al. (2000)	M_s	4.5	7.3	R_{hyp}	7.0	100	483	139
Boore et al. (1997)	M_w	5.3	7.7	R_{jb}	0.0	109	14	112
Campbell, Bozorgnia(2002)	M_w	4.7	7.7	R_{seis}	2.0	60	36	443
Lussou et al. (2001)	M_{JMA}	3.7	6.3	R_{hyp}	4.0	600	102	3,011
Sabetta & Pugliese (1996)[2]	M_s,M_L	4.6	6.8	R_{jb},R_{epi}	1.5	180	95	17
Somerville et al. (2001)	M_w	5.5	7.5	R_{jb}	0.0	500	-	-
Spudich et al. (1999)	M_w	5.1	7.2	R_{jb}	0.0	99.4	38	141
Toro et al. (1997)	M_w	5.0	8.0	R_{jb}	1.0	1000	-	-
Bay (2002)	M_w	5.0	7.5	R_{jb}	1.0	500	-	-
Rietbrock (2002)	M_w	5.0	7.5	R_{jb}	1.0	500	-	-

[1] Distances defined as in Abrahamson & Shedlock (1997)
[2] Equations presented for both distance metrics

2.1.1 Abrahamson & Silva (1997)

Published in Seismological Research Letters.

Derived from regression on database of worldwide strong-motion accelerograms from shallow crustal earthquakes, predominantly in Western North America (WNA): less than 10 out of 58 earthquakes from other parts of the world. None of the earthquakes are from central Europe or SCRs.

Site classification: two site categories. The "rock" category includes sites with shear wave velocity $V_s > 600$ m/s, including sites with soil layers of up to 20 m overlying the rock. The equations include a factor to account for the non-linear response of soils, controlled by the level of PGA. The M-R distributions of the datasets used in this study, indicating the site classification of each record, for regressions on spectral ordinates at 0.2 second and at 1.0 second, are shown in Figure 2.1. The difference between the two figures reflects the fact that because of the filtering required for the removal of long-period noise, there were successively fewer records with increasing response periods.

The equation also includes dummy variables to account for style of faulting, covering the options of reverse, oblique reverse and others; the equation imposes an increase in amplitude for oblique reverse faults that is half of that due to pure reverse faults. The "others" category seems to be dominated by strike-slip earthquakes since normal faulting events are very poorly represented in their data set. The style of faulting factor is strongly magnitude dependent, creating larger increases for small events. This equation is also one of the only two that include a term for sites located above the hanging wall of the fault rupture.

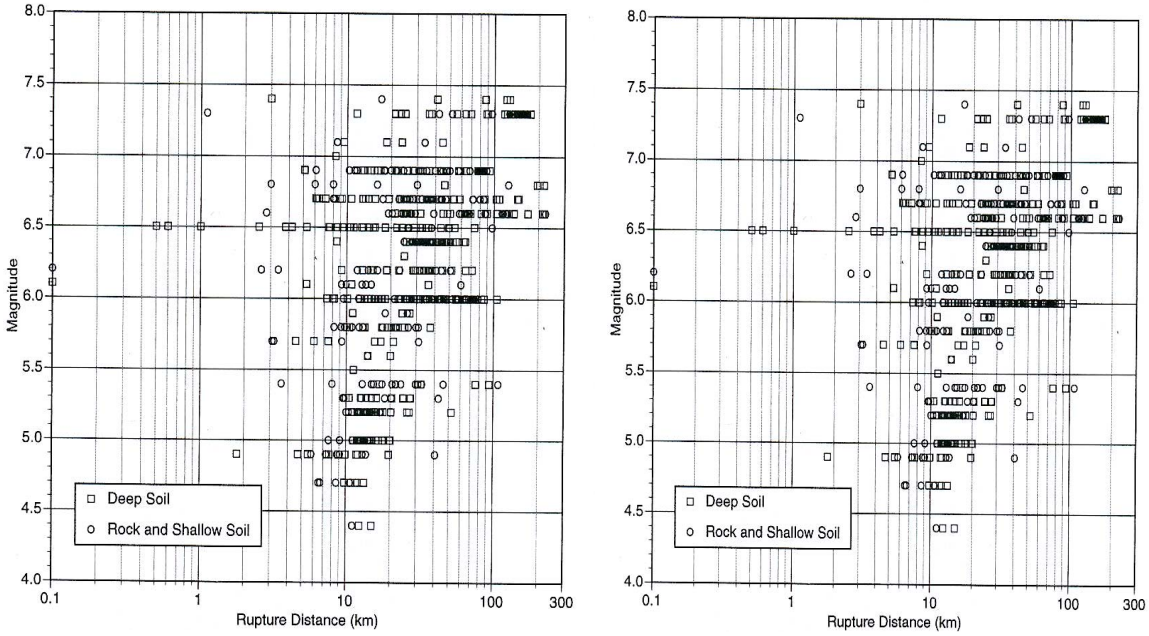

Fig. 2.1: Dataset of Abrahamson & Silva (1997) for regressions on spectral ordinates at response periods of 0.2 second (left) and 1.0 second (right)

The authors do not make any explicit recommendations regarding the magnitude and distance ranges of applicability for the equations.

2.1.2 Ambraseys et al. (1996)

Published in Earthquake Engineering & Structural Dynamics.

The horizontal equations are derived from regressions on a database of records from European earthquakes, predominantly from Italy, Greece, Yugoslavia, Iran, Turkey and the former USSR. Almost none of the earthquakes could be classified as being from SCRs and there are no records from Central Europe or Switzerland in the database.

The site classification is based on $V_{s,30}$, with "rock" sites being those with values greater than 750 m/s, stiff soil sites being those with values between 360 and 750 m/s. Very few of the site

classifications are actually based on *in situ* measurements and several of the classifications have been questioned. The M-R distributions of the data within the three site categories employed are shown in Figure 2.2.

The equations did not include any additional explanatory variables. All styles of faulting are represented in the data set but normal and reverse (including many thrusts) events dominate the data set. The style of faulting of the earthquakes in the data set was not presented in the paper.

The authors specifically recommend that the equations can be used in the range of magnitudes from M_s 4.0 to 7.5 and for source-to-site distances up to 200 km.

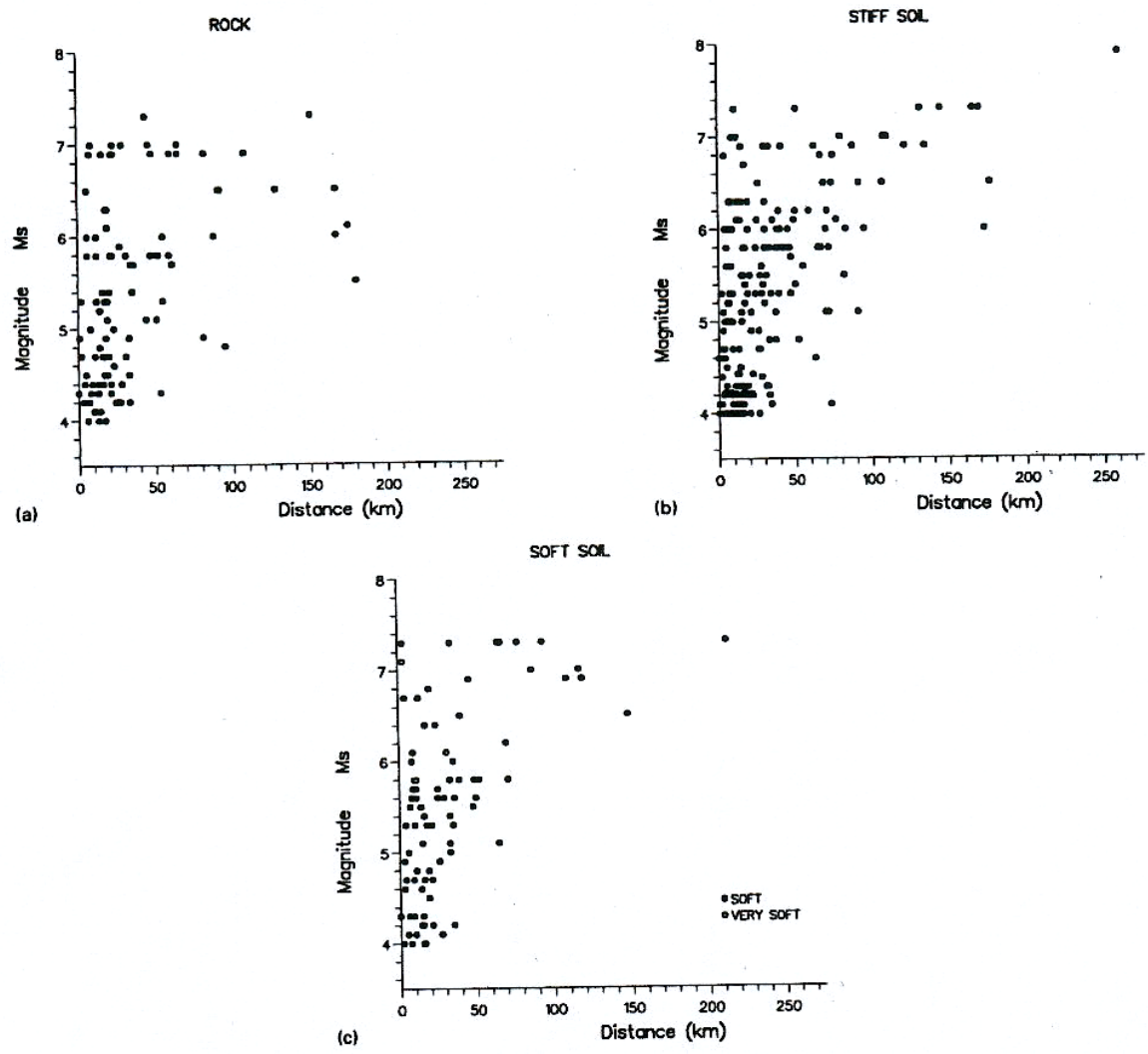

Fig. 2.2: Dataset of Ambraseys et al. (1996) for the three site classes employed in the study

2.1.3 Ambraseys & Douglas (2000, 2003)

Published as ESEE Research Report at Imperial College; rejected for publication in *Earthquake Engineering & Structural Dynamics*, then revised, submitted and accepted for publication in *Soil Dynamics & Earthquake Engineering*.

The publication was primarily focused on vertical spectra but equations for horizontal spectral ordinates are also presented. The equations are based on regression on a worldwide database of

strong-motion records selected on the basis of a minimum magnitude threshold (M_s 5.8), focal depth less than 20 km and distance less than 15 km. Database dominated by records from WNA (72 %), with 22 % from Europe and others from Canada, Nicaragua, Japan and Taiwan.

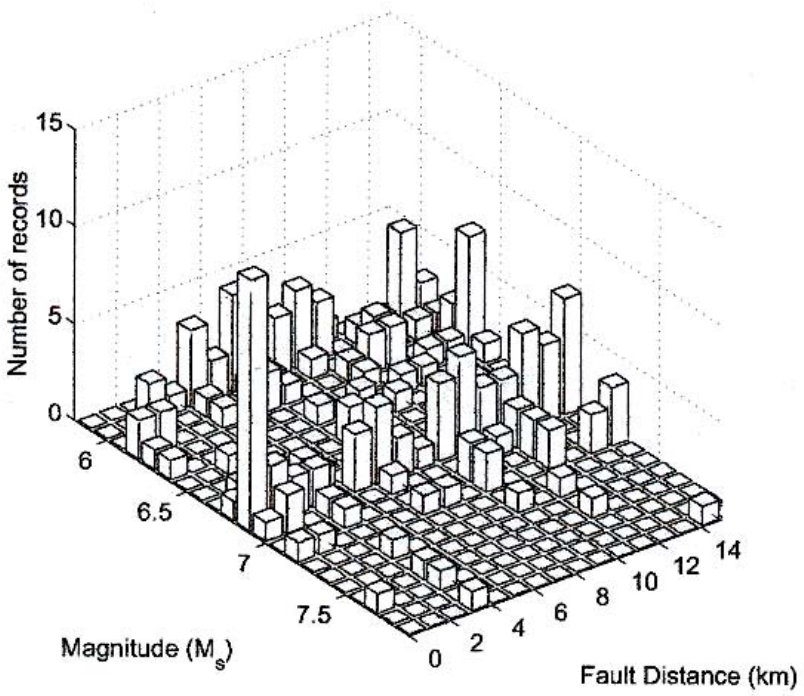

Fig. 2.3: Dataset of Ambraseys & Douglas (2000) in M-R space, without distinction by site category

Equations use the same site categories (rock, stiff and soft) as the Ambraseys et al. (1996) study. Figure 2.3 shows the M-R distribution of the complete dataset employed in this study. The original source reference does not display the distribution in terms of site category but it is stated that there are 91 records from sites classified as soft, 68 from stiff sites and just 23 from rock sites. Since all of the data are from distances of less than 15 km, the lack of information on the M-R distribution for a particular site class is less significant. Inspection of the dataset listing in the original reference reveals that the 23 rock site records are well distributed in the range of distances from 0 to 14 km.

Style of faulting is not included in the attenuation model but the distribution of the records with respect to rupture mechanism is reverse (53 %), strike-slip (39 %) and normal (9 %).

The authors do not make any specific recommendations regarding the range of applicability of their equations, presumably because the focus of the study, and therefore of their conclusions also, is with respect to the importance of the vertical ground motion and its influence on structural response.

2.1.4 Atkinson & Boore (1997)

Published in *Seismological Research Letters*, in a paper that makes comparisons amongst the predictions of various ENA equations as well as comparing ENA and Californian equations. The equations were originally published by Atkinson & Boore (1995) in the *Bulletin of the Seismological Society of America*.

The equations are derived by regression on stochastically generated accelerograms using source and path parameters calibrated for Eastern North America (ENA).

The equation is derived explicitly for "hard rock" sites in ENA, for which it is assumed that the near-surface shear wave velocity is 2,800 m/s.

The style of faulting is not included in the equation, but the equations are calibrated, in terms of derivation of the input parameters to the stochastic model, to thousands of records from hundreds of ENA earthquakes. The authors state that "*based on the regional faulting style the predominant mechanism is believed to be thrust*".

The authors explicitly recommend their equations for use in the range of moment magnitudes from 4 to 7.25, and distances from 10 to 500 km, although they note that the maximum magnitude for which the source spectra are constrained is M_w 6.8.

2.1.5 Berge-Thierry et al. (2000)

Originally presented as an internal report of IPSN, France, in French; now submitted as paper to *Journal of Earthquake Engineering*.

Derived from regression on large database of European strong-motion accelerograms, supplemented by some records from California, which constitute 17 % of the total database. Almost none of the earthquakes are from Central Europe or from SCRs.

The site classification scheme employed uses two site categories: rock and sedimentary sites, the former having V_s values greater than 800 m/s, the latter values between 300 and 800 m/s. In the original French reference provided by the project there is only a table listing the records used for the regressions in this study. However, in English language version subsequently distributed by Fabrice Cotton, which has been prepared for journal publication, there are the graphs presented in Figure 2.4.

Style of faulting is not included in the attenuation model and the rupture mechanisms of the earthquakes are not presented. Inspection of the database listing in the original report indicates that all three mechanisms are represented, with reverse and thrust events probably dominating the data.

The authors recommend, in their conclusions, that the equations are valid for magnitudes between 4.0 and 7.3 and for distances from 5 to 100 km.

2.1.6 Boore et al. (1997)

Published in Seismological Research Letters.

Derived from regression on a database of accelerograms from WNA.

The site classification scheme is based on $V_{s,30}$ with the actual value at the site being used in the predictions if known; recommended values are given for NEHRP classified sites and generic "rock" and "soil" sites. Interestingly, the suggested value for "rock" sites is 600 m/s. Figure 2.5 shows the data from Boore et al. (1997) in magnitude-distance space as used for regressions on PGA and on response spectral ordinates, without distinction by site classification.

From inspection of the listing of records used for the regressions on spectral ordinates, it is possible to determine that only 12 of 112 records used were classified as Class A (rock, with $V_{s,30} > 750$ m/s). Furthermore, of these records only 5 were obtained at distance of less than 11 km.

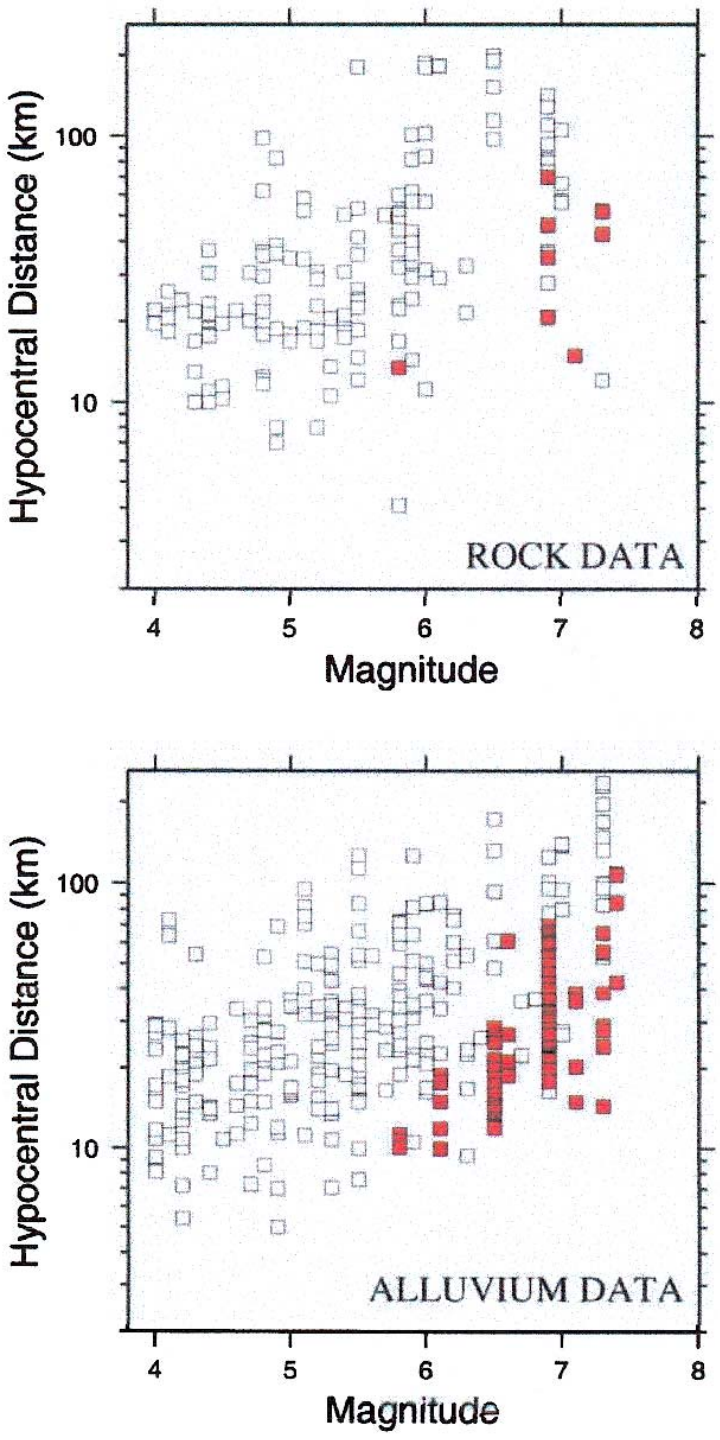

Fig. 2.4: Dataset of Berge-Thierry et al. (2000) in M-R space grouped according to the two site classifications employed in that study

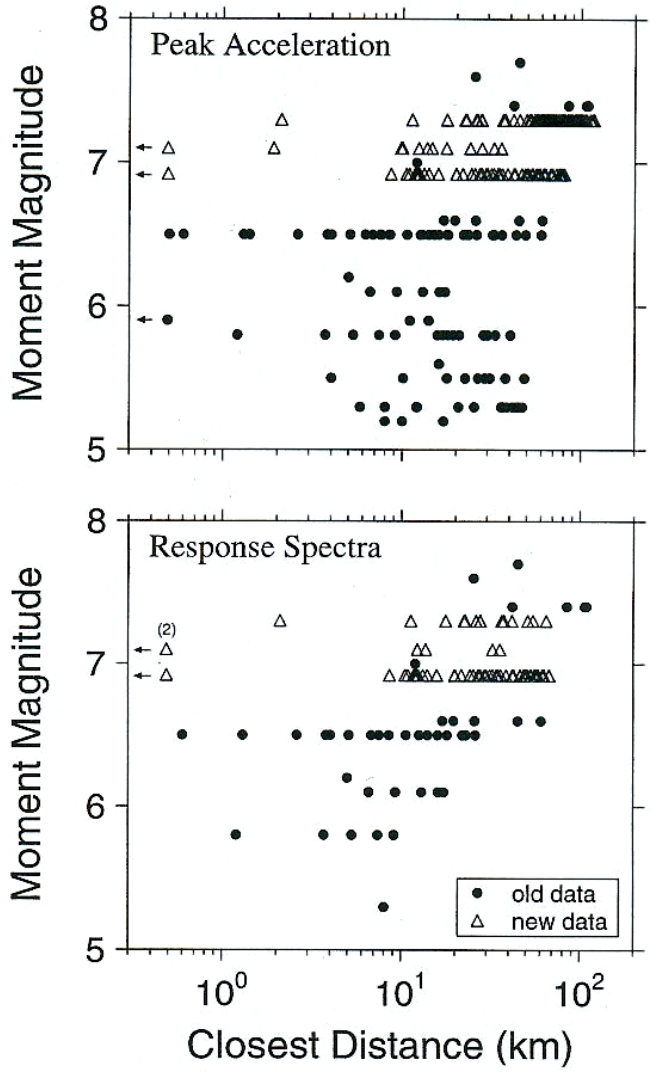

Fig. 2.5: Dataset of Boore et al. (1997) in M-R space as used for the regressions on PGA (upper) and spectral ordinates (lower)

The constant term of the equations is presented for three different cases: strike-slip earthquakes, reverse faulting earthquakes, and independent of style of faulting. The case of normal faulting is not covered, as there is only one normal rupture earthquake in their database.

The authors note that there are very few spectral data below magnitude M_w 6.0. They also point out that there are very few records in their data set that are from distances beyond 80 km and they explicitly recommend that the equations should not be used for greater distances.

2.1.7 Campbell & Bozorgnia (2002)

Submitted for publication in *Bulletin of the Seismological Society of America*. This study is essentially an update of Campbell (1997) and, like the previous study, it is specifically aimed at the estimation of near-source ground motions.

Relations found from regression of large database of near-source accelerograms from around the world, primarily from western USA. The authors argue that near-source attenuation characteristics of shallow crustal earthquakes in regions of active tectonics are the same worldwide. All the earthquakes in the data set have a focal depth of less than 25 km.

Four site categories are used in this study. "Soft rock" sites are stated to correspond to shear wave velocities of approximately 420 m/s, whereas "firm rock" to 800 m/s. The other site classes are "firm soil" and "very firm soil", corresponding to $V_{s,30}$ values of approximately 290 and 370 m/s respectively. Figure 2.6 shows the M-R distribution of the total dataset employed by Campbell & Bozorgnia (2002), without distinction by site class.

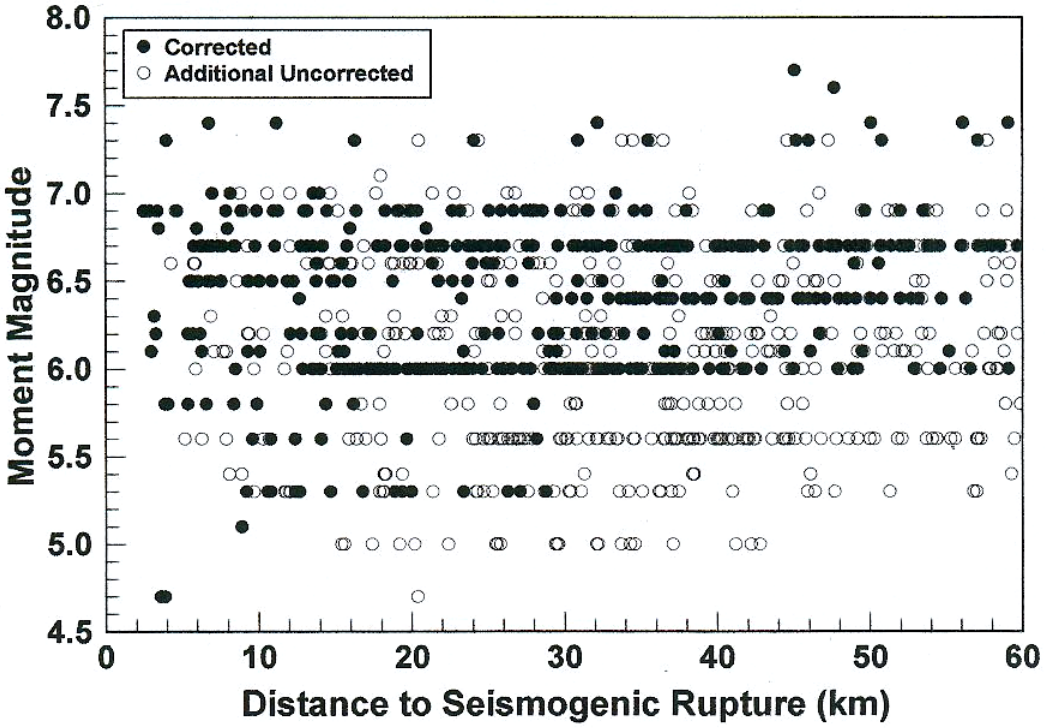

Fig. 2.6: Dataset of Campbell & Bozorgnia (2002) in M-R space

Campbell & Bozorgnia (2002) do not provide in their paper, neither graphically nor in tabular form, the M-R distribution with respect to site classifications, although some inference can be made from distribution of the data employed in the earlier study by Campbell (1997), which itself made use of the same dataset employed by Campbell & Bozorgnia (1994). Figure 2.7 shows the M-R distribution of the earlier dataset, broken down both by site classification and by fault rupture mechanism. However, it must be borne in mind that although only 13 earthquakes were added to the dataset, the total number of horizontal records was doubled with respect to the earlier studies; a number of additional records were included from earthquakes already in their database.

The relations include style of faulting as an additional explanatory variable, with three groups of rupture styles: strike-slip, reverse and thrust. Normal faulting earthquakes are assumed to produce the same amplitudes of ground motion as strike-slip events, but only one earthquake in their database is classified as a normal rupture. The influence of the fault mechanism is modelled to be independent of magnitude and distance, which is different from the model of Campbell (1997).

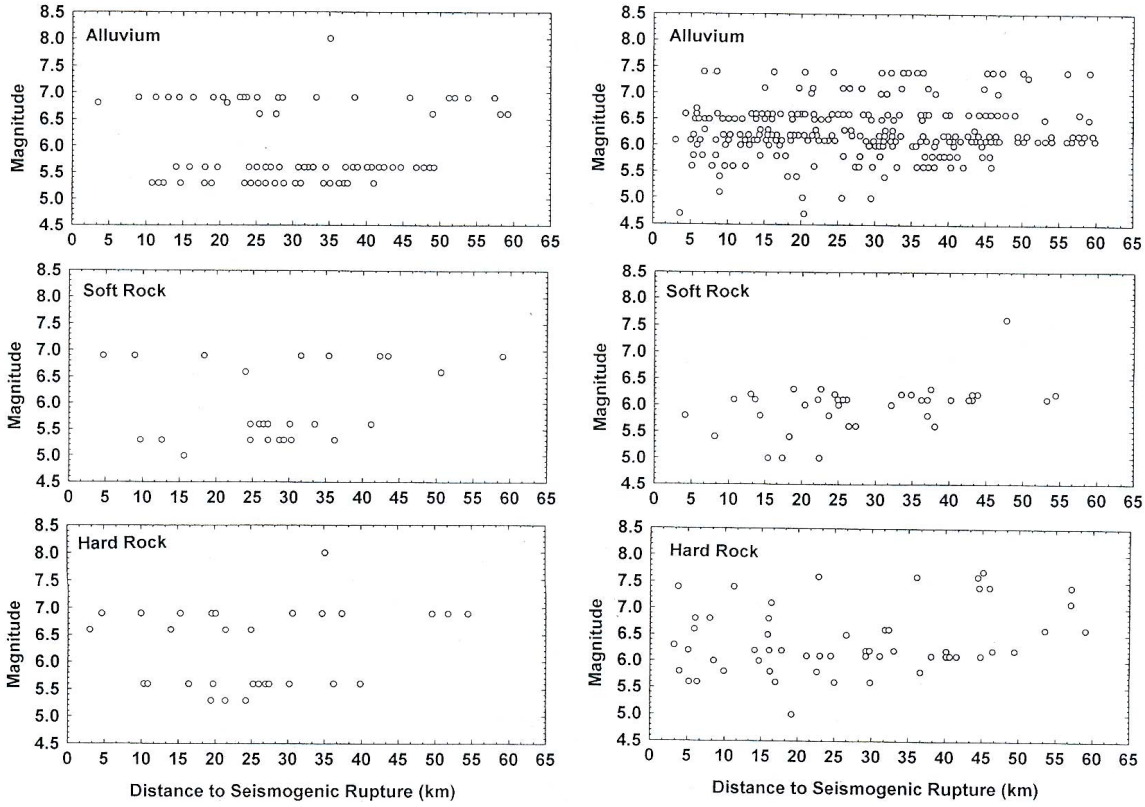

Fig. 2.7: Dataset of Campbell (1997) in M-R space grouped by site classification for strike-slip (left) and reverse (right) earthquakes.

The equations of Campbell & Bozorgnia (2002) also include a term for the hanging wall effect at distances of less than 5 km and magnitudes greater than 5.5.

The authors specifically recommend that the equations are suitable for applications to events of moment magnitude 5.5 and greater and distances less than or equal to 60 km. They go on to say that "*the relations can be extrapolated to a distance of 100 km without serious compromise, but ....they should not be used beyond distance*".

2.1.8 Lussou et al. (2001)

Published in *Journal of Earthquake Engineering*.

Equations founds by regression on a large dataset of records from shallow earthquakes in Japan recorded by K-Net between 1996 and 1998.

Data divided into four site classes, based on measured shear-wave velocities from depths of 10 to 20 m extrapolated to 30 m. Class A sites have values of $V_{s,30}$ greater than 800 m/s and class B sites have values between 400 and 800 m/s.

The M-R distribution of the full dataset employed by Lussou et al. (2001) is shown in Figure 2.8; Figure 2.9 shows the individual M-R distributions for the data in each site class.

This study does not consider style of faulting in the attenuation equation and also does not report the mechanism of the earthquakes in the database. Since the records are all from shallow focus earthquakes in Japan, it may be reasonable to assume that normal ruptures, which would be associated with deeper intra-slab subduction events, are poorly represented if not completely absent, and that the dominant style of faulting is reverse or thrust.

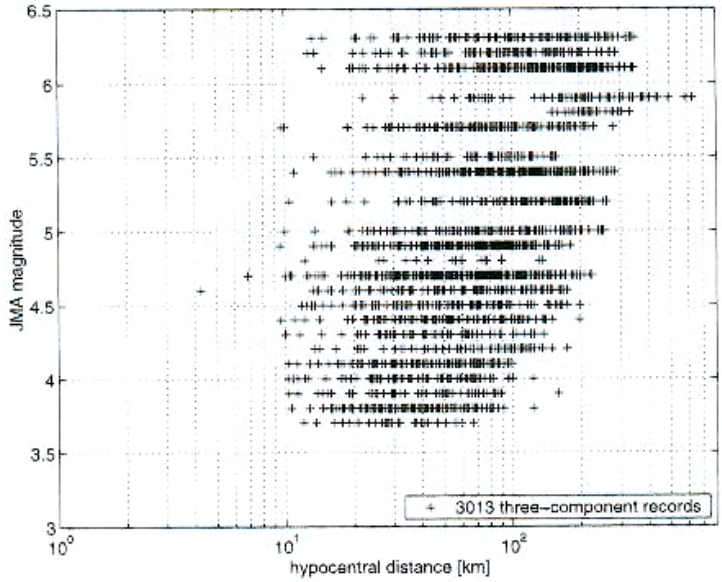

Fig. 2.8: Dataset of Lussou et al. (2001) in M-R space

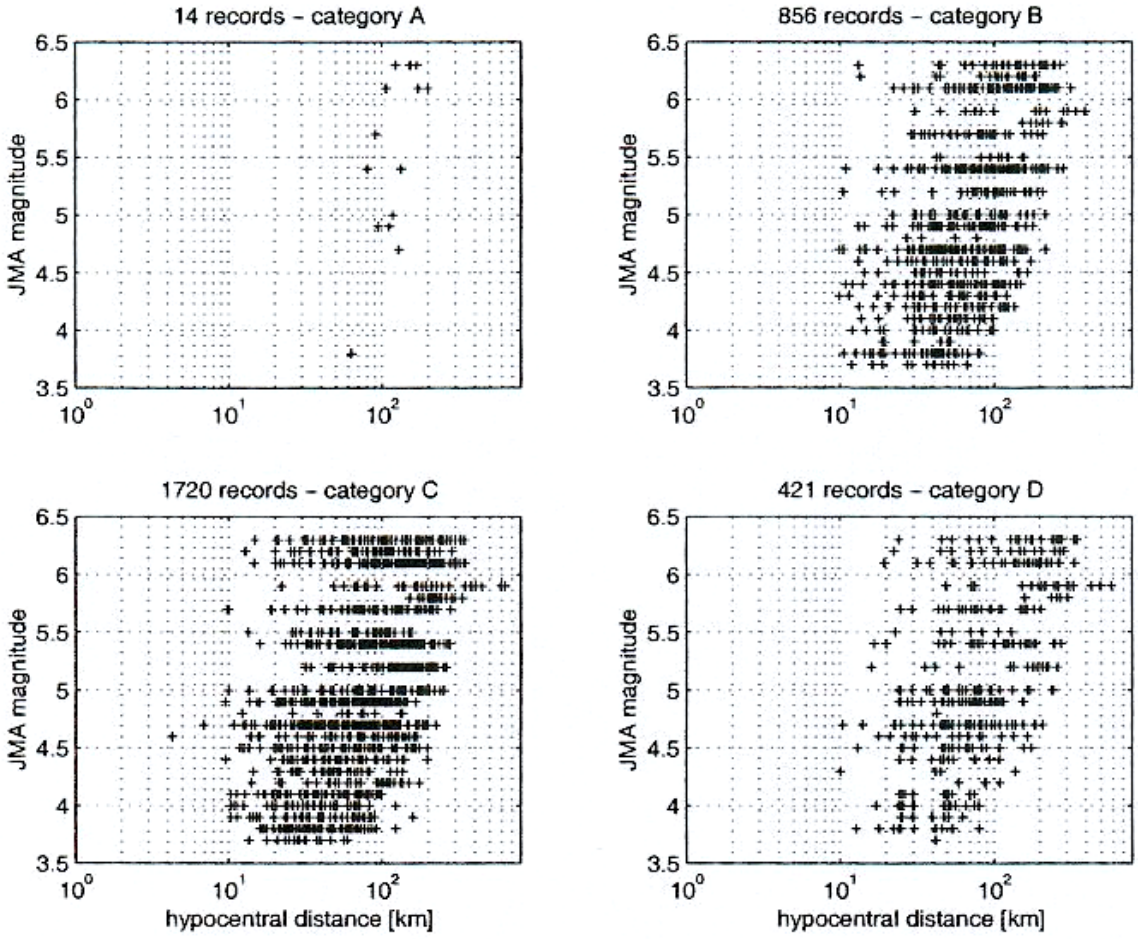

Fig. 2.9: Dataset of Lussou et al. (2001) in M-R space grouped according to site classification

The authors explicitly state the range of applicability of their equations to be for magnitudes from 3.5 to 6.3 and for distances from 10 to 200 km.

2.1.9 Sabetta & Pugliese (1996)

Published in *Bulletin of the Seismological Society of America*.

Based on regressions of the same data set of Italian accelerograms employed in the 1987 study of PGA and PGV by the same authors (Sabetta & Pugliese 1987).

The sites were classed as stiff, shallow alluvium (H < 20 m) and deep alluvium (H > 20 m), with stiff sites having shear wave velocities in excess of 800 m/s and alluvium sites values between 400 and 800 m/s. Figure 2.10 shows the M-R distribution of the Italian dataset of Sabetta & Pugliese (1996); the site classification is also indicated by the symbols used in the plot.

The equations do not include style of faulting as an explanatory parameter. The rupture mechanisms of the earthquakes are not reported but from the list of events given in Sabetta & Pugliese (1987) it is clear that the database consists of reverse and normal events.

The authors recommend that their equations should not be used for earthquakes of magnitudes less than 4.6 or greater than 6.8, and also that they should not be used to predict ground motions at distances greater than 100 km.

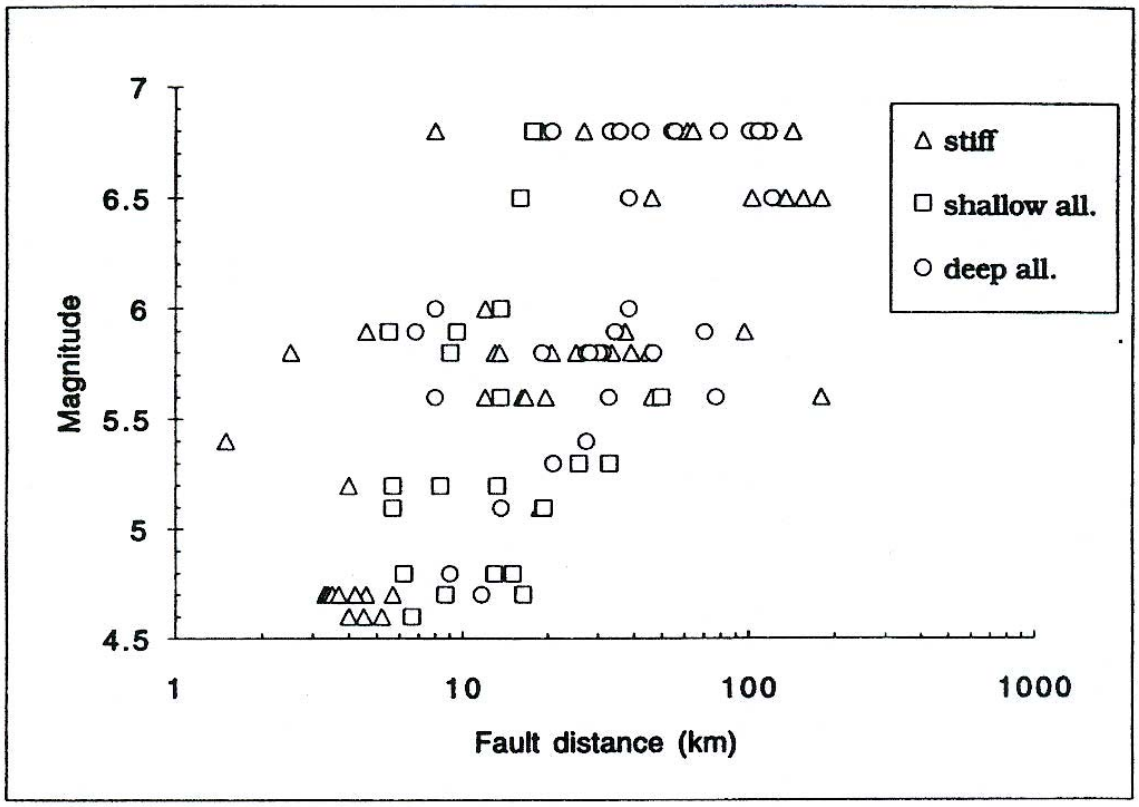

Fig. 2.10: Dataset of Sabetta & Pugliese (1996) in M-R space, with indication of site classification

2.1.10 Somerville et al. (2001)

Published as a report of the UGSG, but not an Open-File Report.

The study is based on a hybrid-empirical approach, in which broadband records are simulated and regressions then formed on the spectral ordinates. Unlike the other equations for the central and eastern United States, which are based on stochastic simulations, Somerville et al. (2001) used deterministic, finite-fault simulations.

The equations are derived specifically for hard rock sites in the central and eastern US, which is stated to correspond to a shear wave velocity of 2,830 m/s.

Separate equations are derived for rifted and non-rifted zones, the former characterised by seismicity distributed over a depth range from 0 to 30 km, whereas in non-rifted zones, the seismicity is concentrated in the uppermost 10 km. In terms of focal depth distributions, these two scenarios may correspond to Alpine Foreland and Alp regions of Switzerland. Apart from this distinction of tectonic regimes, there is no explicit reference to style of faulting in the models.

The authors do not make any categorical statements regarding ranges of applicability of their equations.

2.1.11 Spudich et al. (1999)

Published in *Bulletin of the Seismological Society of America*, these equations are essentially an update of Spudich et al. (1996).

Relations obtained from regressions on dataset of accelerograms from extensional tectonic regimes around the world.

Relations include dichotomous term for site geology, which are crudely grouped because of the lack of detailed information regarding site conditions at a large number of the stations. The "rock" category, which is 25 % of the database, includes hard rock, soft rock and unknown rock stations; the "soil" category includes generic soil sites and all sites with soil deposits of 5 m or more. In comparing their predictions with those from Boore et al. (1997), they assume a value of 620 m/s as the shear wave velocity for the rock sites. Figure 2.11 shows the M-R distribution of the Spudich et al. (1999) dataset divided into the two site classifications employed in that study.

The equations do not include style of faulting as an explanatory variable, but the mechanisms of the earthquakes in the dataset are only strike-slip and normal – as would be expected in extensional tectonic regimes – in approximately equal proportions.

The authors of this study make no specific statement about the ranges of applicability of the equations but they do note that the magnitude dependence is constrained up to M_w 7.7.

2.1.12 Toro et al. (1997)

Published in Seismological Research Letters.

The equations are derived by regression on stochastically generated accelerograms using source and path parameters calibrated for Eastern North America (ENA).

The equation is derived explicitly for "hard rock" sites in ENA, defined in their paper as having a near-surface shear wave velocity is 1,830 m/s; at WS-3/SP2, the lead author, Gabriel Toro, informed EG2 that this was a typographical error and the shear wave velocity was in fact 2,800 m/s (i.e. 9,000 rather 6,000 feet/sec).

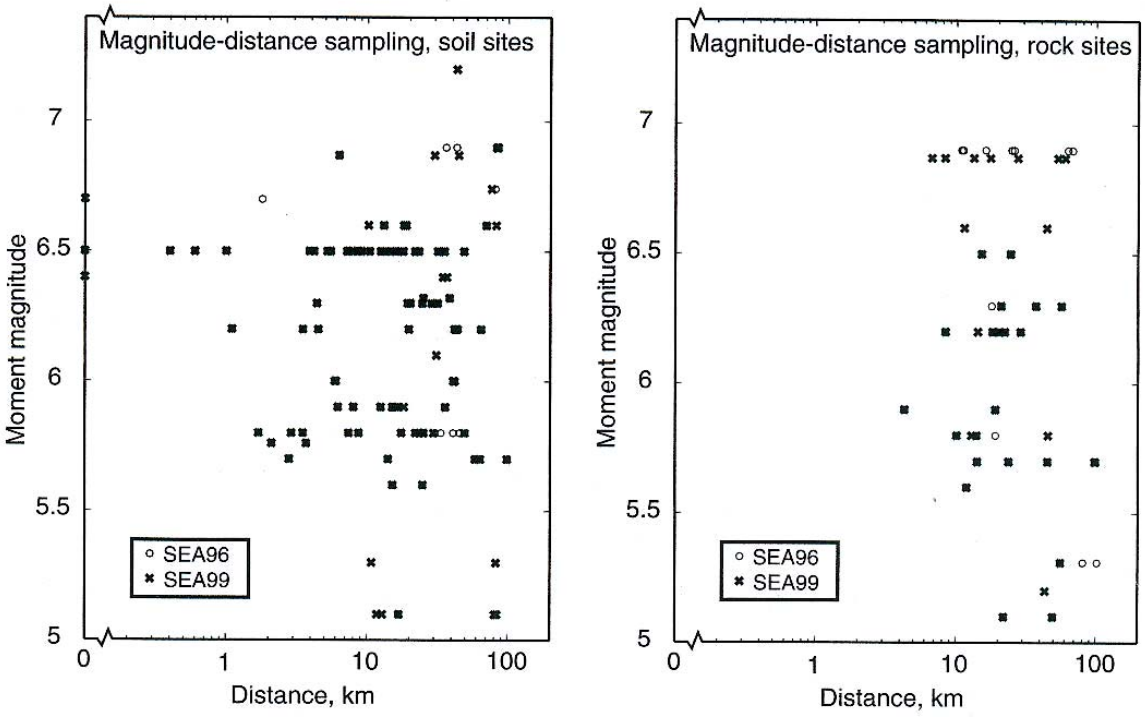

Fig. 2.11: Dataset of Spudich et al. (1999) in M-R space grouped by site classification soil (left) and rock (right) sites

Separate equations are derived for regions defined as "mid-continent" and "Gulf"; most of central and eastern USA and Canada are covered by the mid-continent equations. In common with the ENA equations of Atkinson & Boore (1997) and Somerville et al. (2001), the equations of Toro et al. (1997) do not inclue a factor for the style of faulting.

The authors do not make any explicit statements regarding ranges of applicability of the equations.

2.1.13 Bay (2002)

Originally published as a PhD Thesis from ETH, Zurich, and recently published in the *Bulletin of the Seismological Society of America* (Bay et al. 2003). The work has also been supplemented by a series of technical notes produced within the PEGASOS Project that have explored and re-examined various aspects of the model.

Apart from the attenuation relationship for PGA presented by Smit (1998), this is the first attenuation equation derived specifically for Switzerland. The study employed a dataset of 2,958 waveforms (1,782 vertical and 1,176 horizontal) from 292 events that occurred in Switzerland and in the border regions of Italy, France and Austria from January 1984 to January 2000. All of the records were from digital instruments, including short-period seismometers, broad-band seismographs and strong-motion accelerographs. However, the accelegraph records were not used for the regressions but only to investigate the influence of site conditions on the predictions, since the strong-motion stations are stated to be mainly NEHRP classes C and D, whereas the seismographs are generally from sites classified as NEHRP classes A or B. The records cover a magnitude range from M_L 2.0 to M_L 5.2, but 80 % of the data is from earthquakes no larger than M_L 3.0 (Figure 2.12). The recordings, and the ray paths, provide comprehensive geographical coverage of the Swiss territory (Figure 2.13).

Several selection criteria are applied to define the data set used for the regressions, resulting in the use of about 10 % of the regional data available for the period covered. These criteria include a signal-to-noise ratio of at least 20 and the rejection of all clipped signals; the latter criterion resulted in the removal of most of near-source recordings from larger (M_L > 2.9) events, as shown in Figure 2.12.

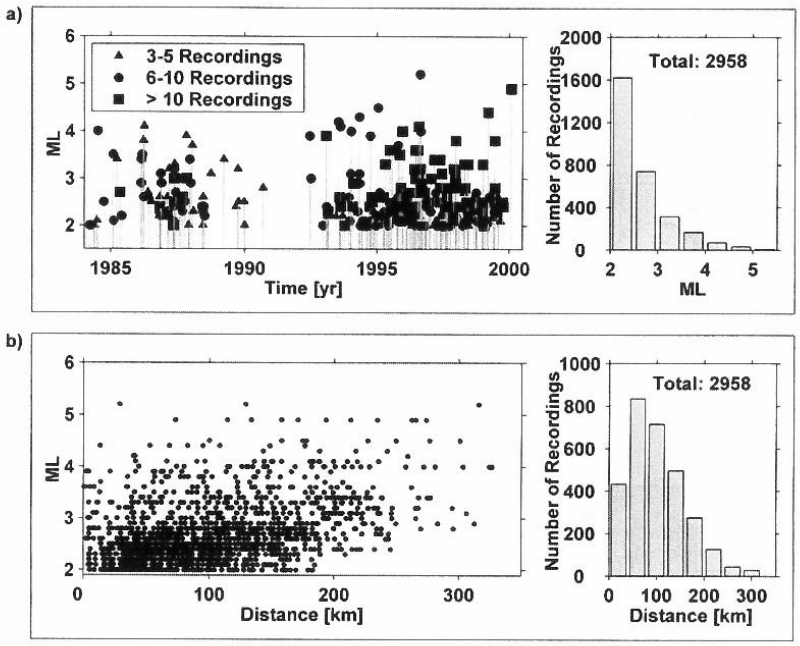

Fig. 2.12: Distributions of data set employed by Bay (2002)

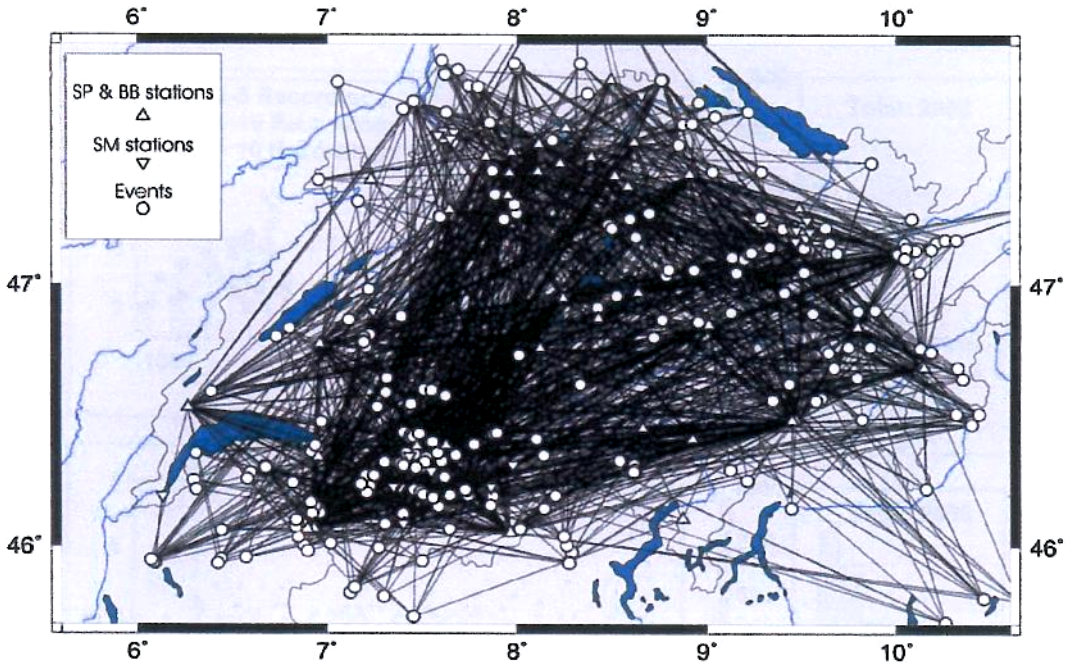

Fig. 2.13: Ray paths of data set used by Bay (2002)

The method employed by Bay (2002) was essentially the same as that used previously by Luca Malagnini and co-workers in studies for Italy and Central Europe (Malagnini et al. 2000a, b; Malagnini & Hermann 2000).

2.1.14 Rietbrock (2002)

Following discussions at WS-3/SP2 regarding concerns expressed by members of EG2 with respect to the work of Bay (2002), Dr Andreas Rietbrock was commissioned by the PEGASOS Project to carry out a re-evaluation of the data set employed in the original study. The work produced a series of brief technical notes, including presentation of the analysis by Andreas Rietbrock (EXT-TN-0306), comments on the work by Frank Scherbaum (EG2-TN-0314) and an interpretation of the Rietbrock model by TFI Norm Abrahamson.

The analysis performed by Andreas Rietbrock made use of a subset of the Bay (2002) data set, using only the vertical components of motion, in order to "*homogenise this very heterogeneous data set*". Furthermore, earthquakes recorded by less than four stations were excluded since a common corner frequency is assumed for all records corresponding to the same event. The main focus of the re-evaluation of the data was to obtain better constraint on the attenuation by using a procedure to decouple the determination of anelastic and geometric attenuation (Rietbrock 2001, Haberland & Rietbrock 2001).

2.2 Applicability of Models to Switzerland

Before discussing the applicability of the different attenuation equations to Switzerland, it is useful to briefly set the scene. Figure 2.14 shows the main tectonic provinces of Switzerland, consisting of the Alpine Foreland, where the four NPP sites are located (see Figure 1.1) in the north and the Alpine Belt to the southwest; the Foreland consists of the Molasse Basin and Jura. The northernmost part of Switzerland lies within the Upper Rhine Graben. Focal depths in the Alpine Belt are limited to less than 20 km, whereas in the Foreland depths reach 30 km (Figure 2.15).

In the first version of this logic-tree prepared for WS-3/SP2, scaling factors for each of the attenuation equations were derived from the residual plots produced using the Swiss records in the WAF database, an example of which is shown below in Figure 2.14. The data available to explore the scaling factors is a very limited collected of recordings from Switzerland and neighbouring areas obtained from strong-motion (SM), short-period (SP) and broadband (BB) instruments. The BB records have been shown to give uniformly lower motions, by a factor of about 9. Given this consistent apparent underestimation of the strong-motion amplitudes from the BB records, it was decided to exclude these from further considerations and to make judgements based primarily on the SM data.

There are only 68 Swiss strong-motion records from rock site available for these analyses, and since residuals have only been calculated for those records for which all of the required parameters (magnitude, distance) used in the equations are available, the numbers used varies considerably from equation to equation. Another important limitation is that the vast majority of the data is from earthquakes of magnitude smaller than M_w 5, which is actually the lower limit that will be used in the hazard integrations. Hence, there is very considerable uncertainty regarding any extrapolation of observed patterns to the higher values of magnitude of relevance to the hazard calculations. This (epistemic) uncertainty would need to be captured by the range of scaling factors adopted for each equation.

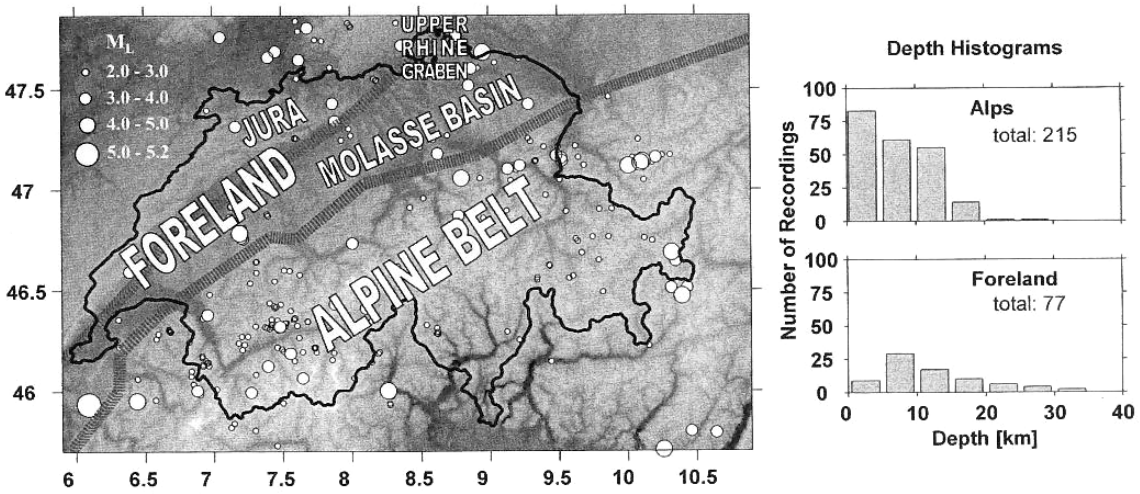

Fig. 2.14: Map of Switzerland, showing tectonic provinces and epicentres of earthquakes used in the Bay (2002) study, together with histograms of the depth distributions of the recordings (Bay et al. 2003)

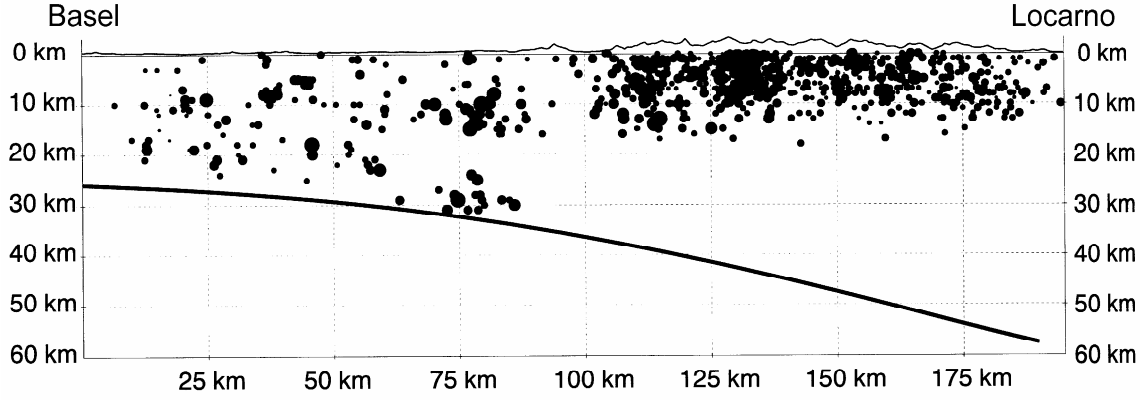

Fig. 2.15: NNW-SSE cross-section of Swiss crust showing focal depth distributions in the Foreland and the Alpine Belt, and the inferred depth of the Moho (PEGASOS Report TP2-RF-0176)

The residual plots, such as that in Figure 2.16, show trend lines, straight lines fitted to the data showing the apparent mean trend of the residuals with magnitude, distance or focal depth. The gradients of these lines are often tenuously constrained and if one focuses exclusively on the strong-motion data (indicated by x in the plots) the trend is often less pronounced and frequently not apparent at all. Equally important to note is the fact that most of the residuals, and in a few cases nearly all of them, correspond to magnitude ranges outside the range of applicability of the attenuation equations. Therefore, the approach that would be adopted here, as a first approximation, is to simply examine, at each period, the residuals in the magnitude range of about 4 to 5 to assess an average value and the spread of the residuals. The residuals are calculated as the logarithm of the observed amplitude minus the logarithm of the predicted median amplitude. The residuals could therefore be interpreted as follows: negative residuals would imply that Swiss data is over-predicted and a scaling factor of less than 1 would need to be applied, and conversely for positive residuals.

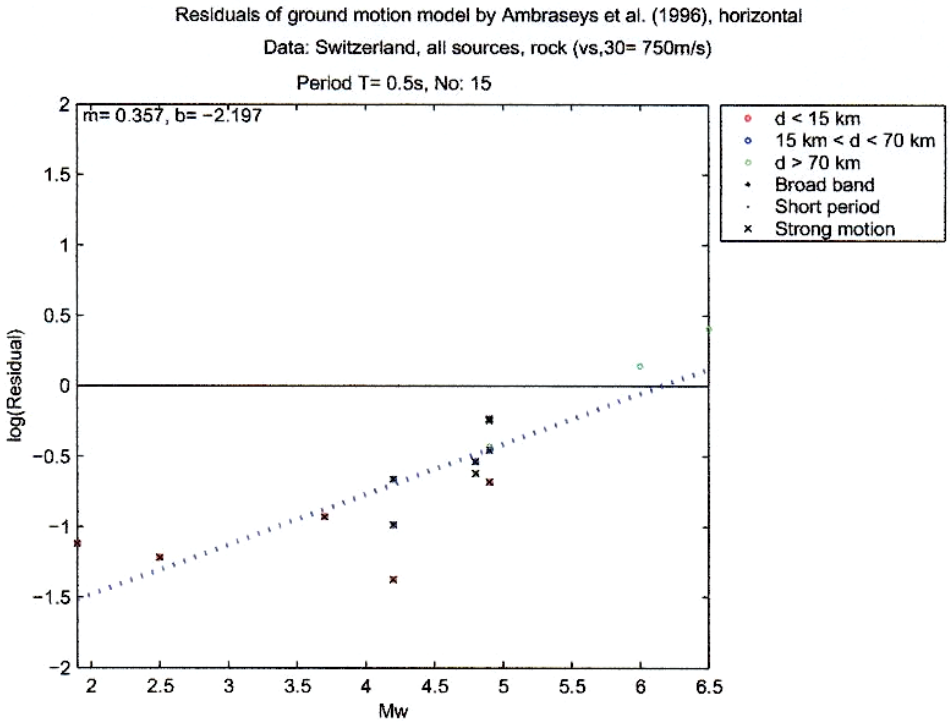

Fig. 2.16: Example of an apparent, but poorly constrained residual trend with magnitude; Swiss data and equation of Ambraseys et al. (1996) at 0.5 second response period

The scaling factors inferred in this way are uniformly less than 0.6, which implies that all of the predictions would need to be reduced by at least 40 % and in some cases by 75 %. There is no compelling reason to believe that earthquakes in Switzerland should produce ground motions that are so much lower in amplitude than other regions of the world, and hence the only conclusion drawn at this stage is that the quality and quantity of the current Swiss strong-motion database is simply insufficient to be used at this stage for calibration or verification of the selected attenuation equations. This approach was therefore abandoned. Support for the Swiss strong-motion data not being exceptionally different from European strong-motion in general is provided by the PGA equation of Smit (1998), which is compared with other equations for Europe and other parts of the world in Figure 2.17.

The conclusions that can be drawn from Figure 2.17, however, are limited, because in plotting the curves no adjustments have been made for different definitions of the horizontal component of motion, the magnitude scale and the distance metric, and furthermore it has been assumed that all "rock" classifications are equivalent. Figure 2.19 shows a comparison of the Smit (1998) PGA equation with the PGA equation of Ambraseys & Bommer (1991) that explicitly includes the focal depth, h, as an explanatory variable:

$$\log(PGA) = -0.87 + 0.217M_s - \log\sqrt{R_{jb}^2 + h^2} - 0.00117\sqrt{R_{jb}^2 + h^2} \qquad (2.1)$$

where PGA is measured in units of *g*. The equation of Smit (1998), in which PGA has units of nm/s^2, is:

$$\log(PGA) = 5.230 + 0.868M_L - \log(R_{hyp}) - 0.001059(R_{hyp}) \qquad (2.2)$$

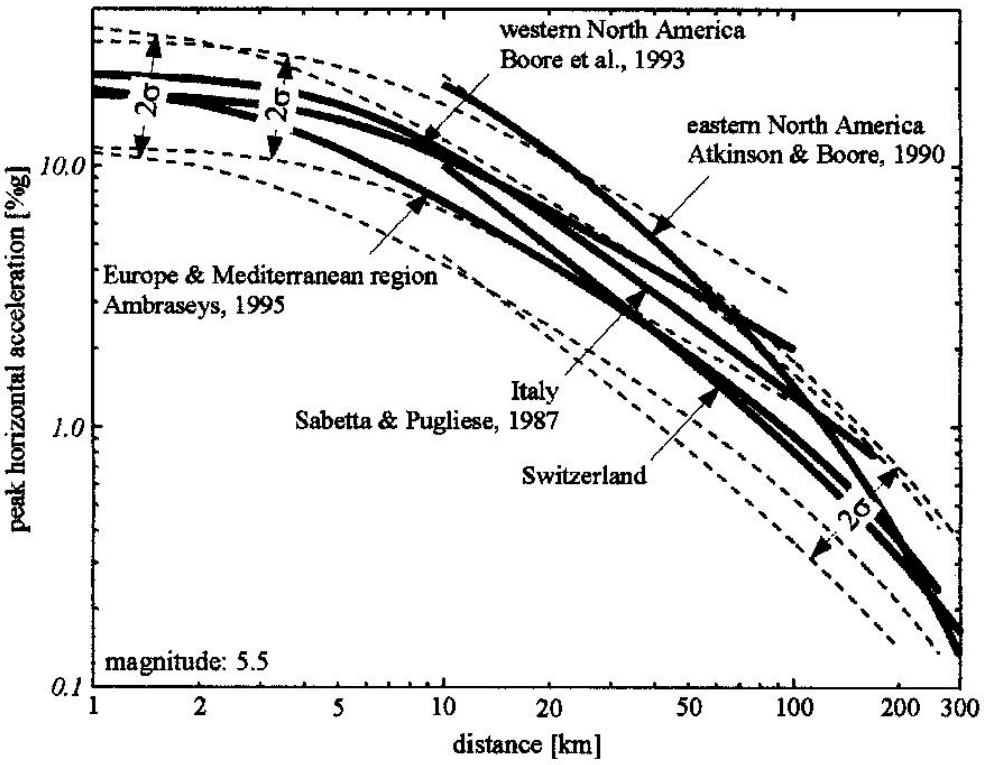

Fig. 2.17: Co*m*parison of predicted PGA values for an earthquake of magnitude 5.5 from the Swiss equations of Smit (1998) with two equations for Europe and others for western and eastern North America

For small magnitude earthquakes, R_{jb} and R_{epi} are equivalent, hence Eqs.(2.1) and (2.2) can be assumed to have the same distance metric. Both equations use the larger horizontal component of motion, but a factor of 0.86 is applied to tranform this to the geometric mean component that is the PEGASOS standard. In Figure 2.19 the two equations are plotted together with the rock data from the St. Dié earthquake (Figure 2.18), which is discussed in greater detail towards the end of this Section. The earthquake is reported to have a moment magnitude M_w of 4.8, which both Eqs.(3.5) and (3.6) convert to M_s 4.3. Eq.(3.7) suggests that the equivalent M_L value is 4.8, but as shown in Figure 2.18 a direct estimate of M_L is available, the reported value being 5.4 (although this is not from the Swiss Seismological Service and it is possible that this M_L value is not compatible with that determined by SSS, but no M_L estimate is available at http://seismo.ethz.ch).

Using M_L 5.4 and M_s 4.3, the equations of Ambraseys & Bommer (1991), derived using data from across southern Europe and the Middle East, and the equation of Smit (1998), derived from Swiss data, are compared in Figure 2.19, together with the rock site recordings from the St Dié earthquake.

Notwithstanding the uncertainty in the magnitude values, and particularly the possibility that the appropriate M_L value for the Smit (1998) equation may be lower than the M_L 5.4 value employed, the differences between the median predictions are less than a factor of 2. This is comparable to the mismatch between the Swiss records and the predictions of Ambraseys et al. (1996) in the region of M_w 4.8 in Figure 2.16. The equation of Smit (1998) is based mainly on vertical component velocity records from seismographs on rock, supplemented by a small number of accelerograph records. The equation of Ambraseys & Bommer (1991) is based on strong-motion records from a range of site conditions, but using a site-independent model, which therefore represents an "average" condition. This alone could explain difference between the two curves in Figure 2.19.

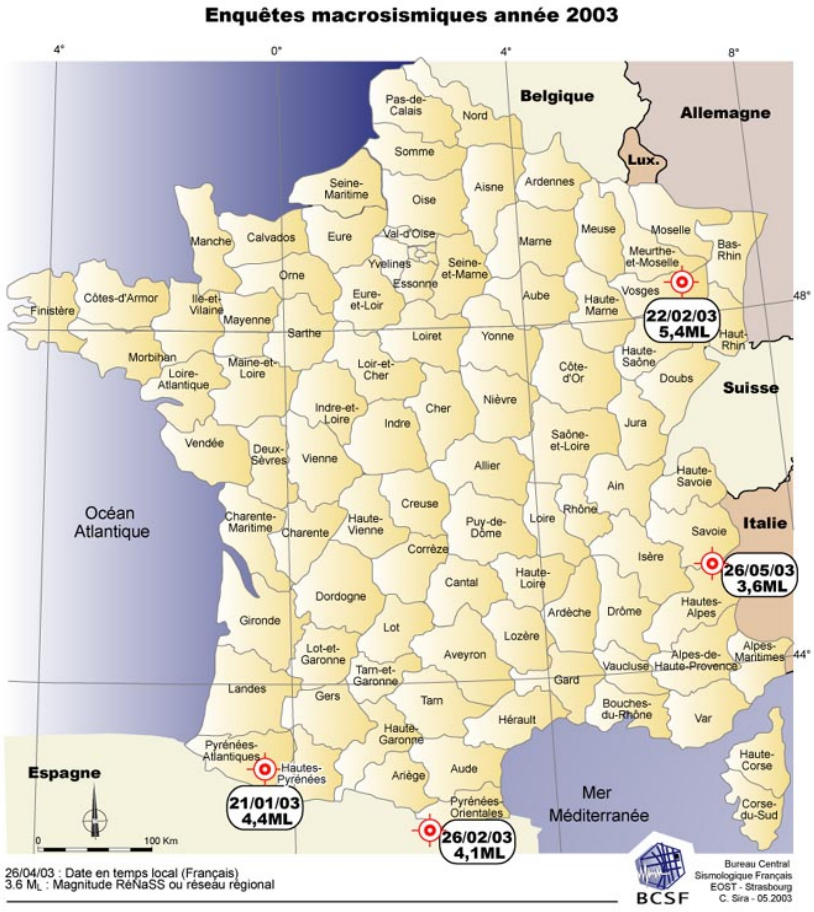

Fig. 2.18: Location map of felt earthquakes in France in 2003 (http://www.seisme.prd.fr)

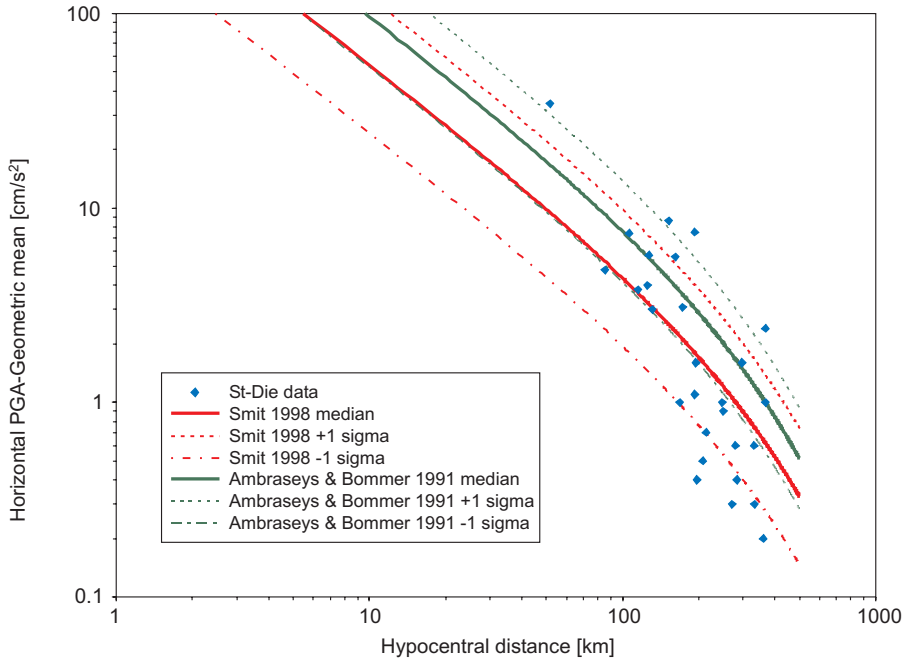

Fig. 2.19: Comparison of Smit (1998) and Ambraseys & Bommer (1991) PGA equations with the rock site data from the St. Dié earthquake

The foregoing discussion is considered to be inconclusive. On the one hand there is an implication that the limited Swiss strong-motion data on average is of much lower amplitude that data from the rest of Europe and from North America. The accelerograph data for Switzerland is currently too limited, in number and in ranges of magnitude and distance, to provide robust estimates for ground-motion models and it is therefore not given significant weight in constructing the ground-motion logic-tree presented herein. This is vindicated by the fact that there are currently no strong-motion attenuation equations for response spectral ordinates derived from these recordings. In passing it is worth noting that with respect to the Swiss seismograph recordings, the location of the instruments may to some extent influence the amplitudes of motion that they display. Data provided in PEGASOS Report TP2-TN-0368 show that at least a third of the stations are buried at some depth in tunnels and shafts (Figure 2.20). Although it is impossible to infer the likely effects on the recordings without much more detailed information, it is also noted in passing that half of the recordings are not located on flat ground (Figure 2.20). Tables 2.2 and 2.3 also show that some of the stations are located at depth.

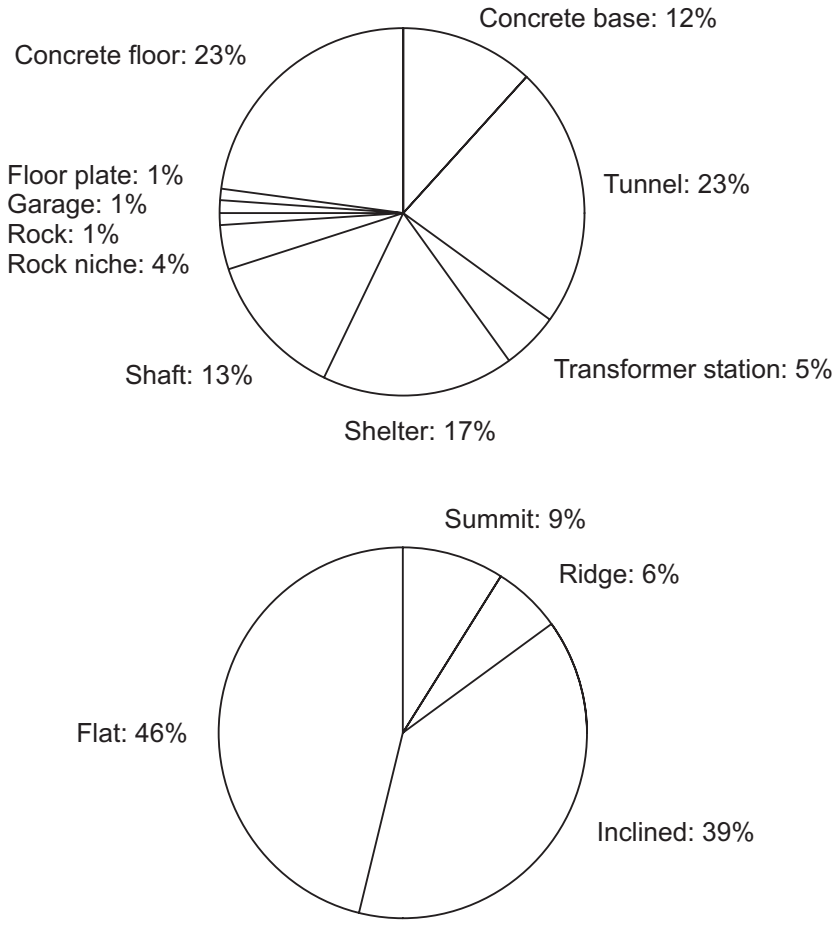

Fig. 2.20: Locations (upper) and topography (lower) of Swiss Seismological Survey instruments

Tab. 2.2: Estimates of vertical overburden (OB) at SSS instrument locations, indicating quality factors with which these estimates are made

OB (m)	Q1 (± 2 m)	Q2 (± 10 m)	Q3 (± 50 m)
0	35	0	0
2 – 4	8	0	0
10	8	0	0
20	1	5	1
30	0	3	1
50	1	3	0
100	0	1	0
150	0	0	1
500	0	0	1

Tab. 2.3: Estimates of shortest depth to the surface (D) at SSS instrument locations, indicating quality factors with which these estimates are made

D (m)	Q1 (± 2 m)	Q2 (± 10 m)	Q3 (± 50 m)
0	18	0	0
$0 < D \leq 1$	8	1	1
$1 < D \leq 2$	9	0	0
$2 < D \leq 5$	8	0	0
$5 < D \leq 10$	7	0	0
$10 < D \leq 50$	1	11	1
100	0	0	1
200	0	0	1

The main issue to be addressed, however, is applicability of the Swiss stochastic models that have recently been derived. Being specifically derived for Swiss conditions, they would be expected to be included in the logic-tree and also assigned a significant proportion of the total weighting, perhaps of the order of one half, the other half of the weight applying to other equations that are better constrained at short distances or higher magnitudes, or include more explanatory variables, thereby capturing the epistemic uncertainty that would be ignored if the Swiss stochastic model were to be used alone.

At the time of finalising this GM logic-tree, there are a few options available to SP2 regarding Swiss stochastic models. The work of Bay (2002) was introduced to the project participant early on in the project but at the SP2 workshops many doubts and concerns were raised about the data, the analysis and the results. In an attempt to resolve the problems regarding the input parameters to the stochastic model Dr Andreas Rietbrock was commissioned to carry out a parallel study employing a technique that decouples the determination of geometrical and anelastic attenuation. His report (EXT-TN-0306), however, is inconclusive, reporting that the geometric spreading is not well constrained, reporting three different distance segmentations with corresponding attenuation coefficients. The average stress drop for those recordings with corner frequencies of less than 15 Hz is reported as 46 bars, with a standard deviation of 8.1

bars. Comments by Frank Scherbaum on the report of Dr Rietbrock were provided in report EG2-TN-0314, but these were also inconclusive, listing additional work that would need to be carried out in order to make a final judgement. As mentioned in sub-section 2.1.14, the main focus of the work by Andreas Rietbrock was to improve the determination of the attenuation parameters, rather than the scaling parameters, of the stochastic model, which – notwithstanding the relationships and trade-offs between the two – are not the main cause of concern. A note by TFI Norm Abrahamson on the study was presented to SP2 in January 2003 under the title "Implementation of the Rietbrock stochastic model for Switzerland". This report makes two important observations, the first being that the mean value of the Brune stress parameter obtained by Rietbrock is 46 bars and that this value is not well constrained. The second observation is that the implemented model gives results (Figure 2.21) that are similar to the implementation of the Bay (2002) model using a value of 20 bars for $\Delta\sigma$. From this it can be concluded that little is added by the Rietbrock model and it can be dropped from further consideration, the key issue remaining the applicability or otherwise of the Bay (2002) model.

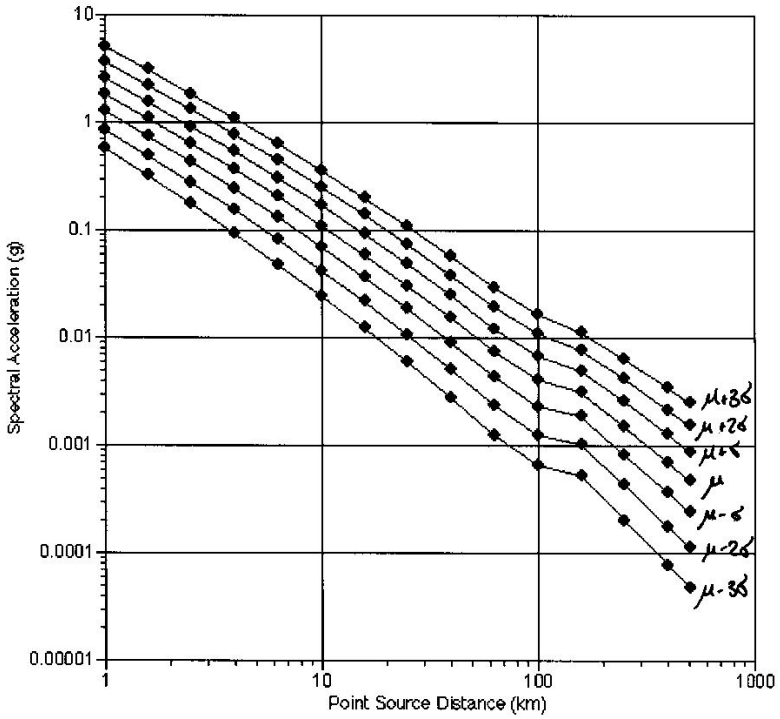

Fig. 2.21: PGA predictions from the implementation of the Rietbrock model with a stress parameter of 46 bars for an earthquake of M_w 7

The stochastic model originally derived by Bay (2002) in her PhD thesis, and subsequently published as Bay et al. (2003), has a kappa value of 0.0125 s and a very low value of $\Delta\sigma$, which is 2.7 bars in the thesis and then given as 5-10 bars in the journal paper. There is general agreement that this value for $\Delta\sigma$ is unexpectedly and unrealistically low, and the models that are being employed in the project are essentially versions of this model adjusted with higher values of $\Delta\sigma$. The key issue then becomes whether the basis for these adjustments are physical and whether they are well constrained.

As a result of the concerns regarding the low stress drop values, Dr Bay was requested to carry out additional work to explore the issue of the stress drop, the findings of which were issued in the Pegasos project reports EXT-TN-0216 and EXT-TN-0251. The first was in response to answer the question of whether or not a stress drop of 100 bars could be discarded as being

incompatible with her data, to which the response was that it could not. The second report focused on forward modelling using ranges of stress drop and kappa to compare simulations with broadband and strong-motion recordings from Switzerland. The conclusion of the second report was that the best results were obtained with a stress drop of 1 bar or even smaller. It was during the process of these exploratory studies, it was revealed that there were many problems with the broadband recordings from Switzerland, since these instruments were generally located at depth in tunnels and were producing consistently much lower motions than the strong-motion instruments. As noted previously, the number of recordings from Swiss strong-motion instruments is very small. The main conclusion that could be drawn from these exploratory studies, however, is that the value of $\Delta\sigma$ is not well constrained.

In the PhD thesis, an exercise is performed using records that were obtained between December 1999 and July 2001, which had not been employed in the analysis. These data, from earthquakes of M_w ranging from 2.9 to 4.9, were used to check the best-fit model with $\Delta\sigma$ of 2.7 bars, as shown in Figure 2.22. The most striking observation from these plots is that for events of magnitude greater than 4.5 M_w, all of the observations lie above the model with kappa 0.0125 and the low stress drop of 2.7 bars, which is essentially the published Bay et al. (2003) model.

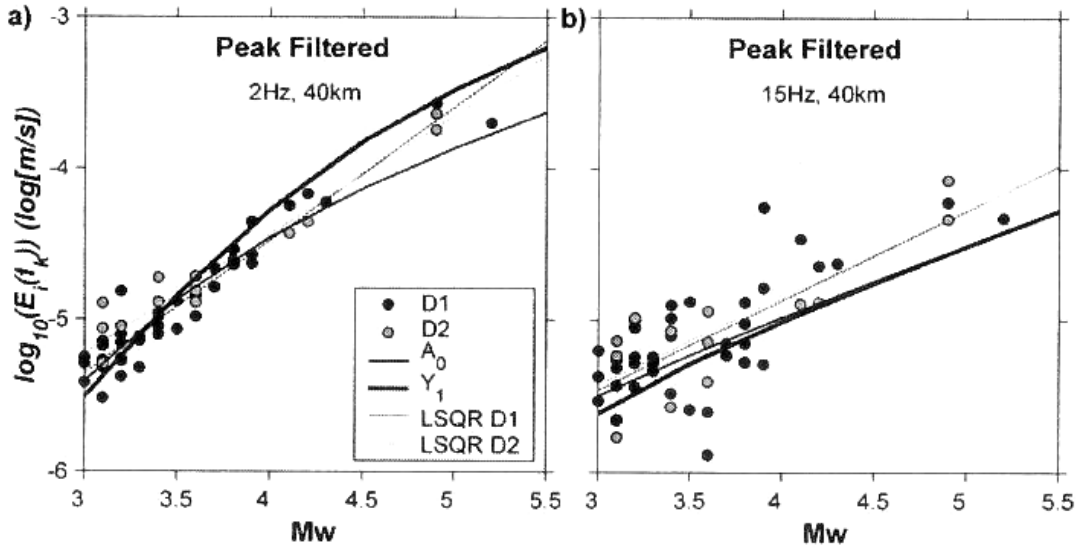

Fig. 2.22: Excitation functions at hypocentral distance of 40 km at two response frequencies and black dots show excitation terms used to calibrate theoretical model

The grey dots are average amplitudes, normalised to 40 km, of the events obtained after the end of the database used to derive the model. The thick black line indicates the excitation model with kappa 0.0125 and stress drop 2.7 bars, the thin bar the excitation model with a different attenuation function, kappa of 0.043 and stress drop 24 bars (Bay 2002).

In the PhD thesis, Bay (2002) explores two avenues for adjusting the value of $\Delta\sigma$, after stating that "a value of $\Delta\sigma$ is low and leads to unreasonable low amplitudes for large events. A number of damaging earthquakes have occurred in Switzerland in historic times, most notable the 1356 Basel event. The EMS98 distributions of these events, reaching intensity IX, also be difficult to explained by stress drops in the 3 bar range, even taking into account site amplification. Therefore, we conclude that model A_0 cannot be extrapolated for computing ground motions for larger (M_w > 4) events. The scaling for larger magnitudes must be different from what we observe for the smaller events". The first alternative model proposed, A_{30}, is based on the work of Ide & Beroza (2001), who use the concept of apparent stress drop, which they find to be con-

stant over 17 orders of seismic moment. Arguing that the Brune stress parameter and the apparent stress drop are related by a constant factor, Bay (2002) uses a factor of 3.3 averaged from two published values in the literature. One of two references cited as sources for this factor gives ratios of 2.3 and 4.3 depending on whether the spectrum is modelled with a rounded or sharp corner at the corner frequency (Singh & Ordaz 1994). The adjustment made in this way by Bay (2002) leads to a stress parameter of 30 bars. The adjustment is judged by the author of this report to be rather arbitrary, and furthermore the resulting model does not provide a good fit to Swiss data of small to moderate magnitudes (Figure 2.23).

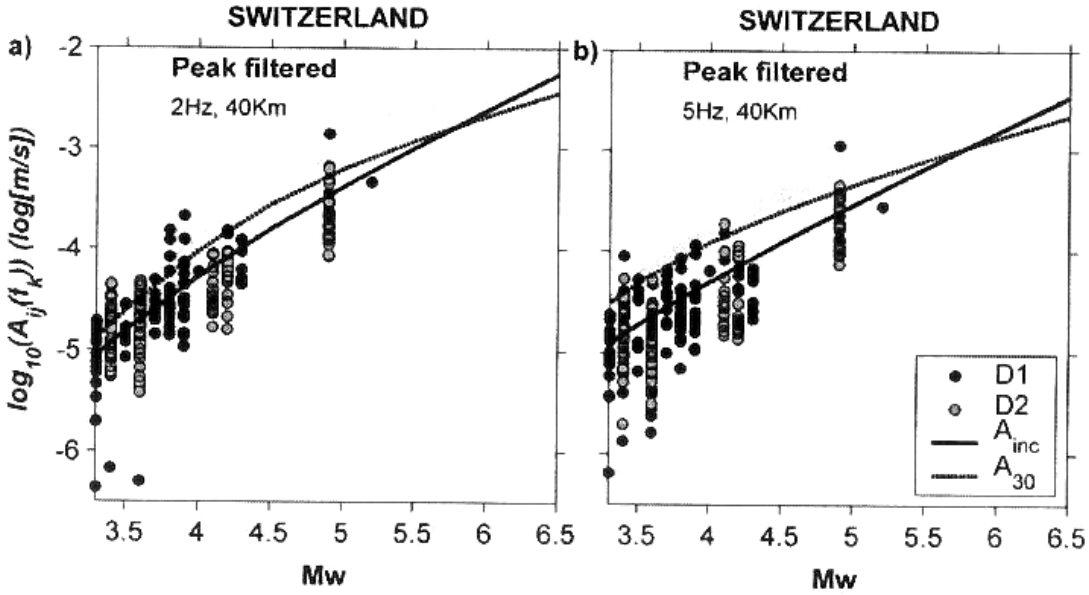

Fig. 2.23: Comparison of the adjusted stochastic models with data, as in Figure 2.22. The dashed line is the A30 model, the solid black line the A_{inc} model

The final alternative model presented, A_{inc}, relies on the work of Mayeda & Walter (1996), who propose that stress drop increases with seismic moment according to the following proportionality:

$$\Delta\sigma \propto M_o^{0.25} \tag{2.3}$$

Bay (2002) calibrates this function to California data – without ever discussing whether or how this might be applicable to Switzerland – with moment magnitudes from 3.4 to 5.6. In Figure 2.23 the A_{inc} model is shown to provide what at first glance looks like a reasonable fit to the Swiss data at lower magnitudes; in fact, the A_{inc} model was shown in PEGASOS Report EXT-TN-0209 to consistently overestimate the broad band data from which the stochastic model was originally derived, although at the same time providing a reasonable fit to the Swiss strong-motion data (Figure 2.24).

Since Bay (2002) herself rejects the basic A_0 model, and the A_{30} model is judged to be an almost arbitrary adjustment, the remaining issue is whether the A_{inc} model should be adopted. The literature on the subject of scaling of stress drop with magnitude is considerable and the issue is unresolved. The core of the controversy is that stress drops calculated for small earthquakes are often very small and therefore, if these values are taken as reliable, it is necessary for the stress drop to increase with magnitude in order to be consistent with the higher values calculated for larger magnitude events. Abercrombie & Leary (1993) present convincing evidence for the apparent breakdown of stress drop from small earthquakes being the result of near surface attenuation. The resolution of this debate is beyond the scope of this report, but it is suffice to

state here that there are good reasons to doubt the proposed model of stress drop scaling with magnitude. Even if the model were valid, in Bay (2002) the scaling is calibrated, for reasons that are not clear, to a suite of data from California. Figure 2.23 shows that the A_{inc} model does not in fact provide a good fit to the low magnitude Swiss data, in fact it is more like an upper bound envelope. The key issue, however, is that the scaling is not validated for larger magnitudes, which is where reliable estimates are required for the hazard calculations that will be performed for PEGASOS. The model gives a value of $\Delta\sigma$ of 7 bars for M_w 3, increasing to 143 bars at M_w 6.5; for a magnitude M_w 4.8 earthquake (i.e. the St. Dié event), the stress bar is lower than 30 bars, so the scaling is particular strong in the range from M_w 5 to M_w 6.5, a range in which stress drop has generally thought to be constant. In view of all of these shortcomings and unexplained features of the A_{inc} model, the author judges it to unsuitable for use in the GM logic-tree and it is therefore, together with the A_0 and A_{30} models, excluded. This decision was not taken lightly since these are the only available equations that have been specifically derived for Switzerland, but the fact remains that the original model (A_0) is rejected even by its author as unsuitable for application to larger magnitude events, and the other two models are adjustments whose validity at larger magnitudes has not been demonstrated. On the other hand, the 12 equations that are being retained have all been directly calibrated for earthquakes in the magnitude range of relevance to the seismic hazard calculations (M_w 5.0 to 7.5).

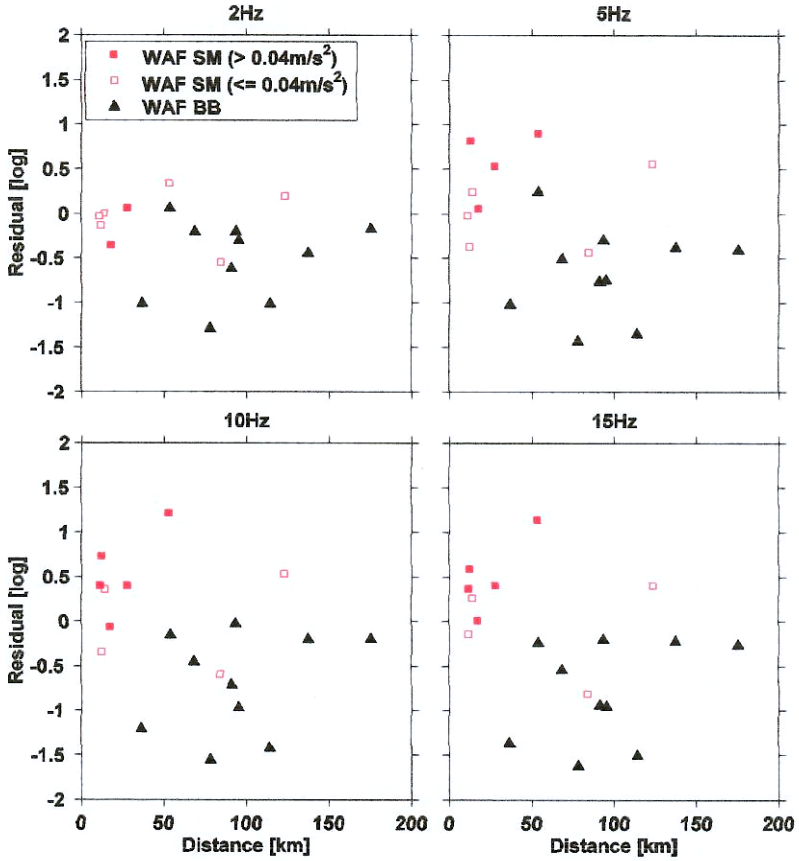

Fig. 2.24: Residuals calculated from the A_{inc} model and the Swiss data in the WAF database, plotted as a function of distance (PEGASOS Document EXT-TN-0209)

The decision not to include the Swiss stochastic models in the GM logic-tree seems to have been vindicated by the M_w 4.8 St. Dié earthquake that occurred on 22 February 2003, two days prior to WS-4/SP2. The earthquake occurred in France, about 120 km north-northwest of Basel, and was recorded by strong-motion instruments in France, Germany and Switzerland. The event is particularly significant because it is just below the lower magnitude limit of the hazard

integrations and at the same time towards the upper limits of applicability of the Swiss stochastic models. Figures 2.25 to 2.27 compare the rock site recordings of the earthquake with the predictions from all of the candidate attenuation equations for PGA and for periods of 0.1 and 0.4 s. In all cases, the Swiss stochastic models provide one of the worst fits to the data; in particular the A_{inc} model is underestimating the recorded amplitudes. The closest recording is at 40 km from the source and the others are all beyond 100 km, so this data does not resolve the applicability at short distances. However, Figure 2.12 also shows that the data set of Bay (2002) provided no constraint for M_w 4.8 at shorter distances and therefore including the stochastic model in the logic-tree would have not improved the near-source estimates of ground motion.

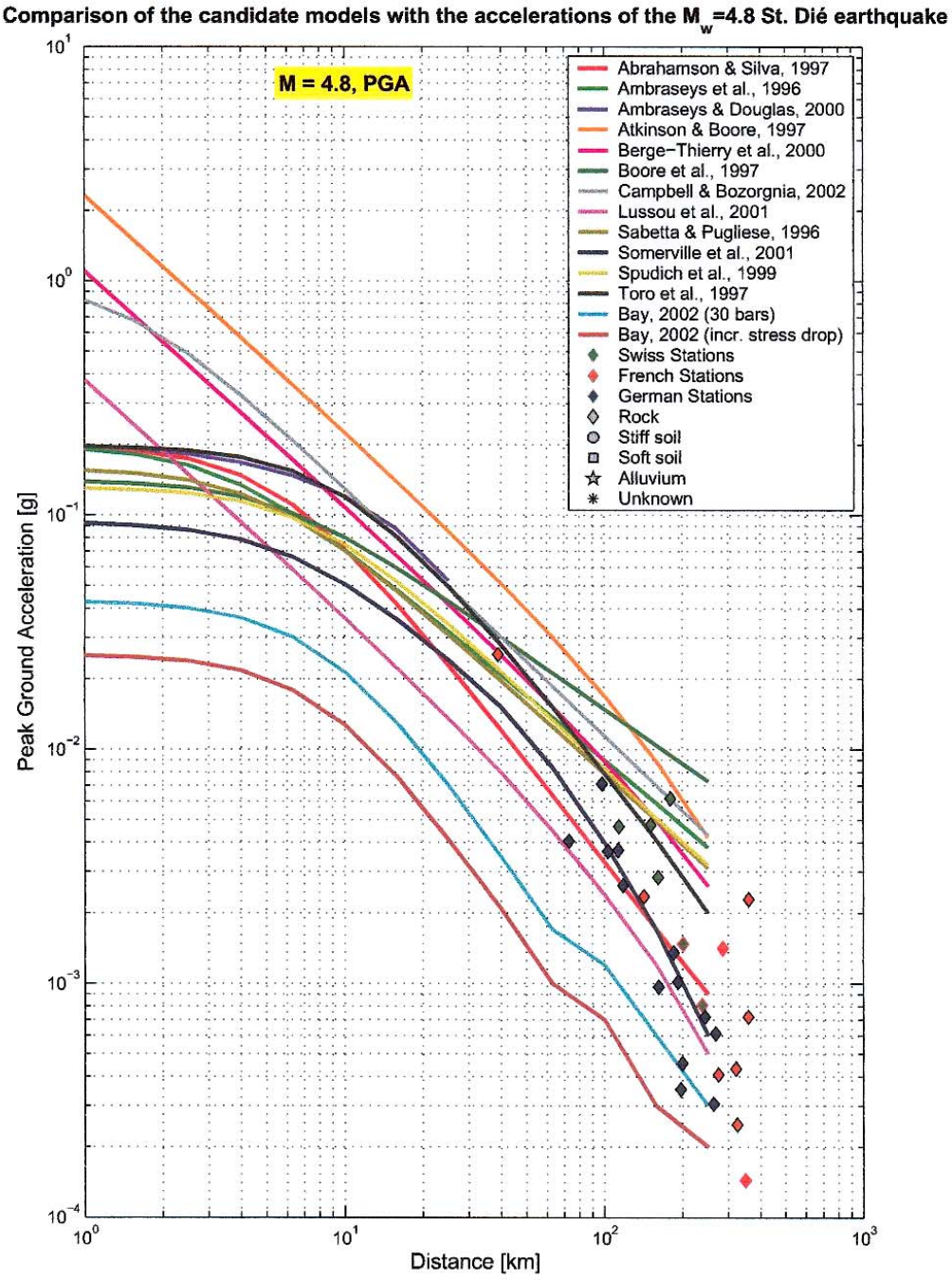

Fig. 2.25: Comparison of St. Dié rock site recordings and candidate ground motion models for PGA

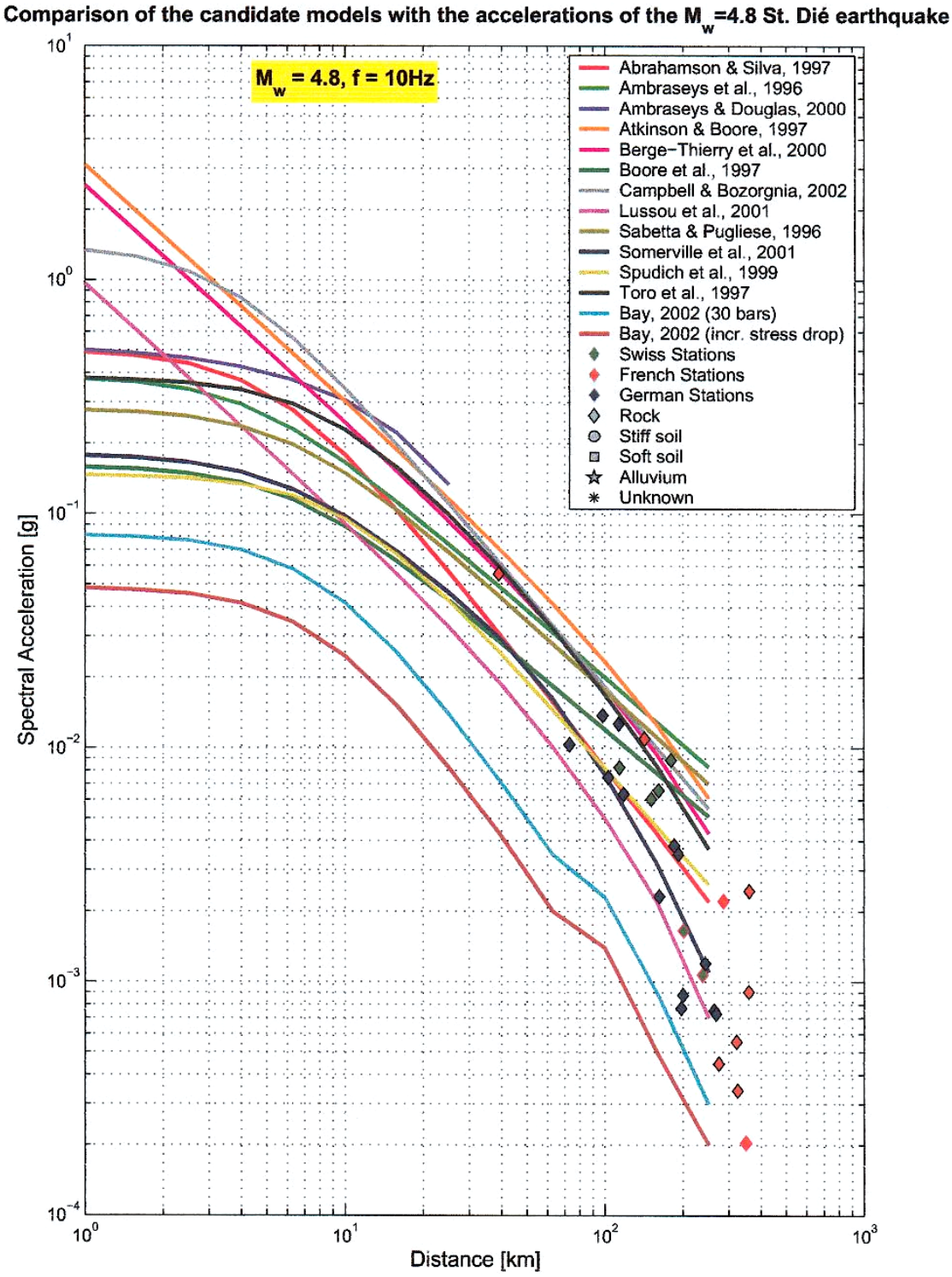

Fig. 2.26: Comparison of St. Dié rock site recordings and candidate ground motion models for spectral acceleration at 0.1 second

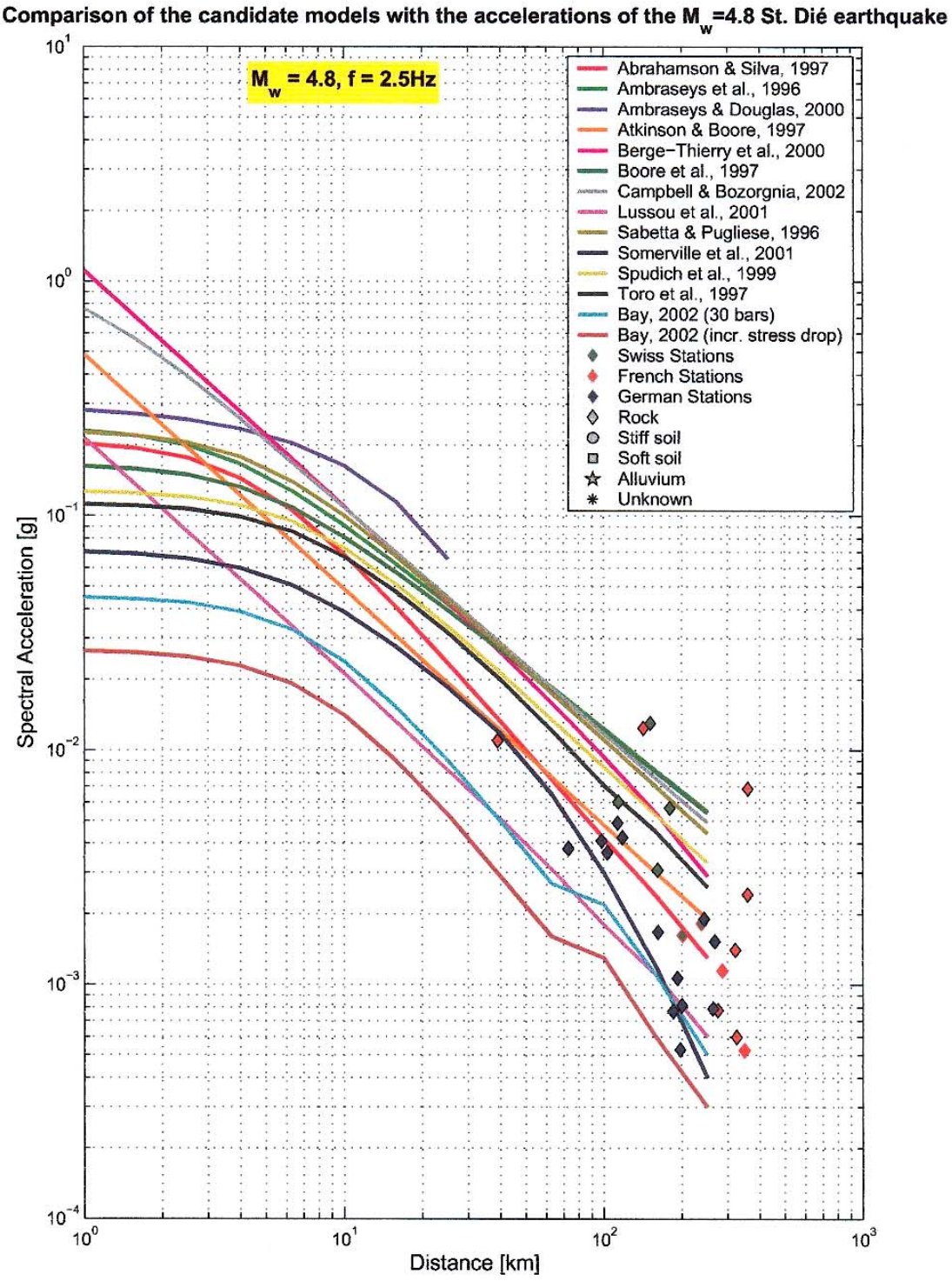

Fig. 2.27: Comparison of St. Dié rock site recordings and candidate ground motion models for spectral acceleration at 0.4 second

3 MEDIAN HORIZONTAL MOTION

This Chapter describes the logic-tree for the median horizontal ground motion. The first step is to choose which equations are to be included in the model, the magnitude-distance bins in which the weights are to be applied, and the criteria for assigning these weights. Other issues that are addressed include the conversions that are required to account for different definitions of the horizontal component of motion and the use of different magnitude scales, the fact that not all of the equations provide coefficients at all of the required response frequencies. The Chapter also addresses the need for the estimates of median horizontal motion from all of the equations to be adjusted to a single reference site condition and the need to include scaling factors for the three specific styles of faulting including in the SP1 seismic source zone models.

3.1 Logic-Tree Structure

All of the equations presented in Section 2.1 have been derived by well respected researchers in the field of engineering seismology and most of them have been published in reputable peer-reviewed journals. On this basis, there is no reason to reject any of them. The only other reason to not select an equation would be because there was a clear and proven proof that it represented conditions that were utterly incompatible with those encountered in Switzerland. Although it does not for a moment imply that western or eastern North America, or southern Europe for that matter, are directly comparable to Switzerland, in seismological terms, there seems to be no compelling reason to drop any of the equations on this basis. The exception to this, paradoxically, was the decision, explained in Section 2.2, not to include either of the two stochastic models derived specifically for Switzerland, Bay (2002) and Rietbrock (2002). This leaves 12 equations, four derived mainly from western US data, 3 derived for central and eastern North America, 3 derived from mainly European data, one from Japanese data, and one from data from extensional regimes, in which the data set is dominated by records from western North America.

One of the main reasons for choosing a large number of equations is that this will help to ensure that the epistemic uncertainty is captured. Since there are judged to be no usable equations available specifically for Switzerland, or indeed for Central Europe, there is a need to include many equations that will be likely to collectively provide predictions that bound the expected levels of ground motion from Swiss earthquakes.

Another reason is that if a large number of equations are included in the logic-tree, the results will not be sensitive to relatively abrupt changes in weights passing from one M-R bin to another, hence the weights can be assigned without worrying about creating "jumps" in the output.

A counter argument to using a large number of equations is that if two or more equations are derived from essentially the same data sets using very similar regression models, the influence of that particular model will be exaggerated. It is precisely for this reason, for example, that the equation of Campbell (1997) has been dropped since it is considered as having been superseded by the equation of Campbell & Bozorgnia (2002). A similar reasoning could be applied to reject the equation of Ambraseys et al. (1996) since the equation of Berge-Thierry et al. (2000) uses the same European data set, expanded and also supplemented by records from California. However, the two data sets are different as are the regression models, hence my judgement is that both should be included. To exclude an equation purely on the basis that it gives similar predictions to another equation, despite being based on a different data set and/or attenuation model, could be artificially increasing or decreasing the epistemic uncertainty, depending on where the predictions from two equations lay with respect to the others.

3.2 Selected Proponent Models and Weights

This section explains the application of the weights to each of the 12 selected attenuation equations. There are reasons to consider making the weights a function of response frequency, these including the fact that it may be desirable to give lower weight to those equations whose coefficients at particular frequencies have had to be interpolated or extrapolated, and the fact that some of the studies have larger data sets for PGA regressions than for SA regressions (Boore et al. 1997) while others use less and less data for longer periods because of filter cut-offs (Abrahamson & Silva 1997). Furthermore, it is apparent from the preceding section that there is greater uncertainty associated with adjustments to the reference site conditions for high-frequency motions. However, the first two factors mentioned above will have very little influence on the assigned weights, and the third factor has been accounted for by capturing greater epistemic uncertainty in the site condition adjustment factors for higher frequencies. Therefore, the weights applied to the equations hold for all nine response frequencies of interest to the project.

The first sub-section explains the selection of magnitude-distance bins for the application of the weights. The five sub-sections that follow thereafter describe the application of "gradings" that reflect the confidence in each equation with respect to its characteristics in terms of the following factors that reflect the reliability of the equation for predicting ground motions in a particular M-R bin in Switerland:

- Coverage of the data set in M-R space
- The source-to-site distance metric used in the equation
- The tectonic environment for which the equation is derived
- The size of the adjustment made for the reference site condition
- The inclusion of additional explanatory variables in the equation

For all of the gradings, the "neutral" value is taken as 10. If there is a low confidence in a particular equation in a particular M-R bin regarding one of the characteristics listed above, it will be assigned a grading of less than 10. Similarly, an equation judged to be particularly well suited or well calibrated with respect to a feature will be assigned a value greater than 10. The gradings are designed to be symmetrical: if an equation judged to be poor in a particular respect is assigned a grading of 4, then another equation judged to be as good as the previous one was poor will be assigned a grading of 25.

The absolute values of the gradings are not important. The important feature is the spread of assigned grades for each feature; those features judged to be particularly important, such as coverage of M-R space, may have gradings from 0 to more than 30, whereas gradings for site condition adjustments may range from 7 to 10.

Once the grades have been assigned, the overall grading of each equation in each M-R bin is determined by simply multiplying the individual grades; an equation judged to be "neutral" in all respects for a particular M-R bin will have an overall grading of 100,000. As described in the final sub-section, the weights are then determined by simply normalising the overall grades so that in each M-R bin their sum is zero.

3.2.1 M-R bins for application of weights

The weights assigned to the different candidate equations are specific to each response frequency and also to bins of magnitude and distance. The minimum magnitude to be used in the integrations has been fixed at M_w 5.0 and the largest magnitude to be considered is M_w 7.5. Some of the equations are based on datasets that contain very little or no data from earthquakes

smaller than magnitude 5.5, so this will be fixed as the lower threshold M1. The upper threshold, M2, is fixed at 6.5 for two reasons: a couple of the equations are poorly constrained above this level and it also represents the level above which it becomes unreasonable to ignore the dimensions of the seismic source by using a point source approximation.

In terms of distance, the lower limit, R1, is fixed at 10 km, since this can unequivocally be considered as "near source" and at least two of the candidate equations are not well constrained in this range. Furthermore, it is a distance over which the focal depth, for small-to-moderate magnitude earthquakes, has been shown to exert a pronounced influence on the ground motions (Ambraseys & Bommer 1999, Bommer et al. 2001). An alternative choice would have been 15 km, but since for very low annual frequencies of exceedance events very close to the site may dominate the hazard, it has been decided to use the lower value of 10 km. The upper limit, R2, is fixed at 60 km since this is the upper limit of applicability of the equation of Campbell & Bozorgnia (2002).

Therefore, in summary, the bins are as defined as in Table 3.1.

Tab. 3.1: Magnitude-distance bins for assigning weight to candidate equations.

Magnitudes	Distances
$M_w < 5.5$	$R_{jb} < 10$ km
	$10 < R_{jb} < 60$
	$R_{jb} > 60$ km
$5.5 < M_w < 6.5$	$R_{jb} < 10$ km
	$10 < R_{jb} < 60$
	$R_{jb} > 60$ km
$6.5 < M_w < 7.5$	$R_{jb} < 10$ km
	$10 < R_{jb} < 60$
	$R_{jb} > 60$ km

3.2.2 Grading for coverage in M-R space

This is a fundamental criterion in selecting and assigning weights to each equation, and is based primarily on how well the equation is constrained by the data in each individual M-R space. This is dictated essentially by whether or not there is data in a particular M-R space and how well represented is that bin. In most cases, for the intermediate magnitude and distance ranges, this will mean that the equations will have equal weighting since they are all well represented between R1 and R2 and M1 and M2.

At short distances (less than R1), two additional criteria may apply, the first being to consider higher weights for those equations specifically derived with an emphasis on near-source conditions, such as Cambell & Bozorgnia (2002) and Ambraseys & Douglas (2000). The second additional criteria may be to consider specifically if the records from the selected site class are well represented for distances less than R1.

The ratings are presented in Table 3.2. Where magnitude or distance limits of the dataset used for the derivation fall within a bin, a slightly reduced weighting is applied to reflect that there may be a small degree of extrapolation. Zero weights are applied to the near-source equations of Ambraseys & Douglas (2001) at distances beyond 60 km, since their dataset is limited to recordings from distances of less than 15 km, and also to the equations of Atkinson & Boore (1997) and Lussou et al. (2001) for distances less than 10 km since in both cases the authors expressly state that the equations should not be applied in these ranges.

Tab. 3.2: Ratings of equations for M-R space coverage

Study	$M_w < 5.5$			$5.5 < M_w < 6.5$			$6.5 < M_w < 7.5$		
	< 10	10-60	> 60	< 10	10-60	> 60	< 10	10-60	> 60
Abrahamson & Silva	10	10	10	10	10	10	10	10	10
Ambraseys et al.	9	10	9	9	10	9	8	8	8
Ambraseys & Douglas	20	2	0	20	2	0	20	2	0
Atkinson & Boore	0	10	10	0	10	10	0	9	9
Berge-Thierry et al.	7	10	10	7	10	10	7	9	9
Boore et al.	7	7	6	10	10	6	10	10	6
Campbell & Bozorgnia	20	15	2	20	15	2	20	15	2
Lussou et al.	0	10	10	0	9	9	0	0	0
Sabetta & Pugliese	10	10	9	10	10	9	5	5	4
Somerville et al.	3	3	3	10	10	10	10	10	10
Spudich et al.	6	10	10	6	10	10	6	8	8
Toro et al.	10	10	10	10	10	10	10	10	10

3.2.3 Grading for distance metric in equation

For this feature, the main criterion applied is that those equations based on hypocentral distance, R_{hyp}, are assigned very low weights for magnitudes greater than 5.5 and distances less than 10 km, and slightly greater weights – but still below the standard – between 10 and 60 km. This simply reflects the inappropriateness of point-source measurements for earthquakes of such magnitude that the source dimensions are significant. However, for small magnitudes and short distances, the equations using hypocentral distance are assigned weights above the "neutral" value because of the importance of focal depth in determining the level of ground motions in the near-field of events of this size (e.g. Bommer et al. 2001). The gradings are given in Table 3.3.

Tab. 3.3: Ratings of equations on the basis of distance metric

Study	$M_w < 5.5$			$5.5 < M_w < 6.5$			$6.5 < M_w < 7.5$		
	< 10	10-60	> 60	< 10	10-60	> 60	< 10	10-60	> 60
Abrahamson & Silva	10	10	10	10	10	10	10	10	10
Ambraseys et al.	10	10	10	10	10	10	10	10	10
Ambraseys & Douglas	10	10	10	10	10	10	10	10	10
Atkinson & Boore	16	12	10	5	7	9	1	4	8
Berge-Thierry et al.	16	12	10	5	7	9	1	4	8
Boore et al.	10	10	10	10	10	10	10	10	10
Campbell & Bozorgnia	10	10	10	10	10	10	10	10	10
Lussou et al.	16	12	10	5	7	9	1	4	8
Sabetta & Pugliese	10	10	10	10	10	10	10	10	10
Somerville et al.	10	10	10	10	10	10	10	10	10
Spudich et al.	10	10	10	10	10	10	10	10	10
Toro et al.	10	10	10	10	10	10	10	10	10

3.2.4 Grading for tectonic environment

This grading factor was subsumed within the grading for distance metric, assigning above neutral grades to equations from SCRs for the greater distance ranges. Since the Swiss stochastic model is currently not included in the logic-tree, this factor has become more important and is almost the only way in which the specific Central European environment can be even partially accounted for in the model. In assigning these grades, it is important to note that "Swiss conditions" are difficult to define, since, as discussed in Section 2,2, there are three different tectonic environments: the Alps, the foreland and the Rhine Graben rift. Notwithstanding this uncertainty, the criteria used to assign the grading for tectonic environment are the following:

- Equations for western USA are graded below the "neutral" level, since California is fundamentally different from Europe and central Europe in particular.
- For the same reason, even lower weights are assigned to the essentially Japanese equations for Lussou et al. (2001).
- European equations are weighted above "neutral" since they may be capturing some of the features of the Swiss tectonic environment.
- The extensional regime equations of Spudich et al. (1999) are also given slightly higher than neutral gradings for the same reason that these are applied to the European equations.
- Equations derived for the intraplate regions of eastern North America (ENA) are assigned the highest gradings. This is not based on any assumption that Switzerland and ENA are tectonically similar but rather an attempt to at least capture the influence of equations from another region of relatively low seismicity. The grades are higher for the longer distance ranges.

The grades, presented in Table 3.4, do not cover a very wide range of values, reflecting the relatively low influence assigned to this particular feature. Scaling to Swiss conditions is discussed further in Section 3.4.

Tab. 3.4: Ratings of equations on the basis of tectonic environment

Study	$M_w < 5.5$			$5.5 < M_w < 6.5$			$6.5 < M_w < 7.5$		
	< 10	10-60	> 60	< 10	10-60	> 60	< 10	10-60	> 60
Abrahamson & Silva	8	8	8	8	8	8	8	8	8
Ambraseys et al.	15	15	15	15	15	15	15	15	15
Ambraseys & Douglas	8	8	8	8	8	8	8	8	8
Atkinson & Boore	12	15	18	12	15	18	12	15	18
Berge-Thierry et al.	13	13	13	13	13	13	13	13	13
Boore et al.	7	7	7	7	7	7	7	7	7
Campbell & Bozorgnia	8	8	8	8	8	8	8	8	8
Lussou et al.	6	6	6	6	6	6	6	6	6
Sabetta & Pugliese	15	15	15	15	15	15	15	15	15
Somerville et al.	12	15	18	12	15	18	12	15	18
Spudich et al.	13	13	13	13	13	13	13	13	13
Toro et al.	12	15	18	12	15	18	12	15	18

3.2.5 Grading for site condition adjustment

This grading was included in the preliminary elicitation report with the objective to simply to reduce slightly the influence of those equations for which large adjustments were being made from the assumed representative site velocity for each equation to the arbitrarily chosen reference site with a shear wave velocity over the uppermost 30 m of 1,000 m/s. The procedures adopted to apply these adjustments are presented in Appendix 2. The grades applied in the earlier versions of this logic-tree to account for the size of the site adjustment were all negative in the sense that they were either the neutral values, if the selected average $V_{s,30}$ value was close to 1 km/s, or smaller if there is a large difference between the two shear-wave velocities. The reduction of the grading from neutral value reflected the size of the difference in site velocities.

This grading is now dropped from the weighting scheme because of the new approach adopted in the project to make the site adjustments, this now being handed over to SP3 (see Section 3.3). Although there will still be some uncertainty in making these site adjustments, they will be smaller using the rigorous site response analyses of SP3 than using the crude schemes presented in Appendix 2.

A question that remains is whether or not account should be taken for any adjustments to Swiss conditions, through a "kappa correction" applied in addition to the V_s profile adjustments to be made by SP3. However, as is explained in Section 3.4, the decision is taken not to apply any such "kappa correction", hence there is no need to weight the relationships to reflect the effects and uncertainties in such an adjustment.

3.2.6 Grading for additional explanatory variables

The main additional explanatory variable included in some of the equations is the style of faulting. A few of the equations include terms that can be adjusted to make predictions for specific types of fault rupture. Following WS-4/SP2, the requirement of adjusting all of the equations to be able to predict motions for all fault rupture mechanisms (normal, reverse, strike-slip), regardless of whether or not the equation actually includes a term related to this factor, has been introduced into the SP2 specifications.

In Section 3.8 the scheme for providing mechanism specific predictions of median horizontal ground motions is presented. Herein, a factor is included in the series of gradings applied to the equations to give greater influence to those which included style-of-faulting coefficients, albeit that these are only applicable to reverse and strike-slip faulting, since none of the equations include predictions for normal faulting events. The basis for this grading is very simply to increase the grades to above neutral values for those three equations that do allow style of faulting to be included as an explicit predictor variable.

Two of the equations, Abrahamson & Silva (1997) and Campbell & Bozorgnia (2002), also include factors to account for the hanging wall effect for dip-slip faults. In the limited magnitude-distance ranges that these factors apply, the grades are increased further to reflect the refinement of the predictions offered by this factor. The final gradings are presented in Table 3.5.

3.2.7 Derivation of weights for equations and M-R bins

As explained in the introduction to this Section, the final weights in each M-R bin are determined by simply multiplying the grades in Tables 3.2 – 3.5 and then normalising so that in each M-R bin the values sum to 1.0. The final weights are in Table 3.6.

Tab. 3.5: Ratings of equations on additional explanatory variables

Study	M_w < 5.5			5.5 < M_w < 6.5			6.5 < M_w < 7.5		
	< 10	10-60	> 60	< 10	10-60	> 60	< 10	10-60	> 60
Abrahamson & Silva	20	20	20	25	25	20	25	25	20
Ambraseys et al.	10	10	10	10	10	10	10	10	10
Ambraseys & Douglas	10	10	10	10	10	10	10	10	10
Atkinson & Boore	10	10	10	10	10	10	10	10	10
Berge-Thierry et al.	10	10	10	10	10	10	10	10	10
Boore et al.	20	20	20	20	20	20	20	20	20
Campbell & Bozorgnia	20	20	20	25	20	20	25	20	20
Lussou et al.	10	10	10	10	10	10	10	10	10
Sabetta & Pugliese	10	10	10	10	10	10	10	10	10
Somerville et al.	10	10	10	10	10	10	10	10	10
Spudich et al.	10	10	10	10	10	10	10	10	10
Toro et al.	10	10	10	10	10	10	10	10	10

Tab. 3.6: Final weights for median horizontal motions at all frequencies

Study	M_w < 5.5			5.5 < M_w < 6.5			6.5 < M_w < 7.5		
	< 10	10-60	> 60	< 10	10-60	> 60	< 10	10-60	> 60
Abrahamson & Silva	0.1141	0.1087	0.1250	0.1292	0.1282	0.1173	0.1406	0.1543	0.1400
Ambraseys et al.	0.0962	0.1019	0.1055	0.0872	0.0962	0.0990	0.0844	0.0926	0.1050
Ambraseys & Douglas	0.1141	0.0109	0.0000	0.1033	0.0103	0.0000	0.1125	0.0123	0.0000
Atkinson & Boore	0.0000	0.0978	0.1406	0.0000	0.0673	0.1188	0.0000	0.0417	0.1134
Berge-Thierry et al.	0.1038	0.1060	0.1016	0.0294	0.0583	0.0858	0.0064	0.0361	0.0819
Boore et al.	0.0699	0.0666	0.0656	0.0904	0.0898	0.0616	0.0984	0.1080	0.0735
Campbell & Bozorgnia	0.2281	0.1630	0.0250	0.2583	0.1539	0.0235	0.2813	0.1852	0.0280
Lussou et al.	0.0000	0.0489	0.0469	0.0000	0.0242	0.0356	0.0000	0.0000	0.0000
Sabetta & Pugliese	0.1069	0.1019	0.1055	0.0969	0.0962	0.0990	0.0527	0.0579	0.0525
Somerville et al.	0.0257	0.0245	0.0422	0.0775	0.0962	0.1320	0.0844	0.1158	0.1575
Spudich et al.	0.0556	0.0883	0.1016	0.0504	0.0833	0.0953	0.0548	0.0803	0.0910
Toro et al.	0.0856	0.0815	0.1406	0.0775	0.0962	0.1320	0.0844	0.1158	0.1575

A few observations can be usefully made regarding the final weights, the first being that by virtue of good data coverage at short distances and across the magnitude range of interest, and furthermore through the use of an appropriate distance metric and the inclusion of both style of faulting and the hanging wall effect as explanatory variables, for distances of less than 60 km the equations of Campbell & Bozorgnia (2002) are dominant, and particularly so for distances of less than 10 km. For the intermediate magnitude range (M_w 5.5 to 6.5) and the shortest distance range (< 10 km), the combined weights of the European equations ins a little above 0.2, as is the combined weight of the three ENA equations; almost half the weight is given to the four equation based primarily on western US data. For the same magnitude category, as the distance

increases the influence of the western US equations drops to less than 0.4 in the 10 – 60 km range and then to 0.2 at greater distances, whereas the collective weight of the European equations increases to 0.25 in the intermediate distance range and to 0.28 beyond 60 km. The ENA equations are dominant beyond 60 km, with a collective weight of almost 0.4.

The dominance of the western USA equations at short distances is the result, primarily, of the fact that two of these equations are derived specifically for near-source conditions using only data obtained at short distances from the fault rupture, and three of them include coefficients for style-of-faulting. This is an acceptable scenario if it is accepted that the primary differences between tectonic regions are in attenuation characteristics rather than source characteristics, which also supports the fact that beyond 60 km, the logic-tree is dominated by the intraplate ENA equations in first place and the European equations in second place.

3.3 Reference Site Velocity Profiles

In earlier stages of the project, a scheme was introduced to adjust all of the attenuation equations to a single reference site condition. For WS-3/SP2, the author had selected nominal 30 m shear wave velocity, $V_{s,30}$, of 550 m/s. After WS-3/SP2, the reference site velocity was increased to 1,000 m/s, partly to reduce the size of the adjustments being made for some of the equations – and in particular those from ENA – but mainly to coincide with the fact that this was the reference site condition used in the numerical simulations performed to explore upper bounds on the ground motions. However, at WS-4/SP2, it was decided to abandon this procedure and to adopt an entirely different approach, which consisted essentially of the following steps:

- Representative $V_{s,30}$ for each attenuation equation to be agreed collectively by the five members of EG2.
- Branches with higher and lower estimates of $V_{s,30}$ for each equation, chosen to represent the epistemic uncertainty in these values, also to be agreed collectively by EG2.
- Weights to be assigned to the three estimates of the representative $V_{s,30}$, values for each equation by each individual expert.
- The adjustments of the ground motion estimates to a reference site velocity of 2,000 m/s to be made by SP3, using generic site profiles.

The selected site classes and representative $V_{s,30}$ values inferred for each of the 12 attenuation equations are presented in Table 3.7. The reasoning followed to assign these $V_{s,30}$ values is very similar to that originally used, and indeed the results are also comparable (see Table A2.2 in Appendix 2). The intervals from the central estimate to the upper and lower bounds reflect the confidence in the estimates, and hence, as in the original scheme presented in Appendix 2, the same weighting scheme can be applied to all of the equations. These weights, also shown in Table 3.7, are unchanged from those in Table A2.2. The values of $V_{s,30}$ in Table A2.2 are those presented in PEGASOS Report TP2-TN-0363.

The soil profiles used are generic rock site profiles that conform to $V_{s,30}$ values and increase the shear wave velocity with depth to the reference condition of 2,000 m/s. The profiles were derived by EG2 member Frank Scherbaum and are based on the generic ENA and California rock profiles presented by Boore & Joyner (1997); examples are shown in Figure 3.1. At the request of SP2, sensitivity studies were performed by SP3 to explore the influence of the damping level assigned to the soil profile, using values of 1 % and 3 %. Results are shown in Figure 3.2 that indicate that the sensitivity is low and for this reason a damping value of 1 % is to be used by SP3 in performing the transformations from the selected site class of each

equation to the reference condition of V_s 2,000 m/s. Sample transfer functions computed using the selected 15 acceleration time-histories that are to be used in all SP3 calculations are presented in Figure 3.3.

Tab. 3.7: Selected site classes for candidate attenuation relations

Study	Site Class	$V_{s,30}$ (m/s)		
		Lower (w = 0.2)	Central (w = 0.6)	Upper (w = 0.2)
Abrahamson & Silva (1997)	Rock	450	600	900
Ambraseys et al. (1996)	Class R (rock)	550	800	1,200
Ambraseys & Douglas (2000)	Class R (rock)	450	800	1,100
Atkinson & Boore (1997)	-	-	2,800*	-
Berge-Thierry et al. (2000)	Rock	550	800	1,200
Boore et al. (1997)	Class A (rock)	550	620	750
Campbell & Bozorgnia (2002)	Firm Rock	450	600	900
Lussou et al. (2001)	Class B	350	500	900
Sabetta & Pugliese (1996)	Stiff	700	1,000*	1,300
Somerville et al. (2001)	-	-	2,800	-
Spudich et al. (1999)	Rock	550	800	1,100
Toro et al. (1997)	-	-	2,800*	-

* For the three ENA equations, there is considered to be no uncertainty, hence a weight of 1.0 is applied to the central value. These equations are only defined for hard rock sites and therefore there is no need to specify the site class to be used in applying the equation.

A question that now arises is whether or not, in addition to the nominal 1 % of damping assigned to the rock profiles, a "kappa correction" is also required, since the SP3 calculations will not account for this effect. In the previous version of this logic-tree presented at WS-4/SP2, at which time the selected reference site had $V_{s,30}$ of 1,000 m/s, adjustments for kappa were made for the ENA equations that had a site velocity of 2,800 m/s. At higher frequencies, these adjustments (see Tables A2.7 and A2.8) were very large, as shown in Figure 3.4. The issue of whether such adjustments need to be applied together with the SP3 transformations to V_s 2,000 m/s is addressed in the following section.

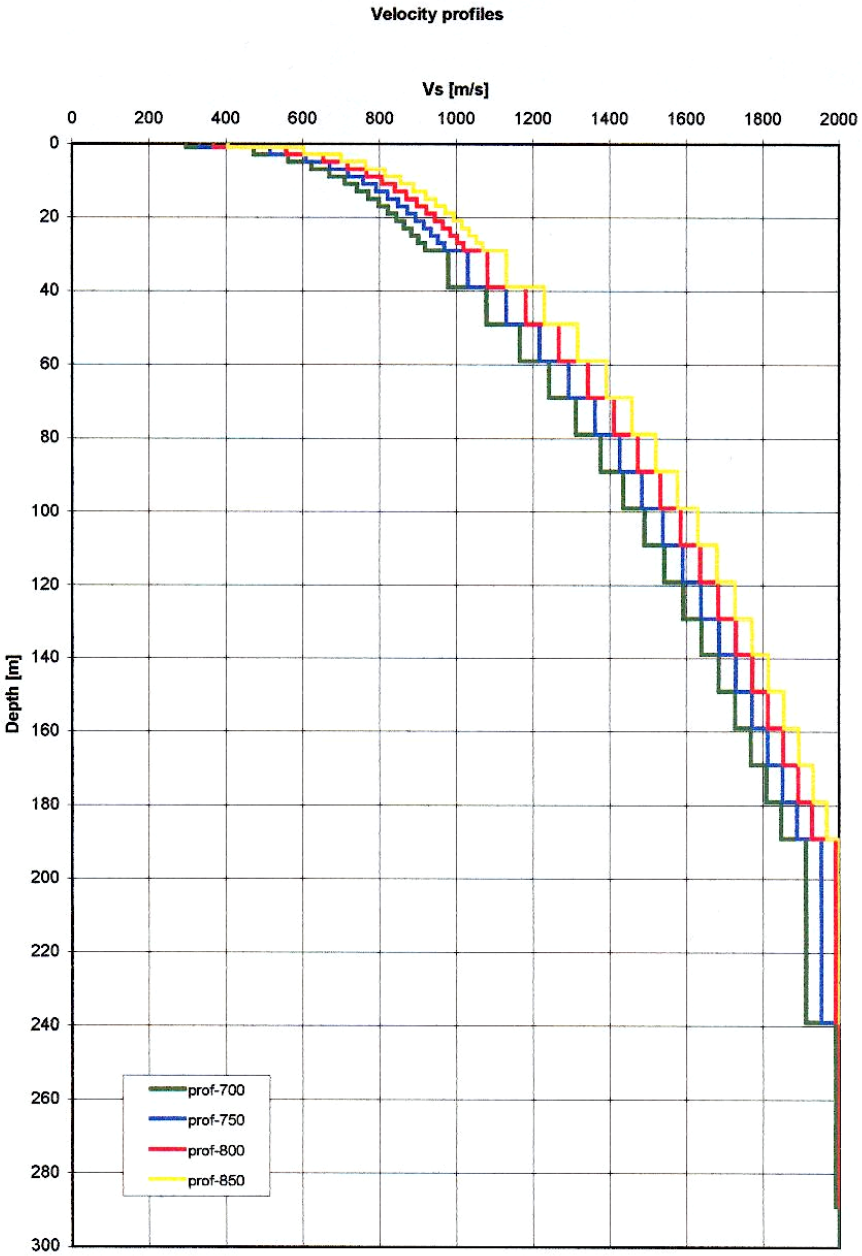

Fig. 3.1: Generic rock site profiles for $V_{s,30}$ values of 700, 750, 800 and 850 m/s (PEGASOS Report TP2-TN-0363).

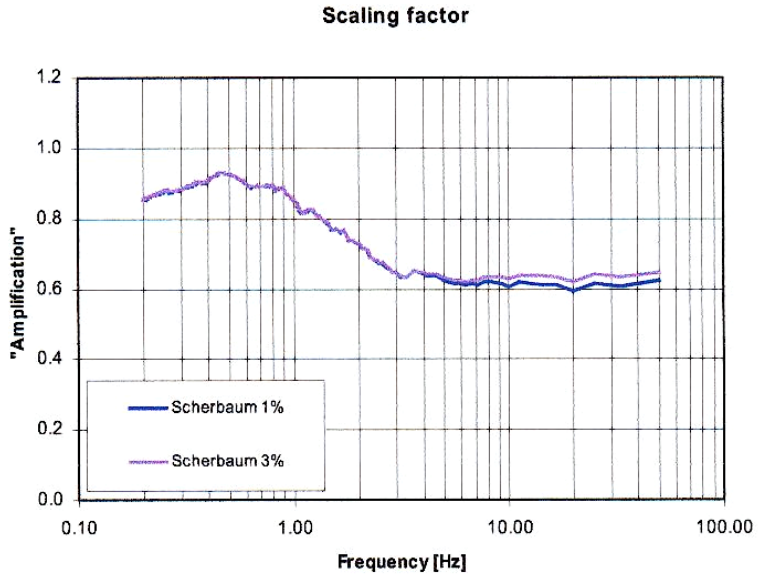

Fig. 3.2: Sensitivity of calculated site response transfer function to assumed damping in rock (PEGASOS Report TP2-TN-0350)

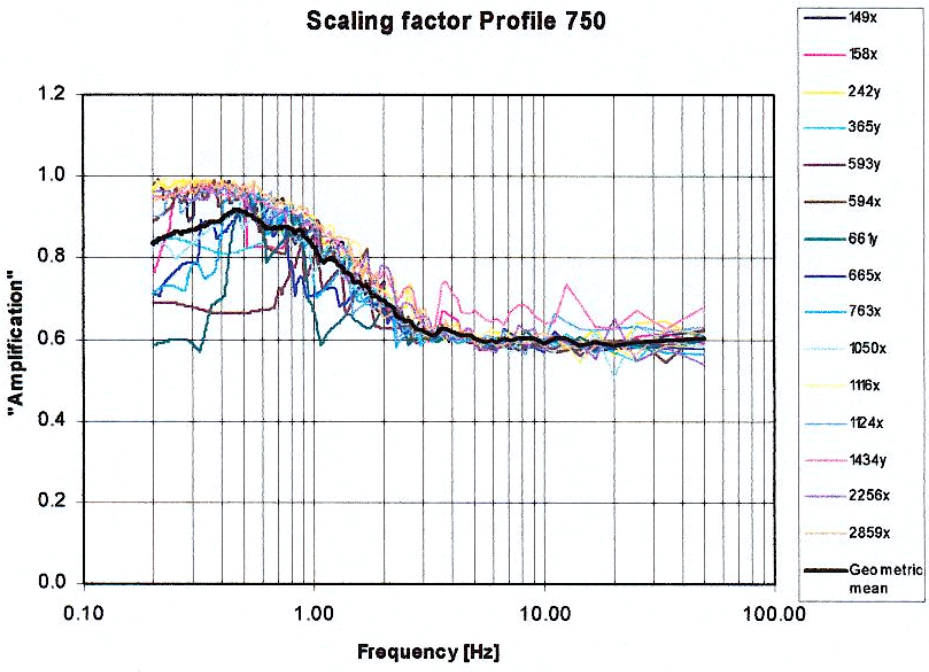

Fig. 3.3: Site transfer functions calculated using time-history analysis and the generic profile for $V_{s,30}$ of 750 m/s (PEGASOS Report TP2-TN-0363)

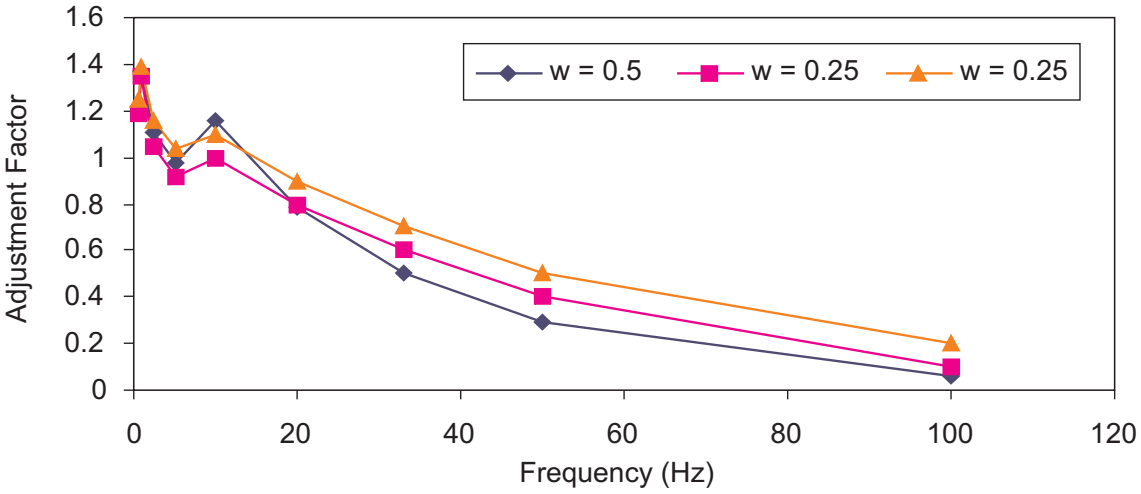

Fig. 3.4: Adjustments made in previous version of logic-tree (see Appendix 2) to transform ENA equations to the reference site condition of $V_{s,30}$ 1,000 m/s accounting for both $V_{s,30}$ and kappa effects

3.4 Adjustment of Proponent Models to Swiss Conditions

In essence, the possible need for a kappa correction arises from the trade-off between site amplification mainly due to impedance contrasts and therefore a function of $V_{s,30}$ and site diminution effects due to the reduced stiffness of the uppermost layers of the crust, modelled by the exponential kappa filter $\exp(-\pi\kappa_0 f)$. The trade-off results from the fact that both filters are frequency-dependent. The correction for Fourier spectral amplitudes (which therefore may not be directly applicable to response spectra) models the difference between the value of kappa assumed for Switzerland and the value of kappa representing the region for which the proponent model was derived:

$$CORR_{\kappa}(f) = \frac{\exp(-\pi\kappa_0^{SWISS} f)}{\exp(-\pi\kappa_0^{MODEL} f)} = \exp\left(-\pi(\kappa_0^{SWISS} - \kappa_0^{MODEL}) f\right) \qquad (3.1)$$

There are, however, a number of issues associated with this correction. Firstly, the reasoning above is entirely based on the assumption that kappa is a site parameter reflecting near-surface effects, which is still a matter of some controversy. The spectral scaling relation derived from the Brune model does not prescribe any upper bound on the frequency range over which the spectral amplitude is constant. Observed seismic spectra however are band-limited in frequency. As a result, an additional filter must be included in the theoretical model to account for high-frequency behaviour.

As for the stress parameter $\Delta\sigma$, there is considerable controversy as to the physical interpretation and hence the functional form of this high-frequency filter. Some authors (e.g. Papageorgiou & Aki 1983) consider the existence of an upper bound on frequency f_{max} as a source effect (i.e. f_{max} is the highest frequency radiated by the source), others, such as (Hanks 1982), consider it to be a site effect (i.e. f_{max} is the highest frequency transmitted by the materials overlying the bedrock beneath the site). An alternative representation of the high-frequency roll-off (Anderson & Hough 1984) uses an exponential filter with decay rate κ. This latter parameter can be measured by fitting recorded spectra, but this will result in distance-dependent values because of trade-

offs with the whole-path anelastic attenuation. When a generic regional kappa value is required, the zero-distance intercept κ_0 of a kappa function averaged over all the sites is used.

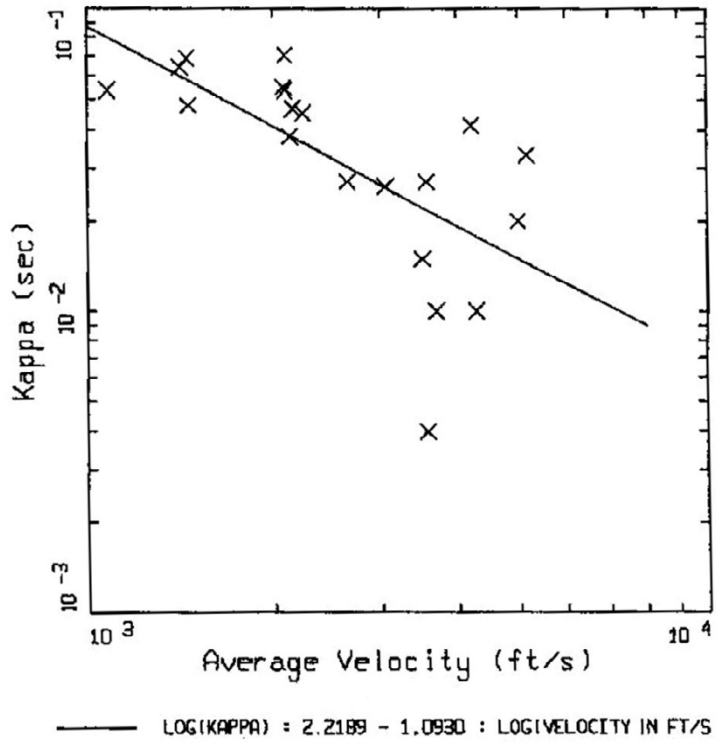

Fig. 3.5: Relationship between kappa and $V_{s,30}$ for western North American rock sites (Silva et al. 1998)

One implication of this is that kappa values determined from spectral fitting will trade off with other model parameters, and also include information about the goodness-of-fit of the Brune model. The trade-off between $\Delta\sigma$ and kappa is one of the main problems in the calibration of the stochastic method and has been investigated by Boore et al. (1992). An interesting point to note is that the best estimate values of $\Delta\sigma$ and kappa for Western North America have been revised several times by the authors as a result of the refinement of the amplification model (Boore & Joyner 1997). A conclusion from this is that although changes in $V_{s,30}$ will affect the value of kappa, the strong trade-off with $\Delta\sigma$ will remain. Figure 3.5 shows kappa and $V_{s,30}$ values from sites in western North America, to which a simple linear function has been fitted although the data distribution seems to suggest a more complex relationship.

The second problem that arises is the determination of appropriate values of kappa for both the regions from where the attenuation equations have been adopted, and also from Switzerland. In his elicitation summary for WS-4/SP2, Frank Scherbaum presented a table with representative $V_{s,30}$ and kappa values for all of the candidate attenuation models, but the sources of this information were not fully documented and it is not known how all of these values have been estimated nor with what degree of confidence. There is also no clear idea of what the appropriate value of kappa for Switzerland should be, since the values suggested in various reports do not always coincide due to the aforementioned trade-off issues and cover quite a considerable range.

Bay (2002) finds a best-fitting kappa of 0.0125 s corresponding to a Brune stress parameter of 2.7 bars. Although this value of $\Delta\sigma$ is considered unacceptably low, the implementations of all three models (A_{10}, A_{30} and A_{inc}) use a value of 0.015 s, which is consistent with the tectonic

setting of Switzerland (between intraplate and active). However, it must be kept in mind that this value was determined using mainly small-magnitude data and might therefore also be affected by scaling effects. The additional fitting exercises requested by the experts seem to confirm this. PEGASOS document EXT-TN-0216 presents an inversion for a fixed $\Delta\sigma$ of 100 bars. The range considered for kappa is 0:0.01:0.1 s; best-fit values lie in the range 0 to 0.07 s (mostly between 0.02 s and 0.04 s). PEGASOS Document EXT-TN-0251, despite being entitled "Forward modelling to investigate stress-drop and kappa values in relation with the model of Bay (2002)", provides conclusions only with respect to $\Delta\sigma$. The range considered for kappa is 0:0.01:0.05; sample best-fit results presented cover the whole of this range (0.03 s and 0.05 s for broadband data, 0.00, 0.01, 0.03 and 0.04 s for data recorded on strong-motion instruments).

Rietbrock (2002) follows a different approach and determines distance-dependent t^* operators (which can be considered equivalent to a distance-dependent kappa). The results are presented in tabular form in PEGASOS document EXT-TN-0306 and summarised in Figure 3.6. The t^* operator can be divided into a path-dependent and a site-dependent component, the latter corresponding to κ_0. This value has been found to vary regionally, as illustrated in Figure 3.7. A constant value of 0.020 s was used in the implementation of the model using SMSIM. The corresponding value of $\Delta\sigma$ is 46 bars.

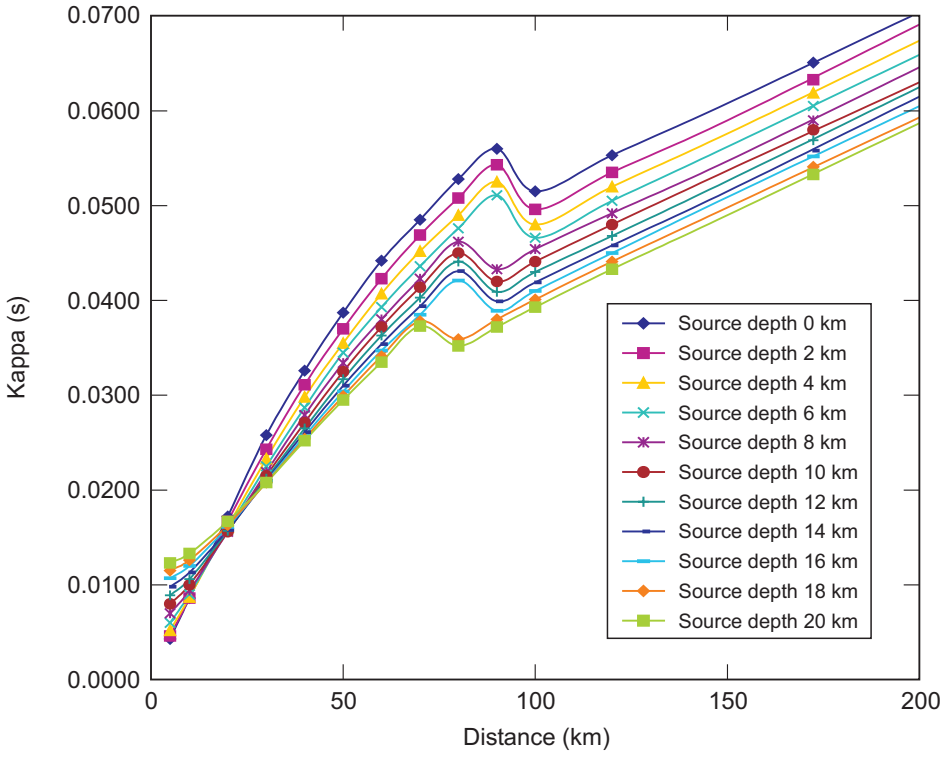

Fig. 3.6: Variation of kappa with distance for Q = 400 and various source depths, as implemented in the Rietbrock (2002) model for Switzerland.

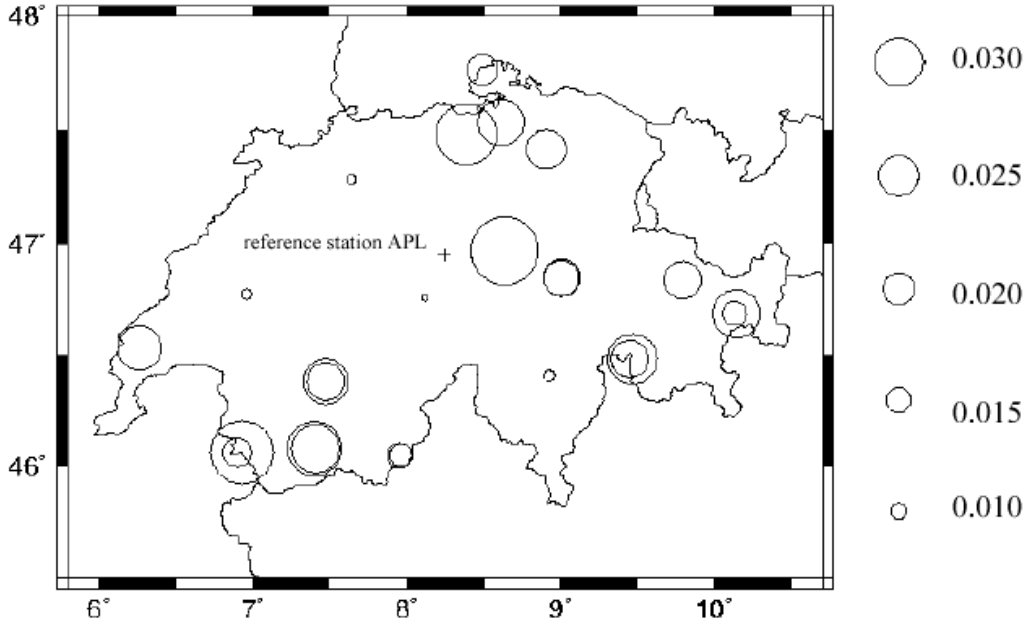

Fig. 3.7: Spatial distribution of station-dependent component of the attenuation operator *t** (Rietbrock 2002, PEGASOS document EXT-TN-0306)

In conclusion, faced with the doubt about the physical interpretation of kappa, particularly when applied in isolation from the other parameters with which its determination has significant trade-offs, coupled with the large uncertainty in the estimation of values for both the candidate equation regions and Switzerland, it is decided not to apply a kappa correction. The fundamental reason for this decision is that it could actually worsen the match between the predicted motions and Swiss conditions.

3.5 Magnitude Scale Conversions

The chosen scale for the seismic hazard analysis, as determined by the characterisation of the earthquake catalogue, is moment magnitude, M_w. Therefore, for those attenuation relationships defined in terms of other magnitude scales it is necessary to provide empirical relationships to convert M_w values to equivalent values on other scales. The conversion needs are summarised in Table 3.8 below.

The selected options for each of these conversions, and the weights assigned to each option, are presented in the following sub-sections. The conversions will be from M_w to the other scales, hence empirical relationships are to be used that are found from regressions of M_w (or M_o) on other magnitude scales, or else on orthogonal regressions between M_w (or M_o) and other magnitude scales.

The conversion options for each of the three conversions required, and their relative weightings, are summarised in the following sub-sections. It is worth pointing out here that in the magnitude range of interest to the project (M_w 5.5 – 7.5) the differences in values reported by different magnitude scales are not large and hence there is justification for making this part of the logic-tree excessively complicated.

Tab. 3.8: Magnitude conversions

Study	Scale	Conversion Required	Number
Abrahamson & Silva (1997)	M_w	None	0
Ambraseys et al. (1996)	M_s	$M_w \rightarrow M_s$	1
Ambraseys & Douglas (2000)	M_s	$M_w \rightarrow M_s$	1
Atkinson & Boore (1997)	M_w	None	0
Berge-Thierry et al. (2000)	M_s	$M_w \rightarrow M_s$	1
Boore et al. (1997)	M_w	None	0
Campbell & Bozorgnia (2002)	M_w	None	0
Lussou et al. (2001)	M_{JMA}	$M_w \rightarrow M_{JMA}$	3
Sabetta & Pugliese (1996)	M_s,M_L	$M_w \rightarrow M_s$ or M_L	2
Somerville et al. (2001)	M_w	None	0
Spudich et al. (1999)	M_w	None	0
Toro et al. (1997)	M_w	None	0

3.5.1 Conversions from M_w to M_s

The most commonly used magnitude scale in the other relationships is M_s and therefore the main requirement is for an empirical conversion between surface wave and moment magnitudes. The ideal situation would be to use equations derived specifically for Switzerland or Central Europe, but failing this to use equations for intra-plate regions, or better yet Stable Continental Regions, in general. Johnston et al. (1994) provide an empirical relationship between $\log(M_o)$ and M_s but this cannot be used for the purpose required. Free (1996) performed regressions using 138 earthquakes from SCRs:

$$M_s = -34.6889 + 2.4593[\log(M_o)] - 0.0336[\log(M_o)]^2 \qquad (3.2)$$
$$\sigma = 0.316$$

The relationship gives very similar results to the European equation, obtained by Ambraseys & Free (1997) from regression on earthquakes of focal depth less than 30 km and magnitudes between 3.5 and 7.5:

$$M_s = -47.379 + 3.41[\log(M_o)] - 0.051[\log(M_o)]^2 \qquad (3.3)$$
$$\sigma = 0.182$$

Substituting the equation of Hanks & Kanamori (1979):

$$M_w = \frac{2}{3}\log(M_o) - 10.7 \qquad (3.4)$$

into Eq.(3.2), yields:

$$M_s = -3.8725 + 2.0712 M_w - 0.0756 M_w^2 \tag{3.5}$$

Bungum et al. (2002) present an orthogonal regression between M_s and M_w for southern Europe, for which the standard deviations are not presented, and this equation was adopted in an earlier version of the elicitation. It was found, however, to yield excessively large estimates of moment magnitude for higher values of M_s. An updated version of the equation was provided to the author, which is quadratic for lower magnitudes and linear above M_s 6.5:

$$M_s \leq 6.5 \qquad M_s = -7.176 + 3.062 M_w - 0.148 M_w^2 \tag{3.6a}$$
$$M_s > 6.5 \qquad M_s = M_w \tag{3.6b}$$

Another empirical equation is provided in the report on the compilation of ECOS (Earthquake Catalogue of Switzerland), Pegasos Document EXT-TB 0043, which provides the following correlations between M_w and M_s values from the USGS Preliminary Determination of Epicenters (PDE). However, this equation is a direct regression of M_w on M_s and hence it is not appropriate for finding M_s values from M_w. Furthermore, the regression is based only on PDE values of M_s, which are not the most reliable and which may often be in error for smaller events because of the USGS policy of the using only surface waves with periods close to 20 seconds. For both of these reasons, the Swiss relation is rejected and only the equations from Free (1996) and Bungum et al. are employed. Since the former is specific to SCRs whereas the latter is mainly derived for the active areas of southern Europe, a weight of 0.6 is applied to Free (1996) and 0.4 to Bungum et al. This is summarised in Table 3.9.

Tab. 3.9: Branch 1 for magnitude conversions (M_w to M_s)

Conversion Formula	Weight
Eq. (3.5) – Free (1996)	0.6
Eq. (3.6) – Bungum et al. (2003)	0.4

3.5.2 Conversions from M_w to M_s-M_L Hybrid

The attenuation relation of Sabetta & Pugliese (1996), in common with their earlier study for PGA and PGV (Sabetta & Pugliese 1987), is based on a hybrid magnitude scale using M_s for larger events and M_L for smaller events; a similar scheme was also used by Campbell (1981). If $M > 5.5$, then the value is M_s, otherwise M_L. In order to apply this scheme, the same procedure as adopted for obtaining M_s values described above is used but with the caveat that if the value turns out to be less than 5.5, an alternative conversion should be applied to obtain M_L instead.

The following equation, derived specifically for Switzerland, is presented in the ECOS report:

$$M_L = 0.58 + 0.87 M_w \tag{3.7}$$

No other relations between M_L and M_w have been found and even if they were it is unlikely that M_L from different regions is actually comparable. An alternative strategy is to convert M_s values of less than 5.5 to M_L via another empirical relationship, such as that derived by Ambraseys & Bommer (1990) through orthogonal regression:

$$0.82M_L - 0.58M_s = 1.20 \tag{3.8}$$

In order to avoid too many branches, Eq.(3.8) is combined with Eq.(3.5) to yield the following conversion:

$$M_L = 1.276 + 1.465M_w - 0.0535M_w^2 \tag{3.9}$$

Eq. (3.9) is found to give unreasonably high estimates of M_L, so it is not used. For the logic-tree, the M_L-M_w relationship from ECOS and the assumption that $M_L = M_w$ will be adopted, applying equal weights of 0.6 to the former (reflecting its derivation specifically for Switzerland) and 0.4 to the latter; this is summarised in Table 3.10.

Tab. 3.10: Branch 2 for magnitude conversions (M_w to M_s-M_L hybrid)

If $M_s \geq 5.5$, then:	If $M_s < 5.5$, then:	
Use Branch 1.	Conversion	Weight
	Eq. (3.7)	0.6
	$M_L = M_w$	0.4

3.5.3 Conversions from M_w to M_{JMA}

The equations of Lussou et al. (2001) are based on M_{JMA} and hence an additional conversion is required to obtain values on this scale from values of moment magnitude. The only empirical relationship between seismic moment magnitude and the magnitude scale of the Japanese Meteorological Agency is that provided by Fukushima (1996), which can be expressed in the following format:

$$M_{JMA} = \frac{1}{1.10}\left[-17.92 - \log(M_o^{-1} + 10^{-17}.M_o^{-1/3}\right] \tag{3.10}$$

in which M_o is given in units of dyn.cm. For a seismic moment of 10^{25} dyn.cm, which corresponds to M_w 5.97, the equation yields a value of 6.29 for M_{JMA}. To employ Eq. (3.10), it would be necessary to first convert moment magnitudes to seismic moment by inverting Eq. (3.4):

$$M_o = 10^{1.5[M_w+10.7]} \tag{3.11}$$

There is a risk, however, in using only a single conversion equation, in so much that epistemic uncertainty is not captured. Lussou et al. (2001) refer to the work of Heaton et al. (1986), who

showed that M_{JMA} is very close to M_s and M_w in the range of M_w values from 6 to 7; in fact, according to the curves of Heaton et al. (1986), M_{JMA} only differs appreciably from M_w above M_w values of 7.5, hence for the purposes of this project it may be assumed that no conversion is required. It is noted, however, that given the way in which M_{JMA} is calculated (Willmore 1979), it would perhaps be expected to be closer to M_s than M_w. The two options, therefore, are to use M_w and M_{JMA} as if they were equivalent, the other to convert to M_s using one of the equations provided in Branch 1 and assume the M_s and M_{JMA} are equivalent. The options and weightings are summarised in Table 3.11.

Tab. 3.11: Branch 1 for magnitude conversions (M_w to M_{JMA})

Conversion Formula	Weight
Eqs. (3.11) and (3.10)	0.6
Assume $M_w = M_{JMA}$ (i.e. no conversion)	0.2
Eq. (3.5) and assume $M_s = M_{JMA}$	0.2

3.6 Component Conversions

The candidate equations do not all use the same approach to define the values of horizontal PGA and spectral ordinates from each triaxial accelerogram. The project organisers have decided to define the input motion required for analysis in terms of the geometric mean of the horizontal PGA values and at each response period. Table 3.12 below summarises the definition of the horizontal component used in each study and the conversions required whenever this is different from the geometric mean value.

Tab. 3.12: Component conversions required for horizontal motions

Study	Component[1]	Conversion Required	Number
Abrahamson & Silva (1997)	Geometric	None	0
Ambraseys et al. (1996)	Larger-env.	$H_{larger\text{-}envelope} \rightarrow H_{random}$	1
Ambraseys & Douglas (2000)	Larger-env.	$H_{larger\text{-}envelope} \rightarrow H_{random}$	1
Atkinson & Boore (1997)	Both	None	0
Berge-Thierry et al. (2000)	Both	None	0
Boore et al. (1997)	Geometric	None	0
Campbell & Bozorgnia (2002)	Geometric	None	0
Lussou et al. (2001)	Both	None	0
Sabetta & Pugliese (1996)	Larger-PGA	$H_{larger\text{-}PGA} \rightarrow H_{random}$	2
Somerville et al. (2001)	Geometric	None	0
Spudich et al. (1999)	Geometric	None	0
Toro et al. (1997)	Geometric	None	0

[1] geometric mean, for two values, is the anti-log of the arithmetic mean of the logarithms; "both" means that the two horizontal components have been treated as independent data points, which is equivalent to the "random" component.

A couple of points of clarification are in order. The first concerns the definition of the "larger" component. Most studies that have used this definition, including Boore et al. (1993, 1994), Ambraseys et al. (1996) and Ambraseys & Douglas (2000), have taken the larger spectral ordinate from the two horizontal components at each response period, which is also the definition previously being employed in the Pegasos project. However, there is a variation from this definition, which was used by Sabetta & Pugliese (1996), which is to take the horizontal component with the larger PGA value from each accelerogram, and then use this component to determine the spectral ordinates. The former approach will be referred to hereafter as the larger-envelope and the latter as the larger-PGA.

The second point of clarification concerns the definitions of geometric mean and both components. Although there are two different treatments, for the purposes of defining the median values of the horizontal motion, the use of both horizontal values and use of the geometric mean are equivalent. This has been confirmed in Pegasos document TP2-TN-0269, as shown in Figure 3.8: the black crosses indicate that the random and geometric mean are essentially equivalent, and the pink crosses (which lie below the black crosses) confirm the equivalence of the random component and the use of both components.

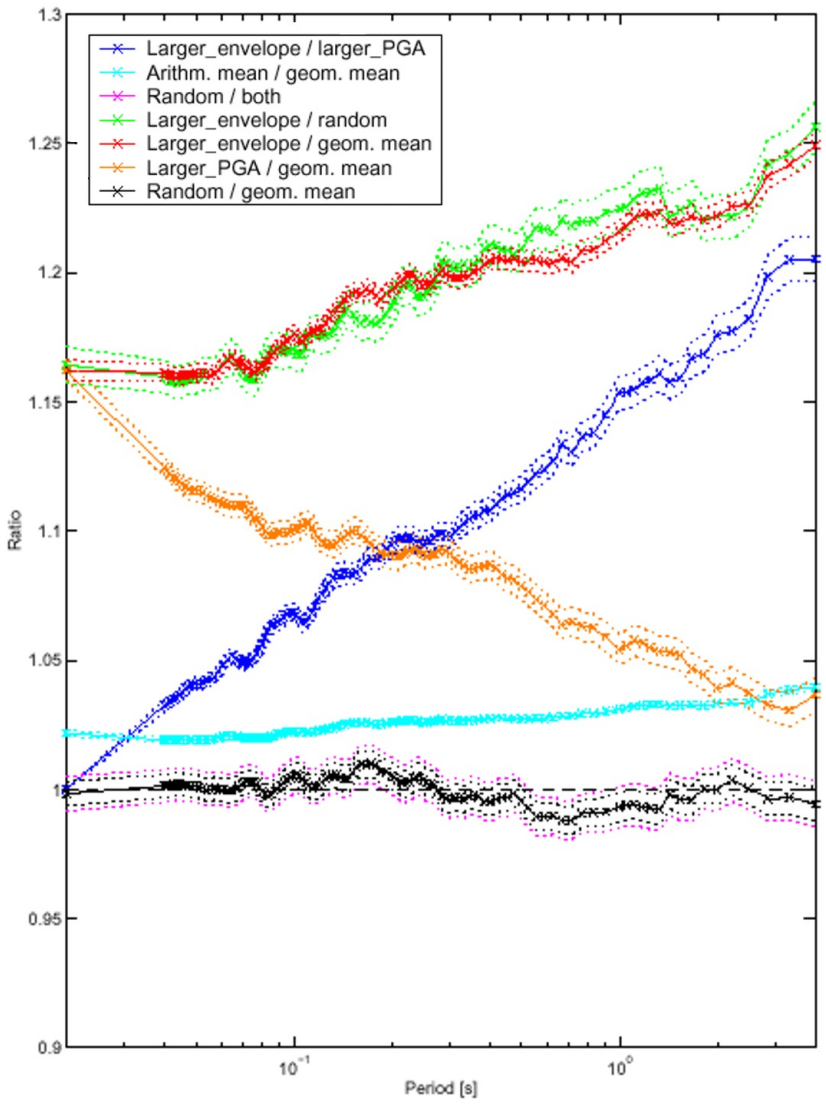

Fig. 3.8: Ratios of spectral ordinates (5 % damping) from the WAF worldwide database using different definitions of the horizontal component of motion

It can be concluded, therefore, that the geometric mean and the use of both components are equivalent. Therefore, only two conversions are required, one to convert from the larger-envelope to the geometric mean or random component, and another to convert from the larger-PGA component to the geomteric mean.

The only information that has been made available regarding the ratio of the larger-PGA component to the geometric mean component is the line of orange crosses in Figure 3.8, which indicates that the ratio is equal to about 1.16 at 50 Hz (i.e. PGA) and decreases to just less than 1.05 at 2.0 seconds. The standard error in the average value of this ratio is small at high frequencies and increases very slightly with period. Therefore, central values of the ratio can simply be read from the curve of blue crosses, taking the reciprocal of the values of the ratios. To capture the uncertainty represented by the standard error at larger periods, additional branches with lower weights could be introduced, although the size of the error does not seem to suggest that such a decision is indispensable. However, there is uncertainty at the high frequencies due to the interpolation, therefore this must be captured in the logic-tree.

Considering now the ratio of the larger to random components, Douglas (2001), using a data set of records recorded at less than 15 km from the source of events in the magnitude range from 5.8 to 7.8, found a range of 1.10 to 1.24 for the ratio of the PGA of the larger component compared to the random component. From a study of 76 horizontal Japanese accelerograms, Ansary et al. (1995) present results from which it can be inferred that the mean ratio of the larger PGA to the mean component (which is not exactly equivalent to the random component but can be taken as a surrogate for this exercise) is 1.12. Boore et al. (1993) present equations, derived from the data set of western North American data, for both the larger component of PGA and the random horizontal component. Neglecting the very small difference in the distance terms of the two equations – which results in only 0.5 % difference between the larger and random components at 10 km from the source – it is possible to obtain the following expression for the ratio of the two PGA values:

$$\frac{PGA_{larger}}{PGA_{random}} = 10^{0.145-0.013M_w} \tag{3.12}$$

For an earthquake of magnitude M_w 5.5, the ratio is 1.18, and for a magnitude M_w 6.0 event the ratio is 1.17; this latter value is the mean of the limits found by Douglas (2001). The ratio must be specified not only for PGA but for all of the specified response periods; the Boore et al. (1993) study gives, for rock motions at 1.0 second, the following equation for the random component:

$$\log(PSV) = 1.724 + 0.450(M-6) - 0.014(M-6)^2 - 0.798\log\sqrt{(d^2+2.90^2)} \tag{3.13}$$

and for the larger horizontal component:

$$\log(PSV) = 1.858 + 0.444(M-6) - 0.016(M-6)^2 - 0.825\log\sqrt{(d^2+2.87^2)} \tag{3.14}$$

The difference in the distance terms is quite small, resulting in a different of just 6 % at 10 km from the source. At the controlling levels of magnitude, the differences in the quadratic magnitude terms are very small, hence can be ignored. Ignoring the last two terms in each equation, it is possible to arrive at the following approximation:

$$\frac{PSV(1.0)_{larger}}{PSV(1.0)_{random}} = 10^{0.17-0.006M_w} \tag{3.15}$$

For an earthquake of magnitude M_w 5.5, the ratio is 1.37, and for a magnitude M_w 6.0 event the ratio is 1.36. The conclusion is that the magnitude and distance variation of the ratio can probably be ignored, but that the increase of the ratio with increasing response period needs to be taken into account. In order to obtain indicative values, the ratio is calculated from the Boore et al. (1993) equations for an earthquake of M_w 6.0 at a distance of 10 km from the source and the results are presented in Table 3.13.

Tab. 3.13: Ratio of larger to random components for M_w 6, d = 10 km (Boore et al. 1993)

Frequency (Hz)	100	10	6.7	5	3.3	2.5	1.0	0.5
Period (s)	PGA	0.10	0.15	0.20	0.30	0.40	1.0	2.0
Larger-to-Random	1.169	1.155	1.158	1.174	1.208	1.236	1.314	1.176

Although the logic-tree is already highly complex and the standard errors in the average ratios are small, it is decided to include additional branches for alternative values of the scaling factors. The reciprocals of the ratios read off Figure 3.8 for the larger-PGA components for each of the response frequencies of interest and taken as the central values. Higher and lower values, weighted at 0.25 each, are assigned by judgement from the information presented in the preceding paragraphs. The resulting component conversions are summarised in Table 3.14.

Tab. 3.14: Branches and weights for horizontal component conversions

Frequency (Hz)	Conversion 1: larger-envelope to random			Conversion 2: larger-PGA to random		
	W = 0.25	W = 0.50	W = 0.25	W = 0.25	W = 0.50	W = 0.25
0.5	0.80	0.82	0.84	0.94	0.96	0.98
1.0	0.80	0.82	0.84	0.93	0.95	0.97
2.5	0.81	0.83	0.85	0.91	0.93	0.95
5.0	0.82	0.84	0.86	0.90	0.92	0.94
10.0	0.83	0.85	0.87	0.89	0.91	0.93
20.0	0.84	0.86	0.88	0.88	0.90	0.92
33.3	0.87	0.86	0.89	0.85	0.88	0.91
50.0	0.82	0.86	0.90	0.82	0.86	0.90
100.0	0.82	0.86	0.90	0.82	0.86	0.90

3.7 Missing Frequencies

Not all of the equations provide equations at all of the required response frequencies, hence in a few cases it becomes necessary to either interpolate or extrapolate to obtain estimates of the median values of the ordinates for those frequencies not covered by the equations. Table 3.15 below indicates the frequencies for which each equation provides direct estimates of the ordinates.

The open circles in Table 3.15 indicate a frequency not explicitly covered by the tabulated coefficients presented in each study. One option is to simply neglect any equation that is not covered at a particular frequency, but this may lead to 'jumps' in the final results and it also means that at some frequencies several equations would be eliminated and hence the epistemic uncertainty would be less well captured. Therefore, rather than rejecting any equation at any particular frequency, rules are developed to interpolate or extrapolate from the coefficients presented in each study to estimate the ordinate at the missing frequency. An additional difficulty with dropping equations because of missing frequencies in the tabulated coefficients, is that all of the weights on the equations would need to be re-assigned in order to still add to unity. This problem is circumvented by always using a scheme for either interpolating or extrapolating to estimate missing values.

Tab. 3.15: Missing frequencies

Frequency (Hz)	100	50	33	20	10	5	2.5	1.0	0.5
Period (s)	PGA	0.02	0.03	0.05	0.10	0.20	0.40	1.0	2.0
Abrahamson & Silva	●	●	●	●	●	●	●	●	●
Ambraseys et al.	●	○	○	○	●	●	●	●	●
Ambraseys & Douglas	●	○	○	○	●	●	●	●	●
Atkinson & Boore	●	○	○	●	●	●	○	●	●
Berge-Thierry et al.	○	○	●	●	●	●	●	●	●
Boore et al.	●	○	○	○	●	●	●	●	●
Campbell & Bozorgnia	●	○	○	●	●	●	●	●	●
Lussou et al.	○	●	●	●	●	●	●	●	●
Sabetta & Pugliese	●	○	○	○	●	●	●	●	●
Somerville et al.	●	○	○	○	●	●	●	●	●
Spudich et al.	●	○	○	○	●	●	●	●	●
Toro et al.	●	○	○	○	●	●	●	●	●

To find missing coefficients at frequencies below 10 Hz, of which there are relatively few, it is a simple procedure to interpolate by fitting polynomial curves to each coefficient plotted against the logarithm of frequency. This is a standard procedure for smoothing coefficients from regression analyses in order to obtain smooth spectra. Figure 3.9 shows examples of such curves fitted to the coefficients of the equations of Atkinson & Boore (1997), from which the coefficients at the missing frequencies of 2.5, 3.3 and 6.7 Hz could be found. It is noteworthy that the curves do not always match the known values exactly, especially for coefficient c_3 in this case, but the differences are small and considered unimportant within the framework of this logic-tree application.

In Pegasos document TP2-TN-0270, such interpolations have been performed for the coefficients of all of the candidate equations and it is proposed that these be adopted wherever needed.

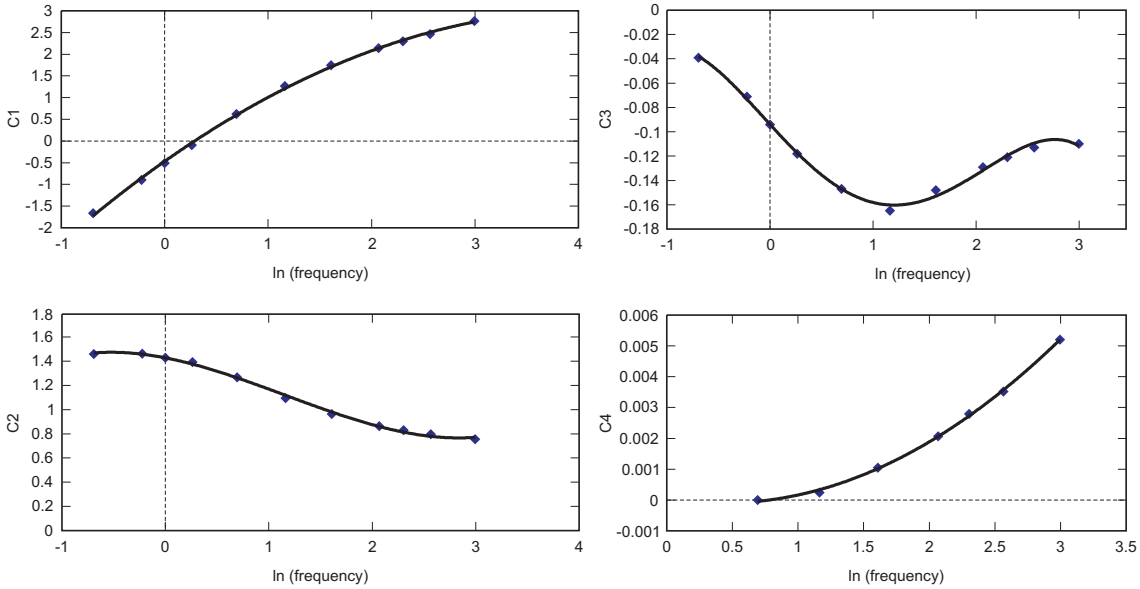

Fig. 3.9: Interpolations of coefficients of Atkinson & Boore (1997)

For coefficients missing at frequencies above 10 Hz the situation is slightly more complicated. The procedure used in the Pegasos document TP2-TN-0270 is to first assume, as has been established for the project, that the spectral acceleration at 100 Hz is equal to PGA. If the coefficient at 50 Hz is missing, it is assumed equal to that at 100 Hz (i.e. PGA), except in two cases:

– Boore et al. (1997) – since coefficients are available at 33 Hz and 100 Hz, the 50 Hz coefficients are found by interpolation.

– Bierge-Thierry et al. (2000) – no PGA equation is given and the highest frequency covered is 33 Hz, hence the coefficients at both 50 Hz and 100 Hz are assumed equal to those at 33 Hz.

The missing coefficients at 33 Hz are then found by linear interpolation in log-linear space. In order to explore the assumptions made in these interpolations, a small experiment is performed using the coefficients of Lussou et al. (2001) and Abrahamson & Silva (1997). In both cases the spectral *shape* is relatively, although not completely, insensitive to distance, hence if distance terms are ignored it is possible to derive simple expressions for the ratio of spectral ordinates at high frequencies to those at 10 Hz, as functions only of magnitude. From the equations of Abrahamson & Silva (1997), the following equation is obtained:

$$\ln\left[\frac{Sa(T)}{Sa(0.1)}\right] = a_1(T) - 2.160 + [a_{12}(T) - 0.028][8.5 - M]^2 \qquad (3.16)$$

and from the equations of Lussou et al. (2001), the following expression is obtained:

$$\log\left[\frac{Sa(f)}{Sa(10)}\right] = [a(f) - 0.351].M + c(f) - 1.562 \qquad (3.17)$$

The functions are plotted for magnitudes 5 and 6 – ignoring the different scales employed in the two equations – in Figure 3.10, from which it can be seen that the assumption of equivalence of spectral ordinates at 50 and 100 Hz is supported, and the differences between these ordinates and those at 33 Hz are sufficiently small for these to taken as equivalent when necessary.

In conclusion, for the logic-tree to be employed at this stage, it is recommended that all missing coefficients be taken from TP2-TN-0270 and that no additional branching be added to account for the uncertainty associated with these interpolations.

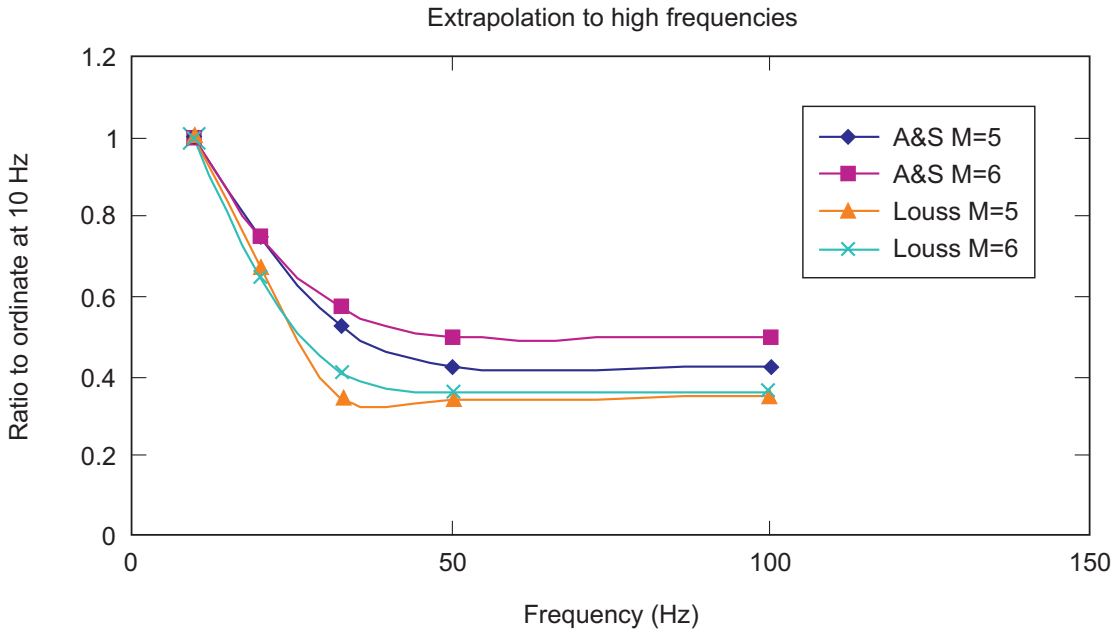

Fig. 3.10: Ratios for spectral ordinates at periods below 0.1s

3.8 Style-of-Faulting Adjustments

At WS-4/SP2, it became clear that all of the source zones defined by the four groups in SP1 specified fault mechanisms, albeit that most sources have been specified to have various possible combinations of mechanism. This necessitates ground-motion predictions that are specific to different styles of faulting, since otherwise the refinement incorporated by the work of SP1 would be largely lost if the spectral ordinates were predicted using equations that are independent of rupture mechanism. However, only 3 of the 12 equations include coefficients that allow the style-of-faulting to be included as a predictor variable, these being Abrahamson & Silva (1997), Boore et al. (1997) and Campbell & Bozorgnia (2002). Furthermore, these equations only allow predictions for the case of reverse or strike-slip ruptures but not normal faults. Therefore, for these three equations factors are required to adjust from, say, strike-slip ground motions to those from normal ruptures.

For the other equations, factors are required to adjust their median predictions, which will generally represent some "average" condition, to each of the three specified mechanisms. In order to apply such adjustments, it is first necessary to determine what actually is the "average" level that corresponds to each equation. The basis for deciding what is the "average" style of faulting for each equation is the distribution of the data set employed to derive the equation with respect to the three rupture mechanisms. Following the special workshop held in London on 13th April 2003, participants in SP2 contributed to a document (TP2-TN-0362) that summarises the

proportions of the data from each relationship in each style-of-faulting category. Table 3.16 presents the proportions by which each rupture mechanism is represented in the data sets of the remaining 9 equations, based on the information presented in the PEGASOS Report just mentioned. Some interpretations were required in order to reduce the classification to the simple three groupings of mechanisms. Firstly, where a proportion of the data from a particular equation was classified as "unknown", which was the case for the three European equations and also Lussou et al. (2001), the percentage was distributed amongst the three categories in the same proportions as the known mechanisms; the largest percentage of records with unknown mechanisms was 6.6 % for Ambraseys et al. (1996). Secondly, for some of the equations, a certain proportion of the data was assigned to "oblique" categories. In the case of Sabetta & Pugliese (1996), some events were classified as "normal strike-slip" or "reverse strike-slip", in which case it was assumed that the dominant mechanism was either normal or reverse and the records assign to appropriate category. A similar procedure was applied by the author in simplifying the data distribution of Ambraseys et al. (1996) in preparing the contributions to TP2-TN-0362. For the case of Berge-Thierry et al. (2000) 10 % of the data is simply defined as "oblique"; two thirds of these records are from the 1989 Loma Prieta earthquake and hence these were incorporated into the strike-slip category, as were the 12 records from 1990 Manjil (Iran) earthquake. The question of classifying oblique fault ruptures into discrete categories is complex and somewhat beyond the scope of this report since a relatively crude adjustment is to be made for style-of-faulting. Boore et al. (1997), for example, use a rake angle of 30° from the horizontal as the criteria to separate strike-slip events, whence in their data set the Loma Prieta earthquake, with a rake angle of 138°, was classified as reverse rupture.

Tab. 3.16: Distributions of candidate datasets amongst style-of-faulting categories

Equation	Strike-Slip	Reverse	Normal
Ambraseys et al.	0.17	0.50	0.33
Ambraseys & Douglas	0.39	0.53	0.09
Atkinson & Boore	0.18	0.81	0.01
Berge-Thierry et al.	0.27	0.31	0.41
Lussou et al.	0.63	0.32	0.05
Sabetta & Pugliese	0.00	0.47	0.53
Somerville et al.	0.00	1.00	0.00
Spudich et al.	0.55	0.00	0.45
Toro et al.	0.18	0.81	0.01

All of the equations contain a mixture of at least two mechanisms, with the exception of the Somerville et al. (2001) relationships that can be considered to represent exclusively conditions of reverse faulting. On the basis of the information in Table 3.16 and the coefficients in the three equations not listed in the table, the predictive cases that are missing can be identified, and these are shown in Table 3.17.

The use of the distributions in Table 3.16 to define the "average" condition represented by each equation is presented later on in this Section. From Table 3.17 it is clear that adjustment factors are required to transfer median motions at each response frequency from any of the three mechanisms to another. In order to simplify the procedures, strike-slip is taken as the base case relative to which the adjustment factors are defined. For the purpose of defining the ratios of spectral accelerations from reverse events to those from strike-slip ruptures, the three equations that provide terms for style-of-faulting can be employed. Figure 3.11 shows the frequency-dependent adjustment factors determined from these equations.

Tab. 3.17: Summary of gaps in predictive capacity of selected attenuation equations for style-of-faulting categories

Equation	Missing scaling factors		
	SS	R	N
Abrahamson & Silva (1997)			●
Ambraseys et al. (1996)	●	●	●
Ambraseys & Douglas (2003)	●	●	●
Berge-Thierry et al. (2000)	●	●	●
Boore et al. (1997)			●
Campbell & Bozorgnia (2002)			●
Atkinson & Boore (1997)	●	●	●
Lussou et al. (2001)	●	●	●
Sabetta & Pugliese (1996)	●	●	●
Somerville et al. (2001)	●		●
Spudich et al. (1999)	●	●	●
Toro et al. (1997)	●	●	●

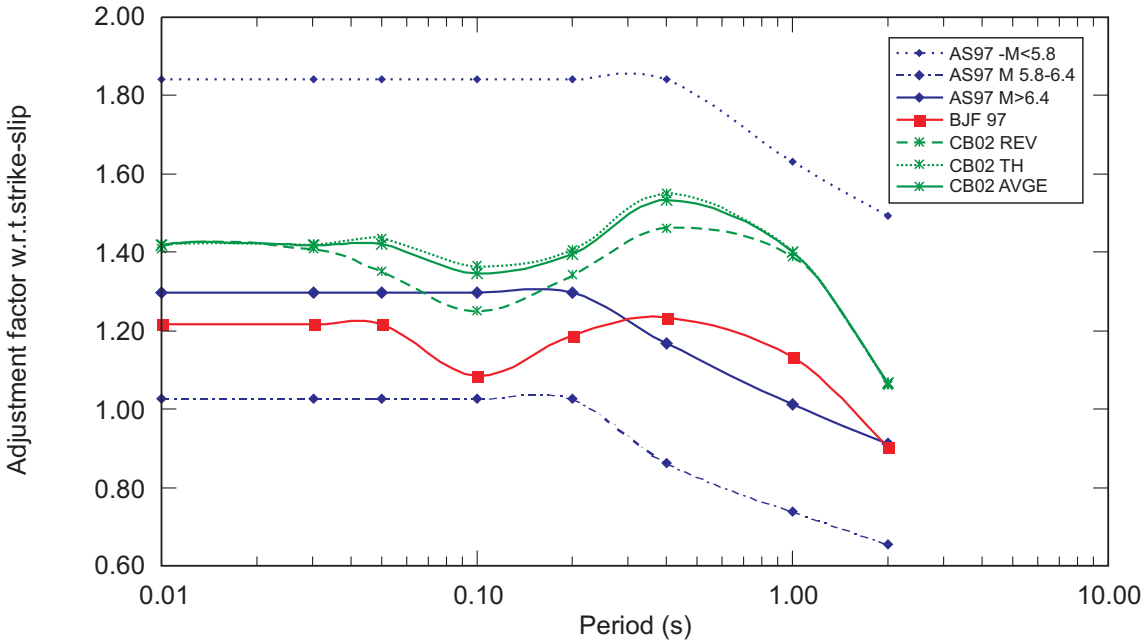

Fig. 3.11: Ratios of accelerations from reverse to strike-slip events using the equations of Abrahamson & Silva (1997), Boore et al. (1997) and Campbell & Bozorgnia (2002)

A large scatter can be observed, with a factor of about 2 between extreme values. However, this is largely due to the moment-dependency introduced in the Abrahamson & Silva (1997) scaling factors. In their paper, the authors state that this strong magnitude-dependency is controlled essentially by the high ground motions recorded during the Coalinga aftershock sequence; as a

consequence, the low magnitude scaling factors from this model are discarded because they are thought to reflect model bias rather than provide representative values. To a lesser extent, this will also affect the estimates at intermediate magnitudes as they are related to the the small magnitude factors via continuity constraints. There is good agreement between the Boore et al. (1997) and the Campbell & Bozorgnia (2002) factors in terms of variation with frequency; the higher values of the Campbell & Bozorgnia coefficients are possibly due to their definition of strike-slip earthquakes, which includes exclusively almost pure strike-slip mechanisms. Another point to note is that although the text states that the strike-slip correction factor is valid for normal events as well, this reflects the opinion of the authors and not an observable trend, since their dataset includes only one record from a normal event. Thrust events accounts for a majority of the reverse category, especially for the corrected dataset (82 %). This explains why the average adjustment factor (defined as the weighted average of the thrust and reverse adjustment factors provided by Campbell & Bozorgnia rather than the half-sum) almost coincides with the adjustment for thrust. The uncorrected records have a somewhat lower thrust to reverse ratio (67 %), which might explain the lower values of the corresponding adjustment factors.The large magnitude (M>6.4) Abrahamson & Silva factors fall within the same range of values as the models just discussed but show a different frequency dependence.

Therefore, the values deemed acceptable for $F_{R:SS}$ range from about 1.1 to 1.5, with a decrease at low frequencies (< 1 Hz). For higher frequencies, a constant factor of 1.3 seems appropriate. Considering the overall pattern and the reservations concerning the Abrahamson & Silva model, the Boore et al. (1997) and Campbell & Bozorgnia (2002) coefficients will be used as bounding values; their arithmetic average will be used as frequency-dependent best estimate. This is illustrated in Figure 3.12.

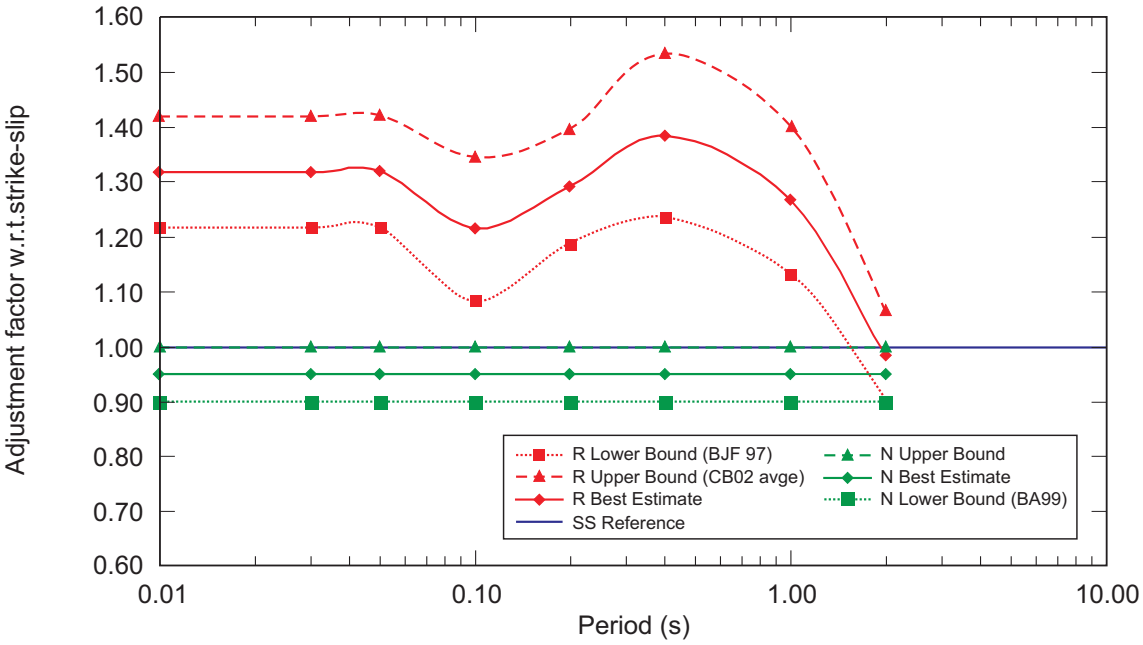

Fig. 3.12: Adopted models for scaling ratios of ground motions from reverse (red) and normal (green) ruptures relative to strike-slip earthquakes

For determining the ratios of normal to strike-slip motions there is far less information available, not least because of the relative scarcity of records from normal faulting events as reflected in Table 3.16. In the earlier version of their equations, Spudich et al. (1999) found that the dif-

ferences identified between motions from the two categories of rupture in SEA96 was a numerical artefact, and therefore imply that the ratio is in fact unity. Westaway & Smith (1989) also concluded that normal faulting earthquakes do not produce systematically lower ground motions than other faulting styles. The study of Becker & Abrahamson (1998) used in the Yucca Mountain Project addressed the apparently lower than average motions from the increasing database of strong-motion records from normal events. The authors recommend to use a factor of 0.9 based on a comparison of median stress drops from strike-slip and normal events. Although they use a fitting method where stress drop and kappa are decoupled, it is doubtful whether the difference of the order of 10 bars can be considered significant considering the large uncertainties associated with stress drop determinations. The crustal attenuation equations presented by McVerry et al. (2000), and used by Stirling et al. (2000) for seismic hazard analysis in New Zealand, includes a specific coefficient for normal faulting. Unfortunately, in neither of the publications cited are the actual numerical values of the equations presented,

In view of the uncertainty regarding the scaling between strike-slip and normal events, a simpler, frequency-independent, model is used. The value of 0.9 proposed by Becker & Abrahamson (1998) is taken as a lower bound, whereas the upper bound of unity reflects the view that strike-slip and normal ruptures produce the same average levels of motion. An intermediate value of 0.95 is added reflect the fact that the lower bound of 0.90 is not robustly determined. The ratios are shown together with those of reverse to strike-slip motions in Figure 3.12.

For the equations of Abrahamson & Silva (1997), Boore et al. (1997) and Campbell & Bozorgnia (2002), estimates from reverse earthquakes and strike-slip earthquakes can be obtained directly by using the appropriate coefficients. To predict ground motions from these three equations for normal faults, the strike-slip coefficient should be used in conjunction with the factors illustrated in Figure 3.12, together with the weighting scheme indicated in Table 3.18.

Tab. 3.18: Logic-tree for factors applied to strike-slip motions from equations of Abrahamson & Silva (1997), Boore et al. (1997) and Campbell & Bozorgnia (2002) to obtain estimates from normal fault ruptures

Factor	Weight
0.90	0.2
0.95	0.4
1.00	0.4

For the remaining 9 equations, the first step is to determine the scaling factor between their "average" condition and the strike-slip base case. A model has been developed (for which Fleur Strasser is acknowledged for a very significant and insightful contribution) to reproduce, in a relatively crude fashion, what the results of the regressions on these equations would have been if the style-of-faulting had been included as a parameter in the attenuation equation. Many simplifying assumptions are made, including that the magnitude-distance-site classification distributions of the subsets for each style-of-faulting are similar. The analysis reduces to a simple expression for the factor to transform motions from the strike-slip base case to the "average" of the equation:

$$F_{SS:eq} = \left(F_{SS:R}\right)^{N_R} \cdot \left(F_{SS:N}\right)^{N_N} \tag{3.18}$$

where $F_{SS:R}$ and $F_{SS:N}$ are ratios illustrated in Figure 3.12 and N_R and N_N are proportions of the dataset from reverse and normal earthquakes respectively. The factors for all of the equations, as well as the Swiss stochastic models, are shown in Figure 3.13 together with the curves already shown in Figure 3.13.

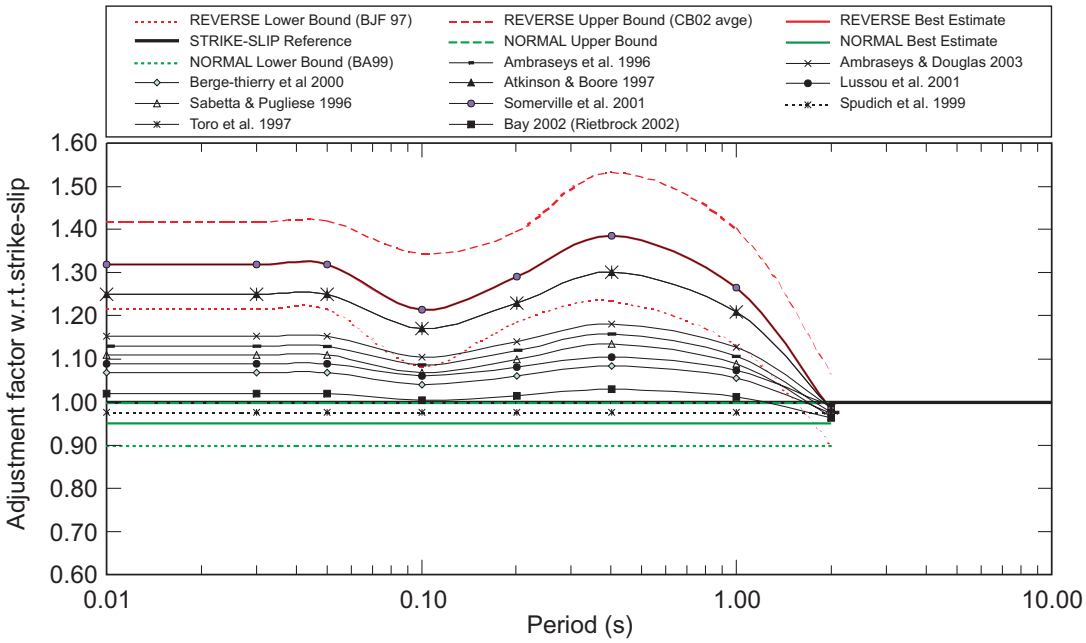

Fig. 3.13: Style-of-faulting scaling factors derived for the candidate attenuation equations without coefficients for accounting for rupture mechanism, together with the scaling factors from Figure 3.12

By inverting $F_{SS:eq}$ we obtain the factor $F_{eq:SS}$ to apply to the ground-motion resulting from the equation to make it representative of strike-slip conditions. Once this operation has been performed, the scaling factors for reverse and normal faulting can be applied as has been done for the equations incorporating a style-of-faulting factor. Tables 3.19 to 3.27 give the multiplicative coefficients to be applied to the ground-motion amplitudes predicted by the candidate model to obtain an estimate for any of the three elementary styles of faulting (strike-slip, reverse, normal).

These coefficients can be interpreted to be similar to the style-of-faulting factors defined previously, except that now the baseline corresponds to the average behaviour of the equation, based on the distribution of the data used for the derivation of the equation and the best estimates for $F_{SS:R}$ and $F_{SS:N}$ defined previously.

The weights for reverse mechanism reflect the higher confidence in the factors from Boore et al. (1997) and the reservations regarding the factors Abrahamson & Silva (1997). In applying the Campbell & Bozorgnia (2002) equations, for any events modelled as reverse faults with low dip angles, the coefficient for thrust events should be used, otherwise that for reverse events. Wherever areal sources are defined within which it is specified that faulting is reverse, but for which dip angles are not given, the reverse coefficients – rather than thrust coefficients – when applying the Campbell & Bozorgnia (2002) equations. For dip-slip events where the site lies on the hanging wall, the appropriate hanging wall factors should be employed in both the Abrahamson & Silva (1997) and Campbell & Bozorgnia (2002) equations.

Tab. 3.19: Style-of-faulting logic-tree for Ambraseys et al. (1996)

Mechanism	Weight	PGA	33 Hz	20 Hz	10 Hz	5 Hz	2.5 Hz	1 Hz	0.5 Hz
Reverse	0.15	1.26	1.26	1.26	1.24	1.25	1.32	1.26	1.09
	0.35	1.17	1.17	1.17	1.12	1.15	1.19	1.14	1.01
	0.50	1.08	1.08	1.08	1.00	1.06	1.07	1.02	0.93
Strike Slip	0.15	0.95	0.95	0.95	0.98	0.95	0.92	0.96	1.09
	0.70	0.89	0.89	0.89	0.92	0.89	0.86	0.90	1.03
	0.15	0.83	0.83	0.83	0.86	0.83	0.80	0.84	0.97
Normal	0.15	0.89	0.89	0.89	0.92	0.89	0.86	0.90	1.03
	0.70	0.84	0.84	0.84	0.88	0.85	0.82	0.86	0.97
	0.15	0.80	0.80	0.80	0.83	0.80	0.78	0.81	0.92

Tab. 3.20: Style-of-faulting logic-tree for Ambraseys & Douglas (2003)

Mechanism	Weight	PGA	33 Hz	20 Hz	10 Hz	5 Hz	2.5 Hz	1 Hz	0.5 Hz
Reverse	0.15	1.23	1.23	1.23	1.22	1.23	1.30	1.24	1.08
	0.35	1.14	1.14	1.14	1.10	1.13	1.17	1.12	1.00
	0.50	1.06	1.06	1.06	0.98	1.04	1.05	1.00	0.91
Strike Slip	0.15	0.93	0.93	0.93	0.97	0.94	0.91	0.95	1.07
	0.70	0.87	0.87	0.87	0.91	0.88	0.85	0.89	1.01
	0.15	0.81	0.81	0.81	0.85	0.82	0.79	0.83	0.95
Normal	0.15	0.87	0.87	0.87	0.91	0.88	0.85	0.89	1.01
	0.70	0.83	0.83	0.83	0.86	0.83	0.80	0.84	0.96
	0.15	0.78	0.78	0.78	0.82	0.79	0.76	0.80	0.91

Tab. 3.21: Style-of-faulting logic-tree for Atkinson & Boore (1997)

Mechanism	Weight	PGA	33 Hz	20 Hz	10 Hz	5 Hz	2.5 Hz	1 Hz	0.5 Hz
Reverse	0.15	1.14	1.14	1.14	1.15	1.14	1.18	1.16	1.08
	0.35	1.05	1.05	1.05	1.04	1.05	1.06	1.05	1.00
	0.50	0.97	0.97	0.97	0.93	0.97	0.95	0.94	0.92
Strike Slip	0.15	0.86	0.86	0.86	0.91	0.87	0.83	0.89	1.07
	0.70	0.80	0.80	0.80	0.85	0.81	0.77	0.83	1.01
	0.15	0.74	0.74	0.74	0.79	0.75	0.71	0.77	0.95
Normal	0.15	0.80	0.80	0.80	0.85	0.81	0.77	0.83	1.01
	0.70	0.76	0.76	0.76	0.81	0.77	0.73	0.79	0.96
	0.15	0.72	0.72	0.72	0.77	0.73	0.69	0.74	0.91

Tab. 3.22: Style-of-faulting logic-tree for Berge-Thierry et al. (2000)

Mechanism	Weight	PGA	33 Hz	20 Hz	10 Hz	5 Hz	2.5 Hz	1 Hz	0.5 Hz
Reverse	0.15	1.33	1.33	1.33	1.29	1.32	1.41	1.33	1.09
	0.35	1.23	1.23	1.23	1.17	1.22	1.28	1.20	1.01
	0.50	1.14	1.14	1.14	1.04	1.12	1.14	1.07	0.93
Strike Slip	0.15	1.00	1.00	1.00	1.02	1.00	0.98	1.01	1.09
	0.70	0.94	0.94	0.94	0.96	0.94	0.92	0.95	1.03
	0.15	0.88	0.88	0.88	0.90	0.88	0.86	0.89	0.97
Normal	0.15	0.94	0.94	0.94	0.96	0.94	0.92	0.95	1.03
	0.70	0.89	0.89	0.89	0.91	0.90	0.88	0.90	0.98
	0.15	0.84	0.84	0.84	0.86	0.85	0.83	0.85	0.92

Tab. 3.23: Style-of-faulting logic-tree for Lussou et al. (2001)

Mechanism	Weight	PGA	33 Hz	20 Hz	10 Hz	5 Hz	2.5 Hz	1 Hz	0.5 Hz
Reverse	0.15	1.30	1.30	1.30	1.27	1.29	1.39	1.30	1.07
	0.35	1.21	1.21	1.21	1.15	1.19	1.25	1.18	0.99
	0.50	1.12	1.12	1.12	1.02	1.10	1.12	1.05	0.91
Strike Slip	0.15	0.98	0.98	0.98	1.00	0.98	0.96	0.99	1.07
	0.70	0.92	0.92	0.92	0.94	0.92	0.90	0.93	1.01
	0.15	0.86	0.86	0.86	0.88	0.86	0.84	0.87	0.95
Normal	0.15	0.92	0.92	0.92	0.94	0.92	0.90	0.93	1.01
	0.70	0.87	0.87	0.87	0.90	0.88	0.86	0.88	0.96
	0.15	0.83	0.83	0.83	0.85	0.83	0.81	0.84	0.91

Tab. 3.24: Style-of-faulting logic-tree for Sabetta & Pugliese (1996)

Mechanism	Weight	PGA	33 Hz	20 Hz	10 Hz	5 Hz	2.5 Hz	1 Hz	0.5 Hz
Reverse	0.15	1.28	1.28	1.28	1.26	1.27	1.35	1.29	1.10
	0.35	1.19	1.19	1.19	1.14	1.18	1.22	1.16	1.02
	0.50	1.10	1.10	1.10	1.02	1.08	1.09	1.04	0.93
Strike Slip	0.15	0.96	0.96	0.96	1.00	0.97	0.94	0.98	1.10
	0.70	0.90	0.90	0.90	0.94	0.91	0.88	0.92	1.04
	0.15	0.84	0.84	0.84	0.88	0.85	0.82	0.86	0.98
Normal	0.15	0.90	0.90	0.90	0.94	0.91	0.88	0.92	1.04
	0.70	0.86	0.86	0.86	0.89	0.86	0.84	0.87	0.98
	0.15	0.81	0.81	0.81	0.84	0.82	0.79	0.83	0.93

Tab. 3.25: Style-of-faulting logic-tree for Somerville et al. (2001)

Mechanism	Weight	PGA	33 Hz	20 Hz	10 Hz	5 Hz	2.5 Hz	1 Hz	0.5 Hz
Reverse	-	-	-	-	-	-	-	-	-
	1.0	1.00	1.00	1.00	1.00	1.00	1.00	1.00	1.00
	-	-	-	-	-	-	-	-	-
Strike Slip	0.15	0.82	0.82	0.82	0.88	0.83	0.78	0.85	1.08
	0.70	0.76	0.76	0.76	0.82	0.77	0.72	0.79	1.02
	0.15	0.70	0.70	0.70	0.76	0.71	0.66	0.73	0.96
Normal	0.15	0.76	0.76	0.76	0.82	0.77	0.72	0.79	1.02
	0.70	0.72	0.72	0.72	0.78	0.74	0.69	0.75	0.97
	0.15	0.68	0.68	0.68	0.74	0.70	0.65	0.71	0.91

Tab. 3.26: Style-of-faulting logic-tree for Spudich et al. (1999)

Mechanism	Weight	PGA	33 Hz	20 Hz	10 Hz	5 Hz	2.5 Hz	1 Hz	0.5 Hz
Reverse	0.15	1.45	1.45	1.45	1.38	1.43	1.57	1.43	1.09
	0.35	1.35	1.35	1.35	1.24	1.32	1.42	1.30	1.01
	0.50	1.24	1.24	1.24	1.11	1.21	1.26	1.16	0.92
Strike Slip	0.15	1.08	1.08	1.08	1.08	1.08	1.08	1.08	1.08
	0.70	1.02	1.02	1.02	1.02	1.02	1.02	1.02	1.02
	0.15	0.96	0.96	0.96	0.96	0.96	0.96	0.96	0.96
Normal	0.15	1.02	1.02	1.02	1.02	1.02	1.02	1.02	1.02
	0.70	0.97	0.97	0.97	0.97	0.97	0.97	0.97	0.97
	0.15	0.92	0.92	0.92	0.92	0.92	0.92	0.92	0.92

Tab. 3.27: Style-of-faulting logic-tree for Toro et al. (1997)

Mechanism	Weight	PGA	33 Hz	20 Hz	10 Hz	5 Hz	2.5 Hz	1 Hz	0.5 Hz
Reverse	0.15	1.14	1.14	1.14	1.15	1.14	1.18	1.16	1.08
	0.35	1.05	1.05	1.05	1.04	1.05	1.06	1.05	1.00
	0.50	0.97	0.97	0.97	0.93	0.97	0.95	0.94	0.92
Strike Slip	0.15	0.86	0.86	0.86	0.91	0.87	0.83	0.89	1.07
	0.70	0.80	0.80	0.80	0.85	0.81	0.77	0.83	1.01
	0.15	0.74	0.74	0.74	0.79	0.75	0.72	0.77	0.95
Normal	0.15	0.80	0.80	0.80	0.85	0.81	0.77	0.83	1.01
	0.70	0.76	0.76	0.76	0.81	0.77	0.73	0.79	0.96
	0.15	0.72	0.72	0.72	0.77	0.73	0.69	0.74	0.91

4 MEDIAN V / H RATIO

The seismic hazard at the four Swiss NPP sites will be defined by horizontal and vertical response spectra at various damping levels.

4.1 Approaches for V / H Ratios

There are basically two different ways in which the V / H ratios can be obtained. The first is to use the estimates from equations that separately predict vertical and horizontal components, and then take the ratio of these at each frequency for each M-R combination. The second approach is to use equations that have been derived to predict directly the ratio V / H as a function of magnitude, distance, site conditions and other explanatory variables, including style of faulting. Although there is no definitive argument in favour of either approach, and certainly both are valid, the use of equations derived specifically for the estimation of V / H ratios is attractive. Some of the available equations for making direct predictions are reviewed in the next section, and then the logic-tree for median V / H ratios is presented in the second section of this Chapter.

4.1.1 Direct Prediction of V / H Ratios

Ambraseys & Simpson (1996) presented equations for the prediction of the maximum ratio of the vertical to the horizontal spectral ordinates of acceleration for periods from 0.1 to 2.0 seconds. Separate equations were derived for thrust, and strike-slip faulting events, plus a third equation in which all fault mechanisms were combined. The equations, valid only for the near-source region (distances < 15 km), are functions of magnitude and distance only, since site conditions were not known for many of the records. Furthermore, the database consisted of only 90 records, so after grouping for style of faulting it is very unlikely, even if the site conditions were known, that the data would have been sufficient to allow reliable determination of the site dependence. Results for small and large earthquakes are shown in Figure 4.1. It is interesting to note that Ambraseys & Douglas (2000) qualified the predictive model of Ambraseys & Simpson (1996) as "non-physical".

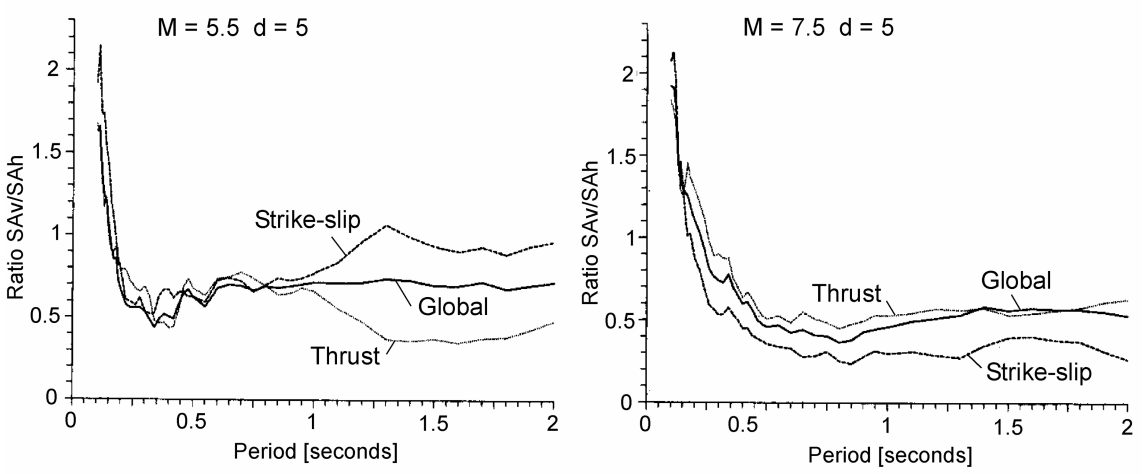

Fig. 4.1: V / H spectral ratios from Ambraseys & Simpson (1996)

Ambraseys & Douglas (2000) present equations for vertical-to-horizontal spectral ordinate ratios that differ from those of Ambraseys & Simpson (1996) in that the larger-envelope horizontal ordinates were used rather than defining the maximum ratio of vertical to horizontal motion considering both horizontal components.

Ambraseys & Douglas (2000) present separate ratios for normal, thrust and strike-slip earthquakes for periods from 0.10 to 2.0 seconds. The ratios are independent of magnitude, distance and site conditions, the first two conclusions being based on the analyses, the third on an assumption in the absence of sufficient information. The data set contained only records at source-to-site distance of less than 15 km. The V/H ratios from their study are shown in Figure 4.2. The authors note that the apparent large difference for normal faulting earthquakes is based on only 15 records and is therefore not conclusive.

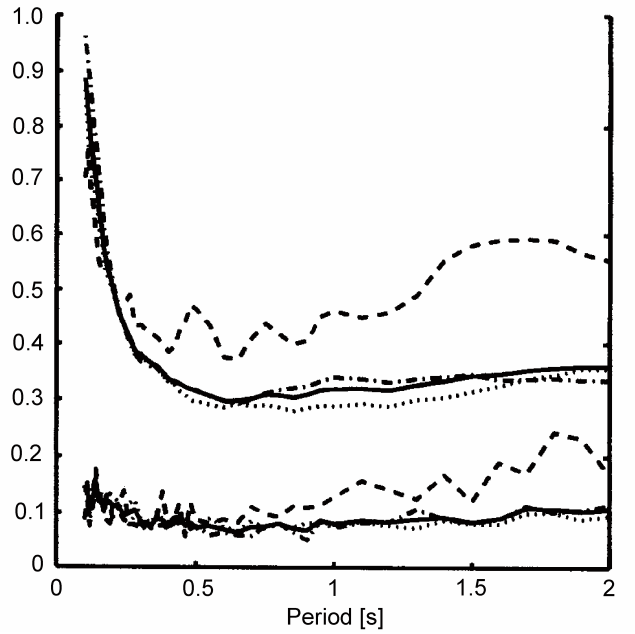

Fig. 4.2: V/H spectral ratios from Ambraseys & Douglas (2000)

Upper curves: solid line – all earthquakes; dashed line – normal ruptures; dotted line – thrust ruptures; dash-dotted line – strike-slip ruptures.

A recent study by Bozorgnia & Campbell (2002) has presented equations for the ratio of vertical to horizontal spectral ordinates, in which the horizontal motion is the geometric mean of the two individual components. Their study is based on the same worldwide (but California dominated) data set of near-source ($R < 60$ km) records as used by Campbell & Bozorgnia (2002). Their equations include the influence of magnitude, distance, style of faulting and site conditions. The relative influence of each of these factors is illustrated in Figure 4.3.

It is worth noting that the Bozorgnia & Campbell (2002) study is not based on direct analysis of the ratios of vertical to horizontal motions but they do perform checks for any bias from examining instead the ratios of vertical and horizontal medians. This does not, however, distract from the value of their paper for the Pegasos project since they provide the only study of response spectral ordinates that considers the influence of all of the relevant explanatory parameters.

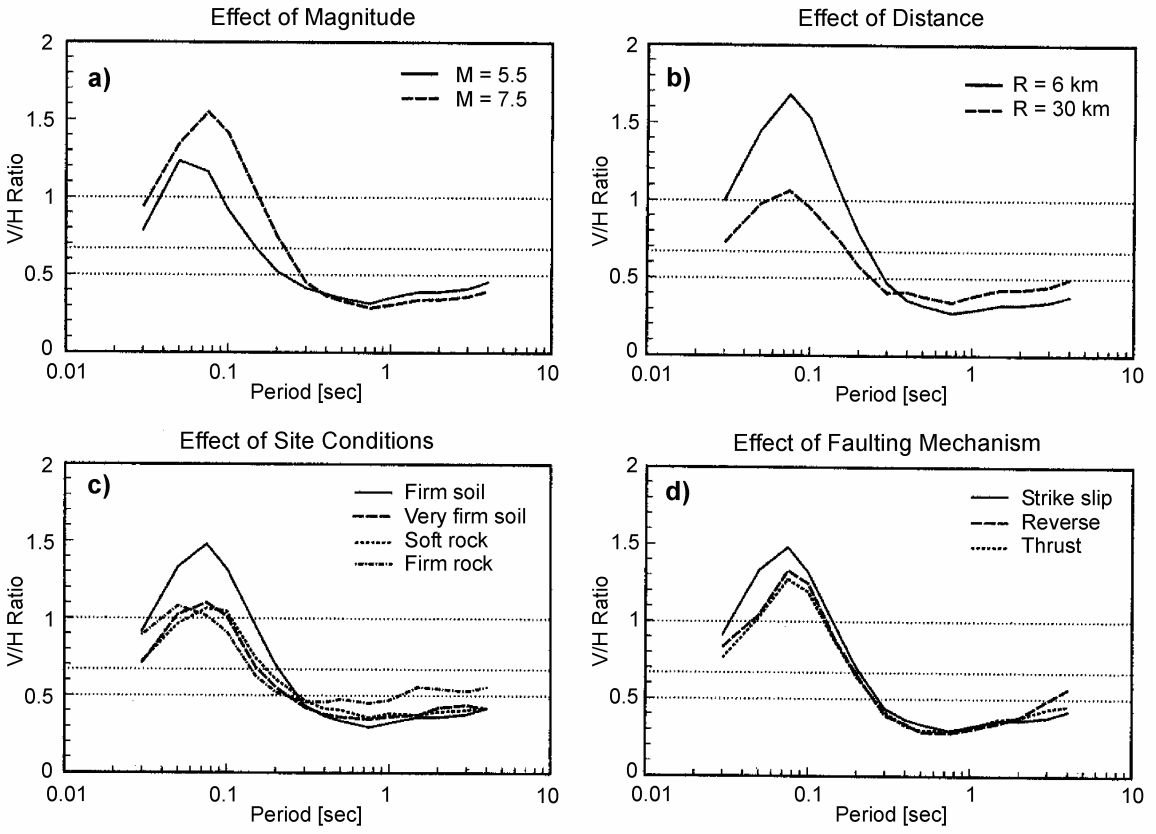

Fig. 4.3 Relative influences of different factors on the V / H spectral ratios (Bozorgnia & Campbell 2002).

A number of interesting observations can be made from Figure 4.3. The influence of magnitude (the figure shows the curves almost at the limits of the magnitude range of interest in the Pegasos project) is relatively small, and the differences amongst the ratios for strike-slip, reverse and thrust events are small. Both of these observations coincide with the conclusions of Ambraseys & Douglas (2000). However, Figure 4.3 also suggests that the ratio is strongly dependent on distance and on site conditions, conclusions that do not match those of Ambraseys & Douglas (2000). It should, however, be recalled that the latter authors did not include site conditions in their analysis and since their data set only covered the range of distances from 0 to 15 km it is unlikely that they would have found a significant dependence on distance.

The question that then arises is whether the Bozorgnia & Campbell (2002) equations can simply be adopted directly, perhaps with some branching to capture epistemic uncertainty, as the basic logic-tree for the V / H ratio. In support of this idea is the fact that in assigning weights to attenuation equations for median horizontal motion in Chapter 3, the equation of Campbell & Bozorgnia (2002), which is essentially the counter part to the Bozorgnia & Campbell (2002) study of the V/H ratio, was given a high rating (see Table 2.16). However, there are also factors that militate against the adoption of such a simple solution, the first being that the equations are based on a data set limited to records obtained at source-to-site distances of less than 60 km. A second factor is that to use only this single study to define the V/H ratios would not capture the epistemic uncertainty in this feature of the ground motion. As mentioned above, branches could be added, presumably defining the same ratios but multiplied by factors both greater than and less than unity, but their basis would be somewhat arbitrary. For these reasons, it is decided that a better approach would probably be to use the ratios obtained from a suite of equations that predict both horizontal and vertical components of motion.

4.1.2 V/H Ratios from Median Horizontal and Vertical Ground Motions

The logic-tree for the median vertical motions is essentially constructed in exactly the same way as that for the median horizontal motions. The magnitude scale conversions and the treatment of missing frequencies are handled in exactly the same way as described in Sections 3.5 and 3.7. Needless to say, no conversion is required for the definition of components since for the vertical motion this is unambiguous. The component conversions for the horizontal components have already been dealt with in Section 3.6.

An important, and complicated, issue that needs to be considered in setting up the logic-tree for the V/H ratio is that the influence of style-of-faulting, as it is for the median horizontal motions (Section 3.8), notwithstanding the apparently relatively small influence of this factor indicated in figures discussed in the previous section. The obvious choice might therefore be to use only those equations that predict both vertical and horizontal components of ground motion, and at the same time include style-of-faulting as a predictor variable in their equations. This would, however, leave only the equations of Campbell & Bozorgnia (2002) and Abrahamson & Silva (1997). The former is limited in applicability to source-to-distances of less than 60 km, and the latter has a very strong magnitude-dependence in the factor for reverse faulting events with respect to strike-slip events (Figure 4.4). This apparently very high scaling factor for smaller magnitude reverse faulting events is driven by the 1983 Coalinga (California) earthquake series and therefore could easily represent any specific peculiarity of those events rather than a general universal trend, at least in degree. In the light of the potential problems with both Campbell & Bozorgnia (2002) and Abrahamson & Silva (1997), it is decided to use a large number of equations, and to consider the issue of style-of-faulting separately.

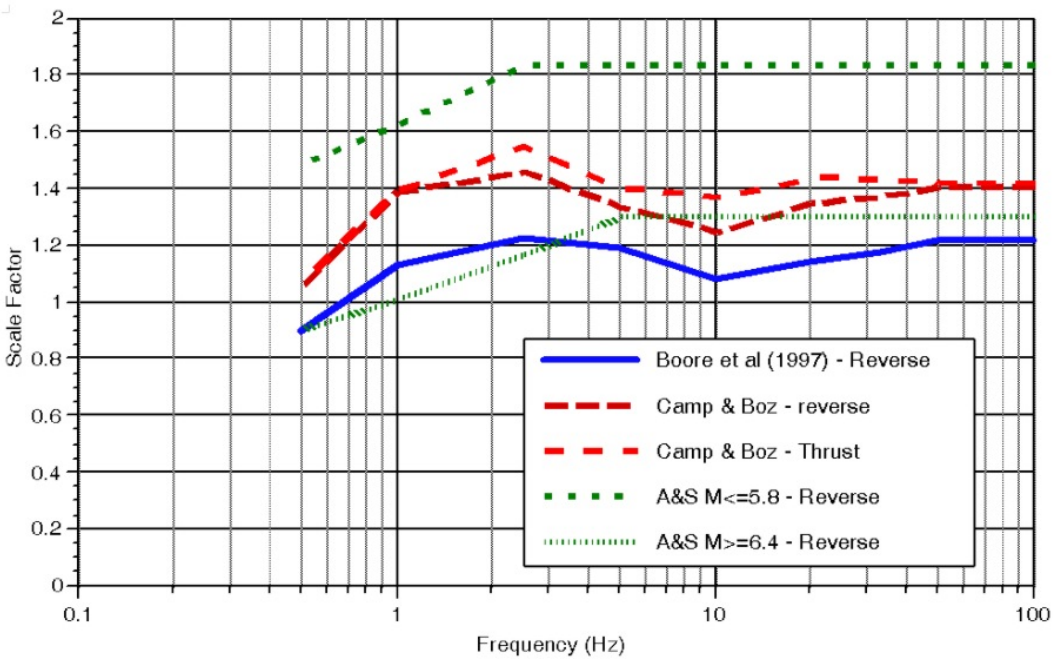

Fig. 4.4: Ratios of horizontal spectral ordinates from reverse and strike-slip events from three attenuation relationships explicitly modelling style-of-faulting effects (from PEGASOS Document TP2-RF-0391red)

4.2 Logic-tree Structure

The same set of attenuation equations is used as for the median horizontal motion, except that four equations, that do not provide coefficients for the vertical component of motion, are dropped: Atkinson & Boore (1997), Boore et al. (1997), Spudich et al. (1999) and Toro et al. (1997). The equations of Ambraseys et al. (1996) are replaced by those of Ambraseys & Simpson (1996). These are based on the same data set as the horizontal equations of Ambraseys et al., but with some reductions compared to the latter study.

A particularly difficult issue to resolve with respect to the vertical motions is the adjustment of the spectral ordinates to the reference site condition. An approximate scheme for achieving this adjustment, when at an earlier stage the reference site had been chosen as having a $V_{s,30}$ equal to 1,000 m/s, is presented in Appendix 2. However, the adjustment to reference site conditions is now to be made as part of SP3, hence in this model it is only necessary to define the V / H ratios for the selected site class for each candidate equation. Therefore, in defining these V / H ratios, the amplifying effect, if any, of the selected site class is explicitly accounted for and no additional adjustments are needed.

The V / H ratios need to include the influence of style-of-faulting, as is done for the median horizontal motion (Section 3.8). The way in which this effect is approached for the vertical to horizontal ratio is addressed below, but the discussion is pre-empted by stating that the equations of Somerville et al. (2001) also need to be dropped since they are applicable to a single style-of-faulting.

As a result of dropping the four equations that do not provide predictions of the vertical component of motion and the Somerville et al. (2001) equations, there are finally seven equations as opposed to 12 in the logic-tree for horizontal motions. However, it is assumed that this number is still sufficient to capture the epistemic uncertainty, whilst also being sufficient in number to avoid sharp jumps due to abrupt changes in weights from one magnitude-distance bin to another. The characteristics of the chosen equations are summarised in Table 4.1, from which it can be easily appreciated that the differences with respect the horizontal equations (Table 2.1) are very minor.

Tab. 4.1: Candidate equations for prediction of vertical median motions

Study	Magnitude			Distance[1]			Data	
	Scale	M_{min}	M_{max}	Scale	R_{min}	R_{max}	EQs	Recs
Abrahamson & Silva (1997)	M_w	4.4	7.4	R_{rup}	0.1	220	58	650
Ambraseys & Simpson (1996)	M_s	4.0	7.9	R_{jb}	0.0	260	157	417
Ambraseys & Douglas (2000)	M_s	5.8	7.8	R_{jb}	0.0	15	44	183
Berge-Thierry et al. (2000)	M_s	4.5	7.3	R_{hyp}	7.0	100	485	139
Campbell & Bozorgnia (2002)	M_w	4.7	7.7	R_{seis}	2.0	60	34	439
Lussou et al. (2001)	M_{JMA}	3.7	6.3	R_{hyp}	4.0	600	102	3,011
Sabetta & Pugliese (1996)[2]	M_s,M_L	4.6	6.8	R_{jb},R_{epi}	1.5	180	95	17

[1] Distances defined as in Abrahamson & Shedlock (1997).
[2] Equations provided in terms of both distance metrics.

The adopted site classes for each equation will be the same as those indicated in Section 3.3, indeed it is essential that the same site classes are considered in generating the median vertical and horizontal motions for the purpose of deriving the ratios of vertical to horizontal spectral ordinates.

In calculating the V / H ratios, the relationships in Table 4.1 are used to generate both median horizontal and median vertical spectral accelerations for the purpose of then calculating the ratios. For both horizontal and vertical motions the weights are as defined in Section 4.3 below. The appropriate conversions for magnitude scale are applied to horizontal and vertical motions using the procedures specified in Section 3.5 and the horizontal components are all adjusted to be equivalent to the geometric mean using the relations specified in Section 3.6. Coefficients for missing frequencies are adopted from the interpolations and extrapolations performed by Proseis, as described in Section 3.7.

The remaining issue is how to account for style-of-faulting in the predictions of V / H ratios. As noted above, two of the 7 equations, those of Abrahamson & Silva (1997) and Campbell & Bozorgnia (2002), include coefficients that allow predictions specifically for strike-slip and reverse faulting events, whereas the other five equations represent the influence of all three mechanisms in differing proportions. The Somerville et al. (2001) relations were dropped because they effectively represent only the case of reverse faulting. A procedure for obtaining scaling factors for the vertical component of motion from reverse ruptures with respect to those from strike-slip events could be carried out along similar lines to that used for horizontal components, as explained in Section 3.8. However, such a complex procedure, with such a high degree of associated uncertainty, may not be warranted. Figures 4.2 and 4.3(d) suggest that for frequencies of 10 Hz and below, the V / H ratio for strike-slip and reverse events is essentially the same for reverse and for strike-slip events. As was explained previously, the apparently strong differences exhibited for normal faulting events in Figure 4.2 are likely to be more due to the lack of constraint as the result of limited number of records from normal faulting events rather than a genuine physical pattern. The explicit assumption is made, therefore, that the V / H ratio for normal faulting earthquakes, for a given combination of magnitude, distance and site conditions, is the same as that for a strike-slip event. The remaining issue, then, is how to include the apparent mechanism dependence, in terms of differentiating reverse events from those with normal or strike-slip rupture, of the V / H ratio for frequencies greater than 10 Hz.

The pattern of the mechanism dependence of the V / H ratio at high frequencies indicated in Figure 4.3(d) are confirmed by comparison of Figures 4.4 and 4.5. The obvious solution would seem to be to use only the Abrahamson & Silva (1997) and the Campbell & Bozorgnia (2002) equations for frequencies above 10 Hz. However, as is explained below in Section 4.3, the weighting scheme applied means that these two equations are dominant amongst the seven relationships in the logic-tree, particularly at short distances, where the effect of style of faulting may be expected to be more pronounced (Figure 4.6). For earthquakes of magnitude 5.5 or less, the two equations carry 0.45 of the total weight, increasing to 0.55 for magnitudes between 5.5 and 6.5, and to 0.62 for the largest category of events. It is therefore considered that unnecessary to make any further adjustment to the logic-tree. In conclusion, the style of faulting in the logic-tree for the V / H ratio will be treated in the following way:

- For reverse faults, Abrahamson & Silva (1997) and Campbell & Bozorgnia (2002) to be used with the appropriate coefficients for reverse faults; all the other equations to be used as published, and without applying the style of faulting adjustments described in Section 3.8.
- For normal or strike-slip faults, Abrahamson & Silva (1997) and Campbell & Bozorgnia (2002) to be used with the appropriate coefficients for strike-slip faults; all the other equations to be used as published, and without applying the style of faulting adjustments described in Section 3.8.

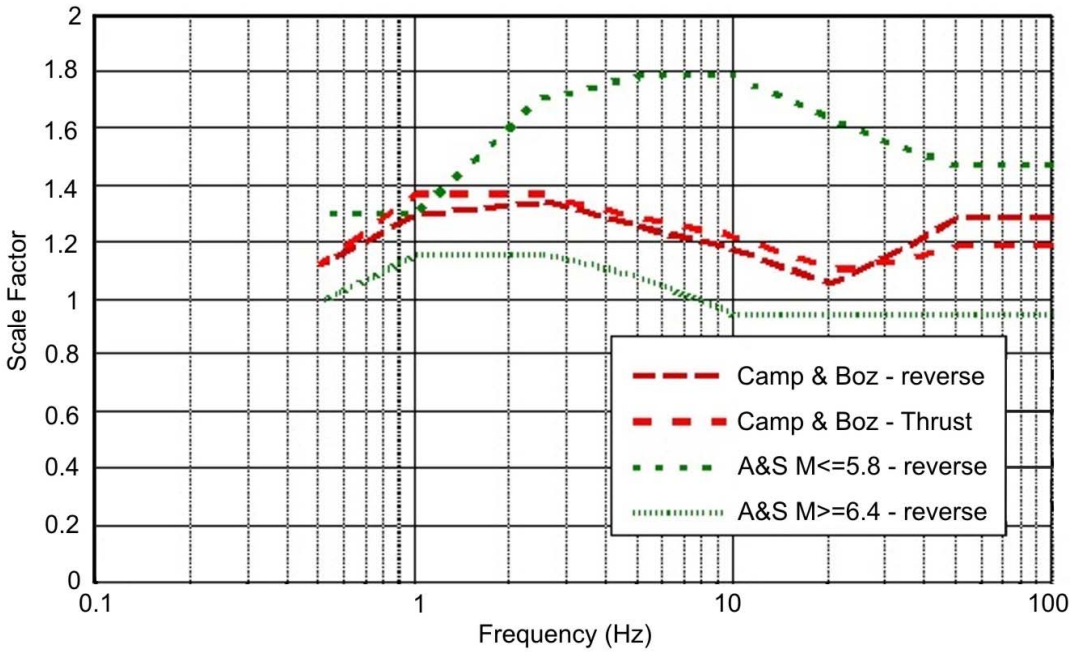

Fig. 4.5: Ratios of vertical spectral ordinates from reverse and strike-slip events from three attenuation relationships explicitly modelling style-of-faulting effects (from PEGASOS Document TP2-RF-0391red)

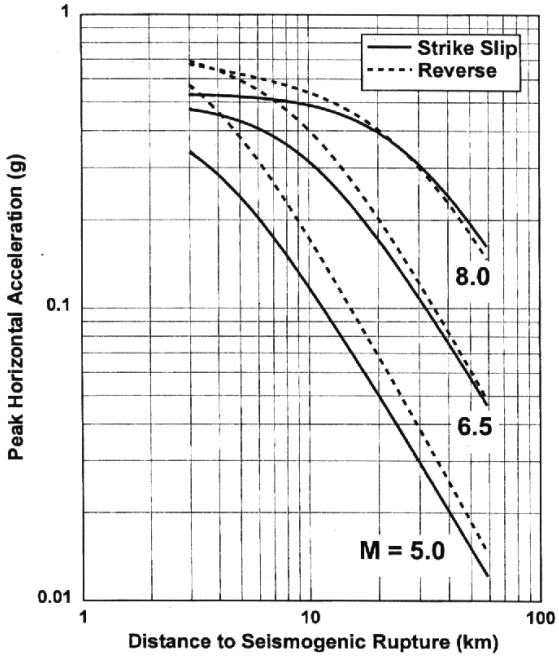

Fig. 4.6: Scaling of PGA with magnitude, distance and source mechanism (Campbell 1997)

4.3 Weights for Proponent Models

The weights for the vertical median motions are assigned in exactly the same way as for the horizontal motions, through four gradings, the rationale for which remains unchanged, which are then multiplied and normalised (see Section 3.2). Since the characteristics of the data sets used to derive the equations for the vertical components of motion are essentially the same as those used for the horizontal equations, the grading applied to each equation under each of the four criteria remain unchanged from those presented in Tables 2.12 to 2.15, for which reason they are not reproduced here. The final weights, however, do change because the overall grades are normalised across the 7 selected equations that consider the vertical component of motion rather than the full suite of 12 equations used for calculating the median horizontal motion. The weights are presented in Table 4.2.

Tab. 4.2: Weights applied to vertical and horizontal ground motions at all frequencies to calculate the V / H ratios

Study	$M_w < 5.5$			$5.5 < M_w < 6.5$			$6.5 < M_w < 7.5$		
	< 10	10 – 60	> 60	< 10	10 – 60	> 60	< 10	10 – 60	> 60
Abrahamson & Silva	0.1494	0.1667	0.2339	0.1834	0.2220	0.2426	0.2074	0.2802	0.3215
Ambraseys et al.	0.1261	0.1563	0.1974	0.1238	0.1665	0.2047	0.1245	0.1681	0.2412
Ambraseys & Douglas	0.1494	0.0333	0.0000	0.1467	0.0355	0.0000	0.1660	0.0448	0.0000
Berge-Thierry et al.	0.1360	0.1625	0.1901	0.0417	0.1010	0.1774	0.0094	0.0656	0.1881
Campbell & Bozorgnia	0.2989	0.2500	0.0936	0.3668	0.2664	0.0970	0.4149	0.3362	0.1286
Lussou et al.	0.0000	0.0750	0.0877	0.0000	0.0420	0.0737	0.0000	0.0000	0.0000
Sabetta & Pugliese	0.1401	0.1563	0.1974	0.1376	0.1665	0.2047	0.0778	0.1051	0.1206

At short distances (< 15 km), as with the median horizontal motion, the equation of Campbell & Bozorgnia (2002) is dominant, but in the intermediate distance range the influence of Abrahamson & Silva (1997) is almost as strong, and Ambraseys et al. (1996) is also significant. There are no ENA equations in the logic-tree for the V / H ratio, and the extensional regime equations of Spudich et al. (1999) are also not included. As for the horizontal motion, the equation with the least overall influence is Lussou et al. (2001), a result of being from a very different tectonic environment, using hypocentral distance, and not being applicable to earthquakes of magnitude greater than 6.3. The logic-tree therefore consists essentially of western US and European equations, the influence in the near-field being in a ratio of about 2:1 in favour of the former, reflecting the superior features of the US-based equations discussed in sub-section 3.2.7. In the intermediate distance range, the two regions have almost equal influence, with the European equations having a collective weight greater than 0.4, and with a collective weight close to 0.6 at distances beyond 60 km, the European equations are dominant.

5 ALEATORY VARIABILITY FOR THE HORIZONTAL COMPONENT

In performing a PSHA, the aleatory uncertainty in the ground-motion prediction equations is as important, if not more so at some of the annual exceedance frequencies of relevance in the Pegasos project, as the median estimates. For this reason, separate logic-trees are required for the aleatory uncertainty associated with the median ground motions.

In the following section, the basic approach for constructing the logic-tree for the aleatory variability of the horizontal ground motion is described. This will involve using the values from several studies that use a definition of the horizontal motion that is different from that to be used as the basis for the Pegasos hazard calculations, namely the larger horizontal component at each response frequency. As a result, conversions then need to be applied to some of the standard deviation values in the logic-tree, and these are defined in the Section 5.2.

5.1 Logic-tree Structure

There is a great deal of evidence in support of magnitude-dependence of the scatter in attenuation equations and it is important that this be included in the analysis. Two relations that includes this effect are those of Abrahamson & Silva (1997) and Campbell (1997), and examples of how the sigma value varies with moment magnitude are given in Table 5.1.

Tab. 5.1: Magnitude-dependent sigma values from Campbell (1997) and Abrahamson & Silva (1997)

M_w	σ [ln(Y)]					
	Campbell	T = 0.10 s	T = 0.50 s	T = 0.75 s	T = 1.0 s	T = 2.0 s
4.5	0.638	0.77	0.80	0.81	0.83	0.85
5	0.607	0.77	0.80	0.81	0.83	0.85
6	0.546	0.635	0.67	0.687	0.717	0.745
7	0.487	0.50	0.54	0.564	0.599	0.64
7.5	0.466	0.50	0.54	0.564	0.599	0.64

The influence is pronounced and there are significant differences between the two models. The conclusion would be to give large weights to both of these models, thus capturing some of the epistemic uncertainty in the problem.

Another issue is whether the sigma values should also vary with the amplitude of the motion, which is also proposed by Campbell (1997), who furthermore finds that this estimate is statistically more stable than that of the magnitude-dependence of the sigma values. The literature is less unanimous on this issue: Douglas & Smit (2001) find a significant dependence of the scatter on magnitude but not on the amplitude of the motion. Boore et al. (1997) note that their results confirm the finding that the scatter in PGA decreases with increasing magnitude (e.g. Youngs et al. 1995) and similarly with increasing PGA. For spectral ordinates they found no clear dependence of variance on magnitude or amplitude but point out that this may be due to there being relatively few low-amplitude spectra and few records from events of magnitude less than 6 in the dataset used for the spectral ordinate regressions. In light of these conflicting

observations, the amplitude-dependent model of Campbell (1997) would also be given a relatively high weight but smaller than the two magnitude-dependent models. However, adopting the magnitude-dependent sigma values from Abrahamson & Silva (1997) and/or from Campbell & Bozorgnia (2002) is sufficient to capture non-homoskedatic measures of the aleatory variability. Although there is support for magnitude-dependence of the variance in ground motion predictions, it is to be noted that few of the models have employed this feature, which may in some cases be a considered decision (e.g. Boore et al. 1997) whereas in many others it appears not to have been explored (e.g. Ambraseys et al. 1996). It is worth noting that Boore et al. (1997) do find a decrease in scatter of PGA with increasing magnitude, reflected by larger values of sigma for magnitude below 6. They also point out that although they do not see the same effect for spectral ordinates that "*this is probably due, at least in part, to the relatively few records in the response spectral data set from earthquakes with magnitude less than 6.0*". The evidence for magnitude-dependent sigma values, on the other hand, is strong and hence such a model is adopted here.

It is decided to use the standard deviations from Abrahamson & Silva (1997) for all the equations. Since this equation is based on the geometric mean definition of horizontal motion, no component conversions are required (see Section 5.3 below); the median values of motion from equations using other definitions of motion are already adjusted to be equivalent to the geometric mean component (Section 3.6). However, it is recognised that the standard deviations may need to be adjusted for some of the other equations, mainly to reflect the influence of error propagation due to conversions of magnitude and distance values. The assumption is made that the error propagation due to component conversions (Section 3.6) is small enough to be neglected. Three other conversions, however, need to be considered:

- Magnitude conversions (Section 3.5): those equations for which it is necessary to apply conversions to obtain M_w values, the sigma values need to be increased (see Section 5.4).
- Distance conversions: conversions need to be applied to various equations since, as shown in Table 2.1, there is not a common distance metric used in all the equations. However, as explained in Section 5.5 below, the distance conversions are now handled entirely by SP4 and SP2 has no input to these adjustments. However, as is also explained in Section 5.5, for those equations based on the R_{jb} definition – which does not account for the actual focal depth of events – it is considered necessary to increase the sigma values at short distances in order to account for the effect of focal depth distributions.
- Style of Faulting: in Section 3.8, adjustments were proposed to allow all 12 equations in the logic-tree to predict median horizontal motions for strike-slip, reverse and normal faulting earthquakes. It could be argued that the sigma values should be increased for those equations where these adjustments are applied to carry across the uncertainty in the adjustments. However, unlike with the magnitude and distance conversions, the adjustments for style of faulting are not altering the definition of a parameter already in the equation but rather adding a new parameter that was previously not included. Therefore, the adjustment could be expected to have the effect of reducing the standard deviation through the addition of an extra explanatory variable. It is assumed that the two effects – increased scatter due to the uncertainty in the style-of-faulting adjustment and decreased scatter because of the additional predictor variable – effectively cancel each out and the effect can therefore be neglected.

The structure of the logic-tree is presented together with the applied weights in the next section. For the two equations with magnitude-dependent sigma values, it is assumed that the actual aleatory uncertainty may be slightly higher or lower than those given by Abrahamson & Silva (1997), and branches are included to reflect possible values either side of those presented in the original paper. For the remaining 10 equations, the same assumption is made but with slightly wider branching. Superimposed on this basic scheme are adjustments to the branches to account

for the effect of the magnitude conversions in increasing the scatter, and at short distances (and moderate to small magnitudes) the sigma values are increased for those equations using the Joyner-Boore definition of distance (see Section 5.3). This effect is only significant at short distances (< 15 km) and further it is only of importance for moderate magnitude events ($M_w < 6.5$) since for larger crustal earthquakes, which rupture through most of the seismogenic layer, the focal depth has no real significance.

An alternative scheme would be to apply the standard deviations from each of the published equations, together with branches to capture possible variations in the calculated values. One disadvantage of this approach is that component conversions would be required for the different definitions of horizontal motion; as shown below in Section 5.3, the adjustments would be small, but this is an additional complication to the logic-tree for no real gain. The main disadvantage of using the published sigma values from each equation is the loss of the magnitude-dependence, which is well supported and of importance for calculating hazard at

5.2 Weights for Proponent Models

Table 5.2 shows the structure of the logic-tree for aleatory uncertainty in the horizontal ground motions and the weights applied. The tendency overall is to increase the estimates of the aleatory uncertainty, mainly to account for the error propagation due to conversions of explanatory variables.

At the same time, for well constrained equations not requiring such conversions, the possibility of the actual aleatory uncertainty being slightly lower is also accounted for by branches having factors less than 1.0 on the standard deviations from Abrahamson & Silva (1997).

The weights in Table 5.2 are to be combined with those for the median values in Table 3.6, which reflect the degree of confidence already determined in each equation.

Tab. 5.2: Logic-tree and weights for aleatory uncertainty of horizontal ground motions

Equation	$M_w < 6.5$ and $R < 15$ km		$M_w > 6.5$ or $R > 15$ km	
	Factor[1]	Weight	Factor[1]	Weight
Abrahamson & Silva	0.95	0.1	0.95	0.1
	1.00	0.8	1.00	0.8
	1.05	0.1	1.05	0.1
Ambraseys et al.	1.05	0.4	1.00	0.4
	1.10	0.4	1.05	0.4
	1.15	0.2	1.10	0.2
Ambraseys & Douglas	1.05	0.4	1.00	0.4
	1.10	0.4	1.05	0.4
	1.15	0.2	1.10	0.2
Atkinson & Boore	0.95	0.15	1.00	0.4
	1.00	0.7	1.05	0.4
	1.05	0.15	1.10	0.2

Tab. 5.2: (Cont.)

Equation	$M_w < 6.5$ and $R < 15$ km		$M_w > 6.5$ or $R > 15$ km	
	Factor[1]	Weight	Factor[1]	Weight
Berge-Thierry et al.	1.00	0.4	1.00	0.4
	1.05	0.4	1.08	0.4
	1.10	0.2	1.15	0.2
Boore et al.	1.05	0.5	0.95	0.15
	1.10	0.3	1.00	0.7
	1.15	0.2	1.05	0.15
Campbell & Bozorgnia	0.90	0.2	0.90	0.2
	1.00	0.7	1.00	0.7
	1.05	0.1	1.05	0.1
Lussou et al.	1.00	0.4	1.00	0.4
	1.05	0.4	1.08	0.4
	1.10	0.2	1.15	0.2
Sabetta & Pugliese	1.05	0.4	1.00	0.4
	1.10	0.4	1.05	0.4
	1.15	0.2	1.10	0.2
Somerville et al.	1.05	0.5	0.95	0.15
	1.10	0.3	1.00	0.7
	1.15	0.2	1.05	0.15
Spudich et al.	1.05	0.5	0.95	0.15
	1.10	0.3	1.00	0.7
	1.15	0.2	1.05	0.15
Toro et al.	1.05	0.5	0.95	0.15
	1.10	0.3	1.00	0.7
	1.15	0.2	1.05	0.15

[1] The factor to be applied to the frequency-dependent sigma values from the equations of Abrahamson & Silva (1997)

5.3 Horizontal Component Conversions

Figure 5.1 shows ratios of the standard deviations of logarithmic residuals calculated using various different definitions of the horizontal component. It can immediately be appreciated that the ratios are in all cases very close to unity, although the patterns of variation of each ratio with response period are somewhat erratic. Since the standard deviations to be applied are taken from a single set of equations that are based on the geometric mean, which is the definition adopted for the PEGASOS project, these adjustments are not needed.

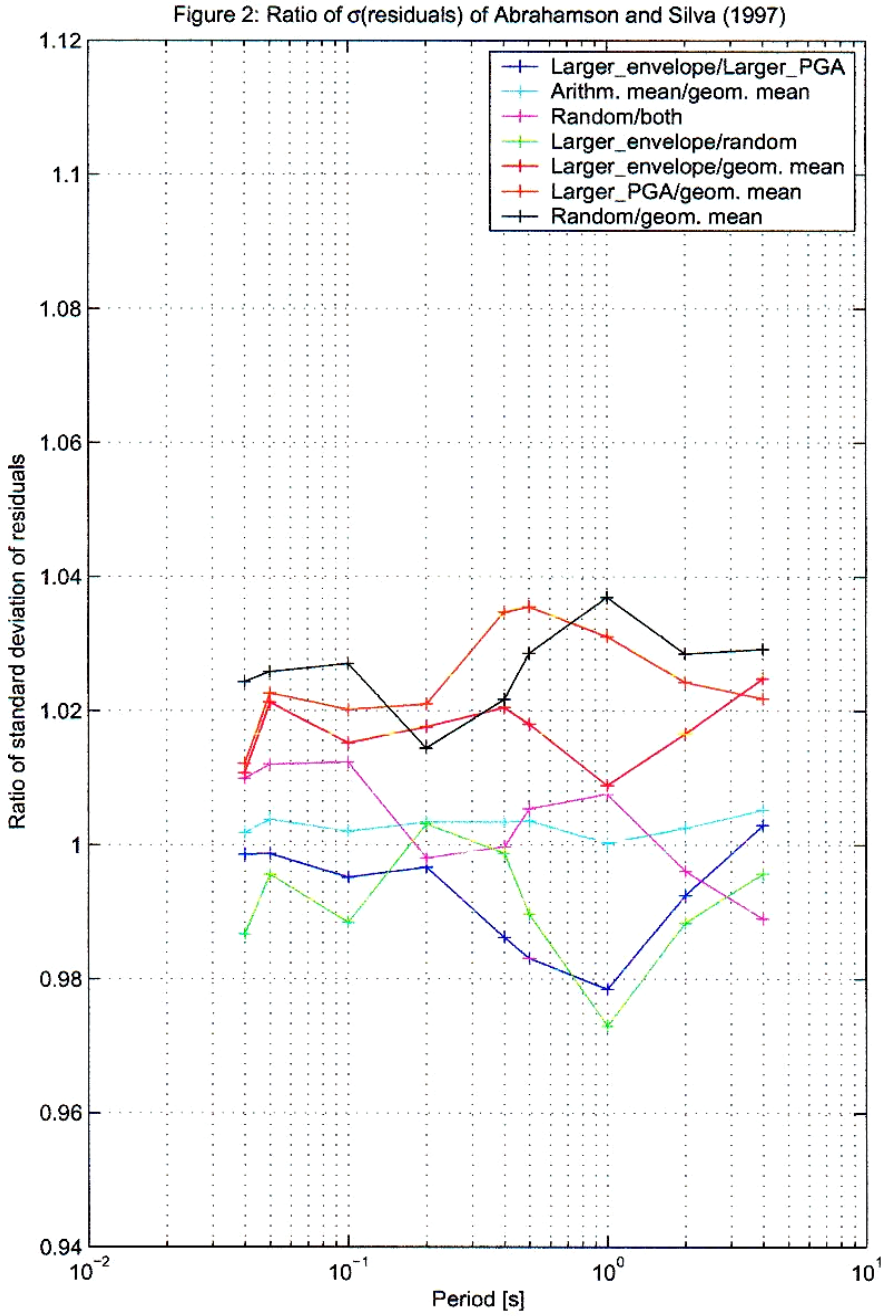

Fig. 5.1: Ratios of sigma values for different definitions of the horizontal components.

The ratios of the residuals shown in Figure 5.1 are useful in identifying why one particular set of published error terms – which in an earlier version of this logic-tree was used as an example of a magnitude-independent scatter term – may not be suitable for use in the hazard calculations. Figure 5.2 shows the ratio of sigma values of geometric mean to larger components from Boore et al. (1993), who used the same data set to derive equations in terms of both definitions of the horizontal component. This curve can be compared with the dark red line in Fig. 5.1; in the latter, the ratio (inverted to match the definition in Fig. 5.2) is always less than unity, whereas in Figuure 5.2 the ratio is consistently above one, and at short periods appreciably so, which is counter intuitive and can lead to physically impossible results in hazard calculations (Fig. 5.3).

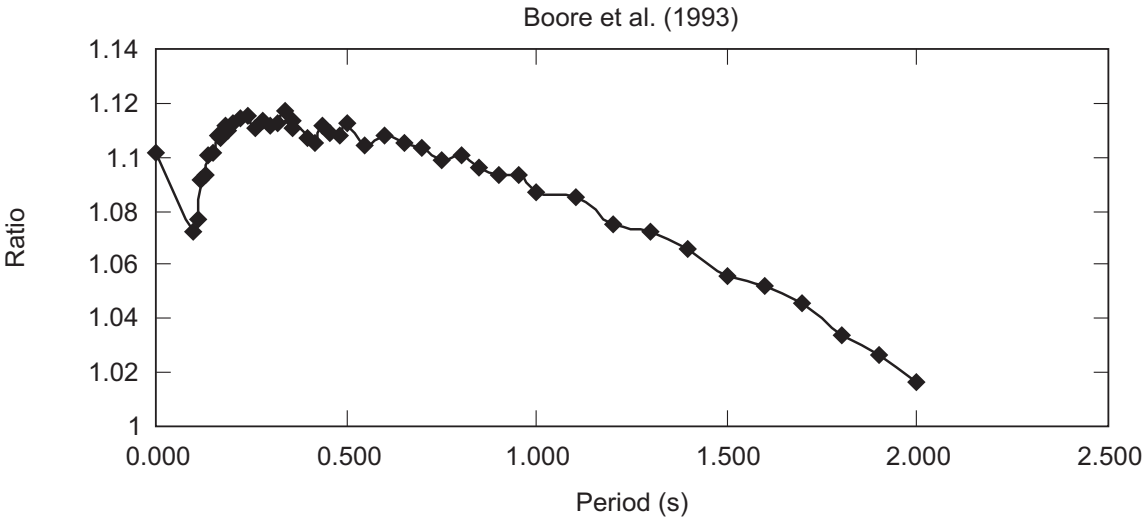

Fig. 5.2: Ratio of sigma values for geometric mean to larger components from Boore et al. (1993)

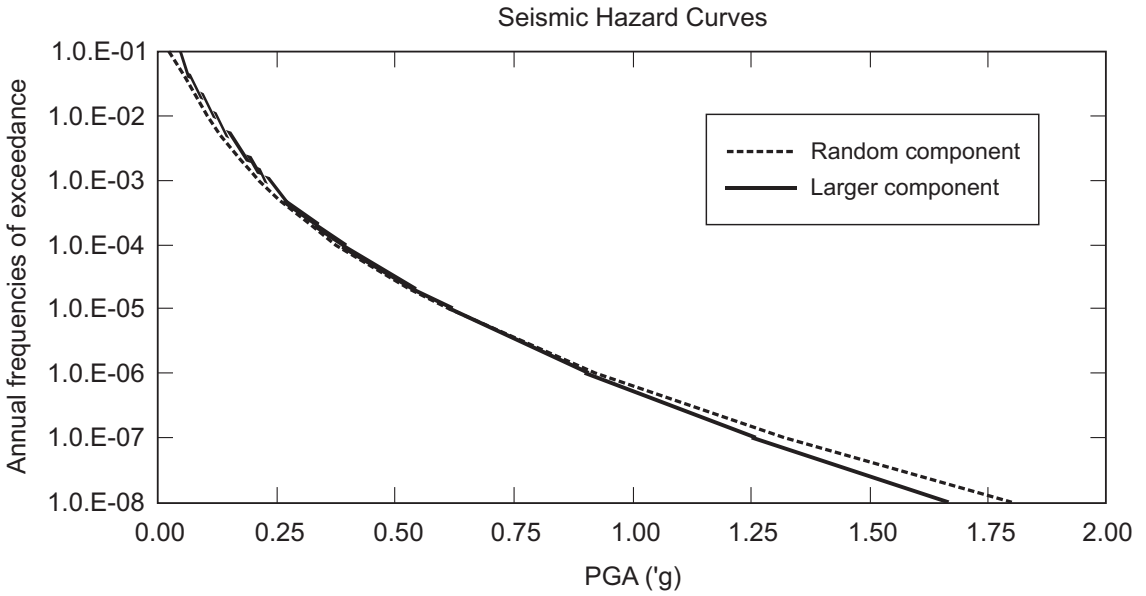

Fig. 5.3 : Hazard curves for Gazantiep (Turkey) using the equations for larger and for geotemtric mean (random) PGA of Boore et al. (1993), showing that at long return periods the geometric mean component motion is greater than the larger component, a physically impossible case (Restrepo-Vélez & Bommer 2003)

5.4 Magnitude Conversion Effect

As noted in Section 3.5, a number of the candidate equations are not derived in terms of M_w and therefore conversions need to be applied in order to obtain magnitude values is other scales (M_s, M_{JMA}, M_L) equivalent to a given value of M_w. These conversions are made using empirical relationships that carry their own associated aleatory uncertainty. Therefore, strictly the effect of the scatter in the magnitude conversion equations should be carried across into the overall sigma values. The equation for calculating the effect of the propagating error is:

$$\sigma_{Total} = \sqrt{\sigma^2 + \left(\frac{\partial \log(Y)}{\partial M}\right)^2 \sigma_M^2} \tag{5.1}$$

where σ_M is the standard deviation of the empirical magnitude relationship. For attenuation equations that do not include a quadratic term in magnitude, the partial derivative term in Eq. (5.1) is simply the coefficient of the magnitude term. For the equations of Ambraseys et al. (1996), this coefficient varies from 0.266 for PGA up to a value aslightly above 0.5 for periods close to 2 seconds, whereas the standard deviation increases from 0.25 for PGA to 0.32 for 2.0 s period. The standard deviation on the empirical relationship between M_s and $\log(M_o)$ by Free (1996) is 0.32. Applying Eq. (5.1), the effect of propagating the aleatory uncertainty in the magnitude conversion increases the sigma value for PGA from 0.25 to 0.264, and the sigma value for spectral acceleration at 2.0 s from 0.32 to 0.36. The effect is therefore not negigible, but it would clearly be complex to define this increase for each of the participating equations, especially since for several of them the resulting model for incrementing the standard deviation would be a function of magnitude, albeit that the coefficient on the quadratic term is generally small. For this reason, the standard deviations are increased with additional branches, as described above in Section 5.1, to account for this and other error propagation effects – including the distance conversion effect discussed below – at once.

5.5 Distance Conversion Effect

In Table 2.1 it was shown that the selected attenuation equations used in the logic-tree for median horizontal motions use four different definitions of source-to-site distance, namley hypocentral (R_{hyp}), Joyner-Boore (R_{jb}), rupture (R_{rup}) and distance to the closest point on the rupture plane within the seismogenic layer (R_{seis}), as illustrated in Figure 5.4. In the hazard calculations, these different definitions require conversions, although these are now defined and handled entirely by SP4 and are no longer part of the responsibility of SP2. The conversions used by SP4 are assumed to be based on those derived by Scherbaum et al. (2003). Since the derivation and application of these conversions are outside the scope of SP2, no attempt is made to carry the uncertainty in the distance adjustments to the aleatory uncertainty, although it is also assumed that the increases in the published sigma values as specified in Table 5.2 to some extent capture any effect of increasing the scatter. It is also assumed that the way in which SP4 will model the sources will use sufficient potential fault locations and orientations for each event, and in particular with respect to the relative location of the hypocentre within the fault plane, to account for a large part of the variability. Nonetheless, the largest uncertainty is likely to be for the case of larger events ($M_w > 6.5$), with fault dimensions measured in 10 km, and distances based on a point source model, which in this case is the hypocentral distance. This is taklen into account in defining the branches on the right side of Table 5.2 for the equations using this definition for the distance metric.

The Expert Groups in SP1 have defined seismic source zones that in distributions of focal depths, which will be included in the integrations performed by SP4. For all of the definitions of distance except R_{jb}, for a given depth and magnitude combination, account is taken of the depth of the seismic source below the ground surface. The Joyner-Boore definition, however, which is the horizontal distance to the surface projection of the fault rupture, does not differentiate between events at different focal depths. One possible solution would be to use those equations based on R_{jb} with the actual focal depth substituted for the constant fictitious depth that is determined as part of the regression of these relationships. The procedure adopted instead is simply to increase the standard deviation applied to these equations for small to moderate earthquakes and for short distances to account for the variability that they effectively neglect. Figures 5.5 and 5.6, respectively, illustrate why this adjustment is necessary only for smaller earthquakes and at short source-to-site distances.

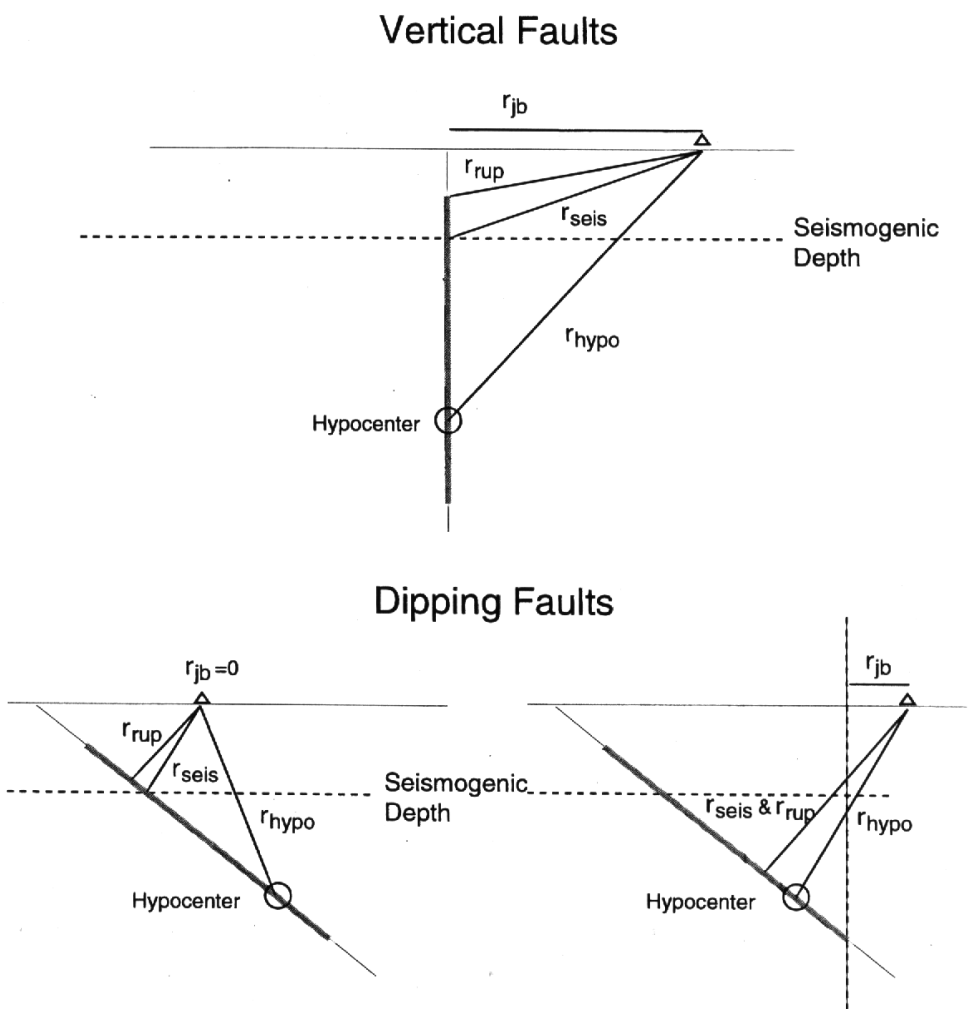

Fig. 5.4: Definitions of source-to-site distance used in attenuation studies (Abrahamson & Shedlock 1997)

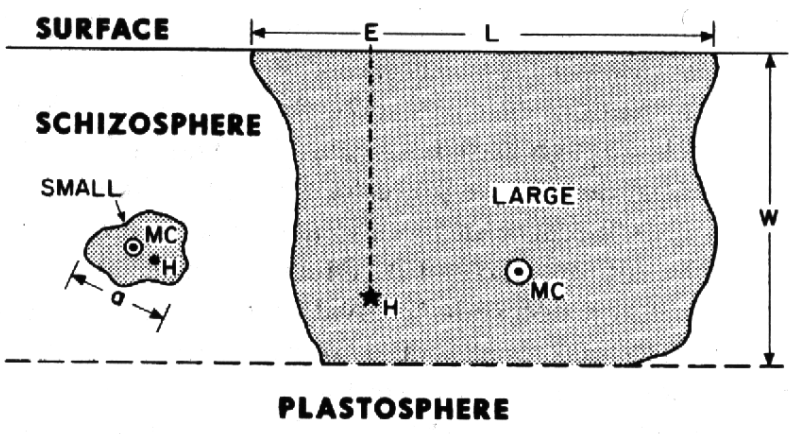

Fig. 5.5: Ruptures for small (left) and large (right) earthquakes (Scholz 1990)

This figure illustrates why the focal depth of crustal earthquakes is only of physical significance for events of sufficiently small magnitude to have rupture dimensions that are significantly less than the thickness of the seismogenic layer.

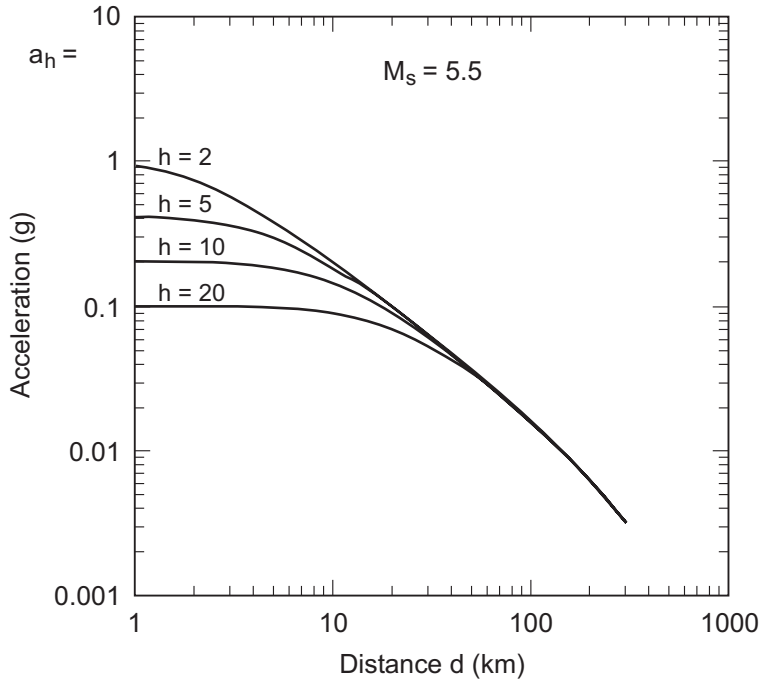

Fig. 5.6: Predicted values of larger component of PGA, from the equation of Ambraseys & Bommer (1991), for an earhquake of M_s 5.5 as a function of distance and focal depth (Bommer et al. 2002)

6 MAXIMUM GROUND MOTIONS FOR THE HORIZONTAL COMPONENT

Since the Pegasos project will be calculating the seismic hazard at annual exceedance frequencies as low as 10^{-7}, the tails of the distribution of residuals in the strong-motion prediction equations may exert a very strong influence. Truncation of the lognormal distribution can result in very different estimates of the design ground motions at return periods of the order of 1,000,000 years or more (Figure 6.1).

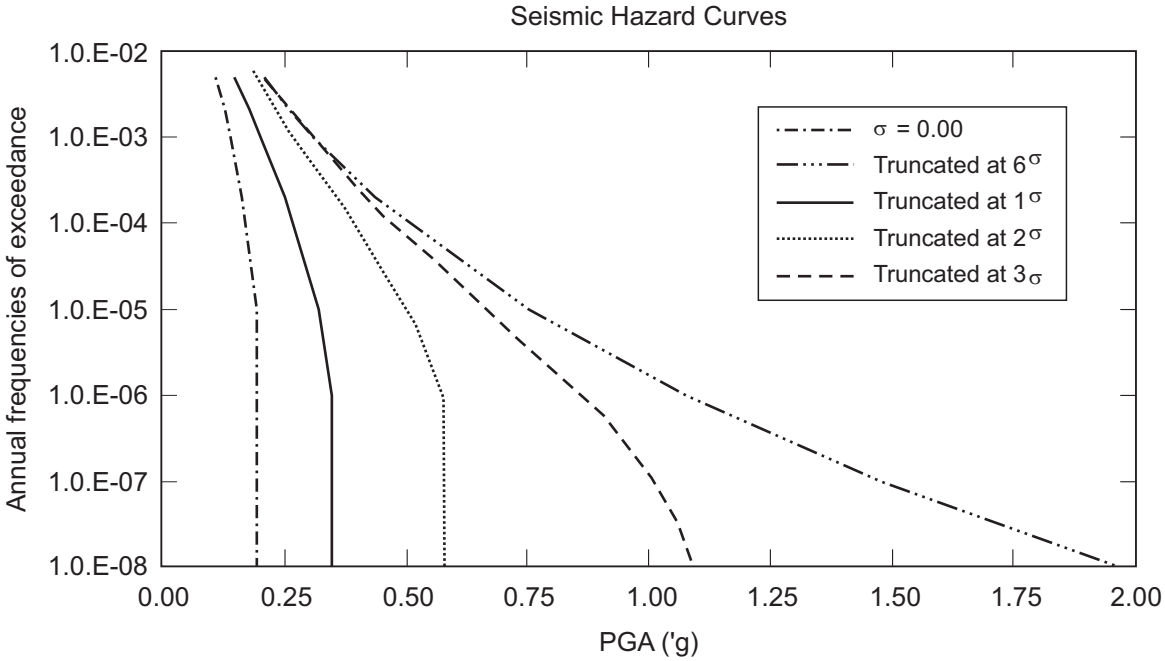

Fig. 6.1: Sensitivity of seismic hazard curves to truncation of the lognormal aleatory variability (Restrepo-Vélez & Bommer 2003)

The failure to truncate the influence of the scatter can lead to physically unrealisable levels of motion at very long return periods, as may have been the case in the Yucca Mountain PSHA (Stepp et al. 2001).

The requirements for the Pegasos project are to provide estimates of the maximum acceleration response ordinates (5 % damped), and the associated epistemic uncertainty, for all the combinations of parameters indicated in Table 6.1. Whereas for the median values of motion and the aleatory uncertainty the logic-trees have been constructed by assigning weights to bins of magnitude and distance, it has been decided to use a different approach for the upper bounds for several reasons. Prominent amongst these reasons is the fact that the M-R bins would need to be much smaller than they were for the median values and aleatory uncertainty. Rather than pay the penalty of an unwieldy logic-tree structure by using a large number of small M-R bins, the approach that is adopted is to extend this to the extreme case of M-R bins defined by single pairs of values, whence the upper bounds are defined as relationships of magnitude and distance, analogous to the attenuation equations used to estimate the median values of horizontal ground motions (Chapter 3).

Tab. 6.1: Parameter combinations for which upper bounds are required

Frequency (Hz)	Magnitudes	Distances
0.5	$5 \leq M_w \leq 7.5$	$0 \leq R_{jb} \leq 200$ km
1.0		
2.5		
5		
10		
20		
33		
50		
100 (PGA)		

The resources available to the ground motion modellers for estimating maximum ground motions is limited, since relatively few studies have addressed the issue of the largest ground motions that could feasibly be produced. It has been noted that a few studies proposing upper limits on PGA and PGV were published in the late 1960's and early 1970's, but with the 1971 San Fernando earthquake triggering more than 200 accelerographs attention became focused on performing regressions to derive attenuation relations (Bommer 2002).

The principal resources available for determining upper bounds within the Pegasos project are the following:

- Quartile plots of residuals from some attenuation equations
- Plots of largest empirical ground motions from WAF database
- Results of numerical modelling by URS (Pitarka) and by OGS (Priolo)

The numerical models are, without doubt, the most important tool available for this task since it is clear that the empirical data is very unlikely to provide anything other than lower bounds on the maximum ground motions. Since the numerical models will provide the main basis for the estimation of upper bounds they are discussed separately in the Section 6.2, and in the next Section attention is given only to the empirical data.

6.1 Evaluation of the Empirical Data

The empirical data is presented in two different ways in the Pegasos documentation: as normal probability plots and as plots of maximum values in M-R bins. The most useful normal probability plots are probably those presented in Pegasos document RDZ-TN-0214 that were derived using the equations of Berge-Thierry et al. (2000), Lussou et al. (2001) and Chang et al. (2001). These equations are derived using data from Europe, Japan and Taiwan, respectively, and their data sets contain 965, 3011 and 4754 records respectively. The results for PGA from the equation of Chang et al. (2001) is shown in Figure 6.2.

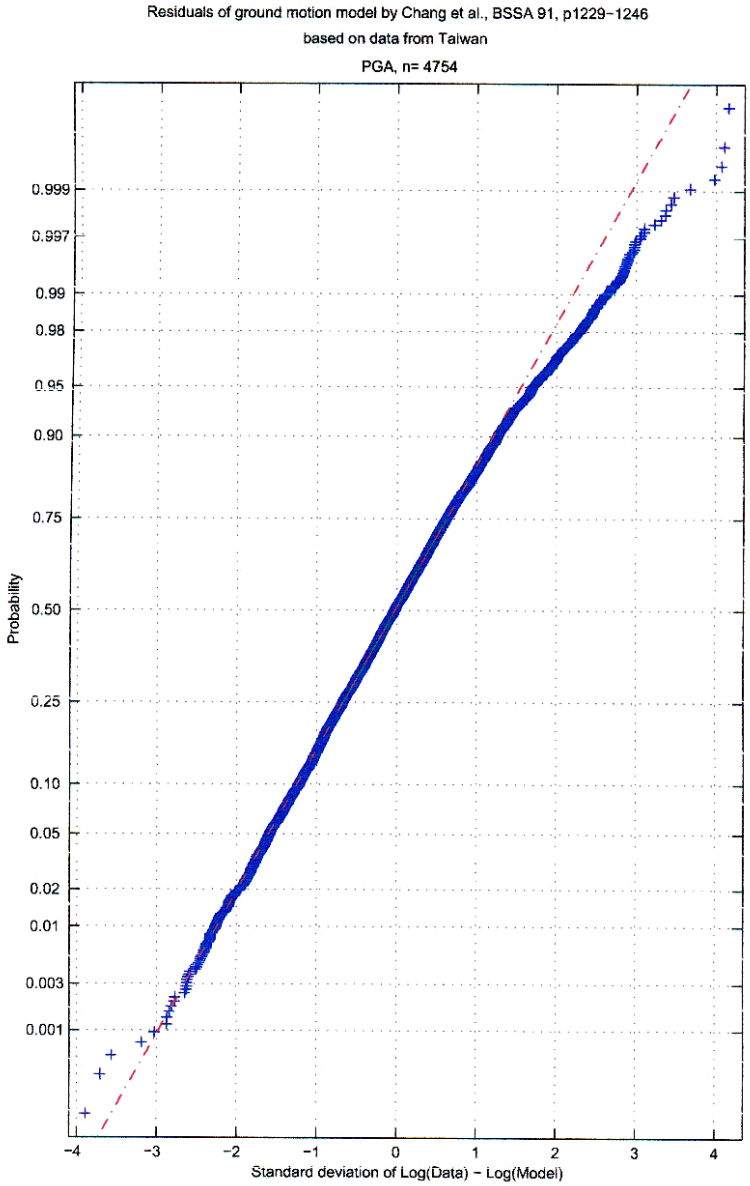

Fig. 6.2: Normal probability plot of PGA residuals from Chang et al. (2001)

The residual plots generally show that the data does conform to a lognormal distribution within limits of ± 2 or ± 3 standard deviations on either side of the mean, but tends to deviate from it beyond these limits. The normal probability plots also show that in many of the data sets there are values of spectral ordinates that are 3, 4 or even 5 standard deviations higher than the median.

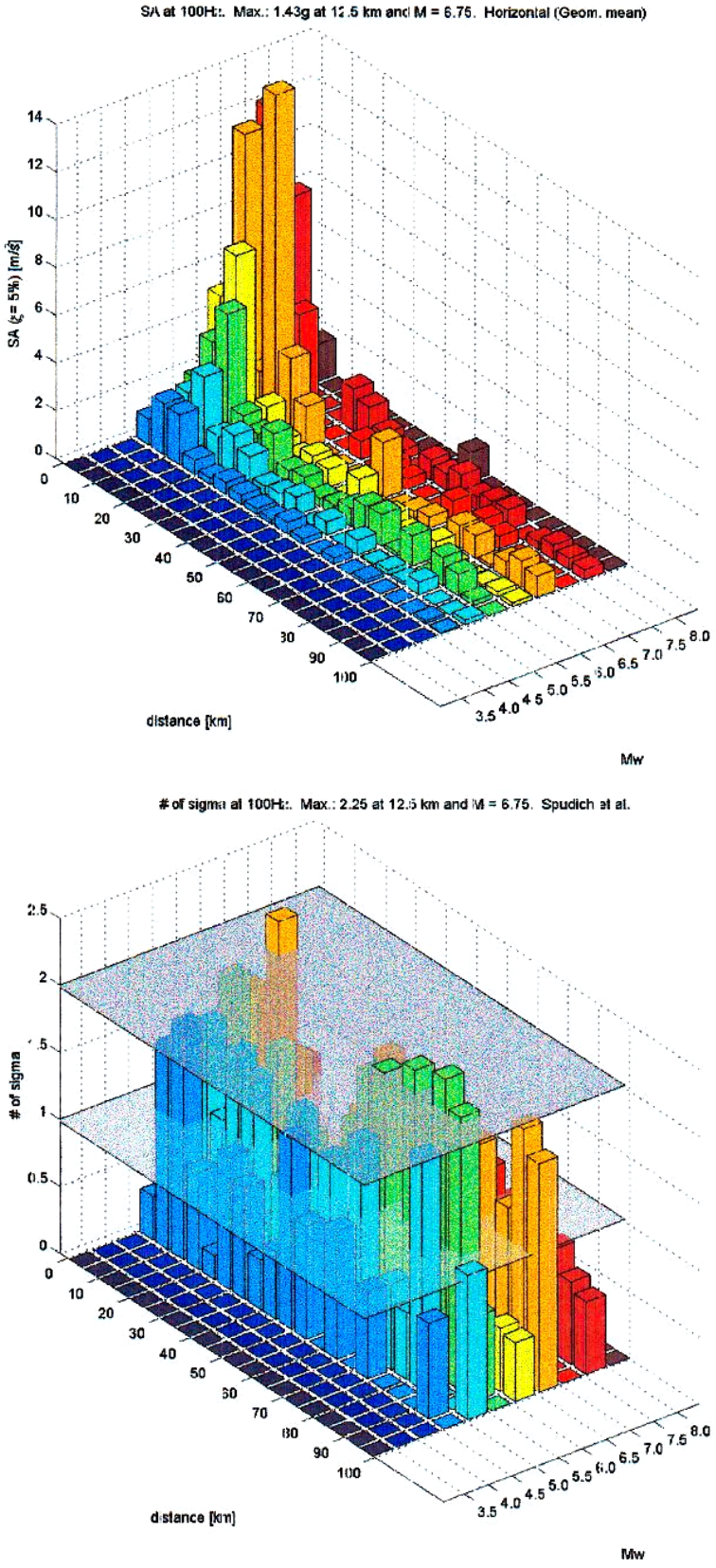

Fig. 6.3: Largest PGA values on rock (top) and number of standard deviations (bottom) above the median values from Spudich et al. (1999) for the M-R bin

It is possible that these extreme values correspond to weak motions generated by small earthquakes or at large distances, and in order to help us in determining which M-R bins are contributing to the largest positive residuals, in addition to document RDZ-TN-0298, Pegasos document TP2-TN-02309 provides plots such as those shown in Figure 6.3, which show the largest amplitudes and the corresponding numbers of standard deviations above the mean for these ground motions in individual M-R bins, calculated using the attenuation equations of Abrahamson & Silva (1997) for spectral ordinates and those of Spudich et al. (1999) for PGA.

The philosophy of the approach being adopted in this model is that the upper bounds should be physical, and therefore plots of the kind shown in the upper part of Figure 6.3 are of greater interest. As explained above, the upper bounds will be defined by absolute values in M-R space rather than in terms of a number of standard deviations above the median, since the latter approach would result in different absolute values for different attenuation equations, which is not consistent with the criteria of physically constrained upper bounds on the motions. Therefore, plots such as the upper plot in Figure 6.3 are useful for this exercise, and can be used to infer lower bounds on the upper bounds. Plots such as that in the lower part of Figure 6.3 and in Figure 6.2 are nonetheless useful when the upper bound estimates are compared to prediction from attenuation relationships since they provide a basis to judge if the upper bounds are too low should they fall below, for example, the median plus two standard deviation values from the equations.

6.2 Evaluation of the Numerical Simulations

Numerical simulations of ground motions have been performed by URS (Arben Pitarka) and by OGS (Enrique Priolo), using combinations of source parameters to search for the maximum feasible ground motions corresponding to a series of magnitude-distance pairs: M_w 5.5 at 5 and 25 km, and M_w 6.5 at 5, 25 and 60 km. At the request of the EG2 experts, Professor Raúl Madariaga, in his capacity as one of the leading developers of dynamic fault models, was asked to assess the input parameters employed in the URS and OGS source models in terms of the feasibility of their being physical realisable. Professor Madariaga was not provided with the output from the two models, in order not be influence his judgement, but merely to judge whether the input parameters were physically realistic. Specifically he was asked to classify the input to the numerical models used to generate upper bound motions according to the following descriptions:

- Possible
- Unlikely
- High unlikely
- Extremely unlikely
- Impossible

In an informal meeting of EG2 held immediately after WS-3/SP2 to discuss joint research work arising from the Pegasos project, the Ground Motion Expert Group conducted an experiment. Each member of EG2 was asked to assign probabilities to each of the five descriptive terms listed above. The experiment was carried out blind so that each expert made a note of their assigned probabilities individually and entirely independently. The probabilities were then compiled into Table 6.2, which reveals a very large range of estimates. The experts all agreed that the distinction between "highly unlikely" and "extremely unlikely" was difficult to define, so these two categories were merged.

Tab. 6.2: SP2 experts' estimates of probabilities associated with likelihood descriptions

Description of Likelihood	Expert[1]				
	1	2	3	4	5
Possible	> 0.1	> 0.03	0.50	> 0.7	> 0.16
Unlikely	$10^{-1} – 10^{-4}$	0.016 – 0.02	0.10	0.05 – 0.02	0.16
Highly or Extremely Unlikely	$10^{-4} – 10^{-7}$	0.001 – 0.005	0.04	0.01 – 0.1	0.023
Impossible	$< 10^{-7}$	0.0	0.0	0.0	0.0

[1] random order

The disparity reflected in Table 6.2 led to a discussion regarding the meaning of the descriptions as well as the appropriate probabilities. An approximate consensus was finally reached, which is summarised in Table 6.3.

Tab. 6.3: EG2 consensus on probabilities for likelihood descriptions

Description	Probability
Possible	> 50 %
Unlikely	< 5 %
Highly or Extremely Unlikely	< 0.1 %
Impossible	0.0 %

The problems that arise from the ambiguity in these definitions is exacerbated by the fact that Raúl Madariaga actually employs different – and presumably equally subjective – descriptive terms in his report.

The evaluation by Raúl Madariaga identifies a number of shortcomings with both studies, as well as pointing out that in both cases the documentation provided by OGS and URS was insufficient to enable a complete and thorough evaluation. These limitations notwithstanding, Madariaga was able to provide some useful guidance on the interpretation of the models. Although not explicitly stated in such terms, he effectively classified the URS model in which super-shear rupture velocity occurs over the entire rupture plane as "impossible". The OGS report arrived at a similar conclusion of its own and discarded the super-shear rupture model as non-physical.

The URS "extreme" and "Max 1" models both include super-shear rupture. The "extreme" model is discarded because in addition to this feature it has combinations of rupture area and rise time that are considered unrealisable, but the "Max 1" model is retained for the time being.

Madariaga classified both models as "very likely" for low frequencies and sub-shear rupture velocities. For higher frequencies, his evaluation of the two models is different. The high frequency motions produced by the OGS model are classified as "not likely" as a result of the use of a zero rise time; I am assuming that "not likely" is equivalent to "unlikely", so from Table 6.3 this would have a less than 5 % probability of being realisable, which means that it is feasible. Madariaga classifies the high-frequency output from the URS models sub-shear rupture velocity models as "likely" but at the same time highlights that there is an unusual resonance in the records at 2 Hz, apparently arising from truncation of the source time functions at 2 Hz.

A joint report prepared by Arben Pitarka and Enrique Priolo on 7 November 2002, and embedded within Pegasos document EXT-TN-0.277, compares the input and the results from the two studies. One of the points noted is the difference between the two studies in terms of the motions at short periods, which is attributed to the fact that the URS model used a stochastic scheme whereas the OGS model was purely deterministic. The numerical simulations did cover almost exactly the same scenarios, as requested by Pegasos, although the common upper magnitude was M_w 7.0 rather than 6.5. The depths to the fault rupture were 3 km in the URS model and 1.5 km in the OGS model.

Another point worth noting is the definition of the horizontal component. Both the empirical data and the URS study present output in terms of the geometric mean of the two horizontal components, which is now the Pegasos standard definition. The OGS study, however, produced results that corresponded to the vector resolution of the two horizontal components, which was adjusted by OGS to be equivalent to the larger horizontal component that was previously the Pegasos standard.

6.3 Logic-Tree Structure

The starting point of the approach is that the upper bounds are to be inferred from the following four sets of information:

- The empirical data plots of maximum ground motions (such as Figure 6.3)
- The numerical simulations from the OGS model
- The numerical simulations from the URS "Max 1" model
- The numerical simulations from the URS "Max 2" model

The confidence that can be assigned in each of these is clearly different and the confidence will vary from one frequency to another. It is also important to point out that the information is not complete in terms of the range of combinations indicated in Table 6.1. It was not expected that the information on upper bounds should be available for the complete magnitude and distance range, and it is therefore inevitable that there will be a degree of interpolation and extrapolation. However, there are other limitations in terms of coverage that are worth noting.

The information on the largest ground motions in the WAF database covers the range of magnitudes from 4.5 to 8, and distances from 0 to 100 km. The numerical modelling studies, however, only cover specific M-R combinations, as was requested by Pegasos, although there was confusion regarding whether the upper magnitude should have been 6.5 or 7.0. The M-R combinations covered by the two numerical models are summarised in Table 6.4: black dots indicate that the scenario is covered, open circles that it is not.

As shown in Table 6.1, estimates of upper bounds are needed at 9 response frequencies for both the vertical and horizontal components. In fact, only eight frequencies are required if it is assumed that the responses at 50 Hz and 100 Hz are assumed to be equal, and this can further be reduced to 7 if the same assumption is extended to 33 Hz. Using the same format as Table 6.4, Table 6.5 shows the coverage from the three different data sources in terms of frequencies, for the horizontal and vertical components.

The first observation that can be made from Table 6.5 is that there is actually no information available at either 33 Hz or at 50 Hz, therefore the assumption is made that the acceleration response at these two frequencies is equivalent to that at 100 Hz and a single set of upper bounds will be provided for these three response frequencies. Therefore, only 14 sets of branches for upper bounds will be given, for horizontal and vertical motions at 7 different response frequencies.

Tab. 6.4: Scenarios covered by the numerical models

Magnitude	Distance					
	5 km		25 km		60 km	
	OGS	URS	OGS	URS	OGS	URS
5.5	●	●[1]	●	●[1]	○	●[1]
6.5	●	○	●	○	●	○
7.0	●	●	●	●	●	●

[1] Only strike-slip rupture case

Tab. 6.5: Response frequencies for which different upper bound estimates exist

Frequency (Hz)	Horizontal		
	Empirical	OGS	URS
0.5	●	●	●
1.0	●	●	●
2.5	●	●	○[1]
5	●	●	●
10	●	●	●
20	●	●	○
33	○	○	○
50	○	○	○
100 (PGA)	●	●	●

[1] Responses provided at 2.0 Hz but not 2.5 Hz.

A few notes are also in order regarding the actual values acceleration values from the three studies. For the empirical data and the OGS studies, acceleration values are tabulated and have been read directly. For the empirical data, since the magnitudes of interest lie on the boundary between bins, for each distance, the larger acceleration from the magnitude bins either side of the control value has been taken. It was noted in the previous section that the OGS report presents acceleration values that correspond to the larger horizontal component, whereas the standard for the project is now the geometric mean. For this application, the central ($w = 0.5$) values for Conversion 1 in Table 2.23 were used to adjust the OGS amplitudes to be equivalent to geometric mean values.

For the URS simulations, the results were presented in two forms. The form of presentation available at the time of preparing the elicitation report for WS-4/SP2 was a series of plots. The maximum amplitudes could be read off from these plots but due to the very small scale of the vertical logarithmic axes, it is inevitable that there will be an appreciable uncertainty in the values obtained in this way. After WS-4/SP2 the numerical values of the URS simulations were provided in digital format, from which it was possible to obtain the exact values. The plots that had been produced to investigate the implied upper bounds were then reproduced using these new values, although it transpired that the plots were visually very similar, no doubt in part due to the use of logarithmic scales.

With the values of maximum spectra acceleration determined from each of the resources listed, plots were prepared for each combination of magnitude and response frequency, for both horizontal and vertical components. On the same plots, the predicted values of spectral acceleration from the equations of Ambraseys et al. (1996) for the horizontal motion are plotted. The median attenuation curve and the 84, 97.7 and 99.9 percentile curves are also plotted, adding respectively one, two and three standard deviations. Since these equations are based on the larger horizontal component, the curves are adjusted by the same factors applied to the acceleration values from the OGS report in order to approximate the geometric mean component. The resulting curves are plotted in Figures 6.4 to 6.24.

In each of the preceding plots, the horizontal values are shown for a given combination of magnitude and response frequency. Straight lines are fitted through the numerical modelling values whenever three points are available, but these are only intended to assist in the interpretation in reading these rather cluttered plots.

Inspection of horizontal motion plots in Figures 6.4 to 6.24 shows that the data for constraining the upper bounds is limited in many senses. It was initially assumed that the empirical values would provide lower bound estimates of the maximum ground motion amplitudes but in many cases these are comparable to estimates from the URS models and frequently much larger than those from the OGS model. Indeed, the OGS model has predicted many "upper bound" values that lie between the median and 84-percentile predictions from the equations of Ambraseys et al. (1996), even at lower frequencies for which they would be expected to be more reliable. This undermines considerably any confidence in these results and hence they do not exert any real influence on the decisions to be taken in terms of defining the upper bounds. This is regrettable because it reduces the available numerical models to one that is excellently documented but judged unreliable and another that is very poorly documented and assumed to be reliable.

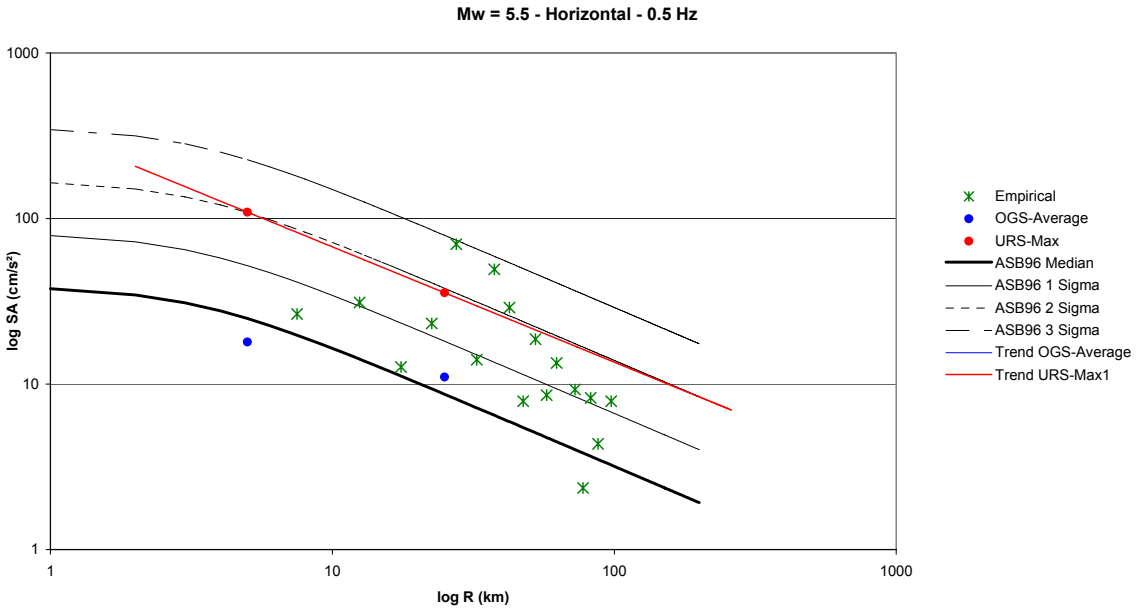

Fig. 6.4: Upper bound estimates of horizontal spectral acceleration at 0.5 Hz frequency for an earthquake of M_w 5.5, compared to predictions of 50, 84, 97.7 and 99.9 percentile values from the equations of Ambraseys et al. (1996)

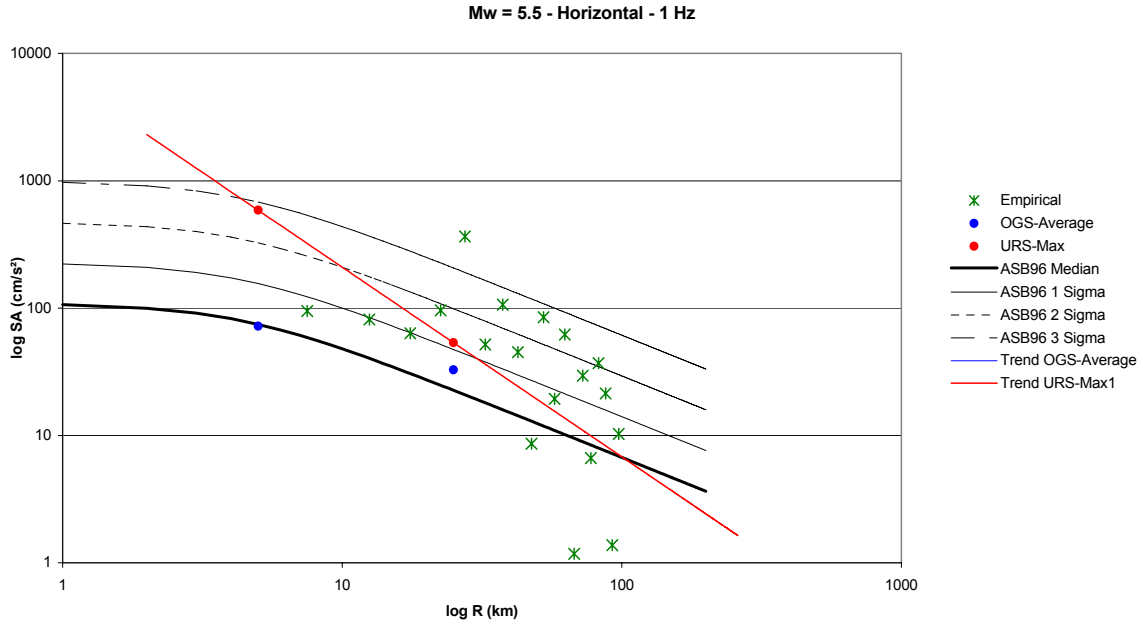

Fig. 6.5: Upper bound estimates of horizontal spectral acceleration at 1.0 Hz frequency for an earthquake of M_w 5.5, compared to predictions of 50, 84, 97.7 and 99.9 percentile values from the equations of Ambraseys et al. (1996)

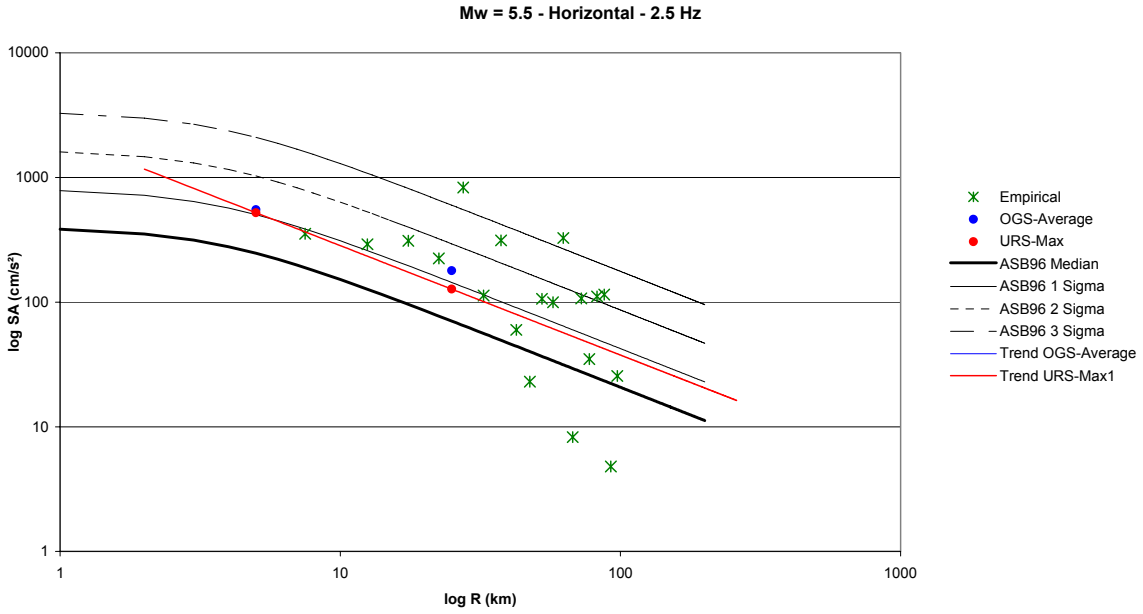

Fig. 6.6: Upper bound estimates of horizontal spectral acceleration at 2.5 Hz frequency for an earthquake of M_w 5.5, compared to predictions of 50, 84, 97.7 and 99.9 percentile values from the equations of Ambraseys et al. (1996)

Note that the URS values on this plot are actually for 2 Hz.

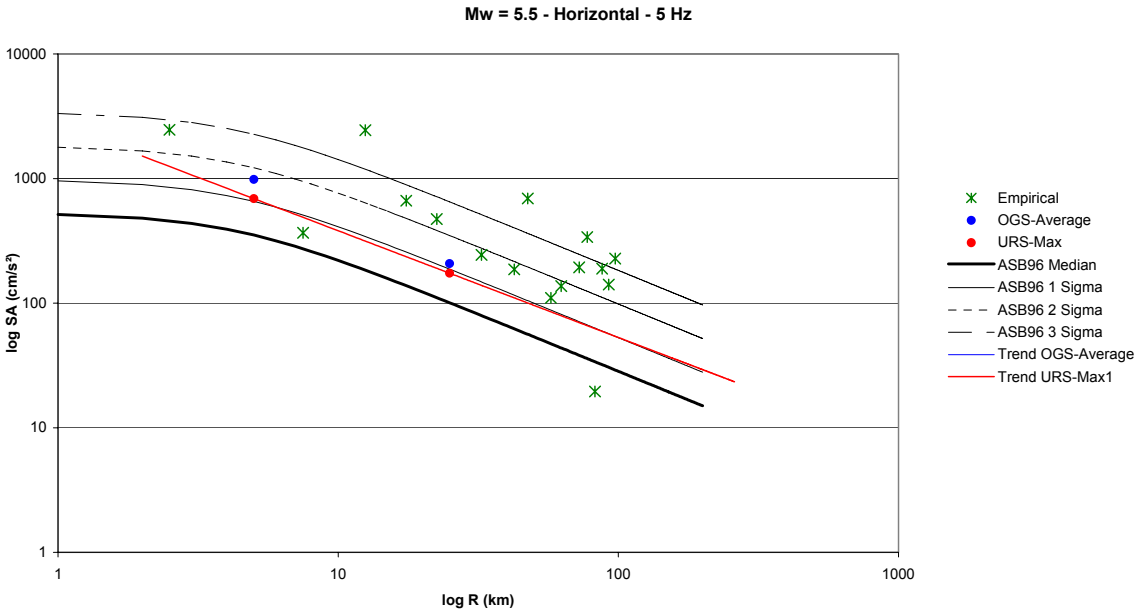

Fig. 6.7: Upper bound estimates of horizontal spectral acceleration at 5.0 Hz frequency for an earthquake of M_w 5.5, compared to predictions of 50, 84, 97.7 and 99.9 percentile values from the equations of Ambraseys et al. (1996)

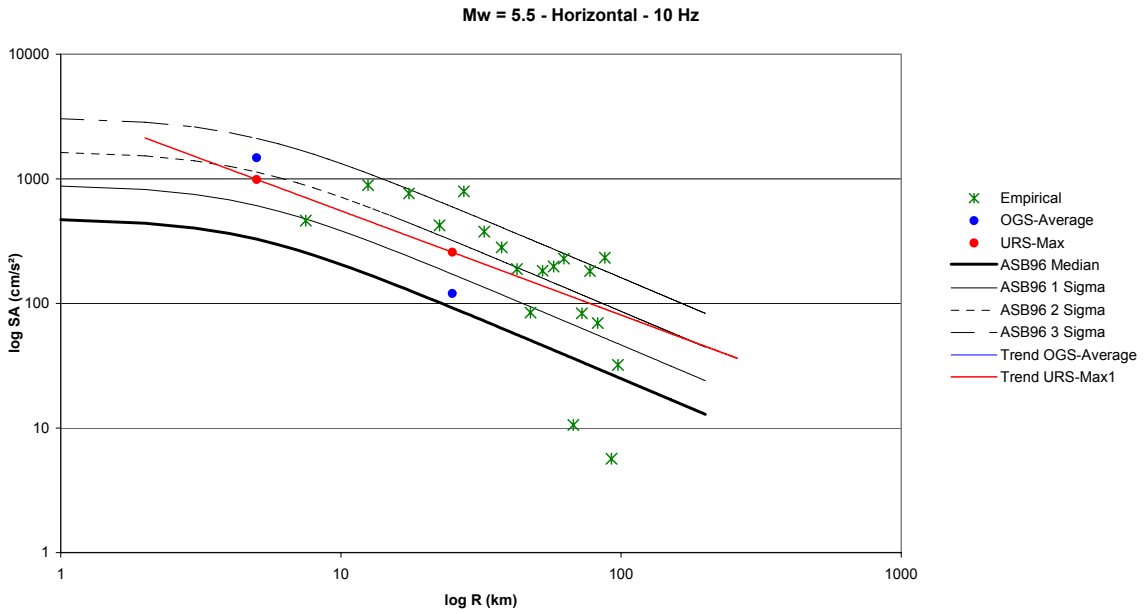

Fig. 6.8: Upper bound estimates of horizontal spectral acceleration at 10.0 Hz frequency for an earthquake of M_w 5.5, compared to predictions of 50, 84, 97.7 and 99.9 percentile values from the equations of Ambraseys et al. (1996)

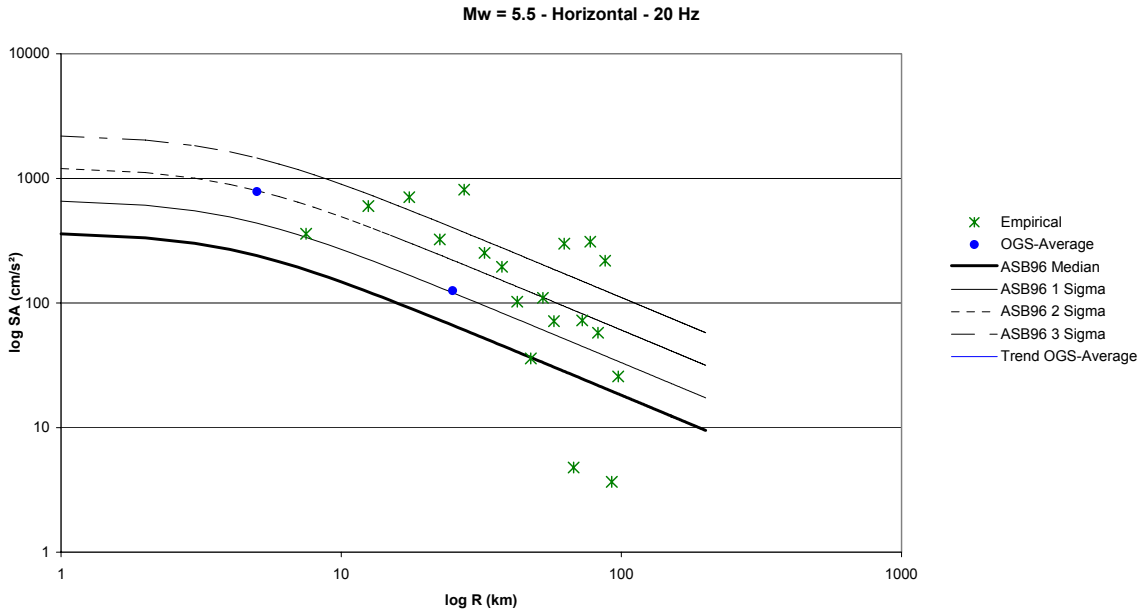

Fig. 6.9: Upper bound estimates of horizontal spectral acceleration at 20.0 Hz frequency for an earthquake of M_w 5.5, compared to predictions of 50, 84, 97.7 and 99.9 percentile values from the equations of Ambraseys et al. (1996)

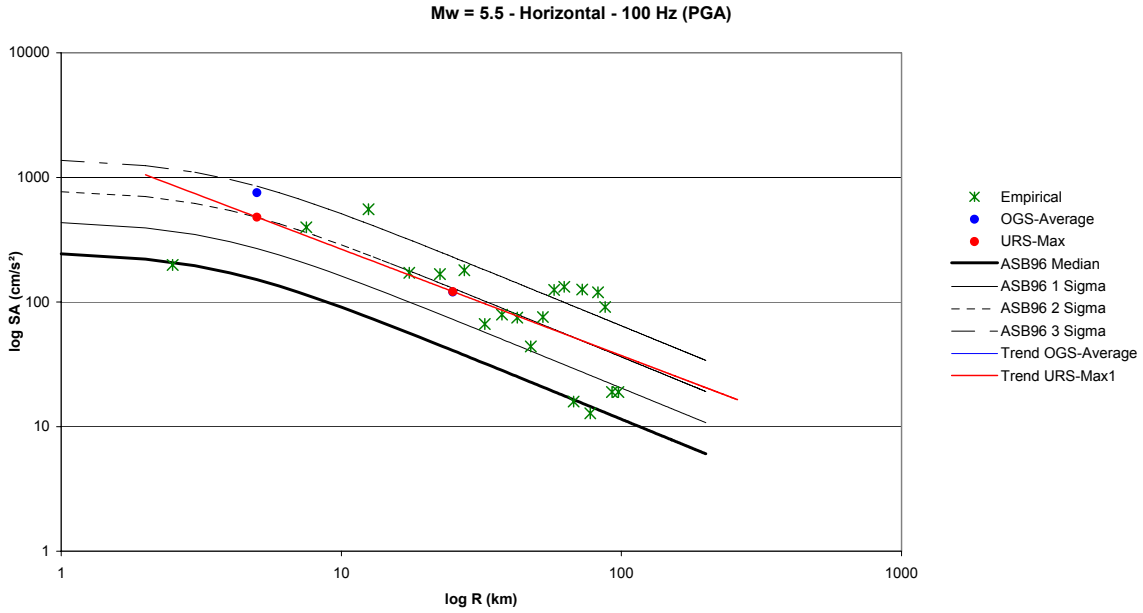

Fig. 6.10: Upper bound estimates of horizontal spectral acceleration at 100.0 Hz frequency (PGA) for an earthquake of M_w 5.5, compared to predictions of 50, 84, 97.7 and 99.9 percentile values from the equations of Ambraseys et al. (1996)

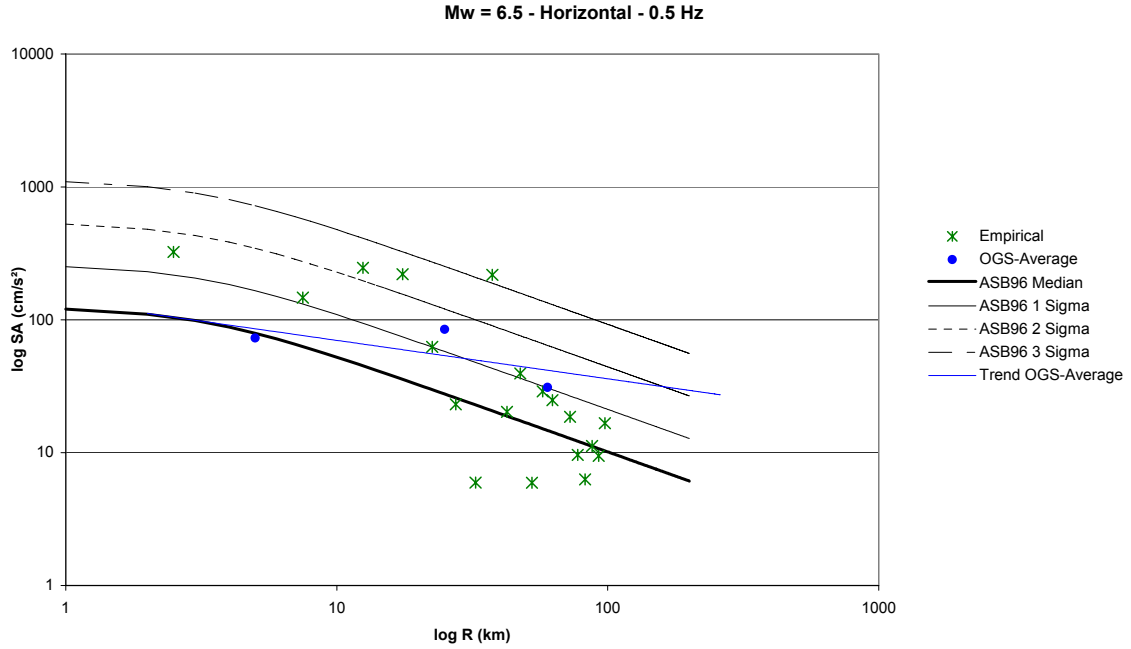

Fig. 6.11: Upper bound estimates of horizontal spectral acceleration at 0.5 Hz frequency for an earthquake of M_w 6.5, compared to predictions of 50, 84, 97.7 and 99.9 percentile values from the equations of Ambraseys et al. (1996)

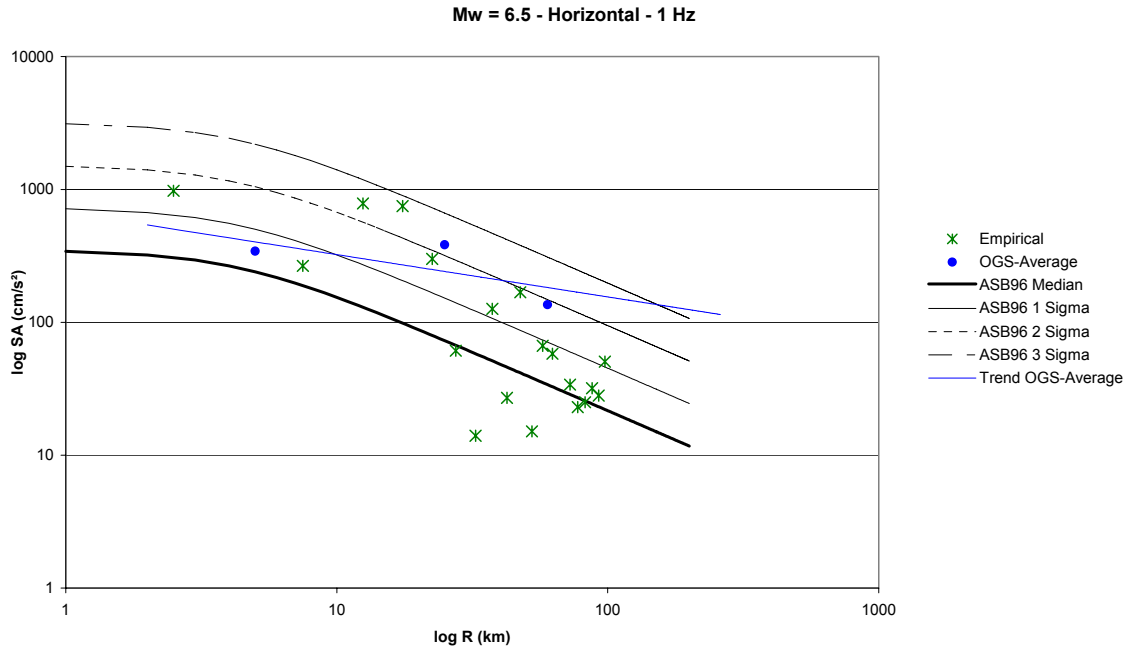

Fig. 6.12: Upper bound estimates of horizontal spectral acceleration at 1.0 Hz frequency for an earthquake of M_w 6.5, compared to predictions of 50, 84, 97.7 and 99.9 percentile values from the equations of Ambraseys et al. (1996)

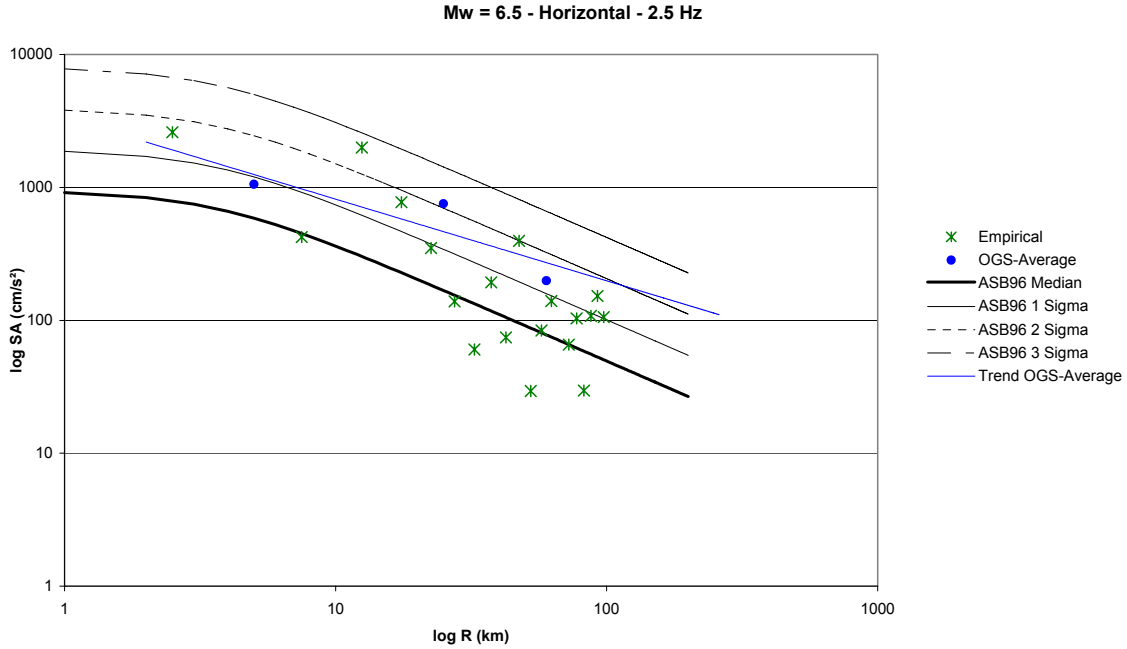

Fig. 6.13: Upper bound estimates of horizontal spectral acceleration at 2.5 Hz frequency for an earthquake of M_w 6.5, compared to predictions of 50, 84, 97.7 and 99.9 percentile values from the equations of Ambraseys et al. (1996)

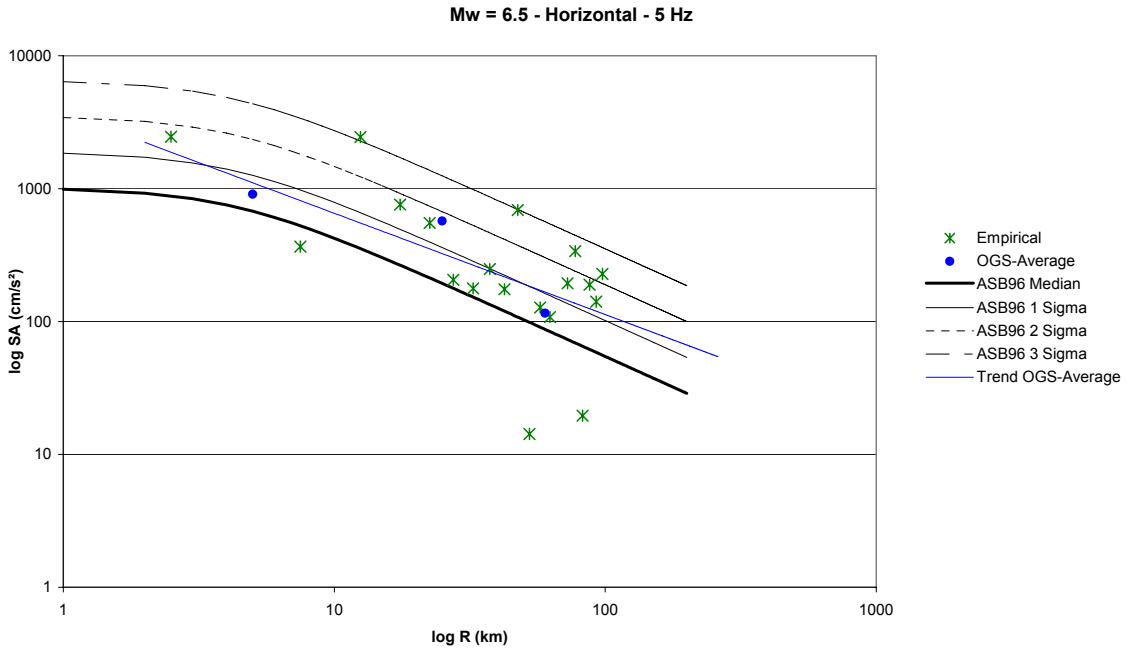

Fig. 6.14: Upper bound estimates of horizontal spectral acceleration at 5.0 Hz frequency for an earthquake of M_w 6.5, compared to predictions of 50, 84, 97.7 and 99.9 percentile values from the equations of Ambraseys et al. (1996)

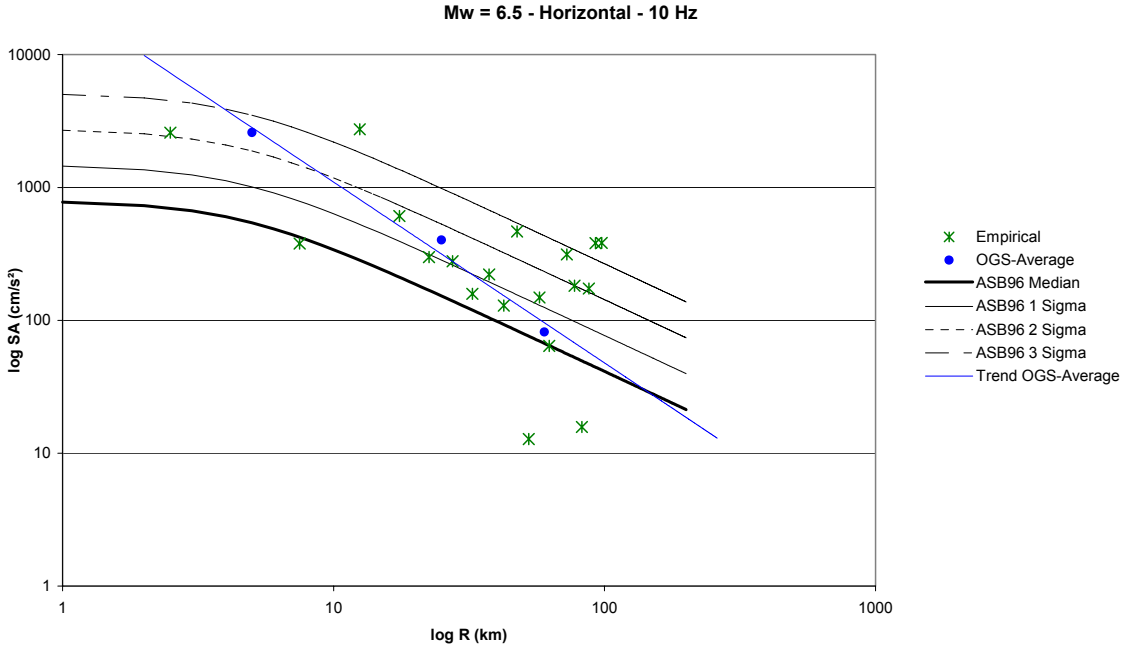

Fig. 6.15: Upper bound estimates of horizontal spectral acceleration at 10.0 Hz frequency for an earthquake of M_w 6.5, compared to predictions of 50, 84, 97.7 and 99.9 percentile values from the equations of Ambraseys et al. (1996)

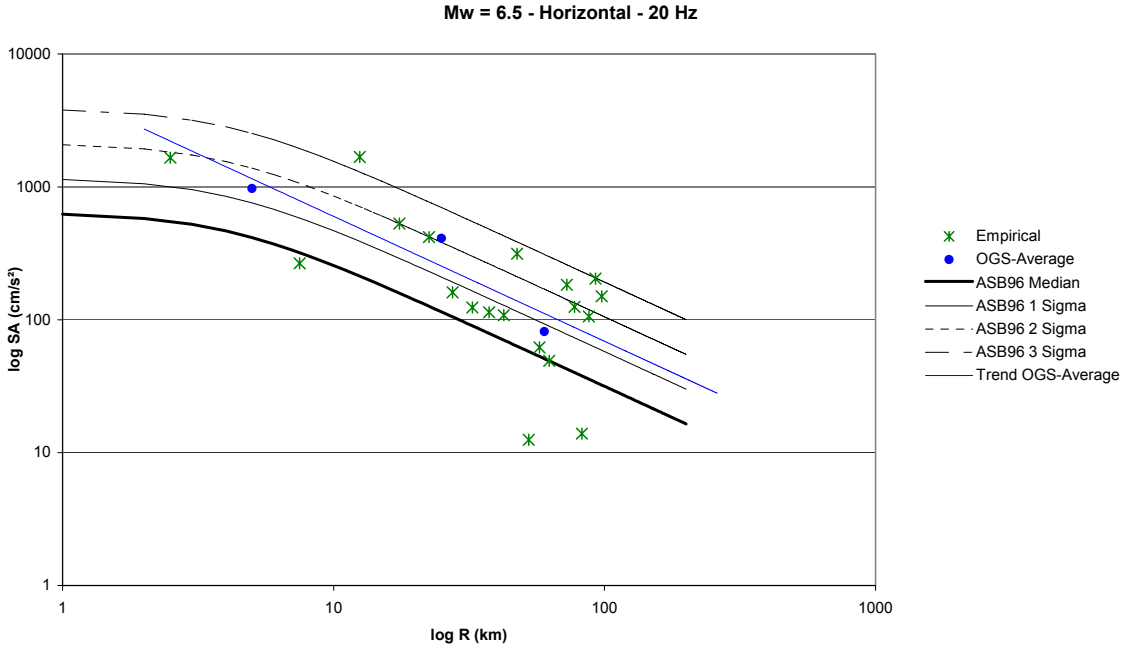

Fig. 6.16: Upper bound estimates of horizontal spectral acceleration at 20.0 Hz frequency for an earthquake of M_w 6.5, compared to predictions of 50, 84, 97.7 and 99.9 percentile values from the equations of Ambraseys et al. (1996)

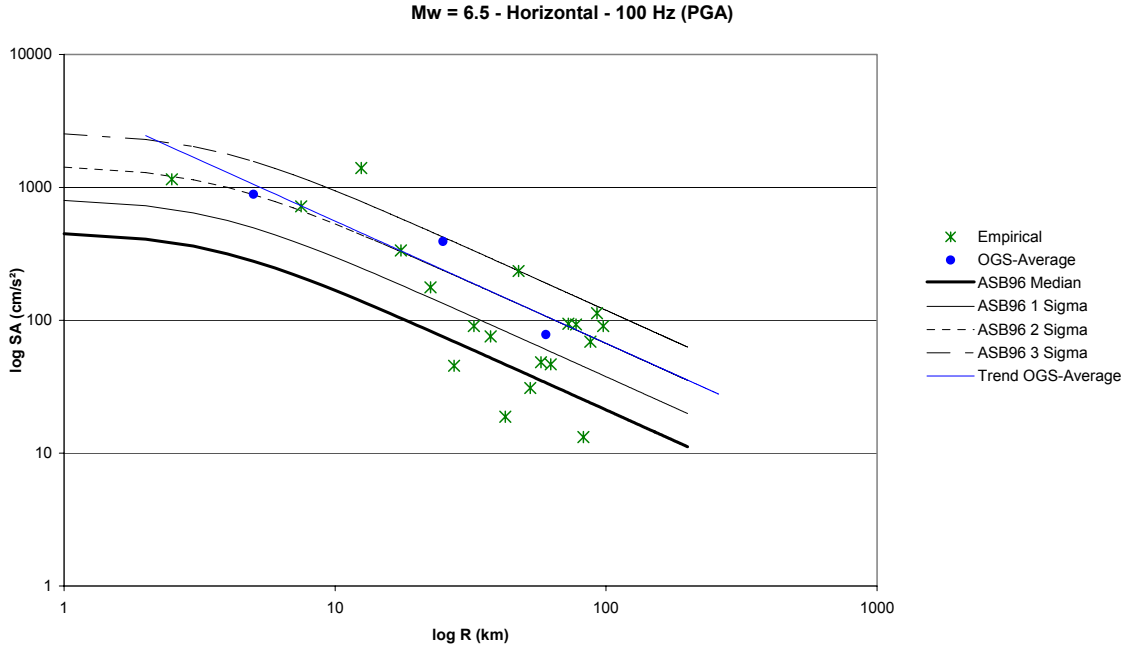

Fig. 6.17: Upper bound estimates of horizontal spectral acceleration at 100.0 Hz frequency (PGA) for an earthquake of M_w 6.5, compared to predictions of 50, 84, 97.7 and 99.9 percentile values from the equations of Ambraseys et al. (1996)

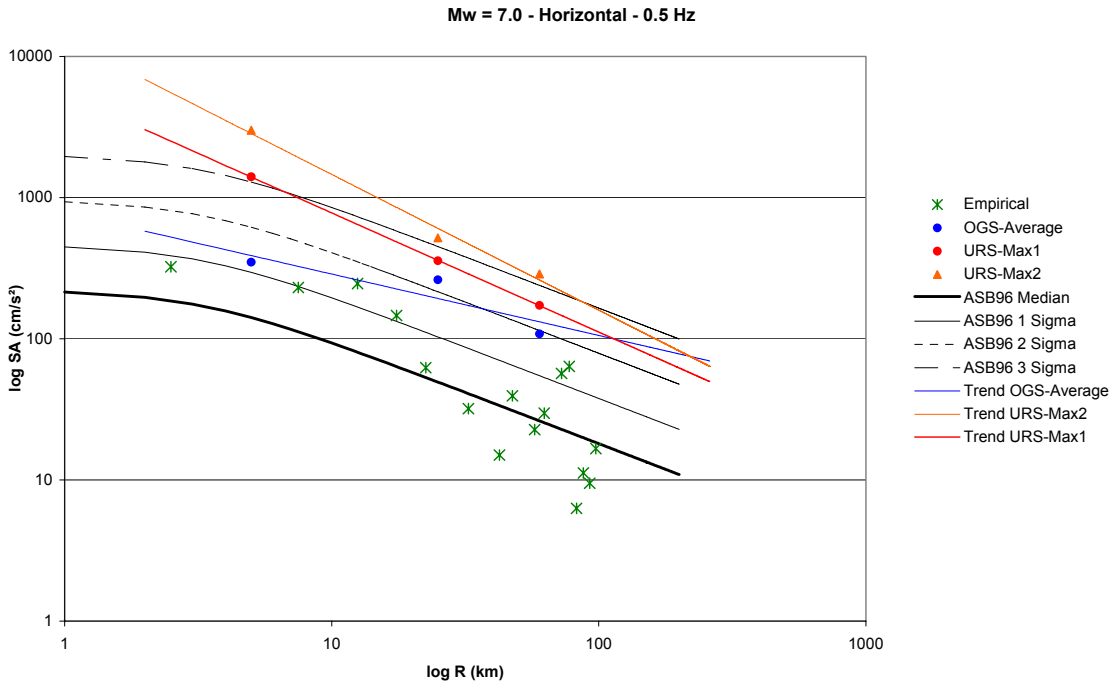

Fig. 6.18: Upper bound estimates of horizontal spectral acceleration at 0.5 Hz frequency for an earthquake of M_w 7.0, compared to predictions of 50, 84, 97.7 and 99.9 percentile values from the equations of Ambraseys et al. (1996)

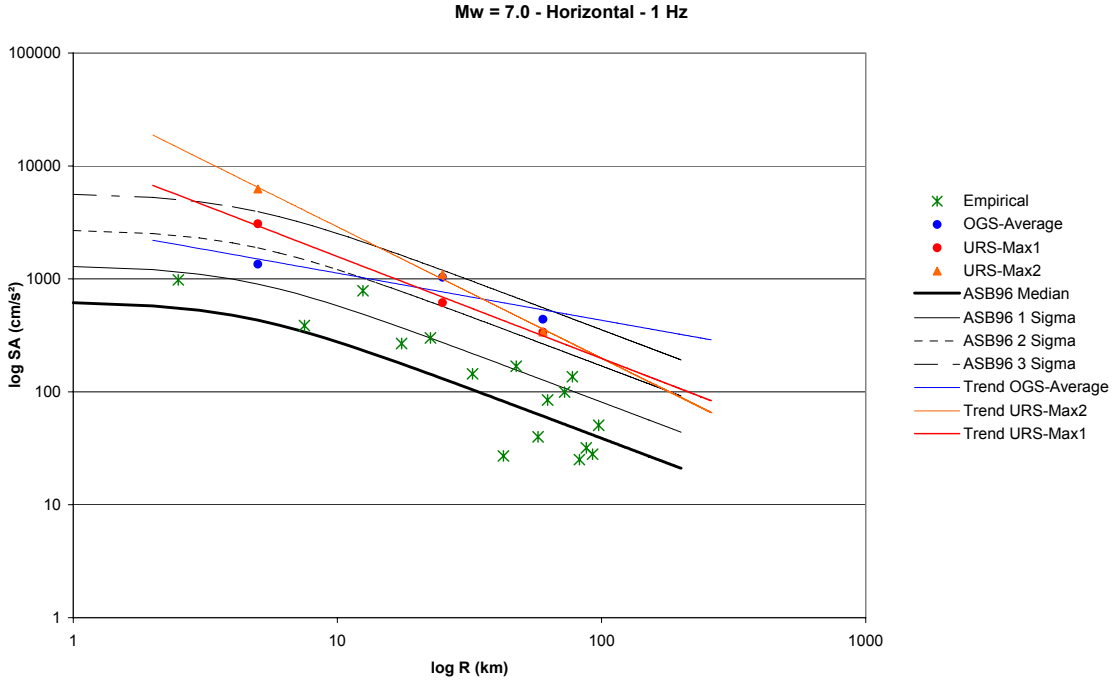

Fig. 6.19: Upper bound estimates of horizontal spectral acceleration at 1.0 Hz frequency for an earthquake of M_w 7.0, compared to predictions of 50, 84, 97.7 and 99.9 percentile values from the equations of Ambraseys et al. (1996)

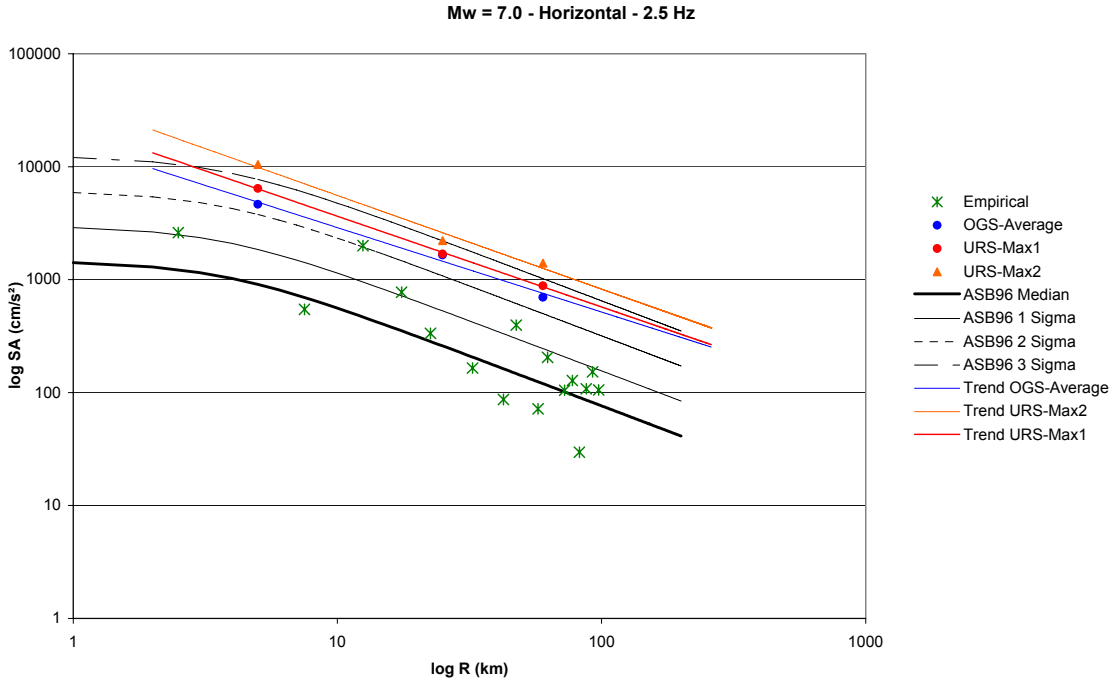

Fig. 6.20: Upper bound estimates of horizontal spectral acceleration at 2.5 Hz frequency for an earthquake of M_w 7.0, compared to predictions of 50, 84, 97.7 and 99.9 percentile values from the equations of Ambraseys et al. (1996)

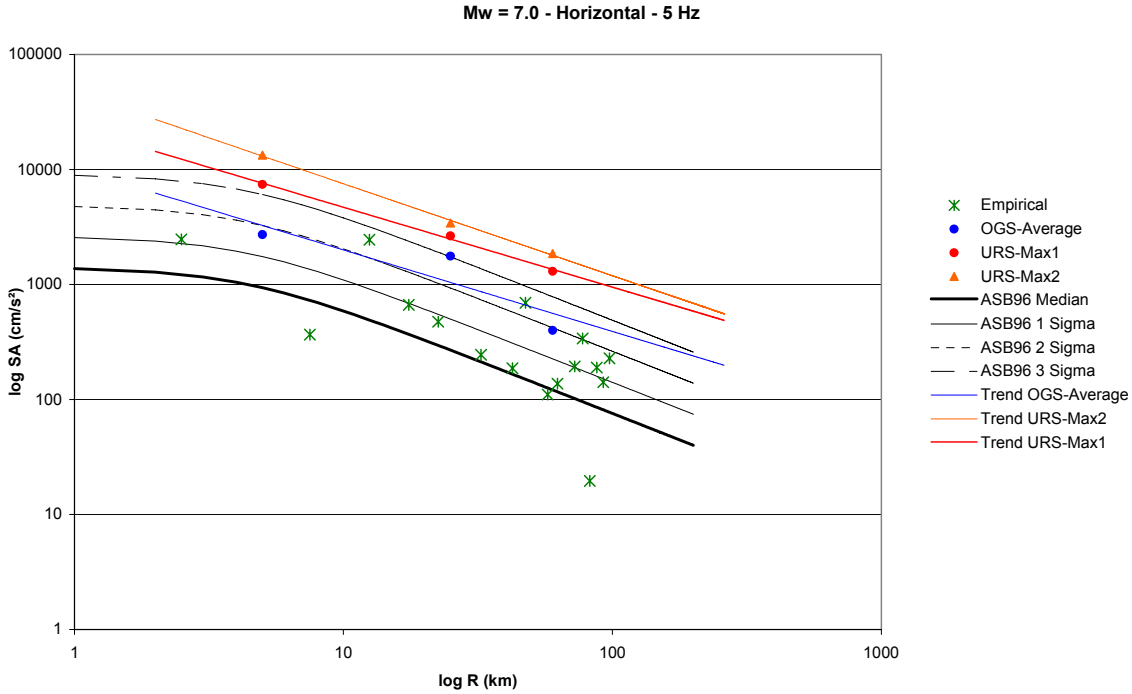

Fig. 6.21: Upper bound estimates of horizontal spectral acceleration at 5.0 Hz frequency for an earthquake of M_w 7.0, compared to predictions of 50, 84, 97.7 and 99.9 percentile values from the equations of Ambraseys et al. (1996)

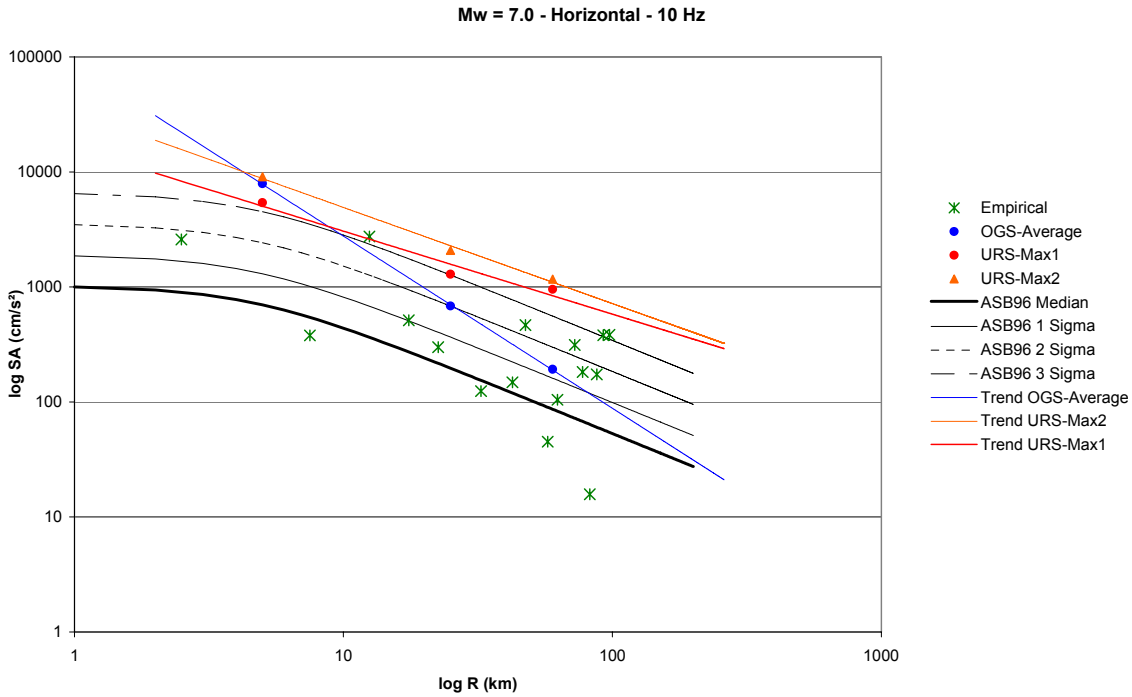

Fig. 6.22: Upper bound estimates of horizontal spectral acceleration at 10.0 Hz frequency for an earthquake of M_w 7.0, compared to predictions of 50, 84, 97.7 and 99.9 percentile values from the equations of Ambraseys et al. (1996)

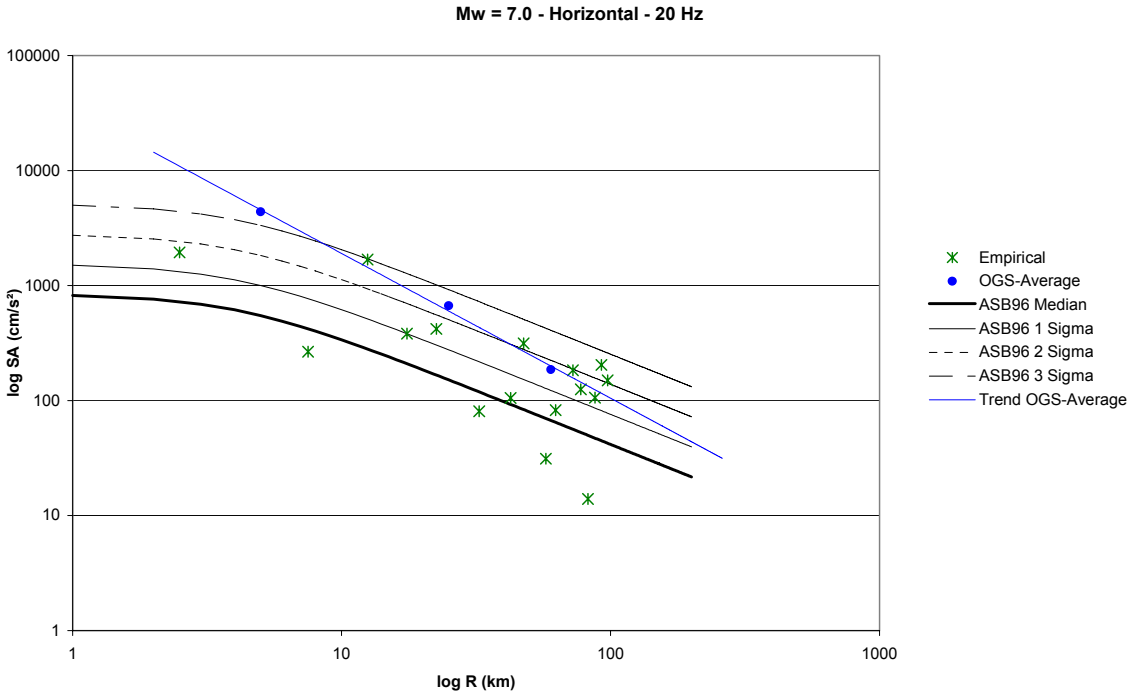

Fig. 6.23: Upper bound estimates of horizontal spectral acceleration at 20.0 Hz frequency for an earthquake of M_w 7.0, compared to predictions of 50, 84, 97.7 and 99.9 percentile values from the equations of Ambraseys et al. (1996)

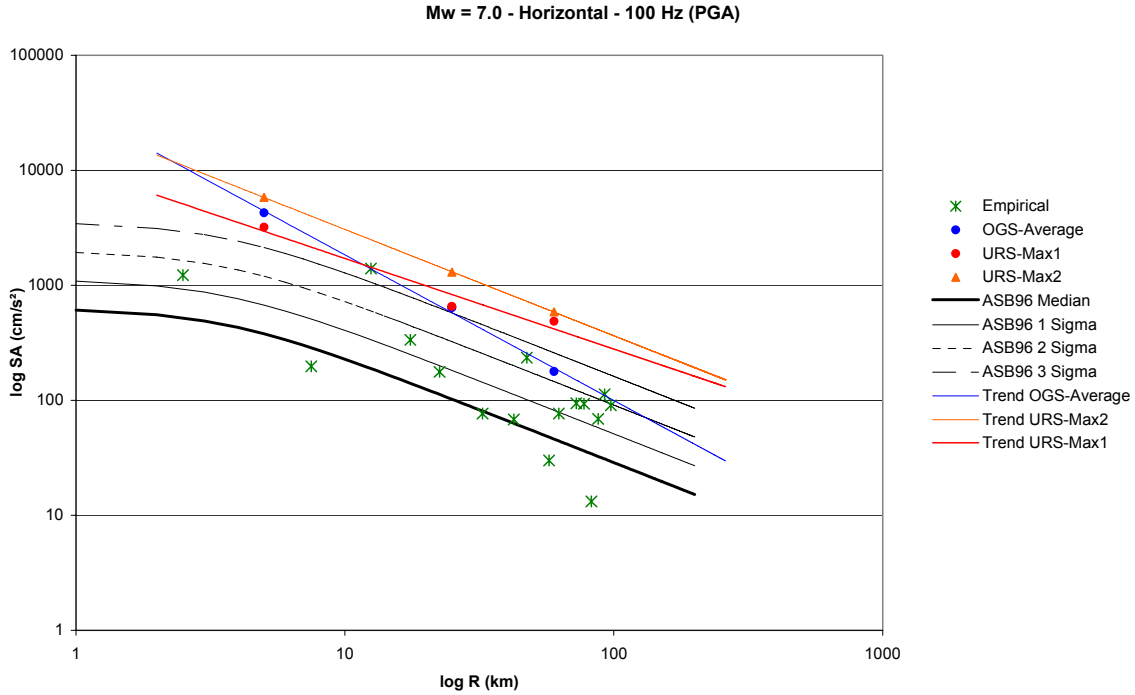

Fig. 6.24: Upper bound estimates of horizontal spectral acceleration at 100.0 Hz frequency (PGA) for an earthquake of M_w 7.0, compared to predictions of 50, 84, 97.7 and 99.9 percentile values from the equations of Ambraseys et al. (1996)

The plots that are most complete in terms of the URS models and the empirical data, since the ORS model is not being taken into account, are those for M_w 7, which are Figures 6.18 to 6.24. In these plots, the URS "Max 2" motions are almost consistently higher than the "Max 1" motions and both are generally above the empirical data points except for a very small number of isolated observations. It is important to recall that the empirical data have been drawn from magnitude bins of 1.0 unit width so these values may correspond to magnitudes above those being represented in the plots. Investigation of individual outliers on the empirical plots has not been carried out because of lack of time.

At short distances (~5 km) the "Max 1" estimates are generally comparable to the median-plus-three-sigma level and the "Max 2" amplitudes are about one standard deviation higher. The upper bounds may be expected to decay with distance more rapidly than the median values from the attenuation equations, if the maximum motions at short distances are caused by near-source effects such as rupture directivity. For shorter frequencies, the URS models predict motions lower than the median-plus-three-sigma levels bit for higher frequencies (> 1 Hz) the motions are above this level.

At short distances from the source (< 5 km) the data is extremely limited and the only constraint is provided by the very small number of empirical data; the extrapolations of the straight lines fitted through the numerical modelling results have no physical significance at all. The empirical observations in this distance range are nearly all bounded by the median-plus-two-standard-deviation curves, with a single exception that lies below the median plus three sigma curves.

There is certainly no scope for fitting meaningful curves through the URS data or the envelope of the empirical data in these plots. Therefore, the approach adopted will be to simply present equations that correspond to different percentiles from the Ambraseys et al. (1996) curves as presented in these figures. The minimum number of standard deviations will be taken as 2.5 and the maximum 4.5. The objective is to ensure that if future work provides more reliable estimates of the upper bound motions, these should lie within the range specified here. Six incremental levels are chosen, including these limiting cases, selected to be separated by uniform intervals in linear space, which means decreasing increments on the logarithmic scale. These intervals are presented for different frequencies in Table 6.6.

Tab. 6.6: Incremental levels adopted to ensure monotonic increase in ground motion

The figures in the table correspond to the number of standard deviations to add to the median for horizontal ground motions

Frequency (Hz)	0.5	1	2.5	5	10	20	33	100
Sigma	0.32	0.32	0.31	0.27	0.27	0.26	0.26	0.25
Incremental level 1	2.5000	2.5000	2.5000	2.5000	2.5000	2.5000	2.5000	2.5000
Incremental level 2	3.1985	3.1985	3.1877	3.1452	3.1452	3.1347	3.1347	3.1243
Incremental level 3	3.6573	3.6573	3.6469	3.6044	3.6044	3.5936	3.5936	3.5826
Incremental level 4	3.9996	3.9996	3.9922	3.9612	3.9612	3.9531	3.9531	3.9449
Incremental level 5	4.2727	4.2727	4.2690	4.2531	4.2531	4.2488	4.2488	4.2445
Incremental level 6	4.5000	4.5000	4.5000	4.5000	4.5000	4.5000	4.5000	4.5000

The approach being used does not mean that the originally philosophy of using absolute values is being abandoned, since the curves will correspond to absolute values that just happen to be inferred from different percentile curves of one particular attenuation relation. The adjustment is

therefore made only to the constant term in the equations by the addition of a number of standard deviations. From the observations made previously, there may be grounds to introduce differences in the coefficients of geometric attenuation but since the observation – that upper bounds on long-period motions decay more rapidly with distance than high-frequency motions – is counter intuitive, this is not done.

In the figures presented above, the attenuation curves for response frequencies of 20 Hz have been plotted using the coefficients interpolated by Pegasos (TP2-TN-0270). For completeness, rather than relying on the assumption that the response at 33 Hz is also equal to that at 50 and 100 Hz, upper bounds are presented for 33 Hz, by again using the equation with the inferred coefficients.

6.4 Weights for Maximum Ground Motions

The weights are assigned uniformly across the frequencies, to reflect the level of confidence that is judged appropriate to these estimates of the upper bounds. In particular, the highest values, corresponding to 4.5 standard deviations above the median from the European attenuation equations, are given very low weights. The weighting scheme is skewed, reflecting the view of the author that the most likely range in which the upper bounds may lie is around 3.5 to 4.0 standard deviations above the median. The weighting distribution is illustrated in Figure 6.25.

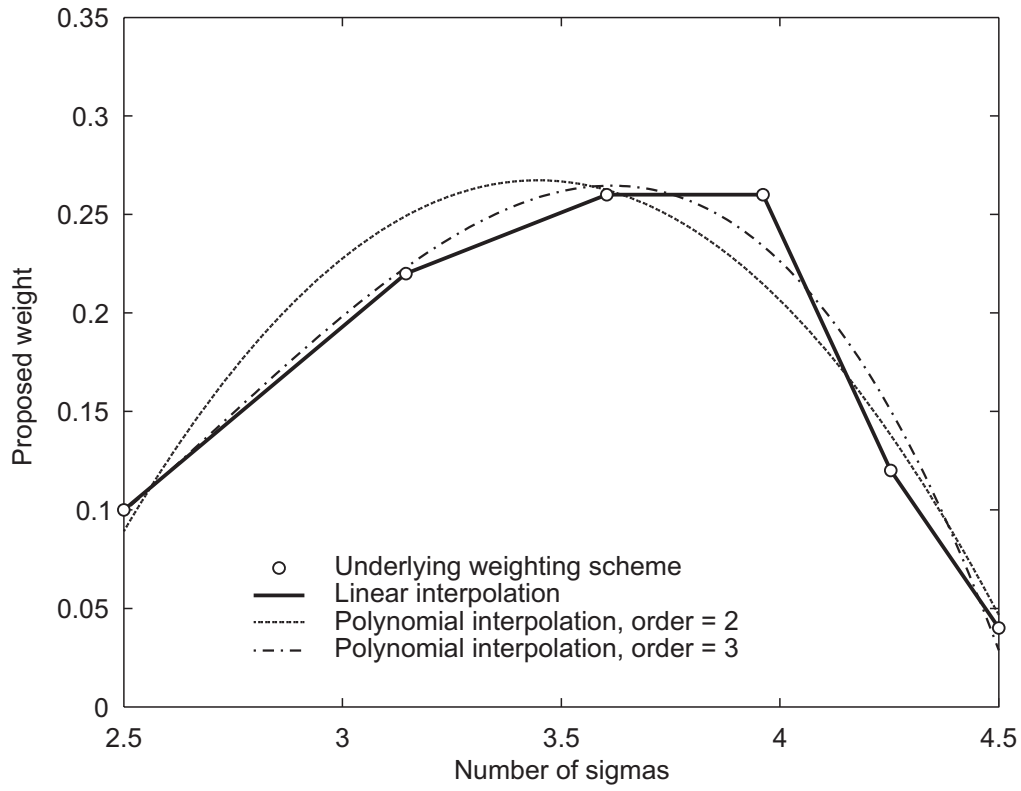

Fig. 6.25: Weighting scheme adopted, illustrated for a sigma value of 0.27 on the common logarithm; the interpolations are only shown to illustrate the shape of the distribution but these curves are not used in assigning weights

The upper bounds are defined by absolute values of spectral acceleration obtained from the following equations:

$$\log_{10}[SA(f)] = C_1 + C_2 M_w + C_3 \log(R) \quad (6.1a)$$

$$R = \sqrt{d^2 + h_o^2} \quad (6.1b)$$

where d is the Joyner-Boore distance and the values of C_1, C_2, C_3 and h_o are tabulated, with their corresponding weights, in Tables 6.7 to 6.14.

Tab. 6.7: Upper bound coefficients for Eq.(6.1) and weights: horizontal motion at 0.5 Hz

Weight	C_1	C_2	C_3	h_o
0.10	-3.076	0.503	-0.728	3.2
0.22	-2.853	0.503	-0.728	3.2
0.26	-2.706	0.503	-0.728	3.2
0.26	-2.596	0.503	-0.728	3.2
0.12	-2.509	0.503	-0.728	3.2
0.04	-2.436	0.503	-0.728	3.2

Tab. 6.8: Upper bound coefficients for Eq.(6.1) and weights: horizontal motion at 1.0 Hz

Weight	C_1	C_2	C_3	h_o
0.10	-2.456	0.508	-0.885	4.3
0.22	-2.233	0.508	-0.885	4.3
0.26	-2.086	0.508	-0.885	4.3
0.26	-1.976	0.508	-0.885	4.3
0.12	-1.889	0.508	-0.885	4.3
0.04	-1.816	0.508	-0.885	4.3

Tab. 6.9: Upper bound coefficients for Eq.(6.1) and weights: horizontal motion at 2.5 Hz

Weight	C_1	C_2	C_3	h_o
0.10	-1.246	0.377	-0.888	3.6
0.22	-1.033	0.377	-0.888	3.6
0.26	-0.890	0.377	-0.888	3.6
0.26	-0.783	0.377	-0.888	3.6
0.12	-0.698	0.377	-0.888	3.6
0.04	-0.626	0.377	-0.888	3.6

Tab. 6.10: Upper bound coefficients for Eq.(6.1) and weights: horizontal motion at 5.0 Hz

Weight	C_1	C_2	C_3	h_o
0.10	-0.611	0.284	-0.922	4.2
0.22	-0.437	0.284	-0.922	4.2
0.26	-0.313	0.284	-0.922	4.2
0.26	-0.216	0.284	-0.922	4.2
0.12	-0.137	0.284	-0.922	4.2
0.04	-0.071	0.284	-0.922	4.2

Tab. 6.11: Upper bound coefficients for Eq.(6.1) and weights: horizontal motion at 10.0 Hz

Weight	C_1	C_2	C_3	h_o
0.10	-0.236	0.219	-0.954	4.5
0.22	-0.061	0.219	-0.954	4.5
0.26	0.063	0.219	-0.954	4.5
0.26	0.159	0.219	-0.954	4.5
0.12	0.238	0.219	-0.954	4.5
0.04	0.304	0.219	-0.954	4.5

Tab. 6.12: Upper bound coefficients for Eq.(6.1) and weights: horizontal motion at 20.0 Hz

Weight	C_1	C_2	C_3	h_o
0.10	-0.518	0.239	-0.940	4.1
0.22	-0.352	0.239	-0.940	4.1
0.26	-0.232	0.239	-0.940	4.1
0.26	-0.138	0.239	-0.940	4.1
0.12	-0.061	0.239	-0.940	4.1
0.04	0.005	0.239	-0.940	4.1

Tab. 6.13: Upper bound coefficients for Eq.(6.1) and weights: horizontal motion at 33.3 Hz

Weight	C_1	C_2	h_o	C_3
0.10	-0.7424	0.2539	-0.9303	3.76
0.22	-0.5805	0.2539	-0.9303	3.76
0.26	-0.4634	0.2539	-0.9303	3.76
0.26	-0.3716	0.2539	-0.9303	3.76
0.12	-0.2962	0.2539	-0.9303	3.76
0.04	-0.2321	0.2539	-0.9303	3.76

Tab. 6.14: Upper bound coefficients for Eq.(6.1) and weights: horizontal motion at PGA

Weight	C_1	C_2	C_3	h_o
0.10	-0.921	0.266	-0.922	3.5
0.22	-0.764	0.266	-0.922	3.5
0.26	-0.650	0.266	-0.922	3.5
0.26	-0.559	0.266	-0.922	3.5
0.12	-0.484	0.266	-0.922	3.5
0.04	-0.421	0.266	-0.922	3.5

In order to obtain an impression of how these upper bounds relate to the numerical modelling, empirical data and median predictions from the attenuation equations, the six upper bound curves are plotted and compared to these other amplitudes in Figures 6.26 to 6.28. These plots only cover horizontal motions and the case of magnitude M_w 7.0 for three selected response frequencies.

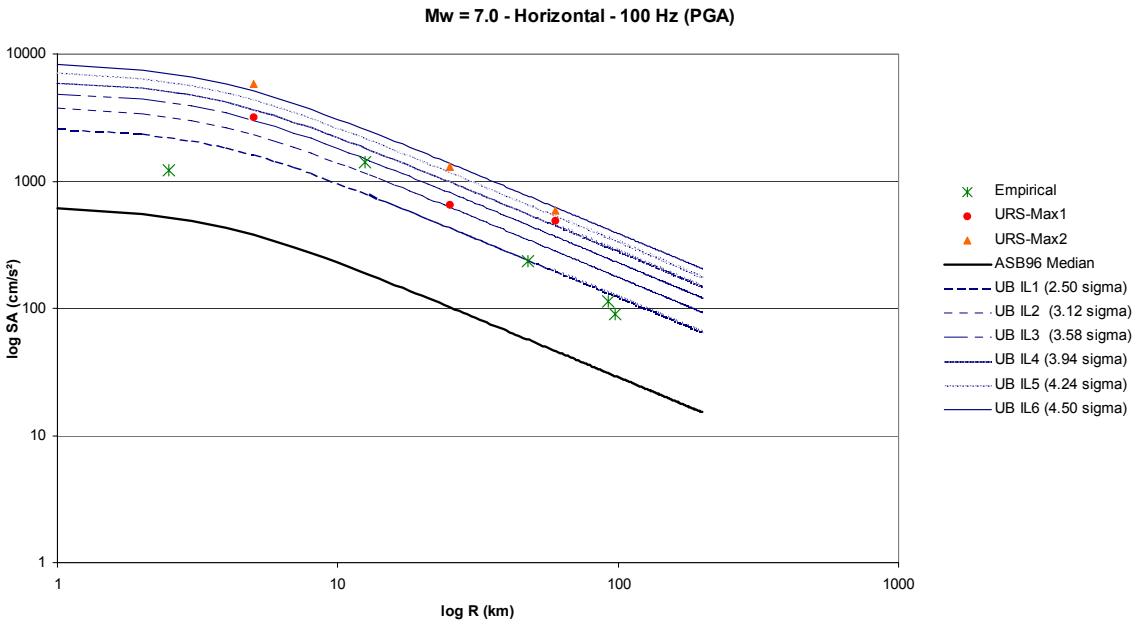

Fig. 6.26: Upper bound branch curves for horizontal PGA from an M_w 7.0 earthquake compared with median motions from Ambraseys et al. (1996), URS numerical models and empirical data from WAF database.

A final point worth noting that these upper bounds have effectively been defined for motions at rock sites with a nominal $V_{s,30}$ value of 1,000 m/s, since this was the reference site for the numerical simulations. The effects of soil layers, in either amplifying these motions further (although soil non-linearity is likely to militate against any very pronounced effect) or providing additional constraints in terms of limiting soil strength, should be accounted for by the work of SP3.

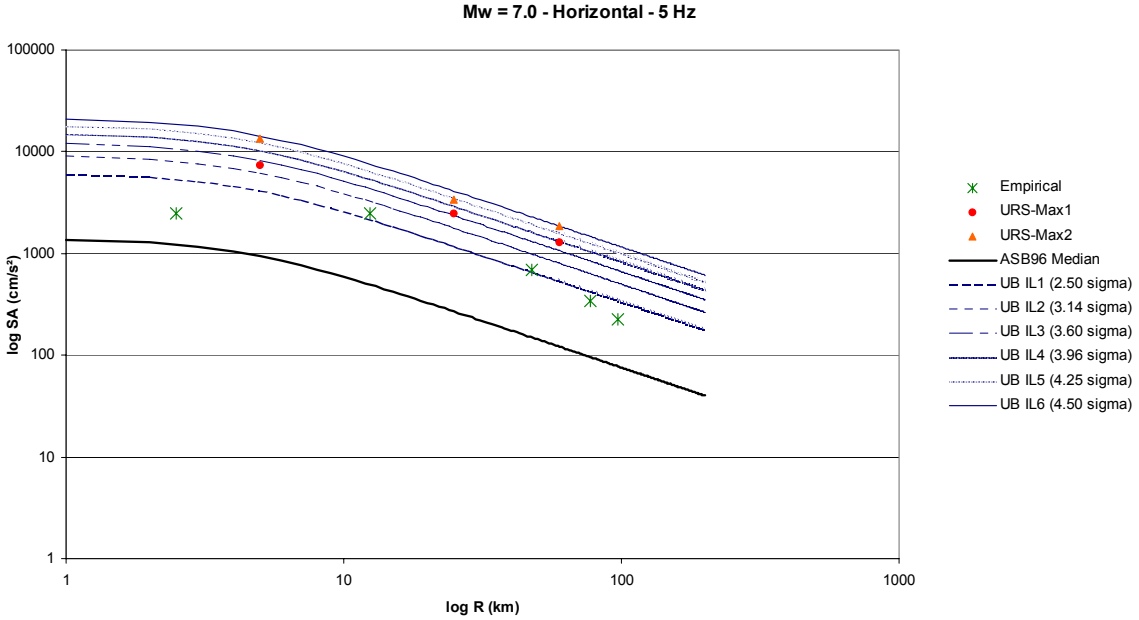

Fig. 6.27: Upper bound branch curves for horizontal spectral acceleration at 5 Hz from an M_w 7.0 earthquake compared with median motions from Ambraseys et al. (1996), URS numerical models and empirical data from WAF database

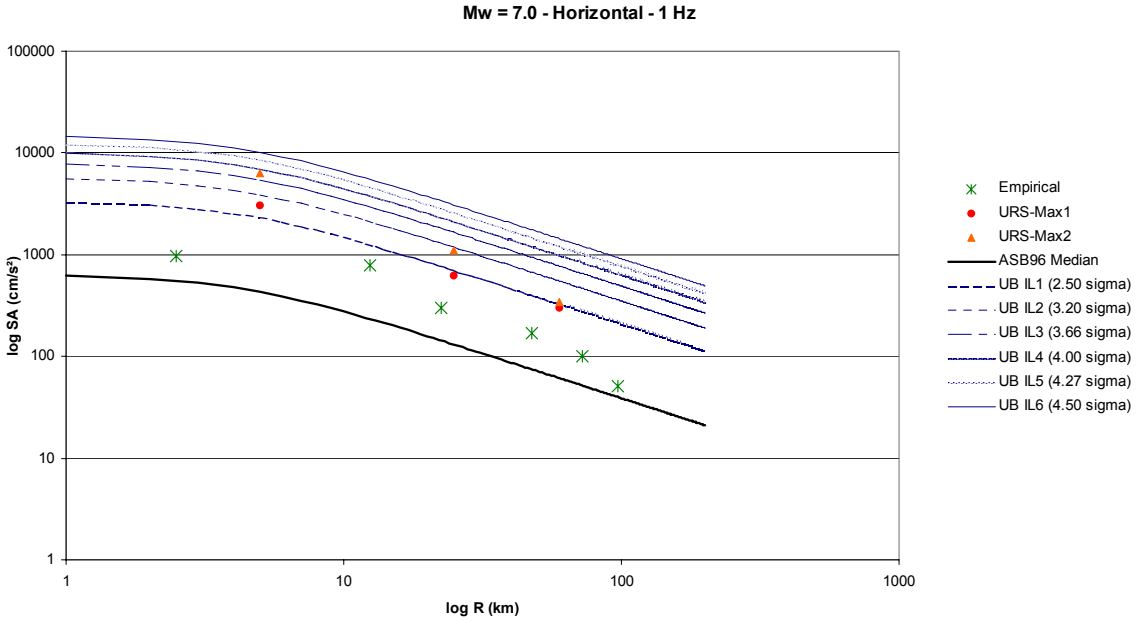

Fig. 6.28: Upper bound branch curves for horizontal spectral acceleration at 1 Hz from an M_w 7.0 earthquake compared with median motions from Ambraseys et al. (1996), URS numerical models and empirical data from WAF database

7 MAXIMUM GROUND MOTIONS FOR THE VERTICAL COMPONENT

Since the Pegasos project requires estimates of both horizontal and vertical response spectra, upper bounds also need to be specified for the vertical component of motion. Estimates of the upper bounds on the vertical component of motion are needed for the same 9 response frequencies and the same ranges of magnitude and distance specified for the horizontal component of motion in Table 6.1 in the previous Chapter.

Analysis of the available data is performed along the same lines s the assessment of tools for evaluating the upper bounds on the horizontal of motion that was presented in the previous Chapter. However, it is found that there is even less data available to constrain the solutions and for this reason the method adopted to define the upper bounds for the vertical component of motion is essentially the same as that employed for the horizontal component of motion.

7.1 Evaluation of the Empirical Data

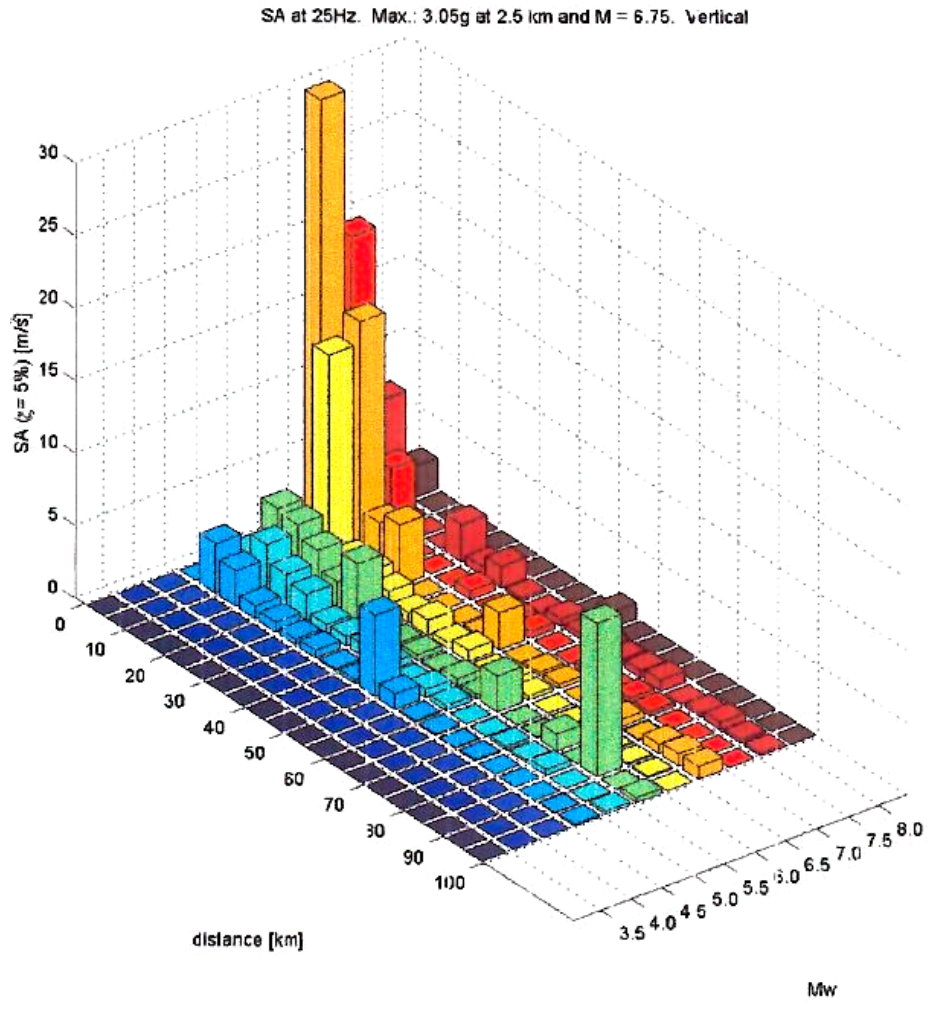

Fig. 7.1: Largest vertical SA at 25 Hz values on rock

The empirical data regarding maximum vertical motions is presented in the same way as for the horizontal motion, in plots showing the largest value of spectral acceleration in M-R bins (Figure 7.1) and the corresponding number of standard deviations above the median value obtained from attenuation equations (Figure 7.2), in this case using the attenuation equation of Abrahamson & Silva (1997) for vertical motions. These plots are useful for the same reasons presented for the corresponding plots of horizontal maxima in Section 6.1, and similarly they are subject to the same limitations: the values presented can only provide lower bounds estimates of the values of the maximum ground motions that could be realised.

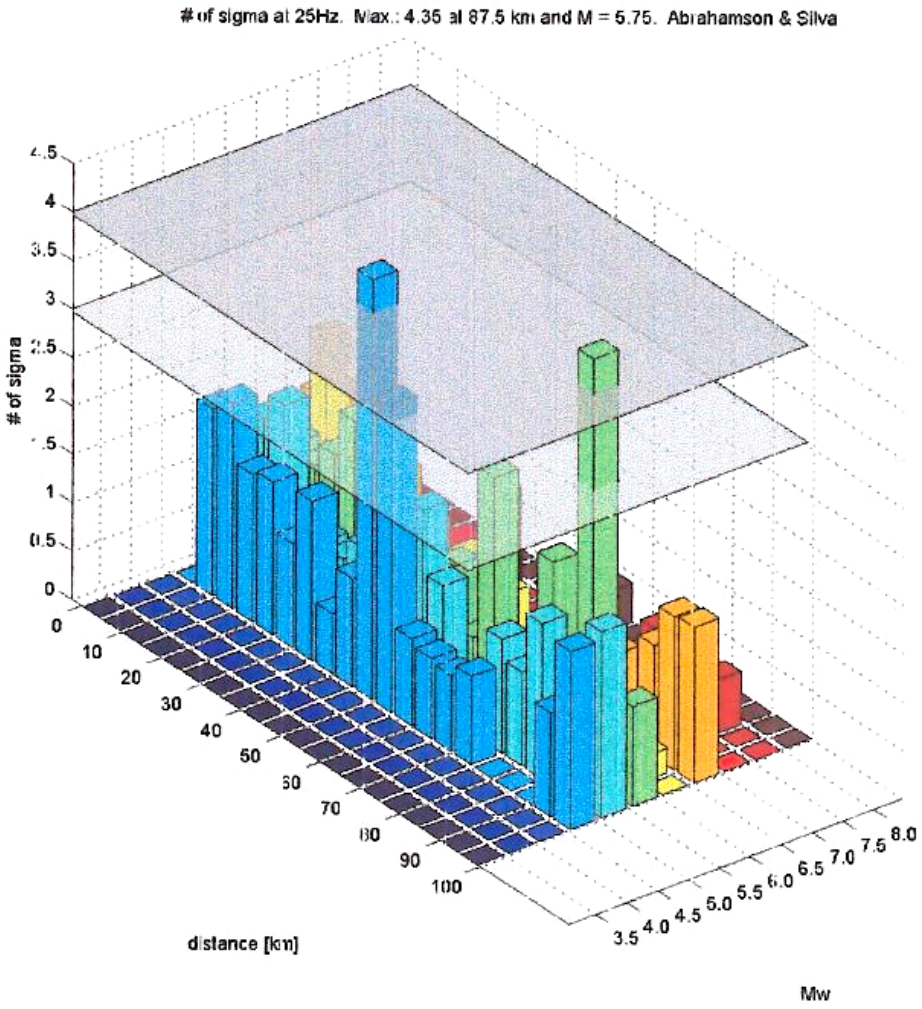

Fig. 7.2: The number of standard deviations above the median values from Abrahamson & Silva (1997), for each M-R bin, for the data presented in Figure 7.1

7.2 Evaluation of the Numerical Simulations

Table 7.1 below summarises the frequencies at which each of the three sources of information (empirical data, URS simulations and OGS simulations) are available for the vertical component of motion.

Tab. 7.1: Response frequencies for which different upper bound estimates exist

Frequency (Hz)	Vertical		
	Empirical	OGS	URS
0.5	●	●	○
1.0	●	●	○
2.5	●	●	○
5	●	●	○
10	●	●	○
20	●	●	○
33	○	○	○
50	○	○	○
100 (PGA)	○	●	○

From Table 7.1 it is immediately apparent that the only information regarding the maximum values of vertical PGA is the OGS numerical modelling, which is deficient for high frequencies. In assessing horizontal upper bounds in Chapter 6 it was concluded that the OGS results are not particularly reliable, hence there can be little optimism about inferring upper bounds on vertical motions using only the empirical data and the OGS numerical simulations.

The lack of constraint on the maximum ground motions for the vertical component is of concern since the largest value of PGA ever was the vertical acceleration of about 2*g* recorded during the 23 December 1985 Nahanni M_w 6.8 earthquake in Canada.

7.3 Logic-Tree Structure

Following the same procedure used for the horizontal motion in Section 6.3, plots were prepared for each combination of magnitude and response frequency for the vertical components. On the same plots, the predicted values of spectral acceleration from the equations of Ambraseys & Simpson (1996) for the vertical motion are plotted. The median attenuation curve and the 84, 97.7 and 99.9 percentile curves are also plotted, adding respectively one, two and three standard deviations. The resulting curves are plotted in Figures 7.3 to 7.23. In each plot the horizontal values are shown for a given combination of magnitude and response frequency. Straight lines are fitted through the numerical modelling values whenever three points are available, but these are only intended to assist in the interpretation in reading these rather cluttered plots.

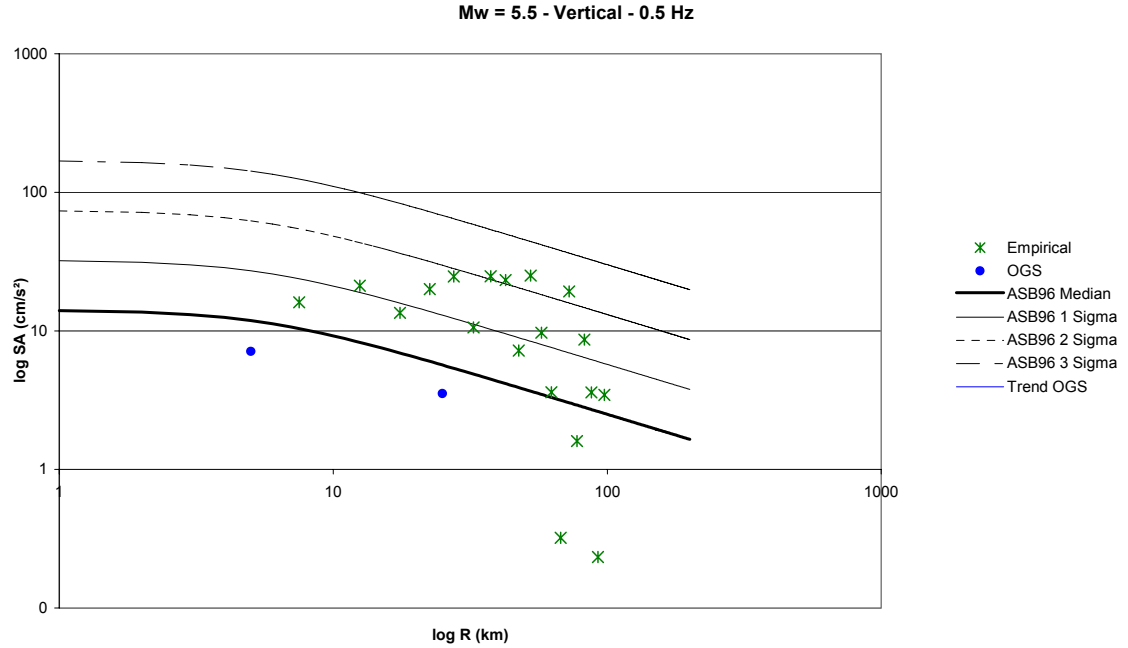

Fig. 7.3: Upper bound estimates of vertical spectral acceleration at 0.5 Hz frequency for an earthquake of M_w 5.5, compared to predictions of 50, 84, 97.7 and 99.9 percentile values from the equations of Ambraseys & Simpson (1996)

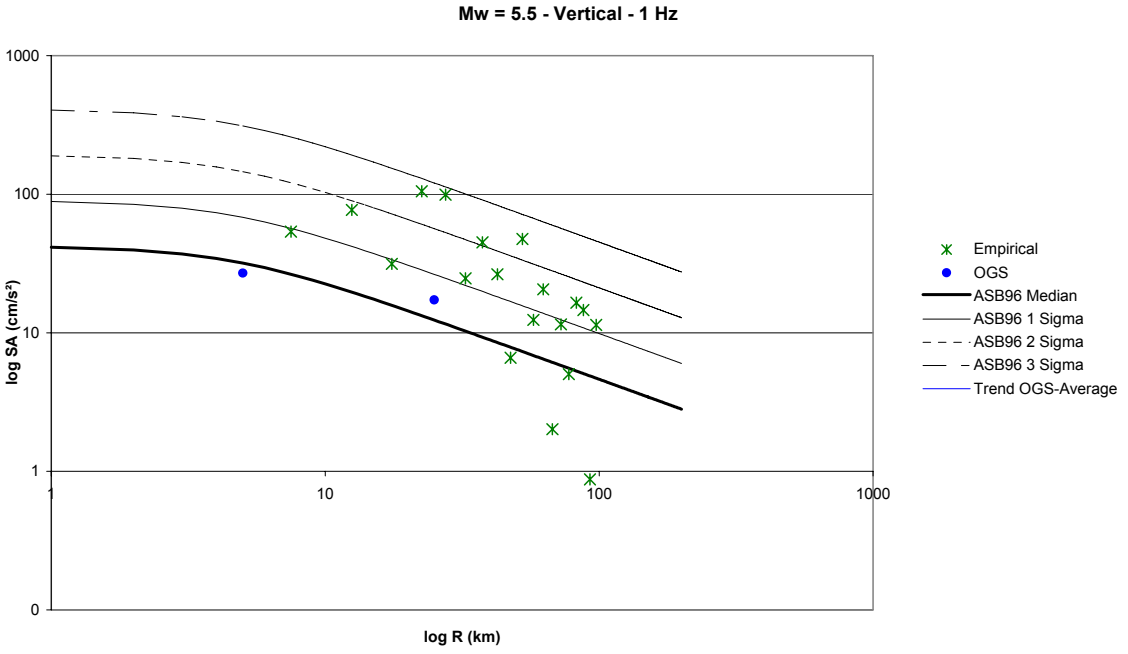

Fig. 7.4: Upper bound estimates of vertical spectral acceleration at 1.0 Hz frequency for an earthquake of M_w 5.5, compared to predictions of 50, 84, 97.7 and 99.9 percentile values from the equations of Ambraseys & Simpson (1996)

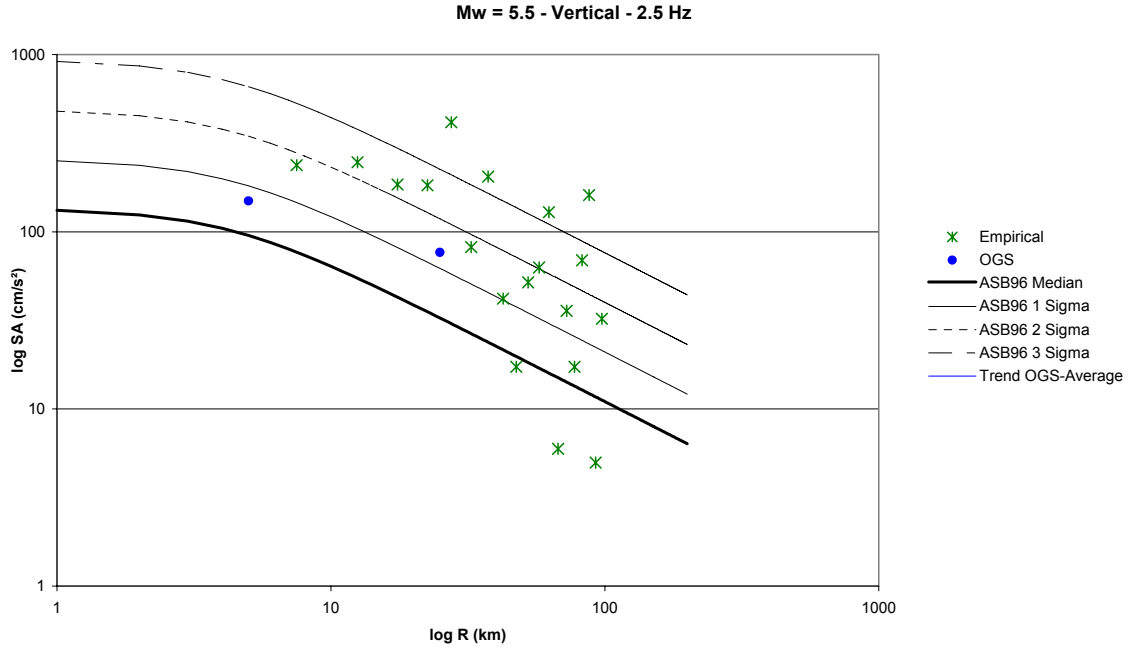

Fig. 7.5: Upper bound estimates of vertical spectral acceleration at 2.5 Hz frequency for an earthquake of M_w 5.5, compared to predictions of 50, 84, 97.7 and 99.9 percentile values from the equations of Ambraseys & Simpson (1996)

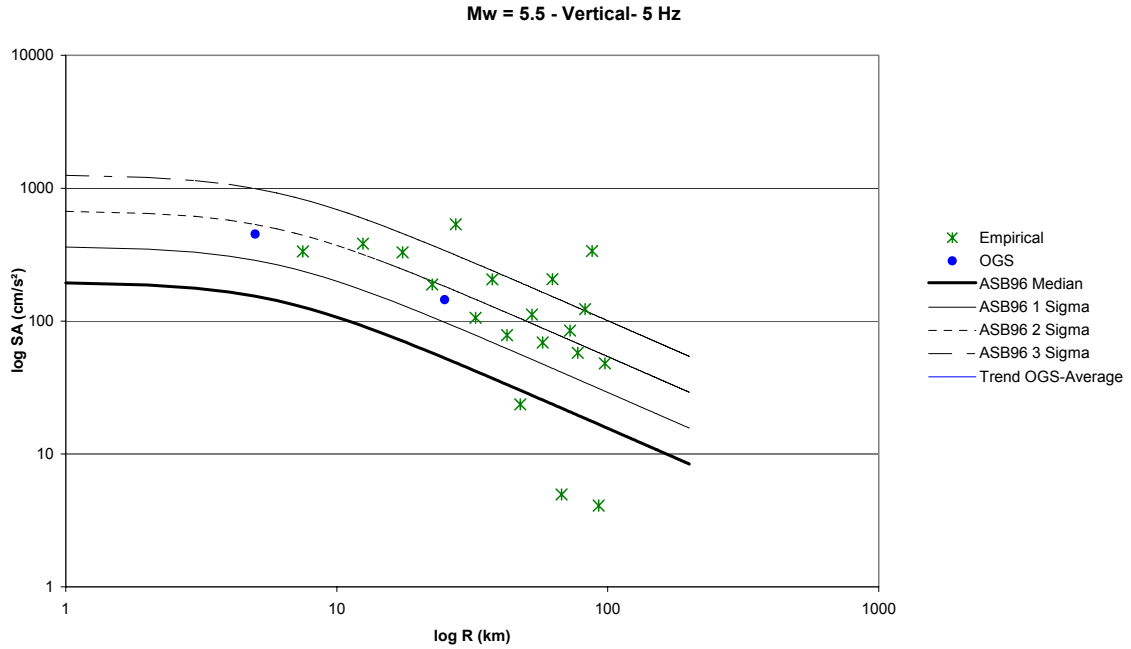

Fig. 7.6: Upper bound estimates of vertical spectral acceleration at 5.0 Hz frequency for an earthquake of M_w 5.5, compared to predictions of 50, 84, 97.7 and 99.9 percentile values from the equations of Ambraseys & Simpson (1996)

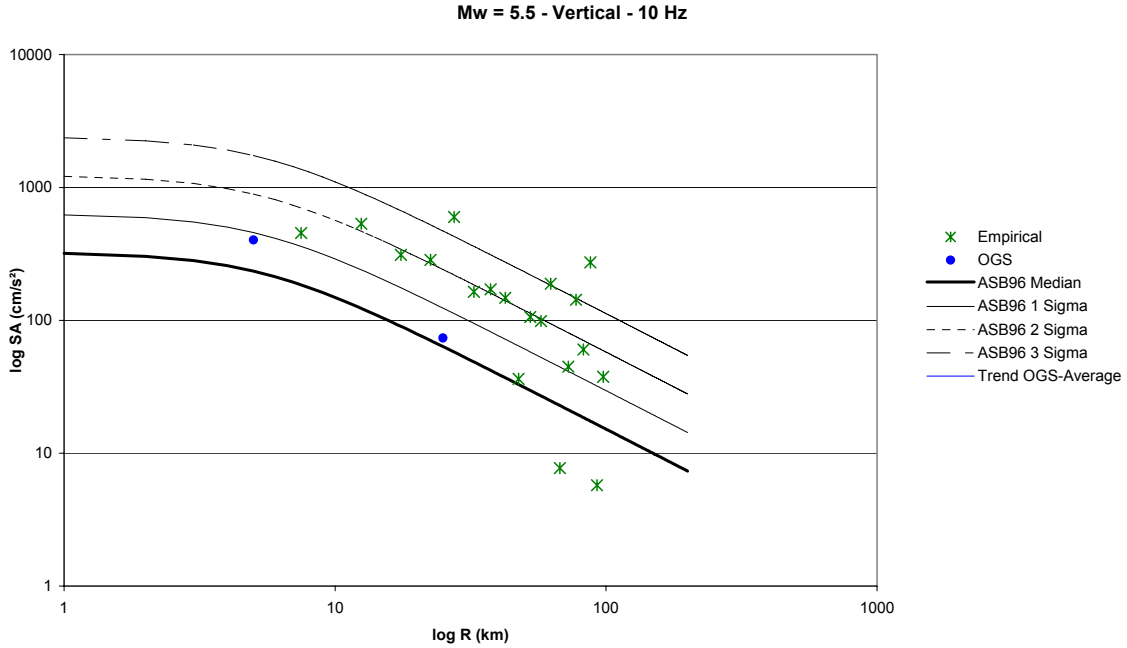

Fig. 7.7: Upper bound estimates of vertical spectral acceleration at 10.0 Hz frequency for an earthquake of M_w 5.5, compared to predictions of 50, 84, 97.7 and 99.9 percentile values from the equations of Ambraseys & Simpson (1996)

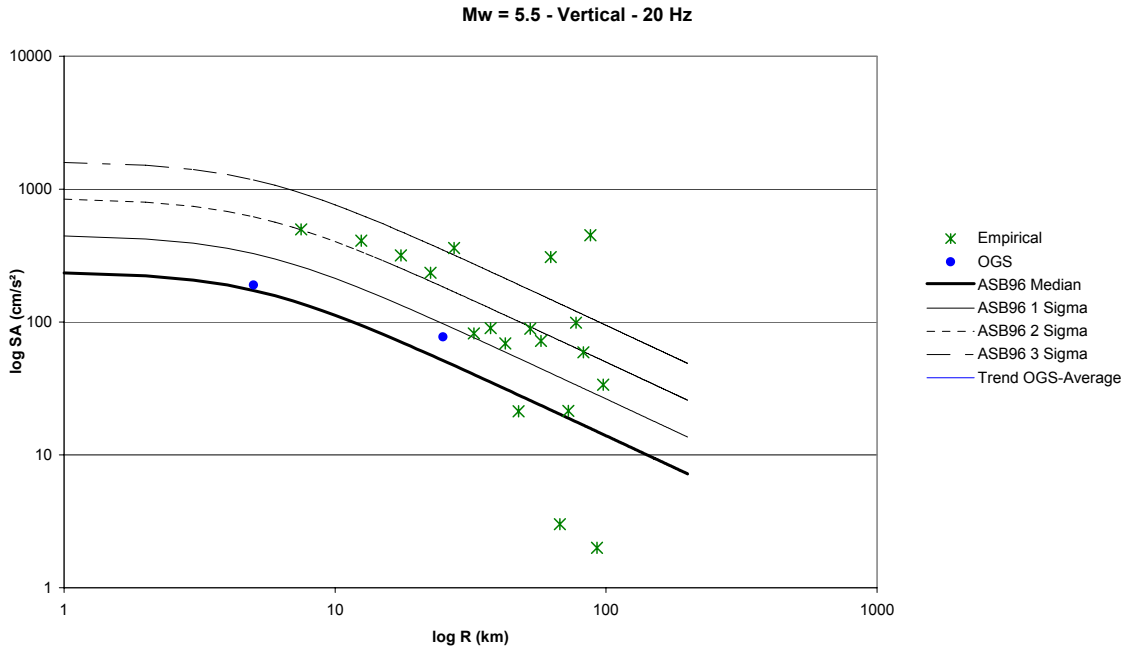

Fig. 7.8: Upper bound estimates of vertical spectral acceleration at 20.0 Hz frequency for an earthquake of M_w 5.5, compared to predictions of 50, 84, 97.7 and 99.9 percentile values from the equations of Ambraseys & Simpson (1996)

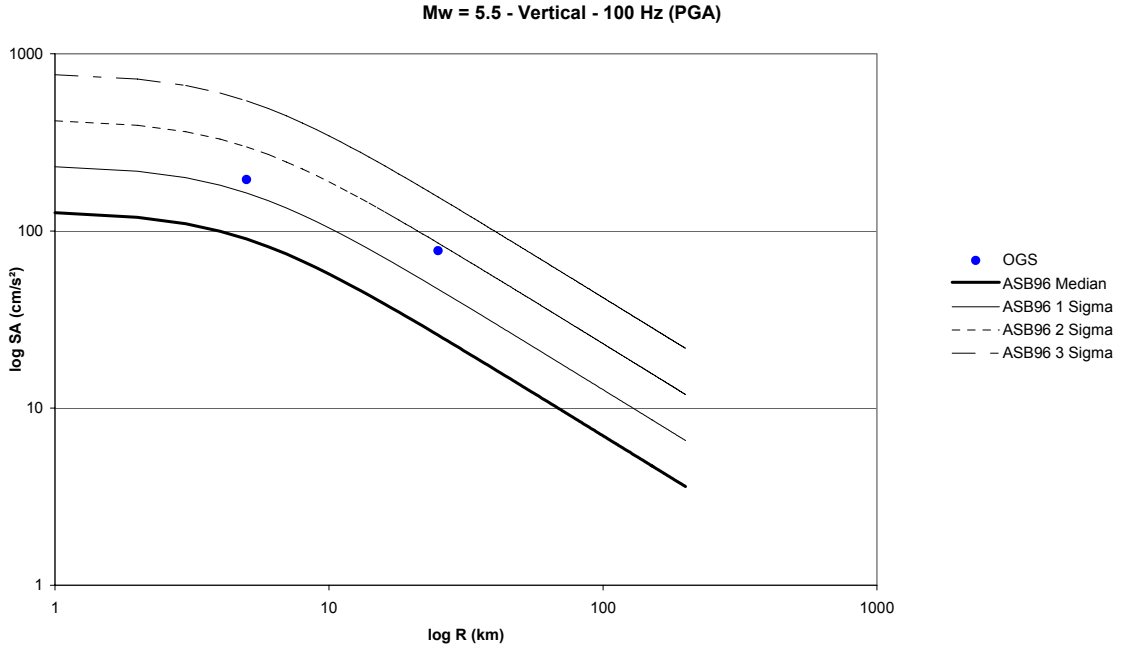

Fig. 7.9: Upper bound estimates of vertical spectral acceleration at 100.0 Hz frequency (PGA) for an earthquake of M_w 5.5, compared to predictions of 50, 84, 97.7 and 99.9 percentile values from the equations of Ambraseys & Simpson (1996)

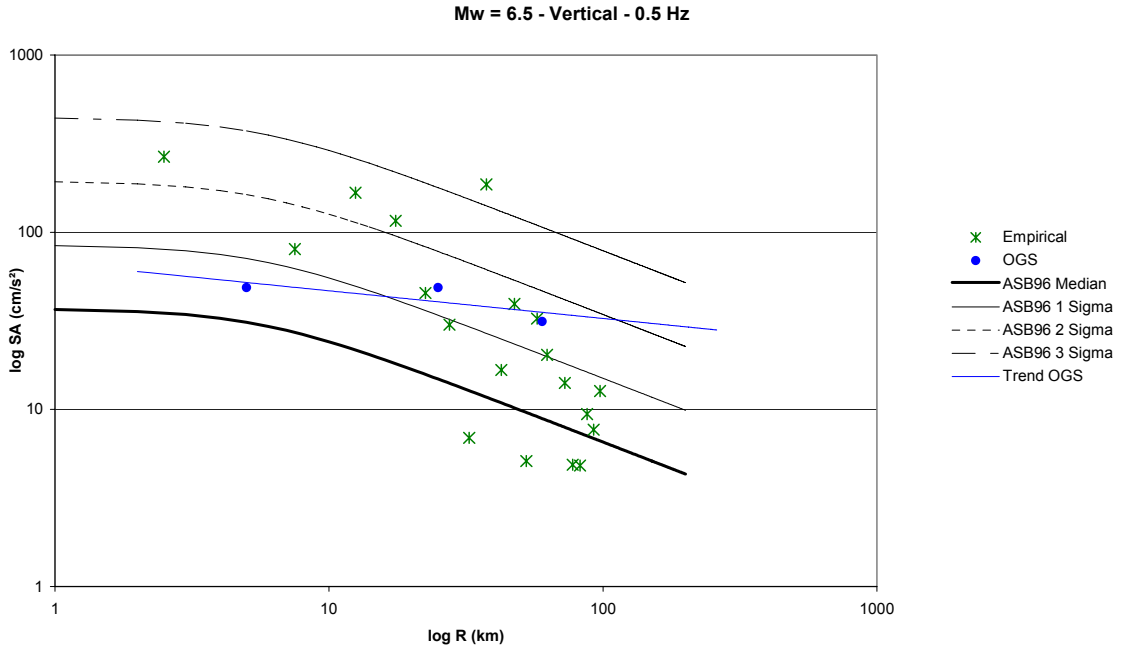

Fig. 7.10: Upper bound estimates of vertical spectral acceleration at 0.5 Hz frequency for an earthquake of M_w 6.5, compared to predictions of 50, 84, 97.7 and 99.9 percentile values from the equations of Ambraseys & Simpson (1996)

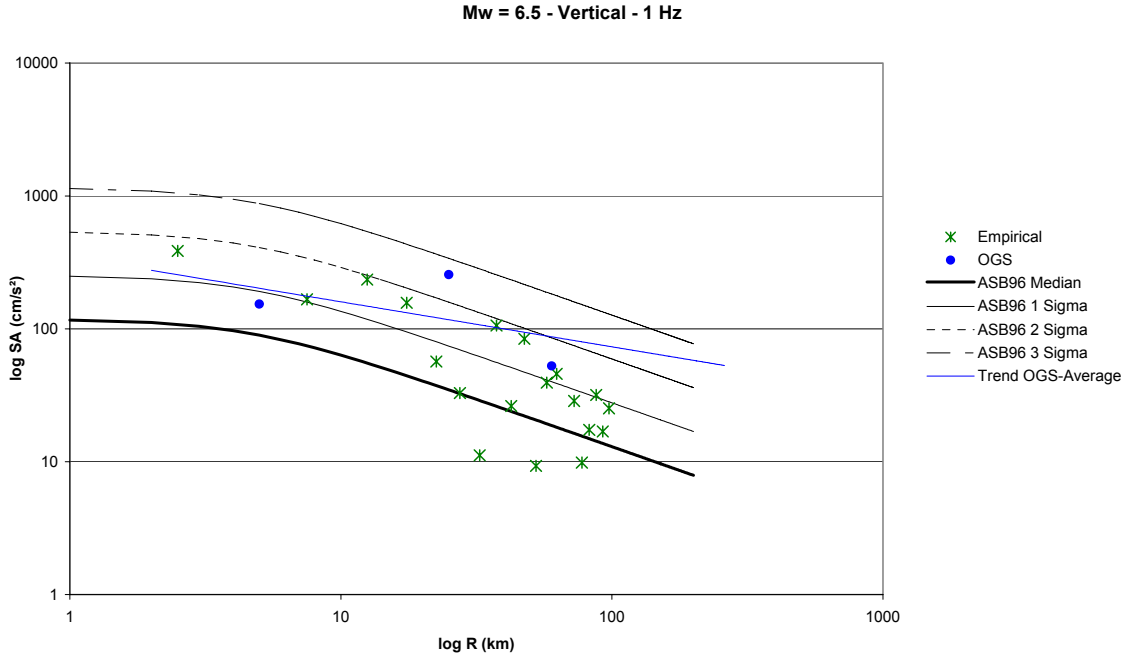

Fig. 7.11: Upper bound estimates of vertical spectral acceleration at 1.0 Hz frequency for an earthquake of M_w 6.5, compared to predictions of 50, 84, 97.7 and 99.9 percentile values from the equations of Ambraseys & Simpson (1996)

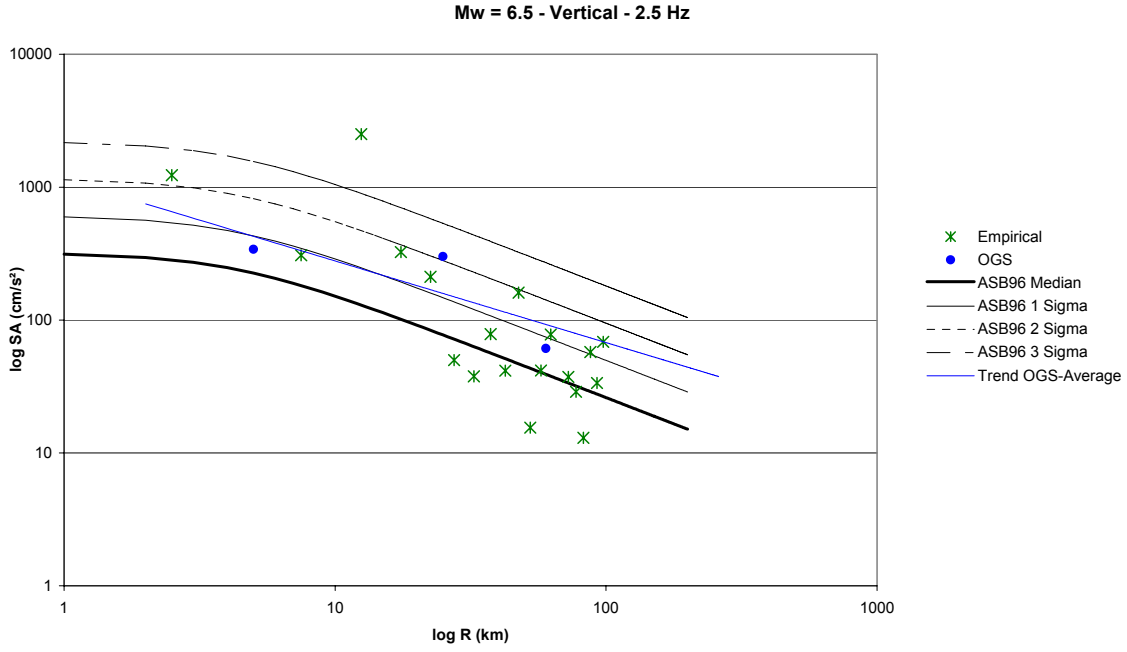

Fig. 7.12: Upper bound estimates of vertical spectral acceleration at 2.5 Hz frequency for an earthquake of M_w 6.5, compared to predictions of 50, 84, 97.7 and 99.9 percentile values from the equations of Ambraseys & Simpson (1996)

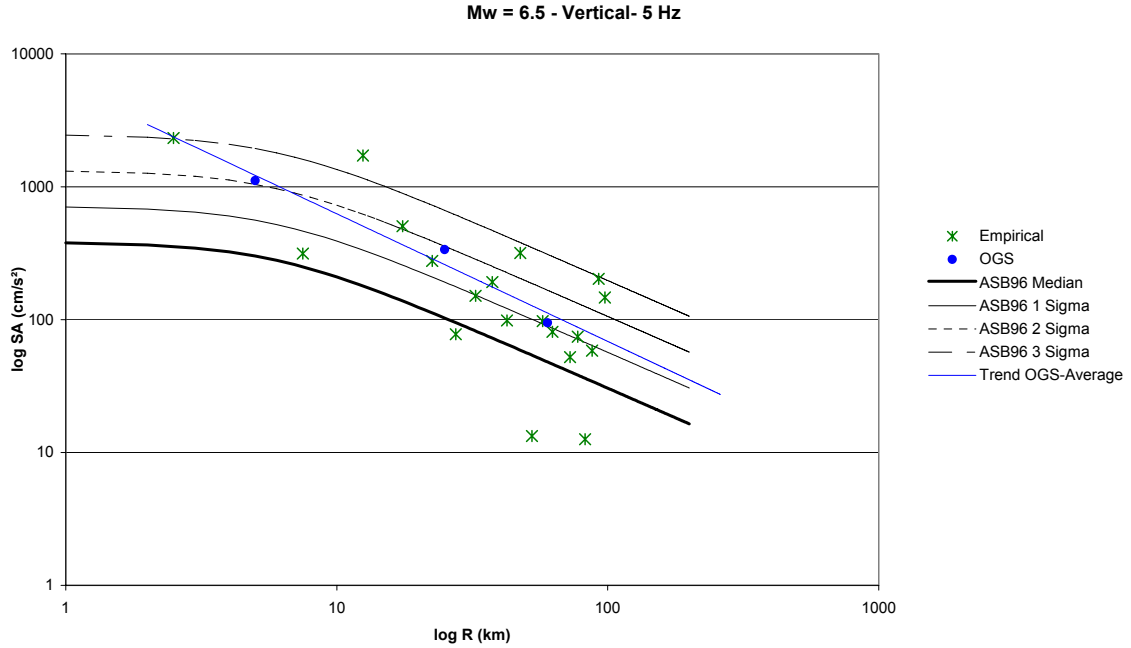

Fig. 7.13: Upper bound estimates of vertical spectral acceleration at 5.0 Hz frequency for an earthquake of M_w 6.5, compared to predictions of 50, 84, 97.7 and 99.9 percentile values from the equations of Ambraseys & Simpson (1996)

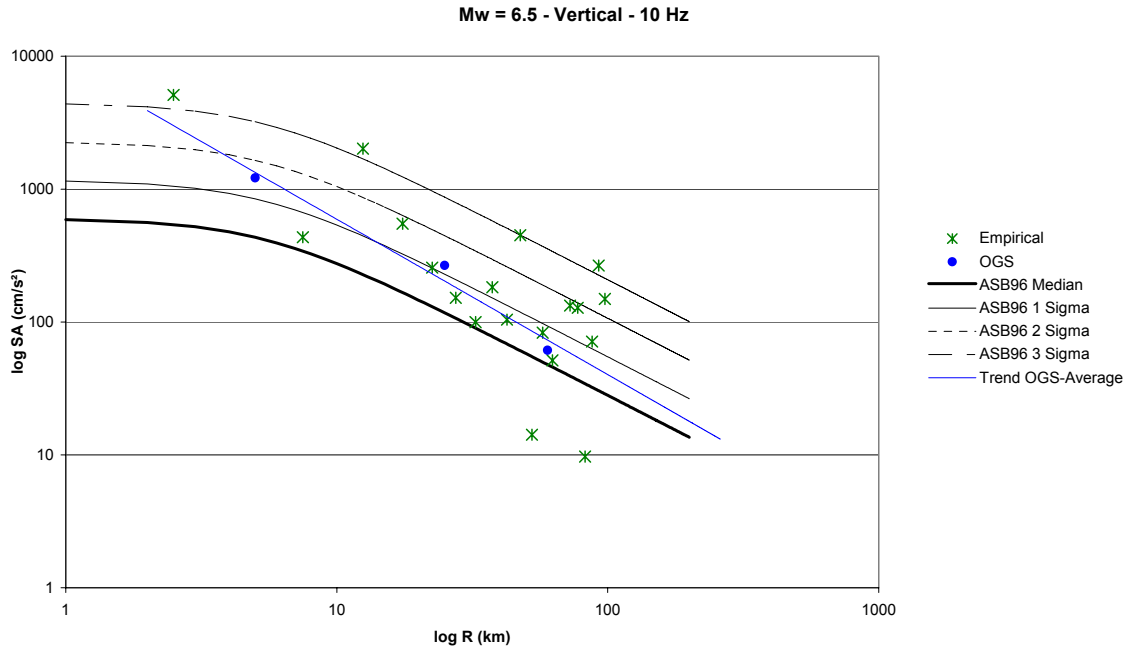

Fig. 7.14: Upper bound estimates of vertical (spectral acceleration at 10.0 Hz frequency for an earthquake of M_w 6.5, compared to predictions of 50, 84, 97.7 and 99.9 percentile values from the equations of Ambraseys & Simpson (1996)

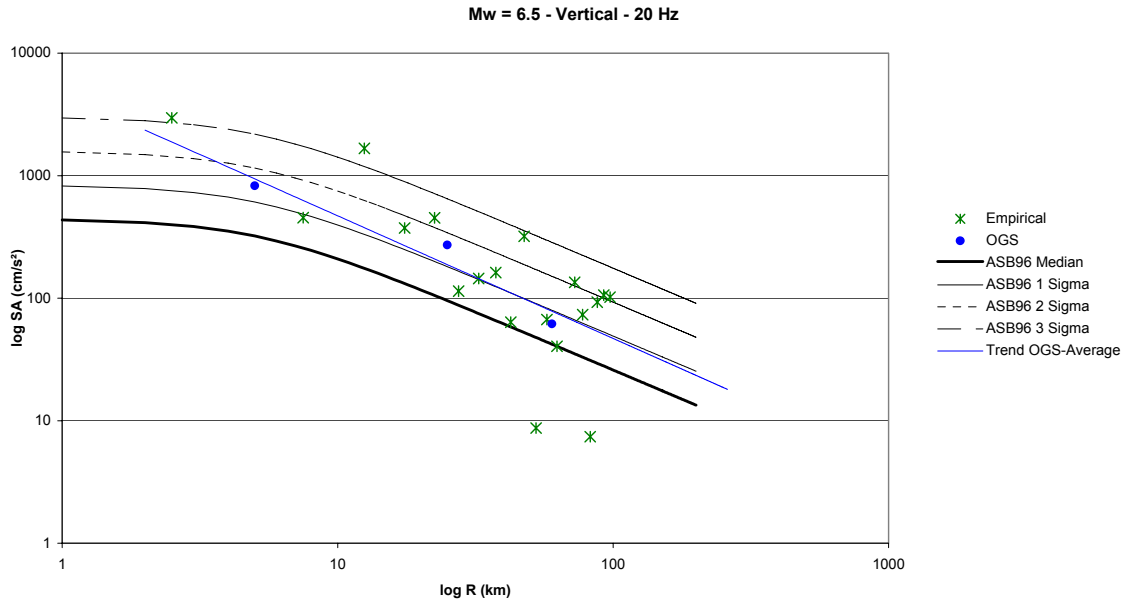

Fig. 7.15: Upper bound estimates of vertical spectral acceleration at 20.0 Hz frequency for an earthquake of M_w 6.5, compared to predictions of 50, 84, 97.7 and 99.9 percentile values from the equations of Ambraseys & Simpson (1996)

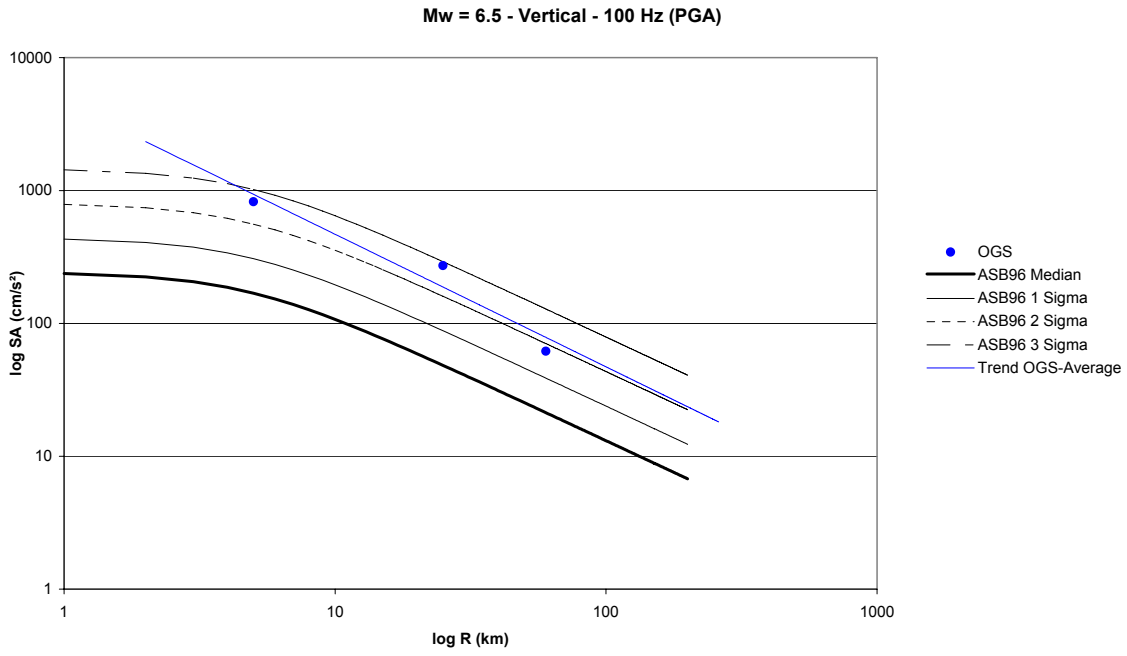

Fig. 7.16: Upper bound estimates of vertical spectral acceleration at 100.0 Hz frequency (PGA) for an earthquake of M_w 6.5, compared to predictions of 50, 84, 97.7 and 99.9 percentile values from the equations of Ambraseys & Simpson (1996)

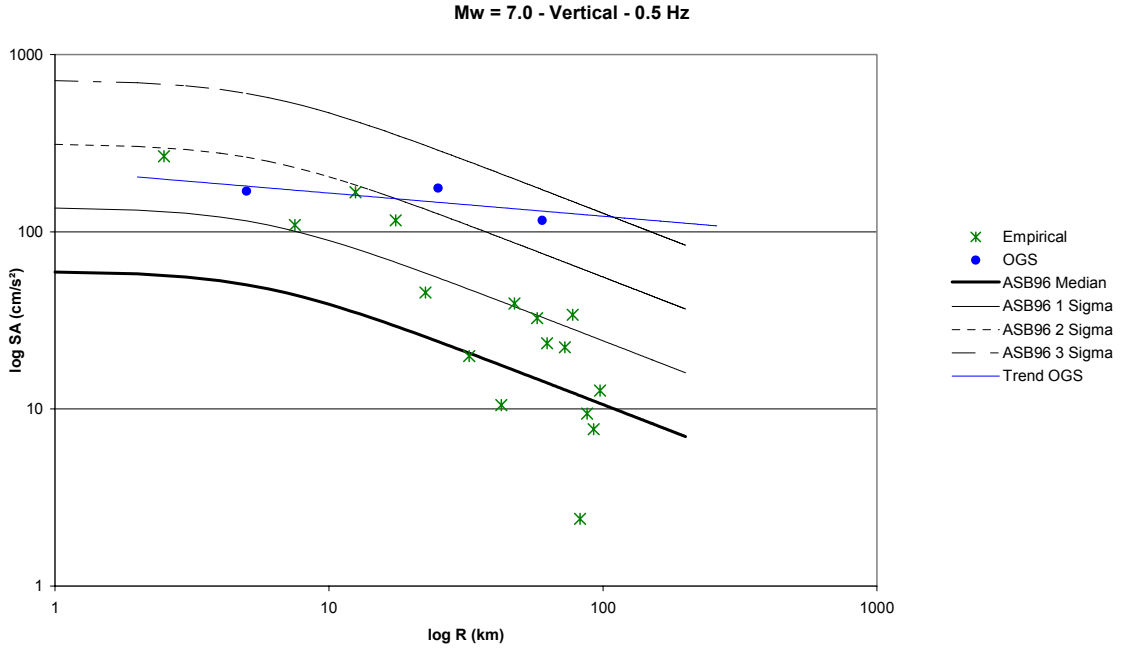

Fig. 7.17: Upper bound estimates of vertical spectral acceleration at 0.5 Hz frequency for an earthquake of M_w 7.0, compared to predictions of 50, 84, 97.7 and 99.9 percentile values from the equations of Ambraseys & Simpson (1996)

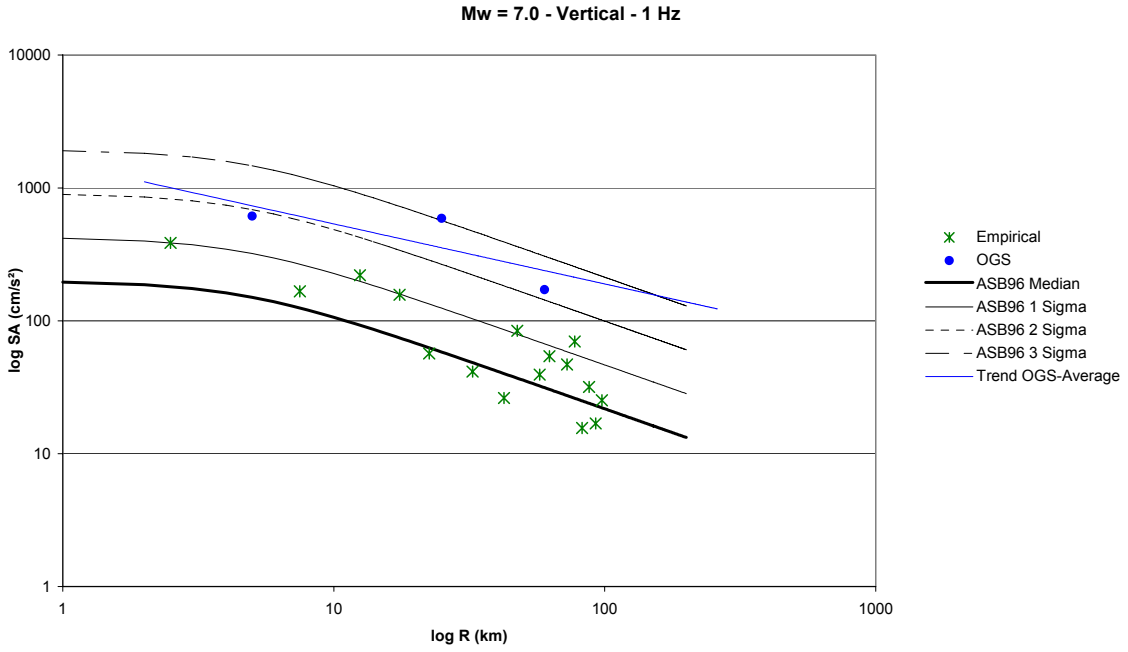

Fig. 7.18: Upper bound estimates of vertical spectral acceleration at 1.0 Hz frequency for an earthquake of M_w 7.0, compared to predictions of 50, 84, 97.7 and 99.9 percentile values from the equations of Ambraseys & Simpson (1996)

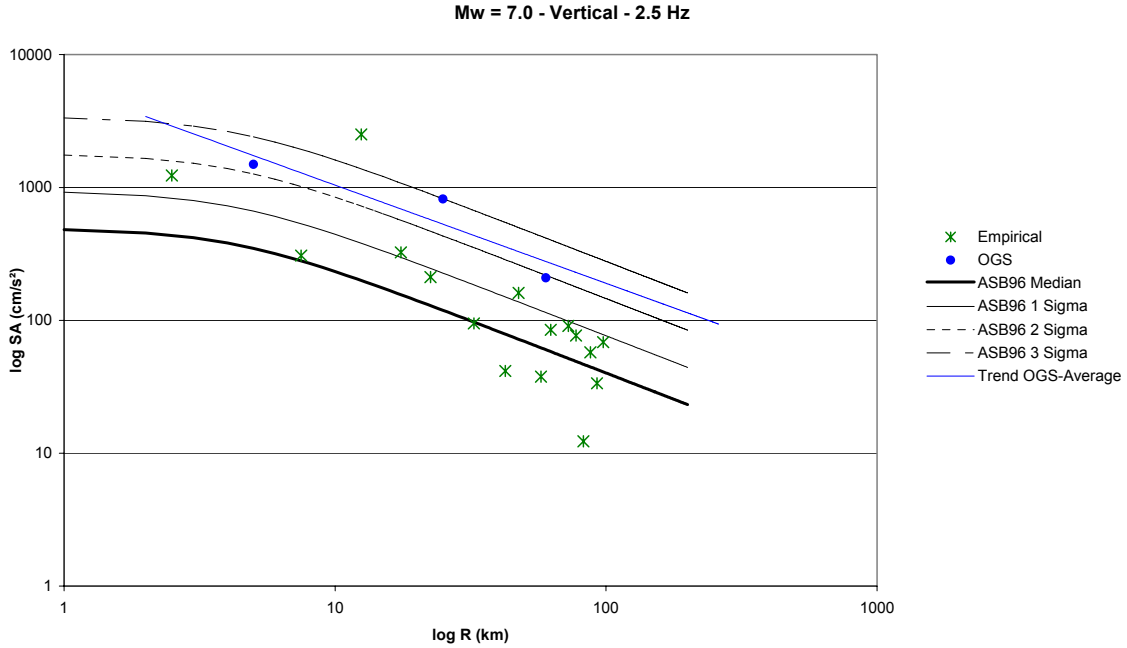

Fig. 7.19: Upper bound estimates of vertical spectral acceleration at 2.5 Hz frequency for an earthquake of M_w 7.0, compared to predictions of 50, 84, 97.7 and 99.9 percentile values from the equations of Ambraseys & Simpson (1996)

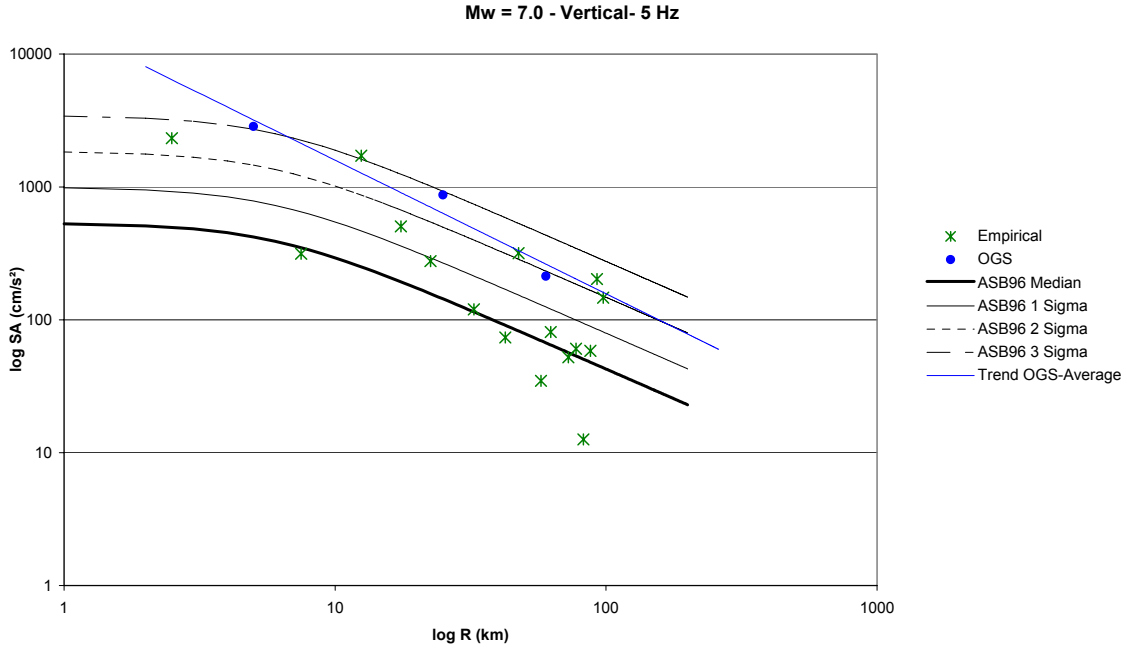

Fig. 7.20: Upper bound estimates of vertical spectral acceleration at 5.0 Hz frequency for an earthquake of M_w 7.0, compared to predictions of 50, 84, 97.7 and 99.9 percentile values from the equations of Ambraseys & Simpson (1996)

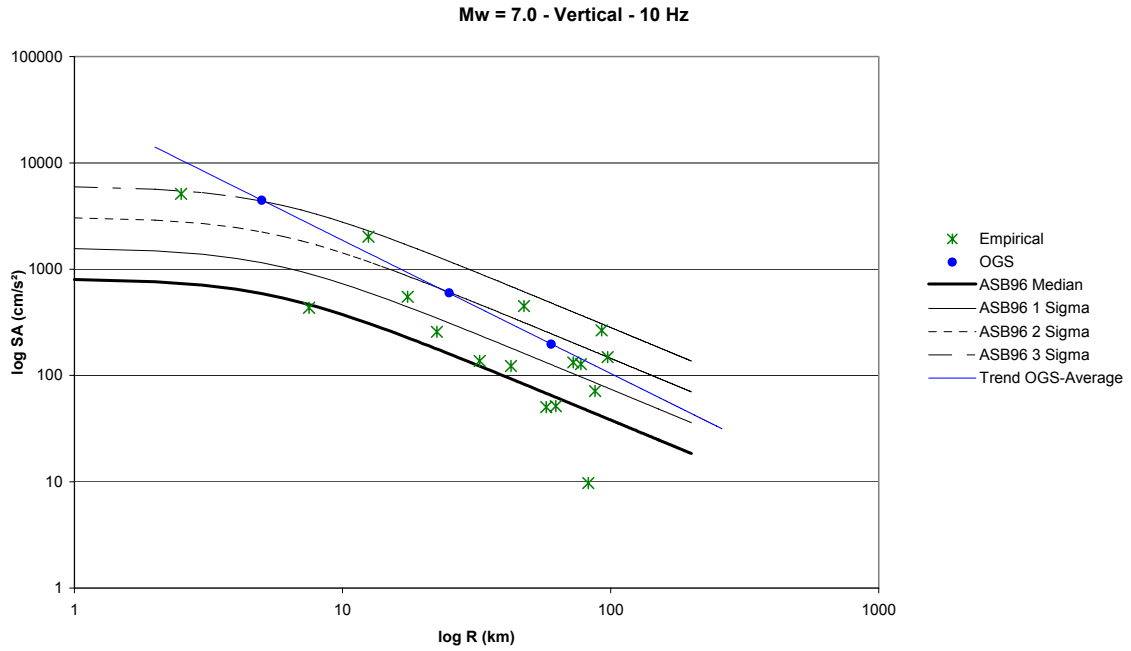

Fig. 7.21: Upper bound estimates of vertical spectral acceleration at 10.0 Hz frequency for an earthquake of M_w 7.0, compared to predictions of 50, 84, 97.7 and 99.9 percentile values from the equations of Ambraseys & Simpson (1996)

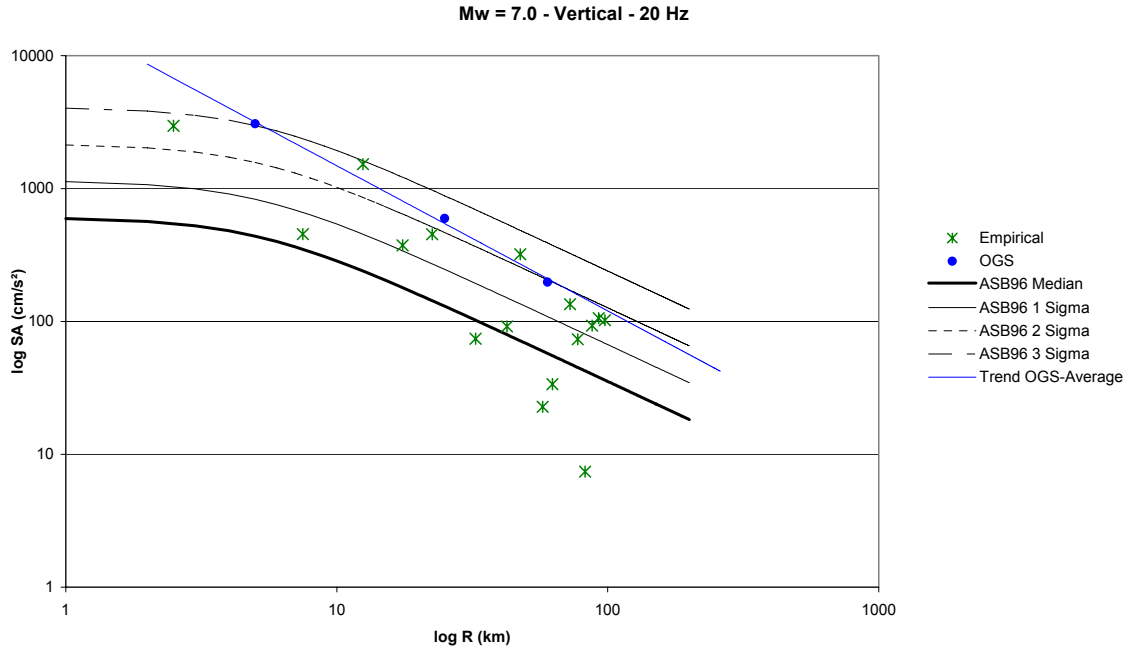

Fig. 7.22: Upper bound estimates of vertical spectral acceleration at 20.0 Hz frequency for an earthquake of M_w 7.0, compared to predictions of 50, 84, 97.7 and 99.9 percentile values from the equations of Ambraseys & Simpson (1996)

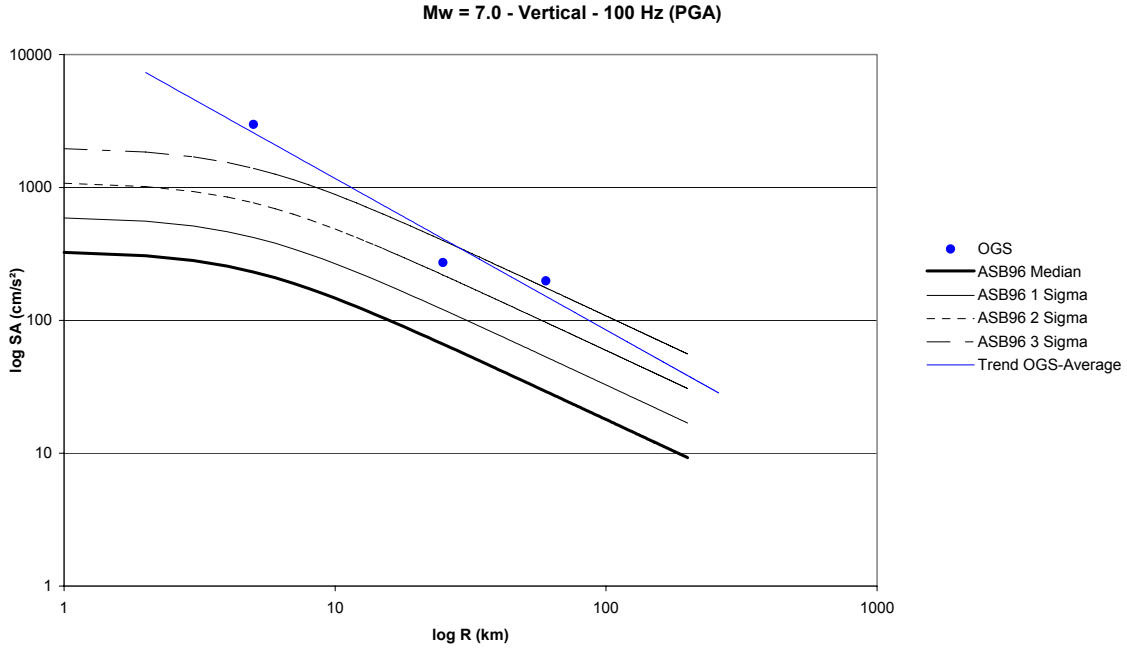

Fig. 7.23: Upper bound estimates of vertical spectral acceleration at 100.0 Hz frequency (PGA) for an earthquake of M_w 7.0, compared to predictions of 50, 84, 97.7 and 99.9 percentile values from the equations of Ambraseys & Simpson (1996)

Tab. 7.2: Incremental levels adopted to ensure monotonic increase in ground motion

The figures in the table correspond to the number of standard deviations to add to the median for vertical ground motions.

Frequency (Hz)	0.5	1	2.5	5	10	20	33	100
Sigma	0.36	0.33	0.28	0.27	0.29	0.28	0.27	0.26
Incremental level 1	2.5000	2.5000	2.5000	2.5000	2.5000	2.5000	2.5000	2.5000
Incremental level 2	3.2419	3.2093	3.1557	3.1452	3.1663	3.1557	3.1452	3.1347
Incremental level 3	3.6979	3.6676	3.6152	3.6044	3.6258	3.6152	3.6044	3.5936
Incremental level 4	4.0280	4.0069	3.9691	3.9612	3.9770	3.9691	3.9612	3.9531
Incremental level 5	4.2869	4.2764	4.2572	4.2531	4.2612	4.2572	4.2531	4.2488
Incremental level 6	4.5000	4.5000	4.5000	4.5000	4.5000	4.5000	4.5000	4.5000

As noted before, the URS study did not consider vertical motions, and in the previous Chapter the reliability of the OGS study was questioned. The only useful data in this case is therefore the maximum vertical motions from the records in the WAF database, which are generally bounded by the curve three sigma values above the median curve, with a few exceptions. However, there are practically no cases where the empirical value reaches, let alone exceeds, the upper limit specified for the horizontal motions of 4.5 standard deviations above the median. One exception to this is in Figure 7.8, which shows the spectral accelerations at 20 Hz for magnitude 5.5 earthquake; a single record appears to be more than 5 standard deviations above the median, but this is at almost 100 km from a moderate magnitude earthquake, and therefore at a level likely to be affected by noise (especially if from an analogue recorder) and certainly of no engineering consequence. It would seem imprudent and unhelpful to allow such values to influence the

levels at which the upper bounds are constrained. The preliminary hazard calculations for the Beznau site, the disaggregations at the 10-7 level, which is where the issue of upper bounds is of most relevance, indicate that events at distances much beyond 30 km do not contribute to the hazard (PEGASOS Report EXT-TN-0293). This is another reason not to allow the definition of the upper bounds to be influenced by observations from such long source-to-site distances.

It can therefore be concluded that for the vertical motions there is simply no useful data to constrain the upper bounds, so exactly the same procedure is adopted as for the horizontal components but using the equations of Ambraseys & Simpson (1996)

7.4 Weights for Maximum Ground Motions

In exactly the same way as was done for the horizontal upper bounds, the upper bounds on the vertical component of motion are defined by absolute values of spectral acceleration obtained from the following equations:

$$\log_{10}[SA(f)] = C_1 + C_2 M_w + C_3 \log(R) \quad (7.1a)$$

$$R = \sqrt{d^2 + h_o^2} \quad (7.1b)$$

where d is the Joyner-Boore distance and the values of C_1, C_2, C_3 and h_o are tabulated, with their corresponding weights, in Tables 7.3 to 7.10.

Tab. 7.3: Upper bound coefficients for Eq.(7.1) and weights: vertical motion at 0.5 Hz

Weight	C_1	C_2	C_3	h_o
0.10	-2.790	0.418	-0.601	5.6
0.22	-2.523	0.418	-0.601	5.6
0.26	-2.359	0.418	-0.601	5.6
0.26	-2.240	0.418	-0.601	5.6
0.12	-2.147	0.418	-0.601	5.6
0.04	-2.070	0.418	-0.601	5.6

Tab. 7.4: Upper bound coefficients for Eq.(7.1) and weights: vertical motion at 1.0 Hz

Weight	C_1	C_2	C_3	h_o
0.10	-2.535	0.449	-0.718	4.6
0.22	-2.301	0.449	-0.718	4.6
0.26	-2.150	0.449	-0.718	4.6
0.26	-2.038	0.449	-0.718	4.6
0.12	-1.949	0.449	-0.718	4.6
0.04	-1.875	0.449	-0.718	4.6

Tab. 7.5: Upper bound coefficients for Eq.(7.1) and weights: vertical motion at 2.5 Hz

Weight	C_1	C_2	C_3	h_o
0.10	-1.730	0.375	-0.791	4.2
0.22	-1.590	0.375	-0.791	4.2
0.26	-1.450	0.375	-0.791	4.2
0.26	-1.310	0.375	-0.791	4.2
0.12	-1.170	0.375	-0.791	4.2
0.04	-1.030	0.375	-0.791	4.2

Tab. 7.6: Upper bound coefficients for Eq.(7.1) and weights: vertical motion at 5.0 Hz

Weight	C_1	C_2	C_3	h_o
0.10	-0.935	0.291	-0.894	5.9
0.22	-0.761	0.291	-0.894	5.9
0.26	-0.637	0.291	-0.894	5.9
0.26	-0.540	0.291	-0.894	5.9
0.12	-0.462	0.291	-0.894	5.9
0.04	-0.395	0.291	-0.894	5.9

Tab. 7.7: Upper bound coefficients for Eq.(7.1) and weights: vertical motion at 10.0 Hz

Weight	C_1	C_2	C_3	h_o
0.10	-0.455	0.267	-1.049	5.4
0.22	-0.262	0.267	-1.049	5.4
0.26	-0.129	0.267	-1.049	5.4
0.26	-0.027	0.267	-1.049	5.4
0.12	0.056	0.267	-1.049	5.4
0.04	0.125	0.267	-1.049	5.4

Tab. 7.8: Upper bound coefficients for Eq.(7.1) and weights: vertical motion at 20.0 Hz

Weight	C_1	C_2	C_3	h_o
0.10	-0.7285	0.2696	-0.9540	5.10
0.22	-0.5468	0.2696	-0.9540	5.10
0.26	-0.4195	0.2696	-0.9540	5.10
0.26	-0.3214	0.2696	-0.9540	5.10
0.12	-0.2416	0.2696	-0.9540	5.10
0.04	-0.1743	0.2696	-0.9540	5.10

Tab. 7.9: Upper bound coefficients for Eq.(7.1) and weights: vertical motion at 33.3 Hz

Weight	C_1	C_2	C_3	h_o
0.10	-0.9260	0.2715	-0.9785	4.88
0.22	-0.7533	0.2715	-0.9785	4.88
0.26	-0.6303	0.2715	-0.9785	4.88
0.26	-0.5348	0.2715	-0.9785	4.88
0.12	-0.4566	0.2715	-0.9785	4.88
0.04	-0.3905	0.2715	-0.9785	4.88

Tab. 7.10: Upper bound coefficients for Eq.(7.1) and weights: vertical motion at PGA

Weight	C_1	C_2	C_3	h_o
0.10	-1.090	0.273	-0.954	4.7
0.22	-0.925	0.273	-0.954	4.7
0.26	-0.806	0.273	-0.954	4.7
0.26	-0.712	0.273	-0.954	4.7
0.12	-0.635	0.273	-0.954	4.7
0.04	-0.570	0.273	-0.954	4.7

8 MODEL FOR UPPER TAIL OF DISTRIBUTIONS

In Workshops WS-2/SP2 and WS-3/SP2, various options for truncating the upper tail of the distribution of logarithmic residuals in the ground motion equations have been discussed. These include various options for tapering the truncation to effect a transition from the standard normal distribution to a value that reaches zero at the cut-off level. A model that has been explored for this application is the upper limit lognormal (ULLN) distribution, but it is judged excessively complicated to warrant application in this project (Restrepo-Vélez & Bommer 2003).

8.1 Evaluation of Empirical Data

Normal probability plots of the residuals used to derive empirical attenuation relationships could be a useful way to obtain insight into the extent and nature of deviation from the lognormal distribution at the upper tail of the distributions. It must be noted, however, that these deviations are generally going to occur at the level of about 3 standard deviations above the mean, which is the 99.9-percentile hence any insight to the correct distribution at the this level requires 1,000 data points. PEGASOS Report RDZ-TN-0214 contains residual plots for three attenuation equations that contain sufficient numbers of records: 965 for Berge-Thierry et al. (2000), 3,011 for Lussou et al. (2001) and 4,754 for Chang et al. (2001). However, to actual capture the true distribution at the median plus 3 standard deviations level, 1,000 data points are probably not sufficient in practice – several thousand records would actually be needed in order to capture the "average" behaviour at the upper tail. Notwithstanding these reservations regarding the usefulness of the empirical data for this purpose of defining the nature of the upper tails, some of the plots from the PEGASOS Report RDZ-TN-0214 are considered herein for the purpose of identifying any observable patterns.

Figure 8.1 shows the residual plots from the Berge-Thierry et al. (2000) and Lussou et al. (2001) equations for spectral acceleration at 34 Hz and 50 Hz respectively, both of which may be considered as equivalent to PGA. These figures are therefore comparable to Figure 6.2 showing the PGA residuals from the Chang et al. (2001) equation. Figures 8.2 and 8.3 show the same information but for spectral acceleration responses at 10 Hz and 1 Hz respectively.

Considering the case of PGA first, and ignoring the case of Berge-Thierry et al. (2000) since it is the smallest of the three data sets, both Chang et al. (2001) and Lussou et al. (2001) show similar patterns at the upper tail, where at about 4 standard deviations above the median, the lognormal distribution seems to overestimate the residuals. However, the Lussou et al. (2001) data conform to the lognormal distribution quite closely right up to 3 sigma above the mean, whereas the Chang et al. (2001) data deviates from the assumed distribution significantly above 2 sigma values above the mean.

Before any inferences are made, however, about what might be the true nature of the distributions of the residuals at 4 standard deviations above the mean, it should be recalled that this corresponds to the 99.9968-percentile level, or the level of the 1 in 33,000 motion; neither of these data sets is actually large enough to capture this level.

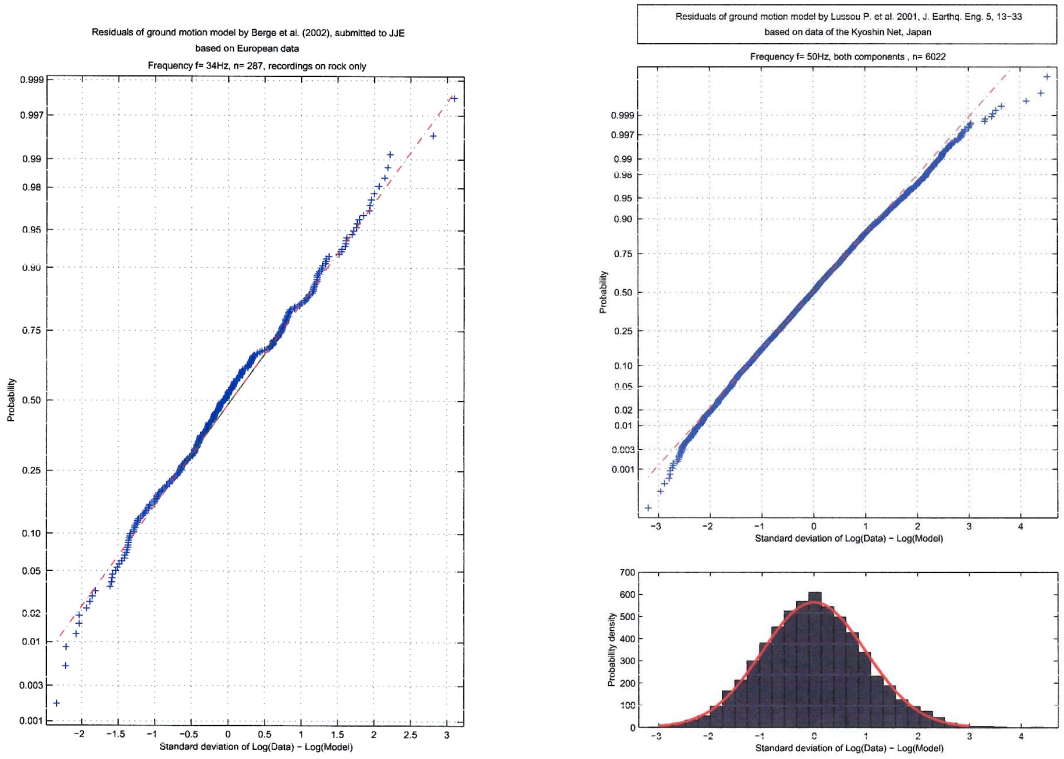

Fig. 8.1: Residual plots for PGA from Berge-Thierry et al. (2000) and Lussou et al. (2001)

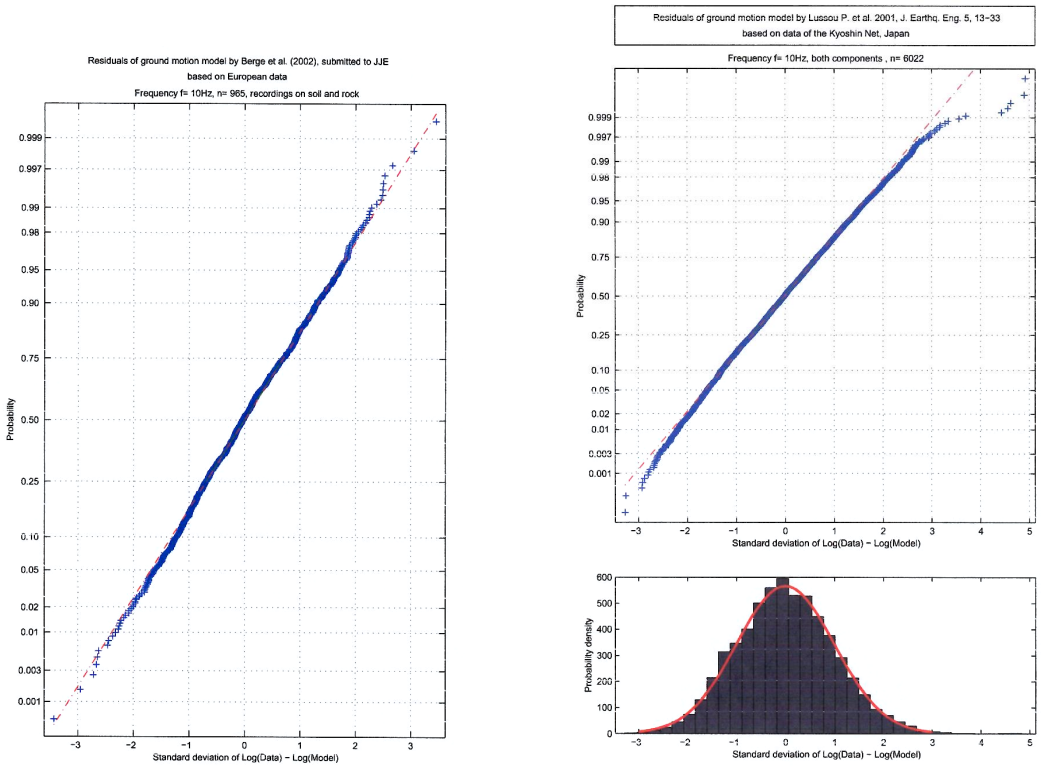

Fig. 8.2: Residual plots for spectral acceleration at 10 Hz from Berge-Thierry et al. (2000) and Lussou et al. (2001)

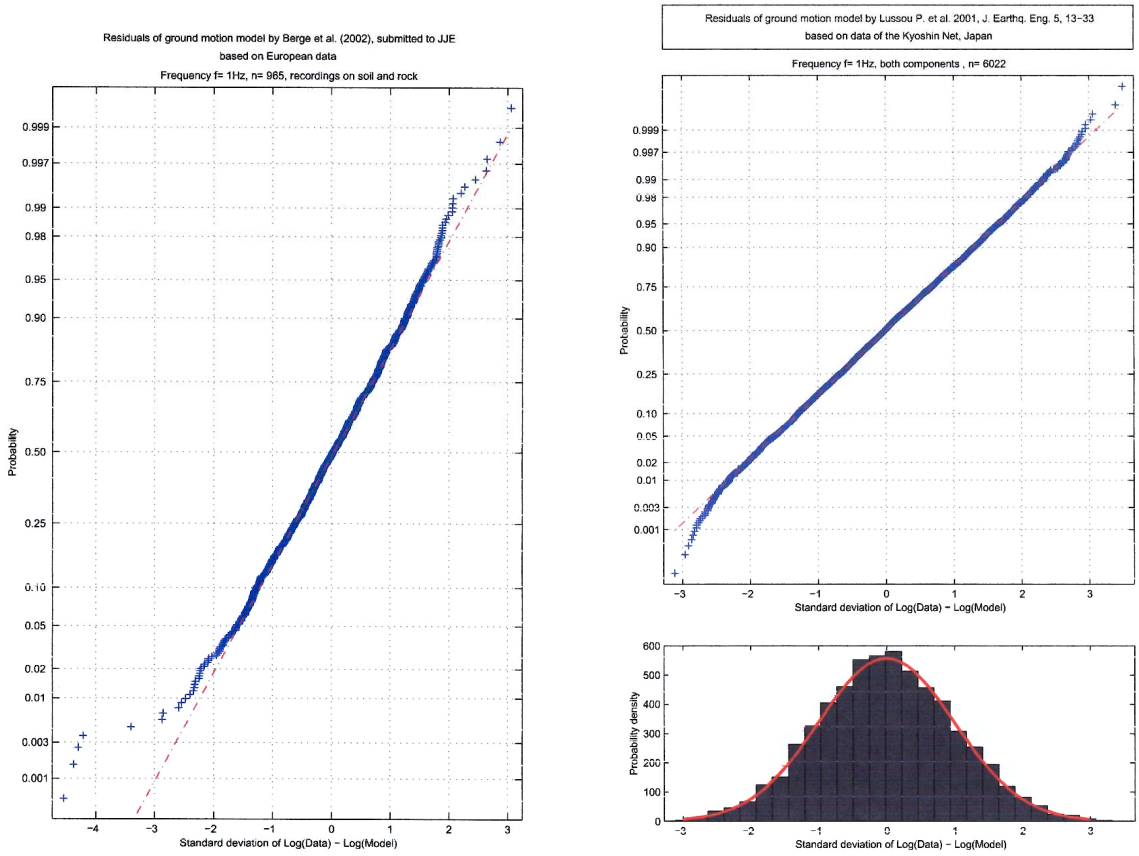

Fig. 8.3: Residual plots for spectral acceleration at 1 Hz from Berge-Thierry et al. (2000) and Lussou et al. (2001)

In Figure 8.2, for spectral accelerations at 10 Hz, the Berge-Thierry et al. (2000) residuals seem to fit the lognormal distribution up to the highest value a little more than 3 sigma above the mean. The Lussou et al. (2001) data also follow the lognormal distribution up to this level, and then deviate significantly at higher values, showing overestimation of the higher residuals in the same way as for PGA. In Figure 8.3, for spectral accelerations at 1 Hz, both datasets seem to follow the lognormal distribution reasonably well and indicate a slight underestimation of the residuals at more than 3 standard deviations above the mean.

Even if the fact that the data is insufficient to constrain distributions of the upper tail that are different from the assumed lognormal distribution, although there are similar patterns observed, there is still uncertainty as to the exact nature of the modifications that would be required to the upper tails. Furthermore, at the levels at which these modifications would be applied, which from Chapters 6 and 7 are at least 2.5 standard deviations above the median, the results are unlikely to be very sensitive to particular way in which the distribution tapers to the cut-off. Since there is no strong evidence for which modification of the upper tails, if any, would be appropriate, it is considered an unnecessary and unjustified complication of the ground motion prediction model.

8.2 Logic-Tree Structure

Consistent with the philosophy expounded in Chapter 6, the physical bounds being proposed in this model are physical rather than statistical, and the value reached should be the same for all equations. For this reason, the upper limits cannot be defined in terms of numbers of standard

deviations above the mean although it is likely that this level will generally correspond to at least three standard deviations above the mean logarithmic value. At these levels, an acceptable model for the truncation is a simple and abrupt cut-off of the distribution, without any tapering or other adjustments. Such abrupt cut-offs should strictly be accompanied by a re-normalisation of the distribution, but since the effect of this would be negligible there is no reason to bring in this additional complication.

8.3 Weights for Upper Tail Models

Since only one model for the upper tail of the distribution of strong-motion residuals is adopted, it automatically carries a weight of unity. The only model proposed is that the upper tail of the distributions be sharply cut at the maximum values of ground motions indicated in Chapters 6 and 7 of this report.

9 REFERENCES

Abercrombie, R. & Levy, P. 1993: Source parameters of small earthquakes recorded at 2.5 km depth, Cajon Pass, Southern California: implications for earthquake scaling. Geophysical Research Letters 20/14, 1511-1514.

Abrahamson, N.A. & Shedlock, K.M. 1997: Overview. Seismological Research Letters 68/1, 9-23.

Abrahamson, N.A. & Silva, W.J. 1997: Empirical response spectral attenuation relations for shallow crustal earthquakes. Seismological Research Letters 68/1, 94-127.

Abrahamson, N.A., Birkhauser, P., Koller, M., Mayer-Rosa, D., Smit, P., Sprecher, C., Tinic, S. & Graf, R. 2002: Pegasos – a comprehensive probabilistic seismic hazard assessment for nuclear power plants in Switzerland. Proceedings of the Twelfth European Conference on Earthquake Engineering, London, Paper No. 633.

Ambraseys, N.N. & Bommer, J.J. 1990: Uniform magnitude re-evaluation for the strong-motion database of Europe and adjacent areas. European Earthquake Engineering 4/2, 3-16.

Ambraseys, N.N. & Bommer, J.J. 1991: The attenuation of ground accelerations in Europe. Earthquake Engineering & Structural Dynamics 20, 1179-1202.

Ambraseys, N.N. & Douglas, J. 2000: Reappraisal of the effect of vertical ground motions on response. ESEE Report No. 00-4, Department of Civil & Environmental Engineering, Imperial College, London (Revised version submitted to Soil Dynamics & Earthquake Engineering).

Ambraseys, N.N. & Douglas, J. 2003: Near-field horizontal and vertical earthquake ground motions. Soil Dynamics & Earthquake Engineering 23, 1-18.

Ambraseys, N.N. & Free, M.W. 1997: Surface-wave magnitude calibration for European region earthquakes. Journal of Earthquake Engineering 1/1, 1-22.

Ambraseys, N.N., Simpson, K.A. & Bommer, J.J. 1996: Prediction of horizontal response spectra in Europe. Earthquake Engineering & Structural Dynamics 25, 371-400.

Ambraseys, N.N. & Simpson, K.A. 1996: Prediction of vertical response spectra in Europe. Earthquake Engineering & Structural Dynamics 25, 401-412.

Anderson, J.G. & S.E. Hough (1984). A model for the shape of the Fourier amplitude spectrum of acceleration at high frequencies. Bulletin of the Seismological Society of America 74, 1969-1993.

Ansary, M.A., Yamazaki, F. & Katayama, T. 1995: Statistical analysis of peaks and directivity of earthquake ground motion. Earthquake Engineering & Structural Dynamics 24, 1527-1539.

Atkinson, G.M. & Boore, D.M. 1995: Ground-motion relations for eastern North America. Bulletin of the Seismological Society of America 85/1, 17-30.

Atkinson, G.M. & Boore, D.M. 1997: Some comparisons between recent ground-motion relations. Seismological Research Letters 68/1, 24-40.

Bay, F. (2002). Ground motion scaling in Switzerland: Implications for hazard assessment. PhD Thesis, ETH, Zurich.

Bay, F., Fäh, D., Malagnini, L. & Giardini, D. 2003: Spectral shear-wave ground-motion scaling in Switzerland. Bulletin of the Seismological Society of America 93/1, 414-429.

Becker, A.M. & Abrahamson, N.A. 1998: Stress drops in extensional regimes (abstract). Seismological Research Letters 69, 172.

Berge-Thierry, C., Griot-Pommera, D-A., Cotton, F. & Fukushima, Y. 2000: New empirical spectra spectral attenuation laws for moderate European earthquakes. Submitted to Journal of Earthquake Engineering (originally published in French as Rapport IPSN/DPRE, SERG/00-53, with slightly different author list).

Bommer, J.J. 2002: Deterministic vs. probabilistic seismic hazard assessment: an exaggerated and obstructive dichotomy. Journal of Earthquake Engineering 6 (special issue 1), 43-73.

Bommer, J.J., Georgallides, G. & Tromans, I.J. 2001: Is there a near-field for small-to-moderate magnitude earthquakes? Journal of Earthquake Engineering 5/3, 395-423.

Boore, D.M. & Joyner, W.B. 1997: Site amplifications for generic rock sites. Bulletin of the Seismological Society of America 87/2, 327-341.

Boore, D.M., Joyner, W.B. & Wennerberg, L. 1992: Fitting the stochastic ω^2-source model to observed response spectra in western North America: trade-offs between $\Delta\sigma$ and κ. Bulletin of the Seismological Society of America 82, 1956-1963.

Boore, D.M., Joyner, W.B. & Fumal, T.E. 1993: Estimation of response spectra and peak accelerations from western North American earthquakes: an interim report. US Geological Survey Open-File Report 93-509.

Boore, D.M., Joyner, W.B. & Fumal, T.E. 1994: Estimation of response spectra and peak accelerations from western North American earthquakes: an interim report – Part 2. USGS Open-File Report 94-127.

Boore, D.M., Joyner, W.B. & Fumal, T.E. 1997: Equations for estimating horizontal response spectra and peak acceleration from western North American earthquakes: a summary of recent work. Seismological Research Letters 68/1, 128-153.

Borcherdt, R.D. 1994: Estimates of site-dependent response spectra for design (methodology and justification). Earthquake Spectra 10/4, 617-653.

Bozorgnia, Y. & Campbell, K.W. 2002: Vertical-to-horizontal response spectra ratio and the vertical design spectrum. Submitted to Earthquake Spectra.

Bungum, H., Lindholm, C.D. & Dahle, A. 2002: Long-period ground-motions for large European earthquakes, 1905-1992, and comparisons with stochastic predictions. Journal of Seismology, in press.

Campbell, K.W. 1981: Near-source attenuation of peak horizontal acceleration. Bulletin of the Seismological Society of America 71/6, 2039-2070.

Campbell, K.W. 1997: Empirical near-source attenuation relationships for horizontal and vertical components of peak ground acceleration, peak ground velocity, and pseudo-absolute acceleration response spectra. Seismological Research Letters 68/1, 154-179.

Campbell, K.W. & Bozorgnia, Y. 2002: Updated near-source ground motion relations for the horizontal and vertical components of peak ground acceleration and acceleration response spectra. Submitted to the Bulletin of the Seismological Society of America.

Chang, T., Cotton, F. & Angelier, J. 2001: Seismic attenuation and peak ground acceleration in Taiwan. Bulletin of the Seismological Society of America 91/5, 1229-1246.

Dobry, R., Borcherdt, R.D., Crouse, C.B., Idriss, I.M., Joyner, W.B., Martin, G.R., Power, M.S., Rinne, E.E. & Seed, R.B. 2000: New site coefficients and site classification system used in recent building seismic code provisions. Earthquake Spectra 16/1, 41-67.

Douglas, J. 2001: A critical reappraisal of some problems in engineering seismology. PhD Thesis, Imperial College, London.

Douglas, J. & Smit, P.M. 2001: How accurate can strong ground motion attenuation relations be? Bulletin of the Seismological Society of America 91/6, 1917-1923.

Free, M.W. 1996: The attenuation of earthquake strong-motion in intraplate regions. PhD Thesis, Imperial College, London.

Fukushima, Y. 1996: Scaling relations for strong ground motion prediction models with M^2 terms. Bulletin of the Seismological Society of America 86/2, 329-336.

Haberland, Ch. & Rietbrock, A. 2001: Attenuation tomography in the western Central Andes: a detailed insight into the structure of a magmatic arc. Journal of Geophysical Research 106, 11151-11167.

Hanks, T.C. 1982: f_{max}. Bulletin of the Seismological Society of America 73, 1867-1879.

Hanks, T.C. & Kanamori, H. 1979: A moment magnitude scale. Journal of Geophysical Research 77/23, 4393-4405.

Heaton, T., Tajima, F. & Mori, A.W. 1986: Estimating ground motions using recorded accelerograms. Surveys in Geophysics 8, 25-83.

Ide, S. & Beroza, G.C. 2001: Does apparent stress vary with earthquake size? Geophysical Research Letters 28/17, 3349-3352.

Johnston, A.C., Coppersmith, K.J., Kanter, L.R. & Cornell, C.A. 1994: The earthquakes of stable continental regions. EPRI Technical Report TR-102261, vol. 1, Electric Power Research Institute, Palo Alto, California.

Lussou, P., Bard, P.Y., Cotton, F. & Fukushima, Y. 2001: Seismic design regulation codes: contribution of K-Net data to site effect evaluation. Journal of Earthquake Engineering 5/1, 13-33.

Mayeda, K. & Walter, W.R. 1996: Moment, energy, stress drop, and source spectra of western United States earthquakes from regional coda envelopes. Journal of Geophysical Research 101/B5, 11195-11208.

McVerry, G.H., Zhao, J.X. Abrahamson, N.A. & Somerville, P.G. 2000: Crustal and subduction zone attenuation relations for New Zealand earthquakes. Proceedings of the Twelfth World Conference on Earthquake Engineering, Auckland, Paper No. 1834.

Papageorgiou, A.S. & Aki, K. 1983: A specific barrier model for the quantitative description of inhomogeneous faulting and the prediction of strong ground motion. I: Description of the model. Bulletin of the Seismological Society of America 73, 693-722.

Restrepo-Vélez, L.F. & Bommer, J.J. 2003: An exploration of the nature of the scatter in ground-motion prediction equations and the implications for seismic hazard assessment. Journal of Earthquake Engineering 7 (special issue no. 1), 171-199.

Rietbrock, A. 2001: P-wave attenuation structure in the fault area of the 1995 Kobe earthquake. Journal of Geophysical Research 106, 4141-4154.

Sabetta, F. & Pugliese, A. (1987). Attenuation of peak horizontal acceleration and velocity from Italian strong-motion records. Bulletin of the Seismological Society of America 77, 1491-1513.

Sabetta, F. & Pugliese, A. 1996: Estimation of response spectra and simulation of nonstationary earthquake ground motions. Bulletin of the Seismological Society of America 86/2, 337-352.

Scherbaum, F., Schmedes, J. & Cotton, F. 2003: On the conversion of source-to-site distance measures for extended earthquake fault models. Submitted to Bulletin of the Seismological Society of America.

Scholz, C.H. 1990: The Mechanics of Earthquakes and Faulting. Cambridge University Press.

Silva, W., Darragh, R., Gregor, N., Martin, G., Abrahamson, N. & Kircher, C. 1998: Reassessment of site coefficients and near-fault factors for building code provisions, Program Element: II. Report 98-HQ-GR-1010.

Singh, S.K. & Ordaz, M. 1994: Seismic energy release in Mexican subduction zone earthquakes. Bulletin of the Seismological Society of America 84, 1533-1550.

Smit, P. 1998: Strong motion attenuation model for Central Europe. Proceedings of the Eleventh European Conference on Earthquake Engineering, Paris.

Somerville, P., Collins, N., Abrahamson, N., Graves, R. & Saikia, C. 2001: Ground motion attenuation relations for the Central and Eastern United States. USGS Report, Award #99HQGR0098.

Spudich, P., Joyner, W.B., Lindh, A.G., Boore, D.M., Margaris, B.M. & Fletcher, J.B. 1999: SEA99: a revised ground motion prediction relation for use in extensional tectonic regimes. Bulletin of the Seismological Society of America 89/5, 1156-1170.

Stepp, J.C., Wong, I., Whitney, J., Quittmeyer, R., Abrahamson, N., Toro, G., Youngs, R., Coppersmith, K., Savy, J., Sullivan, T. & Yucca Mountain PSHA Project Members 2001: Probabilistic seismic hazard analyses for ground motions and fault displacements at Yucca Mountain, Nevada. Earthquake Spectra 17/1, 113-151.

Stirling, M.W., McVerry, G.H. & Berryman, K.R. 2002: A new seismic hazard model for New Zealand. Bulletin of the Seismological Society of America 92, 1878-1903.

Toro, G.R, Abrahamson, N.A. & Schneider, J.F. 1997: Model of strong ground motions from earthquakes in Central and Eastern North America: best estimates and uncertainties. Seismological Research Letters 68/1, 41-57.

Westaway, R. & Smith, R.B. 1989: Strong ground motion in normal-faulting earthquakes. Geophysical Journal 96, 529-559.

Willmore, P.L. 1979: Manual of seismological observatory practice. World Data Center for Solid Earth Physics Report SE-20, US Department of Commerce.

Wills, C.J., Petersen, M., Bryant, W.A., Reichle, M., Saucedo, G.J., Tan, S., Taylor, G. & Treiman, J. 2000: A site-condition map for California based on geology and shear-wave velocity. Bulletin of the Seismological Society of America 90/6B, S187-S208.

Youngs, R.R, Abrahamson, N., Makdisi, F.I. & Sadigh, K. 1995: Magnitude-dependent variance of peak ground acceleration. Bulletin of the Seismological Society of America 85/4, 1161-1176.

APPENDIX 1: ORIGINAL SCHEME FOR SITE CONDITION ADJUSTMENT

At WS-4 / SP2, a decision was taken to completely revise the way in which the candidate attenuation equations would be adjusted to a common reference site. Originally each expert was to devise their own scheme, including the selection of the an appropriate reference site, which would define the hand-over point to SP3 to then perform site response analyses for each of the four nuclear power sites. However, most experts were selecting reference sites with shear wave velocities of the order of 1,000 m/s and using relatively crude schemes to adjust the median predictions from the various attenuation equations to this condition, whereas the first step in the SP2 process will be to adjust the ground motion estimates to a reference velocity of 2,000 m/s. The SP2 experts proposed that this approach was flawed for two reasons:

- There seemed to be no point in making an adjustment to an arbitrarily chosen reference site only for SP3 to then make a second adjustment to 2,000 m/s.
- The simplified adjustments being made by the SP2 experts were judged to be introducing an unwarranted level of approximation when the expertise of SP3 could be used to make more robust site adjustments.

The TFI team agreed to revise the approach so that SP2 would simply define reference site velocities for each of the candidate equations and then hand over to SP3 to make the adjustments directly to the reference condition of 2,000 m/s. The new scheme is presented in Sections 3.3 and 3.4. However, the scheme originally devised is retained in this appendix, primarily to support commentaries made in different parts of the Elicitation Summary for which site conditions are a relevant issue.

A 1.1 References Site Conditions for Candidate Equations

The different attenuation equations employed in the logic-tree do not use the same site classifications and there is no single category of site condition that could be used that would be providing predictions for essentially the same soil conditions. Since the local surface geology can exert a significant effect on the amplitudes of ground motions, the differences amongst the various site classification schemes is considered too important to be ignored. The procedure that is followed is to select a reference rock site condition, defined by an average shear wave velocity over the upper 30 m at the site, $V_{s,30}$. Then, for each attenuation equation, the most appropriate site class is selected to match the reference condition, but noting the most likely average $V_{s,30}$ value for that class. Finally, factors are applied to adjust for any differences between the average shear wave velocity for the site class of the equation and the reference value.

The reference rock site has been chosen to have an average shear wave velocity of 1,000 m/s over the uppermost 30 metres. This classification corresponds unambiguously to a rock site; it is almost twice as high as the value I originally used for the preliminary elicitation. The fundamental reason for adopting this increased value for $V_{s,30}$ of 1 km/s is that this was the assumed site condition that has been employed in the simulations to define upper bounds on ground motions (Chapters 6 and 7). In order not to have to make adjustments to the upper bounds in order to make them compatible with the median predictions of ground, it has been decided that the simplest approach is to adopt the same shear wave velocity as the reference site.

There is an additional advantage in using this higher value of $V_{s,30}$ in that when the lower value of 550 m/s was employed for the preliminary elicitation, some rather large adjustments became necessary, particularly because of the generic 'hard rock' condition used for the three ENA

attenuation equations employed. By using a stiffer reference site, the corresponding adjustments, and the uncertainty that accompanies them, is reduced.

Table A1-1 presents the selected site class for each of the 12 attenuation equations, indicating the definition provided in the relevant study, in terms of $V_{s,30}$ values, and the value judged to be a representative "average" value for that site class. The final column indicates the degree of confidence attached to the assignation of the chosen average $V_{s,30}$ value, as low, medium or high. The selection of the average $V_{s,30}$ values and the degrees of confidence are explained in the remainder of this sub-section.

Tab. A1-1: Selected site classes for candidate attenuation relations

Study	Class	Definition	$V_{s,30}$ [m/s]	Confidence
Abrahamson & Silva (1997)	Rock	$V_{s,30} > 600$ m/s or shallow soil	620	Low
Ambraseys et al. (1996)	Rock	$V_{s,30} > 750$ m/s	1,000	Medium
Ambraseys & Douglas (2003)	Rock	$V_{s,30} < 750$ m/s	850	Medium
Atkinson & Boore (1997)	Hard rock	$V_{s,30} = 2{,}800$ m/s	2,800	High
Berge-Thierry et al. (2000)	Rock	$V_{s,30} > 800$ m/s	1,000	Low
Boore et al. (1997)	Class A	$V_{s,30} > 750$ m/s	1,000	High
Campbell & Bozorgnia (2002)	Firm rock	$555 < V_{s,30} < 1{,}000$ m/s	620	Low
Lussou et al. (2001)	Class A	$V_{s,30} > 800$ m/s	1,000	Low
Sabetta & Pugliese (1996)	Stiff	$V_{s,30} > 800$ m/s	1,000	Medium
Somerville et al. (2001)	Hard rock	$V_{s,30} = 2{,}830$ m/s	2,830	High
Spudich et al. (1999)	Rock	$V_{s,30} > 620$ m/s	750	Low
Toro et al. (1997)	Hard rock	$V_{s,30} = 1{,}830$ m/s	2,830	High

The study of Abrahamson & Silva (1997) uses two categories, rock and soil, the former combining rock sites ($V_s > 600$ m/s) and sites with up to 20 m soil overlying rock. In line with other studies that use the value to define 'rock', the assumed average value is 620 m/s. This value is supported by the average shear wave velocity profile for western US stations reported in Pegasos document TP2-TN-0254. The inclusion of soil layers will tend to reduce the value of $V_{s,30}$, but is also possible that many of the rock sites are much stiffer and have shear wave velocities much higher than 600 m/s. Therefore, it is assumed that the confidence that can be attached to the selected value of 620 m/s is low.

The study of Ambraseys et al. (1996) defines three site categories and the rock category corresponds to sites with shear wave velocities higher than 750 m/s. The average shear wave velocity profiles for strong-motion stations in Italy, Greece, Iran, Yugoslavia and Turkey – which are the principal sources of data used for this study – indicate that a value of 1,000 m/s is probably a reasonable estimate for 'rock' sites in the European and Middle Eastern area. For this reason, the value of 1,000 m/s is assigned. However, not many of the stations are actually classified on the base of shear wave velocity profiles and the distribution of actual $V_{s,30}$ values in each class the Ambraseys et al. data set is not well known. As a consequence, the confidence is medium.

The study of Ambraseys & Douglas (2000), which uses the same site classification scheme as Ambraseys et al. (1996), uses a worldwide rather than European dataset, with western North American data dominating (72 % of the records). Since for many of the sites there is actually a shear wave velocity profile available and since there are several European records (22 %) the value is likely to be higher that for the Abrahamson & Silva (1997) study. The assigned value is

taken to be 850 m/s, as a value between those assigned to Ambraseys et al. and to Abrahamson & Silva. However, the distribution of $V_{s,30}$ values within the rock stations is not known, hence the confidence is medium.

The study of Atkinson & Boore (1997), in common with the studies of Somerville et al. (2001) and Toro et al. (1997), are stochastic simulations for a particular reference site (very hard rock), hence there is a high degree of confidence in the site class and the shear wave velocity of 2,800 or 2,830 m/s.

The study of Berge-Thierry et al. (2000) uses two classes, the selected "rock" class corresponding to sites with values of $V_{s,30}$ in excess of 800 m/s. Despite not being based entirely on European data (17 % of the records come from California), it seems reasonable to apply the same average value as selected for Ambraseys et al. (1996), 1,000 m/s, but reflecting the mixed data set to assign low confidence.

The study of Boore et al. (1997) is unique in that it uses the actual value of $V_{s,30}$ to characterise the site rather than classes, based discrete bands of shear wave velocity, with corresponding coefficients. Figure A1-1 shows the histogram of the $V_{s,30}$ values used in their regressions, which shows that the reference value of 1,000 m/s, although not strongly represented, is a good average for the class A records. Due to the fact that the specific value of $V_{s,30}$ corresponding to the reference site can be applied in the equation means that the confidence is high.

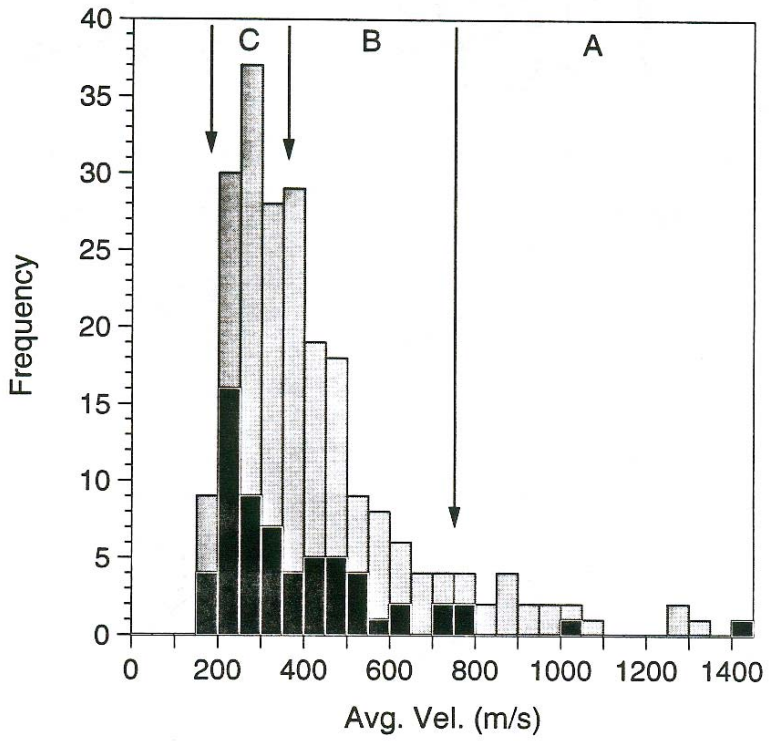

Fig. A1-1: Histogram of average shear wave velocities from Boore et al. (1994)

The black bars represent the data actually used to determine the dependence of the spectral ordinates on the shear-wave velocity; the grey bars represent the distribution of the published shear-wave velocity data.

The study of Campbell & Bozorgnia (2002) uses four site classes, of which the most appropriate for this application is "firm rock". The authors state that the mean and standard deviations of the 30 m-shear wave velocity of this class can be taken to correspond approximately to the BC class defined by Wills et al. (2000). The latter study reports that BC sites, on the basis of 38 profiles,

correspond to $V_{s,30}$ values in the range of 555 to 1,000 m/s, with mean value of 724 m/s and a median value of 583 m/s; the standard deviation is given as 368 m/s. Since the median is the more relevant measure and in view of the fact that the equivalence with the Campbell & Bozorgnia (2002) "firm rock" category is only approximate, it is decided to adopt a value of 620 m/s. Since no information on the distribution of the Campbell & Bozorgnia (2002) data set with respect to actual $V_{s,30}$ values is given and since there is considerable scatter in the measured shear wave values from a limited number of profiles, a low level of confidence is finally assigned.

For the study of Lussou et al. (2001) the selected site class is A, corresponding to "rock". The study is based on K-Net data from Japan, for which shear-wave velocity measurements have been made at every station to depths of between 10 and 20 m. The distribution of the shear-wave velocity values at the stations of the network is shown in Figure A1-2. If it were assumed that all stations are equally represented in the dataset used for the regressions, then this distribution can be taken as a surrogate for the shear-wave velocity distribution of the records. The median value is of the order of 900 m/s. Since there are few records from Class A sites it may be assumed that they are not well represented, hence an average value of 1,000 m/s can be adopted and assigned a low level of confidence. A factor preventing higher confidence being assigned is the fact that the shear-wave velocity measurements are made only to depths of between 10 and 20 m rather than the full 30 m; $V_{s,30}$ values were determined by extrapolating the deeper values of shear-wave velocity.

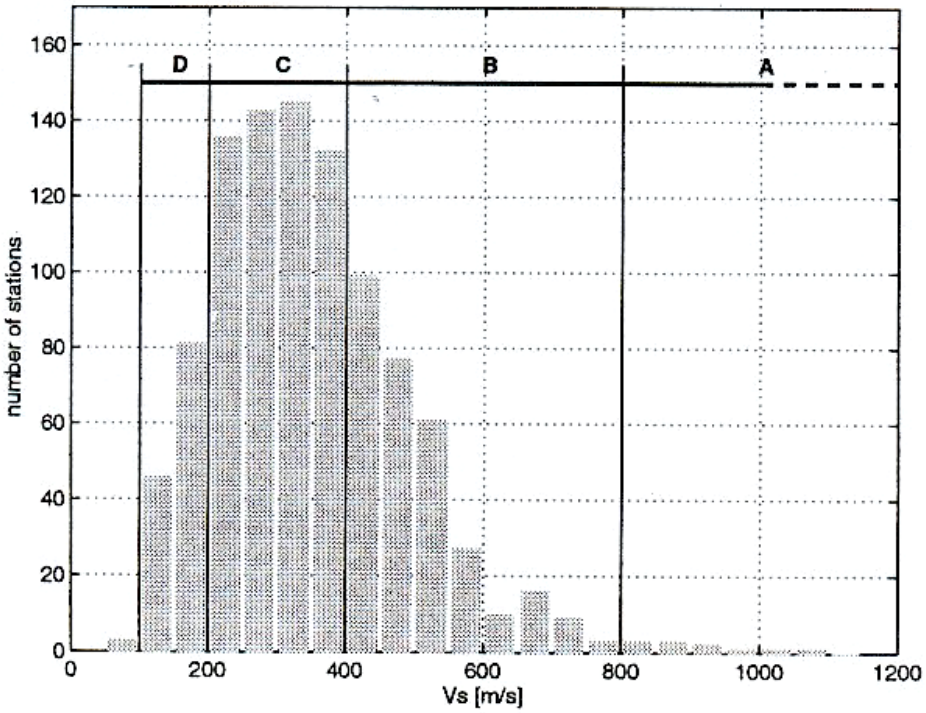

Fig. A1-2: Histogram of average shear wave velocities from the K-Net stations, from which records were used by Lussou et al. (2001)

The study of Sabetta & Pugliese (1996) uses three site classes, the selected class here being "stiff", for which the authors claim that shear-wave velocities are greater than 800 m/s. On the basis of the Italian station profiles presented in TP2-TN-0254, an average value of 1,000 m/s is close to the median shear wave velocity. The geotechnical information on which the classification is based is presented in Sabetta & Pugliese (1987), which implies that the classification of most of the stations is based on geological and geotechnical descriptions rather than direct

measurements of shear-wave velocity. This would suggest that the confidence should be low, but since the spread of V_s values for Italian stations does not appear to be very large, and since the database is in this sense quite homogeneous, the confidence has been assigned as medium.

Finally, the study of Spudich et al. (1999) uses a simple rock-soil classification precisely because shear-wave velocity measurements are not available "*for many recording sites*". For this application, the obvious choice is the "rock" category. Spudich et al. assume that the rock site category can be assumed to be equivalent to a shear-wave-velocity of 620 m/s, as recommended by Boore et al. (1997), although their analysis also suggests that this value is probably too low (although an alternative, higher value is not recommended). Therefore, a higher value of $V_{s,30}$ is selected to represent the average of this class (750 m/s), and a low confidence is assigned.

It is important to acknowledge clearly that most of the assigned $V_{s,30}$ values are judged and therefore carry a degree of uncertainty. The degrees of confidence assigned to each value reflect the likelihood of this being the correct value. The degree, or lack, of confidence in the selected value of $V_{s,30}$ is handled in the same way for every equation, by having three branches, in which the chosen value takes the central branch and is assigned a weight of 0.60. Alternative higher and lower values are assigned values of 0.20 each; the degree of confidence is reflected by the differences between the $V_{s,30}$ values. For those equations for which the confidence in the average $V_{s,30}$ value was judged to be high, no branching is needed and the single value from Table A1-1 is assigned a weight of 1.0.

For the remaining relationships, the upper and lower values are roughly symmetrical about the central value unless the data and distributions discussed above suggest that there is greater likelihood of being on one side or the other. For example, for the equations of Abrahamson & Silva (1997) and Spuidich et al. (1999), the increase in shear wave velocity from the "average" to the upper value will be greater than the difference between the "average" and the lower estimate. The profiles presented in TP2-TN-0254 have also been taken into account in assigning these ranges. The selected values are summarised in Table A1-2 below.

Tab. A1-2: Selected $V_{s,30}$ values for candidate attenuation relations

Study	$V_{s,30}$ (m/s)		
	Lower (w = 0.2)	Central (w = 0.6)	Upper (w = 0.2)
Abrahamson & Silva (1997)	570	620	850
Ambraseys et al. (1996)	900	1,000	1,100
Ambraseys & Douglas (2000)	750	850	1,000
Berge-Thierry et al. (2000)	800	1,000	1,200
Campbell & Bozorgnia (2002)	570	620	850
Lussou et al. (2001)	800	1,000	1,250
Sabetta & Pugliese (1996)	850	1,000	1,100
Spudich et al. (1999)	620	750	1,100

A 1.2 Adjustments to Reference Value of $V_{s,30}$ for Horizontal Component

Since there are differences between many of the $V_{s,30}$ values indicated as representative for each attenuation equation in Table A1-1 and the reference value of 1,000 m/s, adjustments need to be applied to "normalise" the ground-motion predictions to the common reference site conditions. On the one hand, there will be the effect of de-amplification or amplification resulting from the differences in the stiffness of the sites with respect to the reference site. On the other hand, there is the effect of greater or lesser attenuation of high-frequency motions due to differences in the value of kappa. The adjustment needs to consider both of these effects simultaneously.

One model available as the basis for these conversions are the equations of Boore et al. (1997), which characterise sites by their actual value of $V_{s,30}$. If SA_{ref} is the spectral ordinate at the reference site (with $V_{s,30}$ = 1,000 m/s) and SA_{site} is the spectral ordinate at the site with the shear-wave velocity indicated in Table A1-2, then the transformation to be applied is:

$$SA_{ref} = SA_{site}\left(\frac{1000}{V_{s,30}}\right)^{B_V} \tag{A1.1}$$

The values of B_V for the selected response frequencies can be taken directly from the paper of Boore et al. (1997); these are reproduced herein in Table A1-3.

Tab. A1-3: Values of B_V from Boore et al. (1997) for use in Eq.(A1-1)

Frequency [Hz]	0.5	1.0	2.5	3.3	5.0	6.7	10	20	33	50	PGA
Period (s)	2.0	1.0	0.4	0.3	0.2	0.15	0.10	0.05	0.03	0.02	PGA
$-B_V$	0.655	0.698	0.487	0.401	0.292	0.238	0.212	-	-	-	0.371

An immediate problem that becomes apparent is that this scheme does not provide adjustments for response ordinates at 20, 33 and 50 Hz. As is shown in Section 3.7 of this Elicitation Summary, the ordinates of spectral acceleration can be assumed to be the same at 50 and 100 Hz, and in the Pegasos project the response at 100 Hz is being taken as equivalent to PGA. Therefore, the values of B_V that need to be inferred somehow are those at 20 Hz and 33 Hz.

As is discussed in Section 3.7, very few of the candidate equations include coefficients for frequencies higher than 10 Hz and only those of Abrahamson & Silva (1997) and Lussou et al. (2001) cover frequencies higher than 33 Hz. Using the latter study, spectral amplifications of different soil classes with respect to "rock" sites can be inferred from the following equation:

$$SA_{ref} = SA_{site}.10^{[c(A,f)-c(S,f)]} \tag{A1.2}$$

where c(A,*f*) is the constant term for site Class A at frequency *f* and c(S,*f*) is the corresponding coefficient for site Class S.

From Figure A1-2, the mean shear wave velocity for Class A is 1,000 m/s, for Class B 600 m/s, and for Class C 300 m/s. Figure A1-3 shows the adjustment factors that this implies to transpose spectral ordinates estimated for sites of Class B and C to the reference site of Class A. The curve for 600 m/s (Class B), which is the more relevant herein, indicates that from 20 Hz the factor remains almost constant at a value slightly higher than that at 10 Hz. Figure A1-4 shows similar curves derived using Eq. (A1-1) and the values in Table A1-3.

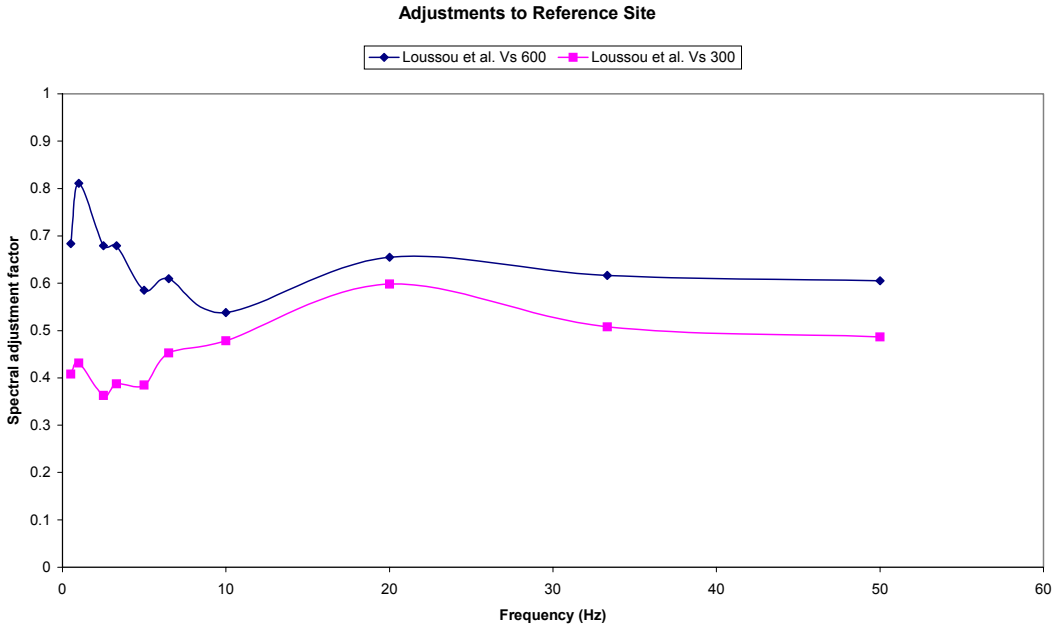

Fig. A1-3: Inferred spectral adjustment factors using the equations of Lussou et al. (2001)

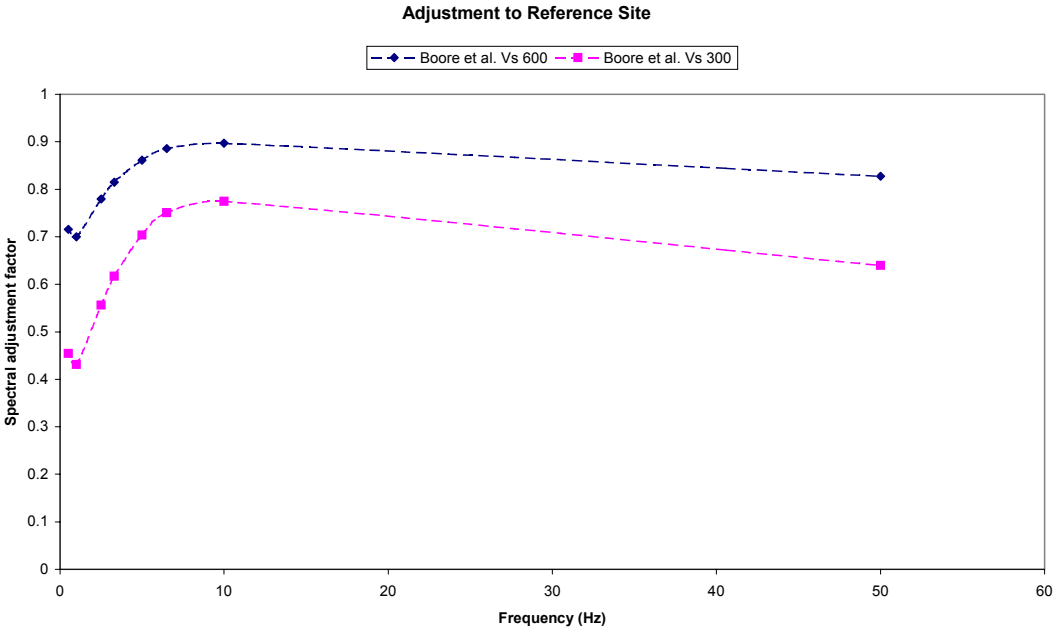

Fig. A1-4: Inferred spectral adjustment factors using the equations of Boore et al. (1997)

In Figure A1-4, the lines are shown dashed since they are not constrained between 10 Hz and 50 Hz. The values of the adjustment are higher than those found from Lussou et al. (2001), although for the 600 m/s site this may in part be due to the fact that the median value of $V_{s,30}$ for the Lussou et al. (2001) Class B is actually lower than 600 m/s, as can be seen in Figure A1-2. The trends of the factors with frequency are also different between the two studies, but it seems reasonable to assume that acceptable estimates of the appropriate B_V values at 20 Hz and 33 Hz could be inferred from the values indicated by the dashed lines in Figure A1-4. This yields values of -0.251 and -0.302 respectively. There is clearly an appreciable level of uncertainty

associated with these values, and the differences between the adjustment factors in Figures A1-3 and A1-4 also reflect the uncertainty associated with this adjustment.

A shortcoming with the Boore et al. (1997) amplification factors is the fact that they do not account for soil non-linearity since the amplification factors are independent of the amplitude of the motion. One scheme that could be used to infer non-linear soil responses is that derived by Borcherdt (1994) and now incorporated into the NEHRP guidelines and the 1997 edition of UBC (Dobry et al. 2000). Table A1-5 shows the classification of sites in these new codes in terms of ranges of shear-wave velocities, from which it can be inferred that the reference site of 1,000 m/s shear wave velocity can be taken as equivalent to Class B.

The NEHRP provisions provide amplification factors, F_A and F_V, for scaling the response spectral ordinates for class B at periods of 0.3 and 1.0 second as a function of the actual level of the spectral ordinate, as shown in Table A1-5.

Another scheme that includes non-linear effects is that of Abrahamson & Silva (1997), in which the ratio of the spectral ordinate at a soil site to that at a rock site is given by the equation:

$$SA_{soil} = SA_{rock} . e^{[a_{10} + a_{11} . \ln(PGA + c_5)]} \quad \text{(A1.3)}$$

For a response period of 0.3 seconds, Table A1-6 compares the adjustments to the reference "rock" site obtained from the Boore et al. (1997) factors, the NEHRP factors in Table A1-5 and from the Abrahamson & Silva (1997) scheme. For the NEHRP classes, the V_s value is simply taken as the mean of the range defined in Table A1-4.

Tab. A1-4: Site classification in 1997 NHERP provisions

Site Class	Description	Shear-wave velocity (m/s)	
		Lower Limit	Upper Limit
A	Hard rock	1500	-
B	Rock	760	1500
C	Very dense soil & soft rock	360	760
D	Stiff soils	180	360
E	Soft soils	-	180

A number of observations and comments can be made regarding the values reported in Table A1-6. Firstly, the conversions for Class D sites are not particularly relevant since the lowest $V_{s,30}$ values in Table A1-2 correspond to Class C sites. The NEHRP factors are designed specifically to provide safe (i.e. conservative) estimates of soil amplification effects for the purpose of obtaining design spectra. As a result, the adjustments from soil to rock sites inferred from these factors are likely to be too small, although for Class C they are consistently higher than those obtained from Boore et al. (1993). This would tend to suggest that the values obtained from Boore et al. (1993) could be close to reliable best estimates.

Tab. A1-5: Soil amplification factors from 1997 NEHRP provisions

(a) Short period site coefficient F_a

Site Class Or Soil Profile Type	Mapped Rock Shaking Level at Short Periods				
	$S_s \leq 0.25$	$S_s = 0.50$	$S_s = 0.75$	$S_s = 1.00$	$S_s \geq 1.25$
	$A_a \leq 0.10$	$A_a = 0.20$	$A_a = 0.30$	$A_a = 0.40$	$A_a \geq 0.50$
A	0.8	0.8	0.8	0.8	0.8
B	1.0	1.0	1.0	1.0	1.0
C	1.2	1.2	1.1	1.0	1.0
D	1.6	1.4	1.2	1.1	1.0
E	2.5	1.7	1.2	0.9	*
F	*	*	*	*	*

(b) Long period site coefficient F_v

Site Class or Soil Profile Type	Mapped Rock Shaking Level at Long Periods				
	$S_1 \leq 0.10$	$S_1 = 0.20$	$S_1 = 0.30$	$S_1 = 0.40$	$S_1 \geq 0.50$
	$A_v \leq 0.10$	$A_v = 0.20$	$A_v = 0.30$	$A_v = 0.40$	$A_v \geq 0.50$
A	0.8	0.8	0.8	0.8	0.8
B	1.0	1.0	1.0	1.0	1.0
C	1.7	1.6	1.5	1.4	1.3
D	2.4	2.0	1.8	1.6	1.5
E	3.5	3.2	2.8	2.4	*
F	*	*	*	*	*

(*) Site-specific geotechnical investigation and dynamic site response analyses shall be performed

Tab. A1-6: Adjustment factors of spectral ordinates (at 0.3 seconds) to reference site

PGA	A&S97	Class A (1500 m/s)		Class C (560 m/s)		Class D (270 m/s)	
(g)	"soil"	BJF97	NEHRP	BFJ97	NEHRP	BJF97	NEHRP
0.1	0.836	1.177	1.25	0.793	0.833	0.592	0.625
0.2	0.935	1.177	1.25	0.793	0.833	0.592	0.714
0.3	1.003	1.177	1.25	0.793	0.909	0.592	0.833
0.4	1.056	1.177	1.25	0.793	1.0	0.592	0.909
0.5	1.010	1.177	1.25	0.793	1.0	0.592	1.0

Another interesting observation from Table A1-5 is that, as would be expected, the relative amplifications between hard rock (Class B) and very hard rock (Class A) are not affected by non-linearity. The difference between the NEHRP and Boore et al. (1997) factors is small and since the NEHRP factor is again probably conservative, this lends further support to the Boore et al. (1997) factors. However, it is important to note that the highest $V_{s,30}$ value in the data set of Boore et al. (1997) is 1,400 m/s, so the extrapolation of their amplification factors to such sites may not be appropriate. An alternative treatment for the Class A sites is discussed below.

One issue that remains to be addressed is the question of differences at high frequencies ($> f_{max}$) due to differences in kappa values, which is not accounted for in the amplification factors considered this far. The largest effect due to differences in kappa will be with respect to the ENA equations of Atkinson & Boore (1997), Somerville et al. (2001) and Toro et al. (1997). However, the method applied to adjust for the high-frequency diminution should be consistent

with derivation of the amplification factors. Boore & Joyner (1997) report significant reductions in high-frequency amplitudes as a result of changes in kappa but they also find relative amplifications on Californian generic rock sites almost three times greater than those on generic ENA very hard rock sites. Therefore, simply calculating ratios of diminution factors from appropriate kappa values for rock sites with shear wave velocities of 1,000 m/s and 2,800 m/s, and combining these with the amplification factors indicated in Table A1-5 would not be appropriate.

Atkinson & Boore (1997) suggest a procedure for converting from California rock sites to ENA rock sites, which accounts for impedance contrast (ignoring differences in rock density) and the "kappa effect" on high-frequency diminution. For the application required here, this results in the following equation, which is quite different from Eq.(A1-1):

$$SA_{ref} = SA_{ENA.}\sqrt{\frac{2800}{V_A}}.\exp(-\pi f/100) \qquad \text{(A1.4)}$$

where V_A is the reference rock velocity for California from Boore et al. (1994), which are essentially the same values as those reported by Boore et al. (1997). The resulting values of the adjustment to be applied to the spectral ordinates from the ENA equations are given in Table A1-7.

Tab. A1-7: Adjustment factors to be applied to spectral ordinates from ENA equations

Frequency (Hz)	V_A	Adjustment Factor
0.5	1795	1.22
1.0	1406	1.37
2.5	1954	1.11
5.0	2118	0.98
10.0	1112	1.16
20.0	1300[1]	0.78
33.3	1396[1]	0.50
50.0 (PGA)	1396	0.29
100.0 (PGA)	1396	0.06

[1] Inferred values

Since there is uncertainty regarding shear wave velocities at generic "rock" sites in California, and Boore & Joyner (1997) indicate that these are closer to 620 m/s than to 1,000 m/s, the factors in Table A1-7 may need further adjustment. Since the values of V_A used are all greater than 1,000 m/s, the effect of lower rock velocities in California is likely to reduce the effect of diminution. For this reason, and since some of the V_A values have been inferred, ranges of adjustment factors are proposed with weightings as indicated in Table A1-8.

For the remaining nine equations, the adjustments are made using Eq. (A1-1) and the values of B_V given in Table A1-9 below, which are based on those in Table A1-3 but include the inferred values at 20, 33 and 50 Hz, and more or less arbitrary ranges to capture the uncertainty, particularly for the higher frequencies where the B_V values have been inferred. The resulting adjustment factors for a site class with shear-wave velocity of 600 m/s are shown in Fig. A1-5.

Tab. A1-8: Adjustment factors to be applied to spectral ordinates obtained from the equations of Atkinson & Boore (1997), Somerville et al. (2001) and Toro et al. (1997)

Frequency (Hz)	Adjustment Factors to Spectral Ordinates		
	Weight = 0.5	Weight = 0.25	Weight = 0.25
0.5	1.22	1.19	1.25
1.0	1.37	1.35	1.39
2.5	1.11	1.05	1.16
5.0	0.98	0.92	1.04
10.0	1.16	1.00	1.10
20.0	0.78	0.80	0.90
33.3	0.50	0.60	0.7
50.0 (PGA)	0.29	0.4	0.5
100.0 (PGA)	0.06	0.10	0.20

Tab. A1-9: Values of B_V to be used in Eq.(A1-1) to obtain factors to adjust ordinates obtained from of all of the equations other than the three listed in Table 2.9

Frequency (Hz)	B_V		
	Weight = 0.25	Weight = 0.5	Weight = 0.25
0.5	-0.680	-0.655	-0.63
1.0	-0.725	-0.698	-0.65
2.5	-0.520	-0.487	-0.46
5.0	-0.310	-0.292	-0.275
10.0	-0.260	-0.212	-0.17
20.0	-0.30	-0.251	-0.18
33.3	0.40	-0.302	-0.20
50.0 (PGA)	-0.47	-0.371	-0.25
100.0 (PGA)	-0.55	-0.371	-0.27

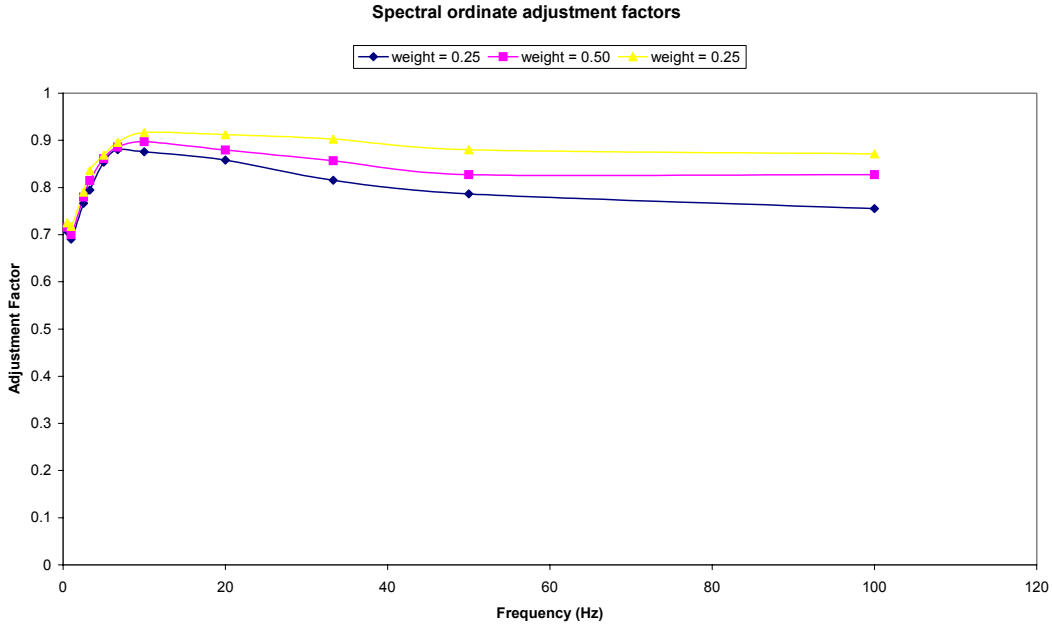

Fig. A1-5: Adjustment factors for spectral ordinates from an equation for which the average $V_{s,30}$ value is 600 m/s, using Eq.(2.1) and the coefficients in Table 2.10

A 1.3 Adjustments to Reference Site $V_{s,30}$ for Vertical Component

The issue of site adjustments is more difficult to resolve for the vertical component, since neither of the resources employed for the horizontal components – Boore et al. (1997) and the NEHRP guidelines – actually give amplification factors for vertical motions. Most studies have found that the effect of site conditions on vertical motions is less pronounced than for horizontal motions (e.g. Ambraseys & Simpson 1996).

In order to explore a possible, albeit unorthodox, method, the ratios of the site coefficients for vertical and horizontal equations are calculated as follows:

$$Ratio = \frac{\frac{Soil_{vertical}}{Rock_{vertical}}}{\frac{Soil_{horizontal}}{Rock_{horizontal}}} \qquad \text{(A1.5)}$$

i.e. it is based on the ratio of actual spectral ordinates, not just site coefficients in the equations that predict the logarithms of the spectral ordinates.

Values of ratio have been determined using the equations for Ambraseys et al. (1996) and Ambraseys & Simpson (1996), which are shown in Figure A1-6, and also using the equations of Lussou et al. (2001), which are shown in Figure A1-7. The soft soil to rock curve is not particularly relevant, since the conversions that are to be applied are more comparable to the transformation from stiff soil to rock. Figure A1-6 suggests that the amplification of vertical motion on stiff soils experiences about 0.9 of the amplification experienced by vertical motions, only reaching higher values (~1.0) at periods of about 0.2 seconds. In Figure A1-7 the most relevant curve is that showing the B-A class ratio and this also indicates that 0.9 is a reasonable average estimate of the ratio of vertical to horizontal site amplification, although the

fluctuations are a little greater than in Figure A1-6. Interestingly, the largest fluctuation is also at 0.2 seconds, but in this case the ratio is reduced to 0.6 at this period.

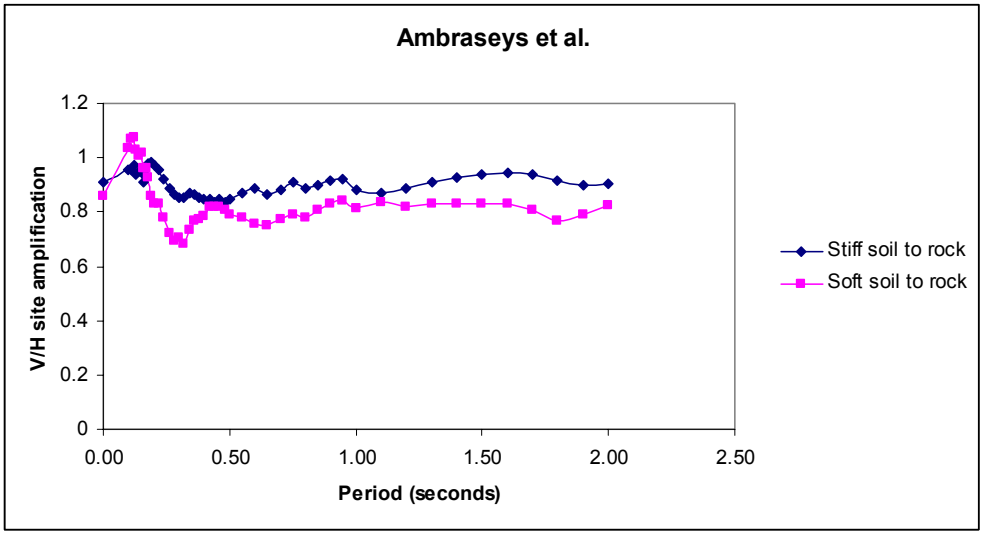

Fig. A1-6: Ratios of vertical-horizontal amplification by soil sites from Ambraseys et al.

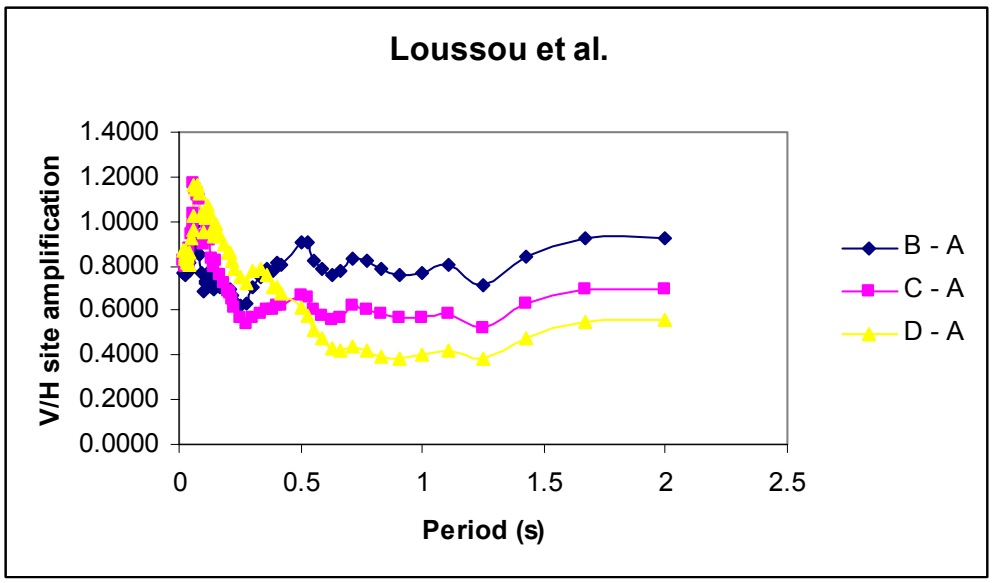

Fig. A1-6: Ratios of vertical-horizontal amplification by soil sites from Lussou et al.

From these curves, the following simple scheme is considered. The factors derived for horizontal motions using Eq.(A1-1) and the values in Table A1-9 could be applied adjusted by factors corresponding to the ratio of about 0.9 inferred from Figures A1-6 and A1-7. This could be achieved by branching at each frequency and each value of B_V to apply values of say 1.0, 1.1 and 1.2 to the adjustment factors, giving these weights of 0.25, 0.50 and 0.25, for example. However, this would result in a logic-tree with a huge number of branches since for each of 7 equations there would be 9 branches just to apply the adjustment factors, meaning that this step alone would require 63 branches on the logic-tree for each of the 11 frequencies. This is considered excessively cumbersome, especially since an improved scheme for this adjustment may yet be encountered.

Therefore, in conclusion, the procedure is simply to use the same adjustment factors as for the horizontal motions, from Eq.(A1-1) and Table A1-9, but multiplying these values by the reciprocal of 0.9, which for this purpose can be taken as 1.10.

APPENDIX 2: HAZARD INPUT DOCUMENT TP2-HID-0027 EXPERT MODEL J. BOMMER

A 2.1 Introduction

This document describes the implementation and parameterization of Julian Bommer's expert model EG2-EXM-0023, as described in the Elicitation Summary EG2-ES-0037 and delivered on 30.05.2003. The purpose of this document is to translate the expert's evaluation of ground motion into an input useable by the hazard software.

A 2.2 Model Implementation

Based on J. Bommer's Elicitation Summary EG2-ES-0037, the logic trees for the median horizontal ground motion, the vertical/horizontal ratio and the aleatory variability of the horizontal component were implemented in FORTRAN and the results displayed graphically.

Key elements in J. Bommer's model are given below (Table A2-1).

Median horizontal ground motion

- 12 of the candidate models have been retained see below:

Tab. A2-1: Final weights for median horizontal motions at all frequencies

	$M_w < 5.5$			$5.5 < M_w < 6.5$			$6.5 < M_w < 7.5$		
	< 10	10–60	> 60	< 10	10–60	> 60	< 10	10–60	> 60
Abrahamson & Silva	0.1141	0.1087	0.1250	0.1292	0.1282	0.1173	0.1406	0.1543	0.1400
Ambraseys et al.	0.0962	0.1019	0.1055	0.0872	0.0962	0.0990	0.0844	0.0926	0.1050
Ambraseys & Douglas	0.1141	0.0109	0.0000	0.1033	0.0103	0.0000	0.1125	0.0123	0.0000
Atkinson & Boore	0.0000	0.0978	0.1406	0.0000	0.0673	0.1188	0.0000	0.0417	0.1134
Berge-Thierry et al.	0.1038	0.1060	0.1016	0.0294	0.0583	0.0858	0.0064	0.0361	0.0819
Boore et al.	0.0699	0.0666	0.0656	0.0904	0.0898	0.0616	0.0984	0.1080	0.0735
Campbell & Bozorgnia	0.2281	0.1630	0.0250	0.2583	0.1539	0.0235	0.2813	0.1852	0.0280
Lussou et al.	0.0000	0.0489	0.0469	0.0000	0.0242	0.0356	0.0000	0.0000	0.0000
Sabetta & Pugliese	0.1069	0.1019	0.1055	0.0969	0.0962	0.0990	0.0527	0.0579	0.0525
Somerville et al.	0.0257	0.0245	0.0422	0.0775	0.0962	0.1320	0.0844	0.1158	0.1575
Spudich et al.	0.0556	0.0883	0.1016	0.0504	0.0833	0.0953	0.0548	0.0803	0.0910
Toro et al.	0.0856	0.0815	0.1406	0.0775	0.0962	0.1320	0.0844	0.1158	0.1575

- For the weighting of the ground motion models, the magnitude – distance plane is subdivided into 9 bins with the following limits:
- Magnitude: $5 \le M < 5.5$, $5.5 \le M < 6.5$, $6.5 \le M < 8$
- Distance [km]: $0 \le R < 10$, $10 \le R < 60$, $r \ge 60$

– To adjust the models to the SP3 reference shear wave velocity of 2000 m/s, ground motion is scaled by factors based on Scherbaum's generic rock profiles and detailed in TP2-TN-0363 (Résonance 2003). Three branches with central, lower and upper velocity values are used to model epistemic uncertainty in the EG2 estimates of V_{S30} for each GM equation, see Table A2-2 below.

Tab. A2-2: Selected site classes for candidate attenuation relations

Study	Site Class	$V_{s,30}$ [m/s]		
		Lower (w = 0.2)	Central (w = 0.6)	Upper (w = 0.2)
Abrahamson & Silva (1997)	Rock	450	600	900
Ambraseys et al. (1996)	Class R (rock)	550	800	1,200
Ambraseys & Douglas (2000)	Class R (rock)	450	800	1,100
Atkinson & Boore (1997)	-	-	2,800*	-
Berge-Thierry et al. (2000)	Rock	550	800	1,200
Boore et al. (1997)	Class A (rock)	550	620	750
Campbell & Bozorgnia (2002)	Firm Rock	450	600	900
Lussou et al. (2001)	Class B	350	500	900
Sabetta & Pugliese (1996)	Stiff	700	1,000*	1,300
Somerville et al. (2001)	-	-	2,800	-
Spudich et al. (1999)	Rock	550	800	1,100
Toro et al. (1997)	-	-	2,800*	-

* For the three ENA equations, there is considered to be no uncertainty, hence a weight of 1.0 is applied to the central value. These equations are only defined for hard rock sites and therefore there is no need to specify the site class to be used in applying the equation.

– No Kappa correction or any other adjustment to Swiss conditions has to be applied.

– Epistemic uncertainties in the magnitude conversion are captured via consideration of either two or three different relationships (depending on the magnitude scale).

– The conversion of the different types of horizontal components to the geometric mean is based on TP2-TN-0269 and the frequency dependent scale factors explicitly given in Table A2-3 below are used. The given factors also account for epistemic uncertainty by the addition of two additional branches with lower and higher scale factors.

– Missing coefficients in the retained ground motion models have been derived according to the procedure described in TP2-TN-0270.

– A conversion to take into account the styles-of-faulting is considered using two different approaches. For the equations of Abrahamson & Silva (1997), Boore et al. (1997) and Campbell & Bozorgnia (2002) only, estimates from normal fault ruptures are adjusted, applying three branches with frequency-independent factors and weights. For the remaining 9 equations, frequency- and equation- dependent scale factors are applied for each faulting mechanism.

Tab. A2-3: Branches and weights for horizontal component conversions

Frequency (Hz)	Conversion 1: larger-envelope to random			Conversion 2: larger-PGA to random		
	W = 0.25	W = 0.50	W = 0.25	W = 0.25	W = 0.50	W = 0.25
0.5	0.80	0.82	0.84	0.94	0.96	0.98
1.0	0.80	0.82	0.84	0.93	0.95	0.97
2.5	0.81	0.83	0.85	0.91	0.93	0.95
5.0	0.82	0.84	0.86	0.90	0.92	0.94
10.0	0.83	0.85	0.87	0.89	0.91	0.93
20.0	0.84	0.86	0.88	0.88	0.90	0.92
33.3	0.87	0.86	0.89	0.85	0.88	0.91
50.0	0.82	0.86	0.90	0.82	0.86	0.90
100.0	0.82	0.86	0.90	0.82	0.86	0.90

V/H Ratio

- V/H ratios are obtained using 7 out of the candidate models that predict both horizontal and vertical components.
- Model weights are used acc. ES, see Tale. A2-4 below.

Tab. A2-4: Weights applied to vertical and horizontal ground motions at all frequencies to calculate the V/H ratios

Study	$M_w < 5.5$			$5.5 < M_w < 6.5$			$6.5 < M_w < 7.5$		
	< 10	10 – 60	> 60	< 10	10 – 60	> 60	< 10	10 – 60	> 60
Abrahamson & Silva	0.1494	0.1667	0.2339	0.1834	0.2220	0.2426	0.2074	0.2802	0.3215
Ambraseys et al.	0.1261	0.1563	0.1974	0.1238	0.1665	0.2047	0.1245	0.1681	0.2412
Ambraseys, Douglas	0.1494	0.0333	0.0000	0.1467	0.0355	0.0000	0.1660	0.0448	0.0000
Berge-Thierry et al.	0.1360	0.1625	0.1901	0.0417	0.1010	0.1774	0.0094	0.0656	0.1881
Campbell, Bozorgnia	0.2989	0.2500	0.0936	0.3668	0.2664	0.0970	0.4149	0.3362	0.1286
Lussou et al.	0.0000	0.0750	0.0877	0.0000	0.0420	0.0737	0.0000	0.0000	0.0000
Sabetta & Pugliese	0.1401	0.1563	0.1974	0.1376	0.1665	0.2047	0.0778	0.1051	0.1206

- Site class adjustments are not taken into account for both components V and H, because only the ratio is of interest.
- Magnitude conversions are applied for both the horizontal component and the V/H ratio.

- The conversion of components to the geometric mean is based on TP2-TN-0269 and applied to the horizontal components only.
- Missing coefficients in the ground motion models predicting vertical components have been derived according to the procedure described in TP2-TN-0270.
- No additional style-of-faulting adjustments are to be made except for those appropriate mechanism parameters as used in the equations of Abrahamson & Silva and Campbell & Bozorgnia.

Aleatory variability for the horizontal component

- Standard deviations computed by the equation of Abrahamson & Silva are used as the base model for all the 12 models retained. The standard deviation from the Abrahamson and Silva model is adjusted to account for the all error propagation effects (e.g. magnitude, component, and distance conversions).
- To account for epistemic uncertainty, model specific scaling along three side branches applying central, lower and higher factors is performed according to ES, see Table A2-5 below for each bin (magnitude and distance dependent).

Tab. A2-5: Logic-tree and weights for aleatory uncertainty of horizontal ground motions

Equation	$M_w < 6.5$ and $R < 15$ km		$M_w > 6.5$ or $R > 15$ km	
	Factor[1]	Weight	Factor[1]	Weight
Abrahamson & Silva	0.95	0.1	0.95	0.1
	1.00	0.8	1.00	0.8
	1.05	0.1	1.05	0.1
Ambraseys et al.	1.05	0.4	1.00	0.4
	1.10	0.4	1.05	0.4
	1.15	0.2	1.10	0.2
Ambraseys & Douglas	1.05	0.4	1.00	0.4
	1.10	0.4	1.05	0.4
	1.15	0.2	1.10	0.2
Atkinson & Boore	0.95	0.15	1.00	0.4
	1.00	0.7	1.05	0.4
	1.05	0.15	1.10	0.2
Berge-Thierry et al.	1.00	0.4	1.00	0.4
	1.05	0.4	1.08	0.4
	1.10	0.2	1.15	0.2
Boore et al.	1.05	0.5	0.95	0.15
	1.10	0.3	1.00	0.7
	1.15	0.2	1.05	0.15
Campbell & Bozorgnia	0.90	0.2	0.90	0.2
	1.00	0.7	1.00	0.7
	1.05	0.1	1.05	0.1

Equation	$M_w < 6.5$ and $R < 15$ km		$M_w > 6.5$ or $R > 15$ km	
	Factor[1]	Weight	Factor[1]	Weight
Lussou et al.	1.00	0.4	1.00	0.4
	1.05	0.4	1.08	0.4
	1.10	0.2	1.15	0.2
Sabetta & Pugliese	1.05	0.4	1.00	0.4
	1.10	0.4	1.05	0.4
	1.15	0.2	1.10	0.2
Somerville et al.	1.05	0.5	0.95	0.15
	1.10	0.3	1.00	0.7
	1.15	0.2	1.05	0.15
Spudich et al.	1.05	0.5	0.95	0.15
	1.10	0.3	1.00	0.7
	1.15	0.2	1.05	0.15
Toro et al.	1.05	0.5	0.95	0.15
	1.10	0.3	1.00	0.7
	1.15	0.2	1.05	0.15

1 The factor to be applied to the frequency-dependent sigma values from the equations of Abrahamson & Silva (1997)

– Equations that correspond to different percentiles from the Ambraseys et al. (1996) ground motion model are used to define alternatives of the maximum horizontal ground motion estimate according to ES, see Table A2-6 below.

Tab. A2-6: Incremental levels adopted to ensure monotonic increase in ground motion

The figures in the table correspond to the number of standard deviations to add to the median for horizontal ground motions.

Frequency (Hz)	*0.5*	*1*	*2.5*	*5*	*10*	*20*	*33*	*100*
Sigma	*0.32*	*0.32*	*0.31*	*0.27*	*0.27*	*0.26*	*0.26*	*0.25*
Incremental level 1	2.5000	2.5000	2.5000	2.5000	2.5000	2.5000	2.5000	2.5000
Incremental level 2	3.1985	3.1985	3.1877	3.1452	3.1452	3.1347	3.1347	3.1243
Incremental level 3	3.6573	3.6573	3.6469	3.6044	3.6044	3.5936	3.5936	3.5826
Incremental level 4	3.9996	3.9996	3.9922	3.9612	3.9612	3.9531	3.9531	3.9449
Incremental level 5	4.2727	4.2727	4.2690	4.2531	4.2531	4.2488	4.2488	4.2445
Incremental level 6	4.5000	4.5000	4.5000	4.5000	4.5000	4.5000	4.5000	4.5000

– The same procedure is used for the maximum ground motion for the vertical component, now using percentiles above the median values from Ambraseys and Simpson (1996), as specified in Table A2-7 below. The upper tail of the distributions is sharply cut at these maximum values of ground motions.

Figures A2-1, A2-2 and A2-3 show the logic trees for the horizontal component, the V / H ratio and the aleatory variability, resp., as they have been implemented in the code.

Tab. A2-7: Incremental levels adopted to ensure monotonic increase in ground motion

The figures in the table correspond to the number of standard deviations to add to the median for vertical ground motions.

Frequency (Hz)	*0.5*	*1*	*2.5*	*5*	*10*	*20*	*33*	*100*
Sigma	*0.36*	*0.33*	*0.28*	*0.27*	*0.29*	*0.28*	*0.27*	*0.26*
Incremental level 1	2.5000	2.5000	2.5000	2.5000	2.5000	2.5000	2.5000	2.5000
Incremental level 2	3.2419	3.2093	3.1557	3.1452	3.1663	3.1557	3.1452	3.1347
Incremental level 3	3.6979	3.6676	3.6152	3.6044	3.6258	3.6152	3.6044	3.5936
Incremental level 4	4.0280	4.0069	3.9691	3.9612	3.9770	3.9691	3.9612	3.9531
Incremental level 5	4.2869	4.2764	4.2572	4.2531	4.2612	4.2572	4.2531	4.2488
Incremental level 6	4.5000	4.5000	4.5000	4.5000	4.5000	4.5000	4.5000	4.5000

A 2.3 Model Parameterization

The ground motion is parameterized for the final Rock Hazard Computations at the following spectral frequencies: 0.5 Hz, 1 Hz, 2.5 Hz, 5 Hz, 10 Hz, 20 Hz, 33 Hz, 50 Hz and at peak acceleration. The implementation of the logic trees results in: (a) a set of alternative estimates of the median horizontal ground motion, aleatory variability of the horizontal ground motion and V / H ratios at each spectral frequency, earthquake magnitude, fault style, and distance and (b) the weight associated to each individual branch of the logic tree.

Ground motions have been modeled for seven magnitudes [5.0 : 0.5 : 8.0] and 14 distances (1.0, 1.6, 2.5, 4.0, 6.3, 10, 16, 25, 40, 63, 85, 100, 160, 250 kilometers).

The ground motion arising from the implementation of the SP2 logic trees has been parameterized using a composite model approach. At each distance, magnitude and spectral frequency and for each fault style, the alternative estimates of the median ground motion are sorted in order of ascending spectral acceleration. The weights associated with the sorted median amplification factors are summed, resulting in a cumulative distribution of the amplification factors. No smoothing of the cumulative distribution has been applied. The values of the ground motion are selected for cumulative distributions corresponding to the following fractiles: 0.13 %, 2.28 %, 16 %, 50 %, 84 %, 97.72 %, and 99.87 %. The seven fractiles correspond to median, $\pm 1\sigma$, $\pm 2\sigma$, and $\pm 3\sigma$ levels. By using the discrete fractiles, no assumption regarding symmetry of the epistemic uncertainty is made.

For the aleatory variability, the same process is repeated but with the sorting performed on the amplitude of the aleatory variability.

A conversion for different distance measures was conducted using the Scherbaum conversion factors. (These conversions may be updated in the final model to incorporate the SP1 depth distributions). Two sets of conversions were done. The first converted the distances to JB distances and the second converted the distances to rupture distance. The main differences between the JB distance and the rupture distance occur for small magnitudes at short distances. However, to avoid potential jumps in the models at bin boundaries, the conversions were

applied to all the bins (unlike what had been done for the sensitivity computations, where the conversion was not applied to the smallest magnitude and shortest distance bin ($M < 5.5$, $D < 10$)).

The values of ground motion resulting from this procedure are directly input into the rock hazard software without further parameterization or fitting.

The Maximum Ground Motion estimates are also parameterized in a similar manner. Tables of the maximum ground motion are developed for the same magnitude and distance bins, for each style of faulting and for the seven fractiles.

Figures 4 to 6 on the next pages of this document show one example (for PGA, the Joyner-Boore distance and strike-slip) of the ground motion for the horizontal component, for the V / H ratio and for the aleatory variability for the horizontal component, respectively. The figures display four subplots. The upper plot shows the median as a distance and magnitude dependent surface. The central plot shows the median ground motion as a distance and fractile dependent surface for magnitude 6.5. The lower left plot shows the median for the 7 magnitudes (magnitude 5.0 to 8.0 in 0.5 magnitude steps) while the lower right subplot shows the 7 fractiles (corresponding to median, $\pm 1\ \sigma$, $\pm 2\ \sigma$, and $\pm 3\ \sigma$) for magnitude 6.5.

Figures 4 to 129 of the associated PDF file (EG2-HID-0027_Bommer_figures_rev1.pdf) show the full set of figures.

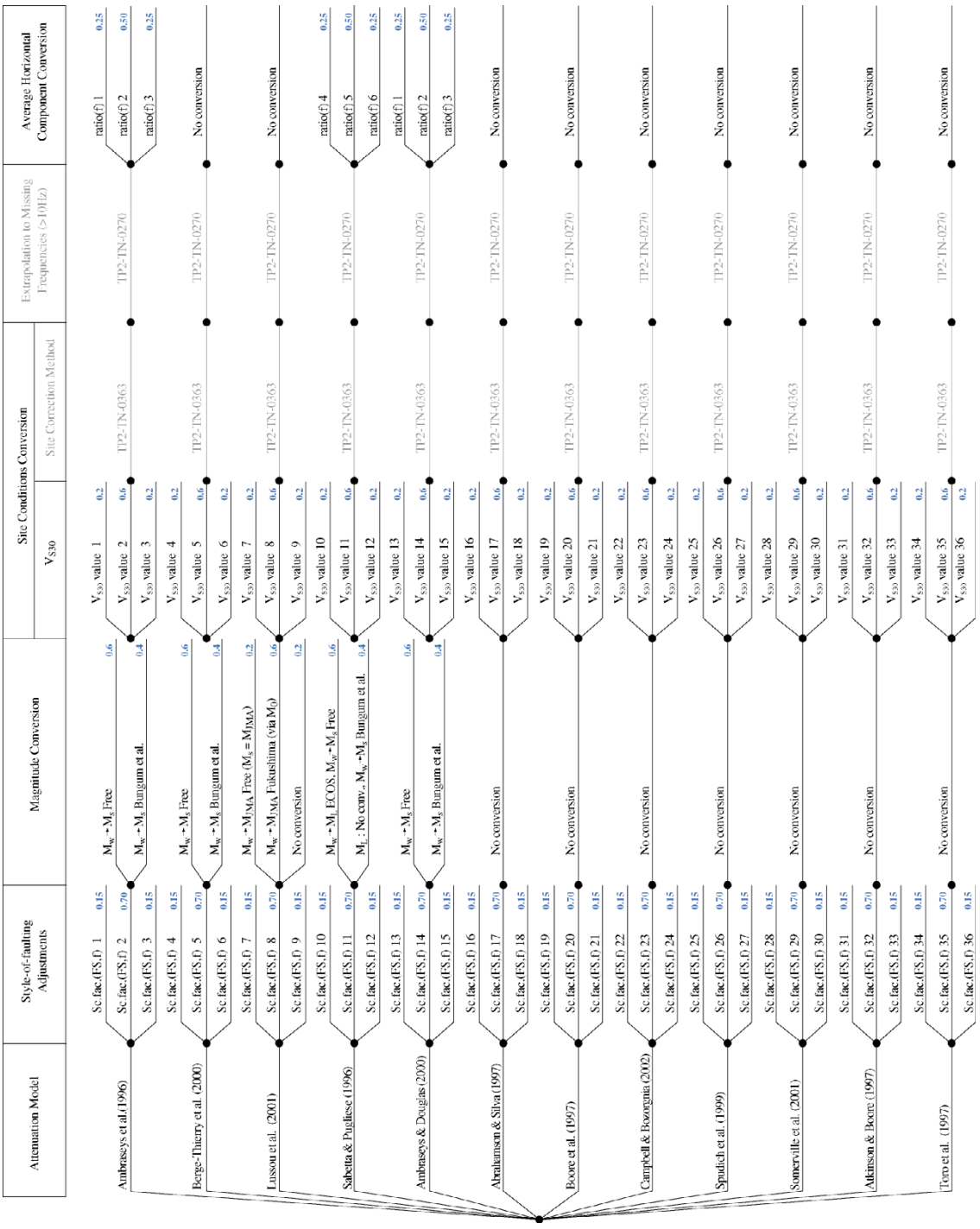

Fig. A2-1: Logic tree for the horizontal ground motion

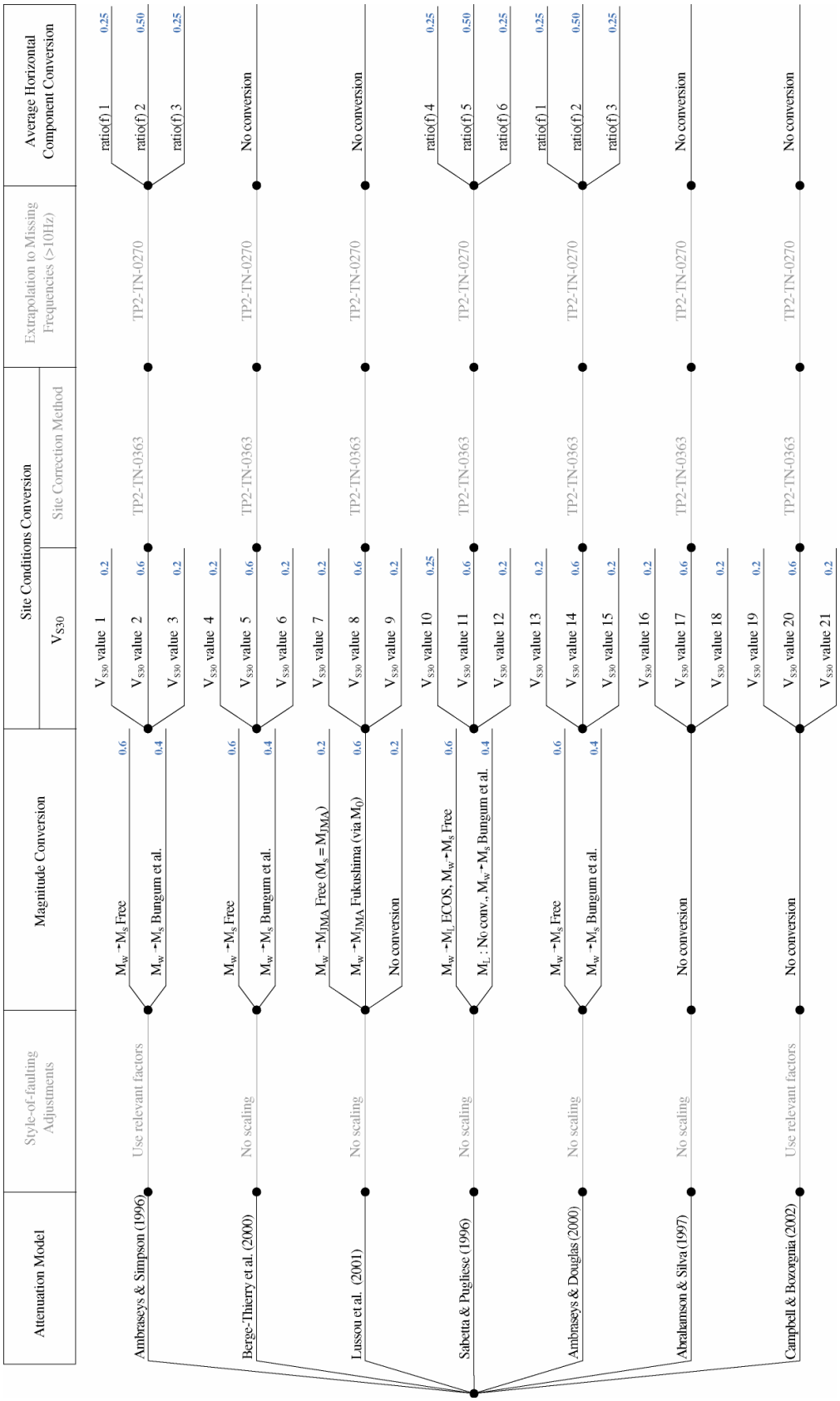

Fig. A2-2: Logic tree for the V/H ratio

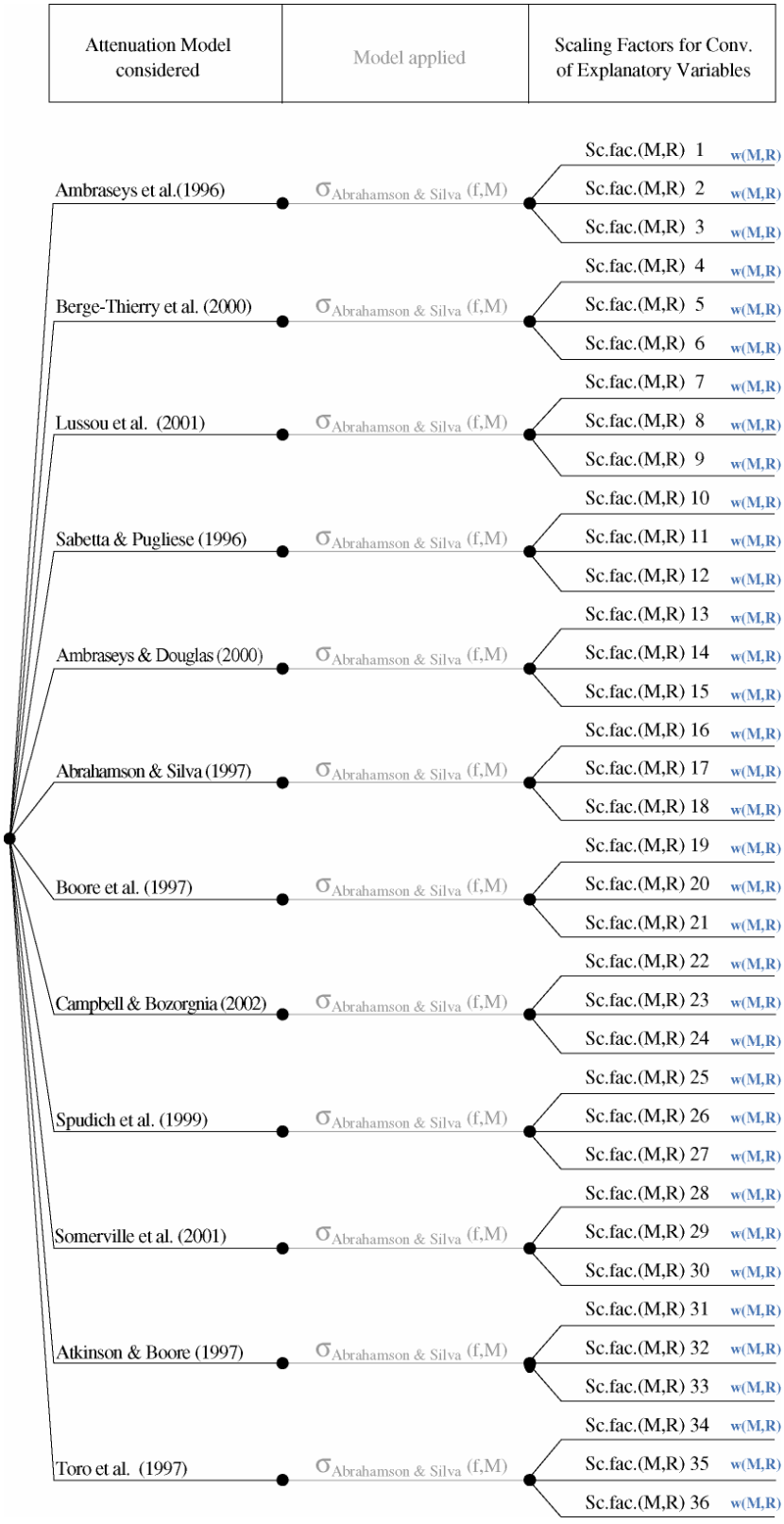

Fig. A2-3: Logic tree for the aleatory uncertainty

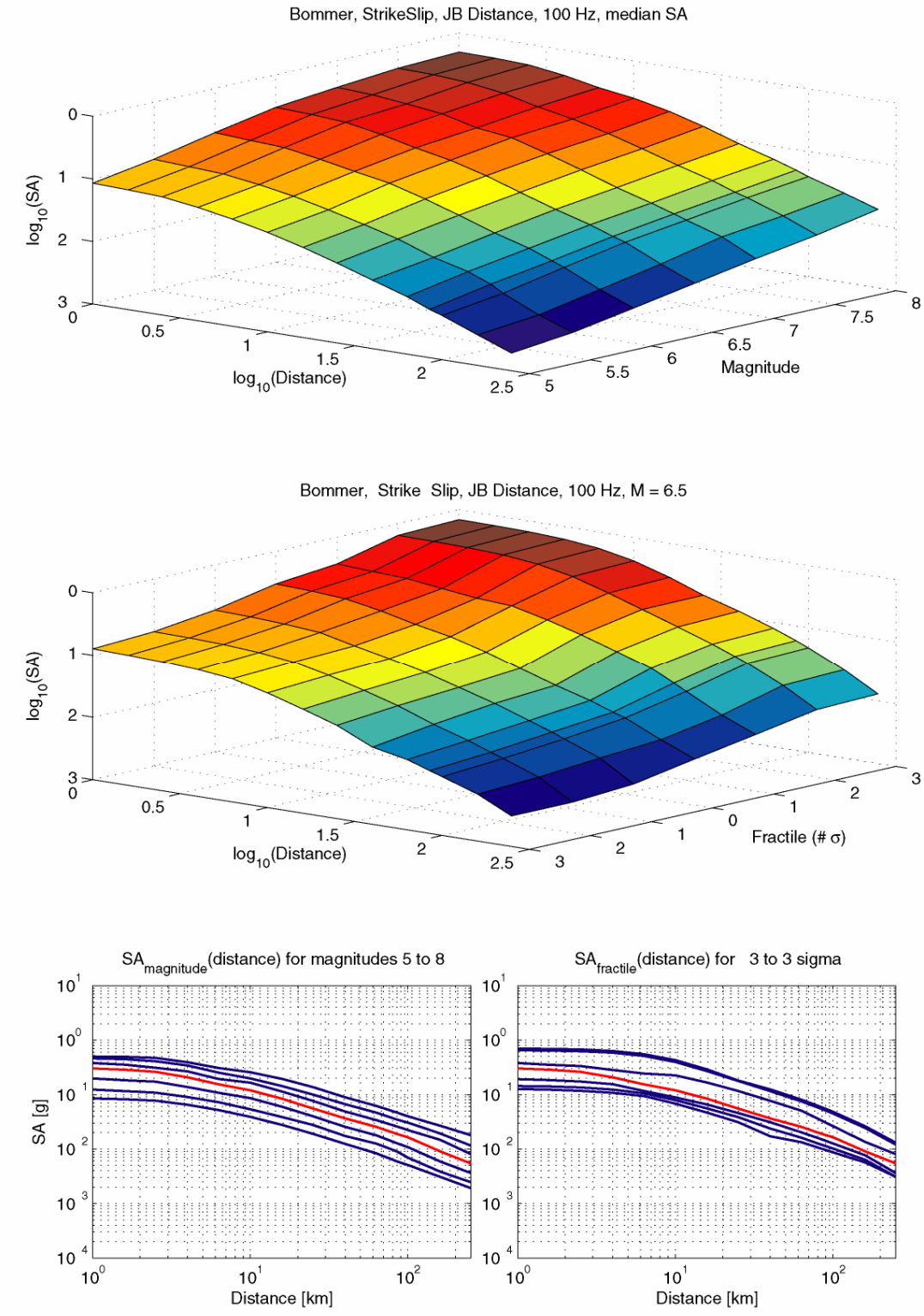

Fig. A2-4: Spectral acceleration (SA) for PGA (100 Hz), assuming strike-slip mechanism and Joyner-Boore distances

The upper plot shows SA (distance, magnitude) for the median. The middle plot shows SA (distance, fractile) for magnitude 6.5. The lower left-hand plot shows the median SA (distance) for different magnitudes. The lower right-hand plot shows SA (distance) for different fractiles and magnitude 6.5

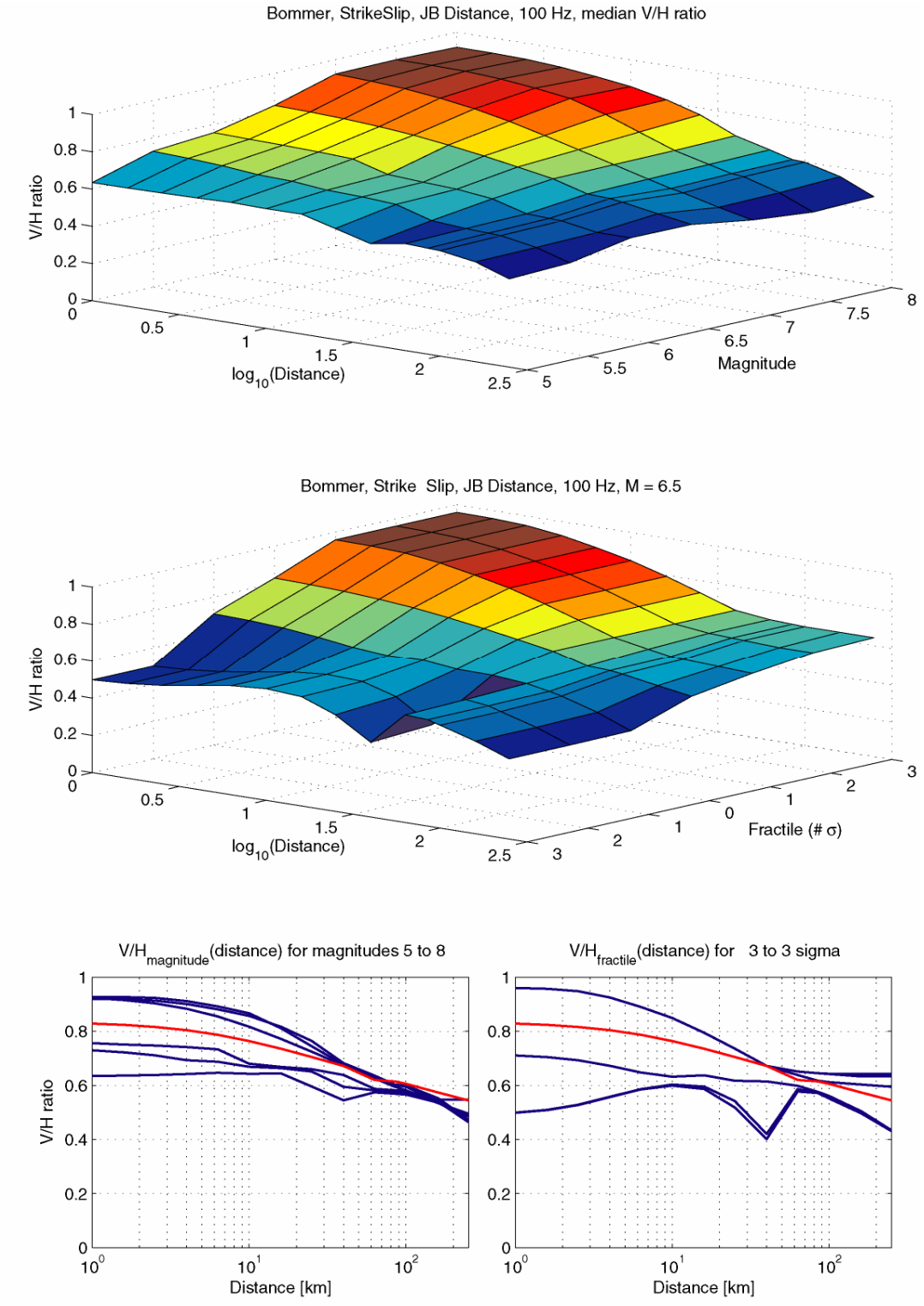

Fig. A2-5: V / H ratio (V / H) for PGA (100 Hz), assuming strike-slip mechanism and Joyner-Boore distances

The upper plot shows V / H (distance, magnitude) for the median. The middle plot shows V / H (distance, fractile) for magnitude 6.5. The lower left-hand plot shows the median V / H (distance) for different magnitudes. The lower right-hand plot shows V / H (distance) for different fractiles and magnitude 6.5

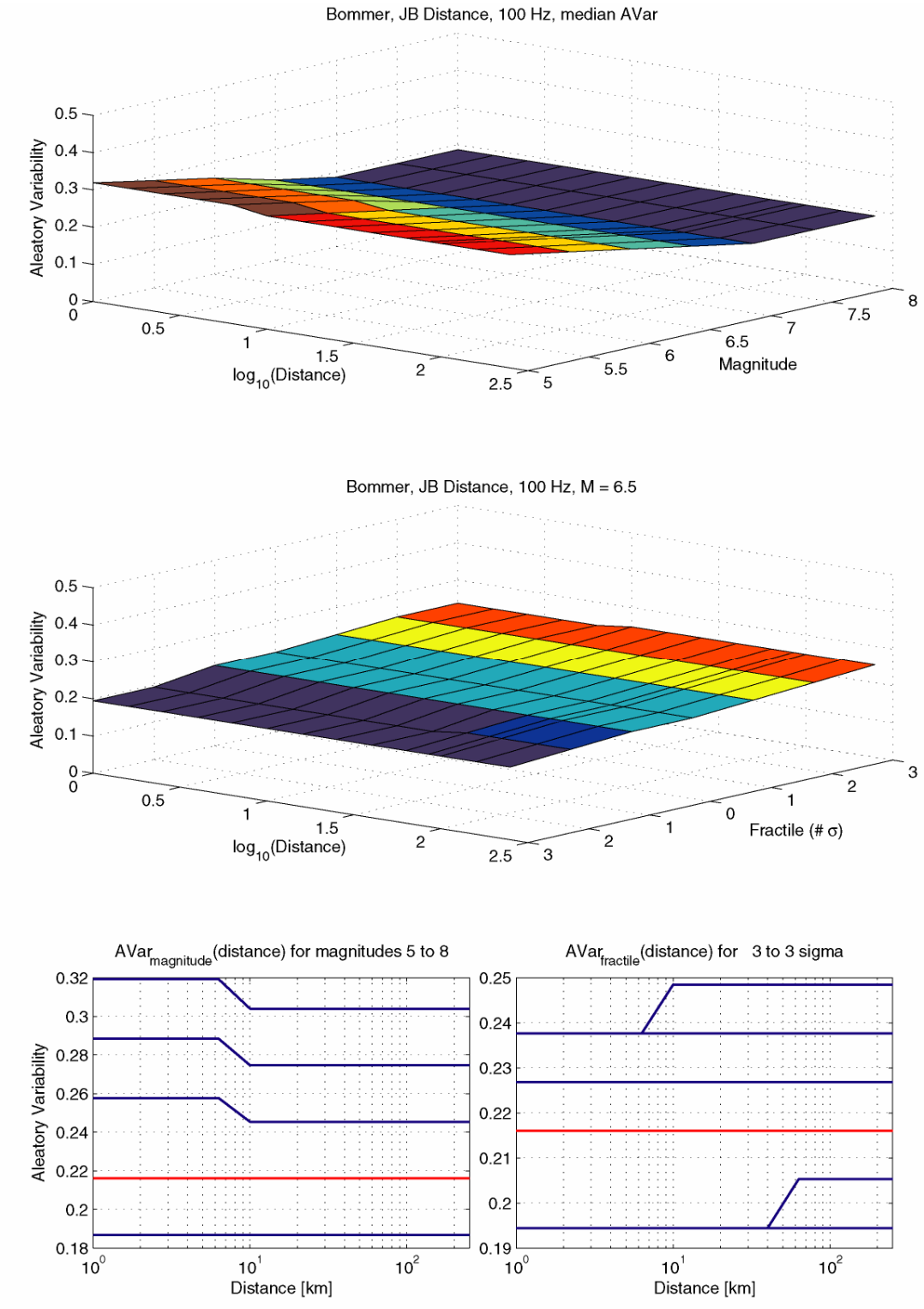

Fig. A2-6: Aleatory variability (AVar) for PGA (100 Hz), assuming strike-slip mechanism and Joyner-Boore distances

The upper plot shows AVar (distance, magnitude) for the median. The middle plot shows AVar (distance, fractile) for magnitude 6.5. The lower left-hand plot shows the median AVar (distance) for different magnitudes. The lower right-hand plot shows AVar (distance) for different fractiles and magnitude 6.5

Part II: Ground Motion Characterisation, Elicitation Summary

Dr. Hilmar Bungum

NORSAR
Kjeller - Norway

Probabilistische Erdbeben-Gefährdungs-Analyse für die KKW-Stand Orte in der Schweiz (PEGASOS)

SP2 Ground Motion Characterisation

Elicitation Summary

Hilmar Bungum

NORSAR
Kjeller – Norway

nagra

PEGASOS

TABLE OF CONTENTS

LIST OF TABLES

LIST OF FIGURES

1 INTRODUCTION

The present document completes the delivery of the final SP2 model, based on and developed from earlier and preliminary models delivered January 10, 2003, October 21, 2002, and September 21, 2002. The present document is, however, self contained, and includes the complete model without reference to the earlier deliveries.

The ground motion models and associated justification presented in the following are resulting from a careful review of the questions posed and the extensive Pegasos documentation that have been offered as a basis for the work, in addition of course to the discussions at the workshops and the interactions with the TFI, in particular at Workshops 3 and 4.

The present report contains, in this respect, only the key relevant reasoning behind the chosen and recommended models, but it is still sufficient for the project to obtain an understanding of the basic philosophy, reasoning, and justifications for the models. The present report also rarely repeats results and arguments contained in project documentation. The main reason for this is that given the allocated budget, it was necessary to use a sufficient amount of the time on working out the model rather than summarizing previously documented results. Even so, I have still used more time for this work than what actually was allotted.

While the model is the direct result of the questions asked and the material provided by Pegasos in support of the work, it also comes out of many years of personal experience in logic-tree based earthquake hazard and loading analyses (of the order of a hundred different projects), as well as underlying research within many parts of such analyses, including strong motion attenuation. There is one important limitation, however, in this background experience, namely that none of the studies have been conducted for an annual exceedance probability below 10^{-4}, which is three orders of magnitudes above the Pegasos level. At those two levels the hazard is driven in quite different ways, calling for attention on different parts of the model.

Among the many (explicit and implicit) guiding principles behind the present ground motion model only two will be mentioned here:

- When faced with two alternatives that equally well can explain some data, preference should be for the simplest one (Occam's razor). There is, however, a delicate balance between this principle and the fact that in the present case I will be using parallel models in order to span properly the space of epistemic uncertainties, but without 'overspanning' this space.
- Branching widely with a logic tree can, however, be used not only to cover the different viable (i.e., more or less viable) alternatives but it can also be used to 'cover one's own back' in the sense that one may be refraining from making a real choice between models which, if not mutually exclusive, at least can be in conflict with each other. Overlapping models is a related problem.

The essential question to be answered here is the selection of attenuation relations to be used, and their individual weights for different magnitudes, distances and frequencies. This addresses in particular the epistemic uncertainty. The second most important question is how to assess the aleatory variability, in terms of sigma values.

The present report complies in full with the recommended outline for the SP2 elicitation summaries.

2 EVALUATION OF PROPONENT MODELS FOR APPLICABILITY TO SWITZERLAND

There are no relations available that are developed specifically for Switzerland or for regions that are quite similar tectonically, except for the new stochastic point source estimations done on the request of the SP2 experts (Bay's and Rietbrock's). This is a common situation for many parts of the world, and the relations adopted in this study will therefore have to be based on a review of attenuation relations for regions with seismotectonic conditions that at least would be reasonably comparable to Swiss conditions.

A specific and challenging problem is this situation is the fact that Swiss seismotectonic conditions include the Alps, the Rhine Graben and the Swiss foreland, with the first one being more plate boundary related, the latter more intraplate related, and the second one somewhere in between. Active rifts constitute plate boundaries while aborted rifts, albeit some times also with significant earthquake potentials, like passive rifted margins, are found in stable continental regions (Johnston et al. 1994, EPRI 1994). This in turn calls for a careful use of the logic tree so as to cover the additional variation in ground motion conditions, and thereby epistemic uncertainty, that this implies.

There are spectral attenuation relations available for the following types of seismotectonic regimes:

1. *Transcurrent or strike-slip regimes* (e.g., Boore et al. 1997, Abrahamson & Silva 1997), in particular California where strong motion data, including in the near field, are in abundance compared to any other region in the world. Such regions include also important compressional conditions (revealed for example in hidden thrusts), as seen in many of the recent larger earthquakes (such as 1989 Loma Prieta and 1994 Northridge).
2. *Subduction zones*, including Cascadia, Japan, Mexico and Central America. Related to this are also relations for back-arc conditions or volcanic chain and shallow crustal events, where there is an important component of compression, but under crustal conditions which are very different from Switzerland.
3. *Extensional regimes*, developing global relations based on data from events revealing normal faulting (e.g., Spudich et al. 1999). In terms of stress regimes this is different from what is generally found in Switzerland, except for some of the earthquakes in the Rhine Graben.
4. *Intraplate (stable continental) regions* (e.g., Atkinson & Boore 1997, Toro et al. 1997), where the conditions are quite different and where relations, because of insufficient empirical data, moreover have to be based more on simulations and (calibrated) theoretical models. Such relations are certainly relevant for Swiss conditions (in particular the foreland).
5. *Compressional tectonics*, where few relations are available, and where the closest we may get is the Mediterranean region (e.g., Ambraseys et al. 1996, Berge-Thierry et al. 2000, 2002). Tectonic conditions are complex and often different, but still close enough to Swiss conditions to be of interest, especially the Alps.

When considering the complex tectonic situation for the Pegasos sites, as documented by SP1, all of the above except No. 2 (subduction zones) could be of interest, as reflected also in the initial selection of candidate relations.

3 MEDIAN HORIZONTAL MOTION

The present ground motion model includes 7 of the 15 relations that initially were selected as candidate relations. In addition, the new point source stochastic model based on Rietbrock's recent inversion of Swiss weak-motion data (Bay 2002) is also included (Abrahamson 2003; TP2-RF-0350). With the exception of the latter one all of the candidate relations are shown in Figures 1 and 2, which are taken from Fabio Sabetta's Elicitation Summary from January, 2003. It is seen there that the scatter is considerable, about one order of magnitude for M = 5 and R = 10 km, and even more for M = 7 and R = 50 km. Correcting for magnitudes, distance and component definitions, etc., does not reduce this scatter in any significant way.

The eight relations selected are listed in the following, with a brief description of each one. A more detailed justification is given in Section 3.2 together with a discussion of the weighting in magnitude-distance space.

1. Ambraseys et al. (1996): Joyner-Boore (JB) distance, horizontal (vertical in Ambraseys & Simpson 1996, and Ambraseys & Douglas 2000), larger component, M_S magnitudes (4.0 – 7.3), distance range 5 – 200 km.
2. Berge-Thierry et al. (2000, 2002): Hypocentral distance, horizontal and vertical, random component, M_S magnitudes (4 – 7.3), distance range 7 – 100 km. Based on the same European data but supplemented with WUS data to stabilize for 'near field' larger magnitudes.
3. Sabetta & Pugliese (1996): JB distance (mixed with Epicentral), horizontal and vertical, larger component, M_S (above 5.5) and M_L magnitudes (below 5.5). Italian data. Distance range 10 – 120 km, magnitude range 4.6 – 6.8.
4. Campbell & Bozorgnia (2002): JB and Rupture (Rup, R_{seis}) distance, horizontal and vertical, average component, M_W magnitudes (4.7 – 7.7). Global data, but with US dominance, distance range 2 – 70 km.
5. Spudich et al. (1999): JB distance, horizontal only, average component, M_W magnitudes (5.0 – 7.5). Global extensional data, mostly US and European, distance range 1 – 100 km.
6. Somerville et al. (2001): JB distance, horizontal and vertical, random component, M_W (6.0 – 7.5). Developed for CAN/ENA conditions, non-rifted (depth 0 – 10 km) and rifted (depth 5 – 30 km), distance range 0 – 500 km.
7. Toro et al. (1997): JB distance, horizontal only, random component, M_W magnitudes.
8. Revised stochastic point source (SPS) relation (see Rietbrock's and Scherbaum's notes plus Abrahamson 2003: TP2-RF-0350). Based on JB distance, horizontal only, random component, M_W magnitudes. Stress drop 46 bars.

Relations 6 and 7 should be corrected for differences in kappa between EUS (0.006 sec) and Switzerland (0.0125 sec, Bay 2002). There are two reasons why kappa corrections are introduced only for these two relations: (1) They are both calibrated-theoretical ones (albeit based on different approaches) where kappa values specific for EUS conditions are explicitly used; (2) The other relations (1 – 5) are empirical ones based on European or global data with siting conditions that overlap more with Swiss conditions, moreover, these variations are reflecting epistemic uncertainties that I specifically want to have included in my model.

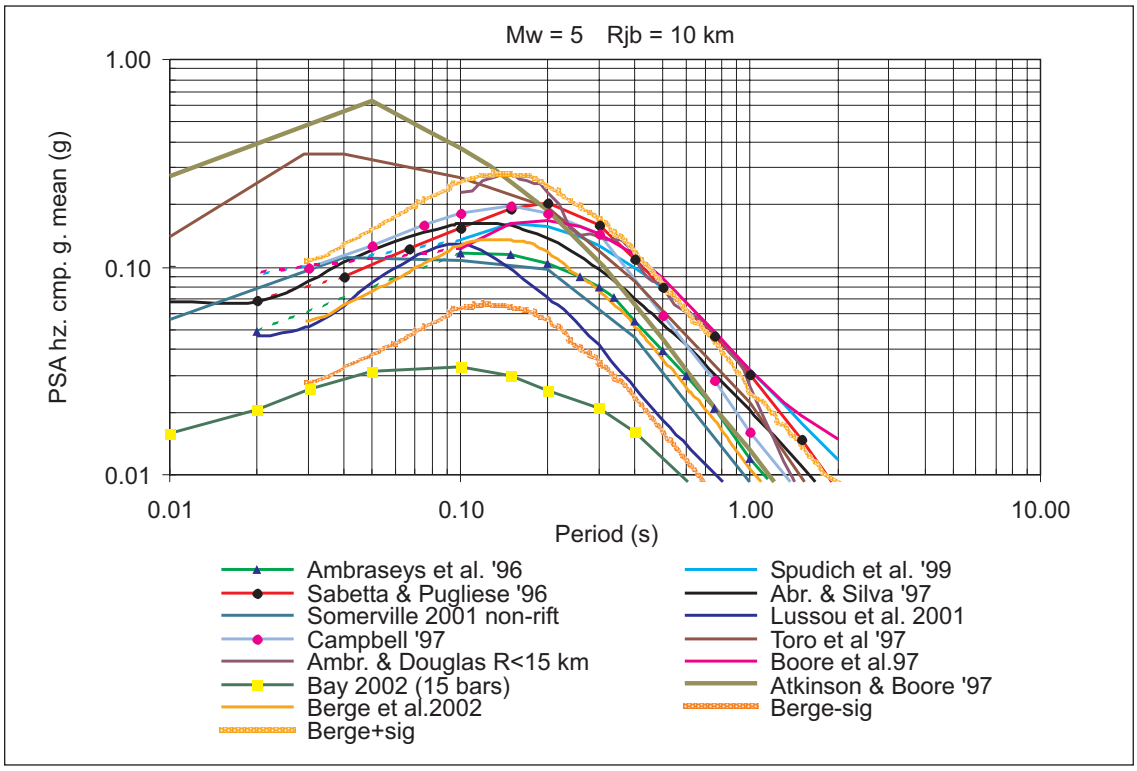

Fig. 1: Acceleration response spectra of the candidate attenuation models, in case of M = 5 and R_{JB} = 10 km compared with the aleatory uncertainty (± 1σ) of Berge-Thierry et al. 2000

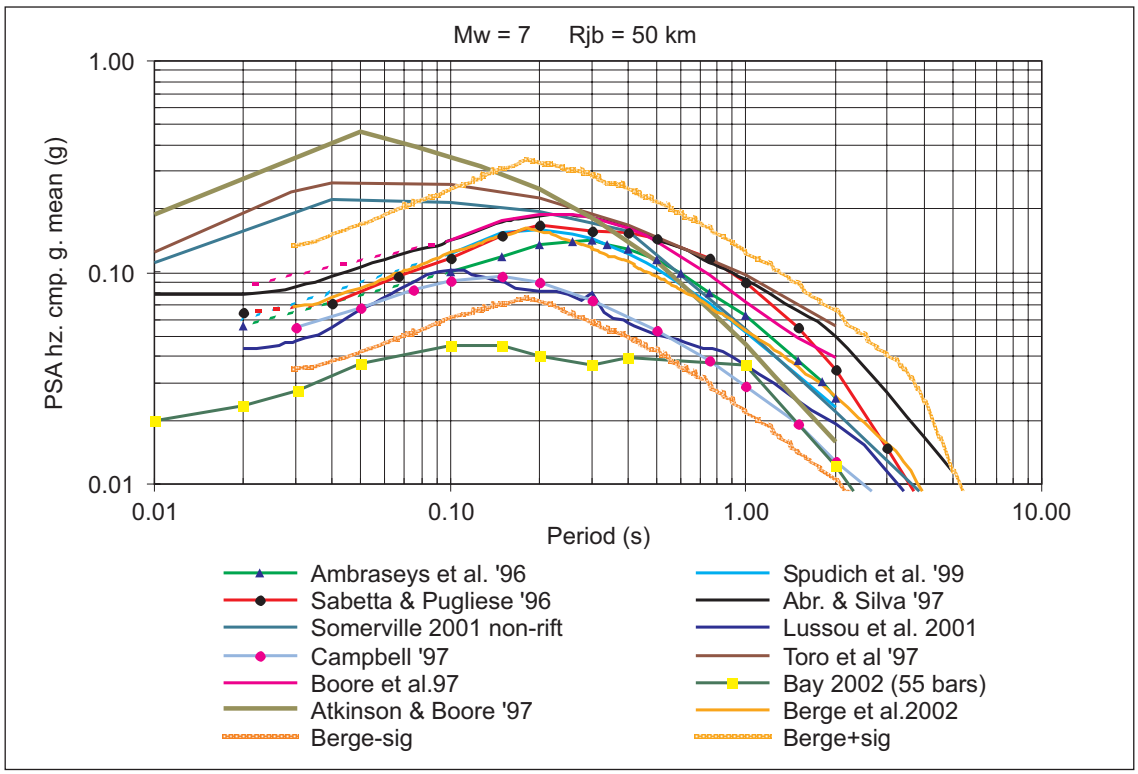

Fig. 2: Acceleration response spectra of the candidate attenuation models, in case of M = 7 and R_{JB} = 50 km compared with the aleatory uncertainty (± 1σ) of Berge-Thierry et al. 2000

The justification for selecting this set of relations also includes establishing a balance between different different types of relations so as to cover properly a sufficient range of epistemic uncertainties, as follows:

- The selected relations provide a balance between European (3 relations) and global (2 relations) data, supplemented with deterministic (1 relation) and stochastic (1 relation) modelling for SCR conditions. In addition, the recently revised (Rietbrock) stochastic point source relation for Swiss conditions has also been included.
- The selected relations imply a European dominance, including the new stochastic relation developed specifically for Swiss conditions, while still taking advantage of the more globally based relations, thereby providing additional robustness and stability.
- There is also a balance between relations that have different strengths in the near and far field, between smaller and larger magnitudes and between lower and higher frequencies.
- The relations have been selected such that one should achieve a sufficient epistemic variability, while at the same time avoiding giving full and independent weight to relations that are essentially based on the same data.

The candidate relations that are *not* used are the following ones (briefly specifying the reasons for not using them):

- Lussou et al. (2001): Japanese data, where the M_J magnitude scale will introduce an additional uncertainty. The distance range is good (10 – 300 km) but the magnitude range (3.5 – 5.0) is a problem. There is a problem also with the different tectonic regime.
- Abrahamson & Silva (1997): Mostly WUS shallow crustal strike-slip events, which are difficult to justify being appropriate for Swiss conditions.
- Boore et al. (1997): Exclusively WUS, same problem as for Abrahamson & Silva (1997).
- Campbell (1997): This relation is essentially replaced by Campbell & Bozorgnia (2002), as concluded also by the authors.
- Atkinson & Boore (1997): This is an Eastern North America (ENA) stochastic (random vibration) relation, moreover with a disputed source spectrum (Haddon 2000). The residual plots (EU399H_Atkinson_Boore) moreover indicate some instabilities over neighbouring frequencies for this relation. It is still appropriate to include relations for Stable Continental Region (SCR) conditions, but to that end Toro et al. is preferred above this one.
- Stochastic Point Source 1 – 3: These relations are weakly documented and not fully peer reviewed, they appear to be unstable, and they are highly sensitive to parameters that are not well constrained. The problems with the Swiss ground motions (SM and BB) as documented by Bay, Smit and Scherbaum underlines this.

However, the since the new inversion of the Swiss data by Rietbrock (EXT-TN-0306), as reviewed by Scherbaum (EG2-TN-0314), appears to be more stable and reliable, handling the tradeoff between geometrical spreading and anelastic attenuation more convincingly and moreover providing more realistic stress drop values, I have decided to include that one, as already noted. It is of considerable importance to be able to include a relation that is developed specifically for Swiss conditions, but only if it can be given a sufficient scientific credibility.

Table 1 is listing the selected relations and summarizes some of their essential characteristics.

Tab. 1: Selected relations and some of their main characteristics

The associated V_{S30} velocities are given in Table 4.

No	Relation	H/V	Comp.	Mag.	Dist.	Site cond.
1	Ambraseys et al.	H	Larger	M_S	JB	Rock
2	Berge-Thierry et al.	H+V	Random	M_S	Hyp	Hard rock
4	Sabetta & Pugliese.	H+V	Larger	M_S/M_L	JB	Stiff alluvium
8	Campbell & Bozorgnia	H+V	Arith_mean	M_W	Seis	Firm rock
9	Spudich et al.	H	Geom_mean	M_W	JB	Rock
11	Somerville et al.	H+V	Random	M_W	JB	'Hard rock'
12	Toro et al.	H	Random	M_W	JB	'Hard rock'
16	Revised SPS	H	Random	M_W	JB	'Hard rock'

3.1 Logic Tree Structure

The logic tree structure in terms of branches and weights is imbedded in this document and can easily be delineated together with the extraction of the model itself.

3.2 Selected proponent models and weights

The magnitude-distance space has been divided into nine (3 by 3) bins as shown in Table 2, representing magnitudes in the low (M < 5.5), intermediate (M = 5.5 – 6.8) and high (M > 6.8) range, and distances in the near field (< 10 km), at intermediate (10 – 60 km) and at far distances (> 60 km). The basis for this division is an assessment of the individual relations in terms of strengths and weaknesses (coverage), as outlined in more detail below.

Tab. 2: Magnitude (M1, M2) and distance limits (R1, R2) for weighting between attenuation relations

This differentiation is defining the nine bins within which the weights in Table 3 are defined.

M1	M_W 5.5
M2	M_W 6.8
R1	10 km
R2	60 km

The weights for the selected relations are given in Table 3, for each of the bins in magnitude-distance space.

Tab. 3: Models and weights for median horizontal ground motion

The magnitude (M1, M2) and distance limits (R1, R2) are defined in Table 2.

Magnitude	< M1			M1-M2			> M2		
Distance	< R1	R1-R2	> R2	< R1	R1-R2	> R2	< R1	R1-R2	> R2
Model	Weights								
Ambraseys et al.	0.150	0.150	0.200	0.150	0.150	0.200	0.150	0.175	0.200
Berge-Thierry et al.	0.050	0.100	0.150	0.050	0.100	0.150	0.125	0.150	0.175
Sabetta & Pugliese	0.150	0.150	0.175	0.150	0.150	0.175	0.050	0.050	0.100
Campbell & Bozor.	0.200	0.150	0	0.200	0.150	0	0.200	0.150	0
Spudich et al.	0.150	0.150	0.175	0.150	0.150	0.175	0.150	0.150	0.175
Somerville et al.	0.050	0.050	0.050	0.125	0.125	0.125	0.225	0.225	0.250
Toro et al.	0.100	0.100	0.100	0.075	0.075	0.075	0.050	0.050	0.050
Revised SPS	0.150	0.150	0.150	0.100	0.100	0.100	0.050	0.050	0.050
Sum weights	1	1	1	1	1	1	1	1	1

More detailed reasons and justifications for the selection of relations and their weights are provided in the following, complementing what was given above along the same line:

- Ambraseys et al.: Since these relations (H and V) are based on a large data base of European data, they represent the backbone of the model, together with Berge-Thierry that is based on much of the same data. Weights between 0.15 and 0.20, balanced against Berge-Thierry in the sense that, since their data bases overlap significantly, one should limit their total weight.
- Berge-Thierry et al.: Because of the data overlap with Ambraseys the weights between the two are combined to give weights between 0.20 and 0.375, lowest for the near field (where other relations are considered to be stronger) and largest for the largest magnitudes, where the Berge-Thierry model is strengthened by US data.
- Sabetta & Pugliese: Italy provides an abundance of strong motion data that are tectonically sufficiently relevant to be used here. The weights go up to 0.175, and lowest (0.05) for largest magnitudes where this relation is considered to be weakest.
- Campbell & Bozorgnia: The data base is dominated by Californian data, but includes also two Turkish (Caldran and Erzincan), two Iranian (Tabas and Manjil), one Armenian (Spitak), one Indian (Koyna) and one Japanese (Kobe) earthquake, all of this without a larger scatter than usually seen for regionally more consistent data. This supports Campbell's earlier idea (Campbell 1989) that near field ground motions are less sensitive to tectonic environment, provided that site affects and magnitude differences are taken into account. The Campbell relation therefore provides important near-field constraints. The highest weights (0.20) are in the near field (< 10 km) where this relation is considered to be strongest, gradually decreasing to zero in the far field (> 60 km).
- Spudich et al.: The data base used here is more globally balanced than Campbell, including an appreciable amount of Italian and Greece data, again without increasing the scatter. The relation therefore offers a useful global average, and the mode of faulting is well defined. Reflecting this, the weights are in the range 0.15 to 0.175 throughout.

- Somerville et al.: Deterministic ground motion simulation based on empirically calibrated source models and scaling relations. Weights ranging from 0.05 for the smallest magnitudes to 0.20 – 0.25 for the largest magnitudes, the latter due to its empirical calibration. Weight-wise balanced against Toro. Kappa correction as indicated above.
- Toro et al.: Stochastic simulations for Canadian / Eastern North America conditions (covering also mid-continent regions), including quantification of uncertainty. The weights are balanced against both Somerville and the revised Swiss SPS relation. For M < 5.5 Toro is considered more reliable than Somerville and has consequently been given higher weights there. Kappa correction as indicated above.
- Revised Swiss stochastic point source (SPS): Since this relation is essentially based on magnitudes below 5, using only more general scaling relations for extrapolation to higher magnitudes, the weights are ranging from 0.15 to 0.05, decreasing with magnitude in a way that reflects the weak-motion basis behind the relation and the associated uncertainties in magnitude scaling. A balance against Toro, the other stochastic relation, has also been done.

3.3 Reference Rock Velocity profiles

Table 4 provides the assessment of the V_{S30} velocities (average shear wave velocities in the uppermost 30 m) for each of the ground motion relations used, as determined in consensus mode by SP2. Those values will in the present model go into a logic tree setup where the central value is given a weight of 0.6 while the lower and higher values each one is given a weight of 0.2.

Tab. 4: Range of V_{S30} velocities assigned in consensus mode by SP2 during WS-4 to the different candidate ground motion relationships

From TP2-TN-0363, page 2.

Candidate attenuation relationship	Range of V_{S30} values [m/s]		
	central	lower	upper
Abrahamson & Silva 1997	600	450	900
Ambraseys et al. 1996	800	550	1200
Ambraseys & Douglas 2003	800	450	1100
Atkinson & Boore 1997	2800	-	-
Berge-Thierry et al. 2000	800	550	1200
Boore et al. 1997	620	500	750
Campbell & Bozorgnia 2002	600	450	900
Lussou et al. 2001	500	350	900
Sabetta & Pugliese 1996	1000	700	1300
Somerville et al. 2001	2800	-	-
Spudich et al. 1999	800	550	1100
Toro et al. 1997	2800	-	-
Bay 2002	1100	750	1500

The correction to a common reference shear wave velocity of 2000 m/s (where SP3 takes over in order to bring the motions up towards the surface again) will be done through a two-step process, firstly a correction to a common reference velocity, here set to 800 m/s, and secondly a correction to the 2000 m/s reference velocity (Figure 3).

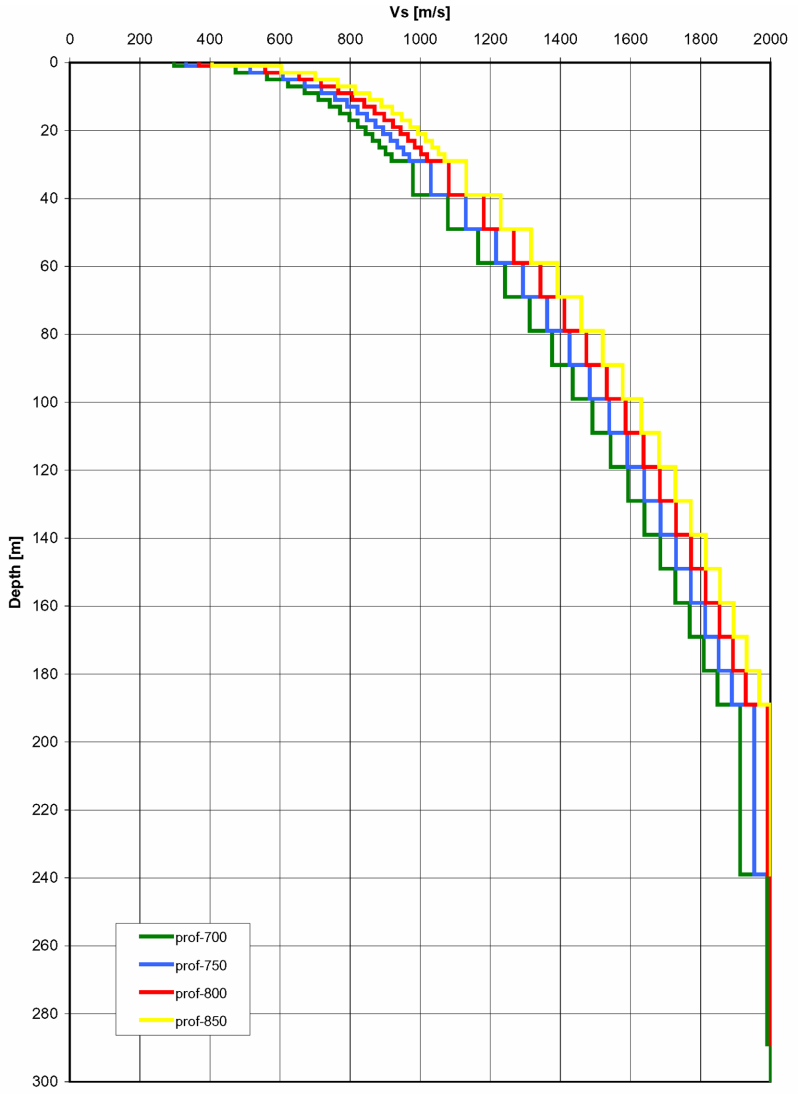

Fig. 3: Scherbaum's generic shear wave velocity profiles down to 2000 m/s, for V_S 700, 750, 800 and 850 m/s

Similar profiles are available for V_S values between 350 and 1500 m/s, referring to 2000 m/s, and between 2000 and 2800 m/s. From TP2-TN-0363, Figure 3.

For the empirical relations in Table 4 the first one of these corrections, to the common reference velocity (800 m/s), is to be based on Boore et al. (1997) (see also Boore & Joyner 1997, in particular Fig. 11), specifying the coefficients in the relation $\ln Y = a + b_V * \ln(V_S/V_{REF})$. The main reason for choosing the Boore model adjustment is that this is a systematic approach based directly on V_{S30} velocities and not on soil classes, thereby being particularly suited to adjust for the site velocity differences in Table 4. The logic tree branching here should be with a weight of 0.6 for the central value and 0.2 for the low and the high values in Table 4, respectively. Since the V_{S30} values for these relations are all fairly close to the chosen reference velocity, these corrections should be expected to be modest.

The second correction is more extensive since reliable velocity profiles for the correction to 2000 m/s are not easily available. A number of velocity profiles are available both from WUS (TP2-TN-0254) and EUS (Odum et al. 2003), while for Europe the best set of profiles are available from Italy (TP2-TN-0254). The consensus solution in this case is to use Frank Scherbaum's generic velocity profiles, based on generic ENA and California rock profiles from Boore & Joyner (1997). These are available from Martin Koller's report TP2-TN-0363 (an example of these profiles is shown in Figure 3), which also is describing the scale factor approach to be used here, in order to be consistent with SP3. For the stochastic relations with velocities of the order of 2800 m/s a suitable generic profile is also available from TP2-TN-0363, thereby providing a means for a direct correction to 2000 m/s. There should be a branching with ± 5 % in velocity and weights of 0.2, 0.6 and 0.2, respectively, justified through the fact that this scatter is largely representative for the uncertainties in such velocity profiles.

3.4 Adjustments of proponent models to Swiss conditions

It has been difficult, from the beginning of the project, to understand and accept that Swiss ground motion should be significantly different from what is obtained elsewhere, under tectonically reasonably similar conditions, even if adjusted for possible differences in siting conditions.

The residual plots for the Swiss data (see Figures 4 and 5, as examples) moreover reveal a considerable instability with respect to both magnitude (albeit decreasing with increasing magnitude), frequency (crossing the zero line over the frequencies analysed) and distance (also crossing the zero line for some frequencies). The large negative residuals are in fact indicated only for magnitudes below the integration limit and there is no solid basis for extrapolating these residuals up to the magnitudes that will drive the hazard in the present case. This is essentially a weak to strong motion scaling problem, and it would be unduly un-conservative to extrapolate the weak-motion residuals up to the magnitudes of engineering importance.

Of great importance in this respect is the Feb. 22, 2003, M_W 4.8 St. Dié earthquake, where Figures 6 and 7, for 1Hz and PGA respectively, show that the recorded ground motions are quite consistent with what is predicted by the candidate ground motion relations. Even though the distances in this case are mostly above 80 km it is difficult to understand that any reasonable ground motion model could imply significantly lower ground motions at shorter distances and more consistent values at larger distances. A supporting argument already noted in this respect is Campbell's earlier idea (Campbell 1989) that near field ground motions are less sensitive to tectonic environment, provided that specific site effects and magnitude differences are taken into account.

Therefore, after a careful review of the Swiss data and their characteristics, including the studies and notes relating to Bay's work (EXT-TN-0209, EXT-TN-0251, TP2-TN-0368, Comments from Smit dated 17.08.02) and the recent St. Dié earthquake results (TP2-TN-0367), my conclusion is not to include any specific modification to Swiss conditions.

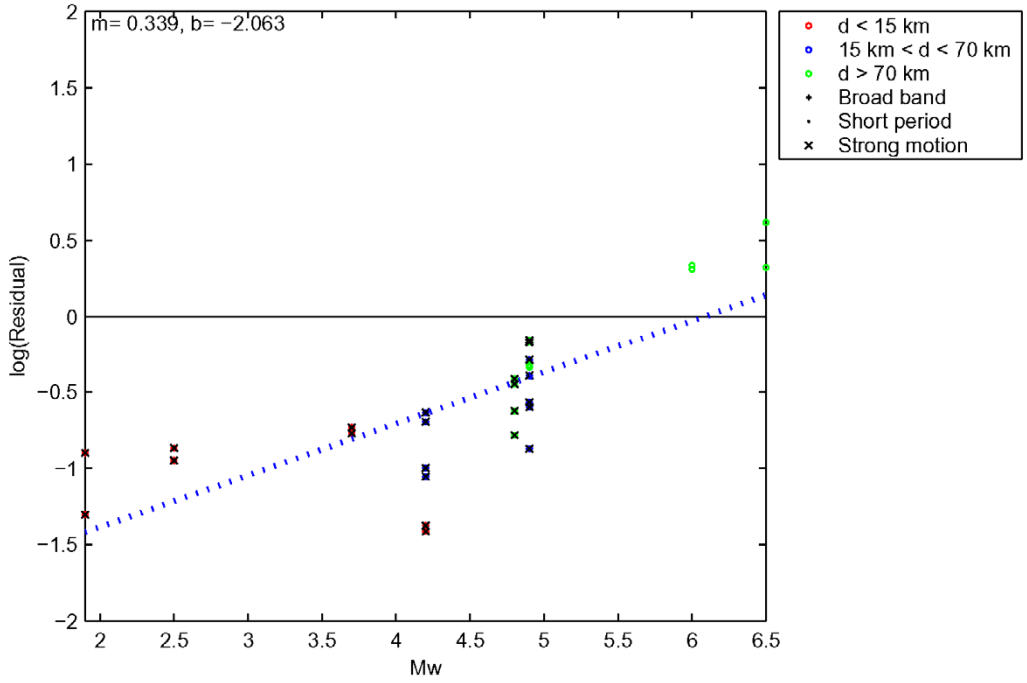

Fig. 4: Residuals of the ground motion model of Ambraseys et al. (1996), horizontal component, with respect to magnitude, based on data from Switzerland, all sources, rock (V_{S30} = 750 m/s), period = 0.5 sec, No = 30

From CH417H_Berge-Thierry_etal, page 9.

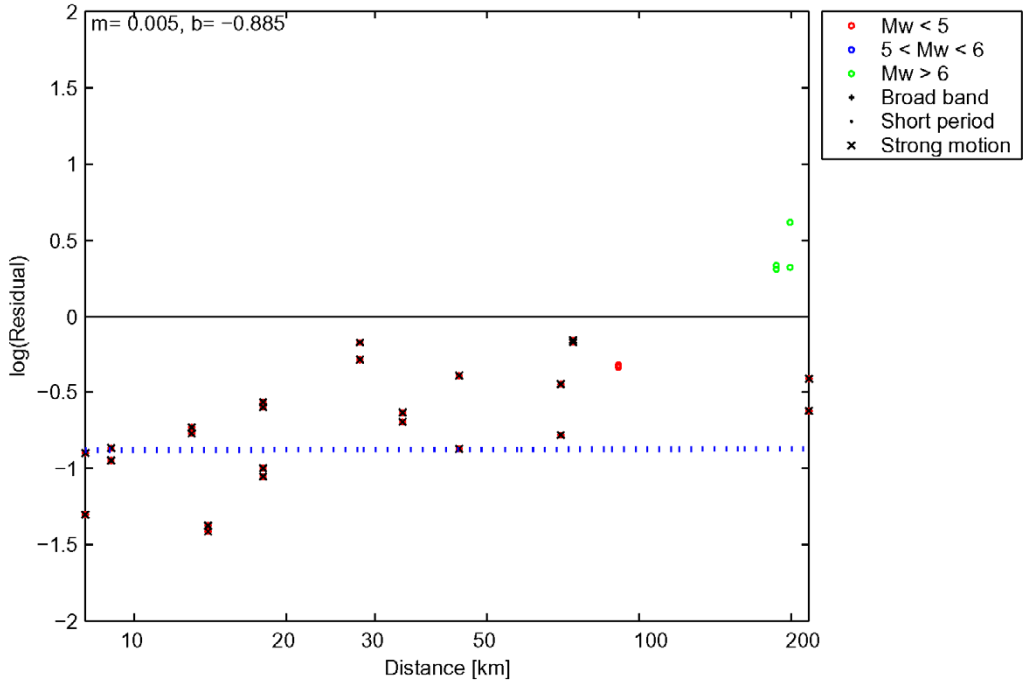

Fig. 5: Residuals of the ground motion model of Ambraseys et al. (1996), horizontal component, with respect to distance, based on data from Switzerland, all sources, rock (V_{S30} = 750 m/s), period = 0.5 sec, No = 30

From CH272H_Ambraseys_etal, page 17.

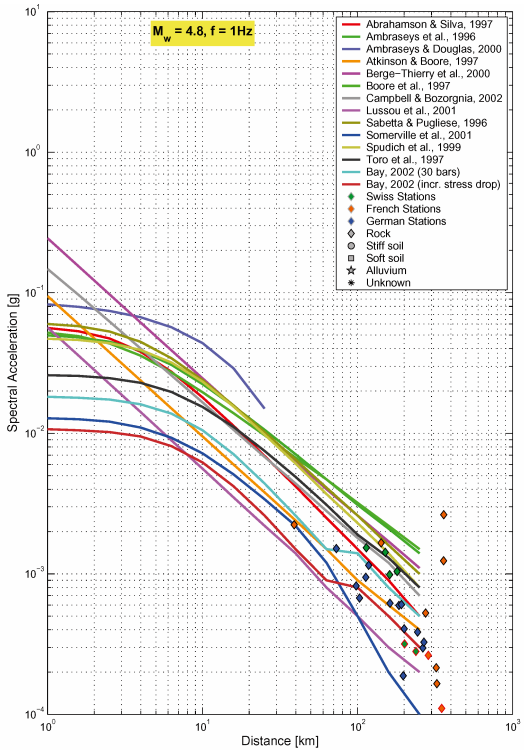

Fig. 6: Comparison between the candidate models and the accelerations of the Feb. 22, 2003, St. Dié earthquake, for 1 Hz

From TP2-TN-0367, page 6.

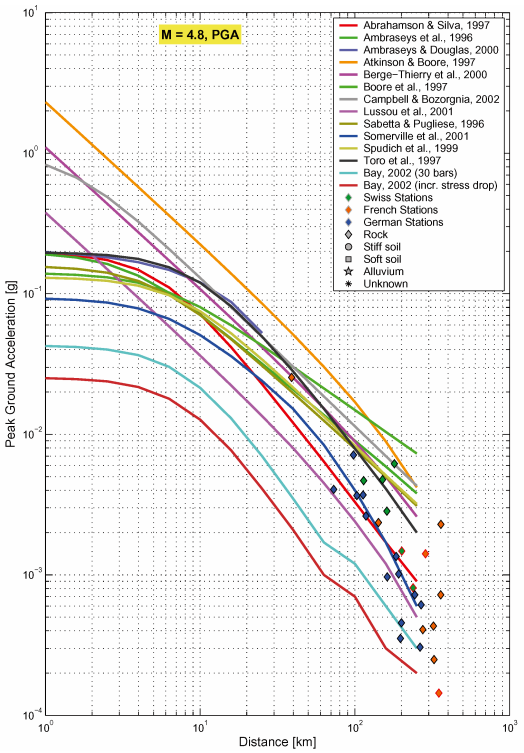

Fig. 7: Comparison between the candidate models and the accelerations of the Feb. 22, 2003, St. Dié earthquake, for PGA

From TP2-TN-0367, page 16.

3.5 Magnitude conversions

The M_W to M_S conversion applies to Ambraseys et al., Berge-Thierry et al. and Sabetta & Pugliese, where the latter magnitudes on the author's recommendation are taken as M_S. Bungum et al. (2003) found for northern Europe very close to an equality between M_S and M_W, an for southern Europe a relation as shown in Figure 8, where the piecewise linear relation has been replaced by the second order one shown in Table 5.

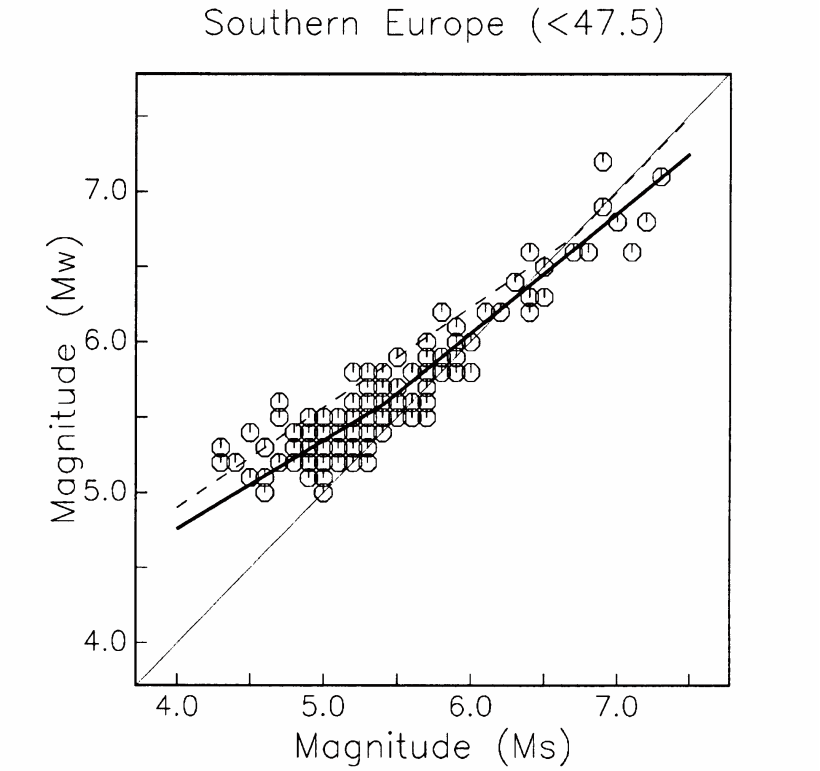

Fig. 8: M_W/M_S relation for southern Europe

The relation used in Table 5 is a new second order relation based on the same data. Note that the piecewise linear relation in this figure is for the purpose of the present study replaced by a new second order relation in Table 4. From Bungum et al. (2003), Figure 5.

Tab. 5: M_W to M_S conversion relations

Weight	Conversion relation	Reference
0.333	$M_S = M_W$	Bungum et al. (2003)
0.333	For $M_S <= 6.5$: $M_S = -7.176 + 3.062*M_W - 0.148*M_W**2$ For $M_S > 6.5$: $M_S = M_W$	
0.333	For $M_S <= 6.1$: $M_S = -2.52 + 1.37*M_W$ For $M_S > 6.1$: $M_S = M_W$	EXT-TB-0043 Figure 6.5

Since southern European relations do not necessarily apply to Swiss conditions I have chosen a balance (1/3 weight for each) between an indicated northern European equality (between M_W and M_S) and a southern European relation, both based on Bungum et al. (2003). The second relation in Table 5 is consistent with the piecewise linear relations of Bungum et al. (2003), both of them quite close to the depth-independent relation of Ambraseys & Free (1997) for southern Europe. An M_W / M_S equality is assumed for magnitudes above $M_S = 6.5$.

However, since Swiss M_S / M_W relations are also available for Switzerland as documented in the Pegasos Earthquake Catalogue report (EXT-TB-0043), the last 1/3 of the weight has been given to that one, as shown in Table 5. The relation chosen here is shown in Figure 9.

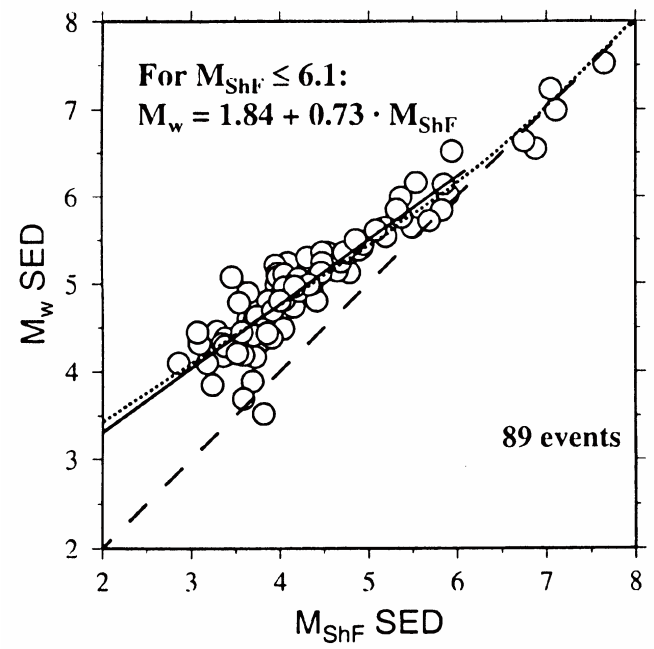

Fig. 9: M_W / M_S relation for Switzerland, based on 89 data points

From the Pegasos Earthquake Catalogue report (EXT-TB-0043), Figure 6.5 (lower left).

3.6 Component conversions

According to the new instructions from the Pegasos project (PMT-AN-0195) the hazard will be computed for the geometric mean (i.e., mean of the logarithms) of the two horizontal components.

An essential question here is to use a consistent definition of 'largest component' either as 'larger_PGA' or 'larger_envelope' as defined and discussed in TP2-TN-0269. These are necessarily similar for PGA, while the former is increasing systematically with respect to the latter, exceeding it by about 20 % at the lowest frequencies. It is important to clarify exactly which definition is used in each of the relations, since this often is not well defined in the papers.

There is also a need for reassessing exactly which type of 'average' definition that has been used in the applied relations, geometric mean or arithmetic mean, since the latter seems to be 2.5 – 3 % higher than the former. This is also sometimes difficult to assess from the papers, and it appears as if the SP2 experts in their earlier elicitation summaries have concluded not quite consistently on this point.

According to the results in TP2-TN-0269 (see Figure 10), based on global data, random component can be considered identical to geometric mean. A useful reference for conversion between random and larger is Boore et al. (1994), while the conversion between larger and geometric mean, for different data sets, is satisfactorily addressed in TP2-TN-0242 (Figure 11).

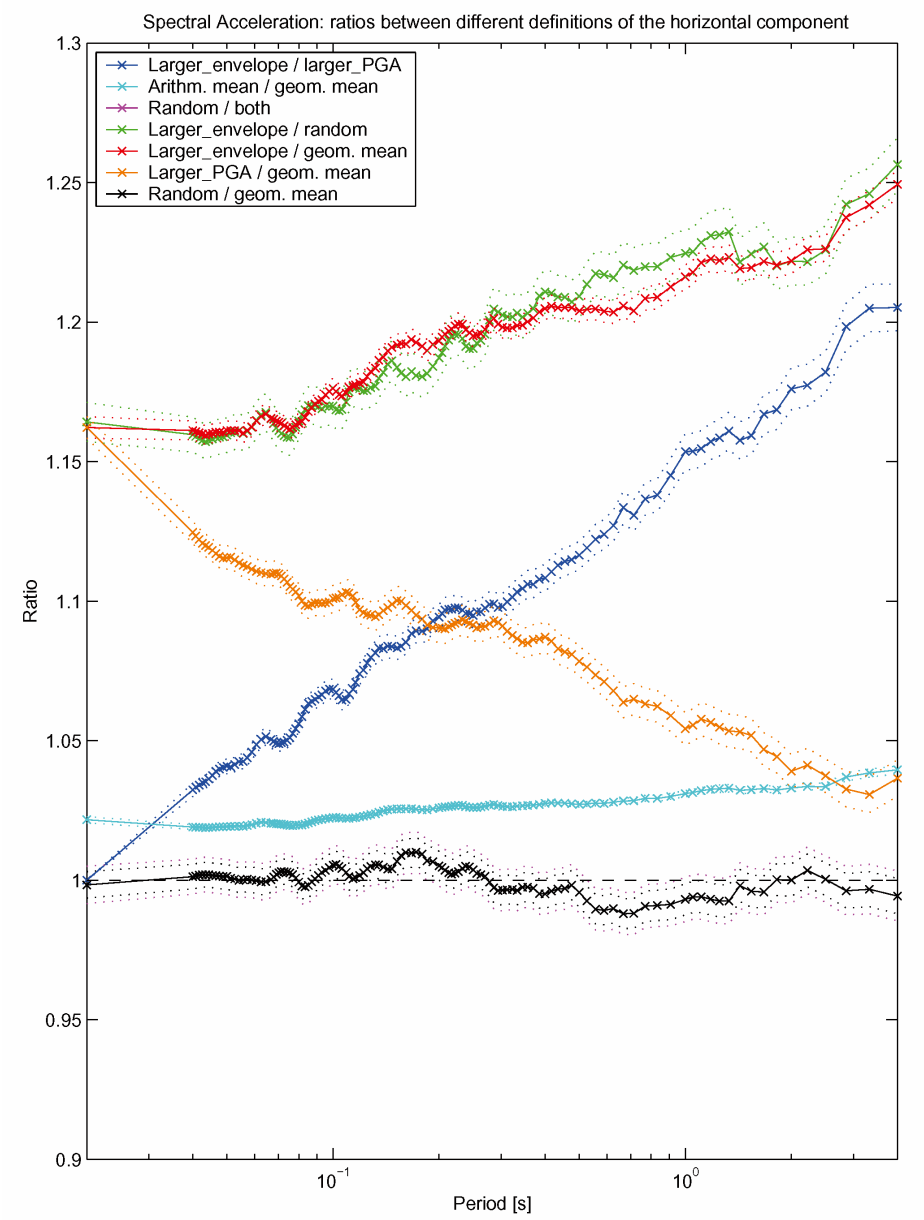

Fig. 10: Spectral acceleration ratios (5 % damping) between different definitions of the horizontal component, based on the worldwide WAF data base. From TP2-TN-0269, page 3.

The present model for conversion to geometric mean introduces another logic tree branch as defined in Table 6. The way this table should be read is that the ratio is increased and decreased by 2.5 %, each one with a weight of 0.2, and that this applies also to the random component, which thereby will range between 0.975 and 1.025. For a ratio of 1.20 the range will correspondingly be between 1.17 and 1.23. The value of 2.5 % has been chosen as representative for the scatter in Figures 10 and 11, reflecting to the assumed epistemic uncertainties in the component conversions.

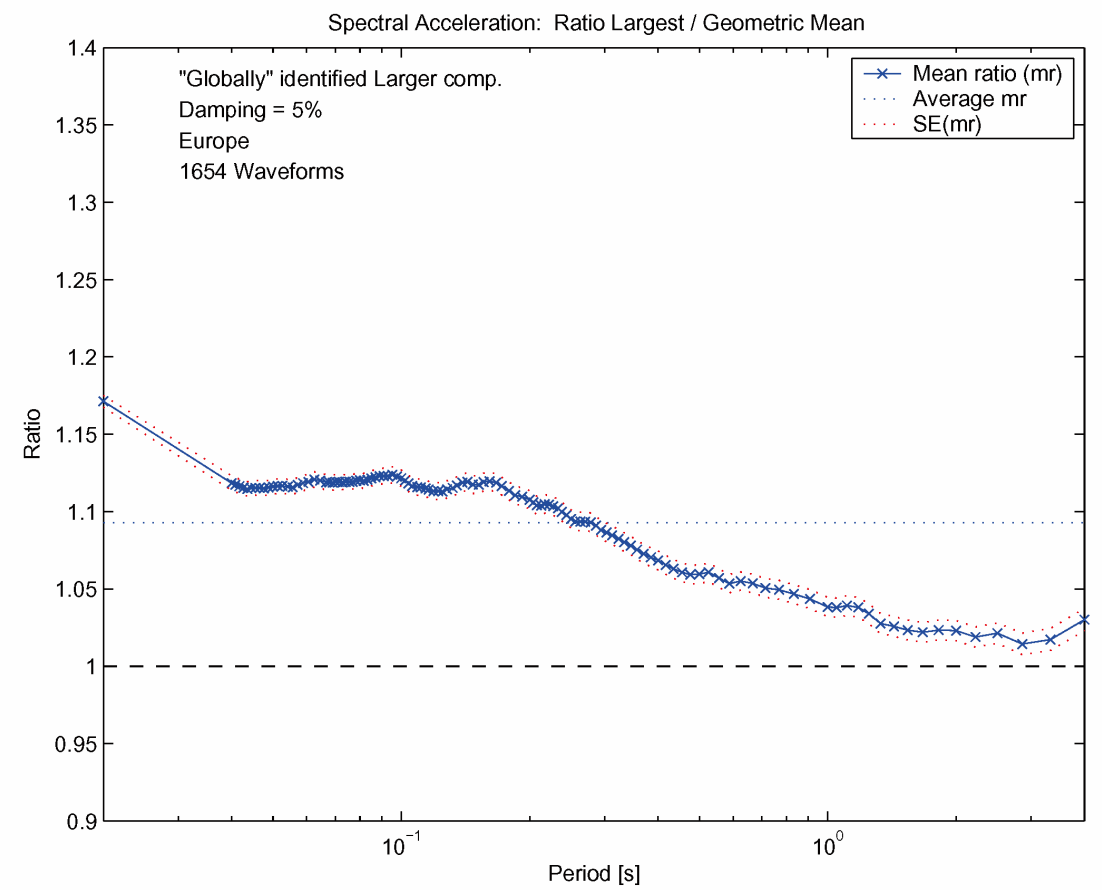

Fig. 11: Spectral acceleration ratios (5 % damping) between the largest horizontal component ('globally' identified) and the geometric mean, based on the worldwide WAF data base

From TP2-TN-0242, page 9.

Tab. 6: Values and weights for conversion to geometric mean for horizontal motion

Conversion to geometric mean from	Model	Weights		
		0.2	0.6	0.2
Random	One-to-one	Coefficient minus 2.5 %	Coefficient as given	Coefficient plus 2.5 %
Larger	TP2-TN-0269			
Arithmetic mean	TP2-TN-0269			

3.7 Missing frequencies

The selected relations have a frequency coverage as shown in Table 7, where 'no' indicates that no coefficients available and where the lighter shading indicates the availability of other frequencies that possibly can be used to constrain the values for the required frequencies.

Tab. 7: Frequency coverage for the selected attenuation relations

Rel. / Freq.	0.5	1.0	2.5	5.0	10	15	20	25	33	35	50	PGA
Ambraseys et al.							no		no		no	
Berge-Thierry et al.											no	no
Sabetta & Pugliese							no		no		no	
Campbell & Bozorgnia									no		no	
Spudich et al.							no		no		no	
Somerville et al.							no		no		no	
Toro et al.							no		no		no	
Revised SPS												

My solution to the missing frequencies is to following the method outlined and tested in TP2-TN-0270. Even so, the following comments, in part written before this report was available, apply with respect to missing frequencies:

- For 20 Hz, the missing values can be computed through interpolation between 10 and 25 Hz, by means of a conventional third order polynomial fit, alternatively a linear interpolation based on $\log_{10}$ frequencies as done in TP2-TN-0270 can be used for Somerville et al., Toro et al., and Sabetta & Pugliese, since 25 Hz is available in all of those relations.
- For 33 Hz the same method could be used by interpolating between 20 (or 25 Hz) and PGA for Ambraseys et al., Campbell & Bozorgnia, Spudich et al., and Somerville et al., as done already in TP2-TN-0270.
- For 50 Hz it is hard to see any real justification for separating this from PGA, since most of the (originally analogue) data that are used in the relations do not resolve such high frequencies anyway (no Fourier energy above 50 Hz).
- For PGA Berge-Thierry et al. there are two possibilities, either (1) to drop it and distribute its weight distributed equally on the weights from the remaining six relations, or (2) to use the 33 Hz value as PGA as suggested in TP2-TN-0270. The latter solution is preferred.

The discussions at WS3 between the experts resolved that a linear interpolation would presumably be more stable that a polynomial fit, which is supported by the behaviour of the coefficients as seen in TP2-TN-0270 (see the example in Figure 12). In conclusion, I therefore include in my model the TP2-TN-0270 procedure for missing frequencies.

3.8 Style-of-faulting adjustments

The source models from SP1 imply different styles of faulting for the different earthquake source zones, usually specified in terms percentages for the different styles of faulting. This calls for a way to make the ground motion models style-of-faulting dependent.

Ideally, this adaption to style-of-faulting models should be done by having style-of-faulting scale factors in each of the ground motion relations. This is not feasible, however, since only one of the relations used here has such scale factors built in, namely Campbell & Bozorgnia (2002), offering a differentiation between all types of faulting.

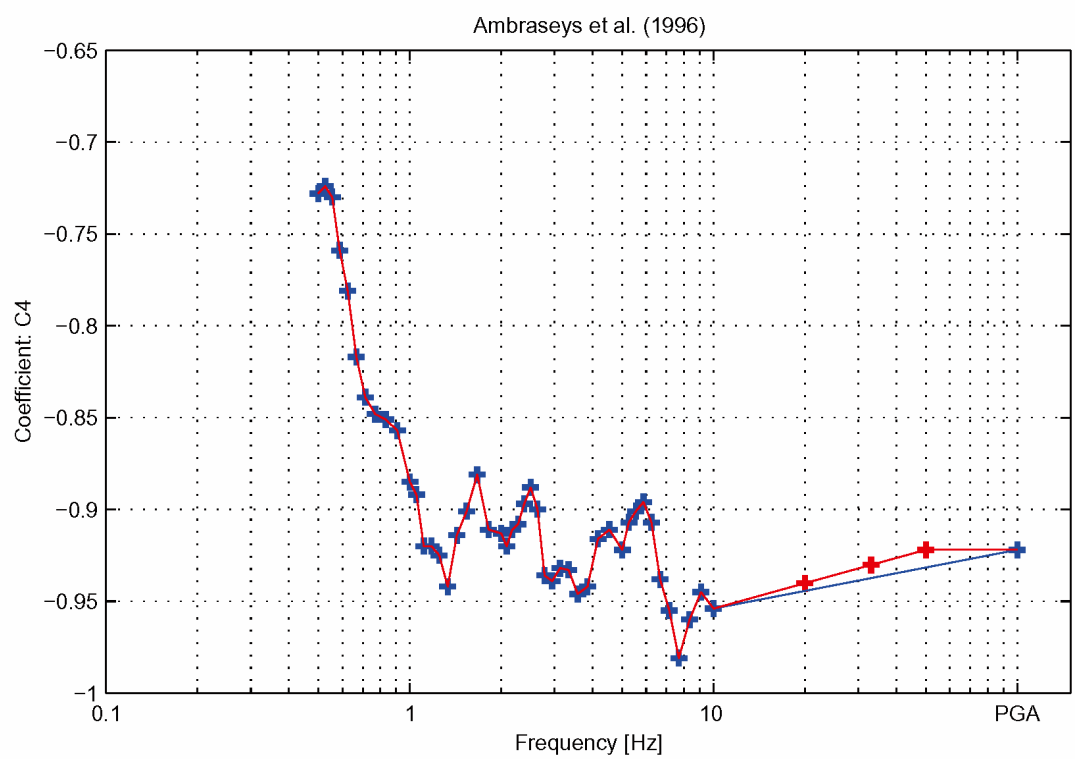

Fig. 12: Interpolation (linear in $\log_{10}$ – lin space between the two nearest values) for coefficient C_4 in Ambraseys et al. (1996), where red indicates interpolated coefficients and blue given ones

From TP2-TN-0270, page 56.

Alternatively, another approach could be based on the distribution of style-of-faulting present in each of the earthquake data bases used for each of the relations. This is summarized in TP2-TN-0362, Table 1, and shown here in Table 8.

Tab. 8: Overview of style-of-faulting in the earthquake databases used for developing the ground motion relations that are included in the present model

Restructured from TP2-TN-0362, Table 1.

Relation	SS	REV	NML	N/SS	R/SS	OBL	UND
Ambraseys et al.	16	47	30				7
Berge-Thierry et al.	17	31	40			10	2
Campbell & Bozorgnia	Factors available						
Sabetta & Pugliese		39	45	5	6		5
Somerville et al.		100					
Spudich et al.	55		45				
Toro et al.	18	81	1				
Bay / Rietbrock	51	5	29	4	3		8

To use the information in Table 8 properly would imply a weighting scheme by which each relation would respond differently to each of the source zones, dependent on the style-of-faulting ratios in both the ground motion relations and in the source zones. This would not really be recommendable since it would imply a logic tree scheme which would be more complicated than the data and the knowledge behind it could support, and a solution like this would also be difficult to justify on the basis that considerable epistemic and aleatory uncertainties already have been built into the model, accounting also for variations over style-of-faulting.

The conclusion that I draw from this is that I do not want to change the basic magnitude-distance-frequency weighting scheme in Table 3, and as a consequence of this I will only add branches to the logic tree that are accounting for style-of-faulting in the same way for all of the ground motion relations. An overview to this end is given in Figures 13 and 14, based on results from Abrahamson & Silva (1997), Boore et al. (1997), and Campbell & Bozorgnia (2002), all three of which are candidate relations (only the last one is used in the present model).

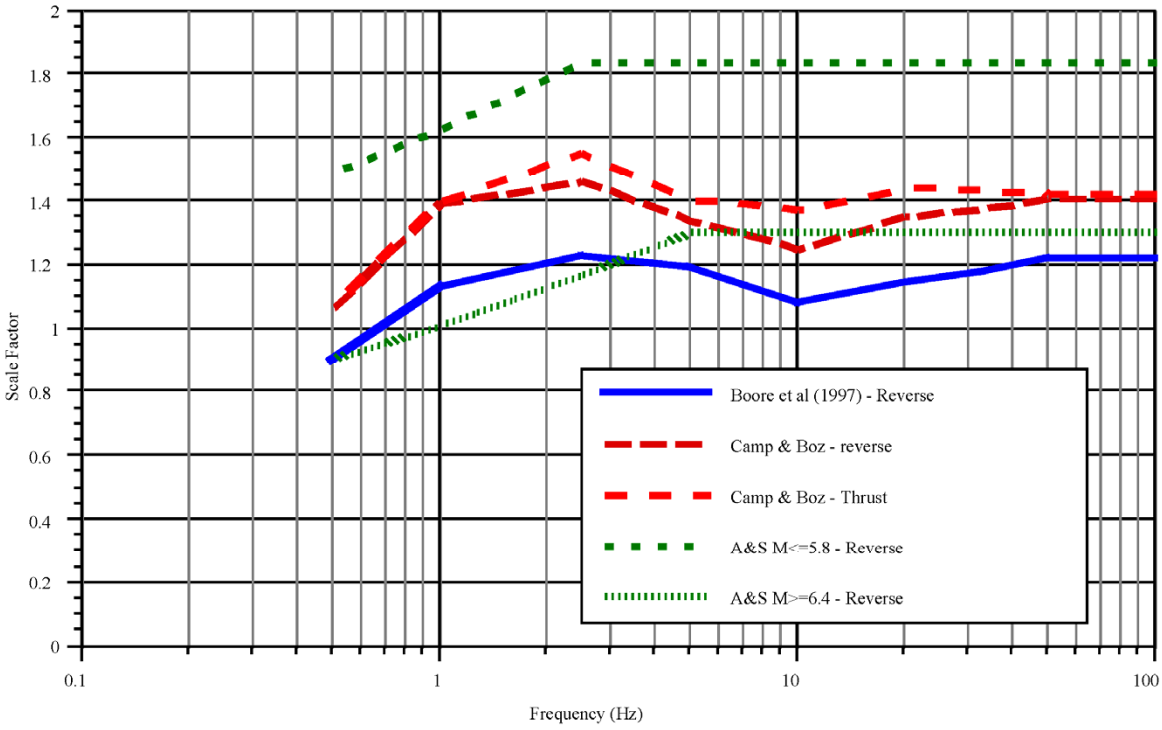

Fig. 13: Published scale factors for style-of-faulting adjustments for horizontal motion
From TP2-RF-0391, slide 2.

I have chosen to interpret these results in terms of the following simple model:

– No factors for normal and strike-slip earthquakes. For reverse faulting, horizontal motion, use frequency and magnitude independent factors of 1.15, 1.40 and 1.65, with weights of 0.2, 0.6 and 0.2, respectively. These numbers cover roughly the range as seen in the available empirical data.

– No effects on the H/V ratios, since such effects are poorly supported by the available data (moreover, vertical factors are not well constrained).

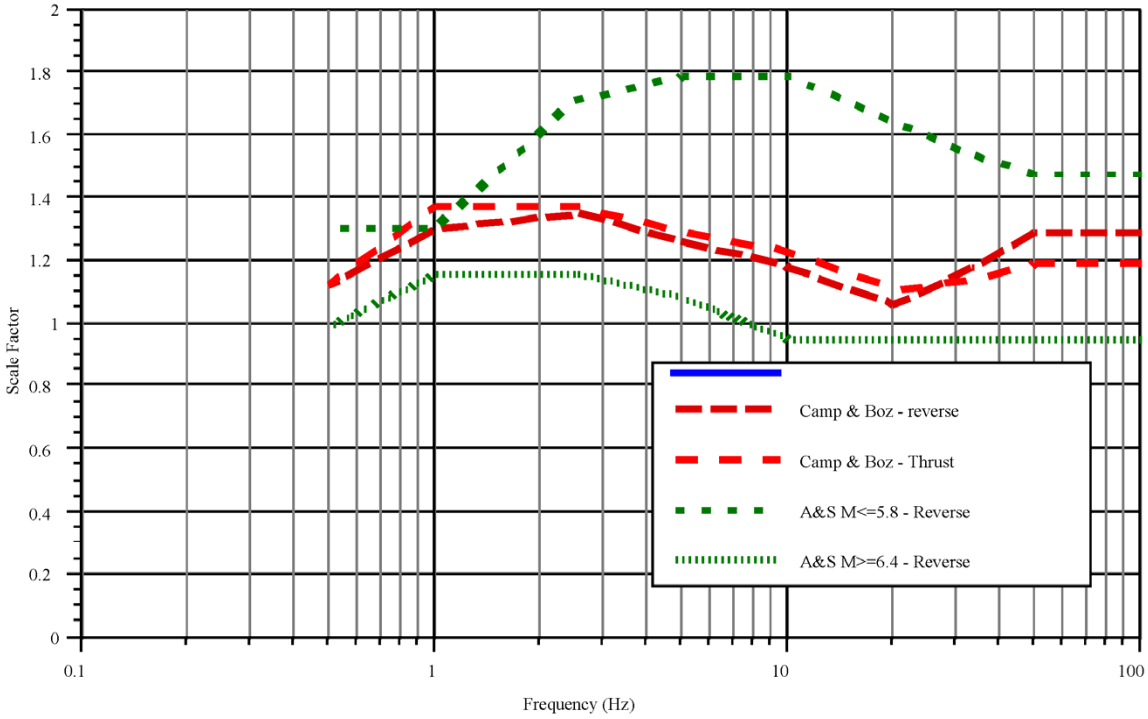

Fig. 14: Published scale factors for style-of-faulting adjustments for vertical motion From TP2-RF-0391, slide 3.

4 MEDIAN V/H RATIO

4.1 Approaches for V/H ratios

There are two viable approaches for estimating vertical ground motions:

1. To compute vertical motions based on vertical relations. Among the relations selected for horizontal motions Spudich et al. (1999) and Toro et al. (1997) do not provide relations for vertical ground motions, while for Ambraseys et al. (1996) a vertical relation, based essentially on the same data, has been published by Ambraseys & Simpson (1996).
2. To use some model for V/H ratio and apply this either by scaling the horizontal relations or by scaling the equal hazard spectrum. A viable approach here is the one used by Bozorgnia & Campbell (submitted to Earthquake Spectra 2002) who developed a scaling relation based on a global database of events with mixed modes of faulting. For rocks and very firm soil their model is as follows: (1) Within 20 km, a ratio of 0.5 below 3.33 Hz and a ratio of 0.9 above 10 Hz, and linearly interpolating for frequencies in between, (2) at 60 km, a ratio of 0.5 below 3.33 Hz and a ratio of 0.65 above 10 Hz, and linearly interpolating for frequencies in between.

My preference here is to use the first one of these methods, using the five available vertical relations as specified in the worksheet. The relative weights are the same as for the horizontal relations, only that they for each bin have been increased proportionally so as to add up to 1.0.

The V/H ratios can be obtained by dividing the vertical Sa from an attenuation relation by the corresponding horizontal Sa for that same attenuation relation.

4.2 Logic tree structure

The logic tree structure in terms of branches and weights is imbedded in this document and can easily be delineated together with the extraction of the model itself.

4.3 Weights for proponent models

Following the methodology outlined above, the results for the vertical relations will be as given in Table 9.

Tab. 9: Models and weights for median vertical ground motion

The magnitude (M1, M2) and distance limits (R1, R2) are defined in Table 2.

Magnitude	< M1			M1-M2			> M2		
Distance	< R1	R1-R2	> R2	< R1	R1-R2	> R2	< R1	R1-R2	> R2
Model	Weight								
Ambraseys et al.	0.250	0.250	0.348	0.222	0.222	0.308	0.200	0.233	0.276
Berge-Thierry et al.	0.083	0.167	0.261	0.074	0.148	0.231	0.167	0.200	0.241
Sabetta & Pugliese	0.250	0.250	0.304	0.222	0.222	0.269	0.067	0.067	0.138
Campbell & Bozorgnia	0.333	0.250	0	0.296	0.222	0	0.276	0.200	0
Somerville et al.	0.083	0.083	0.087	0.185	0.185	0.192	0.300	0.300	0.345
Sum weights	1	1	1	1	1	1	1	1	1

5 ALEATORY VARIABILITY FOR HORIZONTAL GROUND MOTION

An important question to be discussed with respect to aleatory variability is whether or not the scatter derived from a particular empirical relation should be used also when the relation is applied to another region, in fact, the question has also been raised as to whether or not the derived scatter should apply even when it is used in the same region (the ergodicity principle, cf. the Californian 'precarious stones', Brune 1999).

The basic position behind my present model for aleatory variability is that the scatter appearing from the relations in a situation like the present one (California may be different) should be considered only as a guide (admittedly an important one) for what should be used in the hazard computations, and the present solution is therefore to connect a logic tree branch to this parameter as explained in the following. One should still, however, essentially base the values on the relation-derived sigmas, and there are two ways to do this:

- For each relation and frequency, use the derived sigma as a central value in a logic tree variation. The range of variation of the sigmas to be used should depend on an assessment of the source type and tectonic variation in the region of application.
- Another and simpler solution is, for each frequency, to use the range of sigmas in the logic tree branch as derived from an overall assessment of the applied relations.

The preferred solution is the last one, and it is implied here that aleatory variability will be frequency dependent, expected to increase with decreasing frequency. In doing this assessment for individual frequencies one should also aim at maintaining a certain smoothness over frequency.

As a basis for this, the relations have been reviewed in terms of their individual sigma values, resulting in the overview provided in Table 10.

Tab. 10: Sigma values ($\log_{10}$ based) from the different relations

For Campbell & Bozorgnia and Toro et al. there is a magnitude dependence that introduces a range of variability that in this table is indicated only in the first case.

	0.5	1.0	2.5	5.0	10	20	33	50	PGA
Ambraseys et al.	.32	.32	.31	.27	.27				.25
Berge-Thierry et al.	.40	.37	.35	.33	.30	.30	.29		
Sabetta & Pugliese	.30	.30	.26	.22	.19				.17
Campbell & Bozorgnia (range)	.22 .29	.22 .29	.20 .28	.20 .27	.19 .26	.18 .26			.17 .23
Spudich et al.	.31	.27	.24	.23	.27				.20
Somerville et al.	.36	.00	.26	.27	.26	.26			.25
Toro et al.	.39	.39	.34	.33	.38	.47			.30

5.1 Logic tree structure

The logic tree structure in terms of branches and weights is imbedded in this document and can easily be delineated together with the extraction of the model itself.

5.2 Weights for proponent models

The summary of sigma value variations shown in Table 10 were used to estimate average values and ranges. In estimating these average values, support has also been acquired from similar results from other studies. An example here is the study by Schmidt et al. (1997) based on a large data base from Costa Rica, providing a value of 0.34 for PGA and values of 0.28, 0.35 and 0.36 for PSV, for frequencies of 0.25, 2.0 and 10 Hz, respectively.

From both empirical data and modelling results there are clear indications of a magnitude (amplitude) and distance dependence of the variability. While this to some extent could be a combined effect of fewer data points and an upper ground motion limit that (the latter one) will be taken care of elsewhere, the magnitude effect is still significant enough to be included in the model.

My model for magnitude dependence is given in Table 12, where the second row is an average of results published by Youngs et al. (1995), Toro et al. (1997) and Campbell & Bozorgnia (2002), with coefficients converted to $\log_{10}$ basis. However, since there is a solid empirical basis behind the numbers in Table 11, as an average over magnitudes, I have chosen to give the magnitude dependence a weight of 2/3 only, as shown in Table 12.

Tab. 11: Sigma values ($\log_{10}$ based) and weights for different frequencies

	wgt	0.5	1.0	2.5	5.0	10	20	33	50	PGA
σ low	0.2	.21	.21	.21	.21	.21	.21	.21	.21	.21
σ mean	0.6	.30	.29	.29	.28	.27	.26	.26	.25	.25
σ high	0.2	.38	.37	.36	.35	.33	.32	.31	.30	.30

Tab. 12: Magnitude sensitivity of sigma

Weight	Relation
0.333	σ = σ (as in Table 11)
0.667	σ = σ (as in Table 11) - 0.03*(M - 6)

5.3 Horizontal component conversions

The standard deviation of the residuals does vary depending on component definition as shown in TP2-TN-0307. This variation is, however, minor when compared to the range related to the use of different data sets, as shown in Tables 10 and 11. Therefore, it is neglected.

5.4 Magnitude conversion effect

The approach chosen in the above for modelling the aleatory variability is one in which all of the scatter is captured in an overall variability as expressed through the numbers in Tables 11 and 12. This approach is therefore principally different from one in which the variability is propagated through different conversions. Given this, a specific conversion effect for magnitude conversions is therefore not applicable in my model.

5.5 Distance conversion effect

A specific distance conversion effect is not applicable in my model, for the same reason as just given for the magnitude conversion effect.

6 MAXIMUM GROUND MOTIONS FOR THE HORIZONTAL COMPONENT

There are two ways in which this problem can be addressed, based on empirical data and modelling, both of which are extensively explored in this project. My model will be based on a synthesis of both of these approaches. Moreover, a recent paper by Guatteri et al. (2003), exploring the balance between kinematic and dynamic modelling, has been of great additional help in defining my model.

6.1 Evaluation of empirical data

The empirical data have been reviewed in TP2-TN-0309 based on the WAF data base. Essentially, the empirical data show PGA values up to 1.4g and spectral acceleration up to about 2.5 g in the frequency range 2 – 10 Hz. Excerpts from a review of the WAF global data base is shown in Figures 15 and 16.

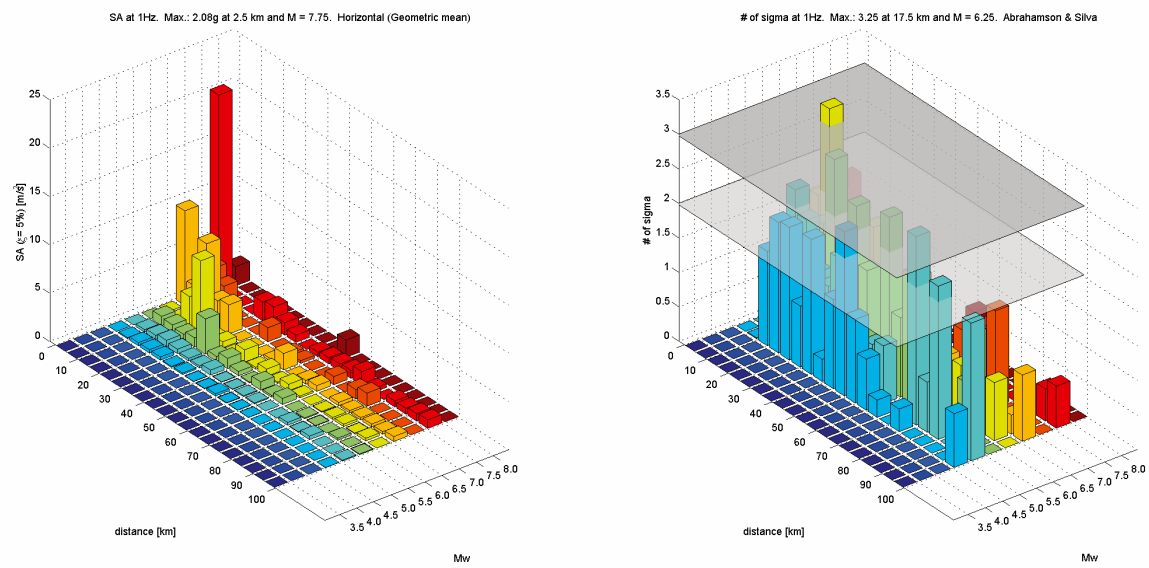

Fig. 15: Maximum observed horizontal (geometric mean) ground motions in magnitude-distance space for a frequency of 1 Hz

The maximum value is 2.08g at a distance of 2.5 km from a M 7.75 earthquake. The corresponding distribution of residuals is given to the right. From TP2-TN-0309, page 5.

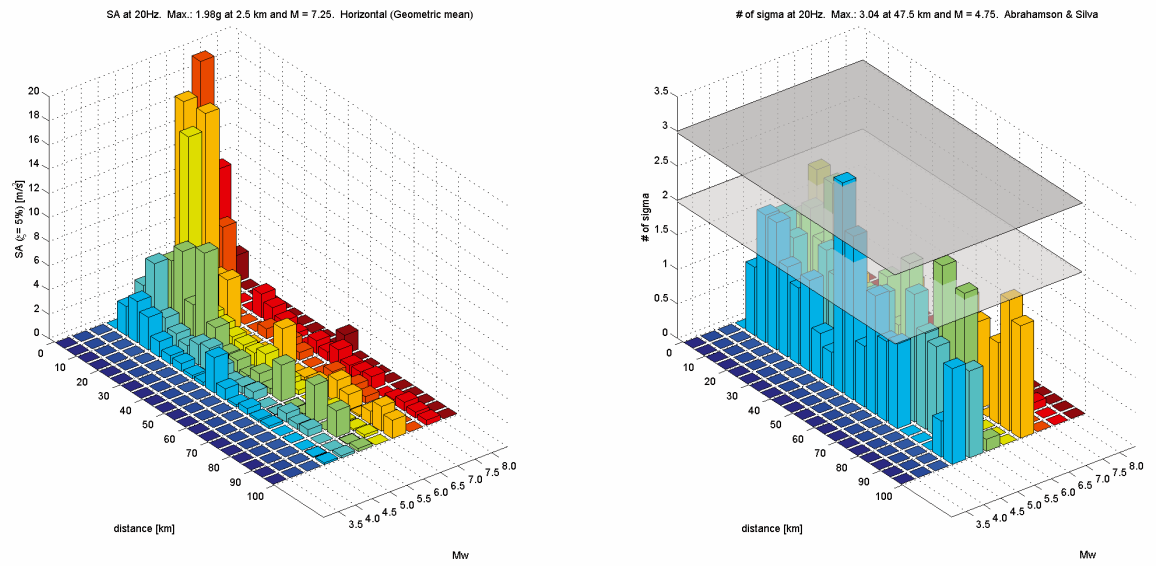

Fig. 16: Maximum observed horizontal (geometric mean) ground motions in magnitude-distance space for a frequency of 20 Hz

The maximum value is 1.98g at a distance of 2.5 km from a M 7.25 earthquake. The corresponding distribution of residuals is given to the right. From TP2-TN-0309, page 10.

6.2 Evaluation of numerical simulations

The theoretical path has been explored through the kinematic modelling of the OGS (Priolo) and the URS (Pitarka) groups (a number of reports from both), subsequently reviewed by Madariaga (EXT-TN-0308). A synthesis of the simulation results are, together with selected empirical maximum ground motion data, shown in Figures 15 and 16. Both empirical data and simulated results are shown in Figures 17 to 20, for 1 and 10 Hz and for magnitudes 5.5 and 7.0. As should be expected, the simulated results range significantly above the empirical values.

The question that arises now is whether or not one could experience, in an extreme case, which means highly unlikely but still physically not impossible, even higher ground motions that have not so far been captured empirically. This was the purpose of the OGS and the URS studies, where I would like to start with the review of Madariaga, who is one of the most competent persons that one could find for a review like this one.

Madariaga's conclusions are as follows:

- At low frequencies both the OGS and the URS models are *very likely*.
- At high frequencies the URS model, with the exception of a 2 Hz peak, is *likely*.
- At high frequencies the OGS model is *not likely*, essentially due to the zero rise time model, causing an instantaneous slip front.
- The supershear models in either study are *not realistic / very unlikely*.

In filtering both the OGS and the URS modelling results through Madariaga's conclusions I find that they are quite consistent with my model for maximum ground motions as given in Table 13, which will be explained in more detail in Section 6.4.

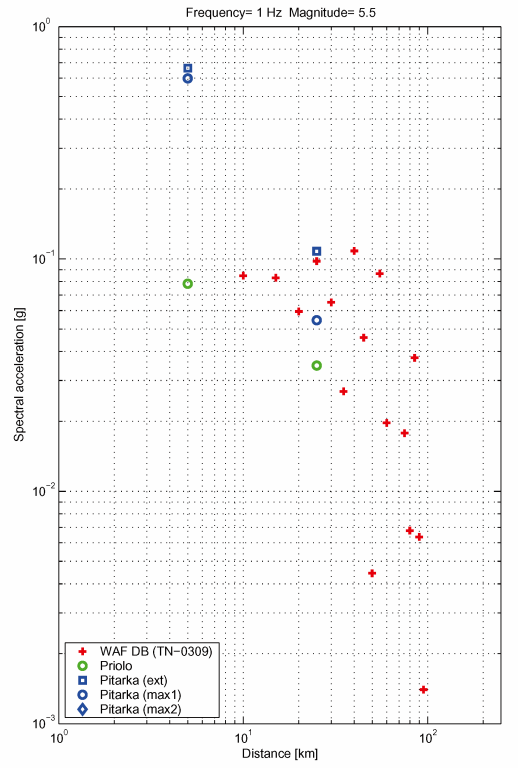

Fig. 17: Maximum empirical and simulated ground motion data for 1 Hz and magnitude 5.5 From TP2-TN-0333 (modified).

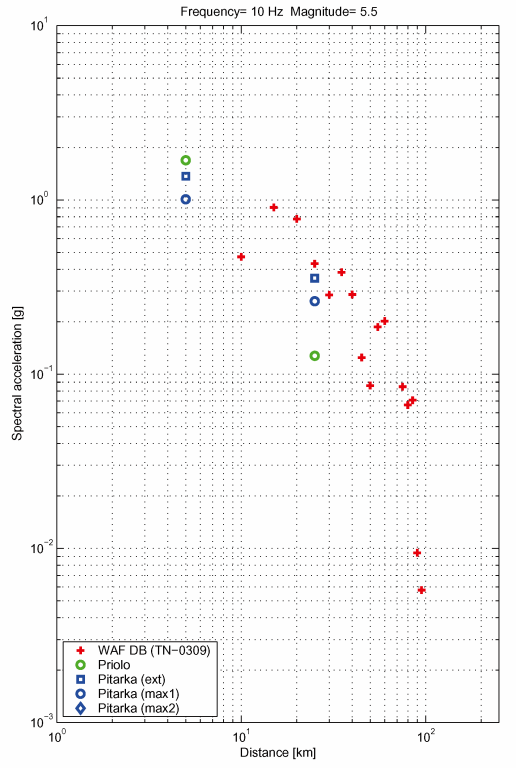

Fig. 18: Maximum empirical and simulated ground motion data for 10 Hz and magnitude 5.5 From TP2-TN-0333 (modified).

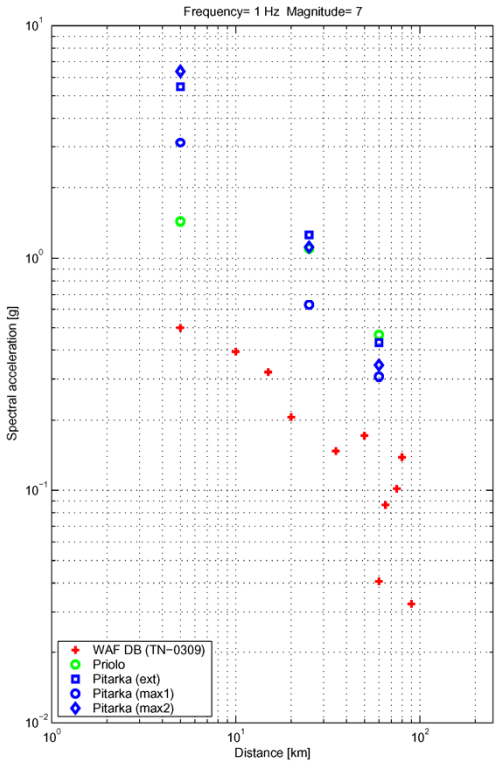

Fig. 19: Maximum empirical and simulated ground motion data for 1 Hz and magnitude 7.0 From TP2-TN-0333 (modified).

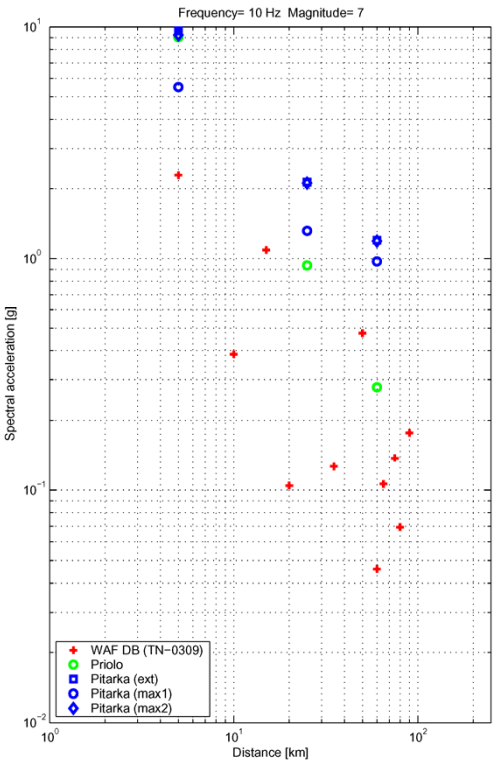

Fig. 20: Maximum empirical and simulated ground motion data for 10 Hz and magnitude 7.0 From TP2-TN-0333 (modified).

Finally I would like to refer also to the Guatteri et al. (2003) paper, using both kinematic and (simplified) dynamic modelling. The dynamic model capture more complexity at the source and thereby also results in more variability in the ground motions, in particular in the near field (< 1 km). This makes the ground motions highly event specific, calling for a sufficient leverage when specifying maximum ground motions. Even so, the one sigma spectral accelerations for magnitude 7 and 2 Hz are around 2g in the near field and 0.1g at 100 km, which also is safely within the limits in Table 13, in particular when considering that the logic tree values range up to twice the tabulated values.

6.3 Logic Tree Structure

The logic tree structure in terms of branches and weights is imbedded in this document and can easily be delineated together with the extraction of the model itself.

6.4 Weights for maximum ground motions

The justification for the values chosen comes as already mentioned from a combined assessment of empirical data and theoretical considerations. I have chosen to answer the request for a break-down of the numbers in frequency, distance and magnitude as shown in Table 13.

The spectral shape, the decay in distance and the magnitude scaling in Table 13 is based on Somerville et al. (2001), on the basis that their relation is well calibrated against larger earthquakes. What I have done then in Table 13 is simply to set the value for near field maximum PGA (M 7.5, D 1 km, highlighted) to 3.0 g, based on my interpretation of empirical and simulated data, and to scale all of the other numbers accordingly based on the Somerville et al. (2001) magnitude-distance surface. If need be, the table can easily be further interpolated (expanded) in magnitude and distance.

Tab. 13: Model for the largest ground motions (absolute limits, all in g), broken down in frequency (PGA, 25, 10, 5, 2.5, 1.0, 0.5 Hz), magnitude (M_W 7.5, 6.5, 5.5) and distance (1, 10, 50, 100 km)

The associated logic tree structure is defined in the main text. The magnitude-distance surface is based on Somerville et al. (2001).

Mag	Dist	PGA	25.0	10.0	5.0	2.5	1.0	0.5
7.5	1	3.0000	5.9276	5.7697	4.9869	4.1797	1.4678	0.6120
	10	2.0867	4.1230	4.0132	3.4687	2.9238	1.0324	0.4293
	50	0.6348	1.2542	1.2208	1.0551	0.9121	0.3352	0.1408
	200	0.0688	0.1360	0.1323	0.0967	0.0663	0.0279	0.0119
6.5	1	1.3372	2.6422	2.5718	1.9030	1.3720	0.4299	0.1517
	10	0.8007	1.5820	1.5398	1.1394	0.8261	0.2603	0.0916
	50	0.2193	0.4334	0.4218	0.3121	0.2321	0.0761	0.0271
	200	0.0217	0.0429	0.0418	0.0261	0.0154	0.0058	0.0021
5.5	1	0.5961	1.1778	1.1464	0.6547	0.3672	0.0952	0.0254
	10	0.3072	0.6070	0.5908	0.3374	0.1903	0.0496	0.0132
	50	0.0758	0.1497	0.1457	0.0832	0.0482	0.0131	0.0035
	200	0.0069	0.0136	0.0132	0.0064	0.0029	0.0009	0.0002

The values in Table 13 should go together with a logic tree defined such that the tabulated values each have a weight of 0.6, while values 50 % lower and 100 % higher both have weights of 0.2. This gives a range of a factor of four between the lowest and the highest brach values, expressing my evaluation of the large uncertainties involved in assessing maximum ground motions.

The model thereby gives near field PGA values in the logic tree range 1.5 to 6 g, centered on 3 g, with spectral acceleration at 25 Hz between roughly 3 and 12 g, centered on 6 g. This is, in my view, sufficiently realistic estimates in relation to both the empirical data, given that I now have a fair number of large earthquakes that have been well captured by near field instruments, and to the simulated results, as discussed and summarized above.

An effect of the way I have chosen to estimate the values in Table 13 is that the magnitude scaling (between M 7.5 and M 5.5) is strictly that of Somerville et al. (2001). Even so, I find that this scaling is of the same order as seen when comparing Figures 17 – 18 with Figures 19 – 20, the large scatter taken into consideration. The values in Table 13 are therefore largely consistent with both of these moment magnitude levels.

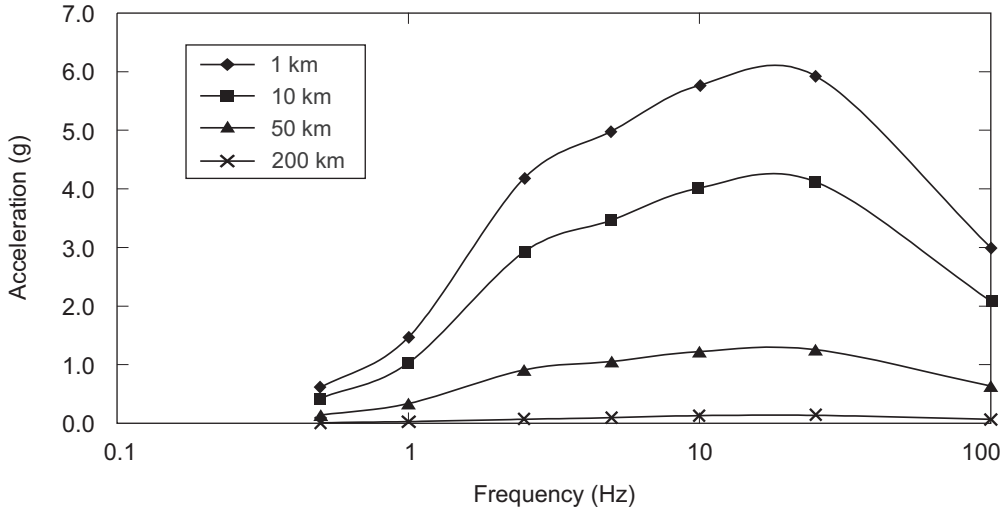

Fig. 21: Model for maximum ground motions for M 7.5 as given in Table 13

This model has a weight of 0.6, while values 50 % smaller and 100 % larger each one has a weight of 0.2.

7 MAXIMUM GROUND MOTIONS FOR THE VERTICAL COMPONENT

The range of variation of the model presented above for maximum horizontal ground motions is a factor of four, reflecting the large uncertainties in the estimation of a parameter where both an empirical and a theoretical (modelling) approach have significant limitations. The same clearly applies to the vertical ground motions, where both empirical and modelling results indicate that one should be well within a factor of two as compared to the horizontal values, which in turn will result in a considerable overlap between the two ranges of variation.

7.1 Evaluation of empirical data

For empirical data it is well known that V / H ratios between 0.5 and 1.0 are common for the largest earthquakes, and even if this cannot be excluded there is no clear indications for the extreme ground motions to have significantly different H/V ratios. A similar uncertainty applies to a possible frequency dependence of the H/V ratio.

7.2 Evaluation of numerical simulations

See above.

7.3 Logic Tree Structure

My position here is therefore that I do not have a sufficient basis for independently assessing horizontal and vertical ground motions in terms of maximum values, also since the V / H ratios in that case easily could become unstable and poorly justified. This applies in particular to the simulations, which are only indicating ballpark levels for maximum ground motions while they are not considered to be sufficiently reliable for a delineation of V / H ratios. Therefore, only a constant scale factor is used.

7.4 Weights for maximum ground motions

For reasons just given, my conclusion from this is that I use a V / H ratio of 2/3 throughout, scaling all of the numbers in Section 6 accordingly (including Table 13).

8 UPPER TAIL OF THE GROUND MOTION DISTRIBUTION FOR THE HORIZONTAL COMPONENT

In addition to the absolute ground motions as just defined I also prefer to introduce a limitation in the number of standard deviations. A central problem here is that there is no solid theoretical justification for such a limit, not even for the distribution. However, after reviewing the residuals provided it is difficult to justify a model that deviates in any systematic way from the lognormal one, even at the tails.

8.1 Evaluation of empirical data

There are three kinds of analyses that have been provided by Pegasos in response to this challenge:

1. The residuals that are provided for practically all of the candidate attenuation relations, evaluated against different data sets, see Figures 22 and 23. These plots have first of all been useful for assessing the appropriateness of the relations but also for understanding the characteristics of the residuals. Naturally, it takes around 1000 values to reach 3 sigma. At that level there are many deviations from the lognormal distribution, but with no systematic trend that would indicate any stable deviation from a lognormal distribution. There are moreover instabilities over frequencies and of course a sensitivity to the relations used. These plots offer little help in assessing the nature and quality of the observations at the very tail of the distribution.
2. The ground motion plots based on the WAF data base (TP2-TN-0309, see Figures 15 and 16) used primarily in assessing the largest ground motions, but also providing associated sigma values. For the Abrahamson & Silva model the maximum sigma values are around 3.0, and slightly less for Spudich. This means that truncating at that level (3 sigma) would be equivalent to an absolute limit at the level of the maximum observed ground motions.
3. The residuals provided for the ground motion models of Lussou et al. and Berge-Thierry et al. (file "residu_top50.xls"), specifically identifying the ten largest residuals. Typically, the largest residuals are for intermediate magnitudes (4 – 6) and for large distances (> 30 km), and the 3 sigma level is usually reached somewhere among the 10 highest values. Most likely, many of these values are associated with quality problems of some sort.

8.2 Logic Tree Structure

I am reluctant to introduce a truncation here that interferes significantly with the maximum ground motion level, while I on the other hand prefer to have one such limit in order to catch excessive deviations from intermediate-magnitude earthquakes. Since another distribution than the lognormal one cannot be properly justified, an abrupt truncation seems to be the most reasonable solution, albeit with a logic tree branching.

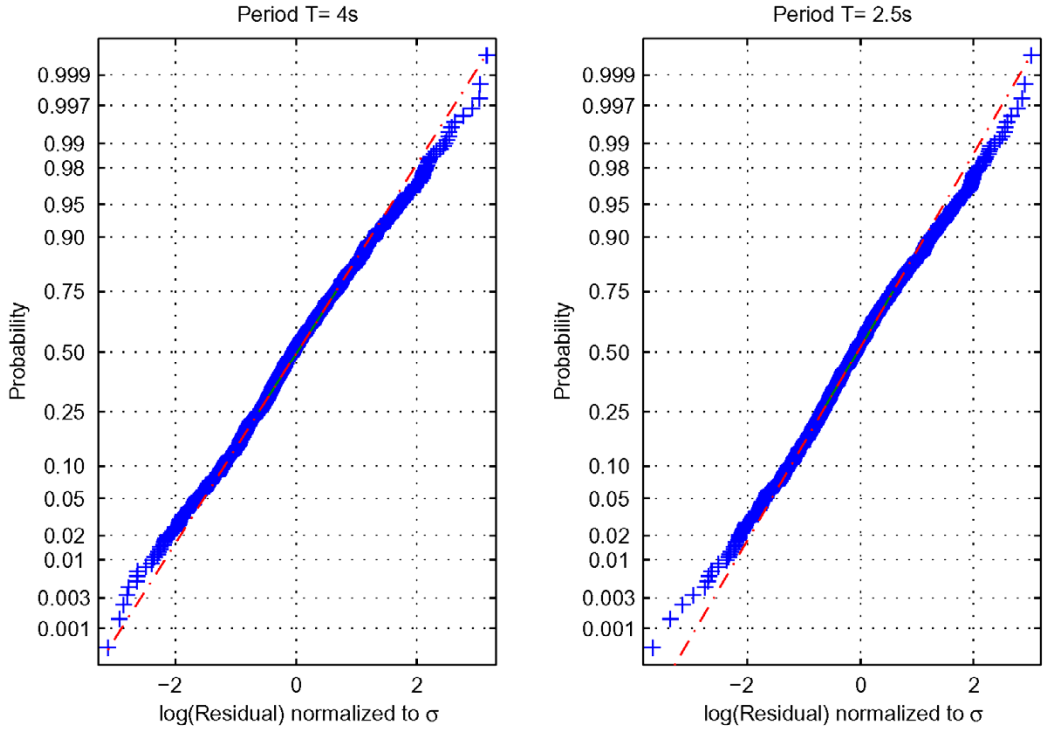

Fig. 22: Residuals of ground motion model by Berge-Thierry et al. (2000), horizontal

Data from Europe and Middle East, all sources, rock (V_{S30} = 750 m/s), frequencies 0.25 and 0.4 Hz. From TP2-TN-0228, page 34.

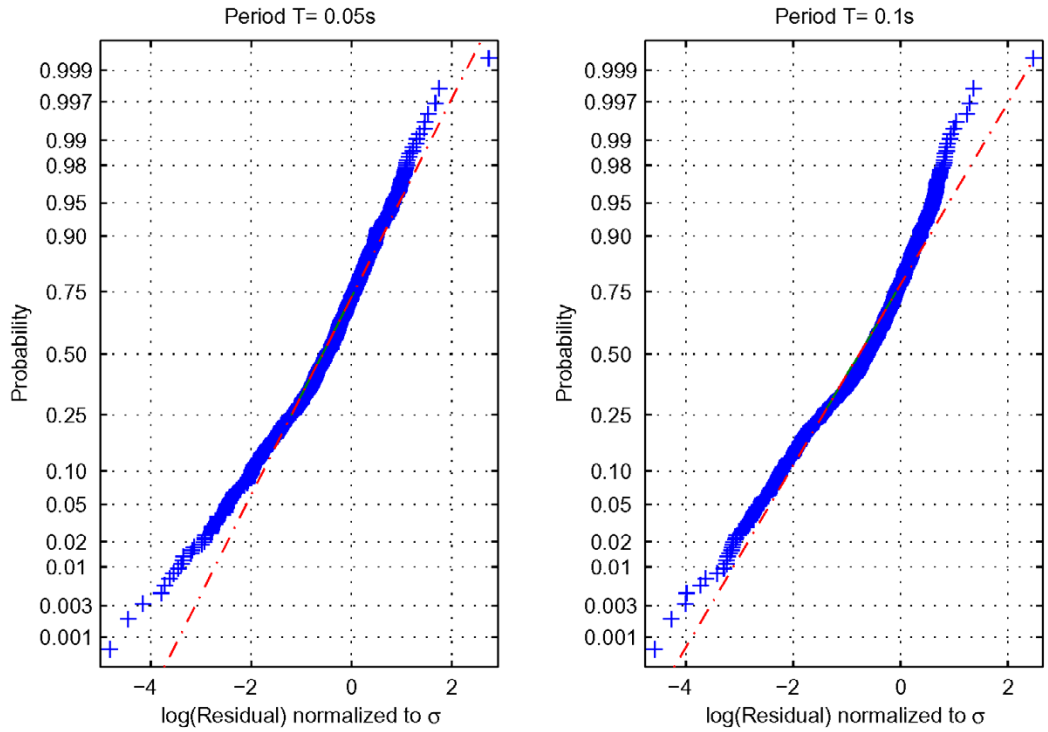

Fig. 23: Residuals of ground motion model by Campbell & Bozorgnia (2002), horizontal

Data from Europe and Middle East, all sources, rock (V_{S30} = 750 m/s), frequencies 20 and 10 Hz. From TP2-TN-0231, page 32.

8.3 Weights for upper tail models

Based on the above data and reasoning my model for truncating the tail of the residual distribution will then appear as seen in Table 14. The main reason for limiting the values to 4 sigma is that values above that level most likely are reflecting quality problems with the data, as already discussed.

Tab. 14: Model for the upper tail of the ground motion distribution, with abrupt truncations at the given sigma levels

Weight	Sigma
0.2	3.0
0.6	3.5
0.2	4.0

9 REFERENCES

Abrahamson, N.A. & Silva, W.J. 1997: Empirical response spectral attenuation relations for shallow crustal earthquakes. Seism. Res. Lett. 68, 94-127.

Ambraseys, N.N. & Douglas, J. 2000: Reappraisal of the effect of vertical ground motions on response. ESEE Report No. 00-4, Department of Civil & Environmental Engineering, Imperial College, London (Revised version submitted to Soil Dynamics & Earthquake Engineering).

Ambraseys, N.N. & Free, M.W. 1997: Surface-wave magnitude calibration for European region earthquakes. J. Earthq. Eng. 1, 1-22.

Ambraseys, N.N., Simpson, K.A. & Bommer, J.J. 1996: Prediction of horizontal response spectra in Europe. Earth. Eng. Struct. Dyn. 25, 371-400.

Ambraseys, N.N. & Simpson, K.A. 1996: Prediction of vertical response spectra in Europe. Earth. Eng. Struct. Dyn. 25, 401-412.

Atkinson, G. & Boore, D.M. 1997: Some comparisons between recent ground-motion relations. Seism. Res. Lett. 68, 24-40.

Bay, F. 2002: Ground motion scaling in Switzerland: Implications for hazard assessment. PhD thesis, ETH Zürich.

Berge-Thierry, C., Cotton, F., Cushing, M., Griot-Pommera, D.-A., Joly, J., Levret, A. & Fukushima, Y. 2000: Methode de determination des verticaux adaptes au site dans le cadre de la RFS I.2.c. Rapport IPSN/Departement de Protection de l'Environment, Sergd/00-53.

Berge-Thierry, C., Griot-Pommera, D.-A., Cotton, F. & Fukushima, Y. 2002: New empirical response spectral attenuation laws for moderate European earthquakes. J. Earthq. Eng., submitted.

Boore, D.M. & Joyner, W.B. 1997: Site amplification for generic rock sites. Bull. Seism. Soc. Am. 87, 327-341.

Boore, D.M., Joyner, W.B. & Fumal, T.E. 1994: Estimation of response spectra and peak accelerations from western North American earthquakes: An interim report, Part 2. USGS Open-File Report 94-127, 40 pp.

Boore, D.M., Joyner, W.B. & Fumal, T.E. 1997: Equations for estimating horizontal response spectra and peak accelerations from western North American earthquakes: A summary of recent work. Seism. Res. Lett. 68, 128-153.

Bozorgnia, Y. & Campbell, K.W. 2002: Vertical-to-horizontal response spectral ratio and vertical design spectrum. Earthq. Spectra., submitted.

Brune, J.N. 1999: Precarious rocks along the Mojave section of the San Andreas Fault, California: Constraints on ground motion from great earthquakes. Seism. Res. Lett. 70, 29-33.

Bungum, H., Lindholm, C. & Dahle, A. 2003: Long period ground motions for large European earthquakes, 1905-1992, and comparisons with stochastic predictions. J. Seism. 7/3, August 2003.

Campbell, K.W. 1989: The dependence of peak horizontal acceleration on magnitude, distance, and site effects for small-magnitude earthquakes in California and eastern North America. Bull. Seis. Soc. Am. 79, 1311-1346.

Campbell, K.W. 1997: Empirical near-source attenuation relationships for horizontal and vertical components of peak ground acceleration, peak ground velocity, and pseudo-absolute acceleration response spectra. Seism. Res. Lett. 68, 154-179.

Campbell, K.W. & Bozorgnia, Y. 2002: Updated near-source ground motion relations for the horizontal and vertical components of peak ground acceleration and acceleration response spectra.. Bull. Seism. Soc. Am., submitted (revised).

Guatteri, M., Martin Mai, P., Beroza, G.C. & Boatwright, J. 2003: Strong ground motion prediction from stochastic-dynamic source models. Bull. Seism. Soc. Am. 93, in press.

Haddon, R.A.W. 2000: Comment on "Evaluation of models for earthquake source spectra in Eastern North America" by Gail M. Atkinson and David M. Boore. Bull. Seism. Soc. Am. 90, 1332-1338.

Johnston, A.C., Coppersmith, K.J., Kanter, L.R. & Cornell, C.A. 1994: The earthquakes of stable continental regions. Tech. Rep. EPRI TR-102261s-VI-V5, Electric Power Research Institute, Palo, Alto, California.

Lussou, P., Bard, P.Y. & Cotton, F. 2001: Seismic design regulation codes: Contribution of K-net data to site effect evaluation. J. Earthq. Eng. 5, 13-33.

Odum, J.K., Williams, R.A., Stephenson, W.J. & Worley, D.M. 2003: Near-surface S-wave and P-wave seismic velocities of primary geological formations on the Piedmont and Atlantic Coastal Plain of South Carolina, USA. USGS Open-File Report 03-043, 14 pp.

PEGASOS EG2-ES-0025: Sabetta, F.: Assoc. EXM. EG2-EXM-0010. Sensitivity Model Elicitation Summary Up-date.

PEGASOS EG2-ES-0035: Bungum, H.: Assoc. EXM. EG2-EXM-0021 Draft of final model H. Bungum.

PEGASOS EG2-EXM-0021: Bungum, H.: Final model H. Bungum.

PEGASOS EG2-TN-0314: Scherbaum, F. 2002: Comments on the report: Determination of input parameters for the stochastic simulation of strong ground motion for Switzerland.

PEGASOS EXT-TB-0043: SED 2002: ECOS: Earthquake Catalogue of Switzerland. Final version.

PEGASOS EXT-TN-0209: Bay, F. 2002: Comparison of WAF Database with Bay et al. 2002 database.

PEGASOS EXT-TN-0251: Bay, F. 2002: Forward Modelling to investigate stress-drop and Kappa values in relation with the model of Bay (2002).

PEGASOS EXT-TN-0306: Rietbrock, A. 2002: Determination of input parameters for the stochastic simulation of strong ground motion for Switzerland.

PEGASOS EXT-TN-0308: Madariaga, R. 2002: Assessment of feasibility of kinematic fault models used for upper limit ground motion evaluations for the Pegasos Project.

PEGASOS PMT-AN-0195: PMT/UAK 2002: Revised specifications of PEGASOS Results; 28.11.02.

PEGASOS TP2-RF-0350: Abrahamson, N. 2003: Rietbrock Model Interpretation.

PEGASOS TP2-RF-0391: Abrahamson, N. 2003: Style of faulting factors.

PEGASOS TP2-TN-0228: Hölker, A. & Roth, Ph.: Revised residuals from GM model of Berge-Thierry et al. 2000.

PEGASOS TP2-TN-0231: Hölker, A. & Roth, Ph.: Residuals from GM model of Campbell & Bozorgnia 2002 (subm.).

PEGASOS TP2-TN-0242: Roth, Ph.: Note on the statistical analysis on average / larger horizontal component from the WAF database.

PEGASOS TP2-TN-0254: Roth, 2002: Average shear wave velocity profiles for Europe and California.

PEGASOS TP2-TN-0269: Roth, Ph.: Note on the statistical analysis of the ratios between different definitions of the horizontal component.

PEGASOS TP2-TN-0270: Hölker, A. 2002: Note on the estimation of coefficients of ground motion models at missing frequencies.

PEGASOS TP2-TN-0307: Hölker, A. 2002: Note on the analysis of standard deviations of residuals computed using different definitions of the horizontal component.

PEGASOS TP2-TN-0309: Roth, Ph.: Note on the plots of the largest ground motion contained in the WAF database TP2-WAF-0008.

PEGASOS TP2-TN-0333: Hölker, A. & Roth, Ph. 2003: Note on Maximum Ground Motion Plots.

PEGASOS TP2-TN-0362: Birkhäuser, Ph. 2003: SP2 inquiry for the style-of-faulting distributions of the selected attenuation relations.

PEGASOS TP2-TN-0363: Lacave, C., Koller, M. & Birkhäuser, Ph. 2003: Final report on the computation of scaling factors for 20 generic "rock" profiles.

PEGASOS TP2-TN-0367: Roth, Ph.: Comparison of the accelerations of the Feb. 22 St. Dié earthquake with the Candidate GM Models.

PEGASOS TP2-TN-0368: Birkhäuser, Ph. 2003: Description of the topography for the stations of the Swiss Seismological Survey used by Bay (2000).

Spudich, P., Joyner, W.B., Lindh, A.G., Boore, D.M., Magaris, B.M. & Fletcher, J.B. 1999: SEA99: A revised ground motion prediction relation for use in extensional tectonic regimes. Bull. Seism. Soc. Am. 89, 1156-1170.

Sabetta, F. & Pugliese, A. 1996: Estimation of response spectra and simulation of nonstationary earthquake ground motions. Bull. Seism. Soc.Am., 86, 337-352.

Schmidt, V.A., Dahle, A. & Bungum, H. 1997: Costa Rican Spectral Strong Motion Attenuation. Technical report under the project Reduction of Natural Disasters in Central America, NORSAR, November 1997, 45 pp.

Somerville, P., Collins, N., Graves, R. & Saikia, C. 2001: Ground motion attenuation relations for the central and eastern United States. Final Report, USGS award number 99HQGR0098.

Toro, G.R., Abrahamson, N.A. & Schneider, J.F. 1997: Model of strong ground motions from earthquakes in central and eastern North America: Best estimated and uncertainties. Seism. Res. Lett. 68, 41-57.

Youngs, R.R., Abrahamson, N., Makdisi, F.I. & Sadigh, K. 1995: Magnitude-dependent variance of peak ground acceleration. Bull. Seism. Soc. Am. 85, 1161-1176.

APPENDIX 1: EG2-HID-0028 HAZARD INPUT DOCUMENT FINAL MODEL H. BUNGUM

A 1.1 Introduction

This document describes the implementation and parameterization of Hilmar Bungums's expert model EG2-EXM-0021, as described in the Elicitation Summary EG2-ES-0035 and delivered on 27.05.2003. The purpose of this document is to translate the expert's evaluation of ground motion into an input useable by the hazard software.

A 1.2 Model Implementation

Based on H. Bungum's Elicitation Summary EG2-ES-0035, the logic trees for the median horizontal ground motion, the vertical/horizontal ratio and the aleatory variability of the horizontal component were implemented in FORTRAN and the results displayed graphically.

Key elements in H. Bungum's model include:

Median horizontal ground motion

- 8 out of 15 candidate models have been retained.
- For the weighting of the ground motion models, the magnitude – distance plane is subdivided into 9 bins with the following limits:

  Magnitude: $5 < 5.5 < 6.8 < 8$

  Distance [km]: $0 < 10 < 60 < 1000$
- To account for site class effects, a two-step process is performed. First, a correction of the representative $V_{s,30}$ for each attenuation equations to a reference velocity of 800 m/s is made based on Boore et al. (1997). Three branches with central, low and high values are used as input to account for epistemic uncertainty. In a second correction step, the scaling factors as provided by TP2-TN-0363 are used as the central branch in the scaling from 800 m/s to 2000 m/s. Two side branches (± 5 % in velocity) cover the uncertainty associated with this correction step.
- Kappa corrections are applied to the relations of Toro et al. and Somerville et al. The corresponding scaling factors are derived using RVT. The point source stochastic model was run using the kappa values of 0.006 and 0.0125 sec for a magnitude 6 earthquake at a distance of 10 km with the Rietbrock model parameters. The ratio of the resulting response spectral values is used for the kappa scaling values. The resulting scale factors for kappa are listed in Table A1-1.
- No further modification to allow for specific Swiss conditions is included in the logic tree.
- Epistemic uncertainties in the magnitude conversion (Ms to Mw, where needed) are captured through consideration of three different relationships.
- The conversion of the different types of horizontal components to the geometric mean definition is based on TP2-TN-0269. Epistemic uncertainty is introduced by the addition of a second and a third branch (+2.5 % and -2.5 %).

Tab. A1-1: Scaling factors for the Toro et al. and the Somerville et al. models derived from the kappa correction

Freq (Hz)	Scale factor for Toro
0.5	0.994
1	0.981
2.5	0.951
5	0.906
10	0.825
20	0.696
33	0.588
50	0.547
100	0.746

- Missing coefficients in the ground motion models considered shall be derived according to the procedure described in TP2-TN-0270.
- Style-of-faulting is accounted for as follows: no scaling of the ground motion is applied in the case of normal and strike-slip earthquakes. For reverse faulting, three branches with frequency and magnitude independent factors are implemented.

V/H Ratio

- V/H ratios are obtained by using 5 out of the 8 candidate models that predict both horizontal and vertical components.
- For the vertical component, the same adjustment with respect to site conditions is applied as described above for the horizontal component case.
- Magnitude conversion is considered for both horizontal and vertical components.
- The conversion of components to the geometric mean is based on TP2-TN-0269 and applied to horizontal components only.
- Missing coefficients in the ground motion models predicting vertical components have been derived according the procedure described in TP2-TN-0270.
- Style-of-faulting adjustments are not applied in computing V/H ratios.

Aleatory variability for the horizontal component

- Aleatory variability is independent of ground motion models.
- Three frequency dependent functions $\sigma(f)$ are considered with different weights.
- Magnitude (amplitude) dependence is considered through two different relations (see logic tree).

Equations that correspond to different scaling factors from the Somerville et al. (2001) ground motion model are used to define alternatives of the maximum ground motion estimate. The base M-R-GM surface is anchored at 3 g for PGA, M = 7.5 and R = 1 km. Epistemic uncertainty is introduced by the addition of a second and a third branch (+100 % and -50 %). The upper tail of the residual distribution is to be truncated according to ES, see Table A1-2 below.

Tab. A1-2: Model for the upper tail of the ground motion distribution, with abrupt truncations at the given sigma levels

Weight	Sigma
0.2	3.0
0.6	3.5
0.2	4.0

Figures A1-1, A1-2 and A1-3 show the logic trees for the horizontal component, the V/H ratio and the aleatory variability, resp., as they have been implemented in the code.

A 1.3 Model Parameterization

The ground motion is parameterized for the final Rock Hazard Computations at the following spectral frequencies: 0.5 Hz, 1 Hz, 2.5 Hz, 5 Hz, 10 Hz, 20 Hz, 33 Hz, 50 Hz and at peak acceleration. The implementation of the logic trees results in (a) a set of alternative estimates of the median horizontal ground motion, aleatory variability of the horizontal ground motion and V/H ratios at each spectral frequency, earthquake magnitude, fault style, and distance and (b) the weight associated to each individual branch of the logic tree.

Ground motions have been modeled for seven magnitudes [5.0 : 0.5 : 8.0] and 14 distances (1.0, 1.6, 2.5, 4.0, 6.3, 10, 16, 25, 40, 63, 85, 100, 160, 250 kilometers).

The ground motion arising from the implementation of the SP2 logic trees has been parameterized using a composite model approach. At each distance, magnitude and spectral frequency and for each fault style, the alternative estimates of the median ground motion are sorted in order of ascending spectral acceleration. The weights associated with the sorted median amplification factors are summed, resulting in a cumulative distribution of the amplification factors. No smoothing of the cumulative distribution has been applied. The values of the ground motion are selected for cumulative distributions corresponding to the following fractiles: 0.13 %, 2.28 %, 16 %, 50 %, 84 %, 97.72 %, and 99.87 %. The seven fractiles correspond to median, $\pm 1\sigma$, $\pm 2\sigma$, and $\pm 3\sigma$ levels. By using the discrete fractiles, no assumption regarding symmetry of the epistemic uncertainty is made.

For the aleatory variability, the same process is repeated but with the sorting performed on the amplitude of the aleatory variability.

A conversion for different distance measures was conducted using the Scherbaum conversion factors. (These conversions may be updated in the final model to incorporate the SP1 depth distributions). Two sets of conversions were done. The first converted the distances to JB distances and the second converted the distances to rupture distance. The main differences between the JB distance and the rupture distance occur for small magnitudes at short distances. However, to avoid potential jumps in the models at bin boundaries, the conversions were applied to all the bins (unlike what had been done for the sensitivity computations, where the conversion was not applied to the smallest magnitude and shortest distance bin ($M < 5.5$, $D < 10$)).

The values of ground motion resulting from this procedure are directly input into the rock hazard software without further parameterization or fitting.

The Maximum Ground Motion estimates are also parameterized in a similar manner. Tables of the maximum ground motion are developed for the same magnitude and distance bins, for each style of faulting and for the seven fractiles.

Figures A1-4 to A1-6 on the next pages of this document show one example (for PGA, the Joyner-Boore distance and strike-slip) of the ground motion for the horizontal component, for the V / H ratio and for the aleatory variability for the horizontal component, respectively. The figures display four subplots. The upper plot shows the median as a distance and magnitude dependent surface. The central plot shows the median ground motion as a distance and fractile dependent surface for magnitude 6.5. The lower left plot shows the median for the 7 magnitudes (magnitude 5.0 to 8.0 in 0.5 magnitude steps) while the lower right subplot shows the 7 fractiles (corresponding to median, $\pm 1\sigma$, $\pm 2\sigma$, and $\pm 3\sigma$) for magnitude 6.5.

Figures 4 to 129 of the associated PDF file (EG2-HID-0028_Bungum_figures_rev1.pdf) show the full set of figures.

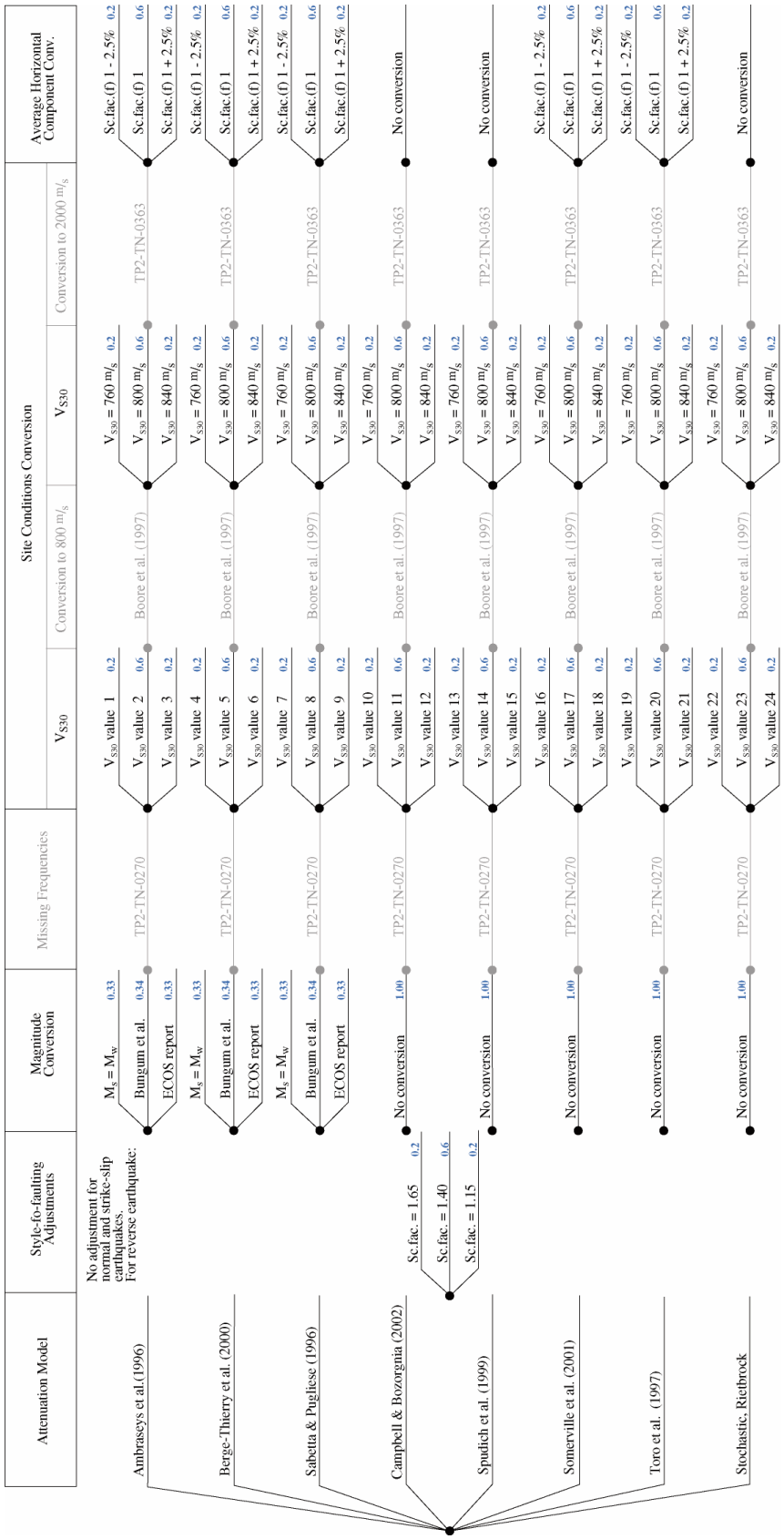

Fig. A1-1: Logic tree for the horizontal ground motion

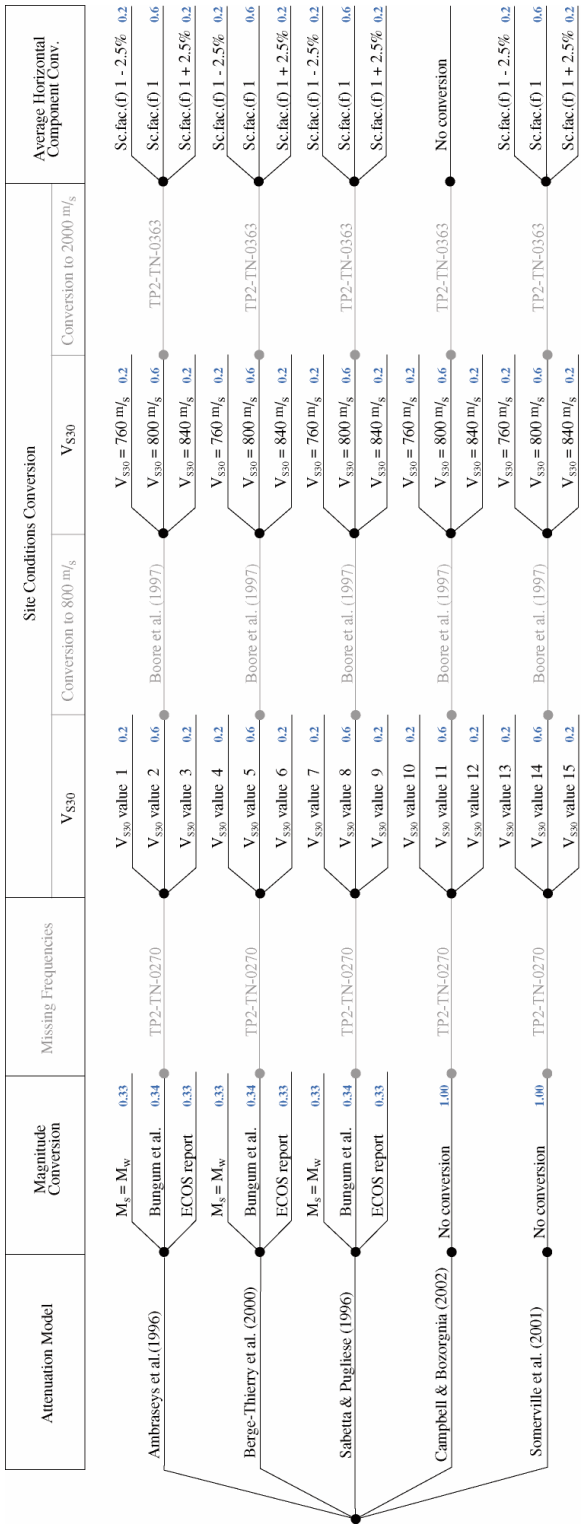

Fig. A1-2: Logic tree for the V / H ratio

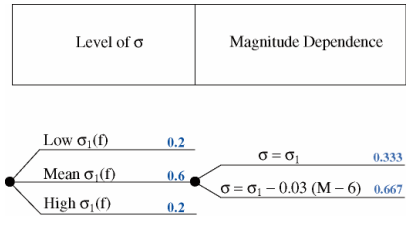

Fig. A1-3: Logic tree for the aleatory uncertainty

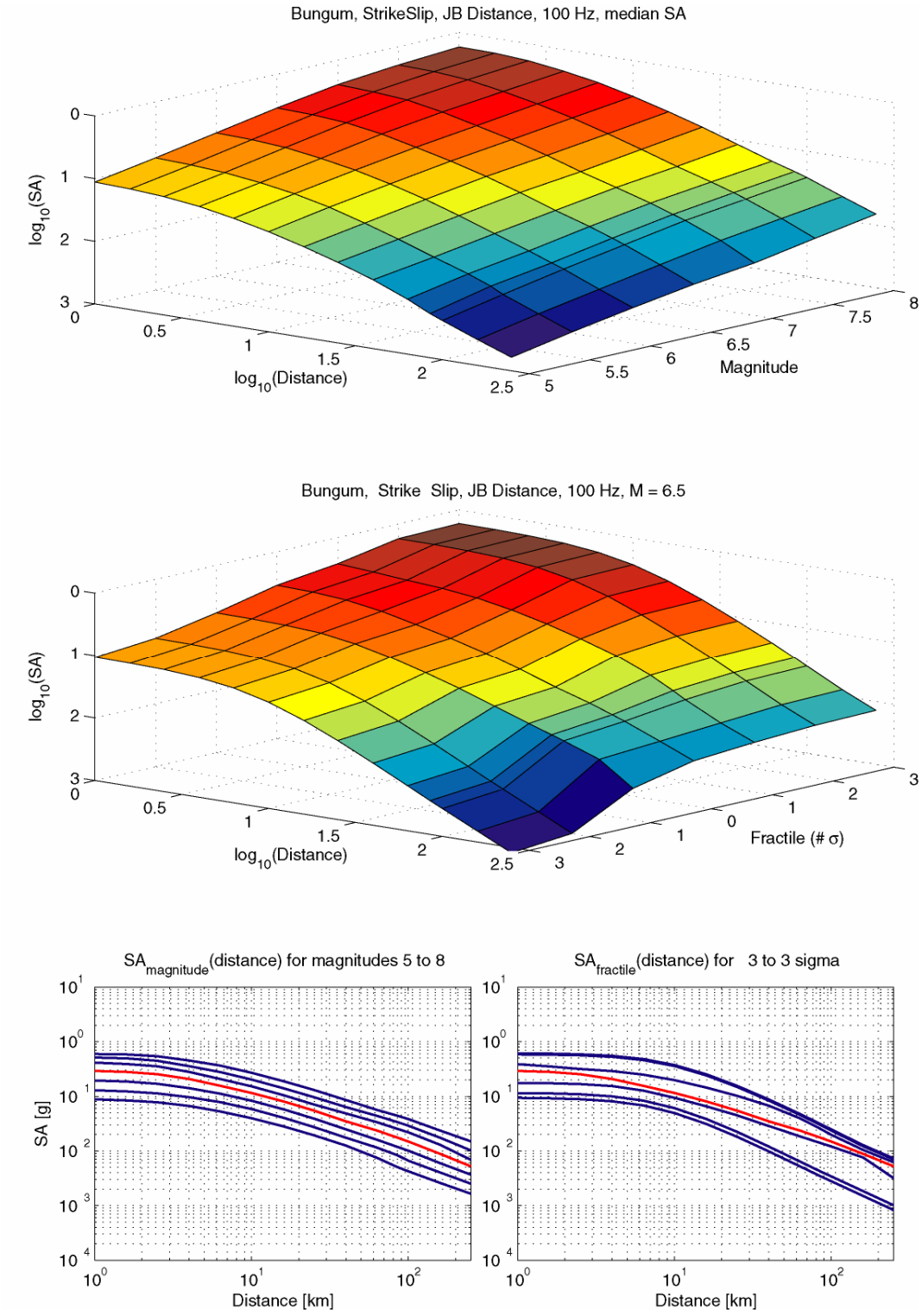

Fig. A1-4: Spectral acceleration (SA) for PGA (100 Hz), assuming strike-slip mechanism and Joyner-Boore distances

The upper plot shows SA (distance, magnitude) for the median. The middle plot shows SA (distance, fractile) for magnitude 6.5. The lower left-hand plot shows the median SA (distance) for different magnitudes. The lower right-hand plot shows SA (distance) for different fractiles and magnitude 6.5.

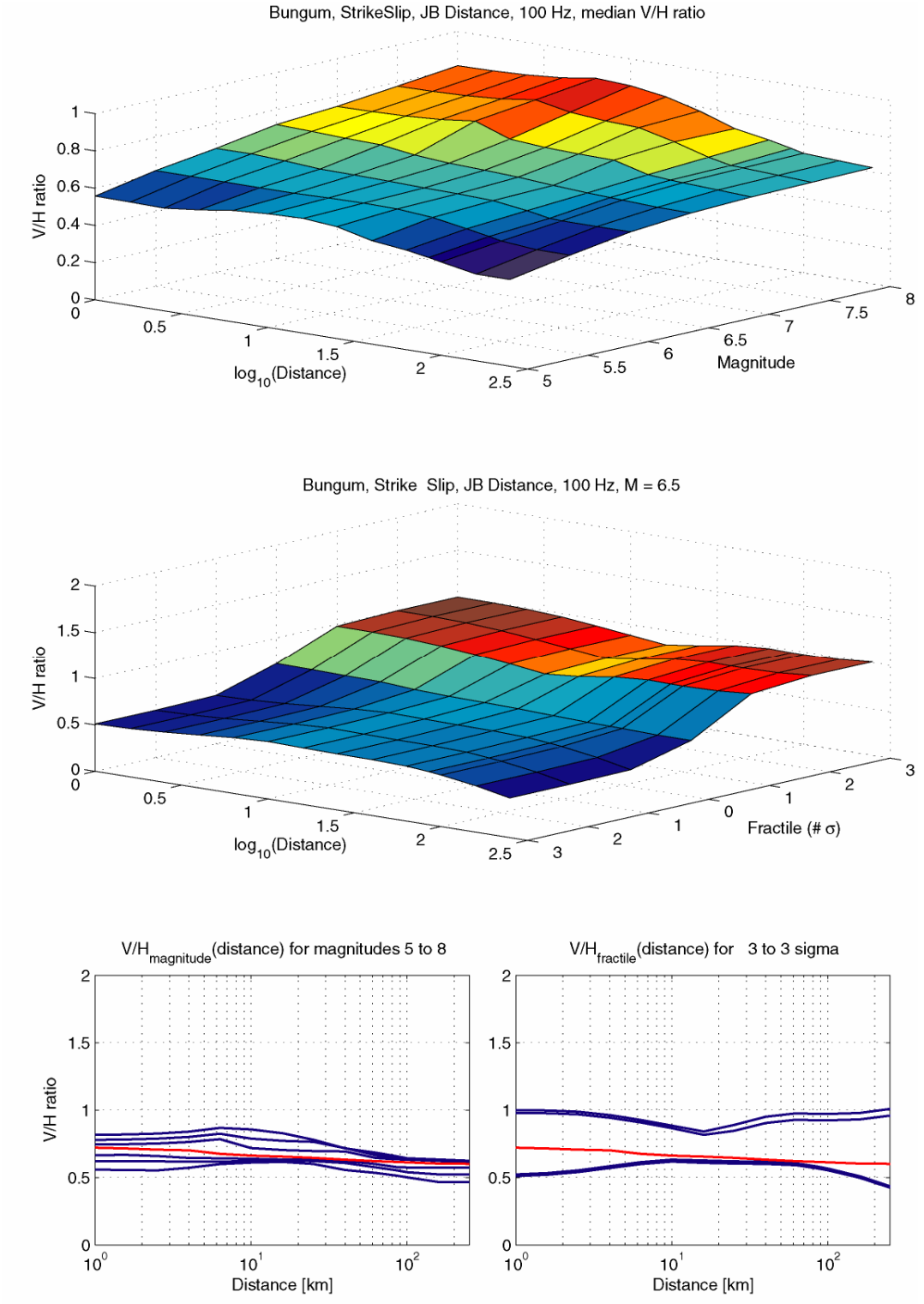

Fig. A1-5: V / H ratio (V/H) for PGA (100 Hz), assuming strike-slip mechanism and Joyner-Boore distances

The upper plot shows V / H (distance, magnitude) for the median. The middle plot shows V / H (distance, fractile) for magnitude 6.5. The lower left-hand plot shows the median V / H (distance) for different magnitudes. The lower right-hand plot shows V/H (distance) for different fractiles and magnitude 6.5.

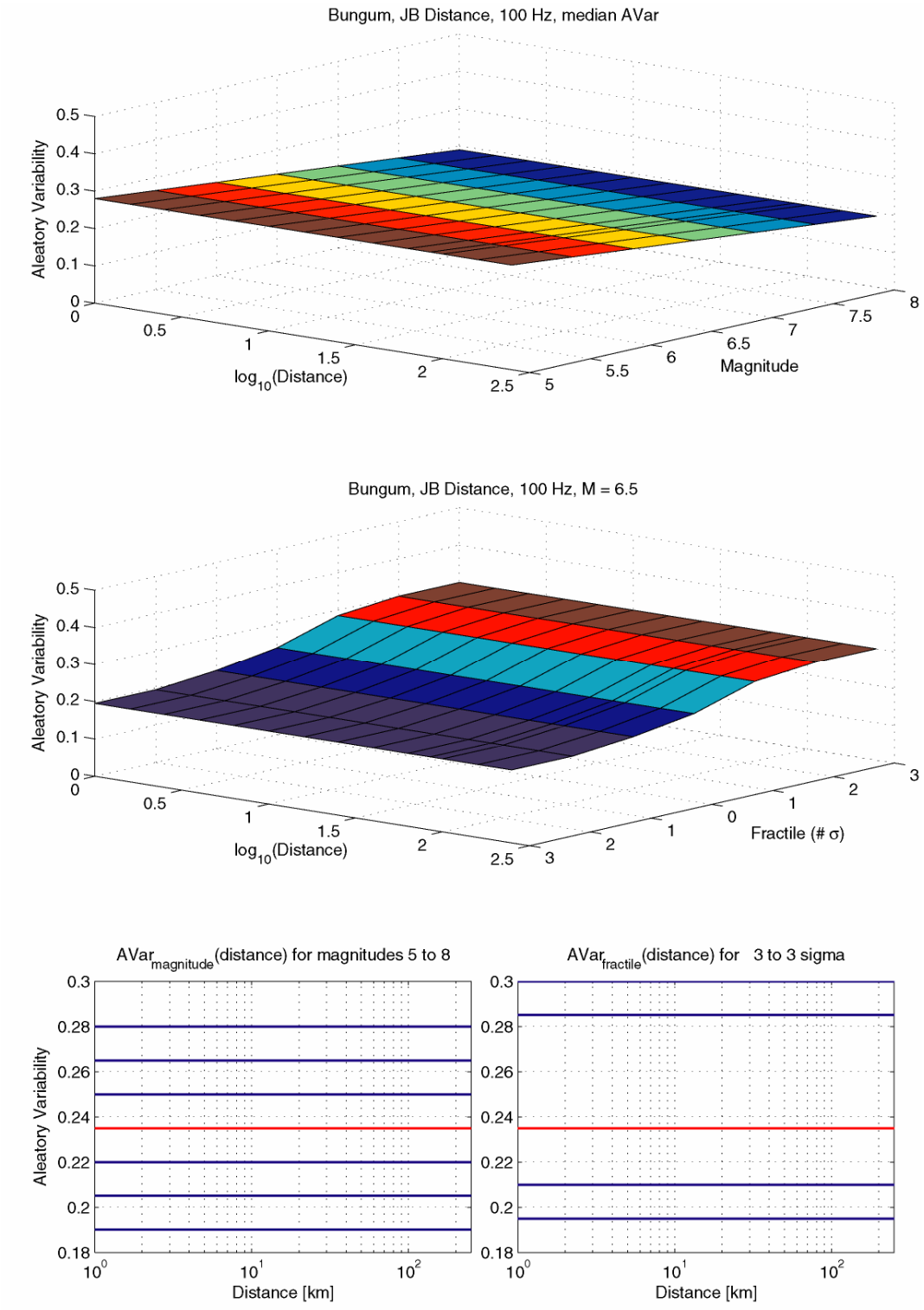

Fig. A1-6: Aleatory variability (AVar) for PGA (100 Hz), assuming strike-slip mechanism and Joyner-Boore distances

The upper plot shows AVar (distance, magnitude) for the median. The middle plot shows AVar (distance, fractile) for magnitude 6.5. The lower left-hand plot shows the median AVar (distance) for different magnitudes. The lower right-hand plot shows AVar (distance) for different fractiles and magnitude 6.5

Part III: Ground Motion Characterisation, Elicitation Summary

Dr. Fabrice Cotton

Université Joseph Fourier
Grenoble – France

Probabilistische Erdbeben-Gefährdungs-Analyse für die KKW-Stand Orte in der Schweiz (PEGASOS)

SP2 Ground Motion Characterisation

Elicitation Summary

Fabrice Cotton

Université Joseph Fourier
Grenoble – France

TABLE OF CONTENTS

LIST OF TABLES

LIST OF FIGURES

1 INTRODUCTION

1.1 What do we know about Swiss earthquake properties ?

1.1.1 Focal mechanism

Focal mechanisms in the foreland are mainly normal and strike-slip. Normal-faulting earthquakes located in extensional stress regimes are associated with lower ground motion than either strike-slip or reverse faulting located in compressional stress regimes. Extensional areas are defined by Spudich et al. (1997) as thinner crust, geothermally active areas (US basin and range). But thin crust and geothermal activity are not present (at least outside the upper Rhine) so I do not think that the Swiss foreland is a pure extensional area as defined by Spudich et al. (1997).

1.1.2 Analysis of deformation rates in Switzerland

The Slip rate of causaltive faults in Switzerland is difficult to evaluate. According to recent geodetic research (e.g Vigny et al. 2002), these slip rates in the alpine area are less than 1 mm/a. In the Foreland these slip rates are probably even less because of lower tectonic activity. According, to Scholz's (1989) classification (Table 1), the Alps, the Jura and the Rhine Graben seems to be a plate boundary related area. The alpine foreland is more an intra-plate related area.

Tab. 1: Swiss tectonic context and associated ground motion empirical models

Description	Slip rate of causaltive fault [cm/a]	Recurrence time [a]	Swiss province	Empirical model
Interplate	$v > 1$	10^2		Global – WUS
Plate boundary related	$1 > v > 0.01$	$10^3 – 10^4$	Rhine Graben – Alps – Jura	European – Global
Intraplate	$v < 0.01$	$> 10^4$	"Real" foreland	Stochastic

(Classification after Scholz 1989)

1.1.3 Analysis of earthquake stress-drops in Switzerland

- Stress-drop analyses performed by different authors are difficult to compare since different definitions of stress-drops exist and because of the trade-off between stress-drop, anelastic attenuation, and geometrical spreading parameters.
- In the French Alps (plate boundary related area) several studies have shown that stress-drops of recent significant ($M > 3.5$) earthquakes are between 30 and 100 bars (Samoens $M = 3.7$, 19/08/2000, stress-drop = 100 bars, Coutant personal communication; Annecy MLDG = 5.3, 15/07/1996, stress-drop = 55 bars (between 30 and 100), Courboulex et al. 1999).
- In the alpine foreland, there is a lack of information about stress-drops of moderate to large earthquakes. Since stress-drop probably increases with the earthquake recurrence interval (stress-drops of intraplate events are higher than stress-drops of interplate events), we cannot exclude large stress-drops in such areas.
- Rietbrock (2002, PEGASOS EXT-TN-0306) has obtained stress-drops which are mostly between 10 and 100 bars.

– Becker's (2003, PEGASOS EXT-TN-0218) results support the fact that small stress-drops are characteristic of small earthquakes recorded on hard rock sites (Figure 1).

– Stress-drop (Figure 1) could be magnitude dependant (Mayeda & Walter 1996)

According to these studies, I recommend including higher stress-drops than the one found by Bay (2002) to simulate strong ground motion in Switzerland.

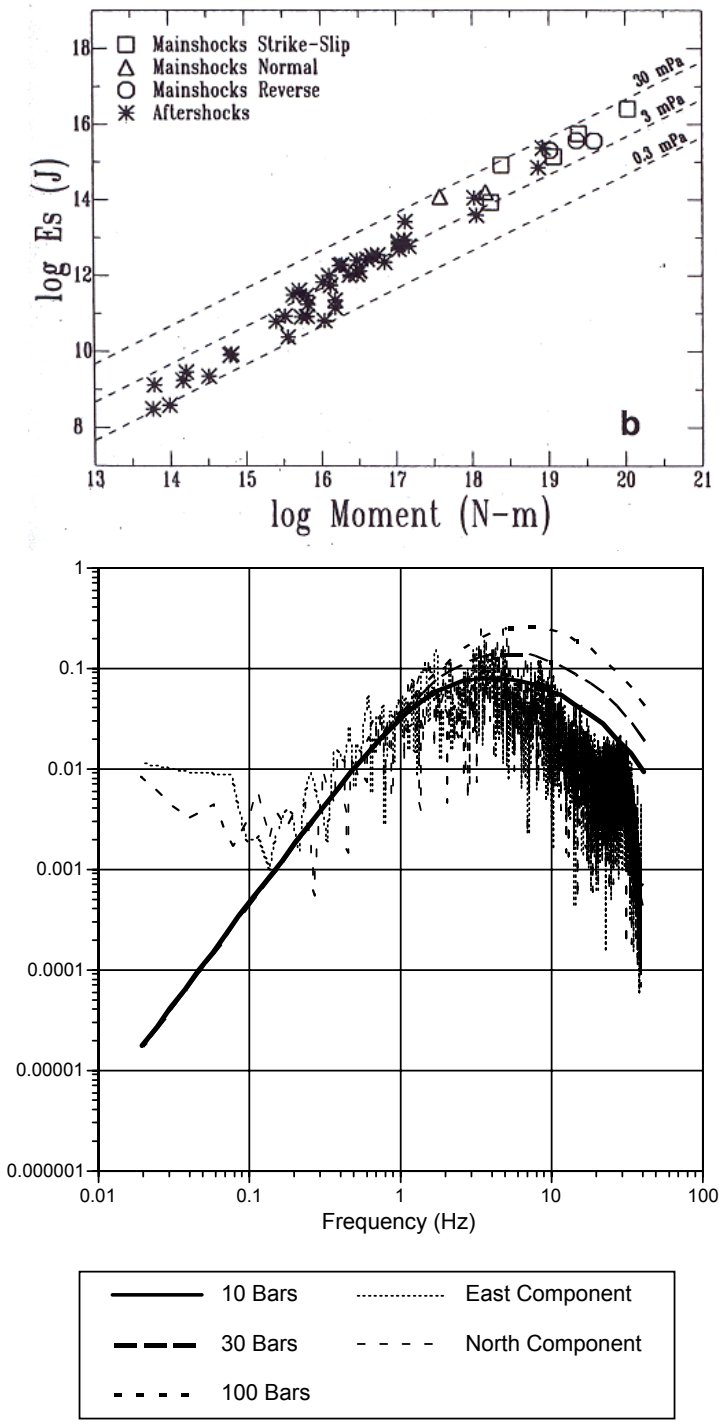

Fig. 1: Evidence of increasing stress-drop with magnitude (above, Mayeda & Walter 1996) and small stress-drop for moderate earthquakes recorded on rock site (below, Becker 2003, PEGASOS EXT-TN-0218)

2 WHAT DO WE KNOW ABOUT WAVE ATTENUATION IN SWITZERLAND ?

2.1 Analysis of macroseismic studies

An analysis of the attenuation of intensity with distance based on more than 6000 macroseismic observations (Rüttener 1995) yields three distinct regions with different attenuation properties. The highest attenuation rate is observed in the subalpine chains (Helvetic and Ultrahelvetic nappes) and the lowest attenuation rate in the crystalline basement and Penninic nappes of the Alps. The northern alpine foreland is characterized by an intermediate attenuation rate.

In order to compare the attenuation in Switzerland with the attenuation of the areas where strong motion empirical models have been derived, I have compared Rüttener analysis with results obtained in eastern US and southern California (Figures 2 and 3).

Results of Figure 3 show that for a hypocentral depth of 10 km, the attenuation of intensities in southern California and in the Swiss foreland are similar. This type of comparison has to be used quite carefully since intensity attenuation ($I - I_0$) is strongly dependent on the hypocentral depth; however, both the comparison with California and the fact that attenuation in the foreland is found to be larger than in the crystalline basement of the alpine chain confirm that attenuation in the foreland is not low and not similar to what is found in a crystalline intraplate area (eastern US).

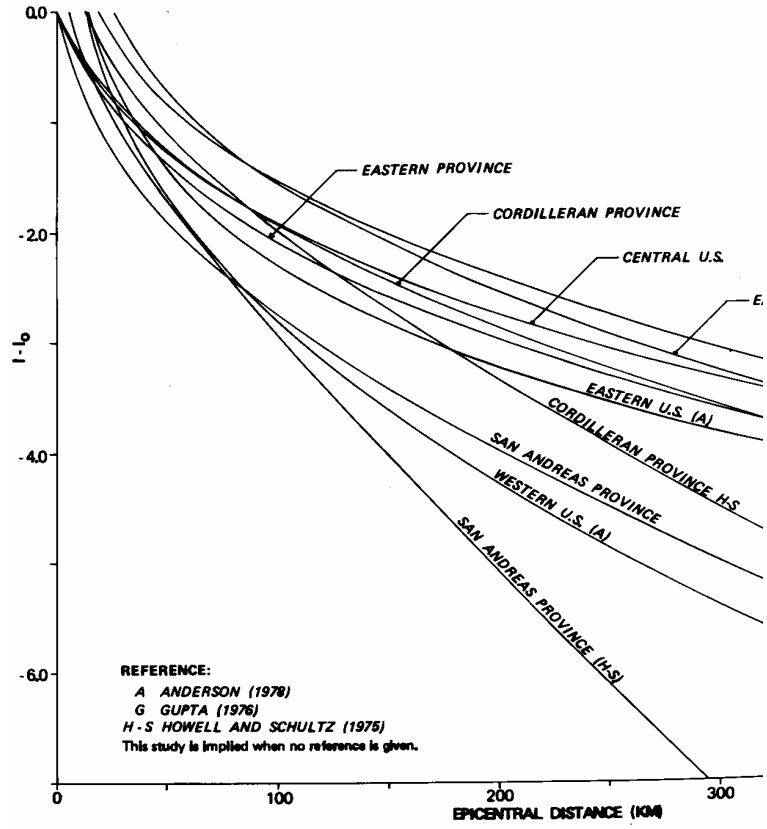

Fig. 2: Intensities attenuation in Eastern and Western US (from Chandra 1979)

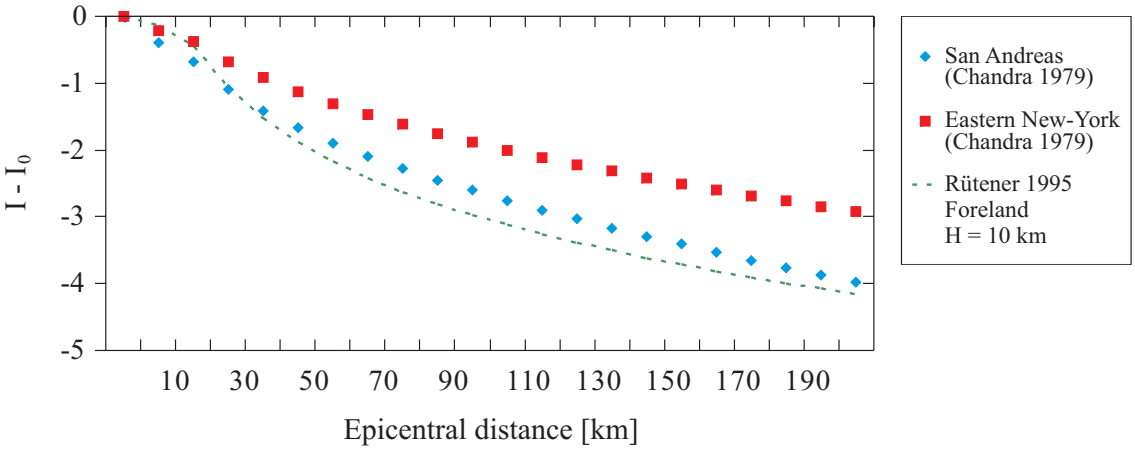

Fig. 3: Comparison between intensities attenuation in Switzerland (Rüttener 1995) and in eastern and western US (Chandra 1979)

2.2 Analysis of weak motion studies

Anelastic attenuation

Weak motions provide some measure of wave attenuation in Switzerland. Bay (2002) suggests an anelastic attenuation model equal to $Q = 270\ f^{0.50}$.

As discussed in the SP2 workshops, using the Bay et al. (2003) method it is difficult to separate the trade-off between geometrical spreading and intrinsic attenuation (Q factor). New results of Rietbrock (2002, PEGASOS EXT-TN-0306) also show (for a similar geometrical spreading to Bay 2002) that the Swiss Q factor (at a frequency of 3 Hz) is intermediate between the one found in California and the one found in eastern US.

In Table 2, I have tried to synthesize and compare Q values and geometrical spreading factors found in Switzerland and in other tectonic areas. These values come from weak motion (direct S wave) measurements at short distances and also on Lg wave measurements for distances larger than 100 km. The Lg wavetrain is particularly well adapted for attenuation measurements since the Lg decay does not depend on magnitude but only on crustal attenuation and a particular station response which can be removed. According to these studies, the mean quality factor in France is $Q = 290\ f^{0.52}$ (Campillo & Plantet 1991). This value is similar to the attenuation model of Bay (2002): $Q = 270\ f^{0.50}$. Like measurements on the direct S-wave of the Lg in Switzerland these results show that the attenuation in France lies between the values typical of active and stable regions.

In my opinion, this summary shows that the anelastic attenuation in Switzerland (and France) lies between the values typical of active and stable regions.

Geometric decay

Bay (2002) suggests a change of the geometric decay near 50 km. For distances less than 50 km the decay is equal to $r^{-1.1}$. This is consistent with macroseismic studies: attenuation is high during the first 70 km, but once the macroseismic field reaches 70 km, intensity decays very slowly with distance. The change of the geometric decay between 50 km and 70 km seems therefore to be common to both strong and weak motions.

Tab. 2: Weak motion attenuation studies

	Qs (value at 3 Hz)	S geometrical spreading (0 – 70 km)	Q Lg (value at 3 Hz)	Lg geometrical spreading
Weak motion in Southern California (Frankel et al. 1990)	800 (frequency independent) 110 (frequency dependant)	$r^{-1.95}$ (free) r-1.0 (a priori choice)	256	$r^{-0.5}$
Weak motion in east US (Frankel et al. 1990)	2099	$r^{-1.27}$	1566	$r^{-0.7}$
Weak motion in France (Campillo & Plantet 1991)			513	$r^{-0.83}$
Swiss weak motion (Bay et al. 2003)	470	$r^{-1.1}$		
Swiss weak motion (Rietbrock 2002)	495 – 639 (for the top 30 km)	$r^{-1.1}$ (strongly variable)		

The geometric decay found by Bay (2002) is high ($r^{-1.1}$) compared to geometrical decays found by strong ground motions empirical studies (regressions done with a 1/r decay lead to negative Q as found by Berge-Thierry et al. 2000, Ambraseys et al. 1996 and Boore et al. 1997). The strong geometrical decay of Bay (2002) is confirmed by Rietbrock (2002, PEGASOS EXT-TN-0306) who also shows a high variability of the geometrical spreading from one event to another. Frankel et al. (1990) show that this steep amplitude decay is caused by the reflection of the upgoing direct wave at the underside of the layer. According to this phenomena, the geometrical decay should therefore be strongly dependant on the depth of the earthquake since this depth will have a strong influence on the interface position and the angle between the upgoing ray and the interface. A recent study in Taiwan (Chang et al. 2001) has found that the geometrical decay is lower for deep events (Figure 4). This could be due to the fact that deep events will have steeper incidence angles and therefore less refection. This hypothesis has to be tested. This depth effect and the fact that this reflection will probably be strongly dependant on the local structure could explain why the geometrical decay is so variable from one event to another and why the Bay (2002) attenuation rate is higher (Figure 5) than that found by Ambraseys et al. (1996).

In the Alpine region, most of the events used by Bay (2002) are shallow which could also have led to an overestimation of the geometrical spreading term.

In order to use both Bay (2002) and/or Rietbrock (2002, PEGASOS EXT-TN-0306) results to simulate strong ground motion we have to answer the following question: will the geometrical spreading of big earthquakes be the same as that measured from small earthquakes? Because big earthquakes are not point sources but extended finite sources which generate seismic waves at different depths, I'm skeptical about the fact that the super-spherical spreading (geometrical spreading greater than 1.0) will also occur for big events.

According to all these results, I believe that the uncertainty on geometrical spreading is quite high and that a lower geometrical spreading than that found by Bay (2002) has to be used to simulate strong ground motion in Switzerland.

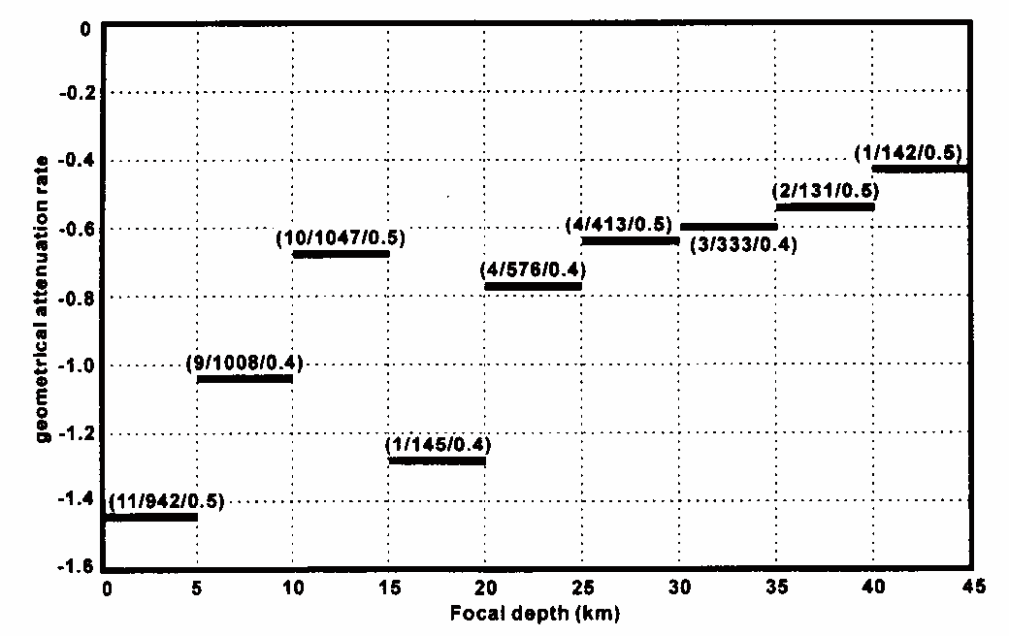

Fig. 4: Evidence of the effet of focal depth on geometric spreading (Chang et al. 2001)

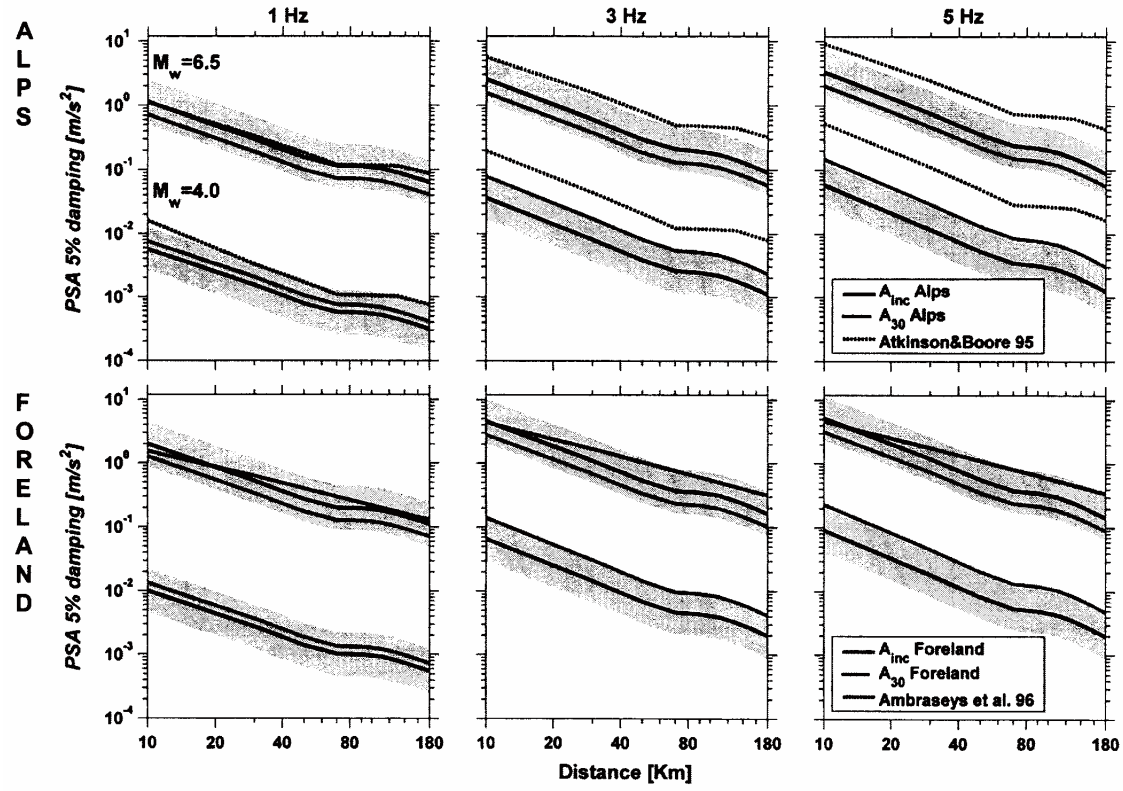

Fig. 5: Comparison of Bay (2002) model with Ambraseys et al. (1996) and Atkinson & Boore (1997)

2.3 Conclusion

According to this analysis of the Swiss case, a balance is needed between:

- European « plate boundary related » attenuation laws (Sabetta & Pugliese 1996, Berge-Thierry et al. 2000, Ambraseys et al. 1996) which are probably close to the Swiss case for « mid » distances and « mid » stress-drops between 30 and 100 bars.
- Globally based on western US relation which provides better data quality, near field, larger magnitude coverage or better site categorization (Campbell et Bozorgnia 2002, Abrahamson & Silva 1997, Lussou et al. 2001, Ambraseys & Douglas 2000).
- Stochastic models based on weak Swiss motions. These stochastic models have to take into account physical parameters of bigger earthquakes (possible lower geometrical decay than suggested by Bay 2002 and Rietbrock 2002, PEGASOS EXT-TN-0306; higher stress-drops than the one used by Bay 2002).
- Eastern US empirical models can not be completely excluded (since very high stress-drop and therefore high frequency motion can not be excluded in such an intraplate environment), but because of the non-crystalline nature of the foreland I suggest very low weights on such models.

3 MEDIAN HORIZONTAL MOTION

3.1 Logic Tree Structure

This logic tree predicts the horizontal ordinates of 5 % damped spectral acceleration at 9 responses period from 0.01 to 20 seconds. The magnitude – distance space has been divided into nine (3 by 3) bins representing magnitudes in the low (M < 5.5), intermediate (M = 5.5 – 6.5) and high (M > 6.5), and distances in the near field (R < 15 km) and far field (R > 70 km). These bins have been chosen according to the strengths and weaknesses (magnitude and distances coverage) of the selected empirical models (see Table 3). A large number of empirical models has been chosen in order to capture the epistemic uncertainty. This large number also helps to avoid large jumps of the predicted motion across the bin boundaries.

3.2 Selected proponent models and weights

3.2.1 European based models

Ambraseys et al. (1996)

Parameters and logic tree conversion needs

- Site factor Sr has to be set to 1 (Rock)
- Need for a conversion from M_w to M_s

Effect of focal depth

Selected earthquakes have depths less than 30 km. The depths found by P-S time analyses show that the depths are between 5 and 15 km. The fictious depth found by the regression is between 2.5 and 5.5. The depths of the earthquakes used in this database seem appropriate to the Swiss case.

Use in Switzerland (stress-drop, faulting style, distance decay, residuals)

Most of the data are from Italian and Greek earthquakes (strike slip and normal mechanism) so the faulting style and possible stress-drops of major earthquakes are probably appropriate to the Swiss case. As already noted, the distance decay is lower than the one found by Bay (2002).

Magnitude, distance and frequency range

- Magnitude: 4 to 7.9
- Distance: 0 to 200 km
- Period range: 0.1 to 2 s, pga is given

Strengths

- The dataset used is large and cover properly all distance and magnitude classes.

Berge-Thierry et al. (2000)

Parameters and logic tree conversion needs

- Site factor c1 has to be chosen (rock)
- Need for a conversion from M_w to M_s
- Need for a conversion to geometric mean horizontal component (horizontal component are independent)

Effect of focal depth

Selected earthquakes have a depth h < 30 km. Since the database is close to the one of Ambraseys et al. (1996), the depth is probably between 5 and 15 km.

Use in Switzerland

The analysis is similar to the one done for the Ambraseys et al. (1996) empirical model.

Strengths and weaknesses

The main weakness is that this empirical model needs many conversions in order to be used in the logic tree. On the other hand, the dataset used is one of the largest and covers properly the study area.

Magnitude, distance and frequency range

- Magnitude: 4 to 7.3
- Distance (Rjb): 7 to 100 km
- Period range: 0.04 to 4 s

Sabetta & Pugliese (1996)

Parameters and logic tree conversion needs

- Site coefficients have to be set to zero (stiff soil)
- Need for a conversion from M_w to $M_{L(Italy)}$ and M_w to M_s
- Need for a conversion to the geometric mean horizontal component

Use in Switzerland

All the data used in this empirical model are from Italian earthquakes (strike slip and normal) so the faulting style is appropriate.

Strengths and weaknesses

The main weakness is that there are no large magnitude earthquakes in the data set and few data have been used to derive this empirical model. On the other hand, the site conditions seem to be well-constrained and only good quality data have been used.

Magnitude, distance and frequency range

- Magnitude: 4,6 to 6.8
- Distance (Rhypo): 10 to 120
- Period range: 0.25 to 25 Hz

Ambraseys & Douglas (2000)

Parameters and logic tree conversion needs

- Site Sr coefficients have to be set to 1 (rock site)
- Need for a conversion from M_w to M_s

Effect of focal depth

Only shallow and intermediate depth earthquakes (H < 20 km) have been used.

Strengths and weaknesses

The main weakness is that only large magnitude data have been used to derive this model.

Magnitude, distance and frequency range

- Magnitude: 5.8 to 6.8
- Distance (Rjb): less than 15 km
- Period range: 0.5 to 10 Hz

3.2.2 Western US / Global based models

Abrahamson & Silva (1997)

Parameters and logic tree conversion needs

- Site factor S has to be chosen equal to zero (rock or shallow soil)
- Need for a conversion from Rjb to Rrup

Effect of focal depth

Selected earthquakes have a depth less than 20 km.

Use in Switzerland

Tectonic context is different but only shallow crustal earthquake have been used. Compared to Campbell (1997), more normal and strike slip events have been used to derive the empirical model.

Strengths

- A large set of data has been used even after excluding recordings with unknown or poor estimation of mechanism, site conditions, distance or magnitude
- 20 Hz, 33 Hz and 50 Hz values are given (the number of records used in the analysis for each of these frequencies is given)

Weaknesses

- Rock site conditions are a mix of soft rock and shallow soil site conditions
- No cut-off for the triggering level has been used

Magnitude, distance and frequency range

- Magnitude: 4,5 to 7.5
- Distance (Rrup): 0.1 to 150
- Frequency range: 0.2 to 50 Hz

Boore et al (1997)

Parameters and logic tree conversion needs

- Average site velocity is chosen equal to 620 m/s (soft rock)
- No need for magnitude conversion
- b1 has to be set to b1rev (reverse faulting) or b1ss (strike slip) . This point will be discussed in the "style-of-faulting part" (in section 3.8).

Site conditions

Rock velocity is a parameter of the empirical model

Use in Switzerland

All the data are either strike slip or reverse slip and do not include normal mechanisms that occur in Switzerland.

Strengths

- No site classes but use of an estimated shear wave velocity (well constrained rock site)
- No distance and magnitude conversion needs
- Cut-off for the triggering level

Weaknesses

- There is a lack of normal faulting records in the dataset used to derive the empirical model
- The dataset is dominated by Imperial Valley and Loma Prieta earthquakes with few events with magnitude less than 6

Magnitude, distance and Frequency range

- Magnitude: 4,5 to 7.5
- Distance (Rrup): 0.1 to 150
- Frequency range: 0.2 to 10 Hz, pga is given

Campbell & Bozorgnia (2002)

Parameters and logic tree conversion needs

- Site coefficient has to be set to Ssr = 0 and Shr = 1 for hard rock
- Need for a conversion from Rjb to Rseis
- Style of faulting coefficient (F) has to be set according to the discussion of the "style-of-faulting" part (in section 3.8)

Effect of focal depth

Selected earthquakes are located in the upper crust (< 25 km). Subduction interface earthquakes used in Campbell (1997) have not been used.

Use in Switzerland

All the data are either strike-slip or reverse-slip and do not include normal mechanisms that occur in Switzerland.

Strengths

- No magnitude conversion needed
- Use of near faults records
- Site conditions are well constrained and show that differences between ground motions on firm and soft rock can be large

Weaknesses

- There is a lack of normal faulting records in the dataset used to derive the empirical model

Magnitude, distance and frequency range

- Magnitude: > 5
- Distance: less than 60 km
- Period range: 0.25 to 20 Hz

Spudich et al. (1999)

Parameters and logic tree conversion needs

- No magnitude conversion
- Conversion from the mean to the larger component
- Site coefficient has to be set to 0 (rock site)

Site conditions

A test made in the paper shows that extensional regime rock sites are harder than western US rock sites (Boore soft rock site Vs = 620 m/s).

Use in Switzerland

Some extensional properties (thin crust, geothermal activity) are not applicable to Switzerland but the database includes numerous normal faulting European records (Roermont, Friuli, Greece, etc.).

Weaknesses

- There is a lack of information on the rock site characteristics (hard, soft and unknown rock are mixed)

Strengths

- No magnitude conversion needed
- European normal faulting records are taken into account

Magnitude, distance and frequency range

- 0.5, 10 Hz and pga
- M from 5 to 7.0
- From 0 to 100 km

Lussou et al. (2001)

Parameters and logic tree conversion needs

- Site factor c(A,f) has to be chosen (rock)
- Need for a conversion from Mm to M_{JMA}
- Need for a conversion from Rjb to Rhypo
- Need for a conversion to geometric mean (horizontal component are independent)

Effect of focal depth

Selected earthquakes have a depth h < 20 km.

Use in Switzerland

Tectonic context is different but only shallow crustal earthquakes have been chosen in this study.

Strengths and weaknesses

- The main weaknesses are that magnitude conversion between M_{JMA} and M_w and distance conversion are needed to use this empirical model. This regression is also based on a database with no large magnitude earthquakes
- On the other hand, this empirical model is mixing both small and large magnitudes earthquakes and rock site conditions are well defined because of systematic geotechnical measurements

Magnitude, distance and frequency range

- Magnitude: 3.5 to 6.3
- Distance (Rhypo): 10 to 200 km
- Period range: 0.02 to 10 seconds

3.2.3 Eastern US based models

Atkinson & Boore (1997)

Parameters and logic tree conversion needs

- No magnitude conversion need
- Distance conversion from Rjb to Rhypo
- Conversion from random horizontal to geometric mean component
- No site or faulting style coefficient

Use in Switzerland

No distinction of focal mechanism type is made but the predominant mechanism is assumed to be thrust.

Weaknesses

- There is no evaluation of the epistemic or aleatory uncertainty of this model

Magnitude, distance and frequency range

- Magnitude from 4.0 to 7.25
- Rhypo from 10 to 500 km

Somerville et al. (2001)

Parameters and logic tree conversion needs

- No magnitude conversion need
- Equations for non-rifted domain have to be used (centroid depth of 5, 10 and 20 km with equal weight)

Effect of focal depth

Earthquake depth is in the range of 0 to 35 km in the non-rifted domain.

Use in Switzerland

The model takes into account slope changes of the attenuation with distance and the slope decrease occurs at the same distance as in Bay (2002); however, as discussed in the introduction, the attenuation properties are probably quite different than those in Switzerland.

Weaknesses

- This empirical model is derived for earthquakes with magnitude greater than 6.0
- The tectonic context is different

Magnitude, distance and frequency range

- M from 6.0 to 7.5
- From 0.25 Hz to 100 Hz

Toro et al. (1997)

Parameters and logic tree conversion needs

- No magnitude conversion
- Conversion from random to geometric mean
- Moment magnitude has to be chosen
- Mid-continent (weight 1/3) and Gulf (weight 2/3). Gulf model has higher anelastic attenuation and is probably more "extensional" than the mid-continent tectonics. For these reasons, this model is preferred.

Strengths

The discussion of the epistemic and aleatory properties can be used to estimate the epistemic uncertainty for other stochastic models.

Magnitude, distance and frequency range

- Magnitude 5 to 8
- Distance 1 to 500 km
- Frequency 1 to 35 Hz

3.2.4 Swiss stochastic model

Two stochastic models have been derived for Switzerland (Rietbrock 2002, PEGASOS EXT-TN-0306 and Bay 2002). I decided to use Rietbrock because his model has a site dependent kappa (t* station) which is more consistent with the fact that kappa is part of the site effect (as demonstrated by Silva et al. 1998).

Parameters and logic tree conversion needs

- Conversion from random to geometric mean

Magnitude, distance and frequency range

- Magnitude: 4 to 7.9
- Distance: 0 to 200
- Frequency range between 1 Hz and 15 Hz

Weaknesses

- The model is calibrated only with small to moderate size events

Evaluation of the point source parameters (see discussion in the introduction part)

Tab. 3: Swiss stochastic models used in the logic tree

Model	Geometric spreading	Anelastic attenuation	Stress drop	K_0
Model1	Geo1	Q400	30	K_0
Model2	Geo1	Q400	80	K_0
Model3	Geo1	Q400	130	K_0
Model4	Geo2	Q400	30	K_0
Model5	Geo2	Q400	80	K_0
Model6	Geo2	Q400	130	K_0

Geo1 $r^{0.9}$ 0 – 80 km, $r^{-0.57}$ > 80 km
Geo2 $r^{0.7}$ 0 – 80 km, $r^{-0.57}$ > 80 km
K_0 : 0.0021

3.3 Reference Rock Velocity profiles

3.3.1 Reference logic tree rock velocity.

The reference rock velocity is equal to 2000 m/s which is the reference velocity of SP3.

3.3.2 Reference profiles

For each of the ground motion models, I decided to use the representative Vs_{30} value assigned by SP2 (Table 4). These values represent consensus values from SP2.

Tab. 4: Range of selected Vs_{30} of the candidate attenuation relationships (Lacave et al. 2003, PEGASOS TP2-TN-0363)

	Lower Vs_{30}	Mean Vs_{30}	Higher Vs_{30}	Representative realistic models
Ambraseys et al. 1996	550	800	1200	Median WAF Italy
Berge-Thierry et al. 2000	550	800	1200	Median WAF Italy
Sabetta & Pugliese 1996	700	1000	1300	Median WAF Italy
Ambraseys & Douglas 2000	450	800	1100	Central western US
Lussou et al. 2001	350	500	900	Central western US Median WAF Italy
Abrahamson & Silva 1997	450	600	900	Central western US
Boore et al. 1997	500	620	750	Central western US
Campbell & Bozorgnia 2002	450	600	900	Central western US
Spudich et al. 1997, 1999	550	800	1100	Central western US
Atkinson & Boore 1997		2800		No site correction
Somerville 1998, Somerville et al. 2001		2800		No site correction
Toro et al. 1997		2800		No site correction
Rietbrock 2002	750	1100	1500	Median WAF Italy

To construct the rock profiles, I decided to use two different methods equally weighted in the logic tree:

- First, I selected the generic Vs_{30} dependent rock models built by Franck Scherbaum and described in Lacave et al. (2003, PEGASOS TP2-TN-0363). These profiles are characterized by a base-rock velocity of 2000 m/s and a surface velocity Vs_{30} varying from 350 m/s to 1500 m/s. The mean velocity value will have a weight of 0.2 in the logic tree. A lower and higher Vs_{30} will account for the epistemic uncertainty in these values (weight of 0.15 each). The scaling factors to the reference base rock velocity of 2000 m/s are provided in Lacave et al. (2003, PEGASOS TP2-TN-0363) through the use of a 1D program identical to SHAKE and a set of 15 accelerograms for each profile.
- The "Scherbaum" rock profiles are rather smooth and Vs increases slowly with depth. I therefore also considered some more realistic profiles as alternatives to the smooth profiles. The number of velocity profiles in the WAF database is known to be low. Furthermore most of the profiles are from Italian stations, limiting the regional applicability of the data coverage (Roth 2002, PEGASOS TP2-TN-0254 and PEGASOS TP2-TN-0242). I selected two "realistic profiles": the median WAF Italy profile (Vs_{30} = 1078) and the central Western US profile (Vs_{30} = 516 m/s). The median WAF Italy profile is to be used for European models (Berge-Thierry et al. 2000, Ambraseys et al. 1996, Sabetta & Pugliese 1996, Bay et al. 2003). The central western US (Vs = 516 m/s) is to be used for western US / Global models (Abrahamson & Silva 1997, Boore et al. 1997, Campbell & Bozorgnia 2002, Spudich et al. 1997 and 1999, Ambraseys & Douglas 2000). The weight for the realistic profile is 0.5. For the Lussou et al. (2001) Model, both profiles are considered applicable and are given equal weight (0.25 for each).
- For EUS models the scaling factors described in Lacave et al. (2003, PEGASOS TP2-TN-0363) for a reference velocity of 2800 m/s is to be used. Since no realistic profiles exist for EUS site conditions, I only selected the factors of Lacave et al. Since these scaling factors are close to a value of one, I decided not to complicate the logic tree unnecessarily and therefore only one branch is used.

These profiles are shown on Figure 6.

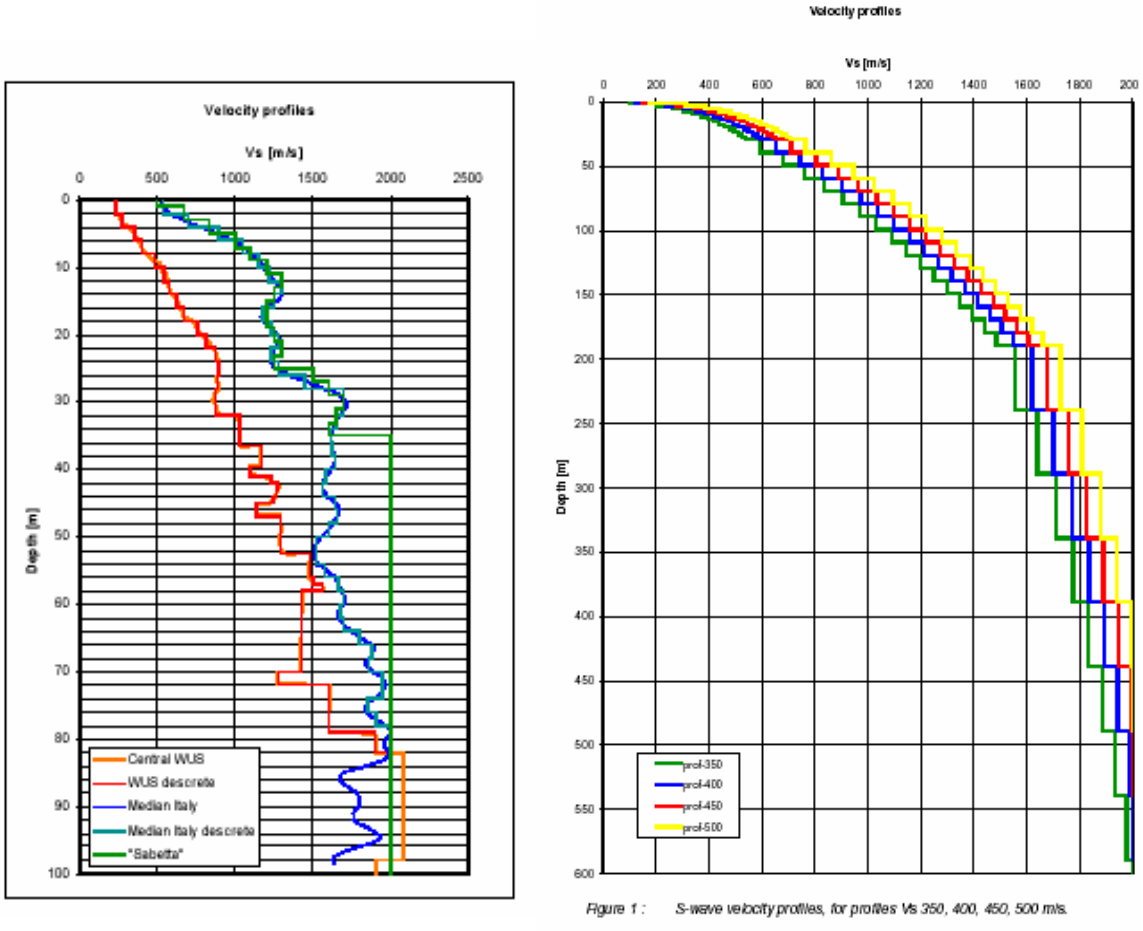

Fig. 6: Velocity profiles used for site corrections (Lacave et al. 2003, PEGASOS TP2-TN-0363 and Roth 2002, PEGASOS TP2-TN-0254)

Kappa correction

Kappa correction has a strong effect on the final values: a factor of two changes in kappa is reflected in about an octave (factor of two) change in the peak frequency (Silva et al., 1998). The effect of this kappa correction (Figure 7) has large effects on the final ground motion calculations as shown very clearly by Silva et al. (1998).

Since the beginning of the project, it has not been clear how to take into account such a correction and what are the physical bases of the kappa filter; however, Silva et al. (1998) clearly show (Figure 7) that there is a trend between rock quality and attenuation. This trend indicates that shallow rock sites are not only a shallow soft layer over a hard rock layer but that the velocity differences (and the effect of the weathering) continue deeper. The correlation between kappa and Vs_{30} therefore indicates that kappa is part of the site effect. This "deep" site effects seems to be highly variable from one site to another: Figure 8 also shows that there is a great variability in the correlation between Vs30 and kappa. This variability is also confirmed by Rietbrock (2002, PEGASOS EXT-TN-0306) who has found a great variation of t* of Swiss stations.

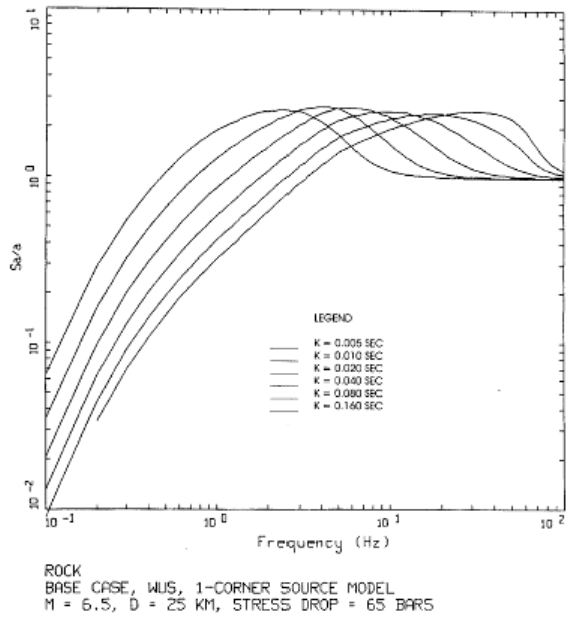

Fig. 7: Effects of the kappa parameter on the ground motion simulation (Silva et al. 1998)

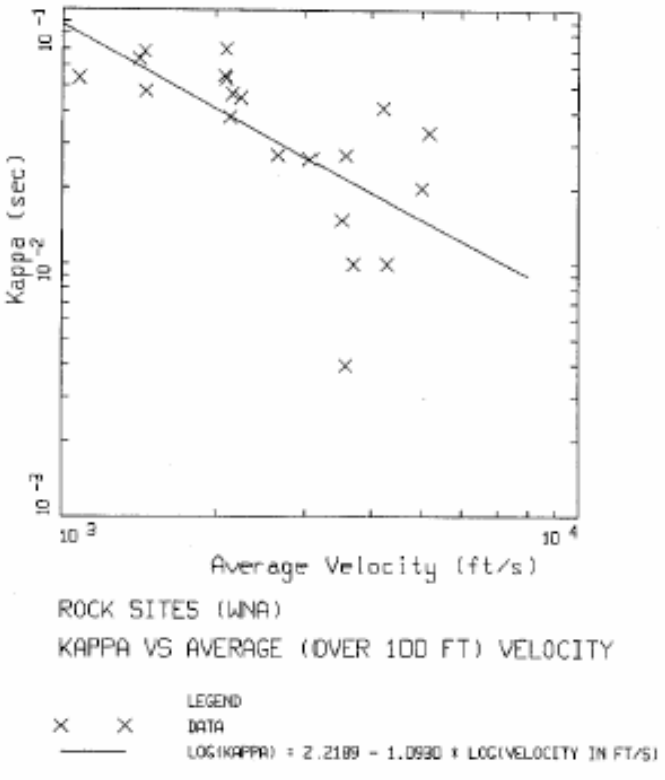

Fig. 8: Relationship between Kappa and Vs_{30} (Silva et al. 1998)

According to these studies, kappa has a site dependent component dependent on deep site properties. This deep site effect cannot be determined by "classical" local site studies and will not be taken into account by SP3. The only way to determine this deep site effect would be to record weak motions at the plants in order to determine the local kappa as it has been done by

Rietbrock (2002, PEGASOS EXT-TN-0306) for Swiss stations. Rietbrock's results are consistent with those of Silva et al. (1998). For a site NEHRP B (1100 m/s) the Silva et al. (1998) empirical relationship gives a kappa value of 0.023 sec. The mean kappa value found by Rietbrock (2002, PEGASOS EXT-TN-0306) is equal to 0.021 sec (value given by the Silva et al. relationship for a Vs30 velocity equal to 1000 m/s). I therefore decided to use a kappa of 0.021 sec as the reference kappa of my logic tree and to consider it as the mean kappa of Swiss Foreland sites (Table 5). The variability of kappa in Switzerland (Figure 9) is also given by Rietbrock. The kappa sigma is equal to 0.011 sec (Tab. 2 of Rietbrock 2002, PEGASOS EXT-TN-0306) which is roughly consistent with the uncertainty given by the Silva et al. (1998) empirical relationship.

Station	$T^{*station}$	Latitude	Longitude
BAL	0.005	47.283	7.644
BIS	0.007	46.412	8.926
BRI	0.004	46.76	8.121
DAV	0.023	46.839	9.794
DAVO	0.023	46.839	9.794
DIX	0.030	46.081	7.409
DIX2	0.034	46.083	7.404
EMS	0.039	46.067	6.931
EMV	0.018	46.064	6.900
IRC	0.029	47.536	8.615
LLS	0.023	46.848	9.009
LLS2	0.022	46.847	9.007
MMK	0.014	46.052	7.965
MMK2	0.015	46.052	7.957
MUO	0.042	46.969	8.638
OSS	0.015	46.69	10.133
OSS2	0.030	46.687	10.144
ROM	0.006	46.775	6.961
SIE	0.023	46.385	7.473
SIER	0.028	46.385	7.473
SLE	0.019	47.766	8.493
STG	0.027	46.535	6.266
TMA	0.000	46.106	8.873
VDL	0.023	46.485	9.451
VDL2	0.031	46.486	9.470
WIL	0.024	47.416	8.909
ZLA	0.038	47.482	8.389
ZUL	0.000	47.481	8.390

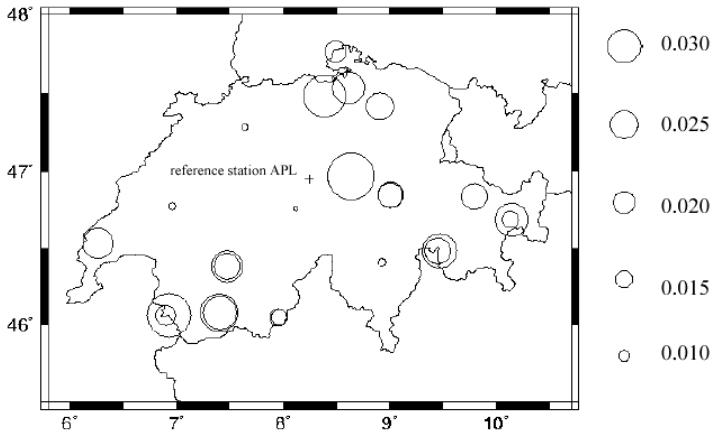

Fig. 9: T*stations determined by Rietbrock (2002, PEGASOS EXT-TN-0306)

The kappa site variability is already included in the aleatory variablity of empirical models. The epistemic uncertainty about the kappa correction comes from the three following hypothesis:

– *Hypothesis 1*. As discussed in the workshops, Kappa is a distance independant filter. Part of it could come from source effects which have not been yet observed in Switzerland but are present in the "kappa-uncorrected" models. Therefore, the first branch 1 of the logic does not take into account any kappa correction. There are no data or observation to support this hypothesis and the weight of the associated branch is therefore low (0.2).

– *Hypothesis 2*. The relationship (Silva et al. 1998) between kappa and Vs_{30} can be applied in Switzerland (this working hypothesis is strongly supported by the fact that the kappa found by Rietbrock (2002, PEGASOS EXT-TN-0306) is similar to the one found by Silva et al. relationship using Vs_{30} = 1000 m/s) and that the variability of $t^*_{stations}$ of Rietbrock is close to the variability of the Silva et al. (1998) relationship. In that case (branch 2) the kappa value due to deep site effect (and therefore not taken into account by SP3) is close to the one found by Rietbrock (even if a superficial site correction does occur) and is chosen equal

to 0.021 sec. This working hypothesis is supported by the Rietbrock (2002, PEGASOS EXT-TN-0306) and the Silva et al. (1998) results and therefore I have chosen to favour it with an associated high weight (0.7).

– *Hypothesis 3*. Swiss rock is not weathered because of the glacier erosion which has deleted the weathered part of rocks (D. Fäh comment during WS4). In that case, we have to take into account the possibility of very low kappa correlated with "very hard rock" deep site conditions. The kappa is then close (branch 3) to a value of 0.012 corresponding to a Vs_{30} of 2000 m/s according to Silva et al. (1998) relationship. This hypothesis is also supported by Rietbrock (2002, PEGASOS EXT-TN-0306) results where some stations (TMA, ZUL) shows a null $t^*_{stations}$ (it would be now very useful to precise the geological history of such sites to confirm or not such hypothesis). The glacier erosion did occur mainly in the alpine part of Switzerland (P. Birkhäuser, personnal communication) and therefore should not be applicable to the Foreland sites; however the results of Rietbrock show very low kappa values for some of the stations located in the Foreland (particularly these located to the western part of the Foreland in Figure 9). Because of the Rietbrock's results, I have chosen not to exclude this hypothesis and to give a small weight to this branch.

Tab. 5: Kappa correction weighting

	Kappa correction
Branch 1 Weight 0.2	No kappa correction
Branch 2 Weight 0.7	From kappa (Vs_{30}) of the host site to kappa (1000 m/s) = 0.021
Branch 3 Weight 0.1	From kappa (Vs_{30}) of the host site to kappa = 0.012

3.4 Adjustments of proponent models to Swiss conditions

Switzerland has no strong ground motion recordings available. Potential strong ground motion will be controlled by source, path and site effects. Some of these parameters have been analysed for small earthquakes at regional distances. In order to adjust the proponent models, there is a need to discuss each of these parameters in order to know if we have a sound technical basis to adjust them to Swiss conditions and large magnitude earthquakes (Table 6).

In conclusion, I decided to adjust the geometrical spreading and the anelastic attenuation of EUS models to the one found by Rietbrock (2002, PEGASOS EXT-TN-0306). The scaling factors are derived from the ratio of theoretical simulation models where the geometric and anelastic attenuation parameters are taken from Rietbrock and theoretical simulations where the geometric and anelastic attenuation parameters are taken from Toro et al. (1997). The other parameters of these two sets of simulations have to be the same so that the ratio is a correction factor which only accounts for the attenuation properties differences. The same factors are to be applied to the Atkinson & Boore (1997) and Somerville et al. (2001) models.

Tab. 6: Adjustments to Swiss conditions

Parameter	Information available from small swiss earthquakes	Proponent models adjustments ?
Stress-drop	Yes	No: stress-drop could be different for large and small earthquakes
Finite source effects at short distances	No	No
Geometrical spreading and anelastic attenuation	Yes	No for purely empirical models because the attenuation of small and large earthquakes could be different. The waves are generated at different depth levels in the case of small and large earthquakes. Large earthquakes break through the whole crust). Moreover, macroseismic attenuation studies in the Foreland do not show such a great difference between Switzerland and Western US Yes for EUS stochastic models which do not include any large earthquakes information
kappa	Is shown to be site dependent by Rietbrock (2002, PEGASOS EXT-TN-0306) and Silva et al. (1998); this information is not available at the plants	This correction is part of the site correction

3.5 Magnitude conversions

3.5.1 From M_w to M_L

Sabetta & Pugliese (1996) use M_L for earthquakes less than 5.5 and M_s for $M_L > 5.5$. The definition of the M_L used in this study is given in Sabetta & Pugliese (1987) and is the one of the "Observatorio Geofisico Sperimentale di Trieste" or from National Earthquake Information Service). In the PEGASOS report (PEGASOS TP1-CAT-0004, PEGASOS EXT-TP-0043 2002) $M_w = M_{L\,(ING)} - 0.3$ (sigma = 0.5, few data).

Sabetta & Pugliese recommend to choice M_w equal to M_L for magnitudes less than 5.5. One branch of the logic is then the equality between these two magnitude scales. A lower weight is given to that branch because there is no precise study to demonstrate this equality (Table 7). The PEGASOS report (PEGASOS TP1-CAT-0004, PEGASOS EXT-TP-0043 2002) provides an up-to-date analysis and has therefore a higher weight in the logic tree.

Tab. 7: M_w to M_L conversion weighting

Logic tree branches	Sigma	Weight
PEGASOS report	0.5	W = 0.6
Equivalence of the scale	0.5	W = 0.4

3.5.2 From M_w to M_s

According to Ambraseys & Free (1997) $M_s = -45.610 + 3.252 \log (M_0) – 0.048 [\log (M_0)]^2$ (sigma = 0.283). The moment (in dyne.cm) is calculated using Kanamori's (1977) formula ($Log_{10} M_0 = 1.5 M_w +16.1$). Note that this conversion is slightly different from Ekstroem & Dziewonski (1988) and from the SED proposed conversion (PEGASOS TP1-CAT-0004) but since the strong motion database uses Ambraseys' M_s definition, I favour the Ambraseys & Free (1997) conversion formula.

Bungum et al. (1996) found for northern Europe that M_s is close to M_w. Another branch of the logic is then the equality between these two magnitude scales. This branch has a lower weight than the one of Ambraseys & Free (1997) since this M_s definition is not the one used in European strong motion databases (Table 8).

Tab. 8: M_w to M_s conversion weighting

Logic tree branches	Sigma	Weight
Ambraseys & Free (1997)	0.283	W = 0.6
Equivalence of the scale	0.283	W = 0.4

3.5.3 From M_w to M_w

The PEGASOS report (PEGASOS TP1-CAT-0004, p. 67) shows that the uncertainty in M_w conversion is about 0.1 magnitude units. I decided not to use a conversion for attenuation laws which are using M_w even if this M_w has been computed by different teams. The epistemic uncertainty is small and will not be taken into account.

3.5.4 From M_w to M_{JMA}

According to Fukushima (1996), the relation between seismic moment and M_{JMA} is:

$\text{Log}(M_0^{-1} + 10^{-17} M_0^{-1/3}) = -1.10 M_{JMA} – 17.92$ (M_0 in dyne.cm)

I have decided to use the Fukushima's conversion formula with a sigma of 0.2. The moment (in dyne.cm) is calculated using Kanamori's (1977) formula ($Log_{10} M_0=1.5 M_w+16.1$). As an alternative model, the M_{JMA} is assumed to be equal to moment magnitude. These two branches are given in Table 9. The equality between the JMA magnitude and the moment magnitude scale is justified by the study of Heaton et al. (1986) where the two scales are shown to be equal between magnitude 5 and 7. However, the Fukushima's study is more recent than the Heaton et al. (1986) analysis and addresses more specifically the problem of the conversion between M_{JMA} and M_w. For this reason, I favour the Fukushima (1996) branch in the logic tree.

Tab. 9: M_w to M_{JMA}conversion weighting

Logic tree branches	Sigma	Weight
Fukushima (1996)	0.2	W = 0.6
Equivalence of the scale	0.2	W = 0.4

3.6 Component conversions

I use the corrections factors described in the PEGASOS document Roth (2002, PEGASOS TP2-TN-0269) since this study is probably the most complete and up-to date analysis done on this subject. The epistemic uncertainty on these conversions is small so I use only one branch for these conversions.

3.7 Missing frequencies

I use the interpolation procedure described in the PEGASOS document (Hölker 2002, PEGASOS TP2-TN-0270).

3.8 Style-of-faulting adjustments

The distinction between ground motions from strike-slip and reverse faults has become common in recent attenuation relations. The difference in ground motion between reverse and strike-slip events is called the style-of-faulting factor. These style-of-faulting factors are taken into account by Abrahamson & Silva (1997), Boore et al. (1997) and Campbell (1997).

3.8.1 Style-of-faulting effect: a fault mechanism's effect or a tectonic stress regime's effect ?

- McGarr (1984) concluded that normal-faulting earthquakes located in extensional regimes are associated with lower ground motion than either strike-slip or reverse faulting earthquake located in compressional stress regimes.
- Northridge and Wittier Narrows earthquakes have shown high motion (Chin & Aki 1994): it could indicate that relatively deep blind thrust faults could systematically produce ground motion that are 50 % higher than those from shallow blind or surface faults with the same style of faulting.
- Spudich et al. (1999) show the similarity of normal motion and strike-slip motion in extensional regimes. They show that motion in extensional regimes is lower than in compressional stress regimes.
- Becker & Abrahamson (1998) have shown that median stress-drop from normal faults is less than median stress-drop of strike-slip faults which contradicts McGarr's hypothesis that the stress-drop of both these mechanisms is less in extensional regime than in compressional stress regime.

Finally, it is not clear if the style of faulting factors is due to source fault mechanism or tectonic stress regime effects. The only clear effect seems to be due to deep blind thrust faults which could systematically produce high ground motion.

3.8.2 Which factors ?

- Distance and magnitude dependencies are not supported by all the datasets.
- H / V style-of-faulting dependency is not supported by all the datasets
- The vertical factors are poorly constrained.

– Frequency dependence of the style-of-faulting factors are consistent in all the datasets; however this frequency dependence is different for horizontal motions and vertical motions. Moreover, the fact that the H / V ratio is constant in some approaches is not consistent with the fact that the frequency dependence of the style-of-faulting factor is different for vertical and horizontal motions.

– Style-of-faulting factors could depend on particular events. For example, Abrahamson & Silva (1997) have found high values of the reverse / strike factors for small magnitudes which could be due to the Coalinga aftershocks.

I have found no clear physical explanations to explain these factors and their dependency with magnitude, distance, and frequency.

3.8.3 Conclusion

– Finally, it is not clear if style-of-faulting factors are due to source fault mechanism or tectonic stress regime effects. The only clear effect seems to be that blind thrust faults systematically produce higher ground motions.

– Therefore, the relative contribution of reverse events (on the one hand) and both normal and strike-slip events (on the other hand) of the resulting composite model have to be the same as in the target region.

3.8.4 Practical solution

The reverse faulting distribution of the resulting logic tree composite model has to be the same as in the target region.

For Abrahamson & Silva (1997), Boore et al. (1997) and Campbell & Bozorgnia (2002), two different equations (Strike Slip or Reverse) of the empirical models can be written. I suggest the following solution: for each of these 3 empirical models, the relative weight of the reverse style-of-faulting equations has to be chosen in order to adjust the composite model reverse distribution (Birkhäuser 2003, PEGASOS TP2-TN-0362) to the one of the target region.

An example is given in Table 10.

The reverse faulting distribution in the Target region is equal to 40 %. The reverse faulting distribution of Boore et al. (1997), Abrahamson & Silva (1997) and Campbell & Bozorgnia (2002) has to be equal to 38.41 % in order to obtain the same reverse distribution in the logic tree composite model than in the target region.

Tab. 10: Example of style-of-faulting adjustment

	Percentage NML and SS	Percentage REV	Logic-tree Weights	Net Weight for NML and SS	Net Weight for REV
Style-of-faulting target (example)	60	40			
Ambraseys et al. (1996)	46.3	47	0.1	0.0463	0.047
Ambraseys & Douglas (2003)	52.7	47.3	0.1	0.0527	0.0473
Berge-Thierry et al. (2000)	58	31	0.1	0.058	0.031
Atkinson & Boore (1997)	19	81	0.05	0.0095	0.0405
Lussou et al. (2001)	35	60	0.05	0.0175	0.03
Sabetta & Pugliese (1996)	50	39	0.05	0.025	0.0195
Somerville et al. (2001)	0	100	0.025	0	0.025
Spudich et al. (1999)	100	0	0.05	0.05	0
Toro et al. (1997)	19	81	0.025	0.00475	0.02025
Bay et al. (2003)	84	5	0.05	0.042	0.0025
Rietbrock (2002)	84	5	0.05	0.042	0.0025
Abrahamson & Silva (1997)	61.6	38.4	0.2	0.1232	0.0768
Boore et al. (1997)	61.6	38.4	0.1	0.0616	0.0384
Campbell & Bozorgnia (2002)	61.6	38.4	0.05	0.0308	0.0192

4 MEDIAN V / H RATIO

4.1 Approaches for V / H ratios

Only Ambraseys & Simpson (1996) and Ambraseys & Douglas (2000) provide equations for the direct V / H ratios of spectral ordinates. The other equations that predict horizontal and vertical spectra separately can also be used to derive such a ratio. These equations have been derived for different site conditions. Most of them are empirical models where rock is a generic soft weathered rock with rock velocity between 450 and 800 m/s (Ambraseys & Simpson 1996, Berge-Thierry et al. 2000, Lussou et al. 2001 (class B site), Sabetta & Pugliese 1996, Abrahamson & Silva 1997, Ambraseys & Douglas 2000, Campbell & Bozorgnia 2002 (soft rock)). Since I do not know any clear method to take into account site correction on vertical ground motion and since my logic tree rock reference velocity has a higher velocity (2000 m/s) than the one of these empirical studies, my approach is to use models that are applicable to hard-rock conditions (Lussou et al. 2001 (class A), Somerville et al. 2001 and Campbell & Bozorgnia 2002 (hard rock)) to build generic hard rock V / H ratios. The obtained logic tree gives the V / H ratio for hard-rock site conditions.

4.2 Logic tree structure

The logic tree has three branches corresponding to the three proponent models that are applicable to hard-rock conditions (Campbell & Bozorgnia 2002, Somerville et al. 2001 and Lussou et al. 2001) and which also predict the ground motion for both horizontal and vertical components.

4.3 Weights for proponent models

The Campbell & Bozorgnia (2002, hard-rock), Somerville et al. (2001) and Lussou et al. (2001, class A) models do not have the same weights for all magnitudes and distances in the logic tree used to predict the horizontal motion. For example, the Campbell & Bozorgnia empirical model includes records at short distances which is not the case for Lussou's model. Therefore, a different weighting of these two models is chosen for the 9 bins defined to predict the horizontal motion (see Table 11).

Tab. 11: H / V (hard rock) weighting

$M_1 = 5.5$; $M_2 = 6.5$ $R_1 = 15$ km ; $R_2 = 70$ km	$M_w < M_1$			$M_1 < M_w < M_2$			$M_w > M_2$		
	$R < R_1$	$R_1 < R < R_2$	$R > R_2$	$R < R_1$	$R_1 < R < R_2$	$R > R2$	$R < R_1$	$R_1 < R < R_2$	$R > R_2$
Model Name	Weight								
Lussou et al. (2001)	0.35	0.4	0.5	0.25	0.35	0.35	0.25	0.3	0.3
Campbell & Bozorgnia (2002)	0.5	0.45	0.35	0.5	0.35	0.35	0.5	0.35	0.35
Somerville et al. (2001)	0.15	0.15	0.15	0.25	0.3	0.3	0.3	0.35	0.35

5 ALEATORY VARIABILITY FOR HORIZONTAL GROUND MOTION

5.1 Logic tree structure

The same bins as used to predict the median ground motion are used for the aleatory variability. I considered the standard deviations from each of the equations used to predict the median ground motion; however the weights given to the models are different than the weights for the median ground motion. The choice of weighting for the aleatory variability is due to the following points:

- the magnitude dependence of the aleatory variability is modeled by recent studies but is not taken into account by all the models,
- the aleatory variability might be overestimated or underestimated due to limited or heterogeneous datasets.

The chosen logic tree also takes into account the rules of error propagation and the effects of magnitude and distance conversions.

5.2 Weights for proponent models

The weighting takes into account the following factors:

Magnitude effect

Peak Ground Acceleration variance is magnitude dependent and the variance decreases when the magnitude increases. Several factors can explain this point:

- *Non-linearity*. As the amplitudes of the motion increases, the high frequency part of the motion is attenuated and the variability of the pga is reduced (Chin & Aki 1991); however, Youngs et al. (1995) have shown that this magnitude dependence also exists for pga < 0.1 g.
- *Shift in the predominant frequency*. Low frequency motion is less variable at short distances than high frequency motions and the predominant frequency is lower for large magnitude earthquakes.
- *Duration*. Increasing the duration could decrease the variability.
- *Magnitude dependence of the stress-drop*. The stress-drop scales the high-frequency part of the motion. Wells & Coppersmith (1994) show that, for a given magnitude, the variability of the fault rupture area (the stress-drop) is less for large magnitude earthquakes than for small magnitude earthquakes.
- *Magnitude and location accuracy*. Magnitude and location determination errors are more frequent for small magnitude events. The measurement errors are treated as variability.

According to these results, higher weights are given to models which take into account this magnitude dependence (Campbell & Bozorgnia 2002 and Abrahamson & Silva 1997).

Dataset effects

- Variance could be underestimated for attenuation laws deduced from limited datasets or from datasets dominated by a few specific events. This could occur for Sabetta & Pugliese (1996) and Boore et al. (1997) who have used good quality but limited datasets.
- Some catalogues deals with a more heterogeneous dataset and associated station parameters where some errors (and then artificially increased variance) can occur because of this heterogeneity (Ambraseys et al. 1996, Berge-Thierry et al. 2000).

Lower weights have been given to models for which the variance could be biased by such data-set effects.

Aleatory uncertainty in Rietbrock (2002, PEGASOS EXT-TN-0306)

The aleatory variability of Rietbrock (2002, PEGASOS EXT-TN-0306) has not been calculated and therefore I assume it to be similar to the value of sigma found by Bay (2002). Sigma is then equal to 0.35 (Bay 2002, p. 58) and is only aleatory. Modelling uncertainties do not take into account the parametric uncertainties (event to event variations due to source path and site properties) since it is estimated with data $3 < M_w < 4$ and only one model A0. I therefore decided to add the parametric uncertainty from Toro et al. (1997) to the modelling variability from Bay (2002).

5.3 Horizontal component conversions

We are dealing with various variance definitions:

- Variance corresponding to a randomly oriented component (Berge-Thierry et al. 2000, Lussou et al. 2001, all stochastic models),
- Variance corresponding to geometric mean (Boore et al. 1997, Abrahamson & Silva 1997, Spudich et al. 1997, 1999) or arithmetic mean (Campbell & Borzorgnia 2002),
- Variance corresponding to the larger component (Ambraseys et al. 1996, Sabetta & Pugliese 1996).

I use the average horizontal uncertainty conversions described in Hölker (2002, PEGASOS TP2-TN-0307). The standard deviation of the residuals calculated using different definitions of the horizontal component are very similar. In other words there is no evidence of a dependence of the standard deviation on the definition of the horizontal component. I have therefore chosen not to take into account a conversion effect on the variability.

5.4 Magnitude conversion effect

The magnitude conversion effect is taken into account (see logic tree) in order to take into account the rules of error propagation.

5.5 Distance conversion effect

The distance conversion issue is not part of the experts models and this point is therefore not adressed in the logic tree.

6 MAXIMUM GROUND MOTIONS FOR THE HORIZONTAL COMPONENT

6.1 Evaluation of empirical data

6.1.1 Analysis of Hölker & Roth (2003, PEGASOS TP2-TN-0333)

The Abrahamson & Silva (1997) empirical model maximum ground motion (expressed in terms of number of standard deviations) has a correct shape to cover maximum observed ground motion at various distances. This point is, for example, supported by the figure which described Cotton's scenario 3 for a magnitude 5.5 at 10 Hz. Moreover, for a given number of sigma (for example 4 sigma, Cotton's scenario 3, see Figure 10), the Abrahamson & Silva model shows a good general agreement with the data comparison among different magnitude, distance and frequencies choices. Therefore, I chose to determine the maximum ground motion using the Abrahamson & Silva model expressed in terms of the number of standard deviations.

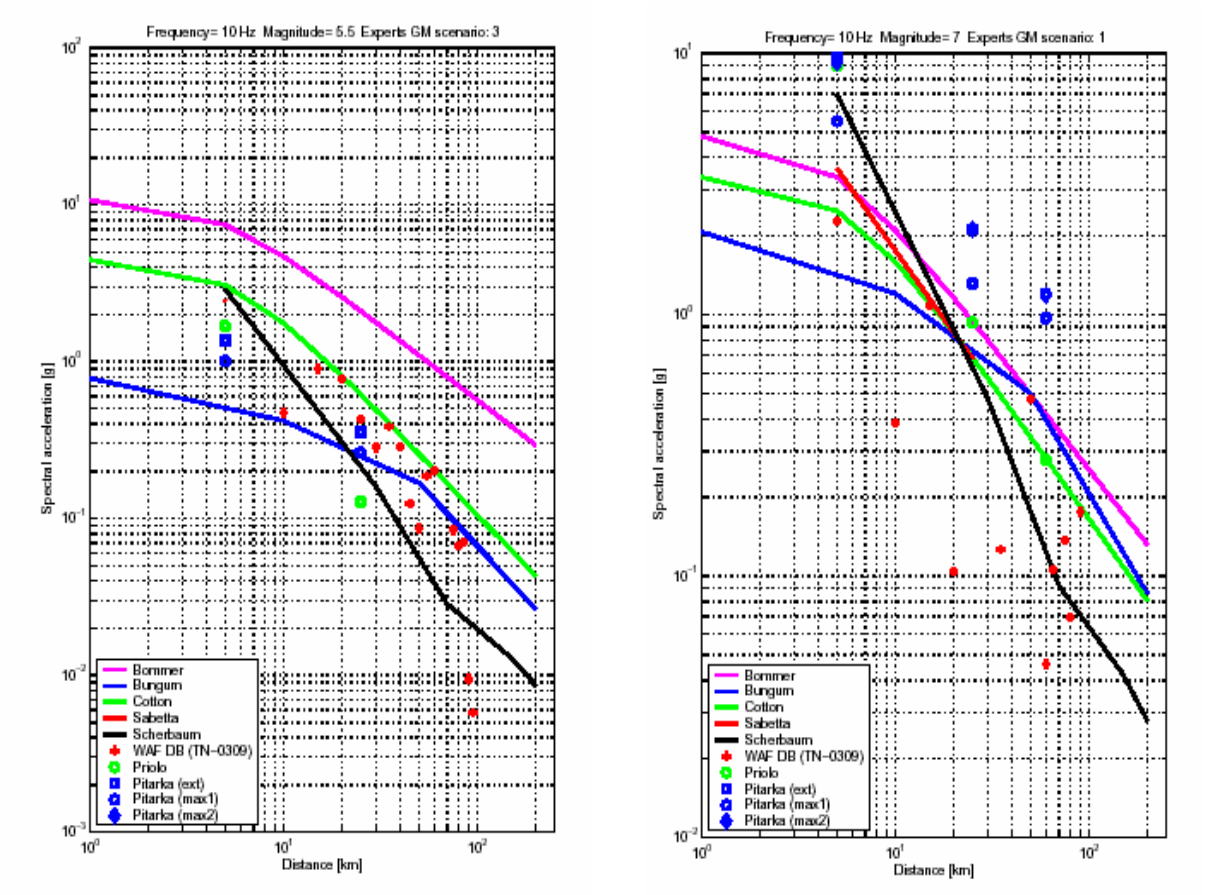

Fig. 10: Comparison between simulated and observed upper ground motion with upper ground motions models (Hölker & Roth 2003, PEGASOS TP2-TN-0333)

Cottons's scenario 3 is built with the Abrahamson & Silva (1997) model + 4 sigma.

6.1.2 Analysis of Roth (2002, PEGASOS TP2-TN-0309)

From the empirical datasets (Roth 2002, PEGASOS TP2-TN-0309) we can also write the two following Tables 12 and 13.

- The maximum observed number of standard deviation (Abrahamson & Silva 1997) is between 2.25 and 3.33 for horizontal motion and between 3.36 and 4.17 for vertical motion. This number is higher at lower frequency for horizontal motion.
- This maximum number of standard deviation is observed for different types of magnitude range and at different distances.
- This maximum number is lower for the horizontal motion than for to the vertical motion.

For horizontal motion, this maximum number is higher at low frequency than at high frequency.

Tab. 12: Interpretation of Roth (2002, PEGASOS TP2-TN-0309) – horizontal motion

Frequency, Hz	Number of sigma	Distance	Magnitude
0.25	3.11	97.5	5.25
0.5	3.33	37.5	6.25
1.0	3.25	17.5	6.25
2.0	2.84	62.5	5.75
2.5	2.65	47.5	4.75
5.0	3.04	47.5	4.75
10	2.89	47.5	4.75
20	3.04	47.5	4.75
25	2.99	47.5	4.75
100	2.25	12.5	6.75

Tab. 13: Interpretation of Roth (2002, PEGASOS TP2-TN-0309) – vertical motion

Frequency, Hz	Number of sigma	Distance	Magnitude
0.25	4.0	27.5	4.75
0.5	3.36	37.5	6.25
1.0	2.56	47.5	4.75
2.0	2.91	27.5	5.75
2.5	2.81	12.5	6.75
5.0	3.66	47.5	4.75
10	3.69	47.5	4.75
20	4.17	47.5	4.75
25	4.35	87.5	5.75

6.2 Evaluation of numerical simulations

Both models, Pitarka (2002) and Priolo et al. (2002), are interesting and well constructed at low frequencies. Both models do present some weaknesses:

- the resonance at 2 Hz of the Pitarka model is questionable,
- high frequency (> 2 Hz) generation of the Priolo et al. model could be overestimated due to instantaneous rise-time and a high fmax.

The easiest way to evaluate (for various frequencies, distances and magnitudes) the maximum ground motion is to express in terms of number of sigma of a given empirical model. I have chosen to use the empirical ground motion of Abrahamson & Silva (1997). This choice is due to several reasons:

- This empirical model is used as reference in the documents of Roth (2002, PEGASOS TP2-TN-0309) and Hölker & Roth (2003, PEGASOS TP2-TN-0333),
- This empirical model use the geometric mean of the two components which is also the project choice,
- Standard deviations have been carefully calculated for this empirical model based on a large amount of data.

However, this model has a magnitude dependant variance and therefore I have also chosen to compare the maximum observed and simulated motions with the empirical model of Ambraseys et al. (1996) which is used in Bommer's scenarios 1, 2 and 3 in Hölker & Roth (2003, PEGASOS TP2-TN-0333).

Table 14 describes the comparison of empirical data and simulated motions with some of the scenarios (Bommer's scenarios 1, 2, 3 and Cotton's scenario 3) described in Hölker & Roth (2003, PEGASOS TP2-TN-0333).

This table and the figures of Hölker & Roth (2003, PEGASOS TP2-TN-0333) show that the simulations reproduce the highest ground motions which have been observed for the magnitude 5.5 case; however, the simulations are much higher than observations for the magnitude 7.0 earthquake. This difference is higher for the 1 Hz case than for the 10 Hz case.

6.3 Logic Tree Structure

- My analysis is that extreme ground motion is mainly due to wave constructive interference of waves. For rock sites, this constructive interference is due to finite sources effects directivity (this effect is increased by super-shear velocity) or waves focusing that could be created also by finite source effects (e.g. Petrolia, see Oglesby & Archuleta 1997) but also by regional deep site effects. This type of focusing or wave trapping by deep geological structures has not been taken into account in our simulations but could exist as suggested by the pockets of localized damage not clearly with surficial soil conditions caused by the Northridge earthquake in Santa Monica (Somerville 1998).
- The fact that simulations are much higher than the maximum observed motion for large magnitudes and not for small magnitudes could indicate that wave constructive interferences (mainly due to finite source effects like directivity or bad source-site location) do not occur so easily as in our simulations. This point is supported by kinematic source inversions which show that the rupture front geometry is irregular and probably reflects stress heterogeneities on fault planes. Madariaga's report (Madariaga 2002, PEGASOS EXT-TN-

0308) also evaluates as unrealistic a constant supershear velocity on the all fault plane. This difference also supports the idea that earth materials are non-linear and that this non-linearity (not taken into account in the simulations) limits extreme ground motions.

– Wave constructive interference occurs more easily at low frequency. However, the decrease of maximum motion (expressed in terms of number of standard deviations) with increasing frequency is only clear for horizontal motions.

Tab. 14: Interpretation of Hölker & Roth (2003, PEGASOS TP2-TN-0333) results

	Empirical data	Simulation	Consistency between data and simulations
2.5 sigma (Ambraseys et al. 1996, 1 Hz, M = 7.0)	All covered	Most not covered	Simulations are much higher than observed data (the difference is higher than at 1 Hz)
2.5 sigma (Ambraseys et al. 1996, 1 Hz, M = 5.5)	Two data are not covered	Two simulations are not covered	Yes
2.5 sigma (Ambraseys et al. 1996, 10 Hz, M = 7.0)	Three data are not covered	Most are not covered	Simulations are always higher than observed data
2.5 sigma (Ambraseys et al. 1996, 10 Hz, M = 5.5)	All covered	Almost covered	Yes
3.5 sigma (Ambraseys et al. 1996, 1 Hz, M = 7.0)	All covered	Almost covered	
3.5 sigma (Ambraseys et al. 1996, 1 Hz, M = 5.5)	All covered	All covered	
3.5 sigma (Ambraseys et al. 1996, 10 Hz, M = 7.0)	All covered	Half are not covered	
3.5 sigma (Ambraseys et al. 1996, 10 Hz, M = 5.5)	All covered	All covered	
5.0 sigma (Ambraseys et al. 1996, 1 Hz, M = 7.0)	Over covered	Over covered	
5.0 sigma (Ambraseys et al. 1996, 1 Hz, M = 5.5)	Over covered	Over covered	
5.0 sigma (Ambraseys et al. 1996, 10 Hz, M = 7.0)	All covered	All covered	
5.0 sigma (Ambraseys et al. 1996, 10 Hz, M = 5.5)	Over covered	Over covered	
4.0 sigma (AS, 1 Hz, M = 7.0)	All covered	Not covered	
4.0 sigma (AS, 1 Hz, M = 5.5)	Almost covered	Almost covered	
4.0 sigma (AS, 10 Hz, M = 7.0)	covered	Not covered	
4.0 sigma (AS, 10 Hz, M = 5.5)	Almost covered	Almost covered	

Table 15 describes the upper bounds weighting.

Tab. 15: Upper bounds weighting

Maximum ground motion expressed in terms of number of sigma (horizontal component) of Abrahamson & Silva's empirical model (1997)	Weight	Working hypothesis
4 sigma	0.6	Extreme source models do not exist and extreme ground motions are due to constructive wave interferences and "bad" source-site geometry. These extreme motions have already been captured by our instruments (e.g. Petrolia, see Oglesby & Archuleta 1997).
5 sigma	0.35	Dynamic physical constraints will limit extreme ground motions generated by extreme kinematic models. These extreme ground motions (e.g. max1 of Pitarka's simulations 2002) have not been captured by our instruments.
6 sigma	0.05	Extreme kinematic models for large earthquakes (without extended supershear velocity) or wave focusing on moderate earthquakes do exist. These extreme ground motions (e.g. ext of Pitarka's simulations 2002) have not been captured by our instruments.

7 MAXIMUM GROUND MOTIONS FOR THE VERTICAL COMPONENT

Extreme vertical ground motion is due, in my opinion, to non-vertical incidence angles. In that case SH waves (which usually are responsible of the maximum ground motion) can control the vertical motion. For this reason I use the same maximum ground motion for both the horizontal and the vertical component.

8 UPPER TAIL OF THE GROUND MOTION DISTRIBUTION FOR THE HORIZONTAL COMPONENT

8.1 Evaluation of empirical data

- From the residuals of Berge-Thierry et al. (2000) and Abrahamson & Silva (1997), departure from the log-normal distribution seems to occur at 3 sigma but there is no systematic shape of the deviation from log-normal above 3 sigma.
- There is a lack of theoretical as well of empirical justification to evaluate the shape of the departure and the maximum number of standard deviations that have to be taken into account.

8.2 Logic Tree Structure

I feel uncomfortable introducing a tail cut-off in excess of what will be indirectly inferred from the ground motion limitation. The trade-off between ground motion limitation and the maximum number of standard deviation is not clear. I therefore decided to only use the upper bound ground motion limitation.

9 REFERENCES

Abrahamson, N.A. & Silva, W.J. 1997: Empirical response spectral attenuation relations for shallow crustal earthquakes. Seism. Res. Lett. 68, 94-127.

Atkinson, G.M. & Boore, D.M. 1997: Some comparison between recent ground-motion relations. Seism. Res. Lett. 68, 24-40.

Ambraseys, N. & Douglas, J. 2000: Reappraisal of the effect of vertical motions on response. ESEE Report 00-4.

Ambraseys, N.N. & Douglas, J. 2003: Near-field horizontal and vertical ground motion relations. Soil dynamics and earthquake engineering 23, 1-18.

Ambraseys, N., Simpson, K.A. & Bommer, J.J. 1996: Prediction of horizontal response spectra in Europe. Earth. Eng. Struct. Dyn. 25, 371-400.

Ambraseys, N.N. & Free, M.W. 1997: Surface-wave magnitude calibration for european region earthquakes. JEE 1/1, 1-22.

Ambraseys, N.N. & Simpson, K.A. 1996: Prediction of vertical response spectra in Europe. Earth. Eng. Struct. Dyn. 25, 401-412.

Bay, F. 2002: Ground motion scaling in Switzerland: implications for hazard assessment. PhD Thesis No. 14567, ETH Zürich.

Bay, F., Fäh, D. Malagnini, L. & Giardini, D. 2003: Spectral shear-wave ground motion scaling in Switzerland. Bull Seism. Soc Am 93, 414-429.

Becker, A. 2003: Brune stress drops for small magnitude california data recorded at hard rock sites. PEGASOS Technical Note EXT-TN-0218.

Berge-Thierry, C., Cotton, F., Cushing, M., Griot-Pommera, D.-A., Joly, J., Levret, A. & Fukushima, F. 2000: Méthode de détermination des spectres horizontaux et verticaux dans le cadre de la révision de la RFS I.2.c. Rapport IPSN/DPRE/SERGD 00-53.

Birkhäuser, Ph. 2003: SP2 inquiry for the style-of-faulting distributions of the selected attenuation relations. PEGASOS Technical Note TP2-TN-0362.

Boore, D.M., Joyner, W.B. & Fumal, T.E. 1997: Equations for estimating horizontal response spectra and peack acceleration from western north american earthquakes: a summary of recents work. Seism. Res. Ltrs. 68/1, 128-153.

Bungum, H., Lindholm, C. & Dahle, A. 2002: Long period ground motion for large European earthquakes, 1905-1992 and comparisons with stochastic predictions. J. Seism. (*in press*).

Bungum, H., Dahle. A. & Lindholm, C.D. 1996: Methodologies, models and uncertainties relating to seismic hazard analyses in Norway. 25th General Assembly of the European Seismological Commission, Reykjavik, Sep. 9-14.

Campbell, W. 1997: Empirical near-source attenuation relationships for horizontal and vertical components of peak ground acceleration, peak ground velocity and pseudo-absolute acceleration response spectra. Seism. Res. Lett. 68, 154-179.

Campbell, W. & Bozorgnia, Y. 2002: Updated near source ground motion relations for horizontal and vertical components of peak ground acceleration, peak ground velocity and pseudo-absolute acceleration response spectra. Bull. Seism. Soc. Am. (*submitted*).

Campillo, M. & Plantet, J.L. 1991: Frequency dependence and spatial distribution of seismic attenuation in France: experimental results and possible interpretation. Phys. of the Earth Planetary Interiors 67, 48-64.

Chandra, U. 1979: Attenuation of intensities in the United States, 1979. Bull. Seism. Soc. Am. 69, 2003-2024.

Chang, T.Y., Cotton, F. & Angelier, J. 2001: Seismic attenuation and peak ground acceleration in Taiwan. Bull Seism. Soc. Am. 91, 1229-1246.

Chin, B.H. & Aki, K. 1991: Simultaneous study of the source, path, and site effects on strong ground motion during the 1989 Loma Prieta earthquake: a preliminary result on persuasive nonlinear site effects. Bull. Seism. Soc. Am. 81, 1859-1884.

Chin, B.H. & Aki, K. 1994: Strong ground motion prediction during the 1994 Northridge earthquake. Seismological Research Letters 65/3-4, 252.

Courboulex, F., Deichmann, N. & Gariel, J.-C. 1999: Rupture complexity of a moderate intraplate earthquake on the Alps: the 1996 M5 Epagny-Annecy earthquake. Geophys. J. Int. 139, 152-160.

Ekstroem, G. & Dziewonski, A.M. 1988: Evidence of bias in estimations of earthquake size. Nature 332, 319-323.

Frankel, A., McGarr, A., Bicknell, J., Mori, J., Seeber, L. & Cranswick, E. 1990: Attenuation of high-frequency shear waves in the crust: measurements from New York State, South Africa and Southern California. J. Geophys. Res. 95, 17441-17457.

Fukushima, Y. 1996: Scaling relations for strong ground motion prediction models with M2 term. Bull. Seism. Soc. Am. 86, 329-336.

Heaton, T., Tajima, F. & Mori, A.W. 1986: Estimating ground motions using recorded accelerograms. Surveys in Geophysics 8, 25-83.

Hölker, A. 2002: Note on the estimation of coefficients of ground motion models at missing frequencies. PEGASOS Technical Note TP2-TN-0270.

Hölker, A. 2002: Note on the analysis of standard deviations of residuals computed using different definitions of the horizontal component. PEGASOS Technical Note TP2-TN-0307.

Hölker, A. & Roth, Ph. 2003: Note on Maximum Ground Motion Plots. PEGASOS Technical Note TP2-TN-0333.

Kanamori, 1977: The energy release in great earthquake. Journal of Geophysical Research 82, 2981-2987.

Lacave, C. 2003: Computation of scaling factors for three "realistic" rock profiles. PEGASOS Technical Note TP2-TN-0350.

Lacave, C., Kohler, M. & Birkhäuser, Ph. 2003: Computation of scaling factors for generic "rock" profiles. PEGASOS Technical Note TP2-TN-0363.

Lussou, P., Fukushima, Y., Bard, PY & Cotton, F. 2001: Seismic design regulation codes: contribution of Knet data to site effect evaluation. J. Earthquake Engineering 5(1), 13-33.

Madariaga, R. 2002: Assessment of feasibility of kinematic fault models used for upper limit ground motion evaluations for the PEGASOS Project. PEGASOS Technical Note EXT-TN-0308.

Mayeda, K. & Walter, W.R. 1996: Moment, energy, stress drop and source spectra of western United State earthquakes from regional code envelopes. J. Geophys. Res. 101, 11195-11208.

McGarr, A. 1984: Scaling of ground motion parameters, state of stress, and focal depth. Geophys. Res. Lett. 89, 6969-6979.

Oglesby, D.D. & Archuleta, R.J. 1997: A faulting model for the 1992 Petrolia earthquake: can extreme ground motion be a source effect ? J. Geophys. Res. 102, 11877-11897.

Pitarka, A. 2002: Numerical Simulations for Evaluation of Median and Upper Limit Ground Motions in Switzerland – Revised Final Report.

Pitarka, A. & Priolo, E. 2002: Comparison of simulations performed by URS Corporation, U.S.A. and OGS, Italy. Joint Report.

Priolo, E., Vuan, A., Klinc, P. & Laurenzano, G. 2002: Results of extended source and full wave-field propagation for strong ground motion modelling. SP2 Workshop 3. PEGASOS TP2-RF-0293.

Rietbrock, A. 2002: Determination of input parameters for the stochastic simulation of strong ground motion for Switzerland. PEGASOS Technical Note EXT-TN-0306.

Roth, Ph. 2002: Note on the statistical analysis of the ratios of different definitions of the horizontal component. PEGASOS Technical Note TP2-TN-0269.

Roth, Ph. 2002: Average shear wave velocitiy profiles for Europe and California. PEGASOS Technical Note TP2-TN-0254.

Roth, Ph. 2002: Note on the statistical analysis of the average / larger horizontal component ratio from the WAF database. PEGASOS Technical Note TP2-TN-0242.

Rüttener, E. 1995: Earthquake hazard evaluation for Switzerland. Matér. Géol. Suisse, Nr. 29, Schweizerische Geophysikalische Kommission, ETH-Zürich, 106.

Sabetta, F. & Pugliese, A. 1987: Attenuation of peak horizontal acceleration and velocity from Italian strong-motion records. Bull. Seism. Soc. Am. 77/5, 1491-1513.

Sabetta, F. & Pugliese, A. 1996: Estimation of ground motion and simulation of nonstationary earthquake ground motions. Bull. Seism. Soc. Am. 86(2), 337-352.

Scholz, C. 1989: The Mechanics of earthquake and faulting. Cambridge, Cambridge Univ. Press.

Silva, W., Darragh, D., Gregor, N., Martin, G., Abrahamson, N. & Kircher, C. 1998: Reassessment of site coefficients and near fault factors for building code provisions. USGS Report 98-HQ-GR-1010.

Somerville, P. 1998: Ground motion attenuation relationships and their application to aseismic design and seismic zonation. The effects of surface geology on seismic motion, Yokohama.

Somerville, P., Collins, N., Graves, R. & Saikia, C. 2001: Ground motion attenuation relations for the Central and Eastern United States. USGS Report 99-HQ-GR-0098.

Spudich, P., Fletcher, J.B., Hellweg, M., Boatwright, J., Sullivan, C., Joyner, W.B., Hanks, T., Boore, D.M., McGarr, A., Baker, L.M. & Lindh, A.G. 1997: SEA96: A new predictive relation for earthquake ground motions in extensional tectonic regimes. Seism. Res. Lett. 68/1, 190-198.

Spudich, P., Joyner, W.B., Lindh, A.G., Boore, D.M., Margaris, B.M. & Fletcher, J.B. 1999: SEA99: a revised ground motion prediction relation for use in extensional tectonic regimes. Bull. Seism. Soc. Am. 89, 1156-1170.

Toro, G.R., Abrahamson, N.A. & Schneider, J.F. 1997: Model of strong ground motions for earthquakes in central and eastern north-america. Seism. Res. Lett. 68, 41-57.

Vigny, C., Chery, J., Duquesnoy, T., Jouanne, F., Ammann, J., Anzidei, M., Avouac, J.P., Barlier, F., Bayer, R., Briole, P., Calais, E., Cotton, F., Duquenne, F., Feigl, K., Flouzat, M., Gamond, J.F., Geiger, A., Harmel, A., Kasser, M., Laplanche, M., Le Pape, M., Martinod, J., Ménard, G., Meyer, B., Ruegg, J.C., Scheubel, J.M., Scotti, O. & Vidal, G. 2002: GPS network monitors the Western Alps deformation over a five year period: 1993-1998. Journal of Geodesy 76, 63-76.

Wells, D.L. & Coppersmith, K.J. 1994: New empirical relationships among magnitude, rupture length, rupture width, rupture area, and surface displacement. Bull Seism. Soc. Am. 84, 974-1002.

Youngs, R.R., Abrahamson, N.A., Makdisi, F.I. & Sadigh, K. 1995: Magnitude-dependent variance of peak ground acceleration. Bull. Seism. Soc. Am. 85, 1161-1176.

APPENDIX 1 EG2-HID-0029 HAZARD INPUT DOCUMENT FINAL MODEL F. COTTON

Introduction

This document describes the implementation and parameterization of Fabrice Cotton's expert model EG2-EXM-0022, as described in the Elicitation Summary EG2-ES-0036 and delivered on 30.05.2003. The purpose of this document is to translate the expert's evaluation of ground motion into an input useable by the hazard software.

Model Implementation

Based on F. Cotton's Elicitation Summary EG2-ES-0036, the logic trees for the median horizontal ground motion, the vertical / horizontal ratio and the aleatory variability of the horizontal component were implemented in FORTRAN and the results displayed graphically.

Key elements in F. Cotton's model are given below:

Median horizontal ground motion

- 13 candidate equations have been retained, where the Swiss stochastic model is included using 6 parameter variants. Including these variations on the Swiss stochastic model, a total of 18 ground motion models are considered.
- The Swiss stochastic model is based on Rietbrock (2002, PEGASOS EXT-TN-0306) and further sub-divided into six equally weighted sub-models, using two different values of geometrical spreading and three different values of stress drop.
- For the weighting of the ground motion models, the magnitude – distance plane is subdivided into 9 bins with the following limits:

  Magnitude: $5 < 5.5 < 6.5 < 8$

  Distance [km]: $0 < 15 < 70 < 1000$
- To adjust the models to the SP3 reference shear wave velocity of 2000 m/s two alternative methods are implemented. First, ground motion is scaled by factors based on Scherbaum's generic rock profiles and provided by Lacave et al. (2003, PEGASOS TP2-TN-0363). Three side branches with mean, lower and upper velocities account for the epistemic uncertainty in the EG2 estimates of Vs_{30} for each GM equation (see Table 4). The second adjustment is based on the "realistic" rock profiles provided along with the corresponding scale factors in Lacave (2003, PEGASOS TP2-TN-0350).
- To account for specific Swiss ground motion conditions, two corrections are made. First, each model is corrected according the differences in κ_0 of the host regions (proponent models) and the Swiss target region. For this reason, representative values for κ_0 have been assigned to each individual ground motion model using the relation of Silva et al. (1998). For the target region a mean κ_0 is used as central branch along with one side branch with a lower value. One additional side branch considers the case where no correction should be applied. The scale factors for the kappa correction are derived using RVT for different kappa values with the source and path parameters from Rietbrock (2002, PEGASOS EXT-TN-0306). The scale factor computation is repeated for each of the nine bins. The scale factors are listed in Tables A1-7 – A1-18.

  Second, the EUS models are corrected for differences in the geometrical spreading and Q between the EUS and Switzerland. To compute these distance dependent scale factors, the response spectra for the Rietbrock model is computed for hypocentral distances covering the range of 10 to 500 km for M = 6 and kappa = 0.006 sec. At each frequency, the resulting

spectral values are then scaled so that at a hypocental distance of 10 km, the spectral values are equal to the spectral values from the Toro et al. model. The ratio of the scaled Rietbrock model to the Toro model gives the scale factor for geometrical spreading and Q. A 10 km value was used for the normalization because the Toro model is based on JB distance with an average depth of about 8 km. The resulting scale factors for geometrical spreading and Q are listed in Table A1-19.

- Each of the magnitude conversion schemes includes two branches: either conversion by Ambraseys & Free (1997) (M_s to M_w), PEGASOS (PEGASOS TP1-CAT-0004) (M_L to M_w) and Fukushima (1996) (M_{JMA} to M_w) or equivalence of scale.
- The conversion of the different types of larger horizontal components to the geometric mean definition is based on Roth (2002, PEGASOS TP2-TN-0269) for spectral acceleration. Epistemic uncertainty is not considered.
- Missing coefficients in the GM models considered are to be derived according to the procedure described in Hölker (2002, PEGASOS TP2-TN-0270).
- A style-of-faulting adjustment is applied to those GM models that account for the faulting mechanism by introducing specific equations for Reverse and Strike-Slip events (i.e. Abrahamson & Silva (1997), Boore et al. (1997) and Campbell (1997)). In order to adjust the Reverse faulting distribution of the composite model to the one of the target region, relative weights (determined by the procedure given in the ES) are applied to the GM Reverse equations according to the distribution of the target region. Because computations for mixed source events are handled by SP4, the style-of-faulting adjustment in SP2 is restricted to cases of pure Strike-Slip / Normal and pure Reverse faulting.

Tab. A1-1: Range of selected Vs_{30} of the candidate attenuation relationships (Lacave et al. 2003, PEGASOS TP2-TN-0363)

	Lower Vs_{30}	Mean Vs_{30}	Higher Vs_{30}	Representative realistic models
Ambraseys et al. 1996	550	800	1200	Median WAF Italy
Berge-Thierry et al.2000	550	800	1200	Median WAF Italy
Sabetta & Pugliese 1987	700	1000	1300	Median WAF Italy
Ambraseys & Douglas 2000	450	800	1100	Central western US
Lussou et al. 2001	350	500	900	Central western US Median WAF Italy
Abrahamson & Silva 1997	450	600	900	Central western US
Boore et al. 1997	500	620	750	Central western US
Campbell & Bozorgnia 2002	450	600	900	Central western US
Spudich et al. 1997, 1999	550	800	1100	Central western US
Atkinson & Boore 1997		2800		
Somerville et al. 2001		2800		
Toro et al. 1997		2800		
Rietbrock 2002	750	1100	1500	Median WAF Italy

V / H Ratio

- V/H ratios are obtained by using 3 out of the 8 candidate models that predict both horizontal and vertical components.
- Model weights are used according to ES, see Table A1-2 below.

Tab. A1-2: H / V (hard rock) weighting

$M_1 = 5.5$; $M_2 = 6.5$ $R_1 = 15$ km ; $R_2 = 70$ km	$M_w < M_1$			$M_1 < M_w < M_2$			$M_w > M_2$		
	$R < R_1$	$R_1 < R < R_2$	$R > R_2$	$R < R_1$	$R_1 < R < R_2$	$R > R2$	$R < R_1$	$R_1 < R < R_2$	$R > R_2$
Model Name	Weight								
Lussou et al. (2001)	0.35	0.4	0.5	0.25	0.35	0.35	0.25	0.3	0.3
Campbell & Bozorgnia (2002)	0.5	0.45	0.35	0.5	0.35	0.35	0.5	0.35	0.35
Somerville et al. (2001)	0.15	0.15	0.15	0.25	0.3	0.3	0.3	0.35	0.35

- Site class adjustments are not taken into account for both components V and H, because it is only the ratio that is of interest.
- Magnitude conversions are applied for both the horizontal component and the V / H ratio.
- The conversion of components to the geometric mean is based on Roth (2002, PEGASOS TP2-TN-0269) and applied to horizontal components only.
- Missing coefficients in the ground motion models predicting vertical components have been derived according to the procedure described in Roth (2002, PEGASOS TP2-TN-0269).
- Style-of-faulting adjustments are applied to both the V and H components, in the same way as described above for horizontal GM.

Aleatory variability for the horizontal component

- The logic tree computations for the aleatory uncertainties are based on the same set of models and weights as used for horizontal ground motion.
- The effect of propagating the aleatory uncertainty in the magnitude conversion is considered by assigning specific values δ_m to each conversion scheme as given in ES, see Tables A1-3 to A1-5 below.

Tab. A1-3: M_w to M_L conversion weighting

Logic tree branches	Sigma	Weight
PEGASOS report	0.5	W = 0.6
Equivalence of the scale	0.5	W = 0.4

Tab. A1-4: M_w to M_s conversion weighting

Logic tree branches	Sigma	Weight
Ambraseys & Free (1996)	0.283	W = 0.6
Equivalence of the scale	0.283	W = 0.4

Tab. A1-5: M_w to M_{JMA}conversion weighting

Logic tree branches	Sigma	Weight
Fukushima (1996)	0.2	W = 0.6
Equivalence of the scale	0.2	W = 0.4

Equations that correspond to different percentiles from the Abrahamson & Silva (1997) empirical ground motion model are used to define alternatives of the maximum ground motion estimate according to ES, see Table A1-6 below. The upper tail of the ground motion distribution is not truncated.

Tab. A1-6: Upper bounds weighting

Maximum ground motion expressed in terms of number of sigma (horizontal component) of Abrahamson & Silva's empirical model (1997)	Weight	Working hypothesis
4 sigma	0.6	Extreme source models do not exist and extreme ground motions are due to constructive wave interferences and "bad" source-site geometry. These extreme motions have already been captured by our instruments (e.g. Petrolia, see Oglesby & Archuleta 1997).
5 sigma	0.35	Dynamic physical constraints will limit extreme ground motion generated by extreme kinematic models. These extreme ground motions (e.g. max1 of Pitarka's simulations 2002) have not been captured by our instruments.
6 sigma	0.05	Extreme kinematic models for large earthquakes (without extended supershear velocity) or wave focusing on moderate earthquakes do exist. These extreme ground motions (e.g. ext of Pitarka's simulations 2002) have not been captured by our instruments.

Figures A1-1, A1-2 and A1-3 show the logic trees for the horizontal component, the V / H ratio and the aleatory variability, resp., as they have been implemented in the code.

Model Parameterization

The ground motion is parameterized for the final Rock Hazard Computations at the following spectral frequencies: 0.5 Hz, 1 Hz, 2.5 Hz, 5 Hz, 10 Hz, 20 Hz, 33 Hz, 50 Hz and at peak acceleration. The implementation of the logic trees results in (a) a set of alternative estimates of the median horizontal ground motion, aleatory variability of the horizontal ground motion and V/H ratios at each spectral frequency, earthquake magnitude, fault style, and distance and (b) the weight associated to each individual branch of the logic tree.

Ground motions have been modeled for seven magnitudes [5.0 : 0.5 : 8.0] and 14 distances (1.0, 1.6, 2.5, 4.0, 6.3, 10, 16, 25, 40, 63, 85, 100, 160, 250 kilometers).

The ground motion arising from the implementation of the SP2 logic trees has been parameterized using a composite model approach. At each distance, magnitude and spectral frequency and for each fault style, the alternative estimates of the median ground motion are sorted in order of ascending spectral acceleration. The weights associated with the sorted median amplification factors are summed, resulting in a cumulative distribution of the amplification factors. No smoothing of the cumulative distribution has been applied. The values of the ground motion are selected for cumulative distributions corresponding to the following fractiles: 0.13 %, 2.28 %, 16 %, 50 %, 84 %, 97.72 %, and 99.87 %. The seven fractiles correspond to median, $\pm 1\ \sigma$, $\pm 2\ \sigma$, and $\pm 3\ \sigma$ levels. By using the discrete fractiles, no assumption regarding symmetry of the epistemic uncertainty is made.

For the aleatory variability, the same process is repeated but with the sorting performed on the amplitude of the aleatory variability.

A conversion for different distance measures was conducted using the Scherbaum conversion factors. (These conversions may be updated in the final model to incorporate the SP1 depth distributions). Two sets of conversions were done. The first converted the distances to JB distances and the second converted the distances to rupture distance. The main differences between the JB distance and the rupture distance occur for small magnitudes at short distances. However, to avoid potential jumps in the models at bin boundaries, the conversions were applied to all the bins (unlike what had been done for the sensitivity computations, where the conversion was not applied to the smallest magnitude and shortest distance bin ($M < 5.5$, $D < 10$)).

The values of ground motion resulting from this procedure are directly input into the rock hazard software without further parameterization or fitting.

The Maximum Ground Motion estimates are also parameterized in a similar manner. Tables of the maximum ground motion are developed for the same magnitude and distance bins, for each style of faulting and for the seven fractiles.

The following Figures A1-4 to A1-6 show one example (for PGA, the Joyner-Boore distance and strike-slip) of the ground motion for the horizontal component, for the V / H ratio and for the aleatory variability for the horizontal component, respectively. The figures display four subplots. The upper plot shows the median as a distance and magnitude dependent surface. The central plot shows the median ground motion as a distance and fractile dependent surface for magnitude 6.5. The lower left plot shows the median for the 7 magnitudes (magnitude 5.0 to 8.0 in 0.5 magnitude steps) while the lower right subplot shows the 7 fractiles (corresponding to median, $\pm 1\ \sigma$, $\pm 2\ \sigma$, and $\pm 3\ \sigma$) for magnitude 6.5.

The full set of figures (4 to 129) are included in the associated PDF file (EG2-HID-0029_Cotton_figures_rev2.pdf).

Tab. A1-7: Scaling factors derived for the kappa correction – Abrahamson & Silva (1997) model

Abrahamson & Silva				Scale factors	
	M, dist	5.25	7.5	Kappa	
freq	0.012	0.021	0.0415	0.012	0.021
0.5	15.45	15.13	14.52	1.064	1.042
1	73.62	71.82	67.54	1.090	1.063
2.5	349.7	325.6	276.8	1.263	1.176
5	726.1	631.1	460.6	1.576	1.370
10	1171	891.6	489.7	2.391	1.821
20	1456	870.3	318.4	4.573	2.733
33	1366	641	225.3	6.063	2.845
50	1098	468.2	204.8	5.361	2.286
100	572.2	365	200.5	2.854	1.820
	M, dist	5.25	30		
freq	0.012	0.021	0.0415	0.012	0.021
0.5	3.45	3.385	3.253	1.061	1.041
1	16.5	16.03	14.99	1.101	1.069
2.5	67.17	62.54	53.21	1.262	1.175
5	123	107	78.32	1.570	1.366
10	173.9	132.9	73.85	2.355	1.800
20	187.4	114.1	45.17	4.149	2.526
33	158.3	80	33.7	4.697	2.374
50	120.9	61.18	31.45	3.844	1.945
100	74.65	51.74	30.86	2.419	1.677
	M, dist	5.25	120		
freq	0.012	0.021	0.0415	0.012	0.021
0.5	1.089	1.071	1.032	1.055	1.038
1	4.149	4.028	3.768	1.101	1.069
2.5	11.48	10.71	9.138	1.256	1.172
5	15.06	13.16	9.747	1.545	1.350
10	14.46	11.3	6.735	2.147	1.678
20	10.43	7.28	4.202	2.482	1.733
33	7.667	5.608	3.743	2.048	1.498
50	6.595	5.165	3.671	1.797	1.407
100	6.016	4.995	3.643	1.651	1.371
	M, dist	6	7.5		
freq	0.012	0.021	0.0415	0.012	0.021
0.5	88.66	87.81	85.58	1.036	1.026
1	274.4	267	250.4	1.096	1.066
2.5	830.7	773.8	659.2	1.260	1.174
5	1493	1299	951.5	1.569	1.365
10	2242	1710	946.4	2.369	1.807
20	2684	1611	606	4.429	2.658
33	2478	1176	437.6	5.663	2.687
50	1978	863.4	400.9	4.934	2.154
100	1042	679.9	390.6	2.668	1.741
	M, dist	6	30		
freq	0.012	0.021	0.0415	0.012	0.021
0.5	20.61	20.36	19.76	1.043	1.030
1	59.2	57.55	53.93	1.098	1.067
2.5	160.3	149.3	127.4	1.258	1.172
5	262.7	228.9	168.1	1.563	1.362
10	354.7	271.8	152.5	2.326	1.782
20	374.6	229.5	94.22	3.976	2.436
33	314.5	161.6	72.16	4.358	2.239
50	240.5	125.2	67.78	3.548	1.847
100	151	106.9	66.47	2.272	1.608
	M, dist	6	120		
freq	0.012	0.021	0.0415	0.012	0.021
0.5	6.459	6.367	6.16	1.049	1.034
1	14.82	14.41	13.5	1.098	1.067
2.5	28.6	26.7	22.86	1.251	1.168
5	34.59	30.32	22.63	1.529	1.340
10	32.51	25.61	15.72	2.068	1.629
20	23.7	16.99	10.47	2.264	1.623
33	17.89	13.53	9.501	1.883	1.424
50	15.66	12.59	9.346	1.676	1.347
100	14.41	12.22	9.287	1.552	1.316
	M, dist	7	7.5		
freq	0.012	0.021	0.0415	0.012	0.021
0.5	411.2	405.7	393.1	1.046	1.032
1	853.3	829.3	777.4	1.098	1.067
2.5	2029	1891	1613	1.258	1.172
5	3348	2916	2140	1.564	1.363
10	4789	3657	2032	2.357	1.800
20	5570	3351	1281	4.348	2.616
33	5075	2423	934.7	5.430	2.592
50	4024	1782	861.8	4.669	2.068
100	2135	1415	837.2	2.550	1.690
	M, dist	7	30		
freq	0.012	0.021	0.0415	0.012	0.021
0.5	92.47	91.21	88.36	1.047	1.032
1	183	177.9	166.8	1.097	1.067
2.5	403.8	376.5	321.5	1.256	1.171
5	619.8	540.5	398	1.557	1.358
10	807.7	619.6	349.7	2.310	1.772
20	835.9	514	215.7	3.875	2.383
33	695.9	361.2	167.5	4.155	2.156
50	531.2	281.4	158.1	3.360	1.780
100	337.1	242.1	154.8	2.178	1.564
	M, dist	7	120		
freq	0.012	0.021	0.0415	0.012	0.021
0.5	28.14	27.75	26.87	1.047	1.033
1	47	45.71	42.92	1.095	1.065
2.5	78.36	73.22	62.86	1.247	1.165
5	91.45	80.33	60.3	1.517	1.332
10	84.81	67.18	42.1	2.014	1.596
20	62	45.22	29.08	2.132	1.555
33	47.47	36.68	26.67	1.780	1.375
50	41.96	34.34	26.28	1.597	1.307
100	38.84	33.39	26.11	1.488	1.279

Tab. A1-8: Scaling factors derived for the kappa correction – Ambraseys et al. (1996) model

Ambraseys et al.				Scale factors	
	M, dist	5.25	7.5	Kappa	
freq	0.012	0.021	0.0303	0.012	0.021
0.5	12.12	11.96	11.81	1.026	1.013
1	53.04	51.76	50.35	1.053	1.028
2.5	208.7	194.4	180.7	1.155	1.076
5	403.7	351.1	304.3	1.327	1.154
10	626.2	477.4	363	1.725	1.315
20	762.5	457.3	281.6	2.708	1.624
33	710.2	336.5	190.3	3.732	1.768
50	570.4	248.1	156.5	3.645	1.585
100	301.7	195.4	144.7	2.085	1.350
	M, dist	5.25	30		
freq	0.012	0.021	0.0303	0.012	0.021
0.5	2.822	2.781	2.739	1.030	1.015
1	11.94	11.61	11.27	1.059	1.030
2.5	41.21	38.39	35.68	1.155	1.076
5	72.13	62.79	54.49	1.324	1.152
10	101.3	77.47	59.12	1.713	1.310
20	111.3	67.69	42.62	2.611	1.588
33	96.38	48.16	29.24	3.296	1.647
50	74.73	36.68	24.94	2.996	1.471
100	44.48	30.61	23.46	1.896	1.305
	M, dist	5.25	120		
freq	0.012	0.021	0.0303	0.012	0.021
0.5	0.833	0.82	0.807	1.032	1.016
1	2.849	2.767	2.686	1.061	1.030
2.5	7.132	6.651	6.19	1.152	1.074
5	9.615	8.402	7.321	1.313	1.148
10	10.1	7.848	6.111	1.653	1.284
20	8.163	5.424	3.861	2.114	1.405
33	6.061	3.992	3.055	1.984	1.307
50	4.913	3.534	2.869	1.712	1.232
100	4.15	3.337	2.805	1.480	1.190
	M, dist	6	7.5		
freq	0.012	0.021	0.0303	0.012	0.021
0.5	64.12	63.5	62.77	1.022	1.012
1	175.7	170.9	166	1.058	1.030
2.5	471.6	439.4	408.7	1.154	1.075
5	807.7	703.2	610.4	1.323	1.152
10	1177	898.9	685.3	1.717	1.312
20	1385	834.1	518	2.674	1.610
33	1271	608.8	352.1	3.610	1.729
50	1015	451.3	292.8	3.467	1.541
100	542.3	358.9	271	2.001	1.324
	M, dist	6	30		
freq	0.012	0.021	0.0303	0.012	0.021
0.5	14.89	14.72	14.52	1.025	1.014
1	38.27	37.21	36.13	1.059	1.030
2.5	94.04	87.67	81.57	1.153	1.075
5	150.2	130.9	113.8	1.320	1.150
10	202.6	155.3	118.9	1.704	1.306
20	218.4	133.5	85	2.569	1.571
33	187.8	95.2	59.23	3.171	1.607
50	145.6	73.3	51.12	2.848	1.434
100	88.2	61.77	48.2	1.830	1.282
	M, dist	6	120		
freq	0.012	0.021	0.0303	0.012	0.021
0.5	4.277	4.217	4.155	1.029	1.015
1	9.093	8.84	8.585	1.059	1.030
2.5	17.05	15.92	14.83	1.150	1.073
5	21.6	18.91	16.52	1.308	1.145
10	22.27	17.39	13.65	1.632	1.274
20	18	12.18	8.898	2.023	1.369
33	13.55	9.212	7.242	1.871	1.272
50	11.16	8.258	6.847	1.630	1.206
100	9.552	7.835	6.709	1.424	1.168
	M, dist	7	7.5		
freq	0.012	0.021	0.0303	0.012	0.021
0.5	260.9	257.4	253.7	1.028	1.015
1	510.3	496.1	481.8	1.059	1.030
2.5	1117	1041	969.2	1.152	1.074
5	1776	1547	1344	1.321	1.151
10	2478	1895	1447	1.713	1.310
20	2842	1716	1071	2.654	1.602
33	2578	1242	728.5	3.539	1.705
50	2046	922.7	610.5	3.351	1.511
100	1102	740.3	566.6	1.945	1.307
	M, dist	7	30		
freq	0.012	0.021	0.0303	0.012	0.021
0.5	59.05	58.25	57.42	1.028	1.014
1	111.3	108.2	105.1	1.059	1.029
2.5	230	214.5	199.7	1.152	1.074
5	346.4	302.2	262.8	1.318	1.150
10	452.2	347	266.2	1.699	1.304
20	478.3	293.4	188	2.544	1.561
33	407.9	208.6	131.8	3.095	1.583
50	315.4	161.4	114.7	2.750	1.407
100	192.5	137.1	108.3	1.777	1.266
	M, dist	7	120		
freq	0.012	0.021	0.0303	0.012	0.021
0.5	16.6	16.37	16.13	1.029	1.015
1	27.28	26.53	25.78	1.058	1.029
2.5	45.37	42.4	39.55	1.147	1.072
5	55.65	48.81	42.72	1.303	1.143
10	56.53	44.32	34.99	1.616	1.267
20	45.5	31.17	23.16	1.965	1.346
33	34.45	23.92	19.15	1.799	1.249
50	28.63	21.62	18.2	1.573	1.188
100	24.74	20.58	17.85	1.386	1.153

Tab. A1-9: Scaling factors derived for the kappa correction – Ambraseys & Douglas (2000) model

Ambraseys & Douglas				Scale factors	
	M, dist	5.25	7.5	Kappa	
freq	0.012	0.021	0.0303	0.012	0.021
0.5	15.45	15.13	14.83	1.042	1.020
1	73.62	71.82	69.89	1.053	1.028
2.5	349.7	325.6	302.4	1.156	1.077
5	726.1	631.1	546.6	1.328	1.155
10	1171	891.6	676.7	1.730	1.318
20	1456	870.3	532.2	2.736	1.635
33	1366	641	356	3.837	1.801
50	1098	468.2	289.3	3.795	1.618
100	572.2	365	266.6	2.146	1.369
	M, dist	5.25	30		
freq	0.012	0.021	0.0303	0.012	0.021
0.5	3.45	3.385	3.323	1.038	1.019
1	16.5	16.03	15.55	1.061	1.031
2.5	67.17	62.54	58.11	1.156	1.076
5	123	107	92.82	1.325	1.153
10	173.9	132.9	101.3	1.717	1.312
20	187.4	114.1	71.87	2.607	1.588
33	158.3	80	48.97	3.233	1.634
50	120.9	61.18	41.95	2.882	1.458
100	74.65	51.74	39.6	1.885	1.307
	M, dist	5.25	120		
freq	0.012	0.021	0.0303	0.012	0.021
0.5	1.089	1.071	1.053	1.034	1.017
1	4.149	4.028	3.908	1.062	1.031
2.5	11.48	10.71	9.963	1.152	1.075
5	15.06	13.16	11.48	1.312	1.146
10	14.46	11.3	8.859	1.632	1.276
20	10.43	7.28	5.448	1.914	1.336
33	7.667	5.608	4.521	1.696	1.240
50	6.595	5.165	4.337	1.521	1.191
100	6.016	4.995	4.272	1.408	1.169
	M, dist	6	7.5		
freq	0.012	0.021	0.0303	0.012	0.021
0.5	88.66	87.81	86.84	1.021	1.011
1	274.4	267	259.4	1.058	1.029
2.5	830.7	773.8	719.4	1.155	1.076
5	1493	1299	1127	1.325	1.153
10	2242	1710	1302	1.722	1.313
20	2684	1611	993.7	2.701	1.621
33	2478	1176	668.3	3.708	1.760
50	1978	863.4	550	3.596	1.570
100	1042	679.9	507.2	2.054	1.340
	M, dist	6	30		
freq	0.012	0.021	0.0303	0.012	0.021
0.5	20.61	20.36	20.09	1.026	1.013
1	59.2	57.55	55.88	1.059	1.030
2.5	160.3	149.3	138.9	1.154	1.075
5	262.7	228.9	198.8	1.321	1.151
10	354.7	271.8	207.9	1.706	1.307
20	374.6	229.5	146.3	2.560	1.569
33	314.5	161.6	101.6	3.095	1.591
50	240.5	125.2	88.15	2.728	1.420
100	151	106.9	83.43	1.810	1.281
	M, dist	6	120		
freq	0.012	0.021	0.0303	0.012	0.021
0.5	6.459	6.367	6.272	1.030	1.015
1	14.82	14.41	13.99	1.059	1.030
2.5	28.6	26.7	24.88	1.150	1.073
5	34.59	30.32	26.52	1.304	1.143
10	32.51	25.61	20.31	1.601	1.261
20	23.7	16.99	13.12	1.806	1.295
33	17.89	13.53	11.2	1.597	1.208
50	15.66	12.59	10.79	1.451	1.167
100	14.41	12.22	10.66	1.352	1.146
	M, dist	7	7.5		
freq	0.012	0.021	0.0303	0.012	0.021
0.5	411.2	405.7	400	1.028	1.014
1	853.3	829.3	805.3	1.060	1.030
2.5	2029	1891	1759	1.153	1.075
5	3348	2916	2531	1.323	1.152
10	4789	3657	2787	1.718	1.312
20	5570	3351	2078	2.680	1.613
33	5075	2423	1397	3.633	1.734
50	4024	1782	1159	3.472	1.538
100	2135	1415	1071	1.993	1.321
	M, dist	7	30		
freq	0.012	0.021	0.0303	0.012	0.021
0.5	92.47	91.21	89.91	1.028	1.014
1	183	177.9	172.8	1.059	1.030
2.5	403.8	376.5	350.4	1.152	1.074
5	619.8	540.5	469.9	1.319	1.150
10	807.7	619.6	475.1	1.700	1.304
20	835.9	514	330.2	2.531	1.557
33	695.9	361.2	231	3.013	1.564
50	531.2	281.4	202	2.630	1.393
100	337.1	242.1	191.4	1.761	1.265
	M, dist	7	120		
freq	0.012	0.021	0.0303	0.012	0.021
0.5	28.14	27.75	27.35	1.029	1.015
1	47	45.71	44.42	1.058	1.029
2.5	78.36	73.22	68.31	1.147	1.072
5	91.45	80.33	70.42	1.299	1.141
10	84.81	67.18	53.69	1.580	1.251
20	62	45.22	35.62	1.741	1.270
33	47.47	36.68	30.89	1.537	1.187
50	41.96	34.34	29.88	1.404	1.149
100	38.84	33.39	29.51	1.316	1.131

Tab. A1-10: Scaling factors derived for the kappa correction – Atkinson & Boore (1997) model

Atkinson & Boore				Scale factors	
	M, dist	5.25	7.5	Kappa	
freq	0.012	0.021	0.0011	0.012	0.021
0.5	5.547	5.443	5.695	0.974	0.956
1	22.67	22.09	23.28	0.974	0.949
2.5	114.9	106.9	124.9	0.920	0.856
5	246.2	214	292	0.843	0.733
10	376.2	286.9	526.1	0.715	0.545
20	428.3	258.7	821	0.522	0.315
33	377.6	185.1	1069	0.353	0.173
50	295.4	139.5	1266	0.233	0.110
100	171.7	114.8	685.5	0.250	0.167
	M, dist	5.25	30		
freq	0.012	0.021	0.0011	0.012	0.021
0.5	1.658	1.629	1.696	0.978	0.960
1	6.693	6.523	6.868	0.975	0.950
2.5	33.32	31.01	36.27	0.919	0.855
5	69.79	60.68	82.77	0.843	0.733
10	102.7	78.46	143.3	0.717	0.548
20	110.4	67.35	210	0.526	0.321
33	92.63	47.32	255.4	0.363	0.185
50	70.9	36.59	281.6	0.252	0.130
100	45.2	31.34	127.3	0.355	0.246
	M, dist	5.25	120		
freq	0.012	0.021	0.0011	0.012	0.021
0.5	0.666	0.657	0.677	0.984	0.970
1	2.586	2.519	2.661	0.972	0.947
2.5	11.76	10.95	12.82	0.917	0.854
5	22.11	19.26	26.17	0.845	0.736
10	27.58	21.24	38.17	0.723	0.556
20	23.65	15.23	43.08	0.549	0.354
33	17.24	10.75	40.18	0.429	0.268
50	13.58	9.267	34.53	0.393	0.268
100	11.37	8.764	18.75	0.606	0.467
	M, dist	6	7.5		
freq	0.012	0.021	0.0011	0.012	0.021
0.5	24.06	23.77	24.32	0.989	0.977
1	84.23	81.89	86.85	0.970	0.943
2.5	259.9	242.2	283	0.918	0.856
5	432.1	376.4	511.7	0.844	0.736
10	585.7	448.6	816	0.718	0.550
20	630.8	385.6	1201	0.525	0.321
33	545.4	276.1	1523	0.358	0.181
50	425.9	213.1	1776	0.240	0.120
100	256.8	179.2	929.8	0.276	0.193
	M, dist	6	30		
freq	0.012	0.021	0.0011	0.012	0.021
0.5	7.899	7.805	7.985	0.989	0.977
1	27.45	26.69	28.33	0.969	0.942
2.5	83.19	77.52	90.6	0.918	0.856
5	135	117.6	159.7	0.845	0.736
10	176.1	135.2	244.8	0.719	0.552
20	179.5	111	338.6	0.530	0.328
33	148.5	78.58	401.7	0.370	0.196
50	113.9	62.35	437.1	0.261	0.143
100	75.14	54.28	196.1	0.383	0.277
	M, dist	6	120		
freq	0.012	0.021	0.0011	0.012	0.021
0.5	3.223	3.184	3.265	0.987	0.975
1	10.75	10.44	11.12	0.967	0.939
2.5	29.8	27.78	32.44	0.919	0.856
5	43.31	37.83	51.12	0.847	0.740
10	47.94	37.19	65.92	0.727	0.564
20	39.32	26.03	70.3	0.559	0.370
33	28.89	19.04	64.28	0.449	0.296
50	23.33	16.81	54.95	0.425	0.306
100	19.95	15.95	30.97	0.644	0.515
	M, dist	7	7.5		
freq	0.012	0.021	0.0011	0.012	0.021
0.5	110.5	109	112.2	0.985	0.971
1	242.5	235.8	250.8	0.967	0.940
2.5	488.9	456	532.1	0.919	0.857
5	708.8	618.7	837.8	0.846	0.738
10	898.9	691.1	1249	0.720	0.553
20	932.8	576.2	1765	0.528	0.326
33	793.6	413.3	2189	0.363	0.189
50	618.1	325.1	2510	0.246	0.130
100	386	278.9	1260	0.306	0.221
	M, dist	7	30		
freq	0.012	0.021	0.0011	0.012	0.021
0.5	43	42.41	43.68	0.984	0.971
1	93.62	91.01	96.84	0.967	0.940
2.5	185.2	172.8	201.5	0.919	0.858
5	262.2	229	309.6	0.847	0.740
10	320.7	247.1	444.3	0.722	0.556
20	316.2	197.8	592.5	0.534	0.334
33	258.3	141.1	690.6	0.374	0.204
50	199	114.1	742.7	0.268	0.154
100	135.2	100.8	330.6	0.409	0.305
	M, dist	7	120		
freq	0.012	0.021	0.0011	0.012	0.021
0.5	18.03	17.78	18.33	0.984	0.970
1	37.69	36.64	39	0.966	0.939
2.5	68.18	63.66	74.12	0.920	0.859
5	86.52	75.78	101.8	0.850	0.744
10	90.03	70.31	123.1	0.731	0.571
20	72.17	48.92	127	0.568	0.385
33	53.47	36.8	114.7	0.466	0.321
50	43.99	33.08	97.7	0.450	0.339
100	38.3	31.53	56.74	0.675	0.556

Tab. A1-11: Scaling factors derived for the kappa correction – Berge-Thierry et al. (2000) model

Berge-Thierry et al.				Scale factors	
	M, dist	5.25	7.5	Kappa	
freq	0.012	0.021	0.0303	0.012	0.021
0.5	12.22	12.07	11.91	1.026	1.013
1	53.59	52.3	50.89	1.053	1.028
2.5	211.9	197.4	183.4	1.155	1.076
5	411.7	358.1	310.4	1.326	1.154
10	642.6	489.8	372.3	1.726	1.316
20	788.5	472.3	290.3	2.716	1.627
33	738.9	348.6	195.9	3.772	1.779
50	595.5	256.3	160.5	3.710	1.597
100	311.5	200.6	148.1	2.103	1.354
	M, dist	5.25	30		
freq	0.012	0.021	0.0303	0.012	0.021
0.5	2.919	2.875	2.831	1.031	1.016
1	12.46	12.11	11.76	1.060	1.030
2.5	43.78	40.77	37.89	1.155	1.076
5	78.06	67.93	58.93	1.325	1.153
10	112.3	85.77	65.37	1.718	1.312
20	127.1	76.88	48.01	2.647	1.601
33	112.5	55.09	32.62	3.449	1.689
50	88.06	41.38	27.47	3.206	1.506
100	50.15	33.85	25.66	1.954	1.319
	M, dist	5.25	120		
freq	0.012	0.021	0.0303	0.012	0.021
0.5	0.951	0.936	0.92	1.034	1.017
1	3.375	3.277	3.18	1.061	1.031
2.5	9.068	8.453	7.863	1.153	1.075
5	13.14	11.47	9.977	1.317	1.150
10	15.11	11.66	9.003	1.678	1.295
20	13.43	8.574	5.802	2.315	1.478
33	10.25	6.067	4.329	2.368	1.401
50	7.935	5.114	3.963	2.002	1.290
100	6.09	4.686	3.834	1.588	1.222
	M, dist	6	7.5		
freq	0.012	0.021	0.0303	0.012	0.021
0.5	64.62	64	63.26	1.021	1.012
1	177.5	172.7	167.8	1.058	1.029
2.5	478.7	446.1	414.9	1.154	1.075
5	823.8	717.2	622.5	1.323	1.152
10	1208	922.1	702.7	1.719	1.312
20	1432	861.3	533.8	2.683	1.614
33	1322	630.3	362.1	3.651	1.741
50	1059	466.8	300	3.530	1.556
100	559.5	368.2	277.2	2.018	1.328
	M, dist	6	30		
freq	0.012	0.021	0.0303	0.012	0.021
0.5	15.37	15.19	14.99	1.025	1.013
1	39.9	38.8	37.68	1.059	1.030
2.5	99.86	93.08	86.59	1.153	1.075
5	162.5	141.6	123	1.321	1.151
10	224.5	171.8	131.3	1.710	1.308
20	249.8	151.5	95.51	2.615	1.586
33	219.1	108.6	65.8	3.330	1.650
50	171.3	82.36	56.07	3.055	1.469
100	98.91	68.06	52.53	1.883	1.296
	M, dist	6	120		
freq	0.012	0.021	0.0303	0.012	0.021
0.5	4.859	4.791	4.721	1.029	1.015
1	10.75	10.45	10.14	1.060	1.031
2.5	21.64	20.19	18.8	1.151	1.074
5	29.45	25.75	22.44	1.312	1.148
10	33.19	25.71	19.96	1.663	1.288
20	29.36	18.97	13.1	2.241	1.448
33	22.54	13.7	10.04	2.245	1.365
50	17.65	11.71	9.273	1.903	1.263
100	13.77	10.8	8.997	1.531	1.200
	M, dist	7	7.5		
freq	0.012	0.021	0.0303	0.012	0.021
0.5	263	259.4	255.7	1.029	1.014
1	515.7	501.3	486.8	1.059	1.030
2.5	1134	1057	983.8	1.153	1.074
5	1811	1578	1371	1.321	1.151
10	2543	1944	1484	1.714	1.310
20	2939	1772	1104	2.662	1.605
33	2681	1286	748.8	3.580	1.717
50	2135	951.7	625.1	3.415	1.522
100	1136	759	579	1.962	1.311
	M, dist	7	30		
freq	0.012	0.021	0.0303	0.012	0.021
0.5	60.95	60.12	59.27	1.028	1.014
1	116	112.8	109.5	1.059	1.030
2.5	244.1	227.7	211.9	1.152	1.075
5	374.6	326.7	284	1.319	1.150
10	501	383.9	294	1.704	1.306
20	545.6	332.5	210.9	2.587	1.577
33	475.5	237.5	146	3.257	1.627
50	370.5	180.8	125.4	2.955	1.442
100	216	150.7	117.7	1.835	1.280
	M, dist	7	120		
freq	0.012	0.021	0.0303	0.012	0.021
0.5	18.83	18.57	18.3	1.029	1.015
1	32.19	31.3	30.42	1.058	1.029
2.5	57.5	53.69	50.04	1.149	1.073
5	75.76	66.3	57.88	1.309	1.145
10	84.02	65.24	50.84	1.653	1.283
20	73.81	48.06	33.59	2.197	1.431
33	56.68	35.02	26.12	2.170	1.341
50	44.64	30.19	24.27	1.839	1.244
100	35.2	27.97	23.59	1.492	1.186

Tab. A1-12: Scaling factors derived for the kappa correction – Boore et al. (1997) model

Boore et al.				Scale factors	
	M, dist	5.25	7.5	Kappa	
freq	0.012	0.021	0.05	0.012	0.021
0.5	15.21	14.89	14.1	1.079	1.056
1	71.95	70.2	64.28	1.119	1.092
2.5	337.2	314	249.7	1.350	1.258
5	701.3	609.5	391	1.794	1.559
10	1141	868.7	375.6	3.038	2.313
20	1442	859.7	225.6	6.392	3.811
33	1372	638.2	172.3	7.963	3.704
50	1113	463.9	163.4	6.812	2.839
100	565.6	356.5	162.2	3.487	2.198
	M, dist	5.25	30		
freq	0.012	0.021	0.05	0.012	0.021
0.5	3.507	3.439	3.251	1.079	1.058
1	16.68	16.21	14.75	1.131	1.099
2.5	68.66	63.91	50.85	1.350	1.257
5	129.4	112.6	72.39	1.788	1.555
10	191.8	146.3	63.96	2.999	2.287
20	220.7	133	37.39	5.903	3.557
33	196.7	95.12	29.43	6.684	3.232
50	153.8	70.62	28.15	5.464	2.509
100	85.94	57.15	27.83	3.088	2.054
	M, dist	5.25	120		
freq	0.012	0.021	0.05	0.012	0.021
0.5	1.221	1.2	1.137	1.074	1.055
1	4.828	4.687	4.262	1.133	1.100
2.5	14.8	13.79	11	1.345	1.254
5	22.13	19.3	12.53	1.766	1.540
10	25.47	19.64	9.05	2.814	2.170
20	22.28	14.22	5.402	4.124	2.632
33	16.77	9.988	4.711	3.560	2.120
50	12.96	8.434	4.607	2.813	1.831
100	10.09	7.755	4.564	2.211	1.699
	M, dist	6	7.5		
freq	0.012	0.021	0.05	0.012	0.021
0.5	85.98	85.15	82	1.049	1.038
1	262.9	255.8	233.5	1.126	1.096
2.5	794.1	739.6	589.8	1.346	1.254
5	1435	1249	804.9	1.783	1.552
10	2178	1661	726.6	2.998	2.286
20	2650	1586	435.6	6.084	3.641
33	2482	1166	340.1	7.298	3.428
50	1999	851.4	323.8	6.174	2.629
100	1025	660.9	319.5	3.208	2.069
	M, dist	6	30		
freq	0.012	0.021	0.05	0.012	0.021
0.5	20.43	20.18	19.33	1.057	1.044
1	58.67	57.03	52.02	1.128	1.096
2.5	162.4	151.3	120.8	1.344	1.252
5	275.1	239.5	154.8	1.777	1.547
10	389.8	297.9	132	2.953	2.257
20	439.3	265.9	78.63	5.587	3.382
33	388.5	190.3	63.36	6.132	3.003
50	303.5	142.7	60.85	4.988	2.345
100	172.1	116.7	60.08	2.865	1.942
	M, dist	6	120		
freq	0.012	0.021	0.05	0.012	0.021
0.5	7.016	6.917	6.601	1.063	1.048
1	16.85	16.38	14.94	1.128	1.096
2.5	36.48	34.03	27.26	1.338	1.248
5	50.43	44.07	28.84	1.749	1.528
10	56.65	43.85	20.75	2.730	2.113
20	49.31	31.9	13.09	3.767	2.437
33	37.39	22.91	11.63	3.215	1.970
50	29.29	19.65	11.41	2.567	1.722
100	23.18	18.19	11.32	2.048	1.607
	M, dist	7	7.5		
freq	0.012	0.021	0.05	0.012	0.021
0.5	390	384.8	367.9	1.060	1.046
1	807.9	785.3	716.6	1.127	1.096
2.5	1929	1798	1436	1.343	1.252
5	3207	2792	1805	1.777	1.547
10	4651	3542	1561	2.980	2.269
20	5487	3293	928.9	5.907	3.545
33	5073	2398	734.4	6.908	3.265
50	4059	1752	701.5	5.786	2.498
100	2095	1371	689.5	3.038	1.988
	M, dist	7	30		
freq	0.012	0.021	0.05	0.012	0.021
0.5	89.71	88.49	84.59	1.061	1.046
1	179.4	174.4	159.2	1.127	1.095
2.5	407	379.4	303.4	1.341	1.250
5	646.3	563.1	365.2	1.770	1.542
10	884.1	676.6	302.2	2.926	2.239
20	976.7	592.8	180.7	5.405	3.281
33	856.1	422.3	147.6	5.800	2.861
50	666.3	318	142.1	4.689	2.238
100	381.1	262.1	140	2.722	1.872
	M, dist	7	120		
freq	0.012	0.021	0.05	0.012	0.021
0.5	29.89	29.48	28.17	1.061	1.047
1	52.82	51.36	46.94	1.125	1.094
2.5	99.22	92.62	74.4	1.334	1.245
5	132.4	115.8	76.19	1.738	1.520
10	146.3	113.5	54.68	2.676	2.076
20	126.5	82.47	35.48	3.565	2.324
33	96.02	59.86	31.9	3.010	1.876
50	75.7	51.78	31.33	2.416	1.653
100	60.54	48.15	31.08	1.948	1.549

Tab. A1-13: Scaling factors derived for the kappa correction – Campbell & Bozorgnia (2002) model

Campbell & Bozorgnia				Scale factors	
	M, dist	5.25	7.5	Kappa	
freq	0.012	0.021	0.04	0.012	0.021
0.5	14.92	14.64	14.12	1.057	1.037
1	70.16	68.43	64.63	1.086	1.059
2.5	321.4	299.3	257.5	1.248	1.162
5	656.5	570.6	426.3	1.540	1.338
10	1043	794.5	456.1	2.287	1.742
20	1273	762.4	299.9	4.245	2.542
33	1173	556.2	211	5.559	2.636
50	931.1	408.3	190.6	4.885	2.142
100	499.7	323.3	186	2.687	1.738
	M, dist	5.25	30		
freq	0.012	0.021	0.04	0.012	0.021
0.5	3.413	3.353	3.237	1.054	1.036
1	15.9	15.45	14.52	1.095	1.064
2.5	62	57.74	49.72	1.247	1.161
5	110.2	95.9	71.86	1.534	1.335
10	149.4	114.4	66.62	2.243	1.717
20	151.2	93.12	40.56	3.728	2.296
33	121	64.27	30.64	3.949	2.098
50	90.83	50.68	28.72	3.163	1.765
100	61.9	44.49	28.22	2.193	1.577
	M, dist	5.25	120		
freq	0.012	0.021	0.04	0.012	0.021
0.5	1.067	1.05	1.015	1.051	1.034
1	3.92	3.807	3.58	1.095	1.063
2.5	10.06	9.387	8.111	1.240	1.157
5	12.1	10.6	8.054	1.502	1.316
10	10.18	8.069	5.176	1.967	1.559
20	6.596	5.022	3.401	1.939	1.477
33	5.162	4.206	3.145	1.641	1.337
50	4.769	4.035	3.107	1.535	1.299
100	4.608	3.975	3.092	1.490	1.286
	M, dist	6	7.5		
freq	0.012	0.021	0.04	0.012	0.021
0.5	84.05	83.23	81.24	1.035	1.024
1	253.6	246.7	232.4	1.091	1.062
2.5	753.4	701.9	605	1.245	1.160
5	1341	1167	874	1.534	1.335
10	1988	1517	876.6	2.268	1.731
20	2337	1406	567	4.122	2.480
33	2122	1017	406.3	5.223	2.503
50	1673	751.1	370.1	4.520	2.029
100	907.4	600.2	359.6	2.523	1.669
	M, dist	6	30		
freq	0.012	0.021	0.04	0.012	0.021
0.5	19.82	19.58	19.03	1.042	1.029
1	55.41	53.86	50.71	1.093	1.062
2.5	146.2	136.3	117.6	1.243	1.159
5	233.9	203.9	153.3	1.526	1.330
10	303.4	233	136.9	2.216	1.702
20	301.2	186.9	84.29	3.573	2.217
33	239.9	130.2	65.28	3.675	1.994
50	180.9	103.8	61.56	2.939	1.686
100	125.2	91.82	60.43	2.072	1.519
	M, dist	6	120		
freq	0.012	0.021	0.04	0.012	0.021
0.5	6.123	6.035	5.853	1.046	1.031
1	13.61	13.23	12.47	1.091	1.061
2.5	24.83	23.19	20.1	1.235	1.154
5	27.73	24.37	18.68	1.484	1.305
10	23.03	18.45	12.24	1.882	1.507
20	15.36	12.05	8.598	1.786	1.401
33	12.41	10.36	8.052	1.541	1.287
50	11.57	9.989	7.971	1.452	1.253
100	11.22	9.86	7.939	1.413	1.242
	M, dist	7	7.5		
freq	0.012	0.021	0.04	0.012	0.021
0.5	376.7	371.6	360.9	1.044	1.030
1	774.4	752.7	708.9	1.092	1.062
2.5	1826	1701	1468	1.244	1.159
5	2990	2604	1955	1.529	1.332
10	4230	3239	1875	2.256	1.727
20	4837	2917	1193	4.054	2.445
33	4335	2092	862.8	5.024	2.425
50	3398	1547	791.1	4.295	1.956
100	1856	1247	766.9	2.420	1.626
	M, dist	7	30		
freq	0.012	0.021	0.04	0.012	0.021
0.5	86.03	84.86	82.38	1.044	1.030
1	168.5	163.8	154.3	1.092	1.062
2.5	365.6	340.9	294.6	1.241	1.157
5	548.6	478.6	360.7	1.521	1.327
10	687.7	528.7	312.5	2.201	1.692
20	669.4	417.1	192.2	3.483	2.170
33	529.3	289.9	150.8	3.510	1.922
50	398.9	233.2	142.9	2.791	1.632
100	279.1	207.5	140	1.994	1.482
	M, dist	7	120		
freq	0.012	0.021	0.04	0.012	0.021
0.5	25.87	25.51	24.77	1.044	1.030
1	42.57	41.4	39.06	1.090	1.060
2.5	67.61	63.21	54.92	1.231	1.151
5	73.03	64.32	49.62	1.472	1.296
10	60.08	48.51	32.94	1.824	1.473
20	40.68	32.5	24.01	1.694	1.354
33	33.41	28.36	22.64	1.476	1.253
50	31.36	27.44	22.43	1.398	1.223
100	30.46	27.09	22.33	1.364	1.213

Tab. A1-14: Scaling factors derived for the kappa correction – Lussou et al. (2001) model

Lussou et al.				Scale factors	
	M, dist	5.25	7.5	Kappa	
freq	0.012	0.021	0.0507	0.012	0.021
0.5	5.4	5.211	4.784	1.129	1.089
1	24.2	23.39	21.08	1.148	1.110
2.5	151.6	140.9	110.9	1.367	1.271
5	371.2	322	203.2	1.827	1.585
10	643.2	488.3	203.9	3.154	2.395
20	830.8	492.3	117.7	7.059	4.183
33	797.3	364	86.31	9.238	4.217
50	647.2	258.8	81.26	7.965	3.185
100	315.9	192.9	80.19	3.939	2.406
	M, dist	5.25	30		
freq	0.012	0.021	0.0507	0.012	0.021
0.5	1.234	1.198	1.109	1.113	1.080
1	5.527	5.341	4.806	1.150	1.111
2.5	31.41	29.18	22.98	1.367	1.270
5	71.66	62.19	39.29	1.824	1.583
10	116.5	88.53	37.16	3.135	2.382
20	141.6	84.3	20.9	6.775	4.033
33	130.2	60.59	15.6	8.346	3.884
50	102.9	43.42	14.77	6.967	2.940
100	53	33.47	14.52	3.650	2.305
	M, dist	5.25	120		
freq	0.012	0.021	0.0507	0.012	0.021
0.5	0.254	0.248	0.233	1.090	1.064
1	0.989	0.957	0.864	1.145	1.108
2.5	4.498	4.183	3.301	1.363	1.267
5	8.687	7.552	4.795	1.812	1.575
10	11.86	9.062	3.892	3.047	2.328
20	11.92	7.277	2.121	5.620	3.431
33	9.56	4.925	1.709	5.594	2.882
50	7.144	3.785	1.648	4.335	2.297
100	4.636	3.258	1.622	2.858	2.009
	M, dist	6	7.5		
freq	0.012	0.021	0.0507	0.012	0.021
0.5	21.92	21.53	20.41	1.074	1.055
1	84.74	82.24	74.58	1.136	1.103
2.5	332	308.9	244.3	1.359	1.264
5	640.5	556.6	353.5	1.812	1.575
10	995.8	757.9	321.5	3.097	2.357
20	1225	730.4	186.7	6.561	3.912
33	1155	535.5	142.6	8.100	3.755
50	931.2	385.3	135.3	6.882	2.848
100	465.1	293.6	133.1	3.494	2.206
	M, dist	6	30		
freq	0.012	0.021	0.0507	0.012	0.021
0.5	5.724	5.623	5.329	1.074	1.055
1	21.2	20.57	18.65	1.137	1.103
2.5	78.33	72.9	57.68	1.358	1.264
5	145	126	80.14	1.809	1.572
10	216	164.6	70.26	3.074	2.343
20	253.9	152.2	40.43	6.280	3.765
33	231.1	109.4	31.47	7.344	3.476
50	182.5	79.71	30.02	6.079	2.655
100	96.43	62.75	29.54	3.264	2.124
	M, dist	6	120		
freq	0.012	0.021	0.0507	0.012	0.021
0.5	1.181	1.161	1.102	1.072	1.054
1	3.831	3.718	3.373	1.136	1.102
2.5	11.86	11.04	8.755	1.355	1.261
5	19.1	16.64	10.64	1.795	1.564
10	24.39	18.7	8.221	2.967	2.275
20	24.04	14.84	4.74	5.072	3.131
33	19.29	10.24	3.97	4.859	2.579
50	14.57	8.071	3.852	3.782	2.095
100	9.753	7.058	3.801	2.566	1.857
	M, dist	7	7.5		
freq	0.012	0.021	0.0507	0.012	0.021
0.5	93.63	92.25	87.89	1.065	1.050
1	231.2	224.5	204.1	1.133	1.100
2.5	600.1	558.9	443.4	1.353	1.260
5	1018	885.7	565.3	1.801	1.567
10	1489	1135	487.6	3.054	2.328
20	1772	1061	284.7	6.224	3.727
33	1644	771.1	223.4	7.359	3.452
50	1316	559	213.3	6.170	2.621
100	669.8	433.5	209.4	3.199	2.070
	M, dist	7	30		
freq	0.012	0.021	0.0507	0.012	0.021
0.5	29.54	29.11	27.73	1.065	1.050
1	71.44	69.4	63.1	1.132	1.100
2.5	180.1	167.8	133.2	1.352	1.260
5	297.9	259.3	165.8	1.797	1.564
10	422.7	322.7	139.5	3.030	2.313
20	484.8	291.7	81.45	5.952	3.581
33	436.6	209.1	65.04	6.713	3.215
50	343.6	153.8	62.37	5.509	2.466
100	184.7	122.8	61.32	3.012	2.003
	M, dist	7	120		
freq	0.012	0.021	0.0507	0.012	0.021
0.5	6.144	6.054	5.77	1.065	1.049
1	13.65	13.26	12.07	1.131	1.099
2.5	30.4	28.34	22.55	1.348	1.257
5	44.95	39.21	25.24	1.781	1.553
10	55.61	42.74	19.15	2.904	2.232
20	54.16	33.68	11.48	4.718	2.934
33	43.39	23.49	9.839	4.410	2.387
50	32.96	18.8	9.581	3.440	1.962
100	22.49	16.61	9.464	2.376	1.755

Tab. A1-15: Scaling factors derived for the kappa correction – Sabetta & Pugliese (1996) model

Sabetta & Pugliese				Scale factors	
	M, dist	5.25	7.5	Kappa	
freq	0.012	0.021	0.0298	0.012	0.021
0.5	8.088	7.886	7.72	1.048	1.022
1	35.03	34	33.04	1.060	1.029
2.5	187.3	174.2	162.3	1.154	1.073
5	423.6	367.8	320.8	1.320	1.147
10	687.2	522.9	402.2	1.709	1.300
20	819.2	490.2	307.5	2.664	1.594
33	741.5	351.6	202.3	3.665	1.738
50	583.4	256.9	164	3.557	1.566
100	315.7	203.6	150.9	2.092	1.349
	M, dist	5.25	30		
freq	0.012	0.021	0.0298	0.012	0.021
0.5	2.532	2.48	2.434	1.040	1.019
1	10.68	10.36	10.06	1.062	1.030
2.5	49.92	46.44	43.29	1.153	1.073
5	101.2	87.94	76.77	1.318	1.145
10	146	111.4	86.03	1.697	1.295
20	152.9	93.04	59.81	2.556	1.556
33	126	64	40	3.150	1.600
50	95.18	48.92	34.07	2.794	1.436
100	60.12	41.65	32.07	1.875	1.299
	M, dist	5.25	120		
freq	0.012	0.021	0.0298	0.012	0.021
0.5	0.772	0.76	0.748	1.032	1.016
1	2.588	2.512	2.441	1.060	1.029
2.5	8.315	7.747	7.232	1.150	1.071
5	12.13	10.59	9.284	1.307	1.141
10	11.93	9.278	7.323	1.629	1.267
20	8.372	5.771	4.312	1.942	1.338
33	6.021	4.35	3.502	1.719	1.242
50	5.149	3.994	3.347	1.538	1.193
100	4.701	3.859	3.29	1.429	1.173
	M, dist	6	7.5		
freq	0.012	0.021	0.0298	0.012	0.021
0.5	35.27	34.77	34.28	1.029	1.014
1	127.9	124.3	120.8	1.059	1.029
2.5	423	393.9	367.6	1.151	1.072
5	750.9	653.4	571	1.315	1.144
10	1090	831.9	642.8	1.696	1.294
20	1234	744.9	474.8	2.599	1.569
33	1095	533.8	319.7	3.425	1.670
50	857.8	397.2	266.2	3.222	1.492
100	480.8	322.5	246.8	1.948	1.307
	M, dist	6	30		
freq	0.012	0.021	0.0298	0.012	0.021
0.5	12.18	12	11.83	1.030	1.014
1	41.52	40.34	39.2	1.059	1.029
2.5	125.1	116.5	108.8	1.150	1.071
5	205.1	178.6	156.3	1.312	1.143
10	271.1	207.8	161.3	1.681	1.288
20	274.9	169.2	111	2.477	1.524
33	225	118.1	77.18	2.915	1.530
50	171.3	92.7	67.24	2.548	1.379
100	112	80.36	63.74	1.757	1.261
	M, dist	6	120		
freq	0.012	0.021	0.0298	0.012	0.021
0.5	3.685	3.631	3.578	1.030	1.015
1	10.17	9.877	9.603	1.059	1.029
2.5	22.13	20.65	19.31	1.146	1.069
5	26.97	23.62	20.78	1.298	1.137
10	24.98	19.65	15.74	1.587	1.248
20	17.73	12.74	9.949	1.782	1.281
33	13.35	10.14	8.465	1.577	1.198
50	11.75	9.465	8.162	1.440	1.160
100	10.87	9.203	8.054	1.350	1.143
	M, dist	7	7.5		
freq	0.012	0.021	0.0298	0.012	0.021
0.5	161	158.8	156.6	1.028	1.014
1	369.4	359	349.1	1.058	1.028
2.5	804.2	749.8	700.4	1.148	1.071
5	1249	1088	952.8	1.311	1.142
10	1695	1298	1007	1.683	1.289
20	1844	1122	725.7	2.541	1.546
33	1604	798.6	497.7	3.223	1.605
50	1248	606	423.4	2.948	1.431
100	725.7	503.5	395.7	1.834	1.272
	M, dist	7	30		
freq	0.012	0.021	0.0298	0.012	0.021
0.5	63.72	62.82	61.95	1.029	1.014
1	140.8	136.9	133.1	1.058	1.029
2.5	288.4	269	251.4	1.147	1.070
5	421.7	368	322.6	1.307	1.141
10	529.5	407.2	317.5	1.668	1.283
20	523.3	325.4	217.2	2.409	1.498
33	424.7	228.9	155	2.740	1.477
50	324.4	183.1	137.3	2.363	1.334
100	218.3	161.1	130.8	1.669	1.232
	M, dist	7	120		
freq	0.012	0.021	0.0298	0.012	0.021
0.5	19.43	19.16	18.89	1.029	1.014
1	36.58	35.57	34.61	1.057	1.028
2.5	57.29	53.55	50.14	1.143	1.068
5	64.17	56.41	49.84	1.288	1.132
10	58.02	46.15	37.49	1.548	1.231
20	41.76	31.05	25.12	1.662	1.236
33	32.49	25.66	22.02	1.475	1.165
50	29.15	24.21	21.36	1.365	1.133
100	27.25	23.62	21.11	1.291	1.119

Tab. A1-16: Scaling factors derived for the kappa correction – Somerville et al. (2001) and Toro et al. (1997) models

Somerville et al., Toro et al.				Scale factors	
	M, dist	5.25	7.5	Kappa	
freq	0.012	0.021	0.0077	0.012	0.021
0.5	5.547	5.443	5.603	0.990	0.971
1	22.67	22.09	22.94	0.988	0.963
2.5	114.9	106.9	118.9	0.966	0.899
5	246.2	214	263.3	0.935	0.813
10	376.2	286.9	429	0.877	0.669
20	428.3	258.7	551.1	0.777	0.469
33	377.6	185.1	559.6	0.675	0.331
50	295.4	139.5	497	0.594	0.281
100	171.7	114.8	229.5	0.748	0.500
	M, dist	5.25	30		
freq	0.012	0.021	0.0077	0.012	0.021
0.5	1.658	1.629	1.673	0.991	0.974
1	6.693	6.523	6.771	0.988	0.963
2.5	33.32	31.01	34.48	0.966	0.899
5	69.79	60.68	74.64	0.935	0.813
10	102.7	78.46	117	0.878	0.671
20	110.4	67.35	141.6	0.780	0.476
33	92.63	47.32	135.5	0.684	0.349
50	70.9	36.59	114.5	0.619	0.320
100	45.2	31.34	58.21	0.776	0.538
	M, dist	5.25	120		
freq	0.012	0.021	0.0077	0.012	0.021
0.5	0.388	0.383	0.391	0.992	0.980
1	1.507	1.468	1.525	0.988	0.963
2.5	6.851	6.38	7.089	0.966	0.900
5	12.88	11.22	13.77	0.935	0.815
10	16.07	12.38	18.25	0.881	0.678
20	13.78	8.873	17.33	0.795	0.512
33	10.05	6.262	13.56	0.741	0.462
50	7.915	5.4	10.51	0.753	0.514
100	6.627	5.107	7.765	0.853	0.658
	M, dist	6	7.5		
freq	0.012	0.021	0.0077	0.012	0.021
0.5	24.06	23.77	24.18	0.995	0.983
1	84.23	81.89	85.33	0.987	0.960
2.5	259.9	242.2	268.8	0.967	0.901
5	432.1	376.4	461.8	0.936	0.815
10	585.7	448.6	666.7	0.879	0.673
20	630.8	385.6	808.9	0.780	0.477
33	545.4	276.1	802.2	0.680	0.344
50	425.9	213.1	704.4	0.605	0.303
100	256.8	179.2	334.7	0.767	0.535
	M, dist	6	30		
freq	0.012	0.021	0.0077	0.012	0.021
0.5	7.899	7.805	7.94	0.995	0.983
1	27.45	26.69	27.82	0.987	0.959
2.5	83.19	77.52	86.04	0.967	0.901
5	135	117.6	144.2	0.936	0.816
10	176.1	135.2	200.3	0.879	0.675
20	179.5	111	229.2	0.783	0.484
33	148.5	78.58	214.8	0.691	0.366
50	113.9	62.35	180.3	0.632	0.346
100	75.14	54.28	94.53	0.795	0.574
	M, dist	6	120		
freq	0.012	0.021	0.0077	0.012	0.021
0.5	1.877	1.854	1.887	0.995	0.983
1	6.258	6.082	6.343	0.987	0.959
2.5	17.35	16.18	17.94	0.967	0.902
5	25.22	22.03	26.92	0.937	0.818
10	27.92	21.65	31.61	0.883	0.685
20	22.9	15.16	28.54	0.802	0.531
33	16.82	11.09	22.19	0.758	0.500
50	13.59	9.794	17.46	0.778	0.561
100	11.61	9.291	13.33	0.871	0.697
	M, dist	7	7.5		
freq	0.012	0.021	0.0077	0.012	0.021
0.5	110.5	109	111.2	0.994	0.980
1	242.5	235.8	245.8	0.987	0.959
2.5	488.9	456	505.4	0.967	0.902
5	708.8	618.7	756.9	0.936	0.817
10	898.9	691.1	1022	0.880	0.676
20	932.8	576.2	1193	0.782	0.483
33	793.6	413.3	1159	0.685	0.357
50	618.1	325.1	1006	0.614	0.323
100	386	278.9	492.3	0.784	0.567
	M, dist	7	30		
freq	0.012	0.021	0.0077	0.012	0.021
0.5	43	42.41	43.28	0.994	0.980
1	93.62	91.01	94.89	0.987	0.959
2.5	185.2	172.8	191.4	0.968	0.903
5	262.2	229	279.9	0.937	0.818
10	320.7	247.1	364.2	0.881	0.678
20	316.2	197.8	402.5	0.786	0.491
33	258.3	141.1	371.4	0.695	0.380
50	199	114.1	309.8	0.642	0.368
100	135.2	100.8	166.9	0.810	0.604
	M, dist	7	120		
freq	0.012	0.021	0.0077	0.012	0.021
0.5	10.48	10.33	10.55	0.993	0.979
1	21.91	21.3	22.21	0.986	0.959
2.5	39.63	37.01	40.96	0.968	0.904
5	50.3	44.05	53.62	0.938	0.822
10	52.34	40.87	59.12	0.885	0.691
20	41.95	28.44	51.89	0.808	0.548
33	31.08	21.4	40.26	0.772	0.532
50	25.57	19.23	32.06	0.798	0.600
100	22.26	18.33	25.15	0.885	0.729

Tab. A1-17: Scaling factors derived for the kappa correction – Spudich et al. (1999)

Spudich et al.				Scale factors	
	M, dist	5.25	7.5	Kappa	
freq	0.012	0.021	0.0303	0.012	0.021
0.5	13.72	13.49	13.27	1.034	1.017
1	63.61	62.1	60.45	1.052	1.027
2.5	276.3	257.3	239.1	1.156	1.076
5	553.2	481	416.8	1.327	1.154
10	874.4	666.2	506.1	1.728	1.316
20	1078	645.5	396.2	2.721	1.629
33	1011	476.5	267	3.787	1.785
50	814.8	350.1	218.3	3.732	1.604
100	426.8	274.1	201.6	2.117	1.360
	M, dist	5.25	30		
freq	0.012	0.021	0.0303	0.012	0.021
0.5	3.187	3.133	3.08	1.035	1.017
1	14.74	14.32	13.9	1.060	1.030
2.5	56.26	52.38	48.68	1.156	1.076
5	102.2	88.91	77.11	1.325	1.153
10	147.2	112.4	85.65	1.719	1.312
20	165.5	100.2	62.57	2.645	1.601
33	145.5	71.52	42.47	3.426	1.684
50	113.5	53.81	35.83	3.168	1.502
100	65.39	44.24	33.52	1.951	1.320
	M, dist	5.25	120		
freq	0.012	0.021	0.0303	0.012	0.021
0.5	1.116	1.098	1.08	1.033	1.017
1	4.268	4.144	4.02	1.062	1.031
2.5	12.15	11.32	10.53	1.154	1.075
5	17.51	15.28	13.3	1.317	1.149
10	19.62	15.16	11.72	1.674	1.294
20	16.85	10.86	7.44	2.265	1.460
33	12.66	7.731	5.628	2.249	1.374
50	9.902	6.616	5.194	1.906	1.274
100	7.866	6.126	5.042	1.560	1.215
	M, dist	6	7.5		
freq	0.012	0.021	0.0303	0.012	0.021
0.5	78.15	77.46	76.62	1.020	1.011
1	230.5	224.3	217.9	1.058	1.029
2.5	648.4	604.2	561.8	1.154	1.075
5	1130	983.9	853.9	1.323	1.152
10	1667	1273	969.6	1.719	1.313
20	1980	1191	737.9	2.683	1.614
33	1828	871.8	500.7	3.651	1.741
50	1464	644.6	414.8	3.529	1.554
100	775.6	510.1	383.4	2.023	1.330
	M, dist	6	30		
freq	0.012	0.021	0.0303	0.012	0.021
0.5	18.55	18.34	18.1	1.025	1.013
1	51.41	49.99	48.55	1.059	1.030
2.5	132.7	123.7	115.1	1.153	1.075
5	216.9	189	164.1	1.322	1.152
10	298.7	228.7	174.8	1.709	1.308
20	329.2	200.3	126.6	2.600	1.582
33	287.4	143.3	87.41	3.288	1.639
50	224	109.2	74.71	2.998	1.462
100	131.2	90.72	70.14	1.871	1.293
	M, dist	6	120		
freq	0.012	0.021	0.0303	0.012	0.021
0.5	6.371	6.281	6.188	1.030	1.015
1	14.78	14.37	13.95	1.059	1.030
2.5	29.87	27.87	25.96	1.151	1.074
5	39.89	34.88	30.42	1.311	1.147
10	43.65	33.89	26.38	1.655	1.285
20	37.35	24.46	17.17	2.175	1.425
33	28.33	17.87	13.41	2.113	1.333
50	22.51	15.53	12.49	1.802	1.243
100	18.19	14.48	12.16	1.496	1.191
	M, dist	7	7.5		
freq	0.012	0.021	0.0303	0.012	0.021
0.5	350.8	346.2	341.3	1.028	1.014
1	704.5	684.9	665.2	1.059	1.030
2.5	1572	1465	1364	1.152	1.074
5	2522	2197	1909	1.321	1.151
10	3548	2712	2070	1.714	1.310
20	4098	2472	1540	2.661	1.605
33	3736	1794	1046	3.572	1.715
50	2973	1329	873.7	3.403	1.521
100	1587	1061	809.5	1.960	1.311
	M, dist	7	30		
freq	0.012	0.021	0.0303	0.012	0.021
0.5	80.7	79.61	78.48	1.028	1.014
1	156.5	152.2	147.8	1.059	1.030
2.5	331.9	309.5	288.1	1.152	1.074
5	508.7	443.6	385.8	1.319	1.150
10	676.8	518.8	397.5	1.703	1.305
20	730.9	446.4	284	2.574	1.572
33	632.7	318.4	197.3	3.207	1.614
50	491.7	243.7	170.1	2.891	1.433
100	291	204.2	160.1	1.818	1.275
	M, dist	7	120		
freq	0.012	0.021	0.0303	0.012	0.021
0.5	26.9	26.53	26.15	1.029	1.015
1	46.15	44.88	43.6	1.058	1.029
2.5	81.14	75.78	70.65	1.148	1.073
5	104.6	91.58	80.01	1.307	1.145
10	112.6	87.69	68.59	1.642	1.278
20	95.81	63.37	45.19	2.120	1.402
33	72.89	46.9	35.92	2.029	1.306
50	58.36	41.15	33.63	1.735	1.224
100	47.71	38.53	32.8	1.455	1.175

Tab. A1-18: Scaling factors derived for the kappa correction – Stochastic models (2001)

Stochastic models				Scale factors	
	M, dist	5.25	7.5	Kappa	
freq	0.012	0.021	0.0214	0.012	0.021
0.5	7.159	7.16	7.159	1.000	1.000
1	25.06	24.55	24.52	1.022	1.001
2.5	80.08	74.67	74.44	1.076	1.003
5	141	122.9	122.1	1.155	1.007
10	197.2	151.4	149.7	1.317	1.011
20	208.1	129.1	126.6	1.644	1.020
33	171.2	92.54	90.5	1.892	1.023
50	130.7	74.39	73.09	1.788	1.018
100	91.01	66.13	65.36	1.392	1.012
	M, dist	5.25	30		
freq	0.012	0.021	0.0214	0.012	0.021
0.5	1.487	1.471	1.47	1.012	1.001
1	5.48	5.328	5.322	1.030	1.001
2.5	15.26	14.23	14.18	1.076	1.004
5	22.98	20.07	19.95	1.152	1.006
10	26.11	20.25	20.02	1.304	1.011
20	20.72	13.86	13.63	1.520	1.017
33	14.53	10.05	9.924	1.464	1.013
50	11.9	9.021	8.932	1.332	1.010
100	10.79	8.722	8.649	1.248	1.008
	M, dist	5.25	120		
freq	0.012	0.021	0.0214	0.012	0.021
0.5	0.386	0.38	0.38	1.016	1.000
1	1.182	1.148	1.147	1.031	1.001
2.5	2.326	2.172	2.165	1.074	1.003
5	2.388	2.102	2.091	1.142	1.005
10	1.601	1.326	1.316	1.217	1.008
20	1.028	0.9	0.896	1.147	1.004
33	0.949	0.853	0.85	1.116	1.004
50	0.938	0.846	0.843	1.113	1.004
100	0.933	0.844	0.84	1.111	1.005
	M, dist	6	7.5		
freq	0.012	0.021	0.0214	0.012	0.021
0.5	32.86	32.72	32.71	1.005	1.000
1	81.12	79.01	78.92	1.028	1.001
2.5	190.7	178	177.4	1.075	1.003
5	299.1	261.1	259.6	1.152	1.006
10	391.1	301.3	297.9	1.313	1.011
20	397.4	248.9	244.1	1.628	1.020
33	322.5	178.4	174.7	1.846	1.021
50	246.3	145.1	142.8	1.725	1.016
100	173.8	129.4	128.1	1.357	1.010
	M, dist	6	30		
freq	0.012	0.021	0.0214	0.012	0.021
0.5	7.326	7.241	7.237	1.012	1.001
1	17.18	16.71	16.68	1.030	1.002
2.5	36	33.61	33.51	1.074	1.003
5	50.21	43.94	43.68	1.149	1.006
10	55.18	42.99	42.53	1.297	1.011
20	43.39	29.5	29.06	1.493	1.015
33	30.8	21.9	21.64	1.423	1.012
50	25.58	19.83	19.65	1.302	1.009
100	23.31	19.19	19.04	1.224	1.008
	M, dist	6	120		
freq	0.012	0.021	0.0214	0.012	0.021
0.5	1.846	1.82	1.819	1.015	1.001
1	3.656	3.555	3.551	1.030	1.001
2.5	5.665	5.298	5.283	1.072	1.003
5	5.572	4.926	4.9	1.137	1.005
10	3.793	3.192	3.169	1.197	1.007
20	2.574	2.292	2.281	1.128	1.005
33	2.4	2.188	2.18	1.101	1.004
50	2.376	2.173	2.165	1.097	1.004
100	2.366	2.168	2.16	1.095	1.004
	M, dist	7	7.5		
freq	0.012	0.021	0.0214	0.012	0.021
0.5	136.9	135.2	135.1	1.013	1.001
1	256.4	249.4	249.1	1.029	1.001
2.5	488.7	456.3	454.9	1.074	1.003
5	699.3	611.3	607.7	1.151	1.006
10	864.5	667.5	660	1.310	1.011
20	849.5	535.4	525.3	1.617	1.019
33	680.6	382.6	375	1.815	1.020
50	518.6	313.5	309.5	1.676	1.013
100	371.2	281.1	278.4	1.333	1.010
	M, dist	7	30		
freq	0.012	0.021	0.0214	0.012	0.021
0.5	29.48	29.09	29.07	1.014	1.001
1	53.14	51.68	51.62	1.029	1.001
2.5	94.6	88.38	88.12	1.074	1.003
5	124	108.7	108.1	1.147	1.006
10	131.6	102.9	101.8	1.293	1.011
20	101.9	70.06	69.04	1.476	1.015
33	72.56	52.61	52.03	1.395	1.011
50	60.76	48	47.6	1.276	1.008
100	55.62	46.41	46.09	1.207	1.007
	M, dist	7	120		
freq	0.012	0.021	0.0214	0.012	0.021
0.5	7.114	7.016	7.011	1.015	1.001
1	11.39	11.08	11.07	1.029	1.001
2.5	16.03	15.01	14.97	1.071	1.003
5	15.42	13.67	13.6	1.134	1.005
10	10.57	8.991	8.931	1.184	1.007
20	7.39	6.656	6.628	1.115	1.004
33	6.933	6.38	6.358	1.090	1.003
50	6.867	6.338	6.316	1.087	1.003
100	6.836	6.319	6.298	1.085	1.003

Tab. A1-19: Scale factors derived from the correction for the spreading factor and Q

JB dist [km]	Hypo dist [km]	Frequency								
		0.5 Hz	1.0 Hz	2.5 Hz	5 Hz	10 Hz	20 Hz	33 Hz	50 Hz	PGA
6.0	10	1.000	1.000	1.000	1.000	1.000	1.000	1.000	1.000	1.000
18.3	20	0.967	0.922	0.880	0.850	0.808	0.733	0.651	0.750	0.750
28.9	30	0.920	0.846	0.783	0.738	0.675	0.578	0.488	0.627	0.627
39.2	40	0.884	0.795	0.724	0.670	0.589	0.477	0.400	0.560	0.560
49.4	50	0.856	0.756	0.677	0.614	0.517	0.397	0.344	0.510	0.510
59.5	60	0.832	0.724	0.638	0.567	0.456	0.337	0.308	0.471	0.471
69.5	70	0.813	0.697	0.605	0.526	0.405	0.292	0.283	0.439	0.439
79.6	80	0.800	0.681	0.585	0.500	0.369	0.263	0.270	0.421	0.421
89.6	90	0.844	0.718	0.613	0.515	0.366	0.261	0.282	0.439	0.439
99.7	100	0.886	0.753	0.639	0.527	0.361	0.261	0.294	0.457	0.457
109.7	110	0.967	0.823	0.700	0.573	0.393	0.306	0.365	0.529	0.529
119.7	120	1.050	0.895	0.761	0.618	0.424	0.357	0.445	0.606	0.606
129.8	130	1.150	1.099	1.073	0.926	0.664	0.607	0.787	1.018	1.018
139.8	140	1.238	1.171	1.116	0.943	0.674	0.659	0.884	1.083	1.083
149.8	150	1.325	1.240	1.157	0.958	0.685	0.715	0.989	1.149	1.149
159.8	160	1.413	1.306	1.196	0.972	0.697	0.775	1.099	1.219	1.219
169.8	170	1.500	1.371	1.233	0.985	0.713	0.839	1.216	1.290	1.290
179.8	180	1.586	1.434	1.268	0.998	0.730	0.906	1.340	1.364	1.364
189.8	190	1.670	1.495	1.303	1.010	0.749	0.978	1.469	1.440	1.440
199.8	200	1.754	1.556	1.336	1.021	0.770	1.054	1.604	1.517	1.517
249.9	250	2.164	1.846	1.490	1.079	0.915	1.487	2.374	1.935	1.935
299.9	300	2.566	2.126	1.631	1.148	1.121	2.015	3.296	2.406	2.406
349.9	350	2.967	2.403	1.764	1.242	1.393	2.645	4.376	2.935	2.935
399.9	400	3.374	2.682	1.896	1.371	1.740	3.386	5.617	3.531	3.531
449.9	450	3.790	2.967	2.031	1.543	2.176	4.254	7.024	4.199	4.199
499.9	500	4.220	3.259	2.173	1.768	2.717	5.263	8.608	4.951	4.951

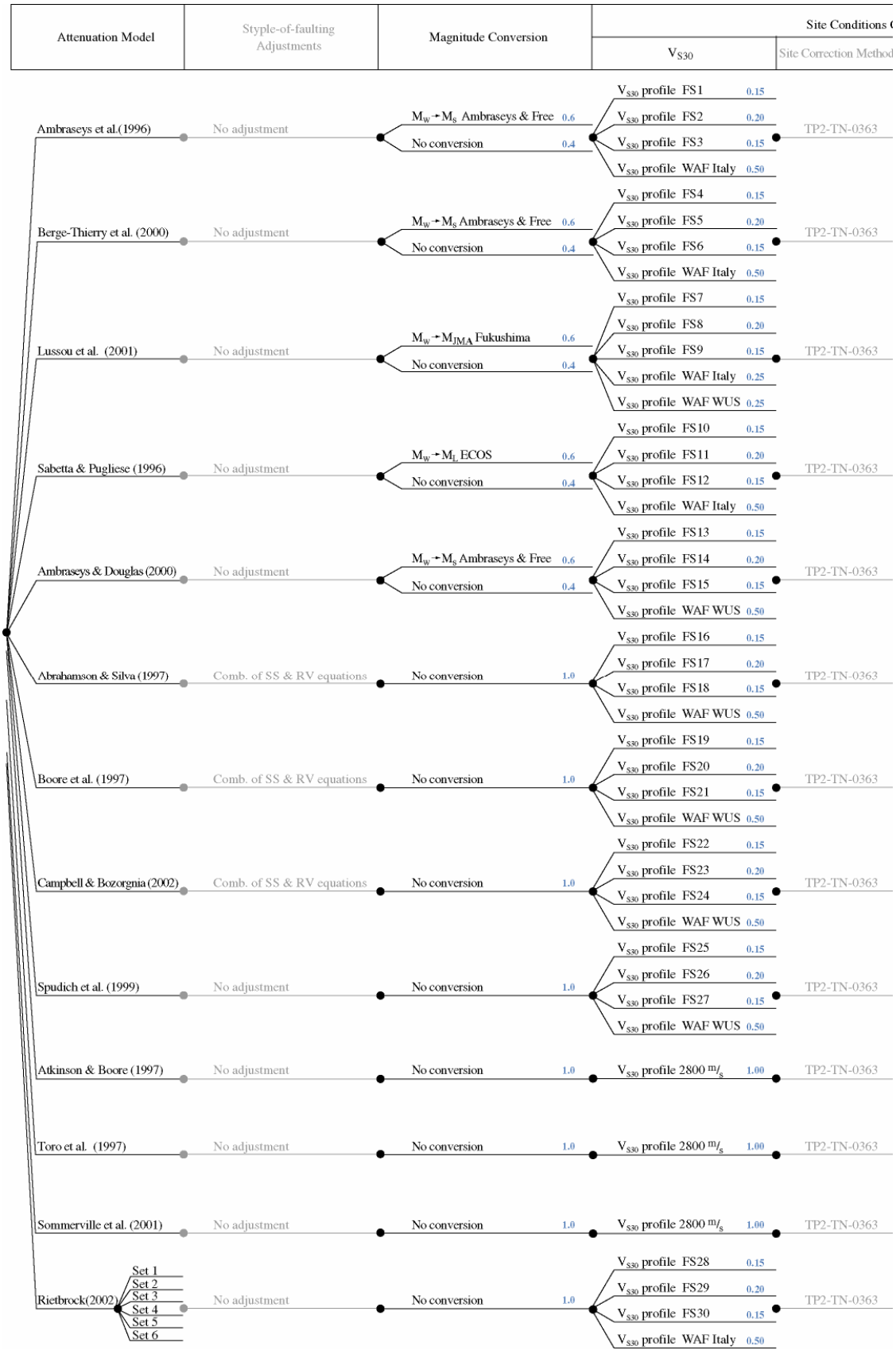

Fig. A1-1: Logic tree for the horizontal ground motion

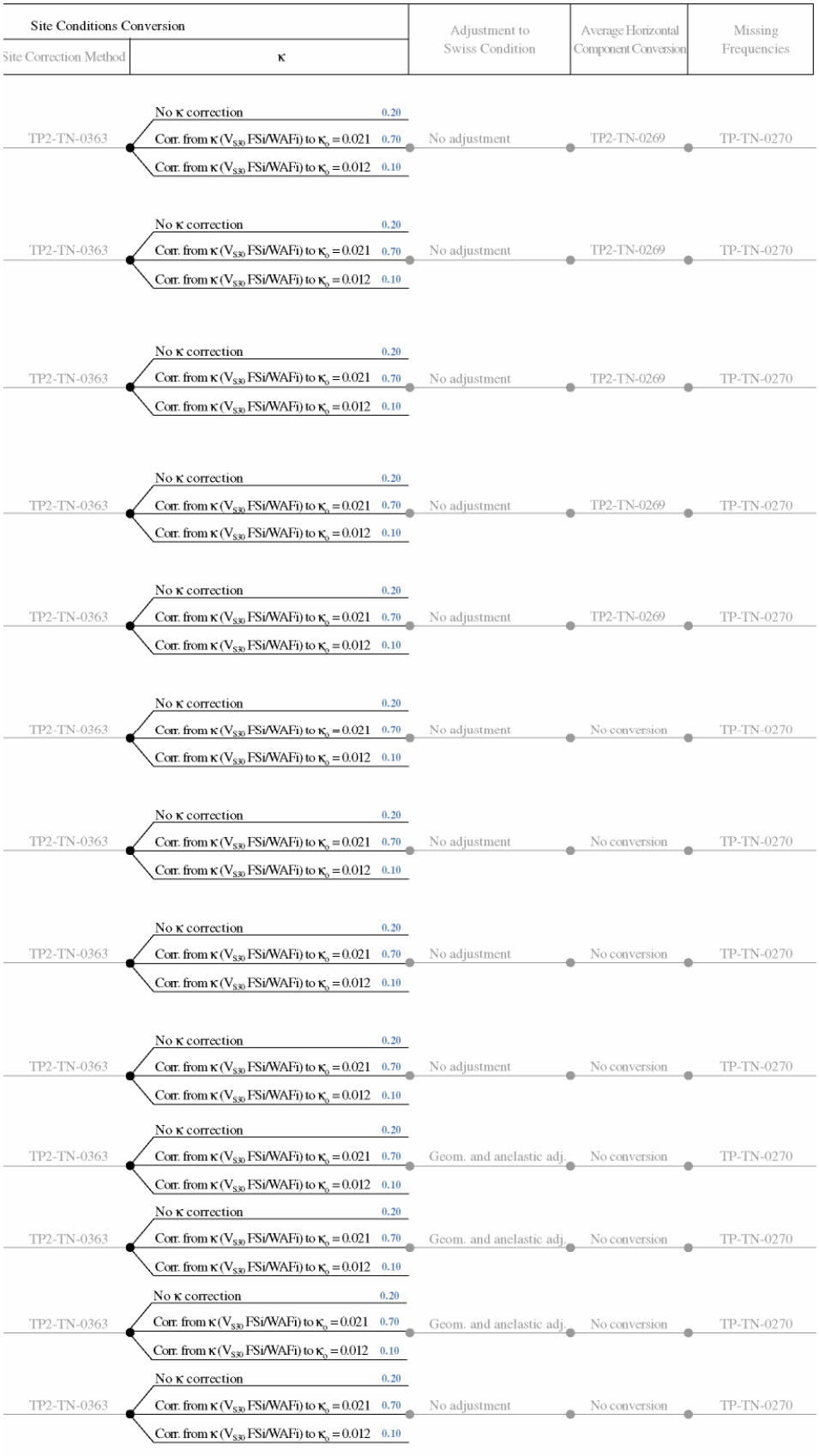

Fig. A1-1: Logic tree for the horizontal ground motion (continued)

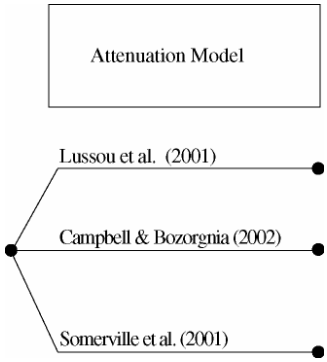

Fig. A1-2: Logic tree for the V / H ratio

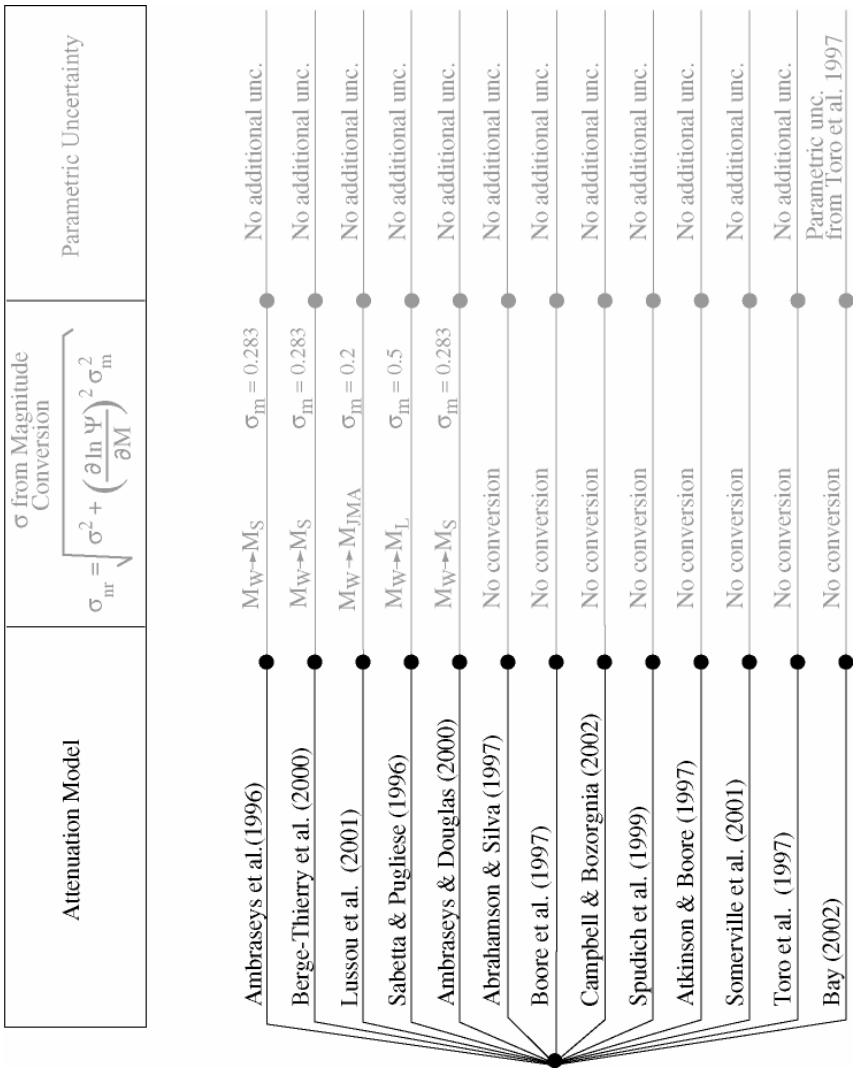

Fig. A1-3: Logic tree for the aleatory uncertainty

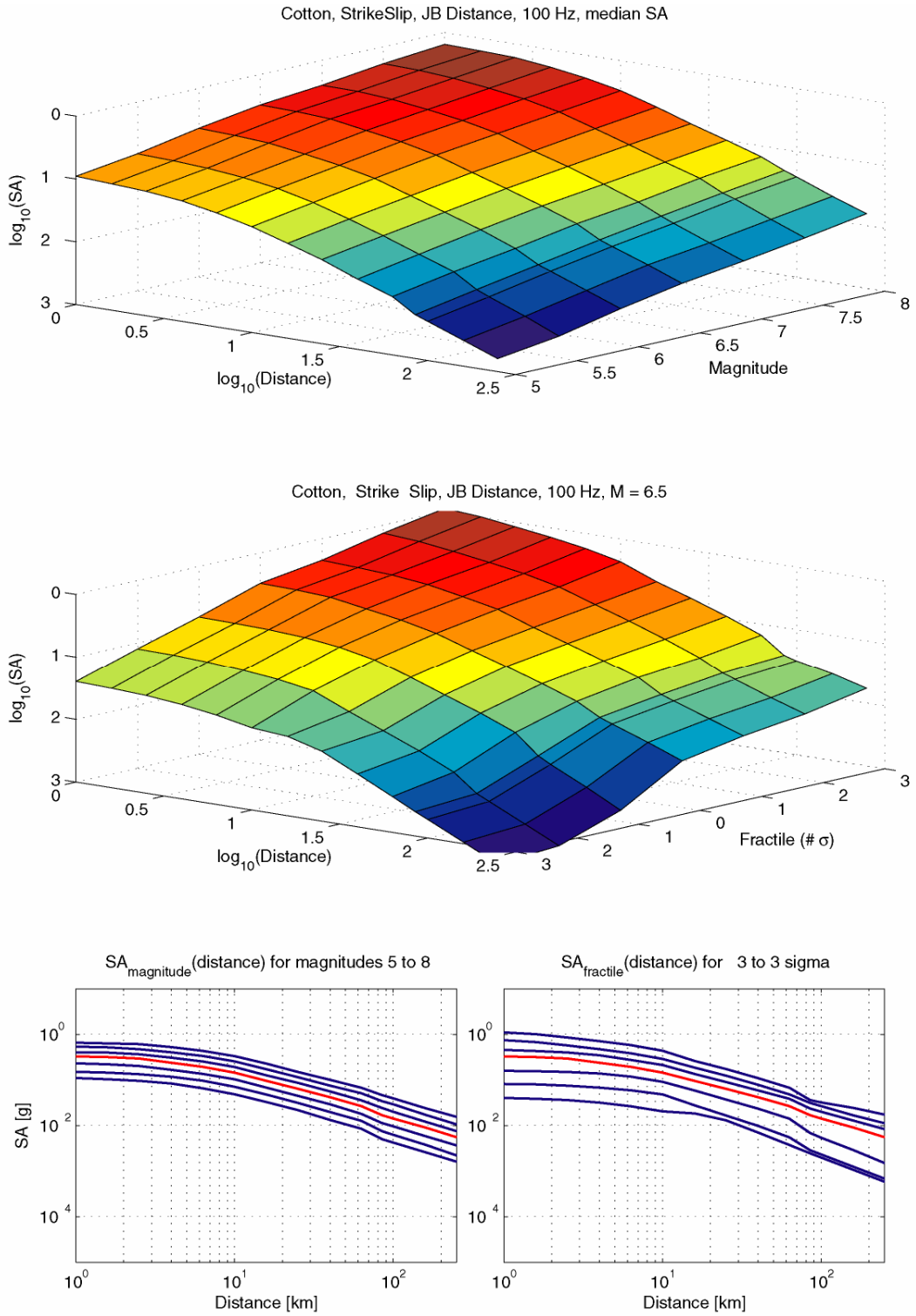

Fig. A1-4: Spectral acceleration (SA) for PGA (100 Hz), assuming strike-slip mechanism and Joyner-Boore distances

The upper plot shows SA (distance, magnitude) for the median. The middle plot shows SA (distance, fractile) for magnitude 6.5. The lower left-hand plot shows the median SA (distance) for different magnitudes. The lower right-hand plot shows SA (distance) for different fractiles and magnitude 6.5.

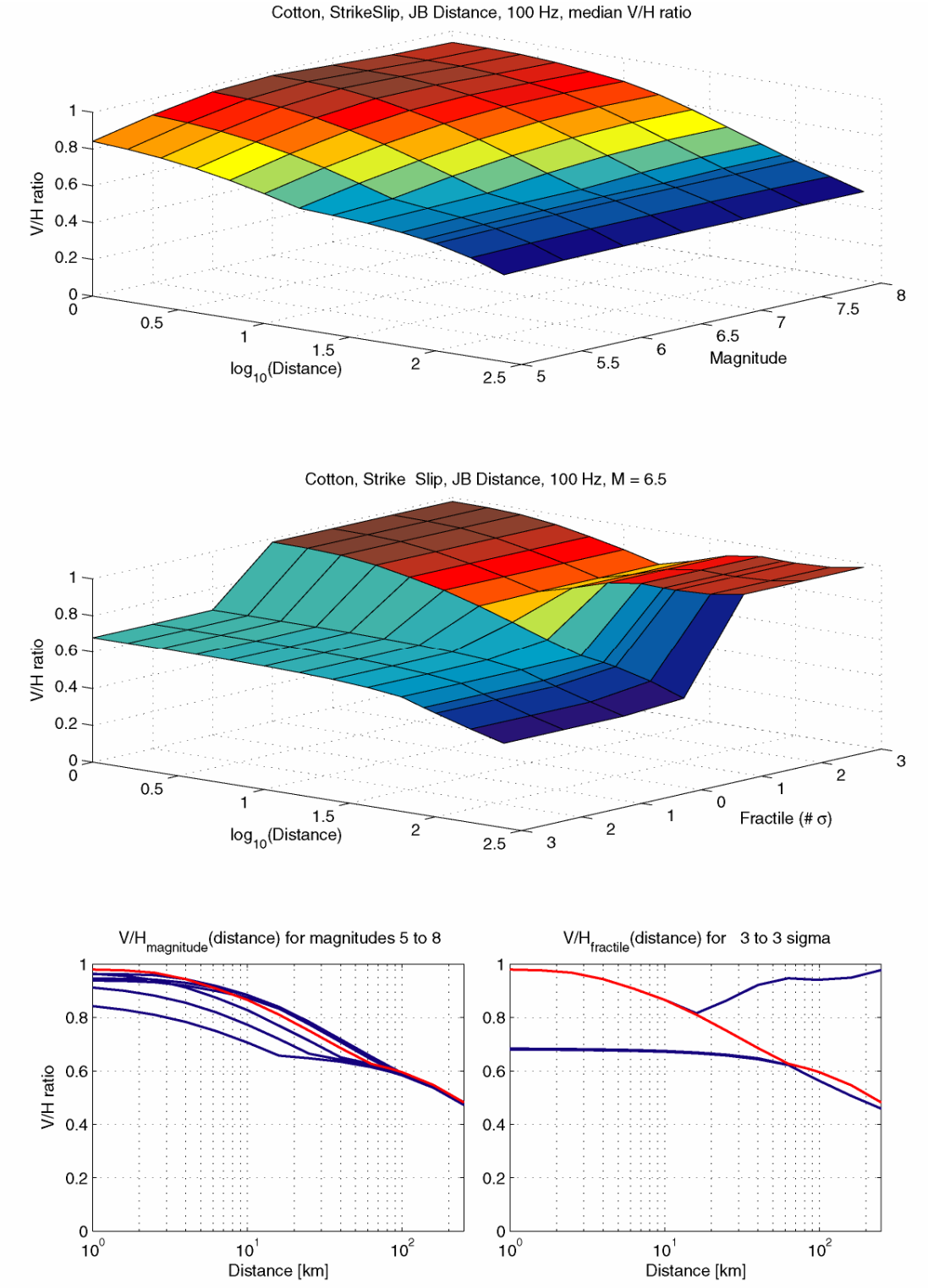

Fig. A1-5: V / H ratio (V / H) for PGA (100 Hz), assuming strike-slip mechanism and Joyner-Boore distances

The upper plot shows V/H (distance, magnitude) for the median. The middle plot shows V / H (distance, fractile) for magnitude 6.5. The lower left-hand plot shows the median V / H (distance) for different magnitudes. The lower right-hand plot shows V / H (distance) for different fractiles and magnitude 6.5.

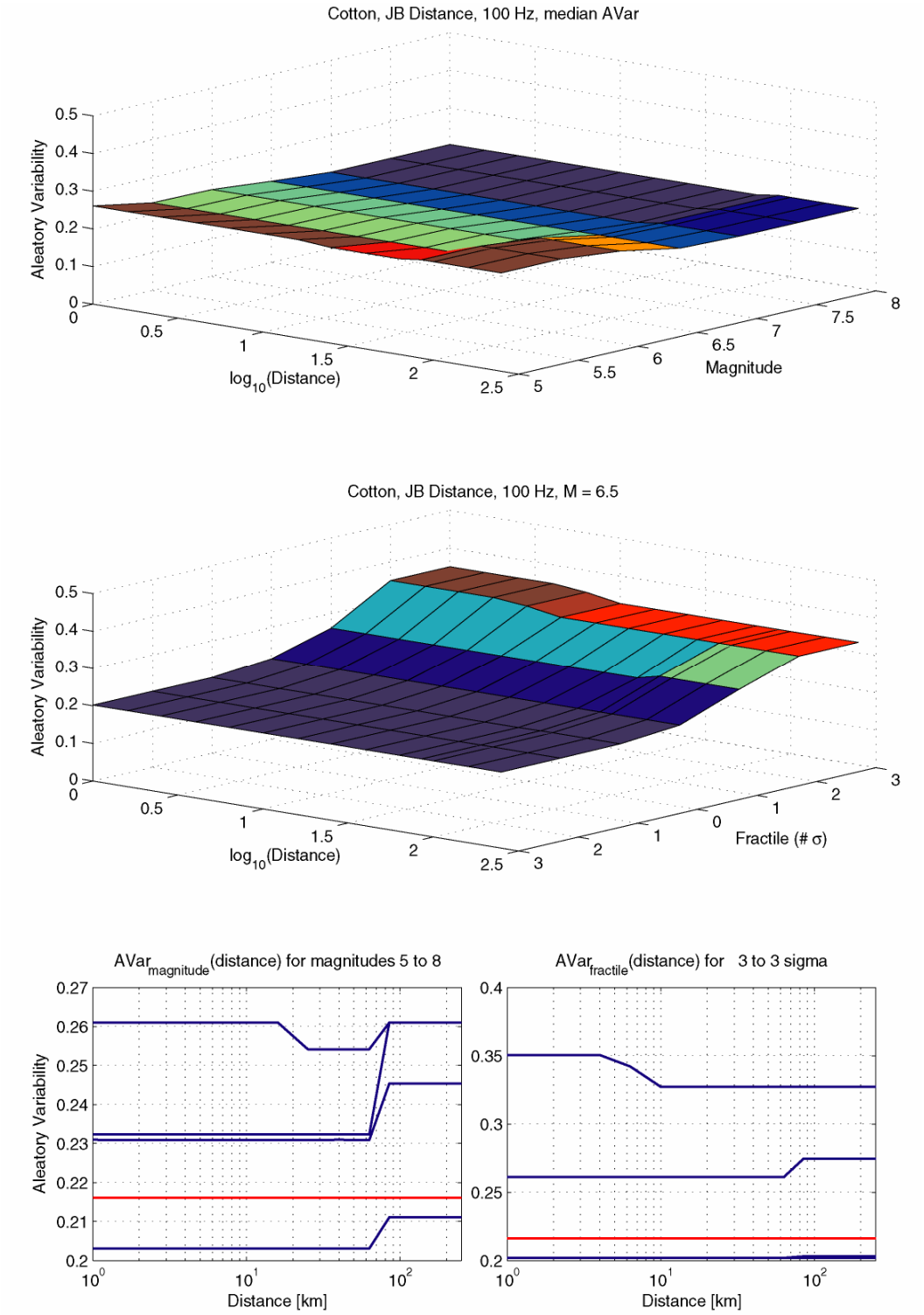

Fig. A1-6: Aleatory variability (AVar) for PGA (100 Hz), assuming strike-slip mechanism and Joyner-Boore distances

The upper plot shows AVar (distance, magnitude) for the median. The middle plot shows AVar (distance, fractile) for magnitude 6.5. The lower left-hand plot shows the median AVar (distance) for different magnitudes. The lower right-hand plot shows AVar (distance) for different fractiles and magnitude 6.5.

Part IV: Ground Motion Characterisation, Elicitation Summary

Dr. Fabio Sabetta

Servizio Sismico Nazionale
Dipartimento della Protezione Civile
Roma – Italy

Probabilistische Erdbeben-Gefährdungs-Analyse für die KKW-Stand Orte in der Schweiz (PEGASOS)

SP2 Ground Motion Characterisation

Elicitation Summary

Fabio Sabetta

Servizio Sismico Nazionale
Dipartimento della Protezione Civile
Roma - Italy

nagra

PEGASOS

TABLE OF CONTENTS

LIST OF TABLES

LIST OF FIGURES

1 INTRODUCTION

A comprehensive overview of the main features and objectives of the PEGASOS Project has been recently published in the Proceedings of 12th European Conference on Earthquake Engineering (Abrahamson et al. 2002). Many of the following introductive remarks have been taken from that document.

The aim of the PEGASOS Project is to develop a Probabilistic Seismic Hazard Assessment (PSHA) for the sites of four nuclear power plants located in northern Switzerland. The PSHA shall be carried out according to the Level 4 procedures for expert elicitation defined in the guidelines of the Senior Seismic Hazard Assessment Committee (SSHAC) on behalf of the US Nuclear Regulatory Committee (SSHAC 1997, NUREG/CR-6372). This is only the second time that the Level 4 procedure has been applied anywhere in the world after the study for the nuclear waste repository at Yucca Mountain, Nevada. In particular, the use of experts and the assessment of epistemic and aleatoric uncertainties receive high priorities in this approach.

The hazard assessment will determine acceleration response spectra, in the frequency range between 0.5 and 50 Hz, for a reference rock site condition, and for the site-specific soil conditions at each plant, for annual probabilities of exceedance as low as 10^{-7}. The inclusion of site-specific soil response and the ground motion upper bound assessment, as part of the expert elicitation, are new aspects that were not considered in the Yucca Mountain study.

The project includes 4 thematic subprojects: "source characterization" (SP1), "ground motion characterization" (SP2), "site response characterization" (SP3), and "seismic hazard computation" (SP4). The subprojects SP1, SP2 and SP3 are assisted by a Technical Facilitator/Integrator (TFI) and are providing the input parameters necessary for the PSHA. SP4 carries out the PSHA by aggregating the models provided by SP1, SP2 and SP3 using the classical Cornell method. Alternative models are considered using the logic-tree method.

Subproject SP2 develops a number predictive regional ground motion models for both the peak ground acceleration and spectral acceleration for rock sites. A single team of 5 experts (EG2) supports SP2. This team sets up the guidelines for the development of predictive ground motion models, evaluates existing strong-motion records and empirical and analytical models, weights the different ground motion models, and estimates the uncertainties of the final models and results.

The summary which follows, aims to illustrate the reasoning for the approach to SP2 objectives and the logic tree structure chosen by the author (EG2 expert). In this respect it contains only a small part of the reasoning and of the work performed on the basis of the extensive documentation provided by the Project.

A special acknowledgement has to be made for the great and extensive work done by PROSEIS within the Computing Modelling and Databank Centre (CMD). Without the data, documents, technical notes, databases and software provided by Philippe Roth, Patrick Smit, Andreas Hoelker and Jim Farrington, the SP2 expert job would have been much more difficult and time consuming.

The essential question that SP2 experts were requested to answer is a selection of attenuation models to be used and their individual weights for different magnitudes, distances and frequencies. This, together with the selection of appropriate conversion rules between different definitions of independent variables, addresses the assessment of epistemic uncertainty. The second issue is to assess the aleatory uncertainty in terms of standard deviation of the selected models. Finally experts will provide estimates of the upper bound of the ground motion in addition to the median and standard deviation.

2 EVALUATION OF PROPONENT MODELS FOR APPLICABILITY TO SWITZERLAND

There are no strong motion attenuation models developed specifically for Switzerland or for regions that are quite similar tectonically, except for the new stochastic point source estimations done on the request by the SP2 experts. The lack of strong motion data is a common situation for many parts of the world, and the models adopted in this study will therefore have to be based on a review of attenuation models for regions with seismotectonic conditions that at least would be reasonable comparable to Swiss conditions.

Tab. 1: Main features of the attenuation models considered

N°		Vt	H comp.	Dist.	M-range	f - range	N° rec.	Site	Area
1	Ambraseys et al. 1996	y	larger envelope	R_{JB} *Repi* *(M_s < 6)*	4.0-7.3 M_s	0.5 -10 Hz	422	Rock > 750 m/s	Europe Middle East 1969-1994
2	Berge-Thierry et al. 2000	y	both	Rhypo	4.5-7.3 M_s	0.1 -33 Hz	485 (965)	Rock > 800 m/s	Europe (17 %) California 1952-1997
3	Sabetta & Pugliese 1996	y	larger PGA	R_{JB}	4.6-6.8 M_s-Ml	0.25-25 Hz	95	Rock > 800 m/s	Italy 1976-1984
4	Ambraseys & Douglas 2000	y	larger	R_{JB} < 15 km	5.8-7.8 M_s	0.5 -10 Hz	186	Rock > 750 m/s	Worldwide (72 % WNA)
5	Lussou et al. 2001	y	both	R_{hypo}	3.5-6.3 M_{JMA}	0.1-50 Hz	3011	400-800 m/s (site B)	Japan 1996-1998
6	Abrahamson & Silva 1997	y	geom. mean	R_{rup}	4.5-7.5 M_w	0.2 -100 Hz	655	Rock > 600 m/s	Worldwide (90 % WNA) 1940-1994
7	Spudich et al. 1999	n	geom. mean	R_{JB}	5.1-6.9 M_w	0.5 -10 Hz	142	Rock > 620 m/s	Worldwide (62 % WNA) extensional 1972-1995
8	Boore et al. 1997	n	random	R_{JB}	5.3-7.7 M_w	0.5 -10 Hz	112	Rock = 620 m/s	WNA 1940-1992
9	Campbell & Bozorgnia 2002	y	geom. mean	R_{seis} < 60 km	4.7-7.7 M_w	0.25-20 Hz	443	firm rock 800 ± 340	Worldwide 1957-1997
10	Atkinson & Boore 1997	n	random	R_{hypo}	4.5-7.0 M_w	0.5 -20 Hz	point s. st. sim.	hard rock 2800 m/s	ENA
11	Toro et al. 1997	n	geom. mean	R_{JB}	5.0-8.0 M_w	0.5-35 Hz	point s. st. sim.	hard rock 2800 m/s	CENA
12	Somerville & Collins 2001	y	both	R_{JB}	6-7.5 M_w	0.25 -100 Hz	deter. sim. finite fault	hard rock 2800 m/s	CENA
13	Point source stochastic (Bay 2002)	y	geom. mean	R_{hypo}	3-6.5 M_w	1 -15 Hz	point s. st. sim.	hard rock NEHRP A-B	Switzerland 2958 rec $2 < M_L < 5.2$

Thirteen attenuation models (originally 14 but Campbell 1997 is superseded by Campbell & Bozorgnia 2002) were selected during Workshop 1 by SP2 experts; the main features are summarized in Table 1.

The first three models are based on European strong motion data coming from inter-plate crustal regions with mixed tectonic regimes (normal, strike-slip, thrust). Models N° 4 to 9 are based on worldwide data (Lussou only Japan), with a clear preponderance of Western North America (WNA) data, always from inter-plate crustal regions with mixed tectonic regimes. Models N° 10, 11, 12 are based on stochastic point source or deterministic finite fault modeling performed for intra-plate stable continental regions of Eastern and Central North America (ENA, CENA). Model N° 13 is the only one developed specifically for Switzerland and based on a stochastic point source simulation calibrated with 2958 weak motions recorded from 1984 to 2000 by short period, broadband, and strong motion instruments in Switzerland and the German border.

The acceleration response spectra of the 13 attenuation models are compared in Figures 1 and 2 for different values of magnitude and distance. To make the comparison, preliminary median conversions for magnitude, distance, horizontal component and style of faulting have been performed as following:

$M_w - M_s \rightarrow$ Ambraseys & Free, 1997; $M_w = M_{jma}$; $M_w = M_L$;

$R_{hypo} = (R_{JB}^2 + h^2)^{1/2}$ $\underline{w = 0.3}$ $R_{hypo} = [(R_{JB}+0.3\cdot RL)^2+h^2]^{1/2}$ $\underline{w = 0.4}$ $R_{hypo} = (R_{JB}+0.7\cdot RL)^2+h^2]^{1/2}$ $\underline{w = 0.3}$

$R_{rup} = (R_{jb}^2+h_{rup})^{1/2}$ $h_{rup} = h-0.5\cdot RW$ $\underline{w = 0.6}$; $h_{rup}= h-0.35\cdot RW$ $\underline{w = 0.2}$; $h_{rup} = h+0.35\cdot RW$ $\underline{w = 0.2}$

$R_{seis} = (R_{JB}^2+h_{seis}^2)^{1/2}$ $h_{seis} = 3$ km

R_{JB} = Joyner & Boore distance; R_{hypo} = hypocentral distance; h = hypocentral depth, RL = fault length ; RW = fault width; h_{rup} = depth to top rupture plane

Scale to geometrical mean horizontal component = Ambraseys and Sabetta scaled respectively from larger envelope and from larger PGA with the frequency dependent factors provided in PEGASOS TP2-TN-0269.

Style of faulting = Somerville divided by 1.1 (from reverse to mixed); Spudich multiplied by 1.1 (from normal to mixed)

More accurate conversions will be provided in the following sections; the above ones have only been used to make simpler the graphical comparisons.

Figures 1 and 2 show that the epistemic uncertainty, taking into account the differences in the models, is lower than the aleatoric one: all the considered empirical models fall inside the ± 1 sigma bound, shown by the thick orange curves, and corresponding to the standard deviation of the Berge-Thierry et al. relation. The exceptions are the theoretical models based on stochastic point source or deterministic finite fault simulations. According to the different values of the parameters (particularly K and $\Delta\sigma$), those developed for ENA and CENA provide higher PSA values at periods shorter than 0.1 sec and that developed for Switzerland provides lower values respect to the other empirical models.

Of course more epistemic uncertainty will be added by more detailed and extensively weighted conversions that will be introduced afterwards, however, in the final hazard assessment, the aleatory variability will be larger than the epistemic uncertainty.

Evaluations of the applicability of the proponent models to Switzerland are given in section 3.4.

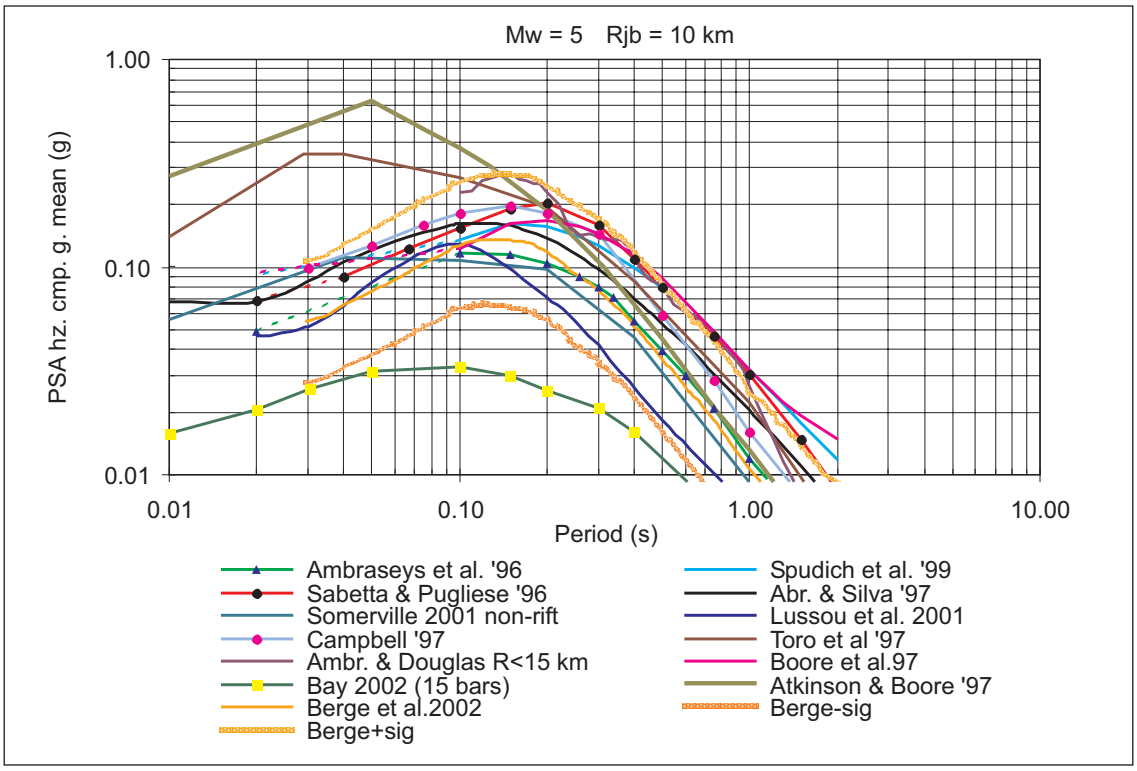

Fig. 1: Acceleration response spectra of the considered attenuation models, in case of M = 5 and R_{JB} = 10 km compared with the aleatory uncertainty (± 1σ) of Berge-Thierry et al. 2000

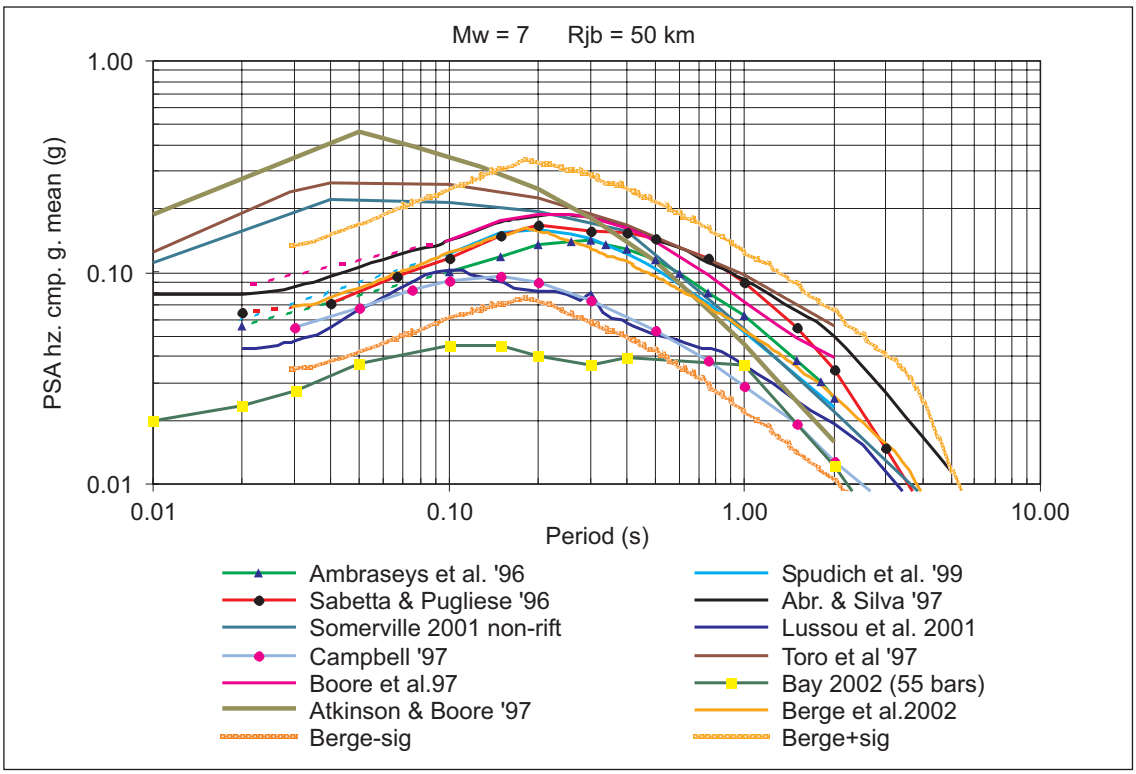

Fig. 2: Acceleration response spectra of the considered attenuation models, in case of M = 7 and R_{JB} = 50 km compared with the aleatory uncertainty (± 1σ) of Berge-Thierry et al. 2000

3 MEDIAN HORIZONTAL MOTION

3.1 Logic Tree Structure – Rejected models

The logic tree structure is summarized in Table 2 and is organized in six main parts with different branches and weights: selected models and corresponding weights for different M-R ranges (section 3.2); site conditions conversion (section 3.3); magnitude conversion (section 3.5); component conversion (section 3.6); missing frequencies (section 3.7); fault type conversion (section 3.8)

Among the 13 proposed attenuation models, 5 have been rejected (zero weight in the logic tree) for the following reasons:

1.-2. Atkinson & Boore (1997) and Toro et al. (1997)

Two of three theoretical simulation models based on data from Eastern and Central North America have been rejected because they are essentially point source stochastic simulation models analogous to that specifically developed for Switzerland (Bay, 2002a) but with different seismological parameters (stress drop, Q, K). These models show a content of high frequencies much greater (max spectral amplification around 0.04 sec) than that of the empirical models for WNA or Europe (NUREG/CR-6372, SSHAC 1997). Therefore, among the Eastern North America models, the choice has been limited to Somerville & Collins (2001) which is also considering a different approach based on finite source simulation.

3. Campbell (1997) and Campbell & Bozorgnia (2002)

The regression models proposed by Campbell are very complicated and with too many parameters (15-17 coefficients). When faced with alternatives that equally well can explain some data, preference should be given to the simplest one (Occam's razor). Furthermore, unless the further parameters are known a priori for future earthquakes, the result of introducing them is only to transfer some modeling uncertainty into parametric uncertainty, without varying the total uncertainty (NUREG/CR-6372, 1997). In this case some parameters linked to the fault geometry, as R_{seis} and the depth to basement rock, are very difficult to predict for future earthquakes. Moreover the attenuation models are valid only up to a distance of 60 km and the standard deviation (Campbell, 1997) is constant with frequency.

4. Ambraseys & Douglas (2000)

This model, as the title says, has been mainly developed for the "Reappraisal of the effect of vertical ground motions on response". It covers only distances up to 15 km. It is mainly based on W.N.A. (72 %) data. It shows very unsmoothed spectral values.

5. Boore et al. (1997)

Between two similar models, mainly based on W.N.A. data, the preference has been given to the Spudich et al. (1999) model which also includes worldwide data. In spite of the use of a cutoff distance for instruments not triggered by S waves, the Boore relation shows higher values at large distances and also some strange increase of the spectral values at long periods probably due to data processing troubles.

3.2 Selected proponent models and weights

3.2.1 Selected models and weights for the intermediate M-R range

Considering that the bulk of the data, in most of the considered models, is included in a magnitude range of 5.5 to 6.5 and a distance range of 10 to 70 km, these values have been selected as intermediate M-R range (M_1-M_2, R_1-R_2).

The 8 selected models provide a balance between European (3 models with mixed tectonic regimes), Worldwide (1 model extensional regime, 1 model mixed regime) and Japanese data (1 model with mixed tectonic regime), supplemented with deterministic (1 model) and stochastic (1 model) modeling for intraplate stable continental regions.

The models have been selected in order to provide a good representation of the epistemic uncertainty, covering the upper and lower bounds in terms of spectral values for different magnitudes and distances (see Figures 1 and 2).

The selection of the weights given to the different models in the intermediate M-R range has been mainly based on:

1. number of records considered in the model;
2. geographical area and representative-ness for Switzerland;
3. regression model and data processing;
4. distribution of the data in M-R space (visual inspection);
5. visual inspection of the plots of the residuals for the different models.

The residual plots provided to the SP2-experts, have been considered with some caution due to the apparent lack of a quality selection criterion in the WAF PEGASOS strong motion records (Bay 2002b). In particular the apparent trends in the residual plots are biased by the unreliable low magnitude Swiss data of which the empirical models are not representative (see section 3.4).

The main features of the selected models together with the main parameters conversions to be used in the logic tree and with the weights selected for the intermediate M-R range, are reported in Table 2. Remembering that the mean weight is 0.125, the reasoning for the weights selection is reported hereafter.

1. Ambraseys et al. (1996)

It represents the most used model to evaluate the ground motion in European seismic hazard studies; it includes 422 records coming from Europe and Middle East; the range of considered frequencies (0.5 – 10 Hz) is rather short; the quality selection criteria of the records are not very accurate; the residuals plots show a better agreement with the European strong motion database (PEGASOS WAF) respect to other models; it provides mean PSA values if compared to the other selected models. The weight assigned is 0.12.

2. Berge-Thierry et al. (2000)

It makes use of an up-to-date and extensive database of European strong-motion records with rigorous selection criteria in terms of quality; it is also integrated by records from crustal events in California (17 % of the total) to cover the high magnitude range (up to 7.3); the residuals plots show a better agreement with the European strong motion database (PEGASOS WAF) respect to other models; it provides mean PSA values (higher in far field and at intermediate periods) if compared to the other selected models. The weight assigned is 0.15.

3. Sabetta & Pugliese (1996)

It's a model developed specifically for Italy. In spite of the fact that it is not really up-to dated (the most recent recordings are of 1984) it gave a good proof in fitting the ground motion data of all the most recent earthquakes; the number of records is small (95) but the selection criteria in terms of accuracy of magnitude and distance determination, free field conditions, recording instruments, and data processing, are very accurate and homogeneous; it has also to be noted that more than 50 % of the European strong motion records are coming from Italy; it provides high PSA values at small magnitudes and long periods if compared to the other selected models. The weight assigned is 0.10.

4. Lussou et al. (2001)

It's the model with the highest number of records (3011) but data are only relative to Japan; the site conditions are much better assessed (V_s profiles) respect to other models; the rock sites ($V_s > 800$) are so few that the use of site category B ($400 < Vs < 800$) is recommended; the M range covers essentially low magnitudes (3.5 – 6.3); it provides low PSA values if compared to the other selected models. The weight assigned is 0.10.

5. Abrahamson & Silva (1997)

It's a very accurate model including 655 worldwide records; it includes more sophisticated features respect to other models such as selection of the data on the basis of the processing, hanging wall effect, saturation with M, non linear site effect; it includes strike-slip and reverse faults but the latter are limited, for $M < 5.8$, to the Coalinga aftershock sequence producing a large style-of-faulting factor for small magnitude events; it provides high PSA values in the near field if compared to the other selected models. The weight assigned is 0.14.

6. Spudich et al. (1999)

It's a model developed specifically for extensional tectonic regimes; it is based on 142 world-wide records very carefully selected and reviewed; the range of considered magnitudes (5.1 – 6.9) and frequencies (0.5 – 10 Hz) are rather short; it provides medium-high PSA values if compared to the other selected models. The weight assigned is 0.10.

7. Somerville et al. non-rifted (2001)

It is one of the two theoretical models selected. It has been specifically developed, using finite fault simulation and slip models, for hard rock (2800 m/s) sites in Central and Eastern U.S. Even if at lower levels respect to other ENA models (Atkinson and Toro), it provides very high spectral values, at high magnitudes, large distances and high frequencies, due to the high $\Delta\sigma$, Q, and low K, peculiar of ENA. I considered the possibility of using this model with $\Delta\sigma$, Q, and K values closer to the Swiss conditions. However, considering the large uncertainty in the above parameters and the trade-off among them and other parameters used in the theoretical models (e.g. density and velocity in the crust) and considering also that "Swiss values" of $\Delta\sigma$, Q, and K are taken into account in the Bay model with a large weight (see point below), I preferred to leave the Somerville model in its original form, to take into account the epistemic uncertainty linked to the possible existence of source, path, and site conditions similar to Eastern U.S. is 0.09.

8. Point source stochastic (Bay 2002a)

It's the only model representing the Swiss conditions and this is the reason of the higher weight given to it (0.2; reaching 0.25 at low magnitudes and large distances).

I also considered the stochastic model developed by Andreas Rietbrock (Rietbrock 2002) using the same data previously analyzed by Bay (2002a). As shown in the comments on Rietbrock's work made by Frank Scherbaum (PEGASOS EG2-TN-0314) the results are basically consistent with the findings of Bay, with some unexplained consequences as the strong scatter and magnitude dependence of the geometrical spreading. I preferred therefore only to use the Bay model which is widely explained and analyzed in her Ph.D. Thesis.

Tab. 2: Main features and weights of the selected attenuation models

N°	Median Horizontal g. m. on rock sites	Logic Tree	Style of faulting	H comp.	Dist.	M range	Freq. Range	N° rec.	Site	Area	Weight 5.5 < M < 6.5 and 10 < R < 70
1	Ambraseys et al. (1996)	correct for: style of faulting, Ms, site cond., larger envelope hz comp.	Reverse, strike-slip normal	larger envel.	R_{JB} R_{epi}	4.0-7.3 Ms	0.5 - 10 Hz	422	Rock > 750 m/s	Europe Middle East 1969-1994	0.12
2	Berge-Thierry et al. (2000)	correct for: style of faulting, Ms, site cond.Rhypo	Reverse, strike-slip normal	both	R_{hypo}	4.5-7.3 Ms	0.1 - 33 Hz	485 (965)	Rock > 800 m/s	Europe 17 % California 1952-1997	0.15
3	Sabetta & Pugliese (1996)	correct for: style of fault. site cond. larger PGA hz comp.	Reverse, normal	larger PGA	R_{JB}	4.6-6.8 M_s - Ml	0.25 - 25 Hz	95	Rock > 800 m/s	Italy 1976-1984	0.10
4	Lussou et al. (2001)	correct for: style of faulting, Mjma, site cond.Rhypo	Reverse, strike-slip, normal	both	R_{hypo}	3.5-6.3 M_{JMA}	0.1 - 50 Hz	3011	400-800 m/s site B	Japan 1996-98	0.10
5	Abrahams. & Silva (1997)	use footwall; correct for: style of faulting, site cond., Rrup	Reverse, strike-slip	geom. mean	R_{rup}	4.5-7.5 M_w	0.2 - 100 Hz	655	Rock > 600 m/s	Worldwide 90 % WNA 1940-1994	0.14
6	Spudich et al. (1999)	correct for: style of faulting, site conditions	Strike-slip normal	geom. mean	R_{JB}	5.1-6.9 M_w	0.5 - 10 Hz	142	Rock > 620 m/s	Worldwide 62 % WNA extensional 1972-1995	0.10
7	Somerville & Collins (2001)	correct for: style of faulting, site conditions	Reverse	both	R_{JB}	6-7.5 M_w	0.25-100 Hz	simul finite fault	hard rock 2800 m/s	CENA	0.09
8	Point source stochastic (Bay 2002)	use different models from dissertation (Ainc, A30, Y1), correct for: style of faulting, site conditions, Rhypo	Reverse, strike-slip, normal	geom. mean	R_{hypo}	3-6.5 M_w	1-15 Hz (0.2 –50 reg. coeff.)	simul. point source	hard rock NEHRP A-B	Switzer-land 2958 rec $2<M_L<5.2$ 80 % $M_L<3$	0.20

The main issue is that the model is calibrated only with small to moderate size events. Consequently, the scaling to higher magnitudes is the source of a large epistemic uncertainty and has to be evaluated carefully. In order to constrain the possible models at large magnitudes, results from worldwide scaling studies (Mayeda & Walter 1996, Ide & Beroza 2001) are evaluated by the author. The parameters uncertainty and the trade off between the parameters are evaluated and discussed in detail in Bay (2002a, chapter 3), showing that a wide range of parameter values can fit the data almost equally well.

In particular a detailed sensitivity analysis, with the parameter combination minimizing the residuals between empirical data and theoretical model, is performed to select the values and analyze the trade off between the five model parameters: $\Delta\sigma$, κ, $G(r_{ref})$, Qo and η. As a result a strong dependence between κ and $\Delta\sigma$ is found, whereas Qo and η trade of in such a way that they do not significantly influence the residuals and they do not significantly trade off with κ and $\Delta\sigma$. Therefore, as shown in Bay (2002a and c), changes in the frequency dependent quality factor $Q(f) = Q_o f^{\eta}$ or in the geometrical spreading $G(r_{ref})$ do not influence the results signifycantly.

Several models are proposed in Bay 2002a to take into account the epistemic uncertainty and in particular two (A_{inc} and A_{30}) are explicitly introduced to scale for larger magnitudes. They are based on the assumption that the small to moderate size earthquakes can be used to constrain the attenuation parameters, but do not provide information about $\Delta\sigma$ for large events. The A_{inc} model, adopts the $\Delta\sigma$-M_0 scaling relation of Mayeda & Walter (1996). The A_{30} model assumes a constant $\Delta\sigma = 30$ bars as found by Ide & Beroza (2001).

All the model parameters, including the $V(f)$ site term for Foreland, the H/V ratio and the sigma, are listed in table 3.1 of Bay (2002a). A third model (Y_1, figure 3.4 of Bay 2002a) is considered, to take into account different values of the parameters.

The weights assigned to these models are summarized in Table 3. The highest weight is given to the A_{inc} model because, as shown in Figure 15, it fits reasonably well the Swiss ground motion data of the PEGASOS WAF database (Smit et al. 2002) if properly selected (Bay 2002b). The A_{30} model has a lower but still high (compared to Y_1) weight because indicated as preferred model for high magnitudes by the author itself and because the parameters values (in particular stress drop) are closer to the values suitable for Switzerland as confirmed by the results of Rietbrock (2002). The Y_1 model is introduced to take into account the epistemic uncertainty and has the lowest weight because the parameters values (in particular Q and κ) are quite far from those expected in Switzerland.

A summary of the main motivation for the different weights assigned to the models is given hereafter:

1. Ambraseys et al.: most used model to evaluate ground motion in Europe; shortcomings due the quality selection criteria of the records. Median weight (0.12).
2. Berge-Thierry: most recent and extended European model; residuals with good agreement with the PEGASOS WAF database. Higher than median weight (0.15).
3. Sabetta & Pugliese: Italian model not really up-to dated; small number of records and very accurate selection criteria. Lower than median weight (0.10).
4. Lussou et al.: only Japanese data; highest number of records but only low magnitudes. Lower than median weight (0.10).
5. Abrahamson & Silva: high number of worldwide records; accurate selection criteria; style-of-faulting factor. Higher than median weight (0.14).
6. Spudich et al.: rather small number of worldwide records very carefully selected from extensional tectonic regimes; short range of magnitudes and frequencies. Lower than median weight (0.10).

7. Somerville & Collins: theoretical model for CENA; seismological parameters very different from Switzerland. Lower than median weight (0.09).
8. Bay: only model representing the Swiss conditions. Higher than median weight (0.2).

Tab. 3: Weights assigned to the different models considered in case of Bay 2002a

Model (as indicated in Bay 2002a)	Attenuation Bay (2002a, table 3.1)	$\Delta\sigma$	K	Weight $5.5 < M < 6.5$ and $10 < R < 70$
A_{inc}	$G(r) = 40^{-1.1}$ $Q(f) = 270f^{0.50}$	Increasing as $M_o^{0.25}$ from 3 bars at $M_w = 3$ to 55 bars at $M_w = 6.5$	0.0125	0.09
A_{30}	$G(r) = 40^{-1.1}$ $Q(f) = 270f^{0.50}$	30 bars	0.0125	0.07
Y_1	$G(r) = 40^{-1.2}$ $Q(f) = 440f^{0.37}$	24 bars	0.0430	0.04

3.2.2 Changes in weights for different M-R ranges

Some examples of the acceleration response spectra of the selected models for different magnitude and distance values are reported in Figures 3 to 8. A short discussion of the change in weighting for the different magnitude and distance ranges is reported hereafter. Attention should be paid to the fact that for $M > 6.5$ the models considered are only 7 (mean weight = 0.143). When only some models are changing weight, the other values are redistributed among the remaining models in order to sum up to 1.

$M < 5.5$ $R < 10$

- All models show very few data at $R < 10$ km.
- *Spudich* has few data for $M < 5.5$ *(lower w.*).
- The near field situation, looking at the data distribution and considering the use of hypocentral distance, is better for *Berge and Lussou* (*higher w.).*
- *Lussou* has a better coverage in the low M range (*higher w.*).
- *Somerville,* as acknowledged in the paper, is biased for $M < 6$ (*lower w.*).
- *Bay* is better calibrated for low magnitudes (*higher w.*).

$M < 5.5$ $10 < R < 70$

Same remarks as the previous distance range apply, except for a slightly lower weight to *Berge and Lussou.*

$M < 5.5$ $R > 70$

Strong motions are generally unavailable for small magnitudes and high distances; *higher weights* to simulations models (*Somerville and Bay*) calibrated for high distances and also including the change of slope (Moho bounce) for $R > 70$ km.

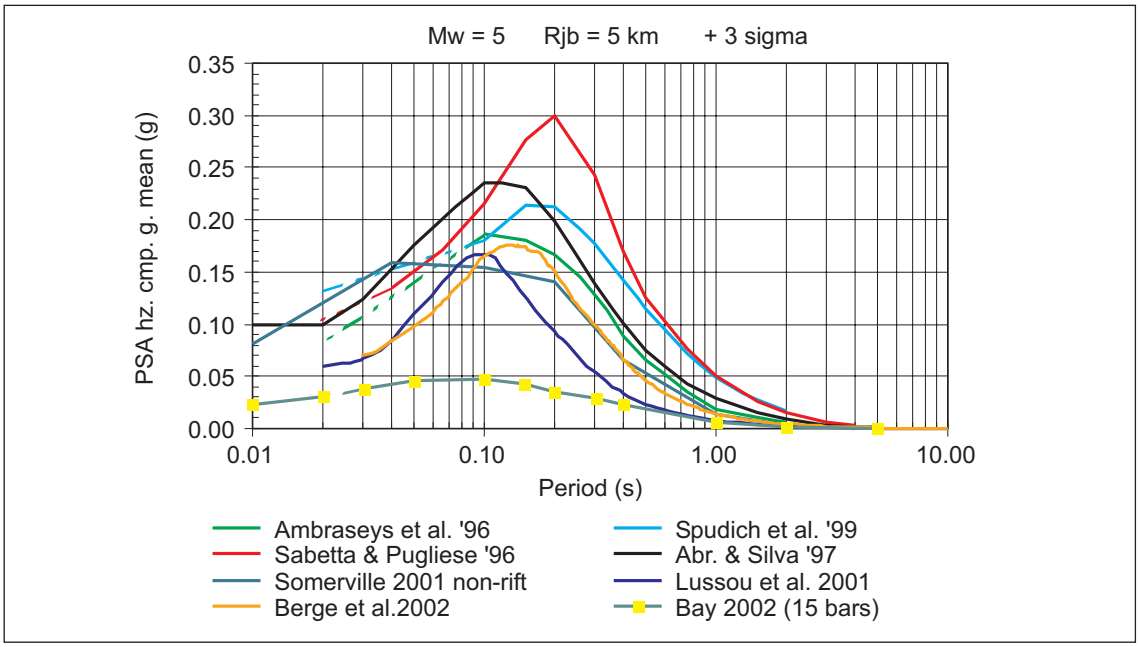

Fig. 3: Acceleration response spectra of the selected models in case of M = 5 and R_{JB} = 5 km

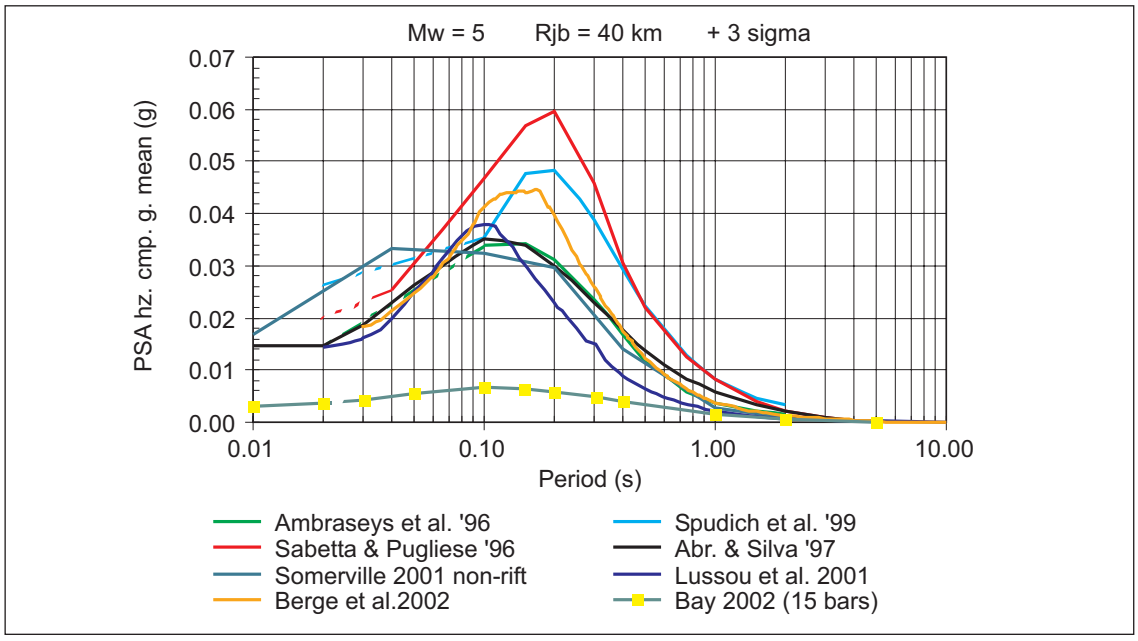

Fig. 4: Acceleration response spectra of the selected models in case of M = 5 and R_{JB} = 40 km

5.5 < M < 6.5 R < 10

Abrahamson and Spudich include more data at intermediate magnitude and distance less than 10 km (*higher w*).

5.5 < M < 6.5 10 < R < 70

Median weights.

5.5 < M < 6.5 R > 70

Higher weights to simulations models (*Somerville and Bay*) calibrated for high distances and also including the change of slope (Moho bounce) for R > 70 km.

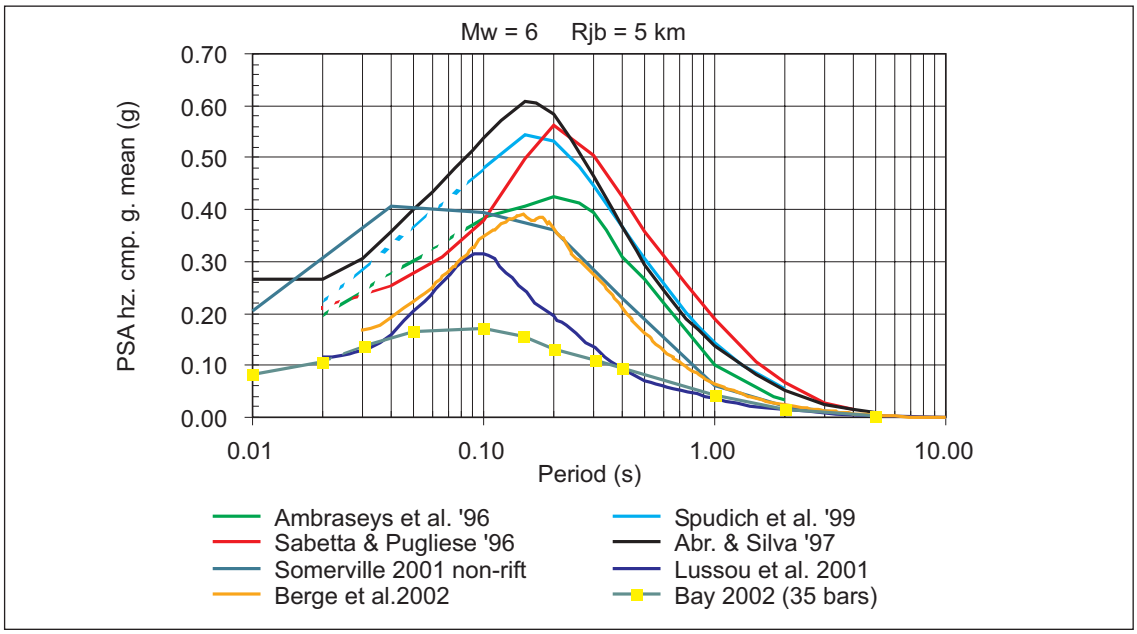

Fig. 5: Acceleration response spectra of the selected models in case of M = 6 and R_{JB} = 5 km

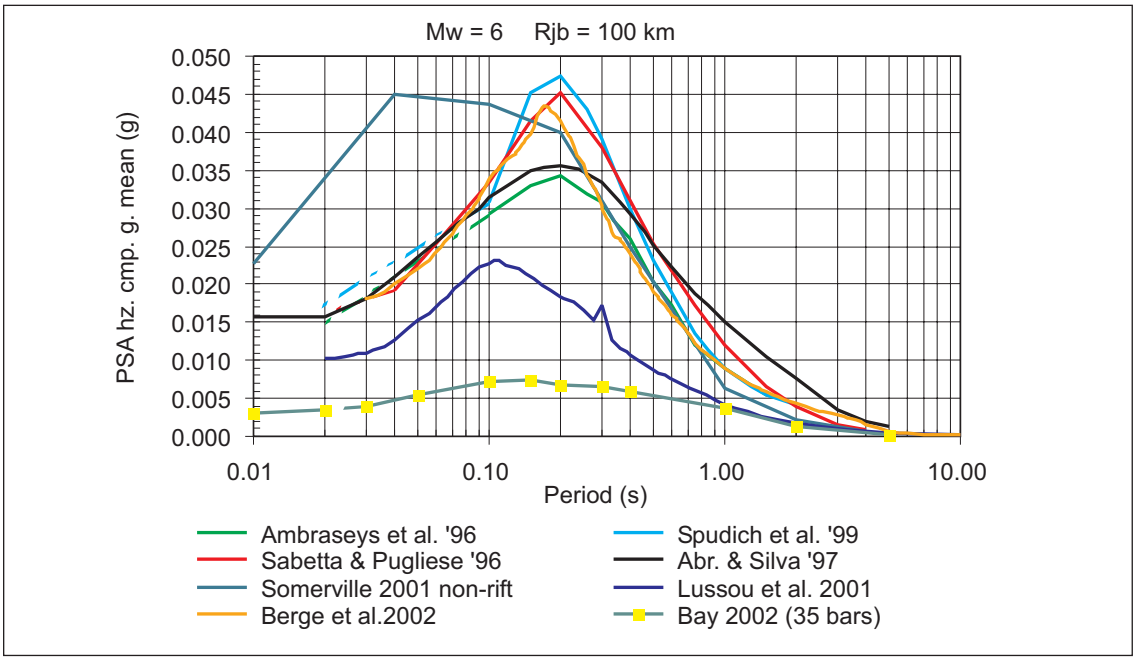

Fig. 6: Acceleration response spectra of the selected models in case of M = 6 and R_{JB} = 100 km

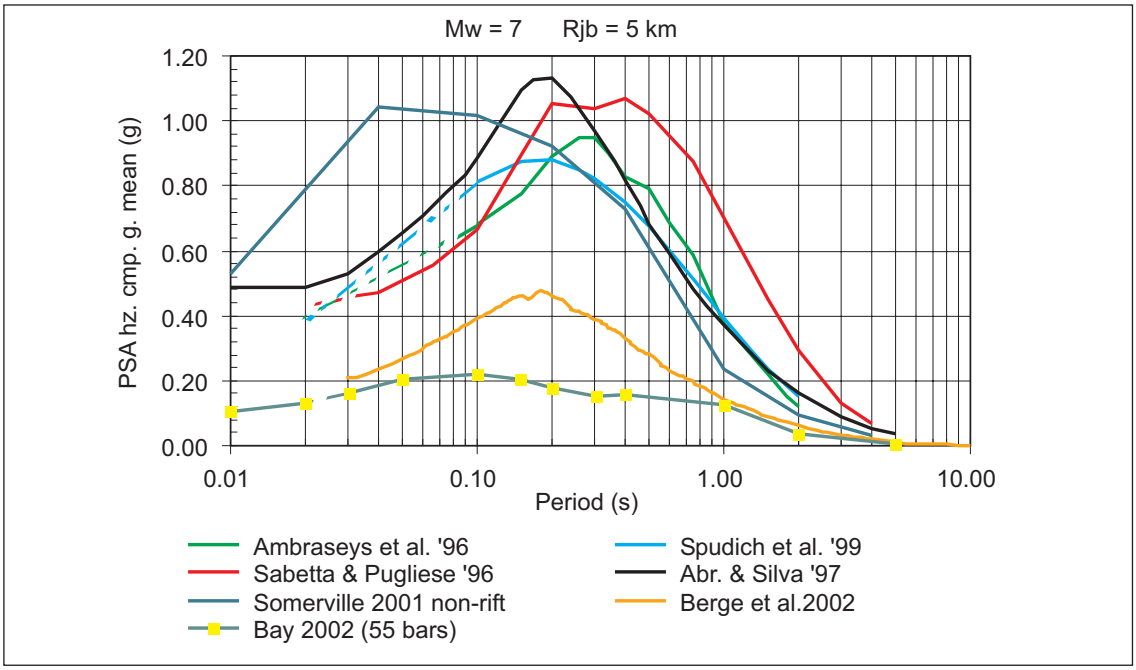

Fig. 7: Acceleration response spectra of the selected models in case of M = 7 and R_{JB} = 5 km

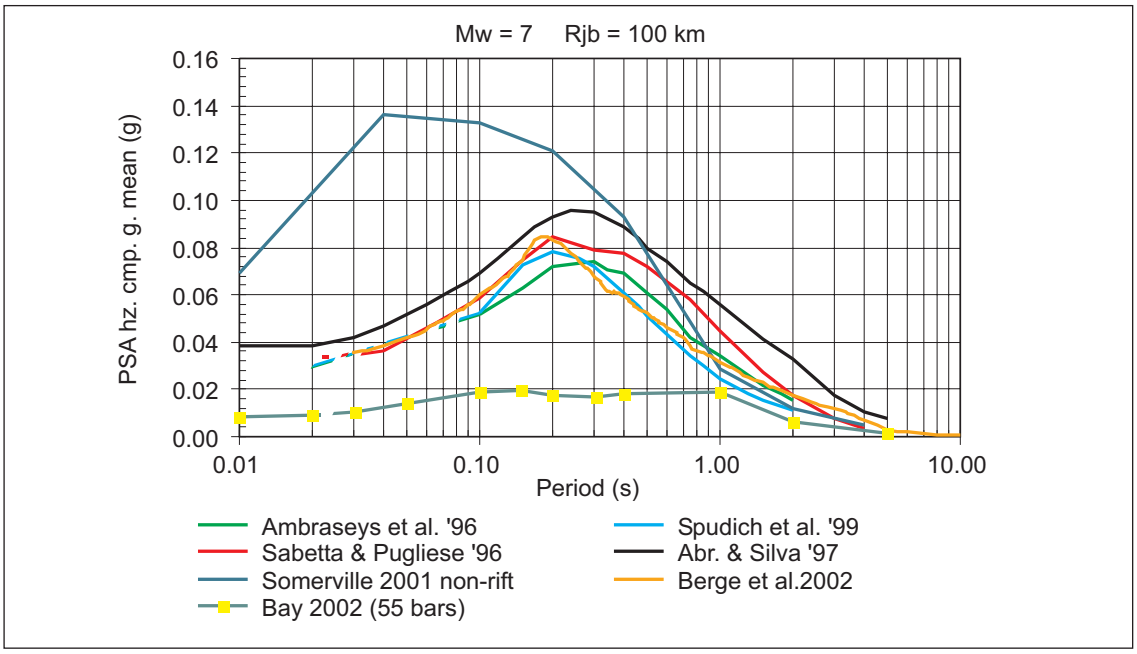

Fig. 8: Acceleration response spectra of the selected models in case of M = 7 and R_{JB} = 100 km

<u>6.5 < M R < 10</u>

- *Lussou* has no data for M > 6.5 *(weight = 0)*.
- *Sabetta* and *Spudich* include only data with magnitude up to 6.8-6.9 (*lower weights*).

- *Lower weights* to models using hypocentral distances (*Berge, Bay*) because for large faults and short distances they can bring to a considerable overestimation.
- *Lower weight* to *Bay* because is badly calibrated for high magnitudes.

6.5 < M 10 < R < 70 and R > 70

Increasing with distance the weights of *Berge, Somerville* and *Bay* for the reasons explained previously.

3.2.3 Summary of Weights as function of magnitude and distance

Table 4 summarizes the weights chosen for the 8 selected horizontal models as a function of magnitude and distance.

Tab. 4: Weights of the horizontal selected models as a function of magnitude and distance

Attenuation model	$M_w < 5.5$			$5.5 < M_w < 6.5$			$M_w > 6.5$		
	$R_{JB} < 10$	$R_{JB} < 10$	$R_{JB} > 70$	$R_{JB} < 10$	$R_{JB} < 10$	$R_{JB} > 70$	$R_{JB} < 10$	$R_{JB} < 10$	$R_{JB} > 70$
Ambraseys et al. (1996)	0.11	0.12	0.12	0.12	0.12	0.12	0.16	0.15	0.14
Berge-Thierry et al. (2000)	0.16	0.15	0.14	0.15	0.15	0.14	0.16	0.17	0.17
Sabetta & Pugliese (1996)	0.10	0.10	0.09	0.09	0.10	0.09	0.10	0.11	0.10
Lussou et al. (2001)	0.12	0.11	0.10	0.09	0.10	0.10	0.00	0.00	0.00
Abrahamson & Silva (1997)	0.14	0.14	0.14	0.15	0.14	0.13	0.19	0.18	0.17
Spudich et al. (1999)	0.08	0.08	0.07	0.11	0.10	0.09	0.12	0.11	0.10
Somerville et al. (2001)	0.07	0.08	0.09	0.09	0.09	0.11	0.11	0.12	0.13
Stochastic-Bay (2002a) *Ainc*	0.11	0.11	0.12	0.09	0.09	0.10	0.07	0.07	0.08
Stochastic-Bay (2002a) *A30*	0.06	0.06	0.07	0.07	0.07	0.08	0.06	0.06	0.07
Stochastic-Bay (2002a) *Y1*	0.05	0.05	0.06	0.04	0.04	0.04	0.03	0.03	0.04
Check: Sum of weights	1.00	1.00	1.00	1.00	1.00	1.00	1.00	1.00	1.00
N° of models- mean weight	8 - 0.12	8 - 0.12	8 - 0.12	8 - 0.12	8 - 0.12	8 - 0.12	7- 0.14	7- 0.14	7- 0.14

3.3 Reference Rock Velocity profiles

The objective is to scale the different attenuation models developed for "rock" conditions, to the reference base rock velocity of 2000 m/s used in SP3 PEGASOS subproject for the computation of local site effects at the different plant sites.

The attenuation models refer to the site conditions indicated in the corresponding paper as "rock" (except Lussou used for site category B $400 < V_s < 800$). This definition (Table 2) is generally based on very poor data (often just a geological description of the site) and rarely are available geotechnical profiles allowing a precise assessment of the shear wave velocity averaged in the upper 30 meters of soil (V_{S30}) that is normally used in the site classification.

Tab. 5: European rock strong motion stations with geotechnical profile

Station Name	Country	Local Geology	Geotech. Profile available?	V_{S30} (m/s)
Kyparrisia	Greece	rock	yes	862
Naghan 1	Iran	rock	yes	757
Arienzo	Italy	rock	yes	912
Auletta	Italy	rock	yes	1092
Bagnoli-Irpino	Italy	rock	yes	1109
Bisaccia	Italy	rock	yes	958
Sannicandro	Italy	rock	yes	840
Sturno	Italy	rock	yes	1100
Tarcento	Italy	rock	yes	847
Tolmezzo-Base Diga	Italy	rock	yes	1043
Tolmezzo	Italy	rock	yes	1021
Hercegnovi Novi	Yugoslavia	rock	yes	834
Ulcinj-Hotel Albatros	Yugoslavia	rock	yes	1083
Mean value				958

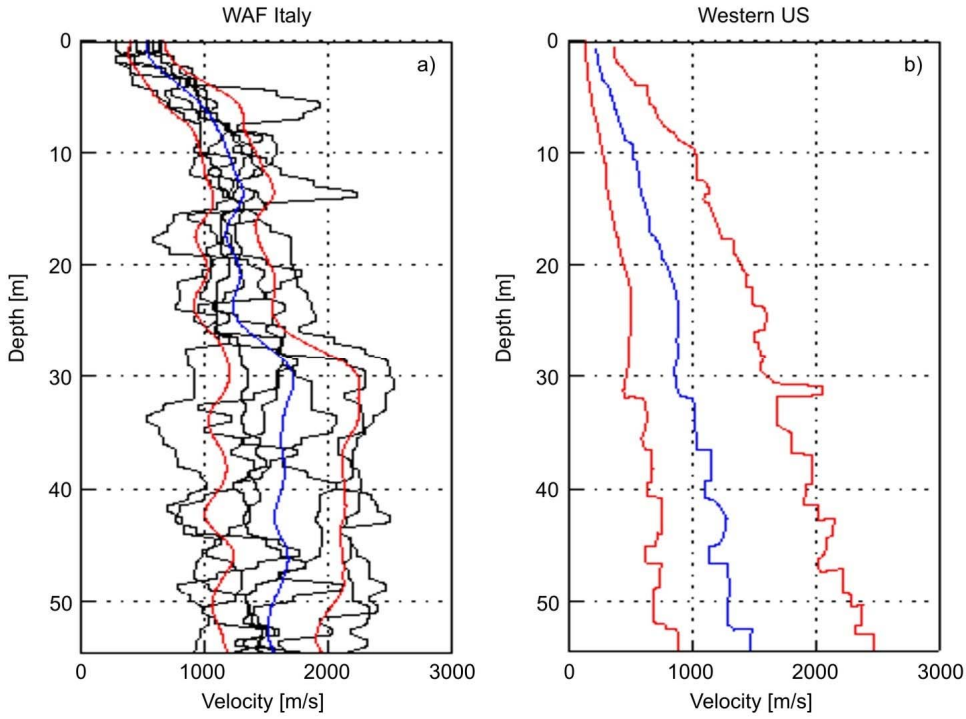

Fig. 9: Shear wave velocity profiles of s.m. stations on rock: a) 9 Italian stations; b) mean values of about 50 WNA stations

Black = observed data; blue = mean profile; red = standard deviation (from PEGASOS TP2-TN-0254, 2002).

For the thirteen European strong motion stations providing a geotechnical profile, the mean V_{S30} value, as shown in Table 5 and Fgure 9a is 958 m/s. If we include further 22 stations without geotechnical profile but with some estimated V_{S30} (PEGASOS TP2-TN-0254; 2002), the mean value becomes 1234 m/s. The authors of the corresponding models declare that rock sites correspond to V_{S30} > 750-800 m/s. In case of the WNA stations considered as "rock", the mean value of V_{S30} appears to be lower and around 600 m/s. This comes out from the literature (e.g. Boore 1997, Abrahamson & ilva 1997, Spudich at al. 1999, Campbell & Bozorgnia 2002) and from the geotechnical profiles of about 50 stations reported in Fgure 9b (McGuire et al. 2001). However the uncertainty in the above values is very large, considering, particularly in the case of European stations, the very small amount of empirical data available (boreholes).

On this basis, during WS-4, mean values and uncertainty bounds for the V_{S30} of each attenuation model have been agreed among SP2 experts and are reported in Table 6. The only change I made is relative to the Bay model because, on the basis of her assessment of rock sites as corresponding to NERHP class A (> 1500 m/s) or B (760 < V_s < 1500 m/s), I believe that the central V_{S30} must be higher than the 1100 m/s agreed among the experts. The weights assigned are skewned toward high V_{S30} values because I'm personally more confident in slightly higher values (Figure 9 and Table 5) respect to those agreed with the experts.

Tab. 6: V_{S30} values and relative weights for the different attenuation models

Attenuation model	V_{S30} [m/s] lower value Weight = 0.2	V_{S30} [m/s] central value Weight = 0.5	V_{S30} [m/s] upper value Weight = 0.3
Ambraseys et al. 1996	550	800	1200
Berge-Thierry et al. 2000	550	800	1200
Sabetta & Pugliese 1996	700	1000	1300
Lussou et al. 2001 (site categ. B)	350	500	900
Abrahamson & Silva 1997	450	600	900
Spudich et al. 1999	550	800	1100
Somerville et al. 2001	-	2800	-
Stochastic-Bay, 2002a (foreland)	750	1500	2000

19 "generic rock profiles" have been calculated (PEGASOS TP2-TN-0363; 2003) on the basis of the work on "site amplification for generic rock sites" carried out by Boore and Joyner (Boore and Joyner, 1997). The profiles are characterized by a base rock velocity of 2000 m/s and a surface V_{S30} velocity varying from 350 to 1500 m/s in steps of 50 m/s. An example is given in Figure 10. The uncertainty is linked to the Vs behavior at depths lower than 30 m because very few of the boreholes of the USGS database used by Boore and Joyner reach a depth larger than 20 – 30 m. However the change in the profile's shape below 30 m affects the scale factors (see PEGASOS TP2-TN-0350; 2003) much less than the uncertainty in the V_{S30} values reported in Table 6.

The scale factors to the reference base rock velocity of 2000 m/s are provided in TP2-TN-0363 through the use of a 1D program identical to SHAKE and a set of 15 accelerograms for each profile. An example, in case of scaling from 600 to 2000 m/s, is provided in Figure 11.

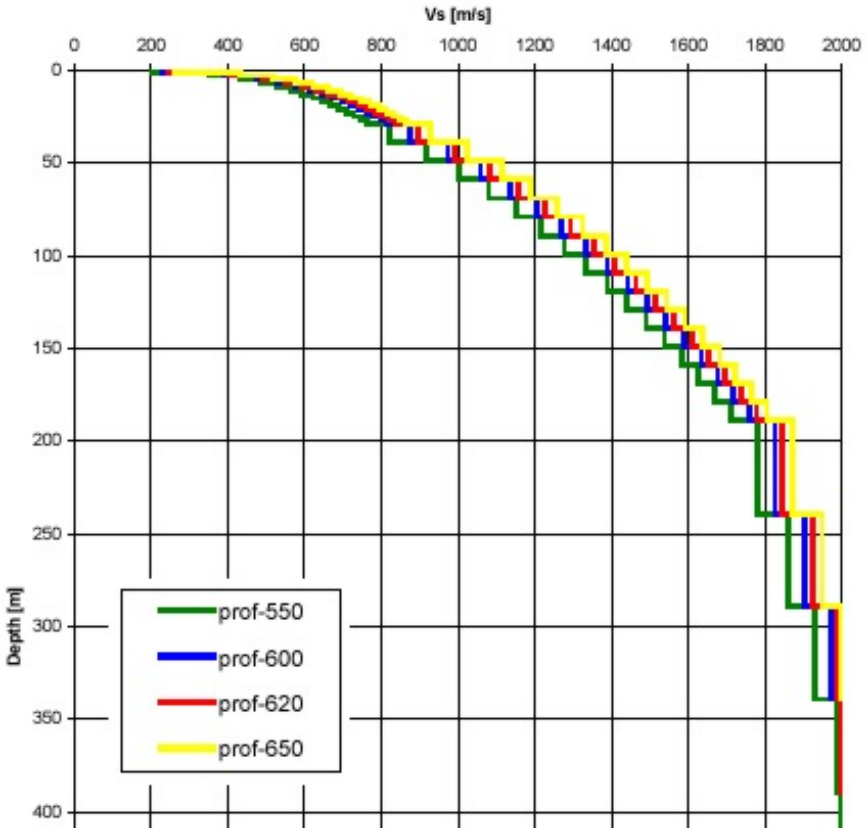

Fig. 10: Generic rock profiles corresponding to different V_{s30} values (from TP2-TN-0363)

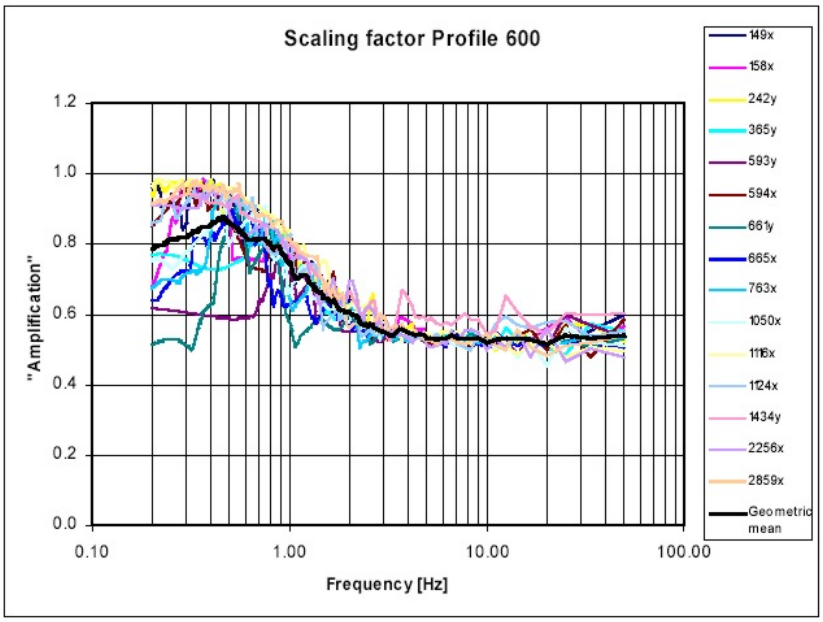

Fig. 11: Scaling factor from 600 to 2000 m/s (from TP2-TN-0363)

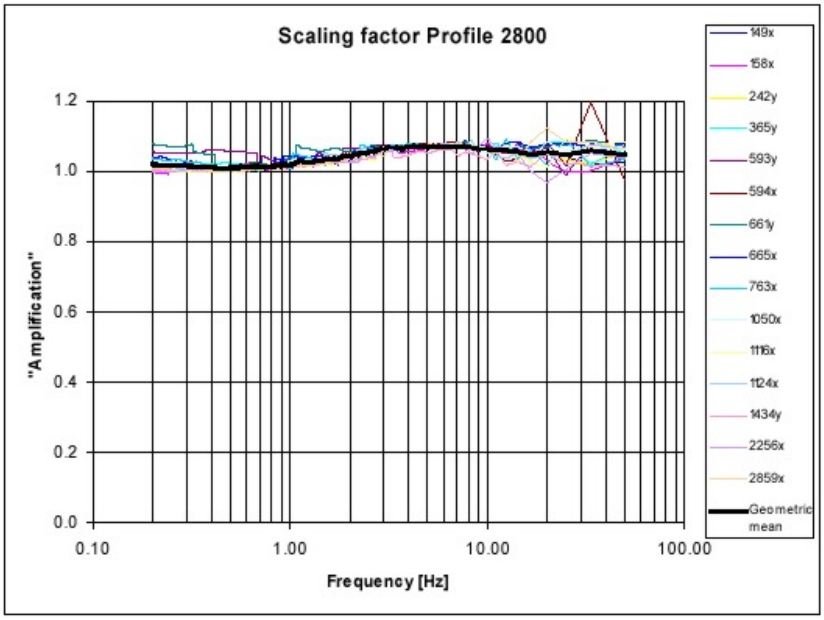

Fig. 12: Scaling from 2800 to 2000 m/s (from TP2-TN-0363)

No "kappa" corrections have been applied because I believe that it's implicitly included in the Vs correction. As shown in Silva et al. (1998), there is a negative correlation between kappa and Vs and the trend obtained from WNA rock sites, even if the data are very scattered, provides values in good agreement to the values used in different models according to the different rock conditions (kappa ~ 0.007 at 2800 m/s; kappa ~ 0.015 at 1500 m/s; kappa ~ 0.04 at 600 m/s). Besides, the scale factor for the only model providing a very different kappa value (Somerville) is very close to unity, as expected if changing V_{S30} from 2800 to 2000 m/s, and as illustrated in Figure 12.

In conclusion the site correction for the different attenuation models can be performed using the values and weights reported in Table 6 and the mean scale factors provided in TP2-TN-0363 as a function of frequency.

3.4 Adjustments of proponent models to Swiss conditions

As discussed previously, Switzerland has no strong ground motion recordings, at least in the meaning of recordings coming from high magnitude earthquakes (M > 5) or characterized by high PGA (> 0.01 g). Currently in the PEGASOS WAF database (Smit et al. 2002) there are 114 time-histories (recorded by strong motion SM, broadband BB, or short-period SP instruments) from Swiss "rock" sites, covering the magnitude range of 1.4 to 4.9 and epicentral distance range of 9 km to 104 km (Smit 2002). However only 11 % of the horizontal and 3 % of the vertical acceleration time histories are fulfilling the criteria indicated (Smit 2002, Bay 2002b) to consider a reliable strong motion record, that is a PGA larger than 0.01g and a frequency range of about 0.5-5 Hz.

Considering the lack of strong motions, a good approach could be represented by the *Hybrid Empirical Approach* suggested by Campbell (2001). The scaling factors are derived from the ratio of theoretical simulation models (e.g. stochastic point source) developed for a "host region" (where the seismological parameters, as stress drop, are well constrained by strong motion data) and for a "target region" (where the seismological parameters can be derived from weak motion data). However, the Hybrid Approach is just a work hypothesis that hasn't yet been proved.

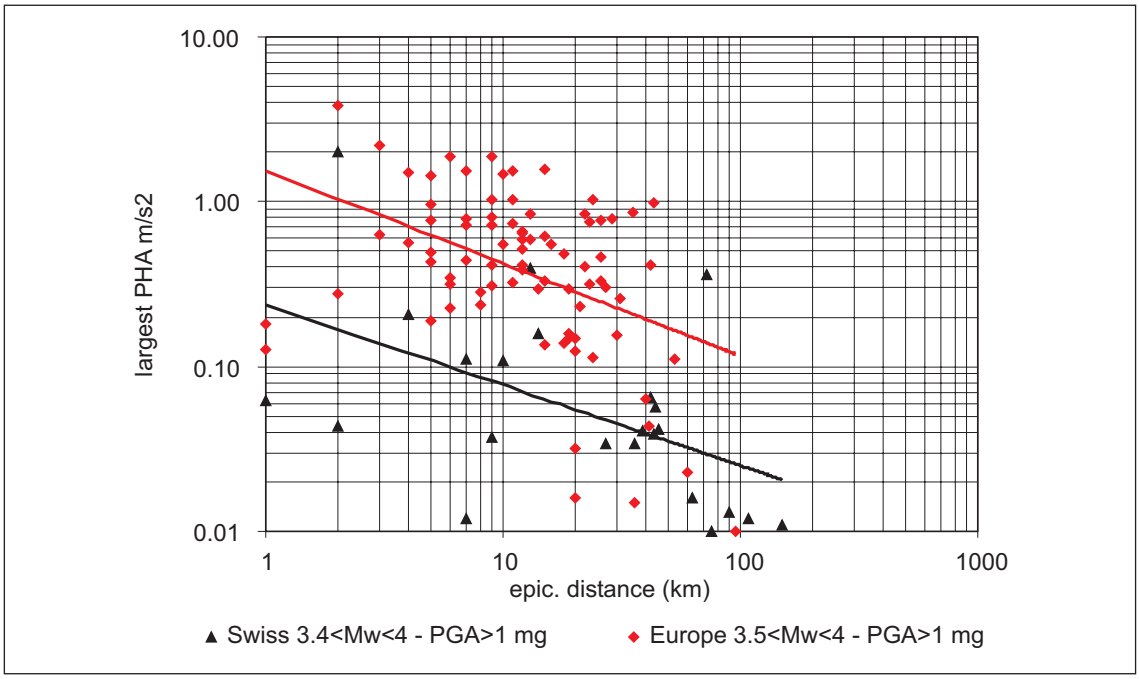

Fig. 13: Comparison of PGA values between Switzerland and Europe in the M range 2.5 – 4.0

No site selection applied. Straight lines represent the regression performed on the data.

In particular, the issue is related to the possibility of using weak ground motion recordings to calibrate models aimed to work for high magnitude earthquakes. As shown in the report of Ann Becker (Becker 2003), many of the small magnitude California data, recorded at hard rock sites, do not even show an omega-squared spectral shape. (The conclusion is however that small magnitude California earthquakes are consistent with low stress drops around 10 bars similar to those found by Bay). Results of papers using weak motion data to calibrate point source stochastic models (Bay 2002a, Rietbrock 2002, Malagnini et al. 2000) show a large variation of the model parameters (in particular stress drop, Q, and K) even for adjacent regions. As noted by Francesca Bay (pp. 52-53 of Bay 2002a) "sizable changes in model parameters can result in only small changes of the residuals. A wide range of models can fit the data almost equally well".

An hybrid empirical model for Switzerland has been developed by the TFI using the results of Bay 2002a. At a first approach this model seems to over predict the Central Europe strong motion data (TP2-TN-0257) but, as discussed afterwards, this is mainly due to the lack of a quality selection in those data.

As shown in Figure 13, the Swiss PGA data extracted from the PEGASOS WAF database (Smit et al. 2002) in the magnitude range 3.5 – 4.0, where there are enough data to be compared with the European ones, seem to provide lower values. I underline "seem" because there are several reasons that can explain this behavior (see also Bay 2002b, 2002c):

1. No quality selection criteria, as discussed above, have been applied to the PEGASOS WAF data. An example is reported in Figure 14, where a record looking like a "white noise", with a PGA of about 1.4 mg and a very low signal to noise (S/N) ratio is shown. The most critical step in developing strong motion attenuation models, is the selection of the data: check of the quality of the record (S/N ratio) and reliability of magnitude, distance and site

evaluations. This is a very time-consuming job that can not be performed when implementing a large database coming from several Institutions. I therefore rely more on the empirical models available in the literature and implemented with smaller sub-sets of the whole database.

2. Swiss s.m. data are in fact weak motions (magnitude not higher than 4 except 2 records of M = 4.9).
3. The difference in magnitude scales ($M_w - M_s$) becomes very important at low M.
4. The recording instruments of Swiss data are often short period seismometers or broadband instruments installed on very hard rock conditions and sometimes underground (tunnels and vaults).
5. The s.m. recordings are biased to high values respect to the weak motions due to the trigger threshold.
6. If a quality selection criterion is applied to the PEGASOS WAF data, the comparison with the stochastic point source model developed for Switzerland (Bay 2002a) becomes quite reasonable: as shown by the residuals plots reported in Figure 15, only the BB data show significantly lower values respect to the model (Bay 2002b).

Furthermore our predictions are requested for high magnitudes (M > 5) and the empirical models are not calibrated for M < 4. There is no plausible reason for which, if Swiss s.m. network recorded a M > 5 earthquake, the s.m. data wouldn't be similar to those recorded in other parts of the world, provided that they are coming from reasonably similar tectonic conditions and velocity models.

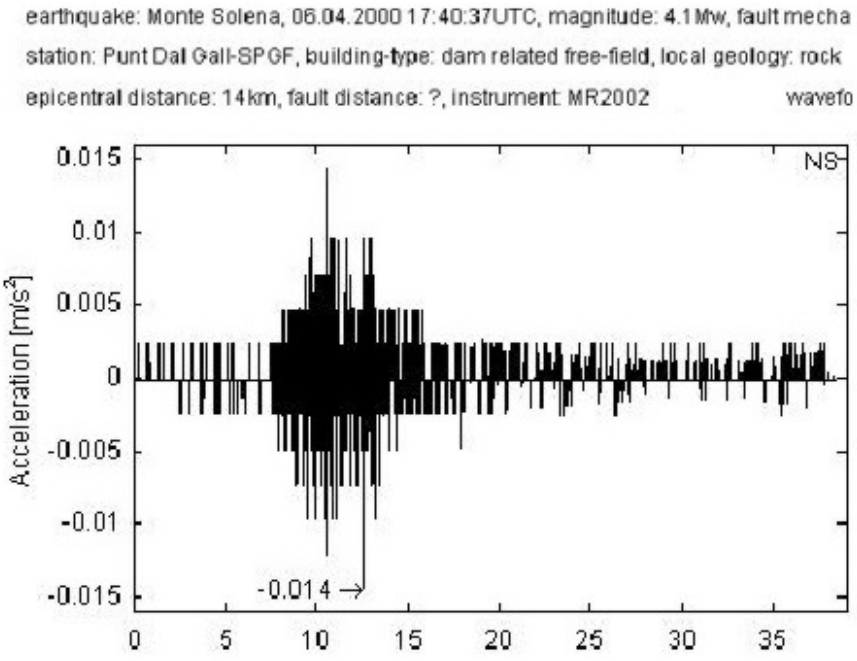

Fig. 14: Example of a Swiss s.m. record included in the PEGASOS WAF database

The better proof of the last sentence (I wrote it in December 2002 in the first elicitation summary) has been given by the strong motion data recorded during the St. Dié earthquake. This event happened on February 22 2003 in the Vosges mountains, at about 120 km NW of Basel, with $M_w = 4.8$. The PGA values recorded during the St. Dié earthquake (TP2-WAF-0009) are compared in Figure 16 with some of the empirical attenuation models calculated for $M_w = 4.8$ and scaled to the largest horizontal component.

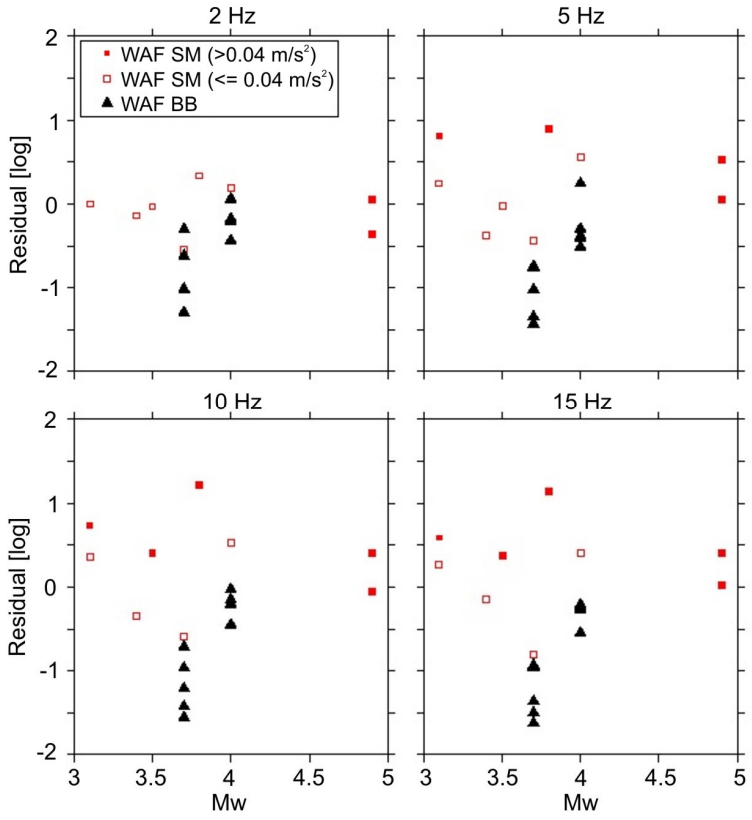

Fig. 15: Residuals of SM and BB data of the PEGASOS WAF database respect to the A_{inc} *model* (NEHRP site class B (developed by Bay (Bay 2002b)

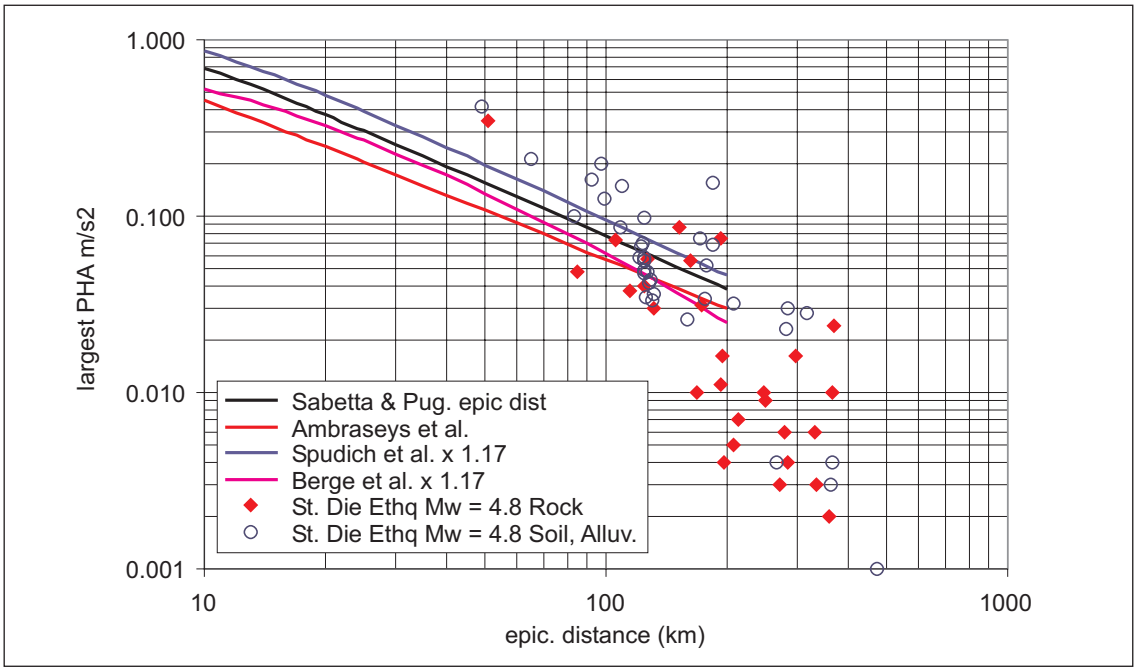

Fig. 16: Comparison of some of the empirical attenuation models (corrected for M, R and largest hz. comp.) with the PGA values recorded during the St. Dié Feb-22-2003 earthquake

Unfortunately most of the St. Dié data are relative to distances higher than 100 – 200 km where the empirical models are not supposed to work. However, it is quite evident that the empirical models fit reasonably well "Swiss" data for an earthquake of magnitude close to 5. The same conclusion can be drawn from the PEGASOS report TP2-TN-0367, where the updated St. Dié data are compared with all the GM models at several frequencies.

The conclusion, for all the reasons discussed above, is not to include any adjustment of the empirical models to Swiss conditions.

3.5 Magnitude conversions

The magnitude scale selected in the PEGASOS Project is the moment magnitude M_W. Magnitude conversions are therefore needed for the attenuation relations not employing M_W. Considering the comparison shown in Figure 17 between different magnitude scales, it follows that, for the intermediate magnitude range (5 – 7) considered in the Project, the magnitude conversions will have a very little impact in the final hazard calculations.

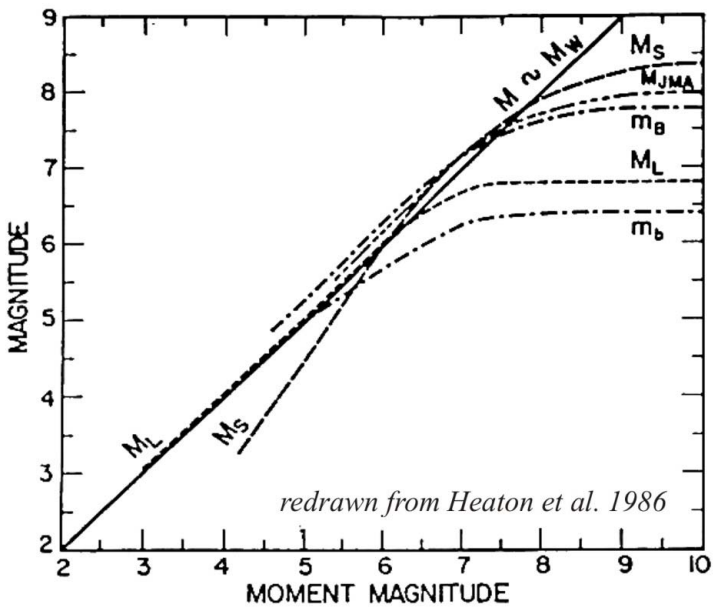

Fig. 17: Comparison of different magnitude scales

3.5.1 $M_W - M_s$ (applies to Berge-Thierry et al. 2000; Ambraseys et al. 1996)

As shown in Figure 18, the difference between M_w and M_s becomes of some relevance only for $M < 5.5$ and the distinction between different $M_w - M_s$ conversions is absolutely negligible up to magnitudes lower than 4, well outside the M range in which we are interested. The conversions selected and the relative weights are reported in Table 7.

3.5.2 $M_W - M_L$ (applies to Sabetta & Pugliese 1996)

The double scale (M_L if < 5.5; M_s if ≥ 5.5) adopted in this relation, as shown in Figure 17, is expressly conceived to linearize with M_W. Therefore no correction is required.

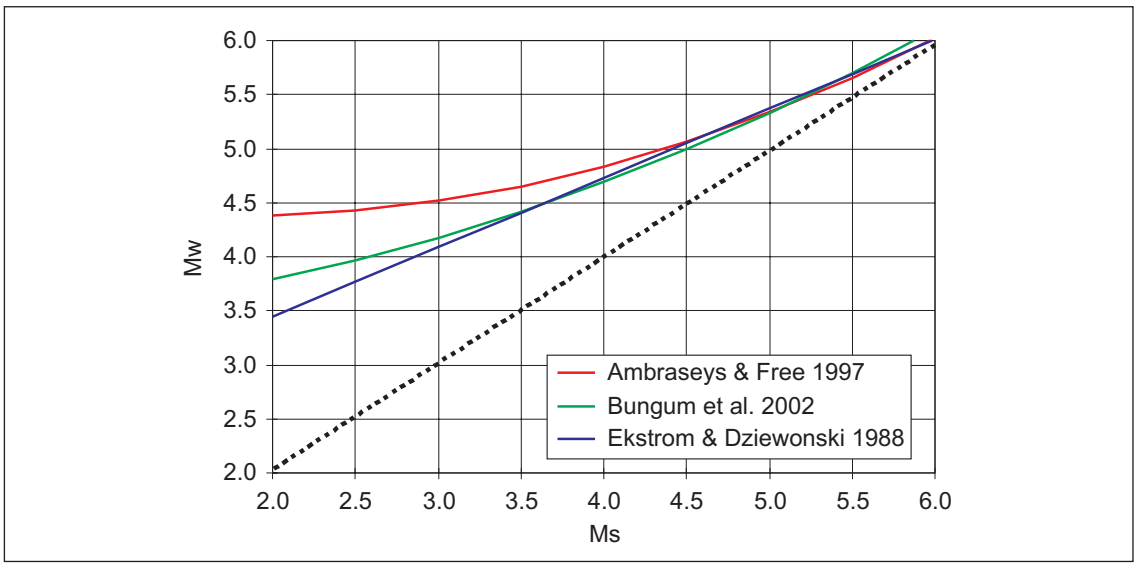

Fig. 18: Comparison of different M_W – M_S conversions

Tab. 7: M_W to M_S conversion relations

Conversion relation		Weight
Free (1996)	M_S = -3.872 +2.071 M_w – 0.076 M_w**2	0.333
Bungum et al. (2002)	for $M_S \leq 6.5$ M_S= -7.176 +3.062*M_W – 0.148*M_W**2 for $M_S > 6.5$ $M_S = M_W$	0.333
Ekström & Dziewonski (1988)	for $M_S \leq 6.1$ M_S = -3.391 + 1.563*M_W for $M_S > 6.1$ $M_S = M_W$	0.333

3.5.3 M_W – M_{JMA} (applies to Lussou et al. 2001)

Some relations indicate $M_W = M_{JMA}$, whereas some others (Fukushima 1996), as shown in Figure 19, indicate slightly higher values of M_{JMA} respect to M_W in the intermediate M range. The conversions selected and the relative weights are reported in Table 8.

3.6 Component conversions

As established in the note PMT-AN-0195 "the hazard will be computed for the geometric mean of the two horizontal components" of the ground motion. The different definitions of the horizontal component normally adopted in the spectral attenuation relations are the following (PEGASOS TP2-TN-0269, 2002):

- *Larger PGA*: the highest PHA value of the two horizontal components is identified and the response spectrum of that component is taken as the larger.
- *Larger envelope*: the response spectra of both components are compared at each individual frequency and the envelope of these two spectra is taken as the larger.

– *Geometric mean*: the geometric mean of the two spectra
– *Random*: one of the two component is randomly selected
– *Both*: both components are taken and considered to be independent.

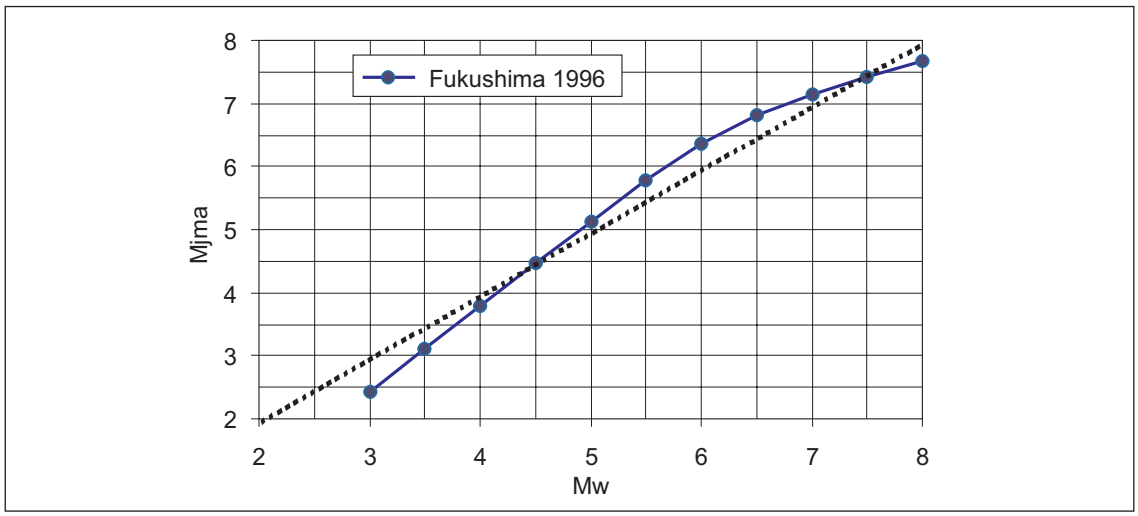

Fig. 19: M_{JMA} versus M_W (conversion of Fukushima 1996)

Tab. 8: M_W to M_{JMA} conversion relations

Conversion relation		Weight
$M_W = M_{JMA}$		0.5
Fukushima (1996)	$M_{JMA} = 1/1.10\ [-17.92 - \log(Mo^{-1} + 10^{-17} \cdot Mo^{-1/3})]$ $Mo = 10^{1.5\,(Mw+10.7)}$ (Mo in dyne·cm)	0.5

Figure 20 (PEGASOS TP2-TN-0269; 2002) shows the ratios between the different definitions given above, calculated from the PEGASOS WAF data, as a function of the spectral period. It's evident that the differences between *geometric mean*, *random*, and *both* are negligible, so that no conversion is needed to make them consistent. Only two of the selected relations (Table 2) are relative to largest horizontal component and are respectively Ambraseys et al. (*larger envelope)* and Sabetta & Pugliese *(larger PGA)*. The range of values and the corresponding weights selected for the horizontal component conversion are reported in Table 9.

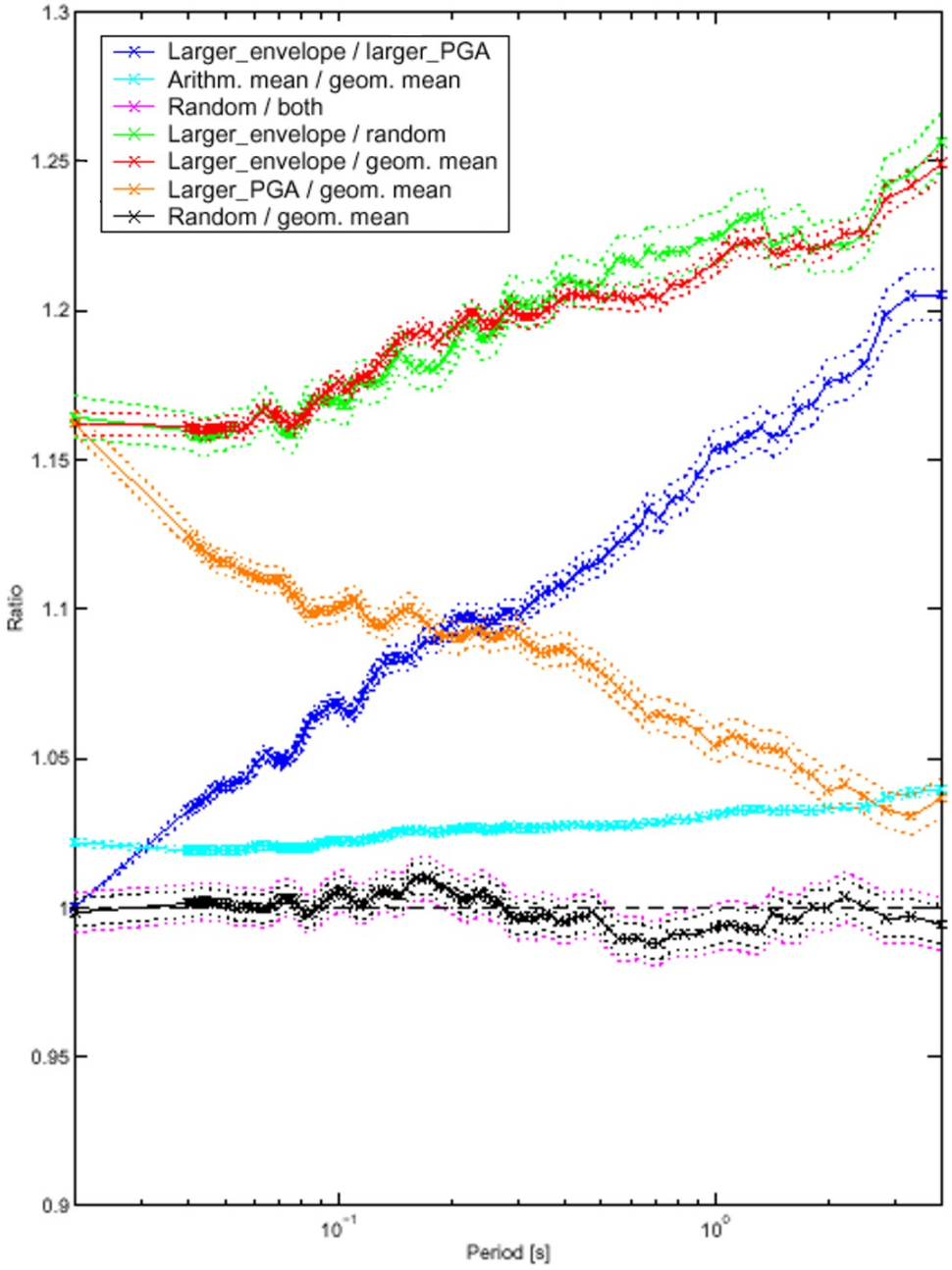

Fig. 20: Rations between different definitions of the horizontal component as a function of the spectral period (from PEGASOS TP2-TN-0269)

Tab. 9: Scale factors for horizontal component conversion

Frequency (Hz)	Larger_PGA/geom. mean (Sabetta & Pugliese)			Larger_envelope/geom. mean (Ambraseys et al.)		
	W = 0.2	W = 0.6	W = 0.2	W = 0.2	W = 0.6	W = 0.2
0.50	0.93	0.96	0.99	0.79	0.82	0.84
1.00	0.92	0.95	0.98	0.80	0.82	0.85
2.50	0.89	0.92	0.95	0.81	0.83	0.85
5.00	0.89	0.92	0.94	0.81	0.84	0.86
10.00	0.88	0.91	0.94	0.82	0.85	0.88
20.00	0.87	0.90	0.92	0.83	0.86	0.89
33.00	0.86	0.89	0.92	0.83	0.86	0.89
50.00	0.83	0.86	0.89	0.83	0.86	0.89
PGA	0.83	0.86	0.89	0.83	0.86	0.89

3.7 Missing frequencies

As reported in PEGASOS TP2-TN-0270 (2002), according to the new project specifications (UAK, 2002) hazard will have to be computed for the spectral frequencies: 0.5 Hz, 1 Hz, 2.5 Hz, 5 Hz, 10 Hz, 20 Hz, 33 Hz, 50 Hz and for PGA. Not all the candidate ground motion models offer coefficients corresponding to these frequencies.

In the same document a stepwise linear interpolation of the coefficients is presented as a two-step procedure. First step: if coefficients for 50 Hz were missing they were set equal to those at PGA; if PGA was not available, coefficients at the maximum available frequency were used for all higher frequencies including PGA. Second step: coefficients at missing frequencies were interpolated between their two nearest neighbors. Linear interpolation was performed in the log10-lin space. The above mentioned interpolation procedure can be used without further modifications and the availability of the coefficients for different attenuation relations is presented in Figure 21.

3.8 Style-of-faulting adjustments

A specific request has been made after Workshop 4 to provide, for each attenuation relation, appropriate scale factors for normal, strike-slip, and reverse faulting earthquakes.

In case of reverse and thrust faulting there is clear evidence (Boore et al. 1997, Abrahamson & Silva 1997, Campbell & Bozorgnia 2002) that the ground motion shows higher amplitudes respect to strike-slip faulting, as shown in Figure 22. This trend is consistent with the expectation that reverse- and thrust-faulting earthquakes, especially from blind thrust faults, might have higher dynamic stress drops than strike-slip and normal-faulting earthquakes. The difference is clearly period-dependent showing the higher values at short-to-mid periods and becoming negligible at periods greater than about 2 sec.

Frequency [Hz]	0.5	1	2.5	5	10	20	33	50	PGA
Abrahamson and Silva, 1997	a	a	a	a	a	a	a	a	a
Ambrayses and Douglas, 2000	a	a	a	a	a	i	i	o	a
Ambrayses et al., 1996	a	a	a	a	a	i	i	o	a
Ambrayses and Simpson, 1996	a	a	a	a	a	i	i	o	a
Atkinson and Boore, 1997	a	a	i	a	a	a	i	o	a
Berge-Thierry, 2000	a	a	a	a	a	a	a	33	33
Boore et al., 1997	a	a	a	a	a	i	a	i	a
Campbell and Bozorgnia, 2002	a	a	a	a	a	a	i	o	a
Lussou et al., 2001	a	a	a	a	a	a	a	a	50
Sabetta and Pugliese, 1996	a	a	a	a	a	i	i	o	a
Somerville et al., 2001	a	a	a	a	a	i	i	o	a
Spudich et al., 1999	a	a	a	a	a	i	i	o	a
Toro et al., 1997	a	a	a	a	a	i	i	o	a

a Coefficients are available
i Coefficients are missing and interpolated
o Coefficients are missing and set equal to those at PGA
33 Coefficients are missing and set equal to those at 33 Hz
50 Coefficients are missing and set equal to those at 50 Hz

Fig. 21: Availability of coefficients of attenuation models at frequencies of interest (from PEGASOS TP2-TN-0270)

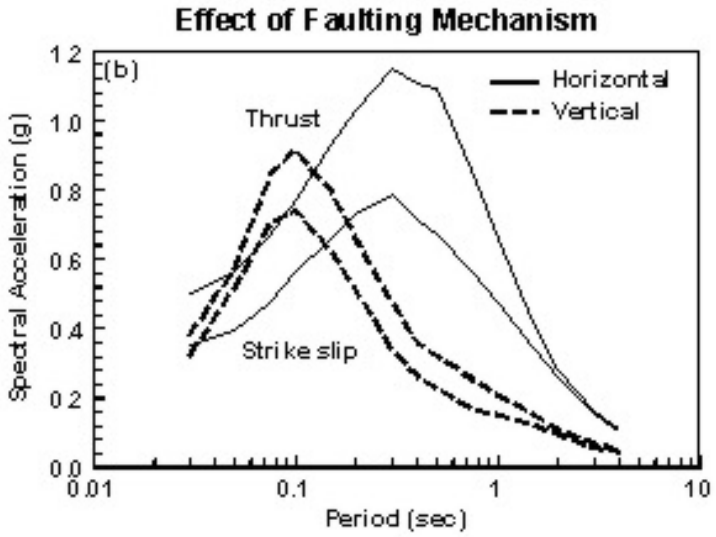

Fig. 22: Response spectra corresponding to different faulting mechanism (from Campbell & Bozorgnia 2002)

The three relations mentioned before provide a scale factor between reverse and strike slip faulting mechanism that, as shown in Figure 23, in case of Abrahamson & Silva exhibits also a significant magnitude dependence. However, as recognized by the authors, the strong increase in the scale factor for $M < 5.8$ is "driven by the Coalinga aftershock sequence that produced larger than average high frequency motion". I will therefore consider, also for Abrahamson & Silva, a magnitude-independent scale factor corresponding to $M \geq 6.4$ which seems to be closer to the results of Boore et al. and Campbell & Bozorgnia. From the results of Figure 23, I derived

the median scale factors and the corresponding uncertainty illustrated in Table 10 for three different frequency intervals.

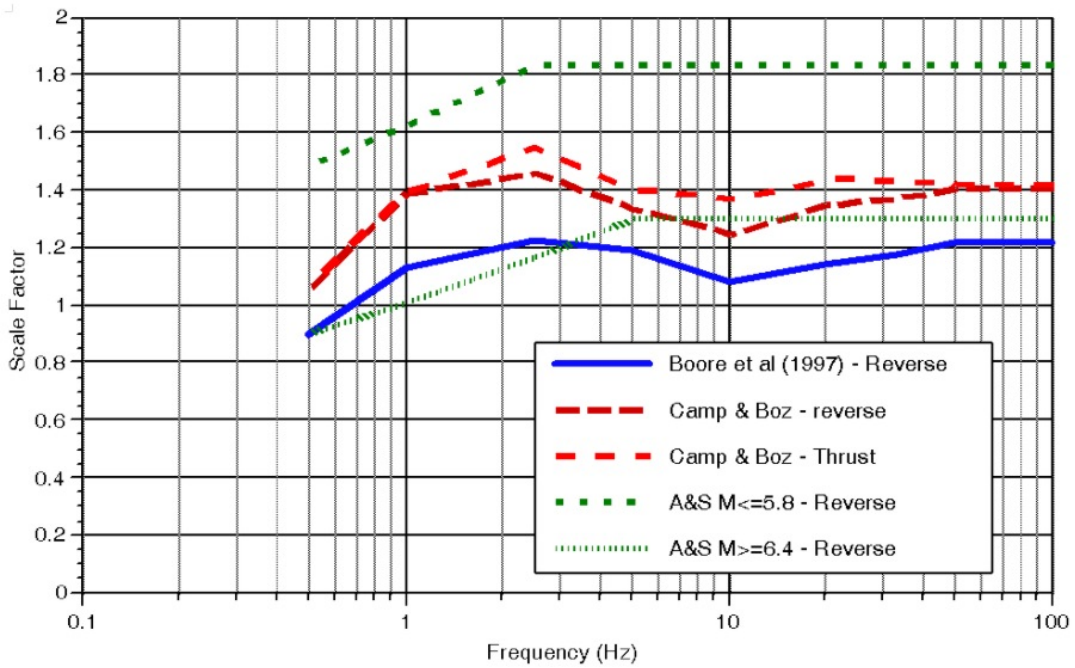

Fig: 23: PSA rations between reverse and strike slip faulting mechanisms of the horizontal components according to the available empirical models (from Abrahamson, April 2003 presentation)

The frequency intervals have been selected in order to reduce the complexity of the model and the ranges of frequencies are chosen mainly based on the behavior of A&S M ≥ 6.4 (green dashed line) in Figure 23. At frequencies > 5 Hz there is no frequency dependence, the mean scale factor is about 1.3 and, allowing for a slight higher epistemic uncertainty respect to the values of Campbell and Boore reported in Figure 23, the lower and upper values have been selected as 1.1 and 1.5. The interval 0.5 – 5 Hz shows a nearly constant decrease of the scale factor with frequency and has been subdivided in two branches. In the 2 – 5 Hz interval, the central value is about 1.2 and, taking the lowest and highest value of the different curves inside the interval, we get 1.1 and 1.5; 1.1 has been lowered to 1.0 to keep the frequency decrease of the central value. In the 0.5 – 2 Hz interval the central value is about 1.1 and, taking the lowest and highest value of the different curves inside the interval, we get 0.9 and 1.5; again 1.5 is reduced to 1.3 to get a lower value respect to the previous interval and to reflect the frequency decrease.

Tab. 10: Style of faulting scale factors for the horizontal components

	Scale factor from strike-slip to reverse			Scale factor from strike-slip to normal		
	lower value	central value	upper value	lower value	central value	upper value
High frequencies (> 5 Hz)	1.1	1.3	1.5	no freq. Dependence		
Intermediate freq. (2-5 Hz)	1.0	1.2	1.5	0.75	0.85	0.95
Low frequencies (0.5-2 Hz)	0.9	1.1	1.3			

The situation is more complicated when comparing normal to strike-slip faults because of the small amount of strong motion data available for normal faulting earthquakes. In most attenuation relations (e.g. Campbell & Bozorgnia 2002), ground motions for normal faulting earthquakes are assumed to be the same as strike-slip earthquakes. However the growing data set of recordings from normal faulting events indicates that ground motions from normal faulting earthquakes are lower than for strike-slip earthquakes.

Spudich et al. (1999) developed a specific relation for extensional tectonic regimes that, if compared to the Boore et al. relation, shows a scale factor (normal/strike-slip) randomly varying with frequency with a mean value of about 0.9.

Abrahamson & Becker (1999), in the frame of the Yucca Mountain project, use two different approaches based respectively on the computation of residuals for normal faulting events (40 recordings, 9 earthquakes) and on point source stress-drops for normal faulting compared to stress-drops for strike-slip earthquakes. Their recommendation is to use a frequency independent scale factor of 0.8 for frequencies higher than 0.5 Hz.

I therefore considered, as shown in Table 10, a central value of 0.85, corresponding to the mean of Boore and Abrahamson results, with an arbitrarily chosen uncertainty (having no other source of information) of about ± 12 %. The values in Table 10 are only the first step to evaluate, as explained hereafter, the scaling factors of the different faulting mechanisms.

The second issue to face is that most selected attenuation relations, as shown in Table 2, are based on data coming from "mixed" seismotectonic regimes. Just two relations are based respectively on extensional tectonic regimes (Spudich et al. 1999) and on reverse faults (Somerville et al. 2001) and one (Abrahamson & Silva 1997) includes, as already mentioned, a scale factor for reverse faults.

The relative percentage of different faulting mechanisms in each attenuation relation has been quantified by SP2 experts (many of them are authors or co-authors of the relative papers) as reported in PEGASOS TP2-TN-0362. On this basis I attributed to each relation the percentages indicated in Table 11 equally sharing among the three mechanisms the "undefined" style of faulting cases and splitting between the corresponding mechanisms the "oblique", "NML/SS", and "REV/SS" cases.

Figure 24 shows the "relative position" of the attenuation models, on the basis of the fault types percentages and central values of the scale factors reported in Tables 10 and 11. The strike-slip mechanism is assumed as "neutral" (scale factor = 1).

Tab. 11: Percentage of different fault types in the selected relations

Attenuation model	% Strike-slip	% Normal	% Reverse
Ambraseys et al. (1996)	18	33	49
Berge-Thierry et al. (2000)	20	45	35
Sabetta & Pugliese (1996)	7	49	44
Lussou et al. (2001)	62	6	32
Abrahamson & Silva (1997)	scale fact.	0	scale fact.
Spudich et al. (1999)	55	45	0
Somerville et al. (2001)	0	0	100
Stochastic-Bay (2002a)	57	33	10

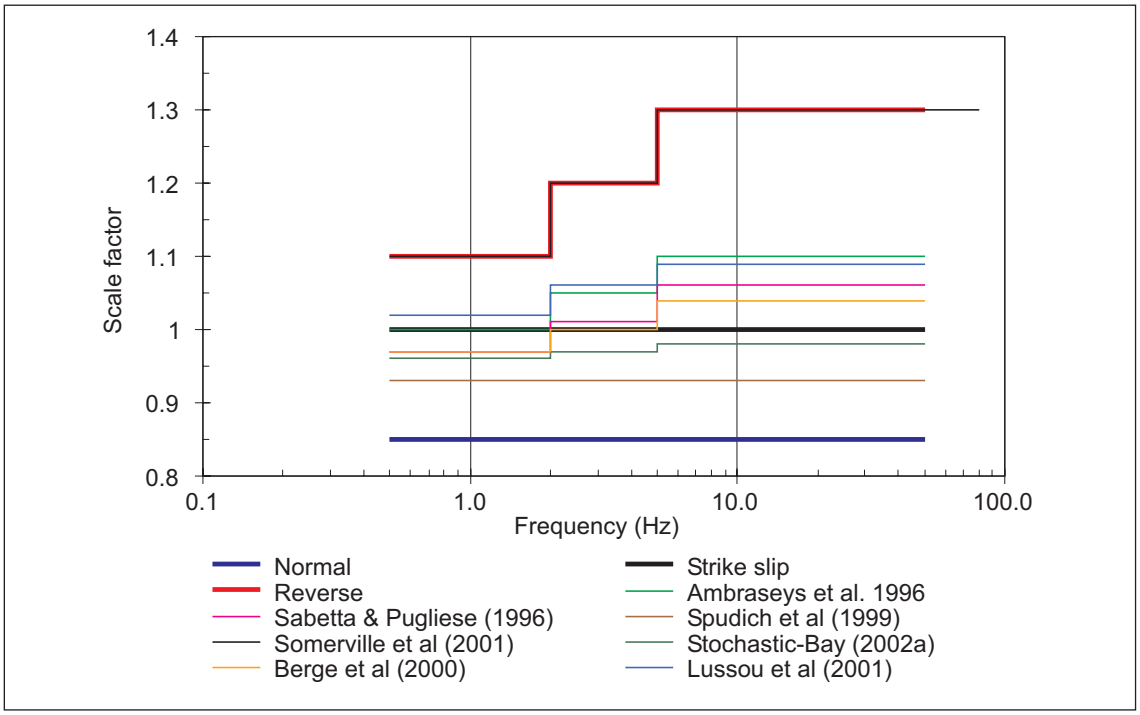

Fig. 24: "Relative position" of the attenuation models, according to the corresponding percentage of fault types, compared to the mean scale factors (bold lines) for reverse, strike-slip (neutral = 1), and normal faults

Tables 12, 13 and 14 provide, respectively in case of normal, strike-slip, and reverse faulting earthquakes, the scale factors to be applied for the attenuation models in different frequency ranges. The epistemic uncertainty in the scale factors is due to the uncertainty in the effect of faulting mechanisms on the ground motion and to the uncertainty in the relative proportion of different fault types in each attenuation model. Having no quantitative information about this latter uncertainty, I arbitrarily chose to fix it at ± 10 % in the lower and upper values of strike slip faulting (Table 13) where the scale factors of Table 10 have no influence.

Tab. 12: Scale factors and relative weights in case of normal faulting (hz. comp.)

	Scale factor 0.5-2 Hz			Scale factor 2-5 Hz			Scale factor > 5 Hz		
Normal Fault	lower W = 0.3	central W = 0.4	upper W = 0.3	lower W = 0.3	central W = 0.4	upper W = 0.3	lower W = 0.3	central W = 0.4	upper W = 0.3
Ambraseys et al. (1996)	0.75	0.85	0.95	0.72	0.81	0.91	0.68	0.77	0.87
Berge-Thierry et al. (2000)	0.78	0.88	0.98	0.75	0.85	0.95	0.72	0.82	0.92
Sabetta & Pugliese (1996)	0.77	0.88	0.98	0.74	0.84	0.94	0.71	0.80	0.90
Lussou et al. (2001)	0.73	0.83	0.93	0.71	0.81	0.90	0.69	0.78	0.87
Abrahamson & Silva 1997 (F = 0 strike-slip)	0.75	0.85	0.95	0.75	0.85	0.95	0.75	0.85	0.95
Spudich et al. (1999)	0.80	0.91	1.02	0.80	0.91	1.02	0.80	0.91	1.02
Somerville et al. (2001)	0.68	0.77	0.86	0.63	0.71	0.79	0.58	0.65	0.73
Stochastic-Bay (2002a)	0.78	0.88	0.99	0.77	0.88	0.98	0.76	0.87	0.97

Tab. 13: Scale factors and relative weights in case of strike-slip faulting (hz. comp.)

	Scale factor 0.5-2 Hz			Scale factor 2-5 Hz			Scale factor > 5 Hz		
Strike-slip Fault	lower W = 0.3	central W = 0.4	upper W = 0.3	lower W = 0.3	central W = 0.4	upper W = 0.3	lower W = 0.3	central W = 0.4	upper W = 0.3
Ambraseys et al. 1996	0.91	1.00	1.10	0.87	0.95	1.05	0.83	0.91	1.00
Berge-Thierry et al. 2000	0.94	1.03	1.14	0.91	1.00	1.10	0.88	0.96	1.06
Sabetta & Pugliese 1996	0.94	1.03	1.13	0.90	0.99	1.09	0.86	0.95	1.04
Lussou et al. 2001	0.89	0.98	1.08	0.86	0.95	1.04	0.84	0.92	1.01
Abrâhamson & Silva 1997 (F = 0 strike-slip)	1.00	1.00	1.00	1.00	1.00	1.00	1.00	1.00	1.00
Spudich et al. 1999	0.97	1.07	1.18	0.97	1.07	1.18	0.97	1.07	1.18
Somerville et al. 2001	0.83	0.91	1.00	0.76	0.83	0.92	0.70	0.77	0.85
Stochastic-Bay 2002a	0.95	1.04	1.15	0.94	1.03	1.13	0.93	1.02	1.12

Tab. 14: Scale factors and relative weights in case of reverse faulting (hz. comp.)

	Scale factor 0.5-2 Hz			Scale factor 2-5 Hz			Scale factor > 5 Hz		
Reverse fault	lower W = 0.25	central W = 0.5	upper W = 0.25	lower W= 0.3	central W = 0.5	upper W = 0.2	lower W = 0.25	central W = 0.5	upper W = 0.25
Ambraseys et al. (1996)	0.90	1.10	1.30	0.95	1.14	1.43	1.00	1.18	1.37
Berge-Thierry et al. (2000)	0.93	1.14	1.34	1.00	1.20	1.50	1.06	1.25	1.45
Sabetta & Pugliese (1996)	0.93	1.13	1.34	0.99	1.18	1.48	1.04	1.23	1.42
Lussou et al. (2001)	0.88	1.08	1.27	0.95	1.14	1.42	1.01	1.20	1.38
Abrahamson & Silva 1997 (F = 1 reverse M_w = 6.5)	1.00	1.00	1.00	1.00	1.00	1.00	1.00	1.00	1.00
Spudich et al. (1999)	0.97	1.18	1.39	1.07	1.29	1.61	1.18	1.39	1.61
Somerville et al. (2001)	0.82	1.00	1.18	0.83	1.00	1.25	0.85	1.00	1.15
Stochastic-Bay (2002a)	0.94	1.15	1.35	1.03	1.24	1.55	1.12	1.33	1.53

In case of Tables 12 and 14, the uncertainty in the effect of faulting mechanisms (upper and lower values of Table 10) is greater than 10 % and therefore overcomes this latter.

The Abrahamson & Silva relation includes a scale factor itself for strike-slip and reverse faulting. This factor should be used, as provided in Eq. 3 and 6 of the corresponding paper, as magnitude independent and only with the values corresponding to $M \geq 6.4$. In case of normal faulting the scale factors of Table 12 apply also to the Abrahamson & Silva relation.

The weighting scheme is slightly different in case of reverse faulting (Table 14), where, due to the large uncertainty in the scale factors of Table 10 particularly at intermediate frequencies, the difference between lower and upper values reaches 50 %; I gave therefore a higher weight to the central values considered more reliable.

4 MEDIAN V/H RATIO

4.1 Approaches for V/H ratios

Within the last decade, several investigators have developed attenuation relations for the horizontal and vertical components of strong ground motion that can be used to evaluate V/H ratios. As shown in Figure 25, for the case of Western U.S., the results are consistent in indicating a strong dependence of V/H on period, with short periods exhibiting higher ratios than long periods.

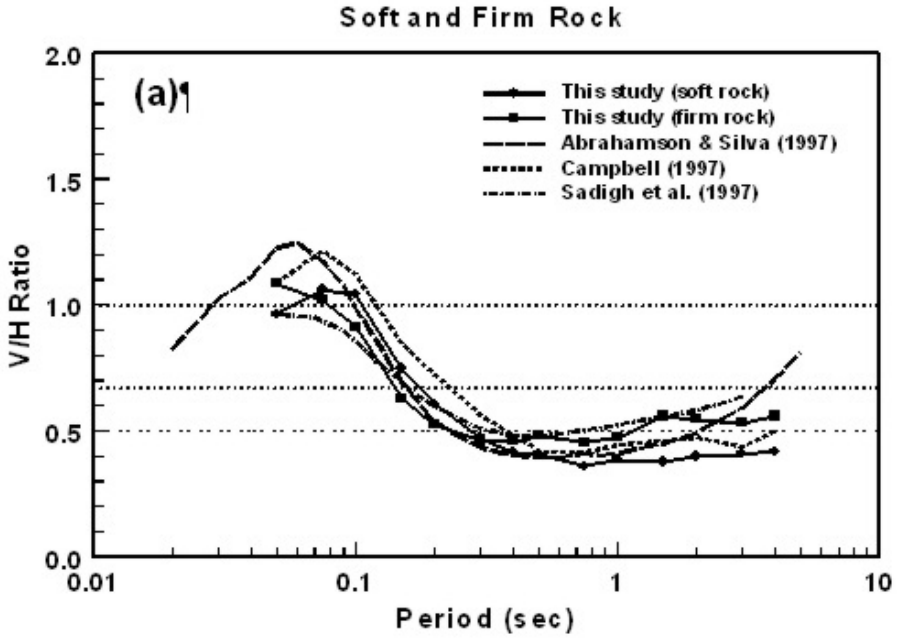

Fig. 25: Comparison of the V/H ratio proposed by Bozorgnia & Campbell (2002) with the results of other WNA relations

The spectra are evaluated for M_w = 7 and R_{rup} = 10 km.

The most recent and accurate study on the V/H ratio is that proposed by Bozorgnia & Campbell (2002). Figure 26 illustrates that the V/H ratio is also dependent on magnitude, distance, site conditions, and faulting mechanism, covering a range of values that may go from 0.3 up to 1.8. It increases with magnitude, decreases with distance and at short periods is higher on soil than on rock, while at long periods is generally higher on rock than on soil.

There are basically two different ways in which the V/H ratios can be obtained:

1. use equations that have been derived to predict directly the V/H ratio;
2. use the estimates from equations that separately predict vertical and horizontal components, and then take the ratio of these at each frequency and for each M-R combination.

The first approach, as discussed in Bozorgnia & Campbell (2002), is "*difficult due to its complex scaling characteristics"*, while a "*statistically robust and unbiased V/H model can be derived from the ratio of the vertical and average horizontal predictive equations"*. Considering that, among the attenuation models selected for the horizontal motions, only Spudich et al. (1999) does not provide vertical relations, the selected approach is the second. The weights of the vertical predictive equations, required to build up the V/H ratio, are provided in section 4.3.

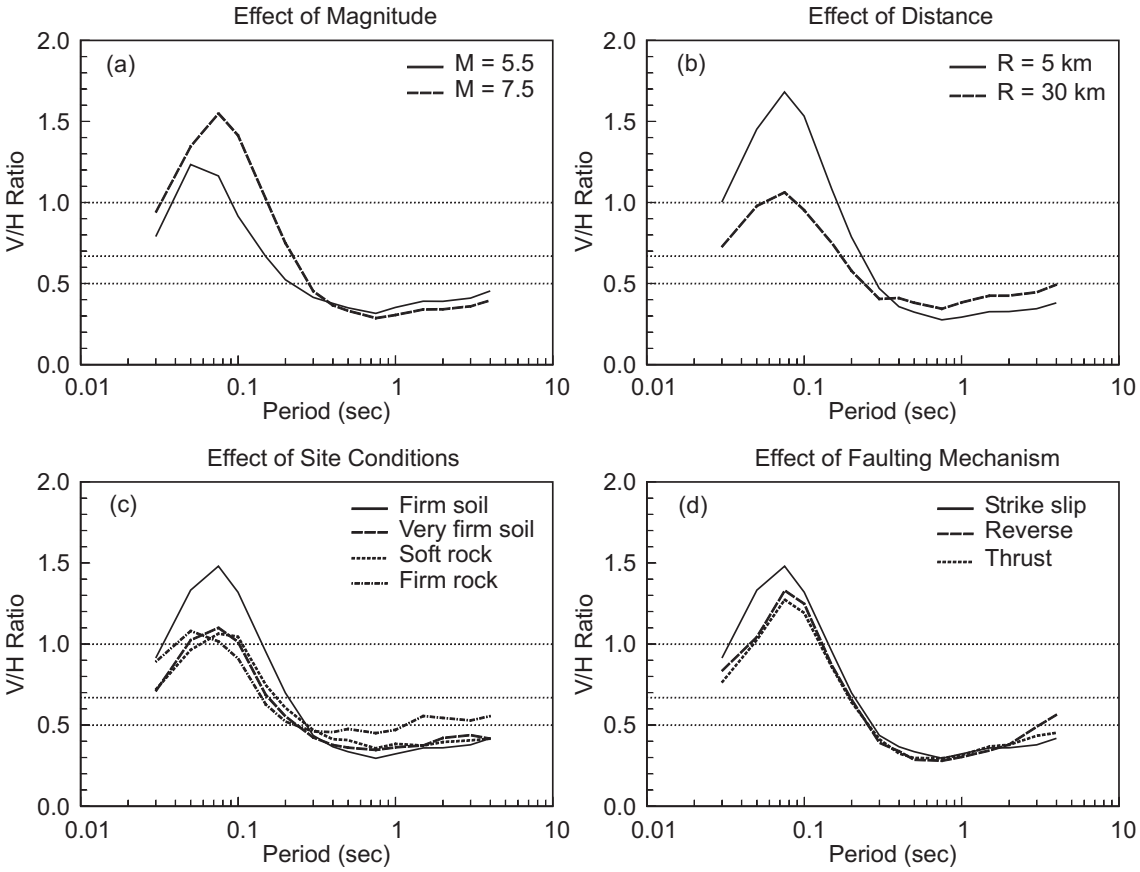

Fig. 26: V / H ratio proposed by Bozorgnia & Campbell (2002) showing the effects of: a) magnitude; b) distance, c) site conditions and d) faulting mechanism

Unless otherwise noted, the V / H is evaluated for $M_w = 7$, $R_{seis} = 10$ km, strike-slip faulting, and firm soil.

4.2 Logic tree structure

The logic tree structure for the vertical components, required to build up the V / H ratio, is the same as that outlined for the horizontal ones (excluding of course the component conversion) except for the site effect and faulting mechanism adjustments. In these cases, as explained in sections 3.3 and 3.8, the corrections employed are not coming from the attenuation equations themselves, so that particular correction factors are required.

4.2.1 Site correction for the vertical components

As discussed previously the site effect in case of vertical motion is generally higher than in case of the horizontal one at short periods, and lower at long periods. Figure 27 shows the V / H ratio of the selected empirical attenuation relations and compares the rock conditions with the soil conditions. The general trend for rock conditions is similar to that shown in Figure 25 for the WNA relations; the differences among the relations are considerable and will be taken into account with the appropriate branching in the logic tree.

The differences between rock and soil are instead similar among the different relations except in case of Abrahamson and Silva. This is better illustrated in Figure 28 where the ratio between the dashed and continuous lines of Figure 27 is shown. Even if the ratio shown in Figure 28 has been developed for soil/soft-rock, lacking other sources of information, I decided to apply it to

quantify the different site effect of the vertical motion also in case of soft-rock/hard-rock. For the sake of simplicity, considering the short range of values, I choose to use the mean value of the empirical attenuation relations (thick line in Figure 28) as reported in Table 15, as the correction factor for the site effect to be applied to the vertical motion.

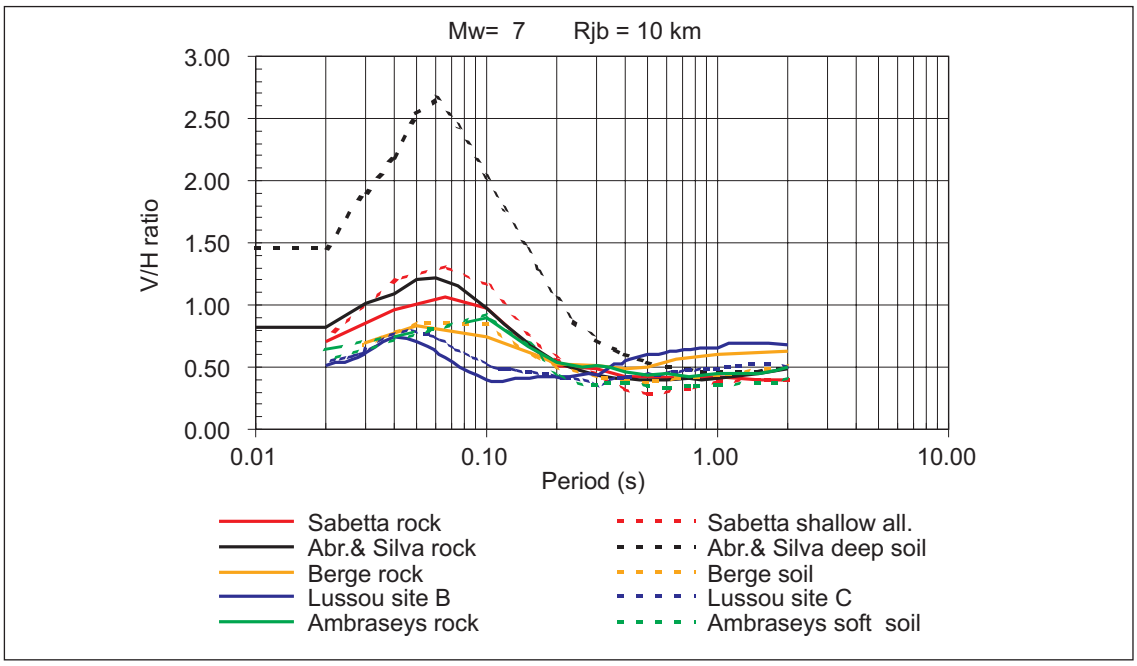

Fig. 27: V / H ratios of the selected attenuation relations for $M_w = 7$ and $R_{JB} = 10$ km

Continuous lines refer to rock conditions and dashed lines refer to soil conditions.

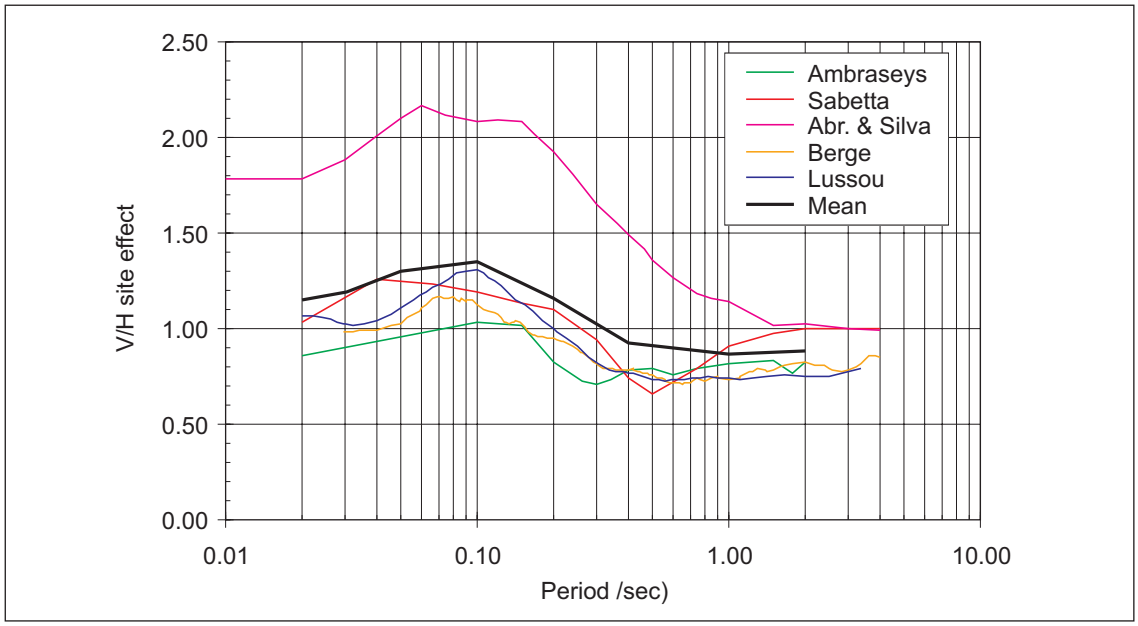

Fig. 28: Correction factor taking into account the different site effect on vertical and horizontal components of the ground motion

The thick black line refers to the mean of the selected attenuation relations.

Tab. 15: Correction factor of the site effect to be applied to the vertical motion

Frequency (Hz)	Correction factor
0.50	0.88
1.00	0.87
2.50	0.92
5.00	1.16
10.00	1.35
20.00	1.30
33.00	1.19
PGA	1.15

In conclusion the site correction for the vertical components can be performed in the same way discussed in section 3.3 for the horizontal components applying the additional site effect correction factors of Table 15.

4.2.2 Style-of-faulting adjustments for the vertical components

As the faulting mechanism is concerned, it has to be remarked that for the vertical components there is no evidence of a different behavior of strike-slip respect to normal faults (Abrahamson & Becker 1999, recommend a scale factor = 1 for frequencies greater than 0.5 Hz; Spudich et al. do not provide vertical relations). As a consequence a scale factor of 1.0 is selected based on the Abrahamson & Becker 1999 results.

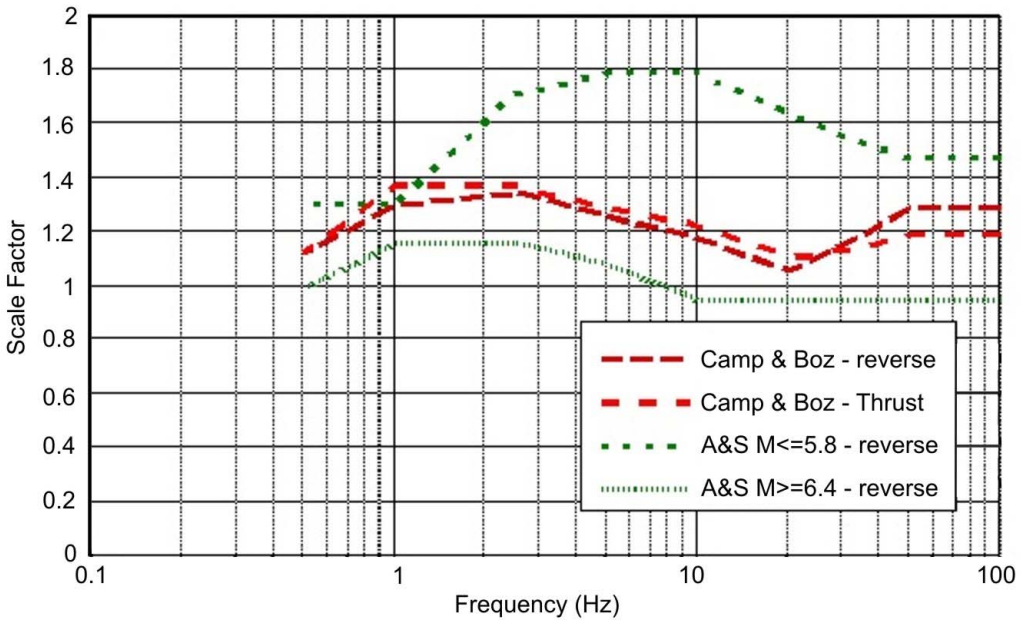

Fig. 29: PSA ratios between reverse and strike slip faulting mechanism for the vertical components according to the available empirical models (from Abrahamson, April 2003 presentation)

In case of reverse and thrust faults, as shown in Figure 29, the vertical components behavior is slightly different respect to the horizontal ones, both in scaling values and in frequency range. A substantial variation of the scale factor is apparent only at intermediate frequencies so that only two frequency intervals have been selected as illustrated in Table 16.

Tab. 16: Style of faulting scale factors for the vertical components

	Scale factor from normal or strike-slip to reverse		
	lower value	central value	upper value
High frequencies (> 5 Hz) and low frequencies (0.5-1 Hz)	0.9	1.1	1.3
Intermediate freq. (1-5 Hz)	1.1	1.2	1.4

The scale factors to be used for the different attenuation models in case of the vertical components of ground motion have been selected using the same approach described in section 3.8 and are reported in Tables 17 and 18. In this case, due to the lower uncertainty in the scale factors of table 16 respect to the horizontal components, the weights 0.3, 0.4, 0.3 are used also for the reverse faulting mechanism (Table 18).

Tab. 17: Scale factors and relative weights in case of normal and strike-slip faulting (vertical components)

	Scale factor 0.5-1 Hz and > 10Hz			Scale factor 1-5 Hz		
Normal and strike-slip faults	lower W = 3	central W = 0.4	upper W = 0.3	lower W = 0.3	central W = 0.4	upper W = 0.3
Ambraseys & Simpson 1996	0.87	0.95	1.05	0.83	0.91	1.00
Berge-Thierry et al. 2000	0.88	0.97	1.06	0.85	0.93	1.03
Sabetta & Pugliese 1996	0.87	0.96	1.05	0.84	0.92	1.01
Lussou et al. 2001	0.88	0.97	1.07	0.85	0.94	1.03
Abrahamson & Silva 1997 (F = 0 strike-slip)	1.00	1.00	1.00	1.00	1.00	1.00
Somerville et al. 2001	0.83	0.91	1.00	0.76	0.83	0.92
Stochastic-Bay 2002a	0.90	0.99	1.09	0.89	0.98	1.08

Tab. 18: Scale factors and relative weights in case of reverse faulting (vertical components)

	Scale factor 0.5-1 Hz and > 10 Hz			Scale factor 1-5 Hz		
Reverse faults	lower W = 0.3	central W = 0.4	upper W = 0.3	lower W = 0.3	central W = 0.4	upper W = 0.3
Ambraseys & Simpson 1996	0.86	1.05	1.24	1.00	1.09	1.28
Berge et al. 2000	0.87	1.06	1.26	1.03	1.12	1.31
Sabetta & Pugliese 1996	0.86	1.05	1.25	1.01	1.10	1.29
Lussou et al. 2001	0.87	1.07	1.26	1.03	1.13	1.32
Abrahamson & Silva 1997 (F = 1 rev. M_w = 6.5)	1.00	1.00	1.00	1.00	1.00	1.00
Somerville et al. 2001	0.82	1.00	1.18	0.92	1.00	1.17
Stochastic-Bay 2002a	0.89	1.09	1.29	1.08	1.18	1.37

4.3 Weights for proponent models

The weights for the vertical models have been obtained from the horizontal ones just removing the Spudich et al. (1999) relation and increasing proportionally the weight of each bin so as to add up to 1. Table 19 summarizes the weights as a function of magnitude and distance bins.

Tab. 19: Weights of the vertical selected models as a function of magnitude and distance

Attenuation model	$M_w < 5.5$			$5.5 < M_w < 6.5$			$M_w > 6.5$		
	$R_{JB}<10$	$10<R_{JB}<70$	$R_{JB}>70$	$R_{JB}<10$	$10<R_{JB}<70$	$R_{JB}>70$	$R_{JB}<10$	$10<R_{JB}<70$	$R_{JB}>70$
Ambraseys & Simpson (1996)	0.120	0.130	0.129	0.135	0.133	0.132	0.182	0.169	0.156
Berge-Thierry et al. (2000)	0.174	0.163	0.151	0.169	0.167	0.154	0.182	0.191	0.189
Sabetta & Pugliese (1996)	0.109	0.109	0.097	0.101	0.111	0.099	0.114	0.124	0.111
Lussou et al. (2001)	0.130	0.120	0.108	0.101	0.111	0.110	0.000	0.000	0.000
Abrahamson & Silva (1997)	0.152	0.152	0.151	0.169	0.156	0.143	0.216	0.202	0.189
Somerville et al. (2001)	0.076	0.087	0.097	0.101	0.100	0.121	0.125	0.135	0.144
Stochastic-Bay (2002a) *Ainc*	0.120	0.120	0.129	0.101	0.100	0.110	0.080	0.079	0.089
Stochastic-Bay (2002a) *A30*	0.065	0.065	0.075	0.079	0.078	0.088	0.068	0.067	0.078
Stochastic-Bay (2002a) *YI*	0.054	0.054	0.065	0.045	0.044	0.044	0.034	0.034	0.044
Check: Sum of weights	1.0	1.0	1.0	1.0	1.0	1.0	1.0	1.0	1.0
N° of models - mean weight	7- 0.143	7- 0.143	7- 0.143	7- 0.143	7- 0.143	7- 0.143	6- 0.166	6- 0.166	6- 0.166

5 ALEATORY VARIABILITY FOR HORIZONTAL GROUND MOTION

5.1 Logic tree structure

All the selected relations (Figure 30) provide a standard deviation dependent on frequency and varying in the range 0.2 – 0.4 (log10 units). As shown by the paper from Douglas and Smit (2001), who used 1484 worldwide strong motion records with the pure error analysis, the scatter is significantly dependent on magnitude (see also Youngs et al. 1995), whereas it does not show dependence on distance and on amplitude of ground motion. The authors also conclude that the current data do not allow a significant improvement in the aleatory uncertainty over what has been found in the published attenuation relations.

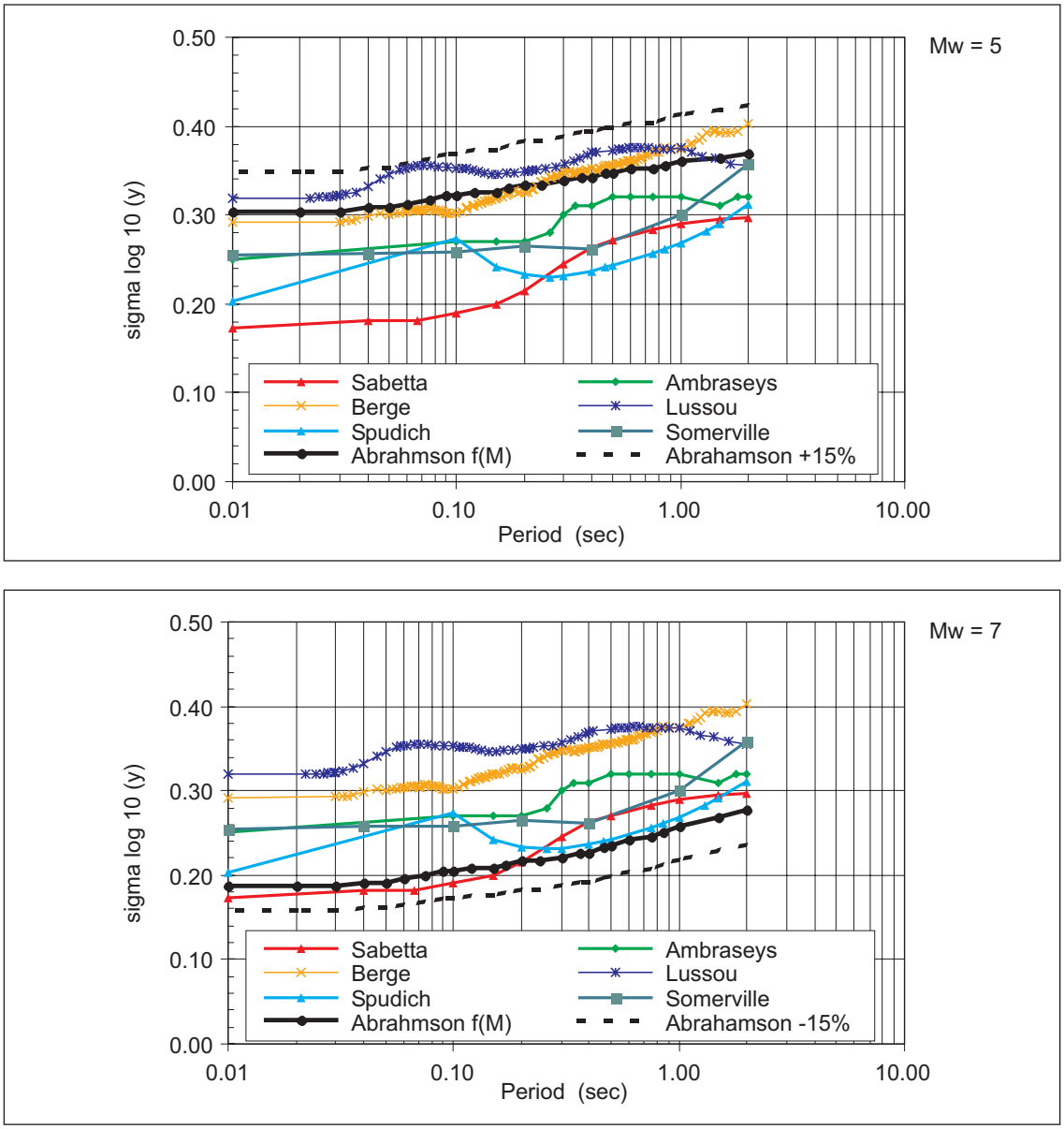

Fig. 30: Standard deviations of the selected attenuation relations compared with sigma from Abrahamson & Silva for $M_w = 5$ and $M_w = 7$

A straightforward approach could be to use, for each relation and frequency, the derived standard deviation as a central value in a logic tree variation. However, as shown in Figure 30, the only relation providing a sigma dependence on magnitude (Abrahamson & Silva 1997), tracks the lowest values of sigma (Sabetta & Pugliese) for M_w = 7 and the highest values (Berge-Thierry and Lussou) for M_w = 5.

The chosen approach is therefore to use just the magnitude dependent standard deviation provided in Abrahamson & Silva (equation 13 in the paper) with a ± 15 % branching (0.3 weight each) in the logic tree to take into account the uncertainty in the standard deviation. The 15 % uncertainty has been selected because, with these bounds, the A&S sigma covers the entire range of variation of the standard deviations proposed by other relations (see Figure 30 dashed lines).

5.2 Weights for proponent models

Example of the sigma values of the Abrahamson & Silva relation, with the corresponding weights (0.4 for central value and 0.3 for lower and upper values) are given in Table 20 in case of magnitudes 5 and 7.

Tab. 20: Standard deviation (log10 based) and weights for different magnitudes and frequencies

	M_w = 5			M_w = 7		
	Abr.& Silva -15 % lower	Abr.& Silva central	Abr.& Silva +15 % upper	Abr.& Silva -15 % lower	Abr.& Silva central	Abr.& Silva +15 % upper
Freq. (Hz)	W = 0.3	W = 0.4	W = 0.3	W = 0.3	W = 0.4	W = 0.3
0.5	0.314	0.369	0.425	0.236	0.278	0.320
1.0	0.306	0.360	0.415	0.219	0.258	0.297
2.5	0.292	0.343	0.395	0.192	0.226	0.260
5.0	0.284	0.334	0.385	0.185	0.217	0.250
10.0	0.273	0.321	0.370	0.174	0.204	0.235
20.0	0.262	0.308	0.355	0.162	0.191	0.220
33.3	0.258	0.304	0.350	0.159	0.187	0.215
50.0	0.258	0.304	0.350	0.159	0.187	0.215
PGA	0.258	0.304	0.350	0.159	0.187	0.215

5.3 Horizontal component conversions

The conversion between different definitions of the horizontal components also affects the standard deviation. In particular aleatory uncertainty is normally greater for random components than for larger component. However, as shown in the note PEGASOS TP2-TN-0307 (2002), the differences in the ratios of sigma residuals among the various component definitions are very small (not higher than 3 – 4 %).

Considering that only the aleatory uncertainty of the Abrahamson & Silva relation (geometric mean of the horizontal components) is employed, no conversion of the horizontal component is required.

5.4 Magnitude conversion effect

The Abrahamson & Silva relation makes use of the moment magnitude so that no magnitude conversion is needed.

5.5 Distance conversion effect

As discussed previously the available studies (Douglas and Smit, 2001; Youngs et al. 1995) do not support a distance dependence of the standard deviation. Moreover the PEGASOS Technical Note TP2-TN-0249, where the WAF database was used to compute the standard deviation of the residuals of each attenuation model at short distances, doesn't show any increase of σ with distance, so that no distance conversion is introduced.

6 MAXIMUM GROUND MOTIONS FOR THE HORIZONTAL COMPONENT

6.1 Evaluation of empirical data

6.1.1 Recorded data

In Table 21 are reported the 6 world highest PHA recordings on rock or stiff soil sites extracted from the PEGASOS database (TP2-WAF-0008) integrated with the 10 strongest GM ever recorded on rock. In Figures 31 and 32 two plots of these recordings are shown. It is interesting to note that 3 of the 4 highest PHA values have been recorded on abutments of dams and are therefore probably affected by soil-structure interaction. Even the "Petrolia" record (Figure 32) is dominated by a single sharp acceleration spike (1.5 g) while the rest of the time history is below 0.5 g. This just to say that the recorded PGA upper bounds are probably already over-estimated.

Tab. 21: List of the 6 world highest PHA recordings on rock or stiff soil sites from the PEGASOS database (TP2-WAF-0008)

Earthquake Name	Date	M_w	Focal Depth	Fault type	Station Name	Local Geology	PHA (g) max hz.	PVA (g)	R_{epi} (km)	R_{JB} (km)
Northridge	17/01/1994	6.7	14 km	reverse	Pacoima Dam-Upper Left Abutment	rock	1.58	1.23	25.0	10.0
Petrolia	25/04/1992	7.2	15 km	reverse	Cape Mendocino	rock	1.50	0.75	4.0	0.0
Morgan Hill	24/04/1984	6.5	9 km	strike slip	Coyote Lake Dam	stiff soil	1.27	0.40	24.0	2.0
San Fernando	09/02/1971	6.6	8 km	reverse	Pacoima Dam-Upper Left Abutment	rock	1.19	0.71	9.0	0.0
Tabas	16/09/1978	7.4	5 km	reverse	Tabas	stiff soil	1.10	0.84	52.0	14.0
Nahanni	23/12/1985	6.7	6 km	reverse	Station 1 (Inverson)	rock	1.02	2.00	7.0	0.0

Table 22 illustrates the largest pseudo-acceleration (PSA) spectral values extracted for different M-R bins from the WAF database (Roth 2002, TP2-TN-0333). As shown in Figure 33, not enough recorded data are available to fill all the M-R bins so that, to cover the magnitudes and distances selected for all the frequencies, I had sometimes to resort to adjacent bins (e.g take, at the same magnitude, higher distances if the acceleration value was higher in a adjacent bin).

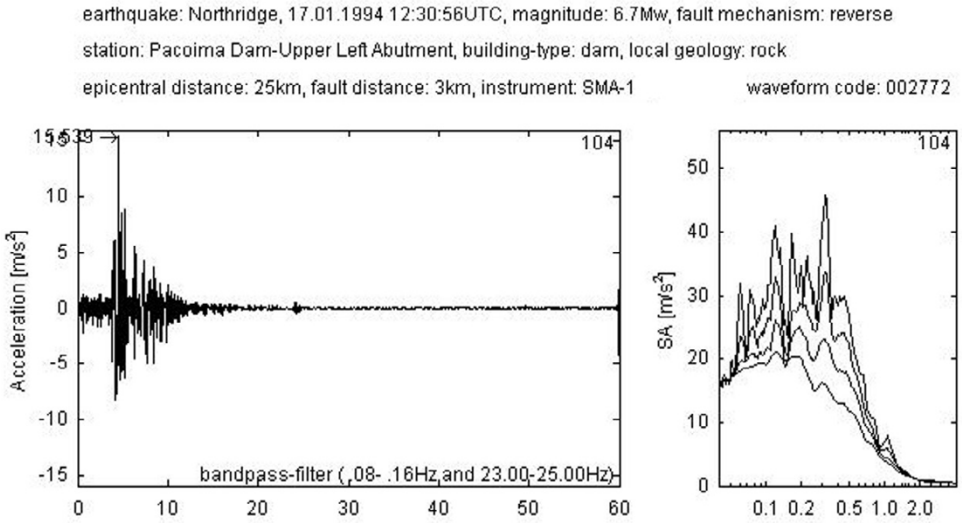

Fig. 31: Accelerogram recorded at Pacoima Dam during the Northridge earthquake

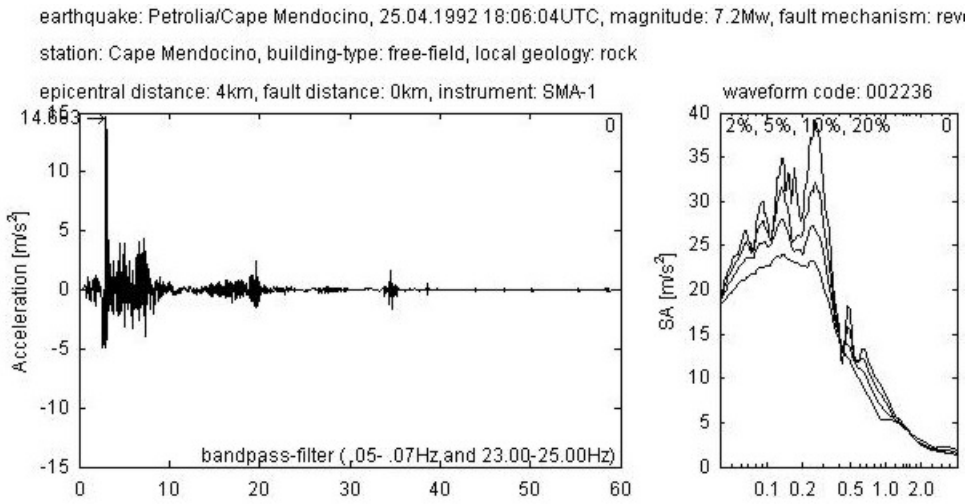

Fig. 32: Accelerogram recorded at Cape Mendocino during the Petrolia earthquake

6.1.2 Empirical relations

In principle upper bounds have to be assessed through the use of physical and not statistical considerations. However the empirical recorded data, as discussed above, are not enough to represent all the required frequencies, magnitudes, and distances. I chose therefore to make use also of the attenuation relations, based on empirical data and covering continuously the M-R-f range. From the numerical simulations and the residual plots, it comes out that the upper motion is of the order of the median + 3 σ (the resulting spectral values are shown in Figure 34). The resulting values from the attenuation relations (Table 23) are often higher than those of numerical simulations or recorded data so that I also took into consideration the median values + 2.5 σ (Table 24).

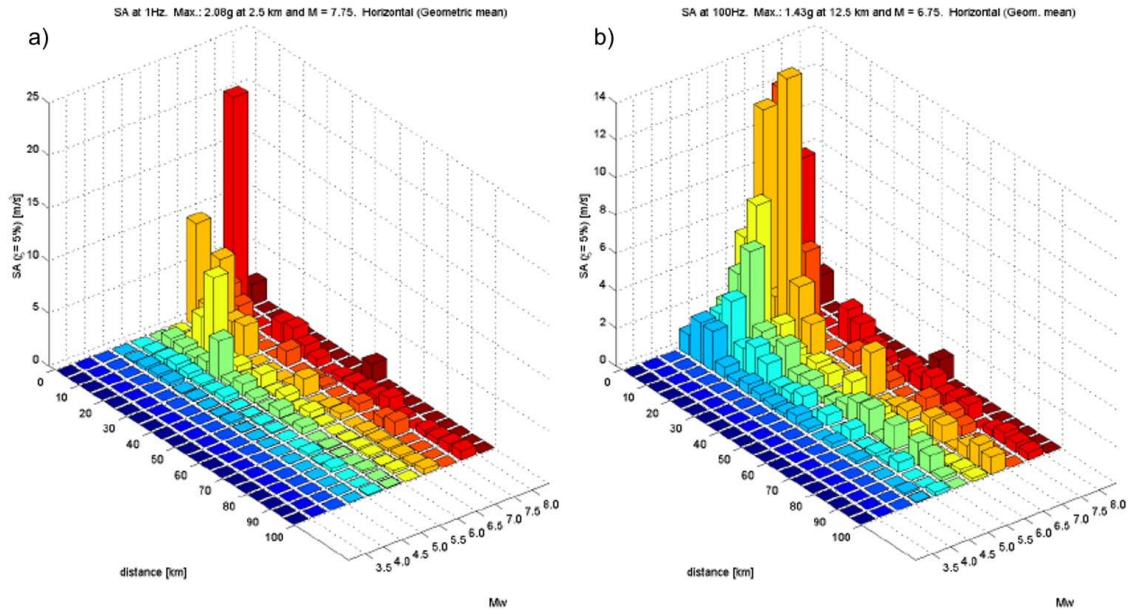

Fig. 33: Largest PSA values (5 %, horiz. comp. geom. mean) of the WAF database grouped in M-R bins: a) 1Hz; b) PGA (Roth 2002)

Tab. 22: Largest PSA (5 %, horiz. comp. geom. mean) contained in the WAF database (Roth 2002, TP2-TN-033)

f (Hz)	T (sec)	M = 7 R = 5 km (g)	M = 7 R = 25 km (g)	M = 5.5 R = 5 km (g)	M = 5.5 R = 25 km (g)
0.5	2.00	0.33	0.25	0.03	0.02
1.0	1.00	1.00	0.28	0.08	0.06
2.5	0.40	2.65	2.04	0.36	0.23
5.0	0.20	2.51	0.68	0.56	0.29
10.0	0.10	2.29	0.52	0.65	0.35
20.0	0.05	1.69	0.43	0.61	0.21
PGA	0.01	1.25	0.34	0.20	0.17

Tab. 23: PSA + 3 σ from the empirical attenuation relations (horiz. comp. geom. mean)

f (Hz)	T (sec)	M = 7 R = 5 (g)	relation	M = 7 R = 25 (g)	relation	M = 5.5 R = 5 (g)	relation	M = 5.5 R = 25 (g)	relation
0.5	2.00	2.18	Sab	0.61	Berge	0.23	Sab	0.08	Berge
1.0	1.00	5.00	Sab	1.28	Sab	0.70	Sab	0.18	Berge
2.5	0.40	7.08	Amb	2.08	Berge	1.67	Sab	0.60	Berge
5.0	0.20	5.83	Amb	2.43	Berge	2.43	Abra	0.97	Berge
10.0	0.10	4.31	Amb	1.67	Berge	2.45	Lussou	0.93	Lussou
20.0	0.05	3.33	Amb	1.15	Berge	1.63	Abr	0.58	Lussou
PGA	0.01	2.13	Amb	0.87	Berge	0.98	Abr	0.36	Berge

Tab. 24: PSA + 2.5 σ from the empirical attenuation relations (horiz. comp. geom. mean)

f (Hz)	T (sec)	M = 7 R = 5 (g)	relation	M = 7 R = 25 (g)	relation	M = 5.5 R = 5 (g)	relation	M = 5.5 R = 25 (g)	relation
0.5	2.00	1.55	Sab	0.38	Berge	0.17	Sab	0.05	Berge
1.0	1.00	3.61	Sab	0.92	Sab	0.50	Sab	0.13	Sab
2.5	0.40	4.93	Amb	1.42	Berge	1.23	Sab	0.40	Berge
5.0	0.20	4.19	Amb	1.67	Berge	1.71	Abra	0.67	Berge
10.0	0.10	3.69	Spud	1.21	Berge	1.71	Abra	0.62	Lussou
20.0	0.05	2.50	Spud	0.83	Berge	1.18	Abra	0.39	Lussou
PGA	0.01	1.67	Amb	0.63	Berge	0.71	Abra	0.25	Berge

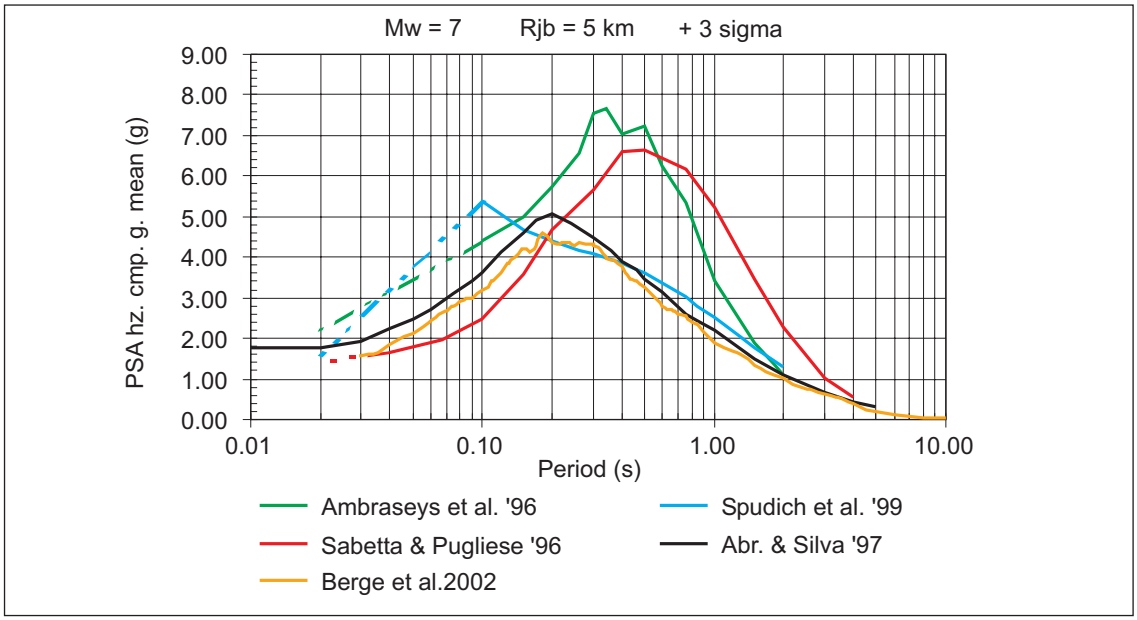

Fig. 34: PSA values of the empirical models increased by 3 sigma for M = 7 and R = 5 km

6.2 Evaluation of numerical simulations

Two different kinematic fault models have been provided to the expert panel EG2 for numerical simulations aimed to evaluate the upper limit ground motion.

The first, developed by URS (Pitarka et al. 2002) is based on the hybrid Green's function method and uses a stochastic approach to generate the high frequency part of the ground motion.

The second, developed by OGS (Priolo et al. 2002) is based on the Wavenumber Integration Method (Herrmann and Wang, 1985) with the source model proposed by Herrero and Bernard (1994) and uses a purely deterministic approach.

Both models have been subjected to a review by a "dynamic modeler" (Madariaga 2002) in order to assess their feasibility. The main remarks made by the reviewer (italic font) are reported hereafter.

6.2.1 URS

The only question that remains is the origin of the monochromatic wave in the source time functions at 2 Hz. Other than that, the assumptions about rise time and k are very reasonable so that I expect accelerograms to be realistic. The median and lower bound rupture speeds of 3.0 km/s and 2.5 km/s are reasonable. *The supershear speed of 4.0 km/s is very unlikely*. I suggest that a more realistic model would be one in which supershear speeds are restricted to the large asperities. The assumption of constant supershear speeds has dramatic effects, producing large shock waves in the near field where slip rate will make a sudden jump of more than a m/s for the models used by the two groups. In my opinion realistic source models may include short bursts of super shear speeds superposed on an average subshear rupture speed. *I thus do not consider the supershear simulations in either report as realistic.*

Other interesting comments are made by the author itself (Pitarka et al. 2002):

The rupture area and rise time as well as their combination with supershear rupture velocity most strongly affect the ground motion.

The Max2 model generates very large ground motions, due to the combined effects of extremely small rupture area and short rise time. We regard this combination as unphysical, because the small rupture area requires a large average displacement, which should be accompanied by a longer than median rise time, not shorter than median rise time.

An even more extreme (and unphysical) set of scenarios adds supersonic rupture velocity to this combination of parameters. Here again the assumption of constant supershear rupture along the entire fault combined with a constant rise time is unrealistic.

For the above reasons I considered the "Max2" and "Extreme" scenarios from Pitarka et al. as being unphysical. In case of M = 7, I only took the values of the "Max1" scenario (figures 4a and 4b in Pitarka et al. 2002) as representative of the largest response acceleration values. In case of M = 5.5, I took the "Max" scenario (figures 11a and 11b in Pitarka et al. 2002). The values are shown in Table 25, where the gray shading indicates the Priolo's values at high frequencies and short distances not considered reliable as explained in the following paragraph.

Tab. 25: Largest PSA (horiz. comp. geom. mean) from the numerical simulations

		M = 7, R = 5		M = 7, R = 25		M = 5.5, R = 5		M = 5.5, R = 25	
f (Hz)	T (sec)	Pitarka Max1 (g)	Priolo/1.2 (g)	Pitarka Max1 (g)	Priolo/1.2 (g)	Pitarka Max (g)	Priolo/1.2 (g)	Pitarka Max (g)	Priolo/1.2 (g)
0.5	2.00	1.50	0.29	0.35	0.23	0.11	0.02	0.03	0.01
1.0	1.00	3.00	1.20	0.60	0.92	0.55	0.07	0.06	0.03
2.5	0.40	6.00	1.91	1.80	1.51	0.55	0.50	0.11	0.69
5.0	0.20	8.00	4.23	2.50	2.15	0.75	0.93	0.19	0.53
10.0	0.10	5.50	7.52	1.30	0.78	1.10	1.41	0.28	0.11
20.0	0.05	4.50	4.44	1.00	0.78	0.80	0.75	0.22	0.39
PGA	0.01	3.50	4.74	0.60	0.78	0.50	0.75	0.13	0.39

6.2.2 OGS

In my opinion the Herrero-Bernard (1994) model needs a finite rise time in order to simulate realistic accelerograms. *It is very likely that the OGS models produce very large high frequencies*. The source models used by OGS are unusual because they were derived from the

Herrero-Bernard model with instantaneous source time functions. I think that the slip function is very likely, but not the instantaneous slip front. *I do not think that it is very realistic at high frequencies, in particular those higher than 2 Hz for a Magnitude 7 event*. At lower frequencies the models are realistic (Madariaga 2002).

Further comments and examples of the over-prediction at high frequencies of the OGS model are presented in the Joint Report on the comparison between OGS and URS models included both in Priolo et al. (2002) and Pitarka et al. (2002).

The stochastic scheme (URS) tends to reduce the coherency of waves at very high frequencies. The deterministic scheme (OGS) may enhance the directivity effect at high frequencies and short distances; particular high frequency phases may be coherent at 5 km distance.

An example is shown in Figure 35 taken from the above mentioned joint report.

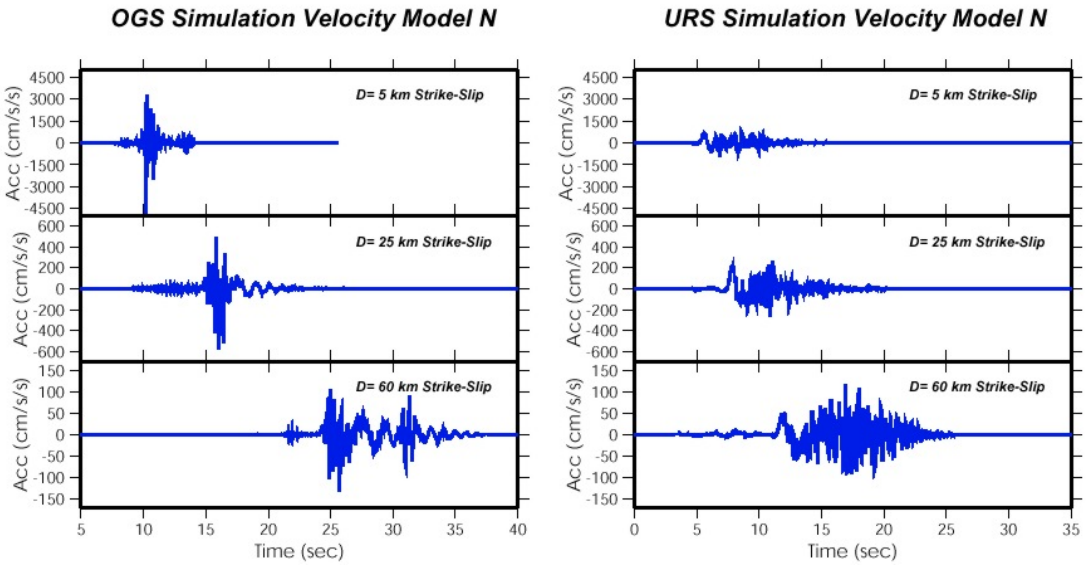

Fig. 35: Comparison between OGS and URS simulations for $M_w = 7$ (Pitarka et al. 2002)

The high frequency pulse with extremely large amplitude that dominates the acceleration at 5 km distance, is caused by a coherent phase which is generated at the source and amplified during the rupture. The pulse is quickly attenuated at longer distances. At 25 km and 60 km the comparison between the two simulations is very favorable.

For the above reasons I did not consider the spectral acceleration values provided by OGS, at a distance of 5 km, for frequencies higher than 2.5 Hz (gray background in Table 25). The values reported in Table 25 have been taken from table 3m at page 33 in Priolo's report and divided by a factor of 1.2 in order to scale down from the largest horizontal component to the geometrical mean used by Pitarka and adopted in the PEGASOS Project.

Further limits of the OGS model are discussed in Sabetta (2002) and only partially answered in the OGS final report (Priolo et al. 2002). An outstanding remark is the huge difference (nearly a factor of 5) between the values at M = 6.5 and M = 7, at 5 km distance, reported in table 3m of Priolo's report. This is probably due to the fact that M = 7 as been added afterwards and *the same fault size has been used for both simulations*. In any case it leaves some doubt on the reliability of the maximum ground motions estimated by OGS (see also the differences in the numerical values reported in different versions of the reports presented by Priolo) and justifies the lower weights assigned to this model (see Tables 26 to 29).

6.3 Logic tree structure

The logic tree structure, as described in the following section, is implemented through the use of an empirical attenuation model incremented by different fractions of standard deviation.

6.4 Weights for maximum ground motions

The weighting scheme chosen for the upper bound values is reported in Tables 26, 27, 28, and 29 for different M-R pairs. The numerical simulations have a global weight of 0.5, with a net preference for the Pitarka model and zero weight to the Priolo model at frequencies larger than 2.5 Hz and short distances, for the reasons discussed previously. The remaining weighting value is subdivided between recorded data and attenuation relations with a preference for the former ones except when they are showing very low values due to a lack in the corresponding M-R bin. The recorded data have been conservatively multiplied by 1.3 to take into account the s.m. recording history of the last years, showing a continuous trend of increasing PGA with time.

Tab. 26: Selected weights of maximum ground motions for M = 7 and R = 5 km

f (Hz)	T (sec)	Pitarka max1 (g)	Priolo (g)	Recorded x 1.3 (g)	Emp.Rel. + 3σ	Emp.Rel. +2.5 σ	weighted value	Max	Min
0.5	2.00	1.50	0.29	0.43	2.18	1.55	1.21	2.18	0.29
Weight		0.35	0.15	0.20	0.15	0.15			
1.0	1.00	3.00	1.20	1.30	5.00	3.61	2.78	5.00	1.20
Weight		0.35	0.15	0.20	0.15	0.15			
2.5	0.40	6.00	1.91	3.45	7.08	4.93	4.88	7.08	1.91
Weight		0.35	0.15	0.20	0.15	0.15			
5.0	0.20	8.00	4.23	3.26	5.83	4.19	5.92	8.00	3.26
Weight		0.45	0.00	0.25	0.15	0.15			
10.0	0.10	5.50	7.52	2.98	4.31	3.69	4.42	5.50	2.98
Weight		0.45	0.00	0.25	0.15	0.15			
20.0	0.05	4.50	4.44	2.20	3.33	2.50	3.45	4.50	2.20
Weight		0.45	0.00	0.25	0.15	0.15			
PGA	0.01	3.50	4.74	1.63	2.13	1.67	2.55	3.50	1.63
Weight		0.45	0.00	0.25	0.15	0.15			

The last three columns of Tables 26, 27, 28 and 29 provide my estimates of mean, maximum and minimum upper bound values for two magnitude and distance values.

To extrapolate these estimates at different M-R values, the chosen approach is to use an empirical attenuation model, Ambraseys et al. 1996, corrected for $M_w - M_s$ and for larger to geometrical mean horizontal component as discussed previously, and incremented by different fractions of standard deviation. As shown in Figure 36 for $M_w = 7$ and f = 1 Hz, a good match of minimum, mean, and maximum upper bound values is obtained using respectively 1.7, 2.8, and 3.6 sigma of the Ambraseys model.

Tab. 27: Selected weights of maximum ground motions for M = 7 and R = 25 km

f (Hz)	T (sec)	Pitarka max1 (g)	Priolo (g)	Recorded x 1.3 (g)	Emp.Rel. + 3 σ	Emp.Rel. + 2.5 σ	weighted value	Max	Min
0.5	2.00	0.35	0.23	0.33	0.61	0.38	0.37	0.61	0.23
Weight		0.35	0.20	0.15	0.15	0.15			
1.0	1.00	0.60	0.92	0.36	1.28	0.92	0.78	1.28	0.36
Weight		0.35	0.20	0.15	0.15	0.15			
2.5	0.40	1.80	1.51	2.65	2.08	1.42	1.85	2.65	1.42
Weight		0.35	0.20	0.15	0.15	0.15			
5.0	0.20	2.50	2.15	0.88	2.43	1.67	2.03	2.50	0.88
Weight		0.35	0.15	0.15	0.15	0.20			
10.0	0.10	1.30	0.78	0.68	1.67	1.21	1.17	1.67	0.68
Weight		0.35	0.15	0.15	0.15	0.20			
20.0	0.05	1.00	0.78	0.56	1.15	0.83	0.89	1.15	0.56
Weight		0.35	0.15	0.15	0.15	0.20			
PGA	0.01	0.60	0.78	0.44	0.87	0.63	0.65	0.87	0.44
Weight		0.35	0.15	0.15	0.15	0.20			

Tab. 28: Selected weights of maximum ground motions for M = 5.5 and R = 5 km

f (Hz)	T (sec)	Pitarka max1 (g)	Priolo (g)	Recorded x 1.3 (g)	Emp.Rel. + 3 σ	Emp.Rel. + 2.5 σ	weighted value	Max	Min
0.5	2.00	0.11	0.02	0.03	0.23	0.17	0.10	0.23	0.02
Weight		0.35	0.15	0.20	0.10	0.20			
1.0	1.00	0.55	0.07	0.10	0.70	0.50	0.39	0.70	0.07
Weight		0.35	0.15	0.20	0.10	0.20			
2.5	0.40	0.55	0.50	0.47	1.67	1.23	0.77	1.67	0.47
Weight		0.35	0.15	0.20	0.10	0.20			
5.0	0.20	0.75	0.93	0.73	2.43	1.71	1.19	2.43	0.73
Weight		0.45	0.00	0.20	0.15	0.20			
10.0	0.10	1.10	1.41	0.85	2.45	1.71	1.37	2.45	0.85
Weight		0.45	0.00	0.20	0.15	0.20			
20.0	0.05	0.80	0.75	0.79	1.63	1.18	1.00	1.63	0.79
Weight		0.45	0.00	0.20	0.15	0.20			
PGA	0.01	0.50	0.75	0.26	0.98	0.71	0.56	0.98	0.26
Weight		0.45	0.00	0.20	0.15	0.20			

Tab. 29: Selected weights of maximum ground motions for M = 5.5 and R = 25 km

f (Hz)	T (sec)	Pitarka max1 (g)	Priolo (g)	Recorded x 1.3 (g)	Emp. Rel. + 3 σ	Emp. Rel. + 2.5 σ	weighted value	Max.	Min.
0.5	2.00	0.03	0.01	0.03	0.08	0.05	0.04	0.08	0.01
Weight		0.35	0.15	0.20	0.10	0.20			
1.0	1.00	0.06	0.03	0.08	0.18	0.13	0.08	0.18	0.03
Weight		0.35	0.15	0.20	0.10	0.20			
2.5	0.40	0.11	0.69	0.30	0.60	0.40	0.34	0.69	0.11
Weight		0.35	0.15	0.20	0.10	0.20			
5.0	0.20	0.19	0.53	0.38	0.97	0.67	0.45	0.97	0.19
Weight		0.35	0.15	0.20	0.10	0.20			
10.0	0.10	0.28	0.11	0.46	0.93	0.62	0.42	0.93	0.11
Weight		0.35	0.15	0.20	0.10	0.20			
20.0	0.05	0.22	0.39	0.27	0.58	0.39	0.33	0.58	0.22
Weight		0.35	0.15	0.20	0.10	0.20			
PGA	0.01	0.13	0.39	0.22	0.36	0.25	0.23	0.39	0.13
Weight		0.35	0.15	0.20	0.10	0.20			

A comparison with the results presented in the note PEGASOS TP2-TN-0333 (2003), illustrates that the values of Ambraseys relation + 3.6 σ are very close to the recorded values (without the multiplication by the factor 1.3) for M = 5.5 f = 10 Hz and intermediate distance. This is also illustrated in Figure 37 where, in case of M = 5.5 and f = 10 Hz, it's shown that a higher fraction of sigma is required to match the max values (red squares) at intermediate distance. Therefore, to capture the uncertainty, I also considered an additional higher value of 4.2 sigma, but with very low weight.

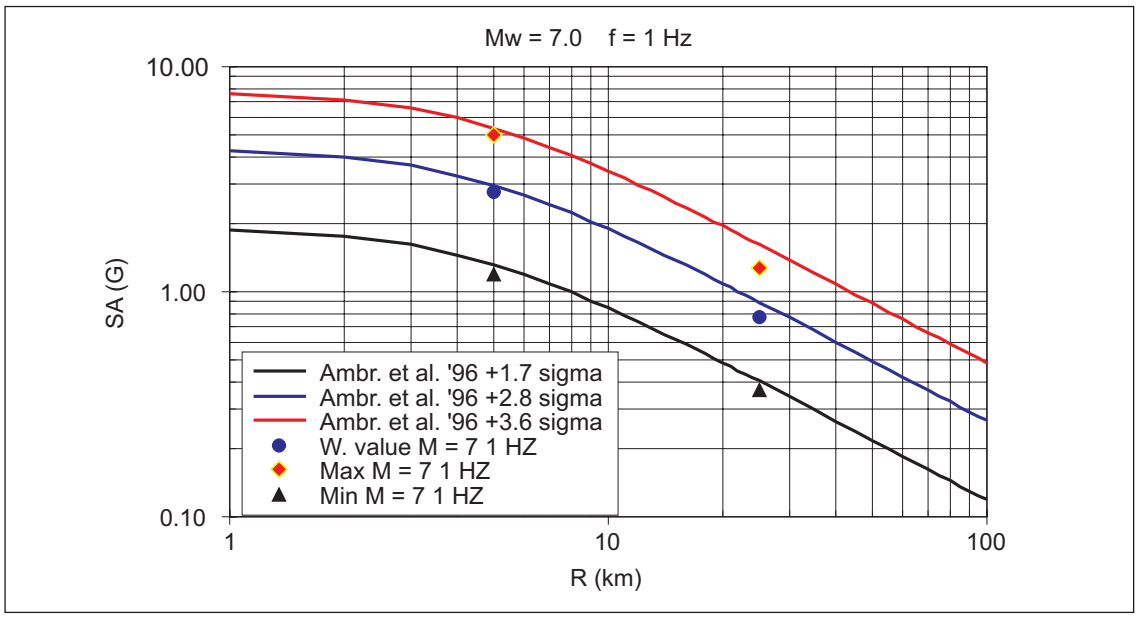

Fig. 36: Upper bound values from Tables 26 and 27 compared with Ambraseys et al. relation (scaled horiz. comp. g. mean and to M_w) incremented by different fractions of standard deviation, for M_w = 7 at 1 Hz

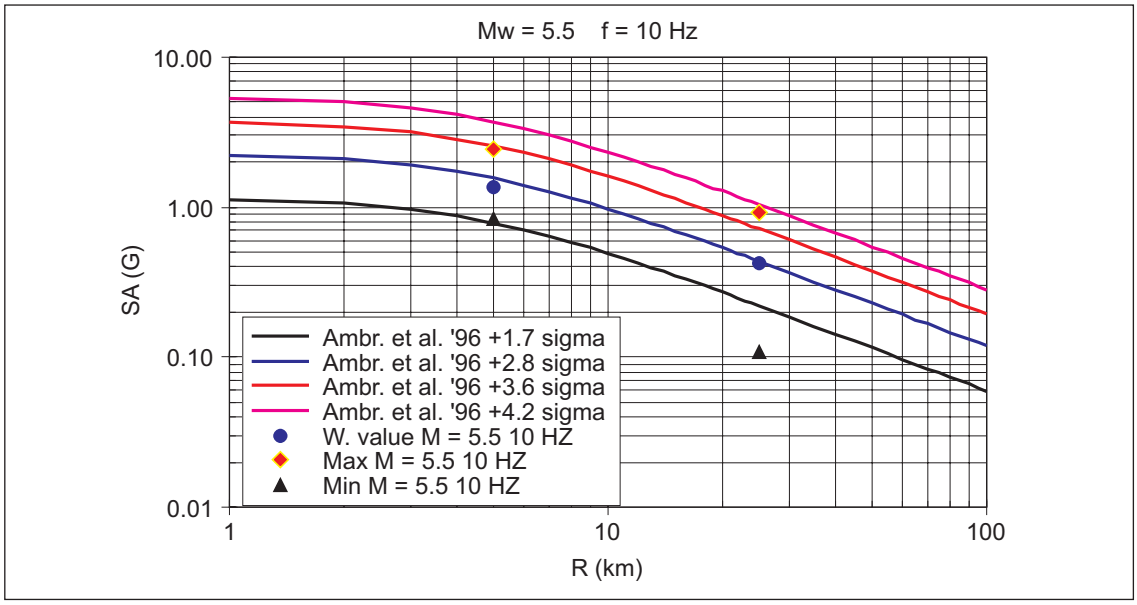

Fig. 37: Upper bound values from tables 28 and 29 compared with Ambraseys et al. relation (scaled to hoiz. comp. mean and to M_w) incremented by different fractions of standard deviation, for M_w = 5.5 at 10 Hz

The final weighting scheme selected for the maximum horizontal ground motions assessment is reported in Table 30. The weights are not related to those of Tables 26 to 29 which were only used to provide my best estimate (called "weighted value" and indicated with blue dots in Figures 36 and 37) of the maximum ground motion. The weights of Table 30 have been selected giving the highest weight (0.60) to the "weighted value", considered more reliable as resulting from the combination of empirical, recorded and simulated data, and corresponding, in terms of the Ambraseys relation, to 2.8 σ. The remaining weights have been assigned fitting a normal PDF on the basis of the distance of the numerical values of the different sigma fractions (1.7, 3.6 and 4.2) from the modal value of 2.8 σ.

Tab. 30: Maximum ground motion expressed in term of number of standard deviations of Ambraseys et al. (1996) relation, scaled to horizontal comp. geom. mean and to M_w

N° of σ (Ambraseys et al.)	Weight
1.7	0.10
2.8	0.60
3.6	0.22
4.2	0.08

7 MAXIMUM GROUND MOTIONS FOR THE VERTICAL COMPONENT

7.1 Evaluation of empirical data

See section 7.4.

7.2 Evaluation of numerical simulations

The most reliable simulation model (Pitarka et al. 2002) does not include vertical motions. The OGS model (Priolo et al. 2002) shows systematically higher values (table 3j page 30) for the horizontal components, contradicting the well known evidence that vertical motions can be higher than horizontal ones for large magnitudes and short distances.

The available numerical simulations are therefore not considered to be reliable for the vertical component.

7.3 Logic Tree Structure

See section 7.4.

7.4 Weights for maximum ground motions

The suggested approach is to scale the maximum ground motions derived for the horizontal components with the V/H ratio discussed in section 4.

8 UPPER TAIL OF THE GROUND MOTION DISTRIBUTION FOR THE HORIZONTAL COMPONENT

8.1 Evaluation of empirical data

The possible truncation of the upper tail of the ground motion distribution, in order to avoid too large acceleration values at very low exceedance probabilities as happened in the Yucca Mountain study, has a natural tradeoff with the selection of the upper bounds.

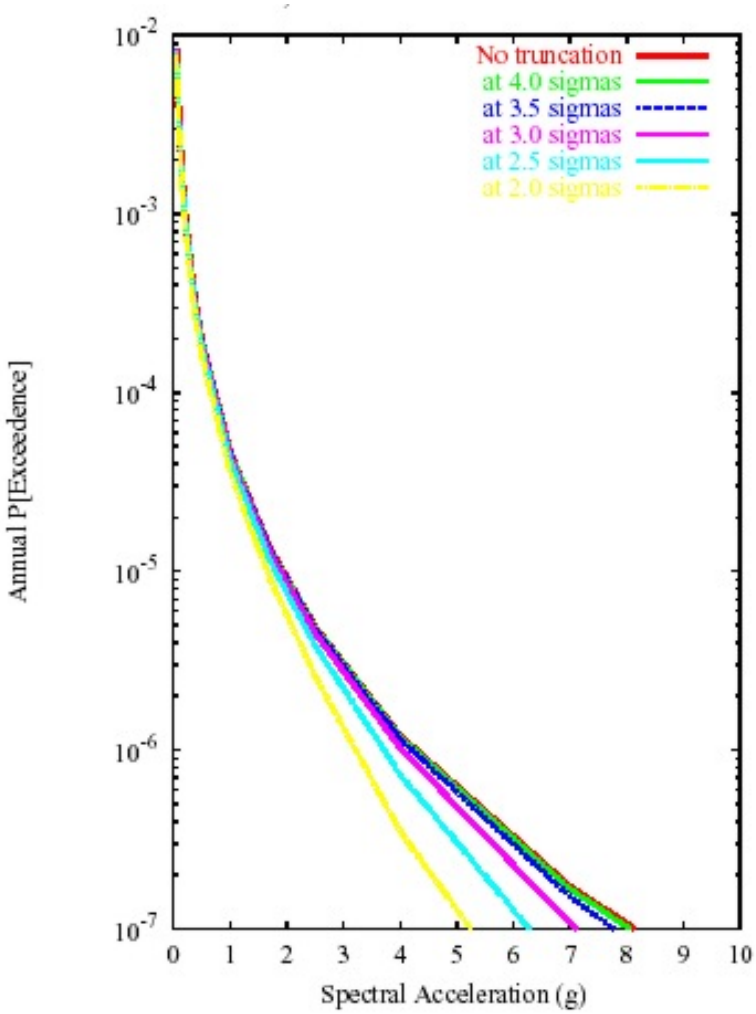

Fig. 38: Effect of ground-motion truncation on mean hazard for 10 Hz spectral acceleration at the Beznau site (EXT-TN-0293)

Figure 38 shows the effect of ground-motion truncation on mean hazard for 10 Hz spectral acceleration at the Beznau site (Toro 2003). The first important remark is that the effect of the truncation, even at 10^{-7} exceedance probability, is null at 4 σ and very low at 3 σ. The second remark, considering that the 10 Hz upper bound weighted values discussed previously are at maximum 4.4 g, is that, in case of the results presented in Figure 38, the truncation of the upper tail produces a lower effect than the upper bound truncation.

8.2 Logic Tree Structure and weights for upper tail models

The analysis of the residual and normal probability plots (TP2-TN-0232), shows that the departure from the log-normal distribution, generally occurs around 3 sigma. It's also worth to note that the outliers generally do not correspond to the highest values (Figure 39).

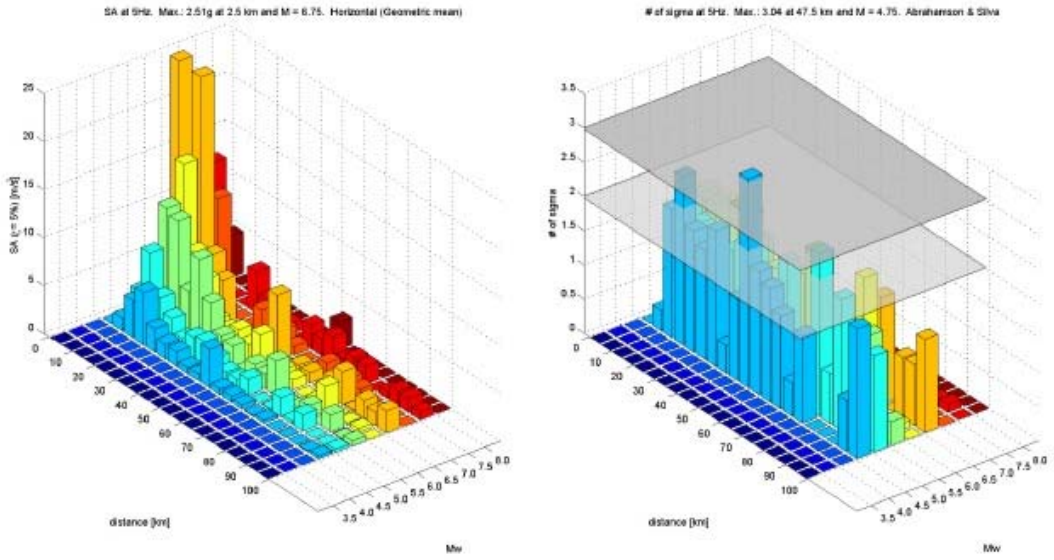

Fig. 39: Largest PSA values (a) and number of sigmas (b) above the attenuation relation of Abrahamson & Silva at a frequency of 5 Hz (Roth 2002)

Considering that more than 1000 s.m. values are needed for getting out to 3 sigma, and that no theoretical or empirical justification is available to select a particular functional form deviating in any systematic way from the log-normal, an abrupt truncation seems to be the most viable solution.

The sigma values selected for the truncation and the corresponding weights are given in Table 31. A low weight (0.1) has been assigned to 3.5 σ because, as shown in Figure 38, this level of truncation has a very little impact on the hazard curve. The remaining weight is subdivided between 3 and 2.5 σ on the basis of the results discussed for the maximum ground motion (section 6.4) and of the results presented in TP2-TN-0309 (Figure 39).

Tab. 31: Model for the upper tail of the ground motion distribution, with abrupt truncations at the given sigma levels

Sigma truncation	Weight
2.5	0.3
3.0	0.6
3.5	0.1

9 REFERENCES

Abrahamson, N.A. & W.J. Silva 1997: Empirical response spectral attenuation relations for shallow crustal earthquakes. Seism. Res. Lett. 68, 94-127.

Abrahamson N.A., P. Birkhäuser, M. Koller, D. Mayer-Rosa, P. Smit, C. Sprecher, S. Tinic & R. Graf 2002: PEGASOS – A comprehensive probabilistic seismic hazard assessment for nuclear power plants in Switzerland. 12th European Conference on Earthquake Engineering, London, paper N° 633, Balkema.

Ambraseys, N.N., K.A. Simpson & J.J. Bommer 1996: Prediction of horizontal response spectra in Europe. Earth. Eng. Struct. Dyn. 25, 371-400.

Ambraseys, N.N. & K.A. Simpson 1996: Prediction of vertical response spectra in Europe. Earth. Eng. Struct. Dyn. 25, 401-412.

Ambraseys, N.N. & M.W. Free 1997: Surface wave magnitude calibration for European region earthquakes. J. Earthq. Eng. 1, 1-22.

Atkinson, G. & D.M. Boore 1997: Some comparisons between recent ground-motion relations. Seism. Res. Lett. 68, 24-40.

Bay, F. 2002a: Ground Motion Scaling in Switzerland: Implications for Hazard Assessment. PhD Thesis, (PEGASOS EXT-RF-0174).

Bay, F. 2002b: Differences between the PEGASOS WAF databases and the dataset of Bay 2002. (PEGASOS EXT-TN-0209).

Bay, F. 2002c: Forward Modeling to investigate stress-drop and kappa values in relation with the model of Bay 2002. (PEGASOS EXT-TN-0251).

Becker, A. 2003: Brune stress drops for small magnitude California data recorded at hard rock sites. Report presented during the SP2 April 2003 meeting in London.

Berge-Thierry, C., F. Cotton, M. Cushing, D.-A. Griot-Pommera, J. Joly, A. Levret & F. Fukushima 2000: Méthode de détermination des spectres horizontaux et verticaux dans le cadre de la révision de la RFS I.2.c. Rapport IPSN/DPRE/SERGD 00-53.

Berge-Thierry, C., D.-A. Griot-Pommera, F. Cotton & Y. Fukushima 2002: New empirical response spectral attenuation laws for moderate European earthquakes. J. Earthq. Eng., submitted.

Boore, D.M., W.B. Joyner & T.E. Fumal 1994: Estimation of response spectra and peak accelerations from western North American earthquakes. USGS internal report, Part 2, 40 pp.

Boore, D.M., W.B. Joyner & T.E. Fumal 1997: Equations for estimating horizontal response spectra and peak accelerations from western North American earthquakes: A summary of recent work. Seism. Res. Lett. 68, 128-153.

Boore, D.M. & W.B. Joyner 1997: Site amplification for generic Rock Sites. Bull. Seism. Soc. Am. 87/2, 327-341.

Bozorgnia, Y. & K.W. Campbell 2002: Vertical-to-horizontal response spectral ratio and vertical design spectrum. Earthq. Spectra., submitted.

Bungum, H., C. Lindholm & A. Dahle 2002: Long period ground motions for large European earthquakes, 1905-1992, and comparisons with stochastic predictions. J. Seism., in press.

Campbell, K.W. 1997: Empirical near-source attenuation relationships for horizontal and vertical components of peak ground acceleration, peak ground velocity, and pseudo-absolute acceleration response spectra. Seism. Res. Lett. 68, 154-179.

Campbell, K.W. 2001: Prediction of Strong Ground Motion Using the Hybrid Empirical Method: Example Application to Eastern North America. Bull. Seism. Soc. Am., submitted.

Campbell, K.W. & Y. Bozorgnia 2002: Updated near-source ground motion relations for the horizontal and vertical components of peak ground acceleration and acceleration response spectra. Bull. Seism. Soc. Am., submitted (revised).

Douglas, J. & P.M. Smit 2001: How accurate can strong ground motion relations be? Bull. Seis. Soc. Am. 91.6, 1917-1923.

Ekström, G. & A.M. Dziewonski 1988: Evidence of bias in estimations of earthquake size. Nature 332, 319-323.

Free, M.W. 1996: The attenuation of earthquake strong-motion in intraplate regions. PhD Thesis, Imperial College, London.

Fukushima, Y. 1996: Scaling relations for strong ground motion prediction models with M2 term. Bull. Seis. Soc. Am. 86, 329-336.

Herrero, A. & Bernard, P. 1994: A kinematic self-similar rupture process for earthquakes. Bull. Seism. Soc. Am. 84, 1216-1228.

Herrmann, R. B. & Wang, C.Y. 1985: A comparison of synthetic seismograms. Bull. Seism. Soc. Am. 75, 41-56.

Ide S. & G.C. Beroza 2001: Does apparent stress vary with earthquake size? Geophys. Res. Letts. 28, 3349-3352.

Lussou, P., P.Y. Bard & F. Cotton 2001: Seismic design regulation codes: Contribution of K-net data to site effect evaluation. J. Earthq. Eng. 5, 13-33.

Madariaga R. 2002: Assessment of feasibility of kinematic fault models used for upper limit ground motion evaluations for the PEGASOS Project. (PEGASOS EXT-TN-0308).

Malagnini, L., R.B. Herrmann & K. Koch (2000). Regional Ground Motion Scaling in Central Europe. Bull. Seism. Soc. Am. 90.4, 1052-1061.

Mayeda, K. & W.R. Walter 1996: Moment, energy, stress drop, and source spectra of western United States earthquakes from regional coda envelopes, J. Geophys. Res. 101, 11195-11208.

McGuire, R., Silva, W. & Costantino, C. 2001: Technical Basis for Revision of Regulatory Guidance on Design Ground Motions: Hazard- and Risk-consistent Ground Motion Spectra Guidelines. NUREG/CR-6728.

NUREG/CR-6372-V1 1997: Recommendations for PSHA: Guidance on uncertainty and Use of Experts.

PEGASOS TP2-TN-0249 2002: Residuals as a function of epicentral distance for ground motions recorded at short JB distances.

PEGASOS TP2-TN-0254 2002: Average shear wave velocity profiles for Europe and California.

PEGASOS TP2-TN-0269 2002: Note on the statistical analysis of the ratios of different definitions of the horizontal component.

PEGASOS TP2-TN-0270 2002: Note on the estimation of coefficients of ground motion models at missing frequencies.

PEGASOS TP2-TN-0307 2002: Note on the analysis of standard deviations of residuals computed using different definitions of the horizontal component.

PEGASOS TP2-TN-0333 2003: Note on maximum ground motion plots.

PEGASOS TP2-TN-0362 2003: SP2 inquiry for the style-of-faulting distributions of the selected attenuation relations.

PEGASOS TP2-TN-0367 2003: Comparison of the measured accelerations of the Feb. 22 Mw 4.8 St. Dié earthquake with the candidate GM Models.

PEGASOS TP2-TN-0363 2003: Final report on the computation of scaling factors for 20 generic "rock" profiles.

PEGASOS TP2-TN-0350 2003: Computation of scaling factors for three "realistic" rock profiles.

Pitarka, A., P. Somerville & N. Collins 2002: Numerical Simulations for Evaluation of Median and Upper Limit Ground Motions in Switzerland – Revised Final Report. (PEGASOS EXT-TN-0277).

Priolo, E., A. Vuan, P. Klinc & G. Laurenzano 2002: Estimation of the Ground Motion Upper Limit in Switzerland: EXWIM Numerical Simulations – Scientific Report Nr.4 - Revised Final Report (PEGASOS EXT-TN-0278).

Rietbrock, A. 2002: Determination of input parameters for the stochastic simulation of strong ground motion for Switzerland (PEGASOS EXT-TN-0306).

Roth, Ph. 2002: Note on the plots of the largest ground motion contained in the WAF database TP2-WAF-0008 (PEGASOS TP2-TN-0309).

Sabetta, F. & A. Pugliese 1996: Estimation of response spectra and simulation of nonstationary earthquake ground motions. Bull. Seism. Soc.Am. 86, 337-352.

Sabetta, F. 2002: Commentary on the Priolo and the Pitarka reports (PEGASOS EG2-TN-0264).

Silva, W., R. Darragh & N. Gregor 1998: Reassessment of site coefficients and near-fault factors for building code provisions (PEGASOS EXT-RF-0394).

Smit, P. 2002: Comments of Smp on Francesca's report regarding expert request 15, (PEGASOS TP2-TN-0393).

Smit, P., A. Hoelker & Ph. Roth 2002: Updated main WAF database, (PEGASOS TP2-WAF-0008).

Somerville, P., N. Collins, R. Graves & C. Saikia 2001: Ground motion attenuation relations for the central and eastern United States. Final Report, USGS award number 99HQGR0098.

Spudich, P., W.B. Joyner, A.G. Lindh, D.M. Boore, B.M. Magaris & J.B. Fletcher 1999: SEA99: A revised ground motion prediction relation for use in extensional tectonic regimes. Bull. Seism. Soc. Am. 89, 1156-1170.

SSHAC (Senior Seismic Hazard Analysis Committee) 1997: Recommendations for PSHA: Guidance on uncertainty and Use of Experts. NUREG/CR-6372-V1.

Toro, G.R., N.A. Abrahamson & J.F. Schneider 1997: Model of strong ground motions from earthquakes in central and eastern North America: Best estimated and uncertainties. Seism. Res. Lett. 68, 41-57.

Toro, G.R. 2003: Sensitivity Analysis on Upper Tail Modification of the Ground Motion Distribution for Switzerland (PEGASOS EXT-TN-0293).

UAK 2002: Revised specifications of PEGASOS Results, 28.11.02 (PEGASOS PMT-AN-0195).

Youngs, R.R., N. Abrahamson, F.I. Makdisi & K. Sadigh 1995: Magnitude-dependent variance of peak ground acceleration. Bull. Seism. Soc. Am. 85, 1161-1176.

APPENDIX 1: EG2-HID-0030 HAZARD INPUT DOCUMENT FINAL MODEL F. SABETTA

A 1.1 Introduction

This document describes the implementation and parameterization of Fabio Sabetta's expert model EG2-EXM-0020, as described in the Elicitation Summary EG2-ES-0034 and delivered on 22.05.2003. The purpose of this document is to translate the expert's evaluation of ground motion into an input useable by the hazard software.

A 1.2 Model Implementation

Based on F. Sabetta's Elicitation Summary EG2-ES-0034, the logic trees for the median horizontal ground motion, the vertical/horizontal ratio and the aleatory variability of the horizontal component were implemented in FORTRAN and the results displayed graphically.

Key elements in the model include:

Median horizontal ground motion

- 8 out of the 15 candidate models have been retained
- The Stochastic Point Source model is based on Bay (2002) and further sub-divided into three sub-models, using three different variable combinations for stress drop and kappa.
- For the weighting of the ground motion models, the magnitude – distance plane is sub-divided into 9 bins with the following limits:
- Magnitude: $5 < 5.5 < 6.5 < 8$
- Distance [km]: $0 < 10 < 70 < 1000$
- To account for site class effects the representative $V_{s,30}$ for each attenuation equation is corrected to the reference of 2000 m/s using the scale factors provided in TP2-TN-0363 (Resonance 2003) as central branch. Epistemic uncertainty is considered by the addition of two side branches with lower and higher $V_{s,30}$.
- No Kappa-Correction is to be made.
- No adjustment to specific Swiss conditions is applied.
- Magnitude conversion from M_s to M_w is computed using three equally weighted relations. Magnitude conversion from M_{JMA} to M_w is computed according to two equally weighted alternative relations (one being equivalence). No conversion is made between M_L and moment magnitude.
- The conversion of the different types of horizontal components to the geometric mean definition is based on frequency dependent scaling factors. Epistemic uncertainty is introduced via the addition of a second and a third branch with smaller and larger scaling factors.
- Missing coefficients in the ground motion models considered shall be derived according to the procedure described in TP2-TN-0270.
- Style-of-faulting adjustment is to be made by applying frequency dependent scaling for normal, strike-slip and reverse faulting. The epistemic uncertainty is modeled by the use of three branches with central, lower and upper scaling factors.

V/H Ratio

- V/H ratios are obtained by using 6 out of the 8 candidate models that predict both horizontal and vertical components
- The site correction for the vertical components is performed in the same way as it was for the horizontal components. In addition, the vertical ground motion is scaled using frequency dependent correction factors.
- Magnitude conversion is applied for both the V and H components.
- The conversion of components to the geometric mean is applied to horizontal components only.
- Missing coefficients in the ground motion models have been derived according the procedure described in TP2-TN-0279.
- Style-of-faulting adjustments are applied using different sets of scaling factors for both horizontal and vertical components. The epistemic uncertainty is introduced by the use of three branches with central, lower and upper values.

Aleatory variability for the horizontal component

- One model is used (Abrahamson & Silva) to provide the standard deviation of horizontal ground motion. Three branches with ± 15 % scaling, account for the epistemic uncertainty, the central branch having a weight of 0.4, the other two of 0.3.

Maximum ground motion and upper tail truncation

- Equations that correspond to different percentiles from the Ambraseys et al. (1996) ground motion model are used to define alternatives of the maximum ground motion estimate, see Tab. A1-1 below.

Tab. A1-1: Maximum ground motion expressed in term of number of standard deviations of Ambraseys et al. (1996) relation, scaled to horizontal comp. geom. mean and to M_w

N° of σ (Ambraseys et al.)	Weight
1.7	0.10
2.8	0.60
3.6	0.22
4.2	0.08

- The upper tail of the ground motion distribution is to be truncated at different values of sigma, see Tab. A1-2 below.

Tab. A1-2: Model for the upper tail of the ground motion distribution, with abrupt truncations at the given sigma levels

Sigma truncation	Weight
2.5	0.3
3.0	0.6
3.5	0.1

Figures A1-1, A1-2 and A1-3 show the logic trees for the horizontal component, the V / H ratio and the aleatory variability, resp., as they have been implemented in the code.

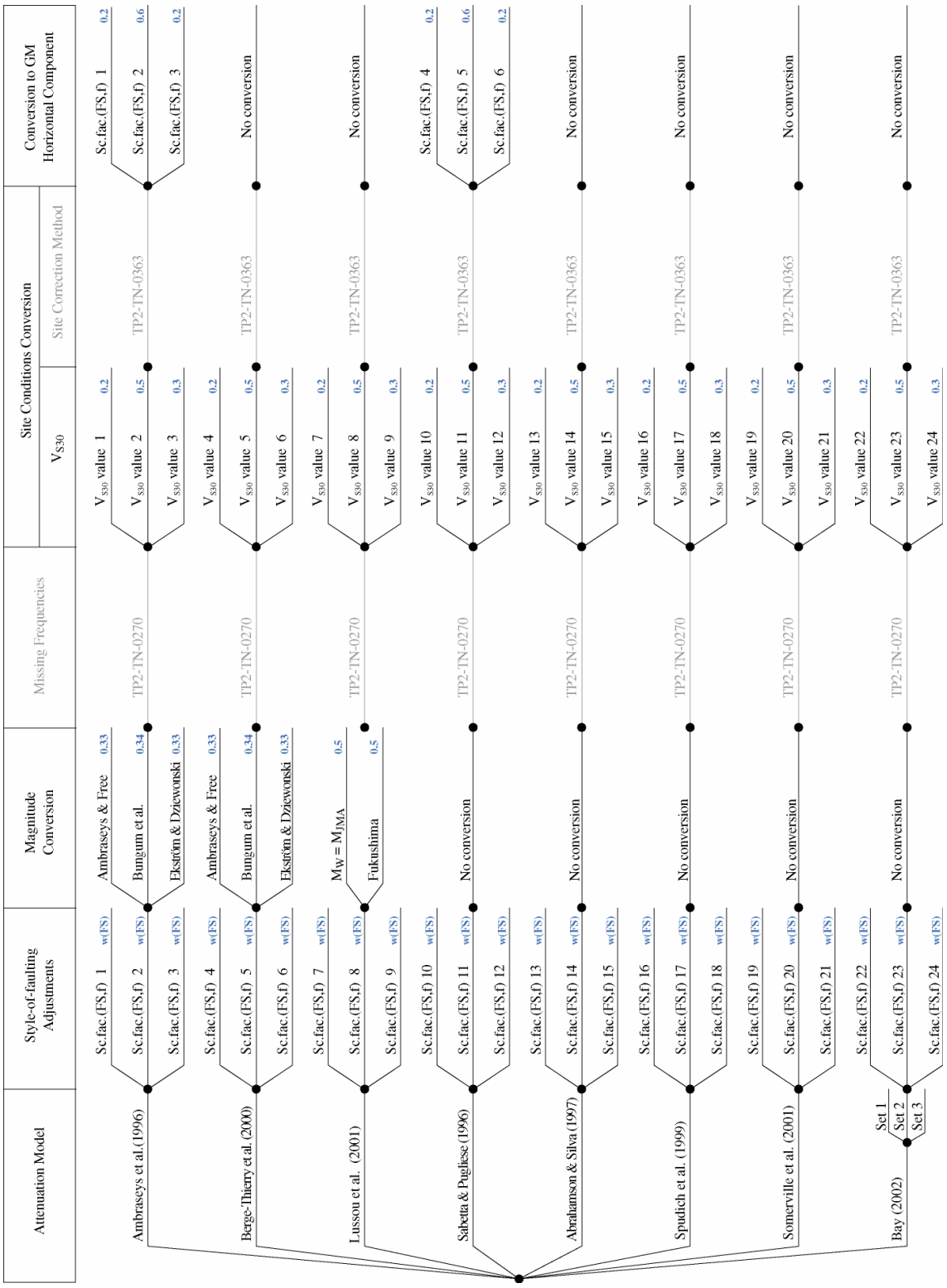

Fig. A1-1: Logic tree for the horizontal ground motion

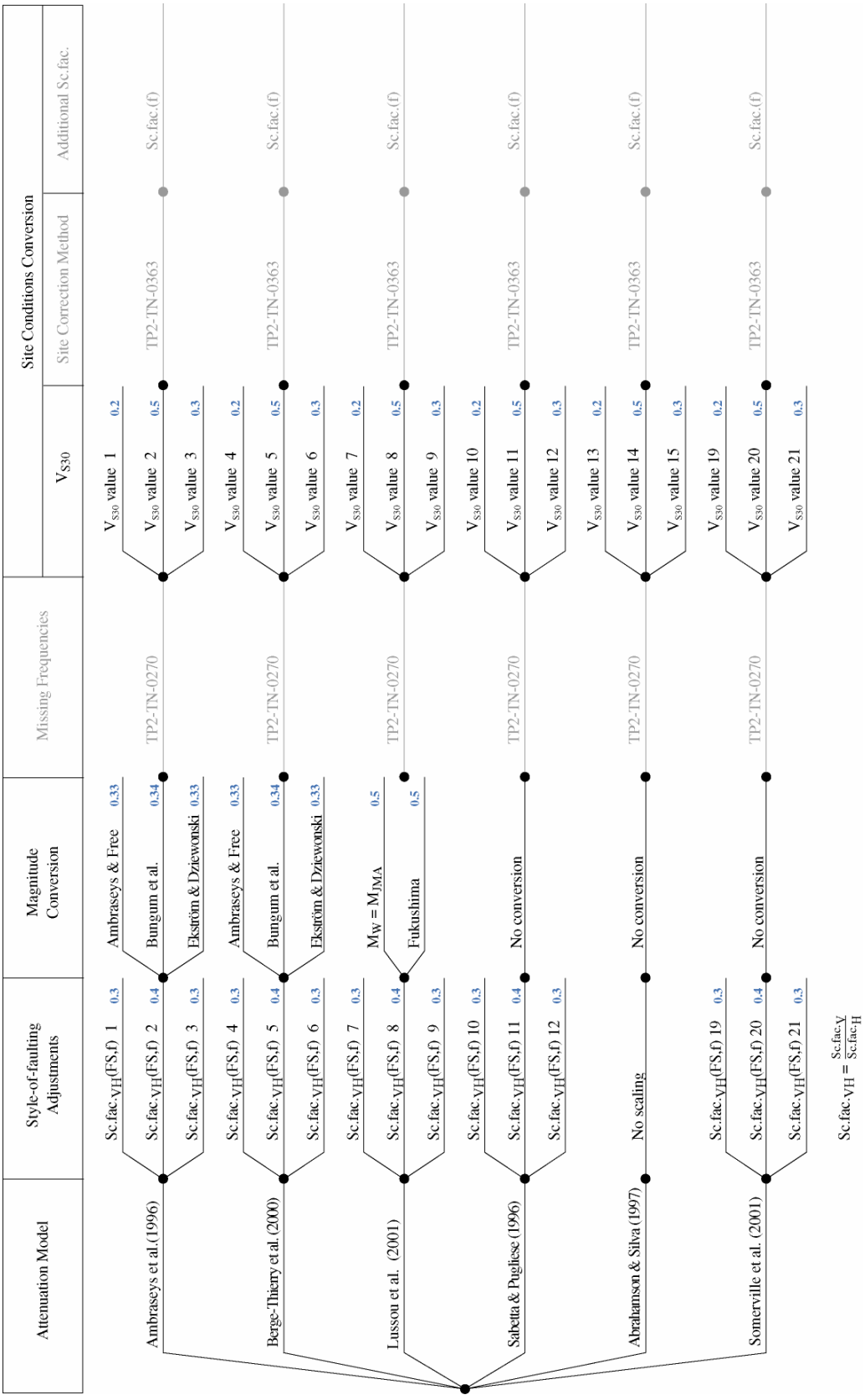

Fig. A1-2: Logic tree for the V/H ratio

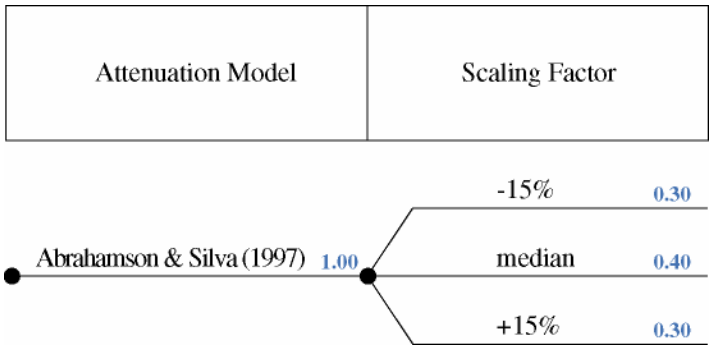

Fig. A1-3: Logic tree for the aleatory uncertainty

A 1.3 Model Parameterization

The ground motion is parameterized for the final Rock Hazard Computations at the following spectral frequencies: 0.5 Hz, 1 Hz, 2.5 Hz, 5 Hz, 10 Hz, 20 Hz, 33 Hz, 50 Hz and at peak acceleration. The implementation of the logic trees results in: (a) a set of alternative estimates of the median horizontal ground motion, aleatory variability of the horizontal ground motion and V / H ratios at each spectral frequency, earthquake magnitude, fault style, and distance, and (b) the weight associated to each individual branch of the logic tree.

Ground motions have been modeled for seven magnitudes [5.0 : 0.5 : 8.0] and 14 distances (1.0, 1.6, 2.5, 4.0, 6.3, 10, 16, 25, 40, 63, 85, 100, 160, 250 kilometers).

The ground motion arising from the implementation of the SP2 logic trees has been parameterized using a composite model approach. At each distance, magnitude and spectral frequency, and for each fault style, the alternative estimates of the median ground motion are sorted in order of ascending spectral acceleration. The weights associated with the sorted median amplification factors are summed, resulting in a cumulative distribution of the amplification factors. The stair-steps cumulative distribution function was somewhat smoothed by interpolating the values between the step centers. The values of the ground motion are selected for cumulative distributions corresponding to the following fractiles: 0.13 %, 2.28 %, 16 %, 50 %, 84 %, 97.72 %, and 99.87 %. The seven fractiles correspond to median, $\pm 1\sigma$, $\pm 2\sigma$, and $\pm 3\sigma$ levels. By using the discrete fractiles, no assumption regarding symmetry of the epistemic uncertainty is made.

For the aleatory variability, the same process is repeated but with the sorting performed on the amplitude of the aleatory variability.

A conversion to account for different distance measures was conducted using the Scherbaum conversion factors. (These conversions may be updated in the final model to incorporate the SP1 depth distributions). Two sets of conversions were done. The first converted the distances to JB distances and the second converted the distances to rupture distance. The main differences between the JB distance and the rupture distance occur for small magnitudes at short distances. However, to avoid potential jumps in the models at bin boundaries, the conversions were applied to all the bins (unlike what had been done for the sensitivity computations, where the conversion was not applied to the smallest magnitude and shortest distance bin ($M < 5.5$, $D < 10$).

The values of ground motion resulting from this procedure are input directly into the rock hazard software without further parameterization or fitting.

The Maximum Ground Motion estimates are also parameterized in a similar manner. Tables of the maximum ground motion are developed for the same magnitude and distance bins, for each style of faulting and for the seven fractiles.

Figures A1-4 to A1-6 on the next pages of this document show one example (for PGA, the Joyner-Boore distance and strike-slip) of the ground motion for the horizontal component, for the V / H ratio and for the aleatory variability for the horizontal component, respectively. The figures display four subplots. The upper plot shows the median as a distance and magnitude dependent surface. The central plot shows the median ground motion as a distance and fractile dependent surface for magnitude 6.5. The lower left plot shows the median for the seven magnitudes (magnitude 5.0 to 8.0 in 0.5 magnitude steps) while the lower right subplot shows the seven fractiles (corresponding to median, $\pm 1\sigma$, $\pm 2\sigma$, and $\pm 3\sigma$) for magnitude 6.5.

The complete set of figures is to be found as a PDF-file on the attached CD-ROM under the designation EG2-HID-0030_Sabetta_ figures.pdf.

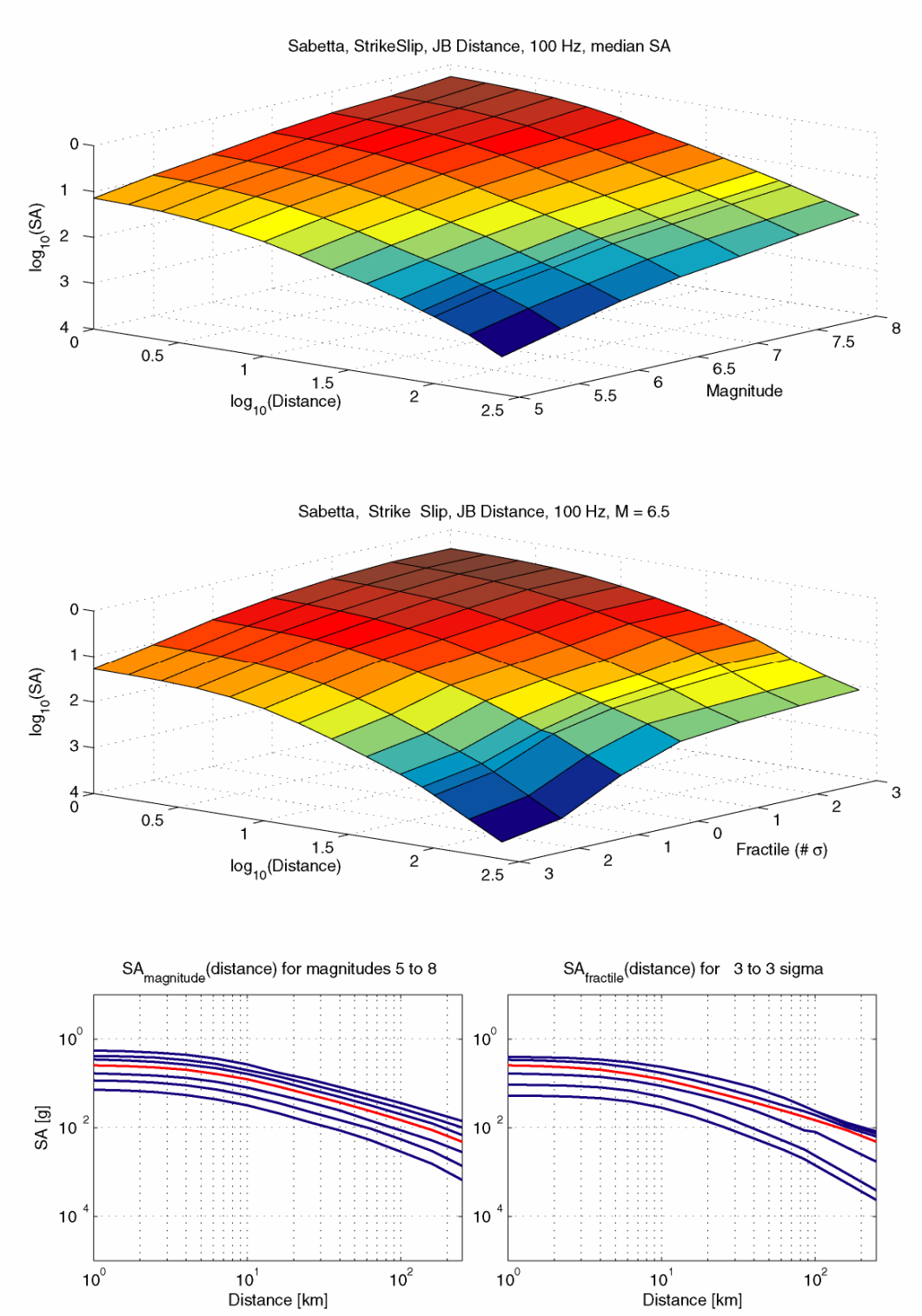

Fig. A1-4: Spectral acceleration (SA) for PGA (100 Hz), assuming strike-slip mechanism and Joyner-Boore distances

The upper plot shows SA (distance, magnitude) for the median. The middle plot shows SA (distance, fractile) for magnitude 6.5. The lower left-hand plot shows the median SA (distance) for different magnitudes. The lower right-hand plot shows SA (distance) for different fractiles and magnitude 6.5.

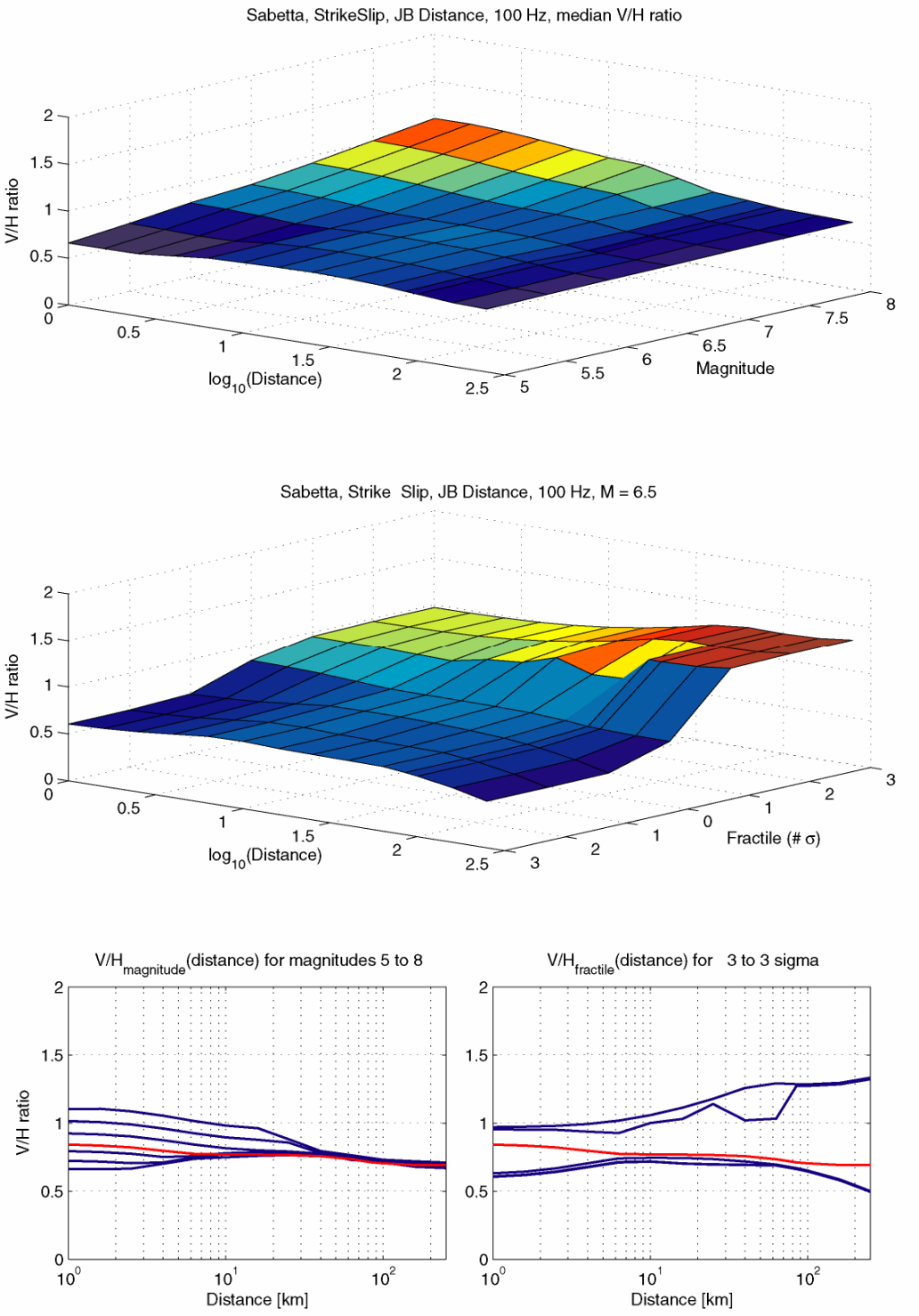

Fig. A1-5: V / H ratio (V / H) for PGA (100 Hz), assuming strike-slip mechanism and Joyner-Boore distances

The upper plot shows V / H (distance, magnitude) for the median. The middle plot shows V / H (distance, fractile) for magnitude 6.5. The lower left-hand plot shows the median V / H (distance) for different magnitudes. The lower right-hand plot shows V / H (distance) for different fractiles and magnitude 6.5

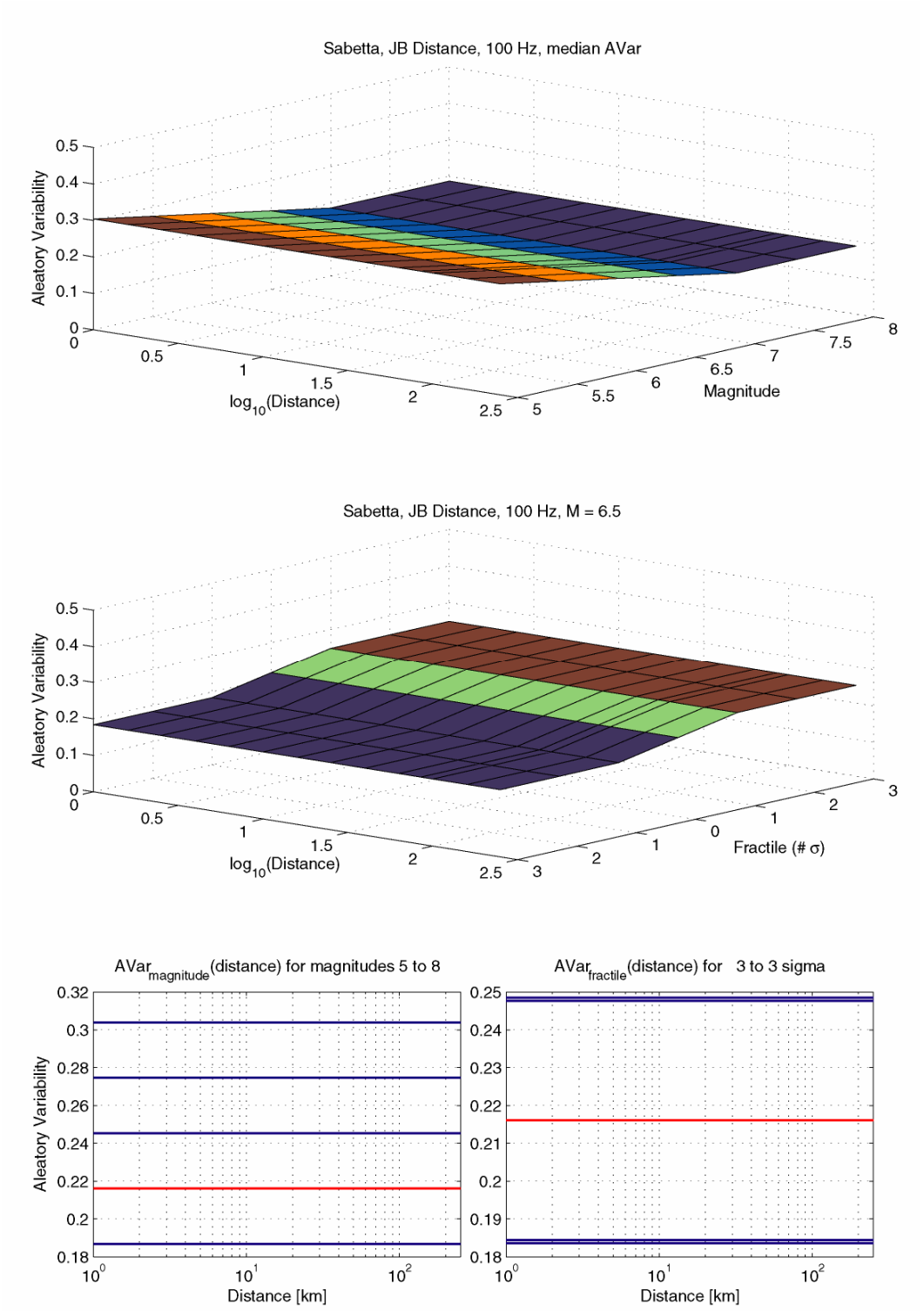

Fig. A1-6: Aleatory variability (AVar) for PGA (100 Hz), assuming Joyner-Boore distances (AVar does not depend on the style of faulting)

The upper plot shows AVar (distance, magnitude) for the median. The middle plot shows AVar (distance, fractile) for magnitude 6.5. The lower left-hand plot shows the median AVar (distance) for different magnitudes. The lower right-hand plot shows AVar (distance) for different fractiles and magnitude 6.5

Part V: Ground Motion Characterisation, Elicitation Summary

Prof. Dr. Frank Scherbaum

Institut für Geowissenschaften der
Universität Potsdam
Potsdam - Germany

Probabilistische Erdbeben-Gefährdungs-Analyse für die KKW-Stand Orte in der Schweiz
(PEGASOS)

SP2 Ground Motion Characterisation

Elicitation Summary

Frank Scherbaum

Institut für Geowissenschaften der
Universität Potsdam
Potsdam - Germany

nagra

PEGASOS

TABLE OF CONTENTS

LIST OF TABLES

LIST OF FIGURES

1 INTRODUCTION

This report summarizes my evaluation of ground motion models for SP2 of the PEGASOS project. My general philosophy has been to derive a *consistent and transparent* weighting scheme which would avoid the subjective juggling of weighting factors based on fuzzy judgments as much as possible. For this purpose, I have developed a fully formalized process of documenting all reasoning. A second focus has been on the applicability to Switzerland. In my approach, match or mismatch of a model to Switzerland is tested in a very rigorous way by comparing the individual ground motion predictions to a regionally observed reference data set (dominated by the St. Dié earthquake). Based on a quantitative goodness-of-fit measure, weighting factors are subsequently readjusted to account for the applicability to Swiss conditions. This adds an objective, data driven quality control mechanism to the selection of ground motion models since models performing poorly on the reference data set will be recognized automatically and will be rejected.

Despite the enormous efforts in SP2 and the excellent support by the PEGASOS PMT, there are a number of issues which still have large uncertainties:

- Kappa: The large scatter of the kappa values in Switzerland demonstrated by the analysis of Rietbrock (Rietbrock, 2002) made me assign a rather large range of kappa values for the target region Switzerland in the context of the host-to-target-region conversion. The possibly rather large scatter of the corresponding ground motion estimates could probably be reduced considerably if the 'kappa effect' would be considered a site specific issue and treated individually of each NPP site. It would also be more consistent with the possibility that kappa and the properties of the reference rocksite could be coupled.
- Site correction for vertical components: Another issue related to the site conditions is the site correction for the vertical component. This is currently treated the same way as for the horizontal component which introduces an unknown amount of bias.
- Dependence of ground motion models: I am aware of the fact, that two of the ground motion models in my logic tree (Ambraseys et al., 1996) and (Berge-Thierry et al., 2000) are not really independent in the sense that they are partially based on the same records. The consequences, however, and to what degree this may be a problem with other ground motion models as well, are not really obvious to me.

Regarding another issue with large uncertainties - maximum ground motions - the project has established the state-of-the-art using available methods. Recently proposed hybrid approaches, however, (Guatteri et al., 2002; Mai and Beroza, 2002; Mai and Beroza, 2002) possibly offer computationally feasible solutions for the not-so-far future.

1.1 Ground motion model weighting Factors

There are two different aspects to the determination of weighting factors which I find conceptually convenient to separate. The first one relates to the overall quality of a particular GMM (ground motion model) while the second one is concerned with the applicability to a particular target region (Switzerland). The first aspect is completely fixed by the GMM and determined (among other factors) 'only' by the quality of the data set on which it was created. The second one depends also on how one can adapt a GMM from the host-region of its data set to a completely different target region (Switzerland).

1.2 Prior GMM weighting factors

The factors corresponding to the first aspect, which I call prior GMM *weighting factors* (*wf*), measure my degree of confidence in a GMM to be appropriate for a given magnitude, distance, and frequency range. In other words, the prior weighting factors (which have to sum up to 1 for all GMMs) reflect my judgment of a particular GMM per se, independent of where the model is going to be applied. The determination of the prior weighting factors was done in four steps. In the first step, I created a knowledge base which contains all the information about a particular ground motion model which I considered relevant. The content of this knowledge base is very similar to the ground motion model summaries which the SP2 expert received at an earlier stage of the project. It contains for example the number of earthquakes in a certain magnitude distances bins, the frequency coverage, remarks about problems, etc. The knowledge base is still kept in a verbose form.

The second step consists of categorization and quantization of the information in the knowledge base. The quantization is still verbose but for each category contains only a limited number of element or judgements. Categories for example are: Magnitude range, Frequency range, distance range, reference rock velocity, dominant faulting style, etc. The quantization of each category is driven by the information which is available (e.g. about different data coverage, etc.).

In the third step, I assign a verbose quality measure (e.g. 'GOOD', 'POOR', 'FAIR', or 'NA') to each of the vector components based on the information in the knowledge base. In order to keep this step completely transparent and flexible, I add a verbose reasoning field to the knowledge base explaining the reasons for giving a particular quality assignment.

Example: For the (Abrahamson & Silva, 1997) relationship, the category 'MAG' of the knowledge base consists of the following vector:

('MAG', ((-1,4.4,'NA'),(4.4,5.0,'POOR'),(5.0,7.0,'GOOD'),(7.0,7.4,'POOR'),(7.4,999,'NA')))

The first element consists of the category label (here 'MAG' for magnitude). Separated by comma is a vector with 5 elements, each of which is a magnitude bin. The two numerical elements define the bin margins (-1 and 999 marks absolute lower and upper bound, respectively) while the string element describes the quality assignment.

The corresponding reasoning field for this example is shown below:

('REASONING', (('MAG',' The total magnitude range is 4.4 - 7.4. Since only 6 events with M < 5 and 4 events with M > 7 are present in the dataset, I judge the range 5 – 7 as GOOD, the ranges 4.4 – 5.0 and 7 – 7.4 as POOR. The rest as NA.')))

This way, I assure that the reasoning is documented and can be reevaluated independently. As a result of the last step, I obtain verbose quality assignments for each category bin to judge.

Appendix A and B contain the complete documentation of the knowledge base for the horizontal and the vertical ground motion models, respectively.

In the next step, the verbose quality assignment are run through a parser which converts each of the quality measures into a number. This is done by the following set of conversion rules:

NA → 0.
GOOD → 1
FAIR → 0.66
POOR → 0.33

A second set of conversion rules defines the relative weighting of individual categories:

MAG → 1.
DISTRANGE → 1.
FREQ → 1.

In case a certain category should be given a higher weight, the corresponding number simply has to be increased. The reasoning behind the assignment of the individual labels is documented in Appendix A and B.

After parsing, each real value in each category is assigned a number representing my personal judgement of the strength of the model at that particular value of the category resulting in a quality function for each ground motion model.

The last step consists of the calculation of the actual weighting factors for the requested magnitude, distance and frequency bins. For this purpose, the distance range was subdivided into those distance bins which were showing different geometrical spreading rates in (Bay, 2002) plus a near source bin. The overall magnitude range to be covered (5-7.5) was subdivided into three bins (5-6, 6-7, 7-7.5). The central bin was chosen according to the magnitudes of those events which were found dominant in previous hazard studies. The frequency range was separated into octave bands with the center frequencies corresponding to those for which an estimate is required. The weighting factor for PGA is assumed to be the same as for the highest frequency bin present. The weighting factor for a particular ground motion model (GMM) in the magnitude bin, distance bin and frequency bin is determined by the following ("quality density") integral:

$$wf_{i,j,k} = \frac{\int_{\Delta M_i}\int_{\Delta R_j}\int_{\Delta f_k} qual_{GMM}(M,R,f)\,dM\,dR\,df}{\Delta M_i \cdot \Delta R_j \cdot \Delta f_k} \qquad (1\text{-}1)$$

Finally, all non-zero weighting factors for a particular magnitude, distance and frequency bin are normalized such that they sum up to 1, if the sum is taken over all ground motion models.

1.3 Relative ground motion model adjustment factors

The second set of factors - which I call GMM *adjustment factors* (*af*) - describe my confidence in the applicability of a particular GMM to Switzerland *after* the GMMs have potentially gone through a whole set of corrections such as magnitude corrections, site condition conversions, attenuation conversions etc. They essentially judge the success of all these modifications and describe how the weighting factors of those models which perform poorly at the end should be reduced (adjusted). The determination of the adjustment factors is data driven as will be described below. Since at present the adjustment factors are independent of frequency, magnitude or distance, they consist only of a single value per GMM. While this makes it for example easy to change procedures for site conversion or host-to-target-region conversion, a price to pay is that the weighting factors have to be renormalized across the branches of the logic tree for each magnitude, frequency and distance bin.

2 EVALUATION OF PROPONENT MODELS FOR APPLICABILITY TO SWITZERLAND

Empirical ground motion models – independent of the quality of the data base from which they were generated – will never describe exactly the properties of a target region for which the model is going to be applied. In the set of methods to deal with this problem two strategies stand out:

- In the pure ranking approach, the ground motion models are left untouched but are weighted differently based on the degree of applicability of the model to the target region.
- In the hybrid approach (Campbell 2001, #3688), the differences between the host region for each ground motion model and the target region are completely modeled and the ground motion models are modified.

In order to maximize the applicability of the candidate models to Swiss conditions, I have tried to generate host-to-target-region conversion filters for the implementation of the full hybrid approach. Equivalent stochastic models for all empirical ground motion models which were considered in SP2 were derived using a combination of trial and error and partial grid search. Although this attempt was successful in the sense that the median empirical models for $5 < M_w < 7$ and distances below 150 km for essentially all attenuation relations could be well represented by what seemed reasonable stochastic models, this exercise also demonstrated that the model parameters are highly non-unique. As a consequence, their uncertainty would be essentially unknown. For this reason I decided to drop the full hybrid model from further considerations and use only a "mild version" in which the host-to-target-region conversion is restricted to the conversion for the local rock site conditions and for differences in kappa. The judgment of how well the resulting models (including all the modifications) match Swiss conditions are taken care of by the calculation of *relative adjustment factors af* whose purpose it is to reduce the overall weight on those models that perform only poorly in terms of being applicable to Switzerland. In order to obtain the *absolute weighting factors wf* for the corresponding branches, the relative adjustment factors have to be normalized together with the prior weighting factors from chapter 1.

2.1 Data driven approach to determine relative adjustment factors for Swiss conditions

The rule based approach used for the determination of the prior weighting factors and of the data less determination of the ground motion model adjustment factors minimizes the risk of inconsistent assignment of judgment on different GMMs in cases where the number of models becomes large. Since the reasoning process is completely transparent and all steps are fully documented (actually the reasoning uses the documentation), posterior quality control is not an issue. It would be very desirable to perform the evaluation of the applicability to Switzerland in a similar transparent and reproducible way e.g. by using strong motion data from the target region. Basically one has to find some quantitative measure which describes how well a particular ground motion model predicts the reference data set (observed response spectra). There are several conceivable candidates for goodness-of-fit measures such as likelihood based measures (Edwards 1992), different flavors of variance reduction estimators (e.g. Cotton & Campillo 1995), or correlation coefficients to describe the degree of linear correlation between model and data vectors (e.g. the Pearson correlation coefficient, Press et al. 2001). In addition, statistical tests such as the Chi-square test or the Kolmogoroff-Smirnov test can be used to check if the data residuals follow the anticipated distribution (Restrepo-Velez et al. 2002). I have tested these measures on subsets of the generating data sets of several attenuation relations

(Abrahamson & Silva 1997, Ambraseys & Douglas 2000, Berge-Thierry et al. 2000, Sabetta & Pugliese 1996). These subsets had been flagged in the PEGASOS database or had been provided to me separately (Abrahamson pers. comm.). A good measure should allow the successful identification of the corresponding ground motion model as well as separate good from bad models. Ideally, if the spread of the measure would be between 0 for an unacceptable model and 1 for a perfect model, the measure could directly be used as ground motion model adjustment factor.

The results of this comparison for the (Abrahamson & Silva 1997) data set are shown in Figure 1 and Table 1. Only those ground motion models have been used for the comparison for which the data set falls into their validity range in terms of magnitude, distance and frequency coverage. In order to match the properties of the particular data set, distance metrics, magnitudes as well as components had to be converted for some of the ground motion models following the procedures described below. For the true ground motion model, the data residuals (scaled by model mean and model variance) should be normally distributed with zero mean and unit variance if the data are assumed to be independent (e.g. ignoring correlations of recordings from the same earthquake).

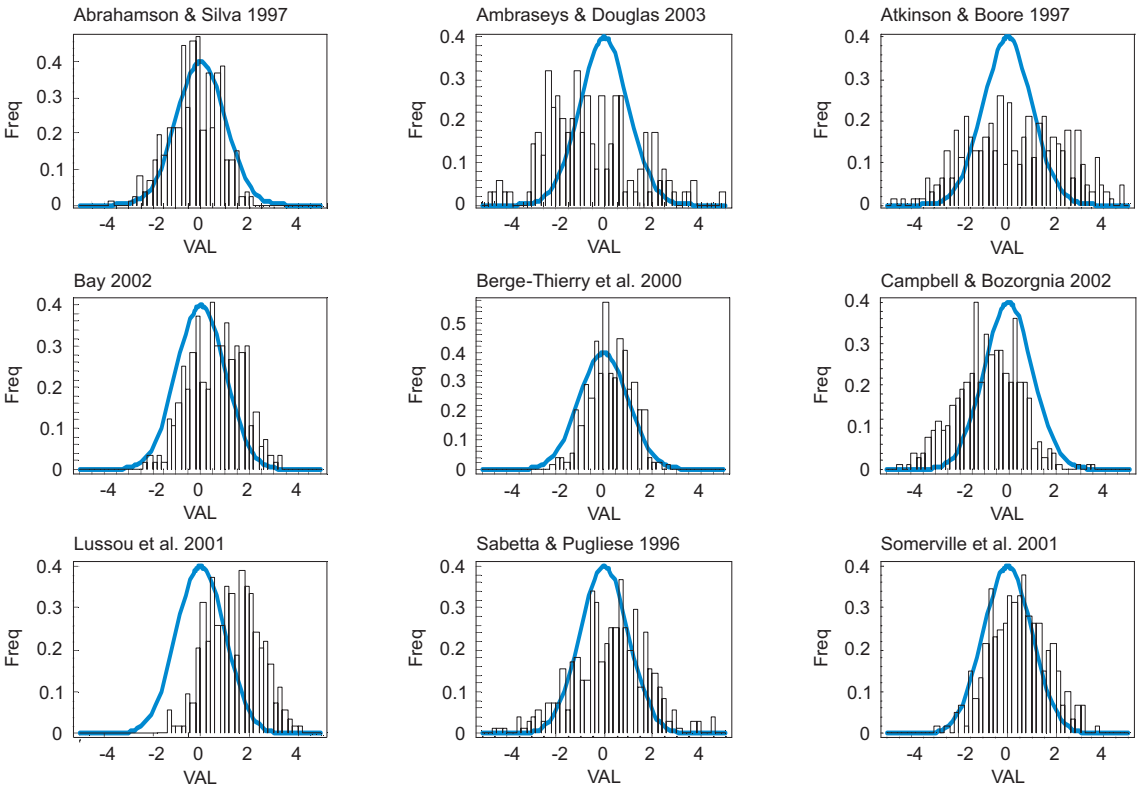

Fig. 1: Residual distribution (scaled by model mean and model variance) of a subset of the generating data set of the Abrahamson & Silva (1997) ground motion model with respect to different attenuation relations

The blue curve shows the expected distribution function for a unit variance normally distributed random variable.

With exception of the likelihood based measure referred to as *LH values*, all the test quantities in Table 1 are well described in the literature (Cotton & Campillo 1995, Press et al. 2001, Restrepo-Velez et al. 2002). The *LH values* have been derived in the following way. It is assumed that each ground motion model can be described by a lognormal distribution, in other words a normal distribution for $\ln(Y)$. If the model would be perfect, any observation can be seen as a random sample drawn from this distribution.

Tab. 1: Comparison of different attenuation relations to model a subset of the generating data set of the Abrahamson & Silva (1997) ground motion model

The goodness-of-fit measures used are: likelihood (LH), variance reduction (VARRED), the median of the sigma scaled deviation (MSSDEV), the Chi-Square statistics (CSQ), the Kolmogoroff-Smirnov statistics (KS), the P-value of the mean test (M-Test), the P value of the variance test (V-Test), and the Pearson correlation coefficient (CC).

Model Name	LH	LH-Ratio	VARRED	MSSDEV	MSSDEVR-ratio	CSQ-Test-Ratio	KS-Test-Ratio	M-Test-Ratio	V-Test-Ratio	CC-Ratio	#
Berge-Thierry et al. 2000	0.51	1.	0.957	0.293	0.743	1.	0.00498	0.000536	0.000497	0.96	61
Abrahamson & Silva 1997	0.466	0.914	0.984	0.218	1.	3.35e-6	1.	0.0187	1.	0.963	73
Somerville et al. 2001	0.396	0.775	0.673	0.451	0.483	0	0.0000149	6.94e-10	6.32e-6	0.916	51
Bay 2002	0.333	0.653	0.677	0.666	0.327	0	0	0	0.0168	0.763	47
Campbell & Bozorgnia 2002	0.321	0.629	0.696	0.806	0.27	0	0	0	0	0.748	65
Sabetta & Pugliese 1996	0.295	0.577	1.	0.323	0.675	0	0.000053	1.	0	1.	59
Lussou et al. 2001	0.178	0.348	-0.623	1.34	0.162	0	0	0	0.1	0.771	45
Atkinson & Boore 1997	0.123	0.242	0.247	0.232	0.937	0	0	0.0000234	0	0.59	52
Ambraseys & Douglas 2003	0.112	0.22	0.987	0.835	0.261	0	0	0	0	0.84	29

If for a given magnitude M, distance R, and frequency f, $\mu(M,R,f)$ is the predicted value for $\ln(Y)$, the probability of a single observation $x = \ln(Y_x)$ to fall into the interval $(x,x+dx)$ is:

$$dF = \frac{1}{\sigma\sqrt{2\pi}} \cdot \exp\left(\frac{-(x-\mu)^2}{2\sigma^2}\right) \cdot dx \qquad (2\text{-}1)$$

Here, $\sigma(M,R,f)$ is the standard error of the ground motion model which in general depends on magnitude, distance and frequency. If we normalize the sample by model mean μ and standard deviation σ we obtain $z = (x-\mu)/\sigma$ for which the distribution function would be:

$$f(z) = \frac{1}{\sqrt{2\pi}} \cdot \exp\left(\frac{-z^2}{2}\right) \qquad (2\text{-}2)$$

A convenient likelihood based quality measure for a ground motion model is the probability for a sample from the normalized distribution to be larger or equal to an observation y:

$$G(y) = \frac{1}{\sqrt{2\pi}} \int_{y}^{\infty} \exp\left(\frac{-z^2}{2}\right) \cdot dz = \frac{1}{2}\left(1 - Erf\left(\frac{y}{\sqrt{2}}\right)\right) = \frac{1}{2} Erfc\left(\frac{y}{\sqrt{2}}\right) \tag{2-3}$$

Here *Erf*(*x*) and *Erfc*(*x*) are the error function $\frac{2}{\sqrt{2\pi}} \int_{0}^{x} \exp(-t^2) \cdot dt$ and complementary error function *Erfc*(*x*) = 1 - *Erf*(*x*) respectively. If one considers both tails of the distribution, the corresponding quantity to consider is the probability for the modulus of a sample from the normalized distribution to be larger or equal to *y*:

$$LH(y) = Erfc\left(\frac{y}{\sqrt{2}}\right) \tag{2-4}$$

In the following, *LH*(*y*) will be referred to as the likelihood of a single observation *y*. *LH*(*y*) has several interesting properties:

- For *y = 0* we obtain *LH*(*0*) = 1. In other words, the observation of the mean value of the distribution corresponds to a likelihood value of 1.
- For y = ∞ we obtain *LH*(*0*) = 0. The poorer the observations become, the smaller the corresponding likelihood value becomes.
- Using the transformation properties of probability distributions, it can be shown that for samples *y* drawn from a normal distribution with unit variance (model assumptions matched exactly), *LH*(*y*) is evenly distributed between 0 and 1. The properties of the *LH* distribution are further illustrated in Figure 2.

Figure 2a shows the case in which the model matches the data exactly in terms of both mean and variance. Here, *LH(y)* is evenly distributed between 0 and 1 and both mean and median of *LH*(*y*) become 0.5. In case the model matches the data only in terms of mean but the sample variance is smaller than the model variance (Figure 2b), the distribution of *LH*(*y*) becomes skewed and the median will increase to values above 0.5. In case the sample variance becomes larger than the model variance (still with the proper mean, Figure 2c) the frequency of low *LH*(*y*) values will increase and the median of the distribution will decrease below 0.5. The decrease of the median of the *LH*(*y*) distribution will be especially strong for simultaneous increase in sample variance and a shift of the mean value (Figure 2f).

Because of these properties, the distribution of *LH*(*y*) seems to be a good indicator for the goodness-of-fit of ground motion models to observed response spectral values as well as for how well the model assumptions are met. The median of the *LH*(*y*) distribution seems to conveniently describe the overall quality of goodness-of-fit by a single number. For the (Abrahamson & Silva 1997) data subset, *LH value* distributions for those attenuation relations with the sufficient validity range are shown in Figure 3.

For the (Abrahamson & Silva 1997), the (Berge-Thierry et al. 2000), and the (Somerville et al. 2001) ground motion model, the shape of distribution resembles an even distribution between 0 and 1 as would be expected for a good model. For the remaining models, there is an increased frequency of small *LH* value, indicating a large number of poorly predicted data points. The median of the *LH*(*y*) distributions, subsequently referred to simply as the *LH value* of a ground motion model, for the individual attenuation relations to match the (Abrahamson & Silva 1997) data set are displayed on top of each panel and are additionally given in the first column of Table 1.

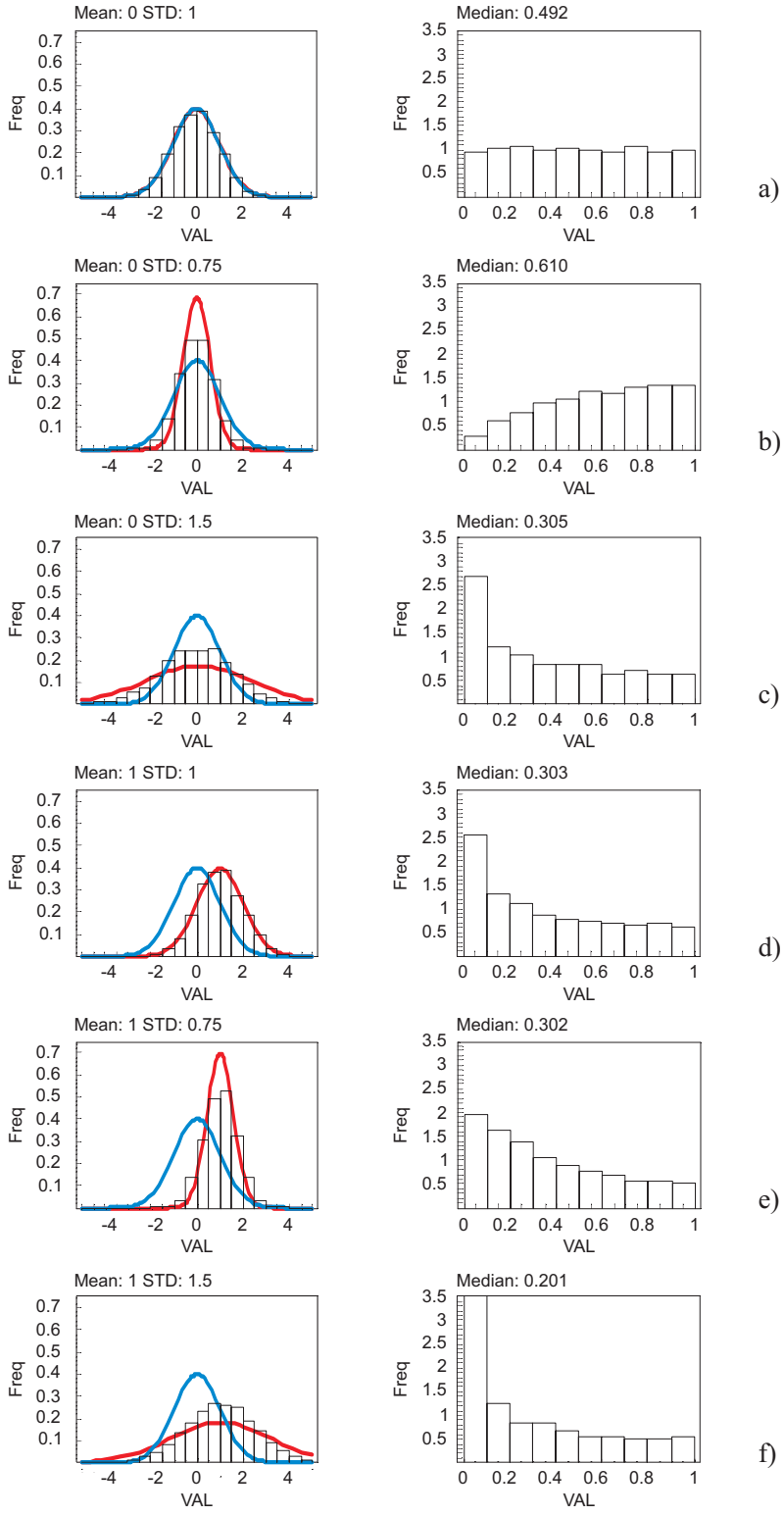

Fig. 2: Distribution of assumed Figure 2 residuals *y* (left panels) and corresponding *LH*(*y*) distribution (right panels)

Mean values and standard deviations of the residual distributions are indicated on top of the left panel. The blue and red distribution functions in the left panel indicate the unit variance normal distribution and the actual residual distribution, respectively. On top of each right panel, the median of the resulting *LH*(*y*) distributions are displayed.

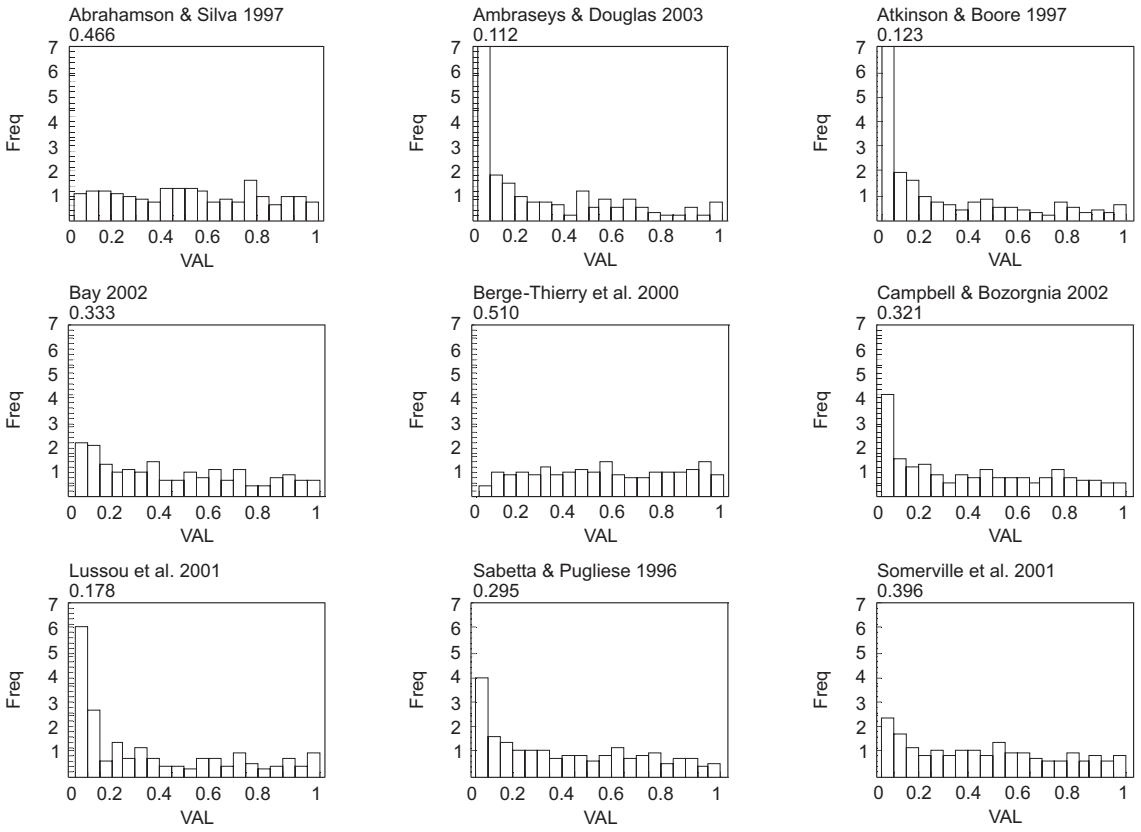

Fig. 3: Distribution of $LH(y)$ for a subset of the generating data set of the Abrahamson & Silva (1997) ground motion model with respect to different attenuation relations

All panels are scaled to the same maximum value.

From the discussion above one would expect an *LH value* close to 0.5 for the model generating data set. As can be seen in Table 1 this is actually the case for the (Abrahamson & Silva 1997) model. The *LH value* larger than *0.5* for the (Berge-Thierry et al. 2000) model probably indicates the sample variance being smaller than the model variance.

A slightly different way of looking at the *LH values,* which is implemented in column 2 of Table 1, is by normalizing the individual values with respect to their overall maximum. This so-called *LH ratio* can be interpreted as a parameter expressing the *relative* strengths of the models, since according to the likelihood axiom, all the information concerning the relative merits of two hypothesis/models is contained in their likelihood ratio (Edwards 1992, p. 31). Figures 4 – 13 and Tables 2 – 6 give the distributions of the residuals, the corresponding *LH values* and the compilation of the goodness-of-fit measures for a number of additional ground motion models for which subsets of the generating data set were available.

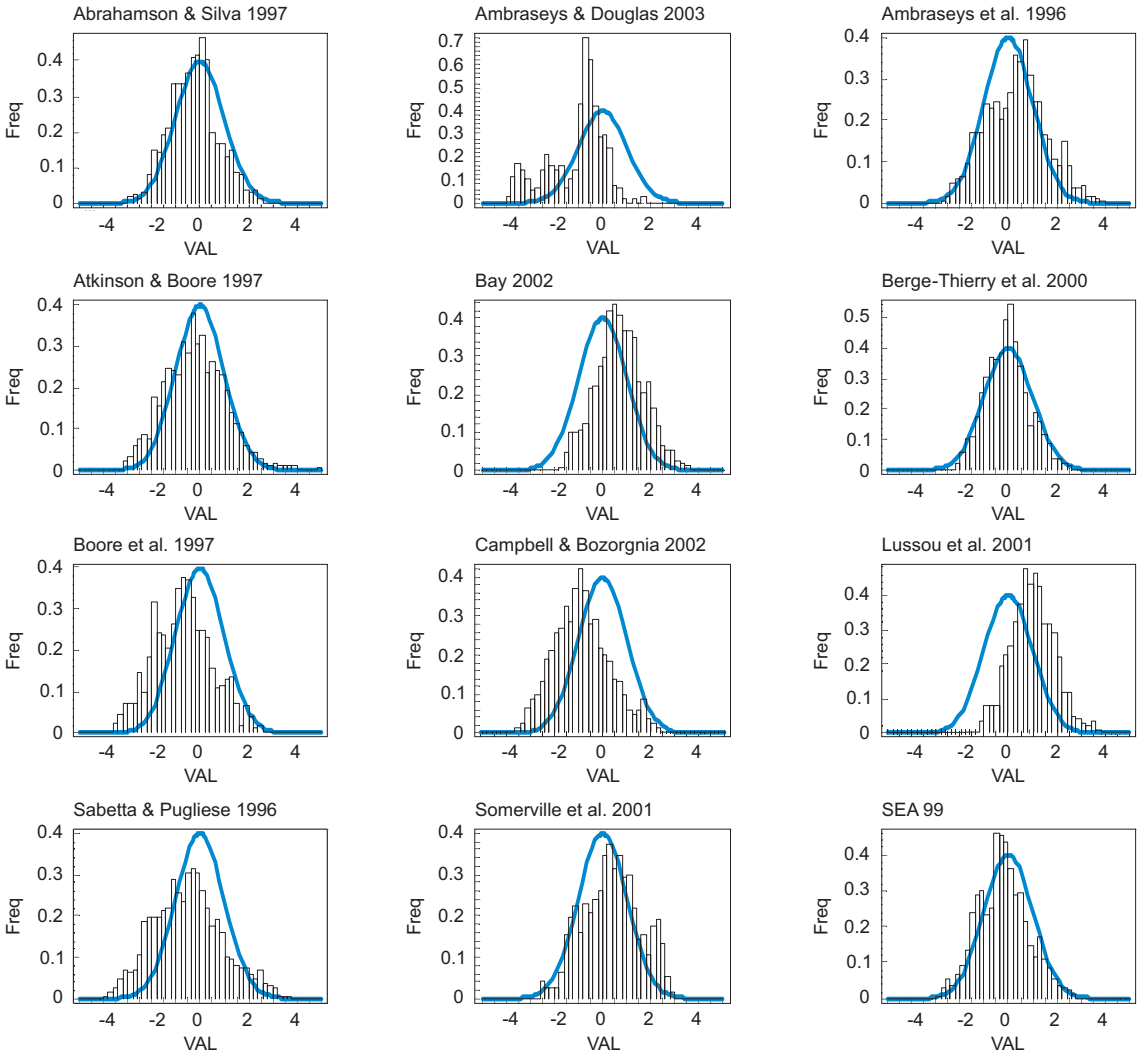

Fig. 4: Residual distribution (scaled by model mean and model variance) of a subset of the generating data set of the Ambraseys et al. (1996) ground motion model with respect to different attenuation relations

The blue curve shows the expected distribution function for a unit variance normally distributed random variable.

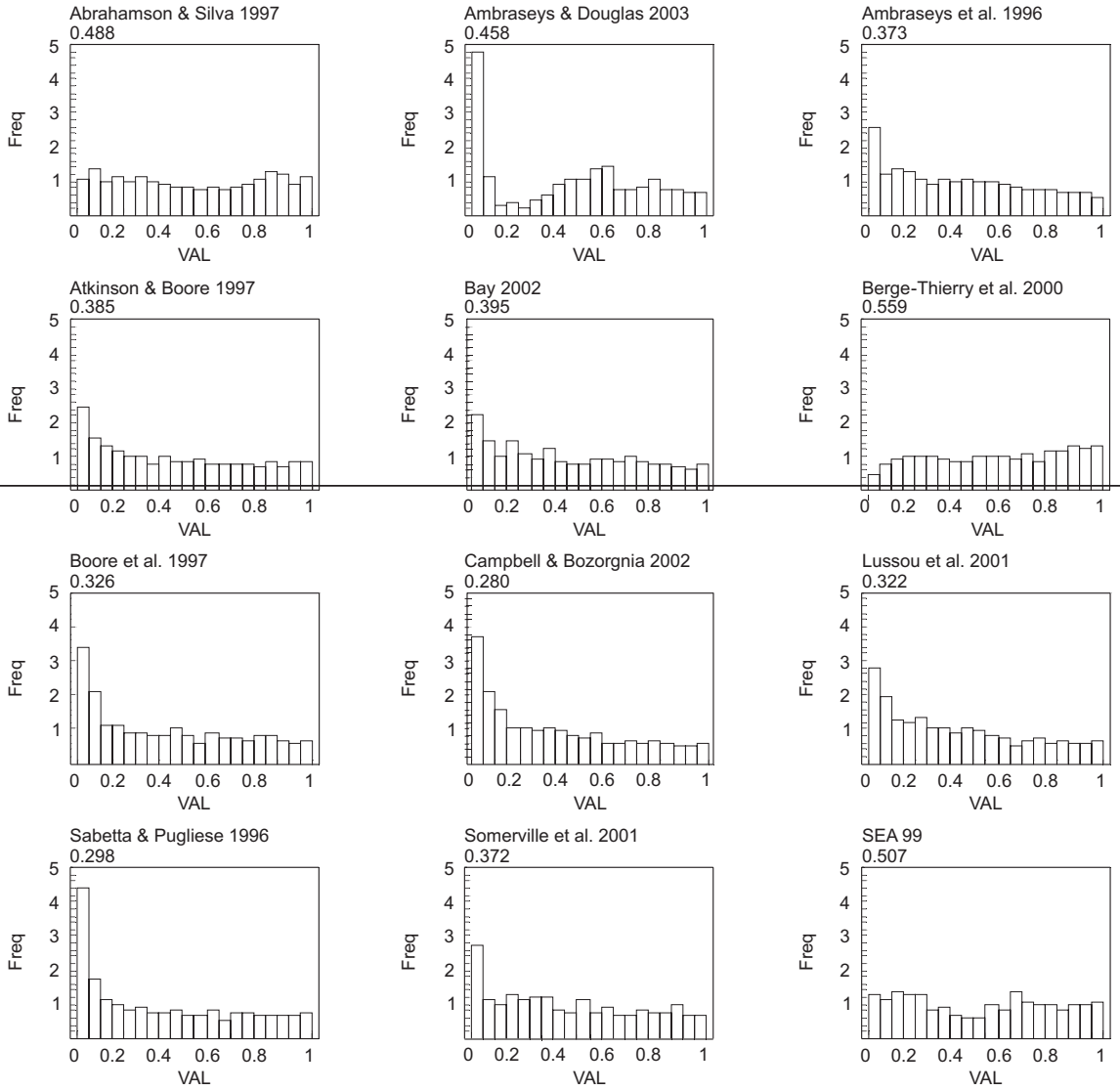

Fig. 5: Distribution of $LH(y)$ for a subset of the generating data set of the Ambraseys et al. (1996) ground motion model with respect to different attenuation relations

All panels are scaled to the same maximum value.

Tab. 2: Comparison of different attenuation relations to model a subset of the generating data set of the Ambraseys et al. (1996) ground motion model

The goodness-of-fit measures used are: likelihood (LH), variance reduction (VARRED), the median of the sigma scaled deviation (MSSDEV), the Chi-Square statistics (CSQ), the Kolmogoroff-Smirnov statistics (KS), the P-value of the mean test (M-Test), the P value of the variance test (V-Test), and the Pearson correlation coefficient (CC).

Model Name	LH	LH-Ratio	VARRED	MSSDEV	MSSDEV-ratio	CSQ TestRatio	KS-Test Ratio	M-Test Ratio	V-Test Ratio	CC-Ratio	#
Berge-Thierry et al. 2000	0.559	1.	0.931	0.0601	1.	0	0	1.	0	0.709	58
SEA 99	0.507	0.907	0.802	0.257	0.234	0	0	0	0.0269	0.686	50
Abrahamson & Silva 1997	0.488	0.873	0.966	0.249	0.242	0	0	0	0.497	0.717	65
Ambraseys & Douglas 2003	0.458	0.819	0.7	0.731	0.0823	0	0	0	1.84e-6	1.	8
Bay 2002	0.395	0.708	0.448	0.673	0.0894	0	0	0	1.	0.67	60
Atkinson & Boore 1997	0.385	0.689	0.821	0.239	0.251	0	0	0	0	0.673	69
Ambraseys et al. 1996	0.373	0.667	1.	0.37	0.163	0	0	0	0	0.737	68
Somerville et al. 2001	0.372	0.665	0.474	0.374	0.161	0	0	0	0	0.829	27
Boore et al. 1997	0.326	0.584	0.349	0.731	0.0823	0	0	0	0	0.648	35
Lussou et al. 2001	0.322	0.576	-0.381	0.98	0.0614	0	0	0	0	0.685	54
Sabetta & Pugliese 1996	0.298	0.533	0.865	0.537	0.112	0	0	0	0	0.688	62
Campbell & Bozorgnia 2002	0.28	0.501	0.315	0.936	0.0643	0	0	0	0	0.646	60

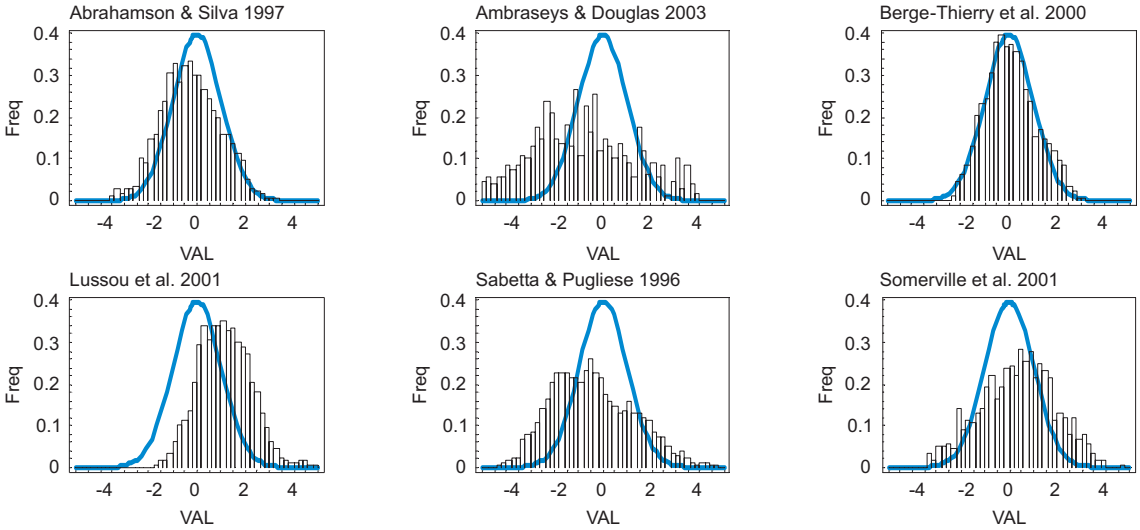

Fig. 6: Residual distribution (scaled by model mean and model variance) of a subset of the generating data set of the Berge-Thierry et al. (2000) ground motion model with respect to different attenuation relations

The blue curve shows the expected distribution function for a unit variance normally distributed random variable.

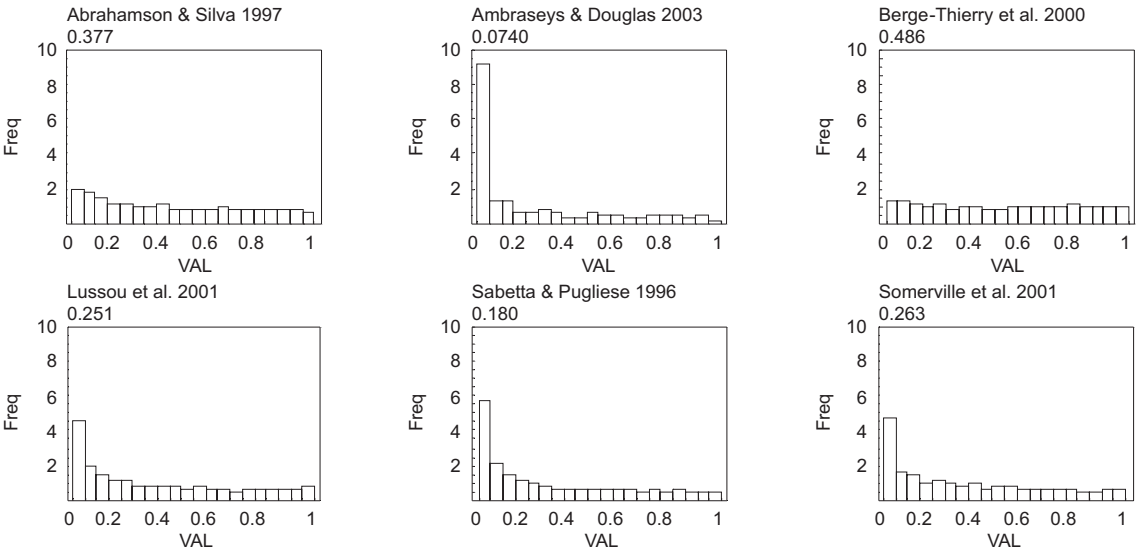

Fig. 7: Distribution of $LH(y)$ for a subset of the generating data set of the Berge-Thierry et al. (2000) ground motion model with respect to different attenuation relations

All panels are scaled to the same maximum value.

Tab. 3: Comparison of different attenuation relations to model a subset of the generating data set of the Berge-Thierry et al. (2000) ground motion model

The goodness-of-fit measures used are: likelihood (LH), variance reduction (VARRED), the median of the sigma scaled deviation (MSSDEV), the Chi-Square statistics (CSQ), the Kolmogoroff-Smirnov statistics (KS), the P-value of the mean test (M-Test), the P value of the variance test (V-Test), and the Pearson correlation coefficient (CC).

Model Name	LH	LH-Ratio	VARRED	MSSDEV	MSSDEV -ratio	CSQ TestRatio	KS-Test Ratio	M-Test Ratio	V-Test Ratio	CC-Ratio	#
Berge-Thierry et al. 2000	0.486	1.	0.996	0.0246	1.	0	1.	1.	1.	0.919	95
Abrahamson & Silva 1997	0.377	0.775	1.	0.296	0.0829	0	0	0	0	0.932	107
Somerville et al. 2001	0.263	0.541	0.686	0.444	0.0554	0	0	0	0	0.747	36
Lussou et al. 2001	0.251	0.516	0.471	1.12	0.0219	0	0	0	6.68e-7	1.	96
Sabetta & Pugliese 1996	0.18	0.371	0.957	0.571	0.0431	0	0	0	0	0.911	104
Ambraseys & Douglas 2003	0.074	0.152	0.82	1.03	0.0238	0	0	0	0	0.843	15

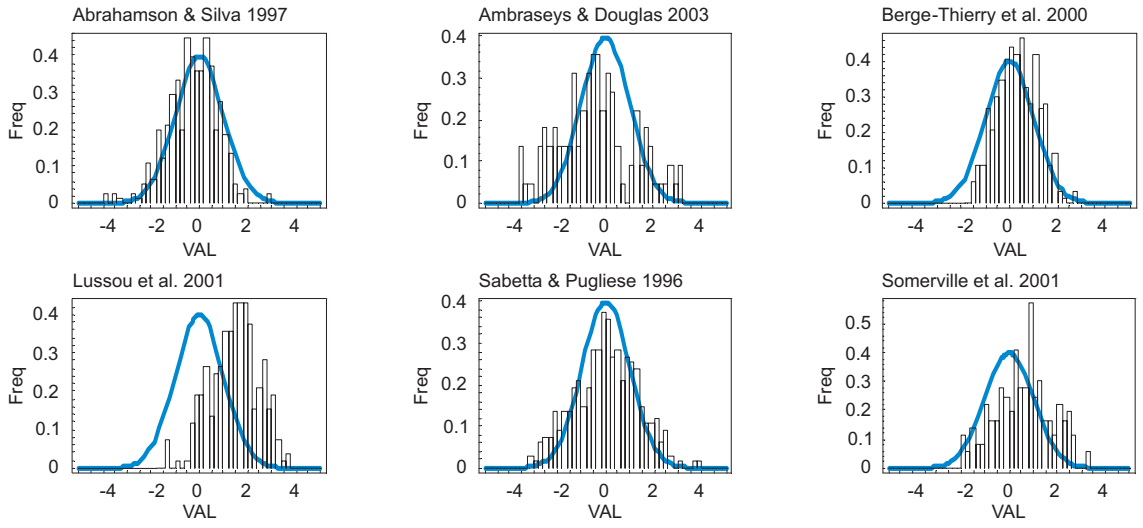

Fig. 8: Residual distribution (scaled by model mean and model variance) of a subset of the generating data set of the Sabetta & Pugliese (1996) ground motion model with respect to different attenuation relations

The blue curve shows the expected distribution function for a unit variance normally distributed random variable.

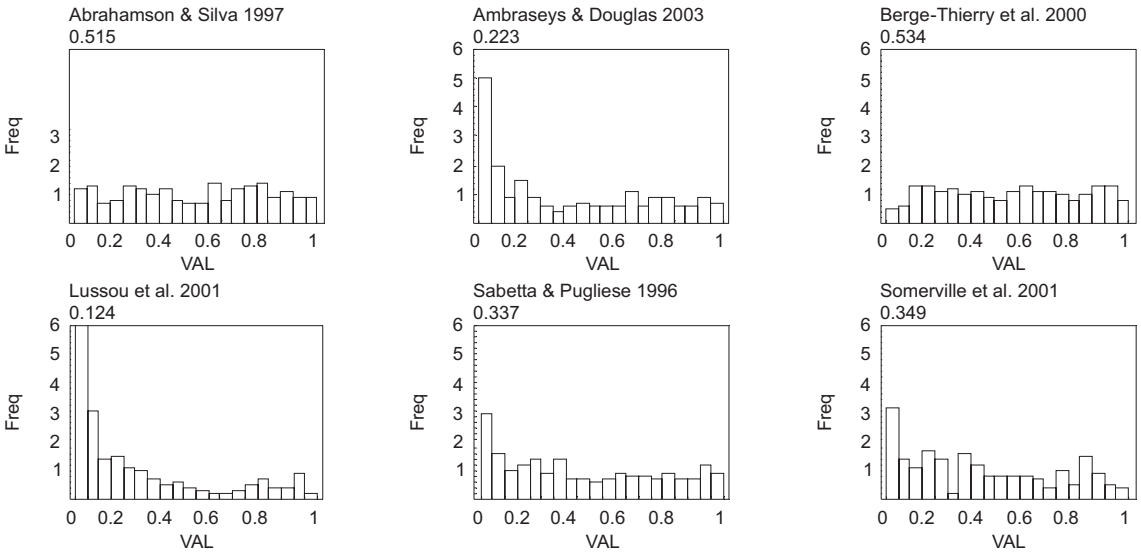

Fig. 9: Distribution of $LH(y)$ for a subset of the generating data set of the Sabetta & Pugliese (1996) ground motion model with respect to different attenuation relations

All panels are scaled to the same maximum value.

Tab. 4: Comparison of different attenuation relations to model a subset of the generating data set of the Sabetta & Pugliese (1996) ground motion model

The goodness-of-fit measures used are: likelihood (LH), variance reduction (VARRED), the median of the sigma scaled deviation (MSSDEV), the Chi-Square statistics (CSQ), the Kolmogoroff-Smirnov statistics (KS), the P-value of the mean test (M-Test), the P value of the variance test (V-Test), and the Pearson correlation coefficient (CC).

Model Name	LH	LH Ratio	VARRED	MSSDEV	MSSDEV -ratio	CSQ Test-Ratio	KS-Test Ratio	M-Test Ratio	V-Test Ratio	CC-Ratio	#
Berge-Thierry et al. 2000	0.534	1.	0.957	0.347	0.0837	1.	0.0000197	8.18e-10	0.000253	0.837	23
Abrahamson & Silva 1997	0.515	0.966	0.972	0.219	0.133	0	0.144	1.55e-7	0.416	0.85	27
Somerville et al. 2001	0.349	0.654	0.819	0.69	0.042	0	3.08e-9	0	0.00124	0.809	13
Sabetta & Pugliese1996	0.337	0.632	1.	0.029	1.	0	1.	1.	0	0.859	24
Ambraseys & Douglas 2003	0.223	0.417	0.894	0.461	0.0629	0	0.0141	0.0000486	0	0.996	8
Lussou et al. 2001	0.124	0.233	0.591	1.54	0.0189	0	0	0	1.	1.	19

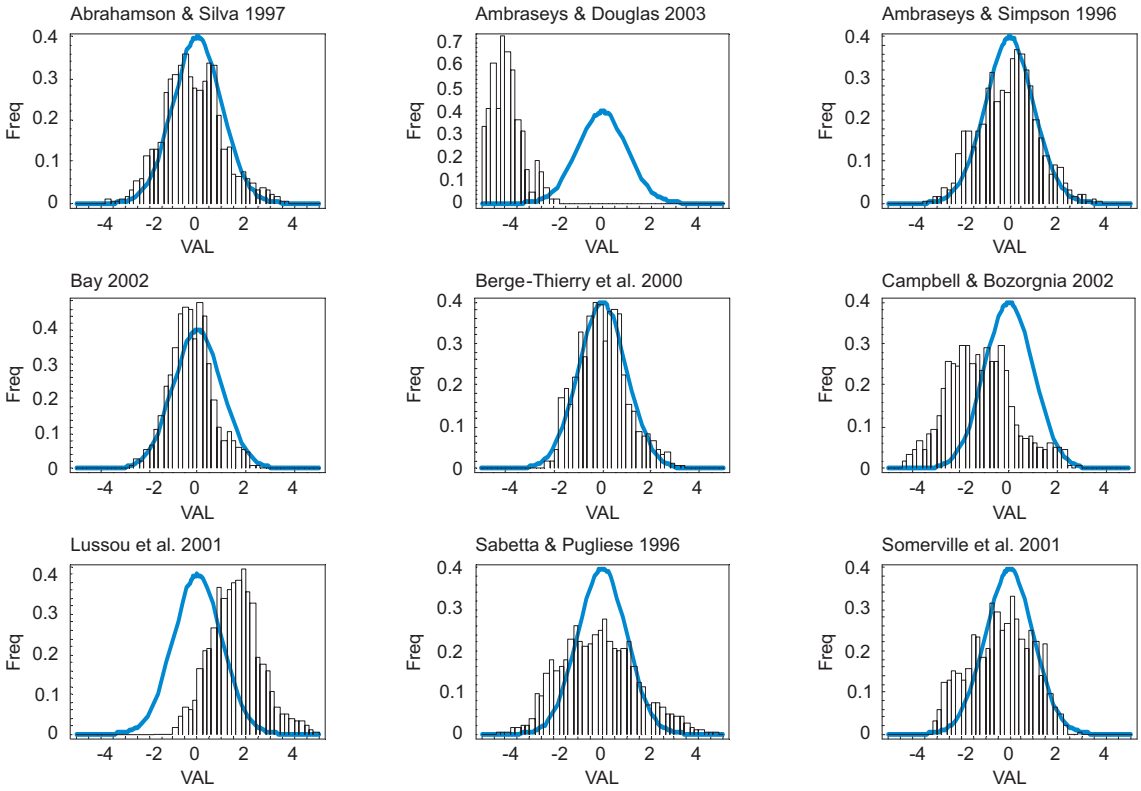

Fig. 10: Residual distribution (scaled by model mean and model variance) of a subset of the generating data set of the Ambraseys & Simpson (1996) ground motion model with respect to different attenuation relations

The blue curve shows the expected distribution function for a unit variance normally distributed random variable.

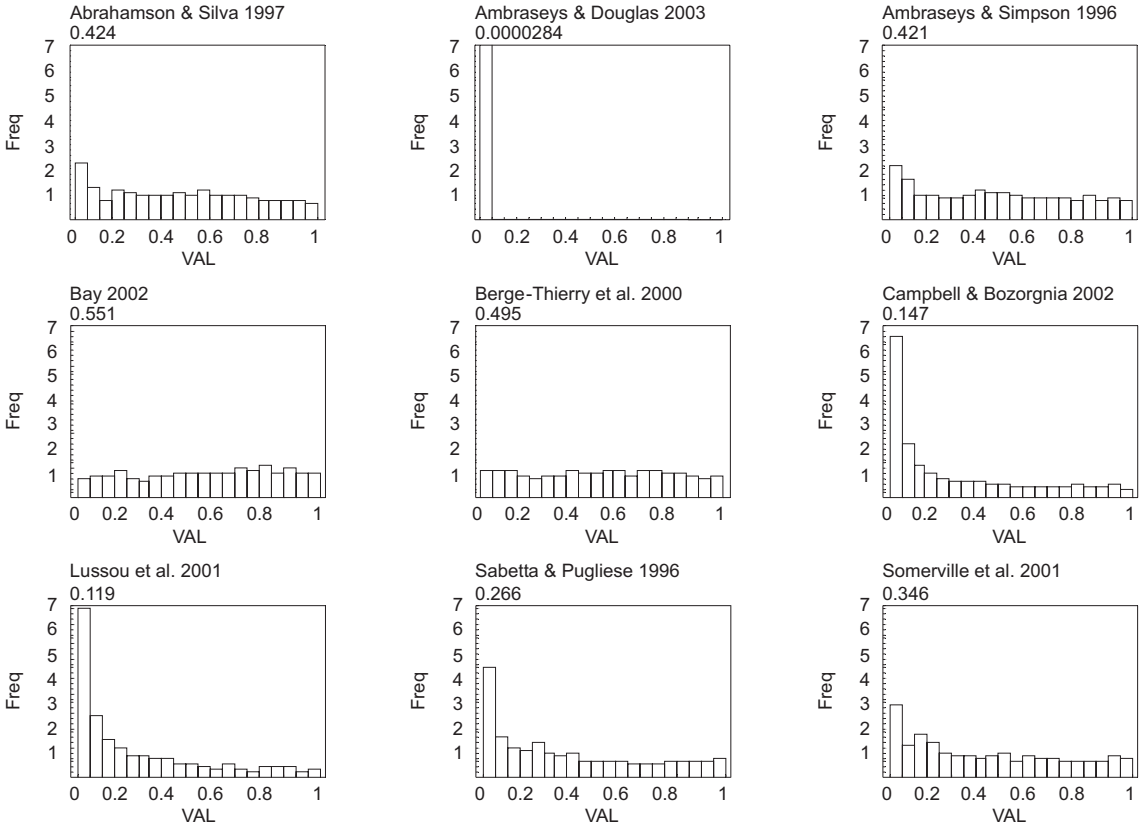

Fig. 11: Distribution of $LH(y)$ for a subset of the generating data set of the Ambraseys & Simpson (1996) ground motion model with respect to different attenuation relations

All panels are scaled to the same maximum value.

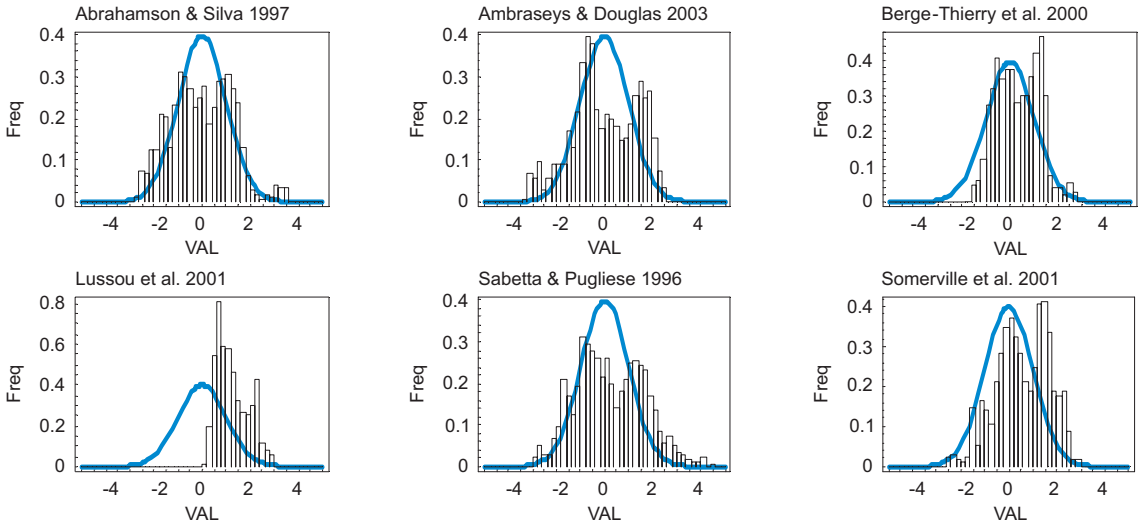

Fig. 12: Residual distribution (scaled by model mean and model variance) of a subset of the generating data set of the Ambraseys & Douglas (2003) ground motion model with respect to different attenuation relations

The blue curve shows the expected distribution function for a unit variance normally distributed random variable.

Tab. 5: Comparison of different attenuation relations to model a subset of the generating data set of the Ambraseys & Simpson (1996) ground motion model

The goodness-of-fit measures used are: likelihood (LH), variance reduction (VARRED), the median of the sigma scaled deviation (MSSDEV), the Chi-Square statistics (CSQ), the Kolmogoroff-Smirnov statistics (KS), the P-value of the mean test (M-Test), the P value of the variance test (V-Test), and the Pearson correlation coefficient (CC).

Model Name	LH	LH Ratio	VARRED	MSSDEV	MSSDEV -ratio	CSQ Test-Ratio	KS Test Ratio	M-Test Ratio	V-Test Ratio	CC-Ratio	#
Bay 2002	0.551	1.	0.968	0.271	0.0488	0	0	0	0	0.7	59
Berge-Thierry et al. 2000	0.495	0.898	0.942	0.0347	0.381	0	1.	1.	0.0261	0.811	58
Abrahamson & Silva 1997	0.424	0.77	0.965	0.243	0.0543	0	0	0	0	0.815	65
Ambraseys & Simpson 1996	0.421	0.765	1.	0.0132	1.	0	0	0.00156	0	0.813	68
Somerville et al. 2001	0.346	0.627	0.896	0.321	0.0412	0	0	0	0	0.899	27
Sabetta & Pugliese 1996	0.266	0.482	0.931	0.2	0.0658	0	0	0	0	0.806	62
Campbell & Bozorgnia 2002	0.147	0.268	0.617	1.25	0.0105	0	0	0	0	0.727	59
Lussou et al. 2001	0.119	0.216	0.287	1.56	8.46e-3	0	0	0	4.98e-4	0.753	53
Ambraseys & Douglas 2003	2.84e-5	5.16e-5	-9.08	4.19	3.15e-3	0	0	0	1.	1.	8

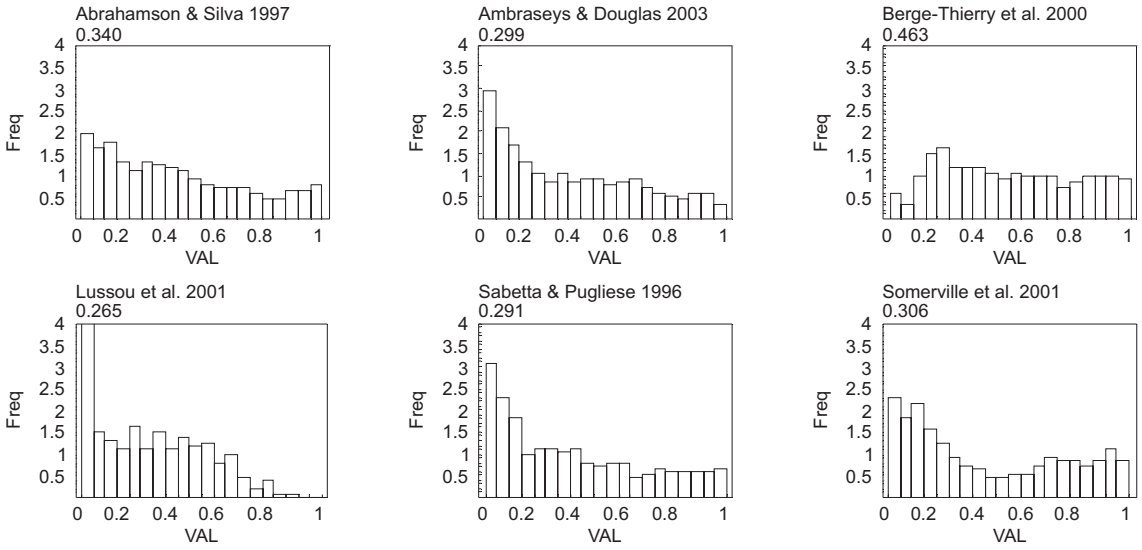

Fig. 13: Distribution of $LH(y)$ for a subset of the generating data set of the Ambraseys & Douglas (2003) ground motion model with respect to different attenuation relations

All panels are scaled to the same maximum value.

Tab. 6: Comparison of different attenuation relations to model a subset of the generating data set of the Ambraseys & Douglas (2003) ground motion model

The goodness-of-fit measures used are: likelihood (LH), variance reduction (VARRED), the median of the sigma scaled deviation (MSSDEV), the Chi-Square statistics (CSQ), the Kolmogoroff-Smirnov statistics (KS), the P-value of the mean test (M-Test), the P value of the variance test (V-Test), and the Pearson correlation coefficient (CC).

Model Name	LH	LH Ratio	VARRED	MSSDEV	MSSDEV -ratio	CSQ Test Ratio	KS-Test Ratio	M-Test Ratio	V-Test Ratio	CC-Ratio	#
Berge-Thierry et al. 2000	0.463	1.	0.893	0.308	0.0639	0	0	0	1.85e-5	0.83	17
Abrahamson & Silva 1997	0.34	0.733	0.818	0.0197	1.	0	0	0.641	0	0.282	14
Somerville et al. 2001	0.306	0.661	0.84	0.581	0.0339	0	0	0	1.	0.905	15
Ambraseys & Douglas 2003	0.299	0.645	1.	0.124	0.158	0	0	1.	0	0.938	10
Sabetta & Pugliese 1996	0.291	0.628	0.893	0.109	0.181	0	0	0	0	0.777	13
Lussou et al. 2001	0.265	0.573	0.379	1.11	0.0177	0	0	0	0	1.	5

Regarding the distribution of *LH*(*y*), I have drawn the following conclusions from the interpretation of Figures 1 – 13:

- The *LH*(*y*) distribution seems to be a good indicator for the goodness-of-fit of ground motion models to observed response spectral values as well as for how well the model assumptions are met. Its median conveniently describes the overall quality of goodness-offit by a single number and allows to easily identify good (*LH approx.* > *0.45*) and unacceptable (*LH approx.* < *0.2*) models.
- A particular ground motion model is not always identified from the subset of its generating data set by an *LH value* close to *0.5*. For two attenuation models (Ambraseys and Douglas, 2003; Sabetta and Pugliese, 1996), the corresponding *LH values* become as low as *0.3*. In both of these cases, the data subsets have become very small and the corresponding residual distributions show obvious deviations from the expected unit variance normal distributions. It has to be kept in mind, however, that the 'test data subsets' were restricted to records obtained on 'rock sites' and an *LH value* lower than *0.5* should not be seen as too surprising. On the other hand this can be taken as an argument that *LH values* between *0.3* and *0.45* should still be seen as describing a fair fit. Finally, I interpret the range of *LH values* between *0.2 – 0.3* to describe poor fit.

Regarding the other goodness-of-fit measures given in Tables 1 to 6 my current interpretations are:

- Due to the lack of successful identifications, the Pearson correlation coefficient as well as the P-value statistics for mean and variance tests have not been found to be very useful in the present context.
- The Chi-square and the Kolmogoroff-Smirnov tests sometimes do and sometimes don't allow the recognition of the right ground motion model. Both tests are too strict in rejecting acceptable models and hence don't seem to provide sufficient robustness for the present task.
- The amplitude normalized variance reduction (VARRED) described by (Cotton & Campillo 1995), as well as the median of the sigma scaled deviation (MSSDEV), have been found to be additional promising candidates to describe the goodness-of-fit of ground motion models to observed spectra. MSSDEV can simply be interpreted as quantifying the shift of the sample median and hence being rather insensitive to deviations of sample and model variance. VARRED quantifies the data residuals scaled by both data variance and data amplitude. Both MSSDEV and VARRED were quite successful in often giving high scores to the proper ground motion models, although their diagnostic power in identifying how well the model assumptions are met is less than for the *LH values*. VARRED often identifies the original ground motion model from among the good models (in terms of *LH values*) but in some cases a high score on VARRED was found to correspond to obviously weak models in terms of residuals (e.g. the Sabetta & Pugliese mode for the Berge-Thierry et al. or the Abrahamson & Silva data set). I feel that in order to make better use of the VARRED parameter in the present context, further studies are needed which are beyond the purpose of the present considerations.

2.1.1 Reference data set

The strategy which I have decided to follow in order to obtain data driven relative adjustment factors for Swiss conditions is based on the interpretations of *LH values* for a reference data set considered appropriate for Switzerland. Regarding the reference data set, there are not really a lot of options. Therefore, I have selected those records from the PEGASOS database which fall into the EZ2B-region and which have distances less than 200 km and moment magnitudes larger than 4.5. The inclusion of larger distances and smaller magnitudes did not seem to be appropriate. Setting temporarily aside all considerations of validity range in terms of magnitude,

distance and frequency coverage of the individual models, I have compared the resulting spectra to all proponent models. The results are shown in Figure 14. The corresponding residual and *LH*- value distributions are shown in Figures 15 and 16. Table 7 lists the corresponding goodness-of-fit values.

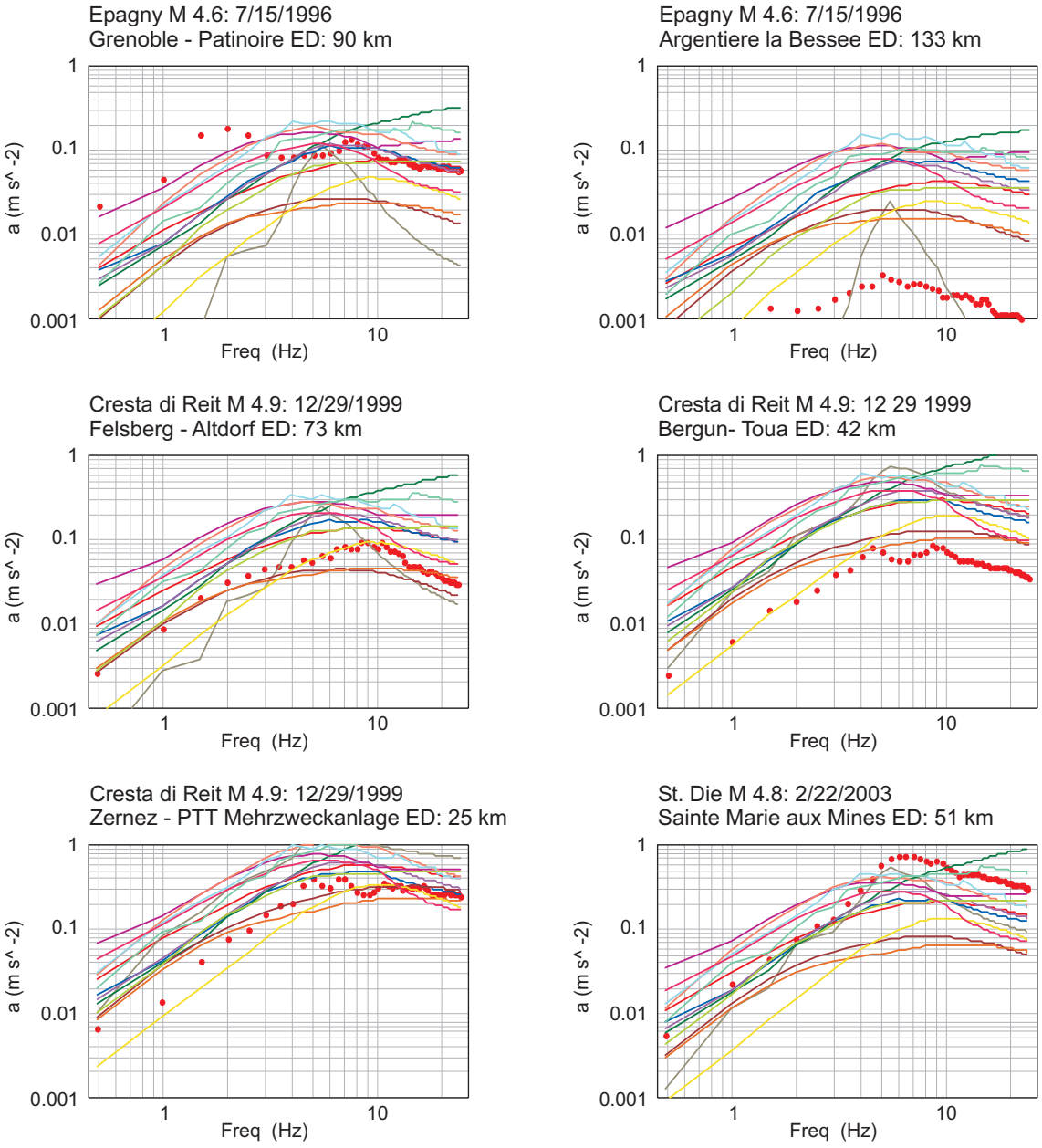

Fig. 14: Comparison of the original proponent models (without modifications for site or kappa differences) to the reference data set (EZ2B region, r < 200 km, M_w > 4.5)

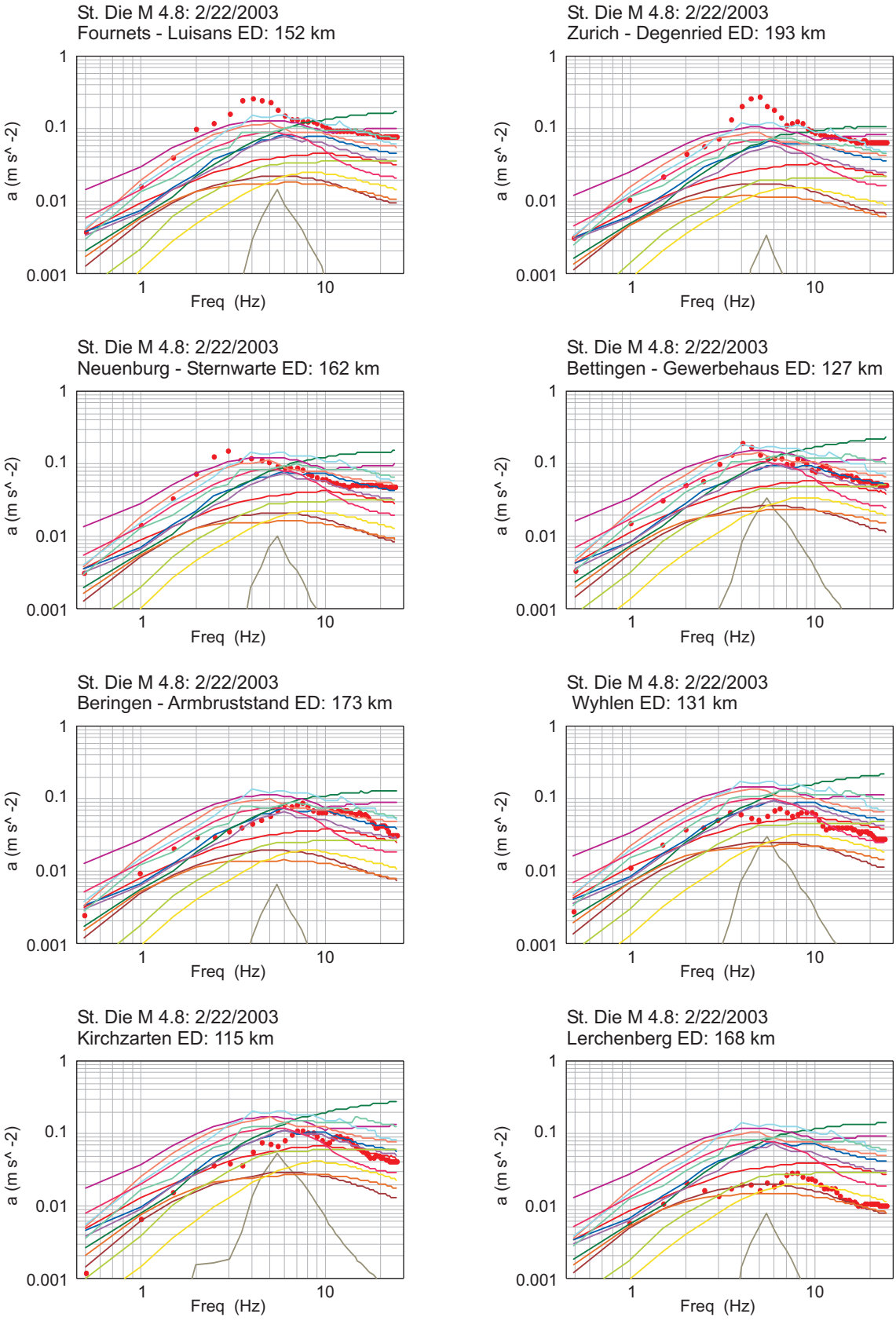

Fig. 14: (Cont.) Comparison of the original proponent models (without modifications for site or kappa differences) to the reference data set (EZ2B region, r < 200 km, M_w > 4.5)

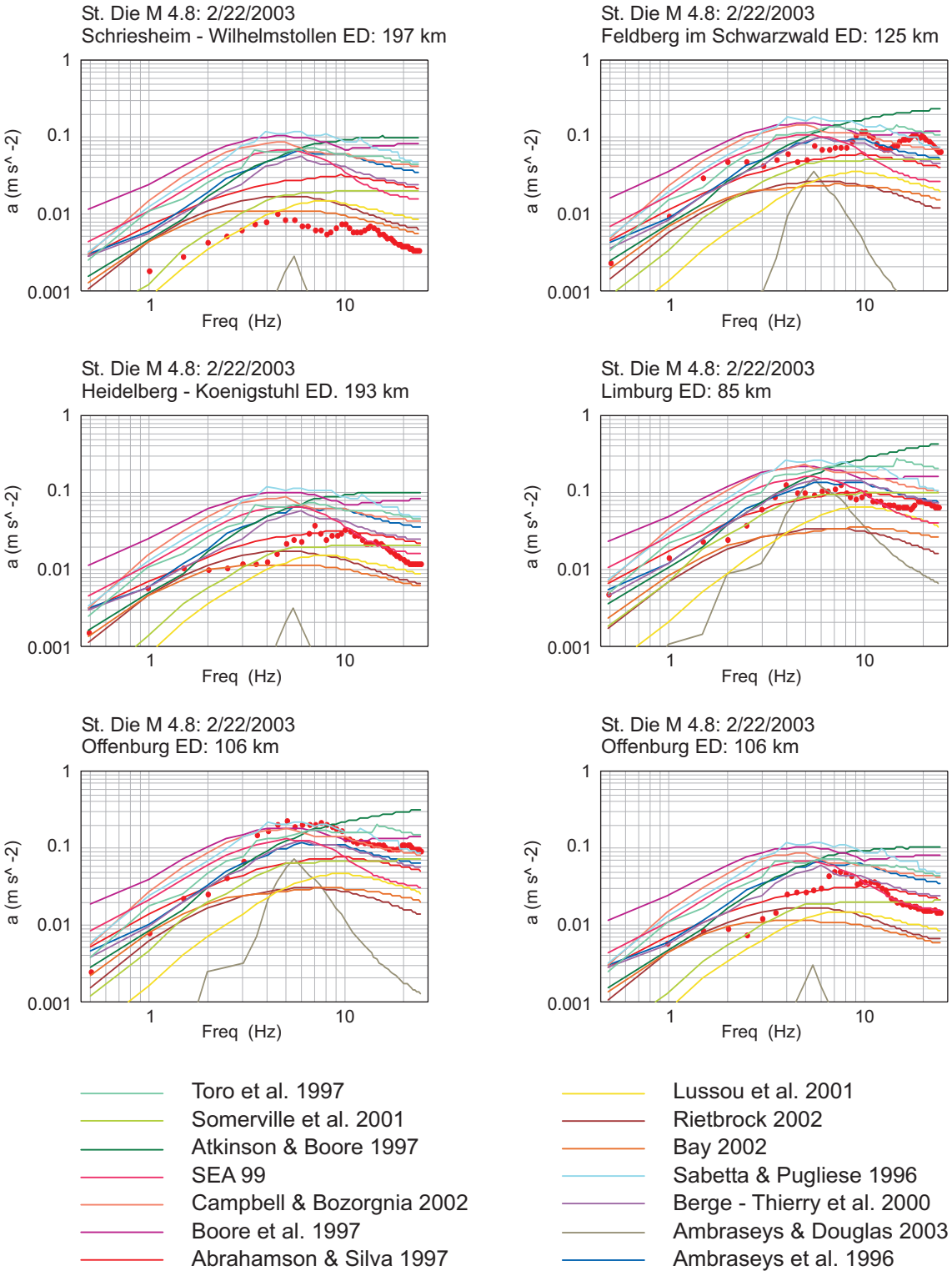

Fig. 14: (Cont.) Comparison of the original proponent models (without modifications for site or kappa differences) to the reference data set (EZ2B region, r < 200 km, $M_w > 4.5$)

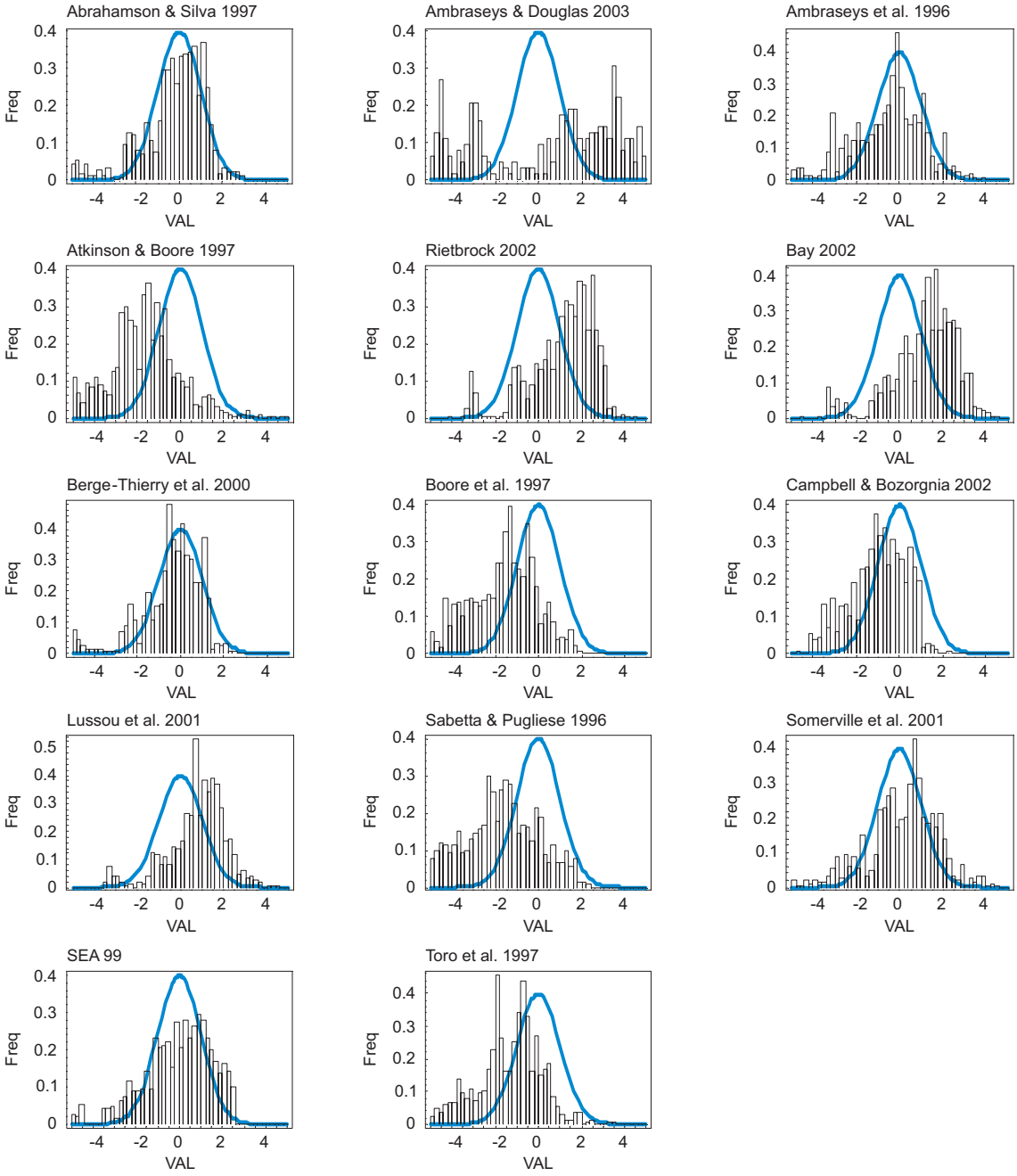

Fig. 15: Residual distribution (scaled by model mean and model variance) for the EZ2B reference data set with respect to different attenuation relations

The blue curve shows the expected distribution function for a unit variance normally distributed random variable.

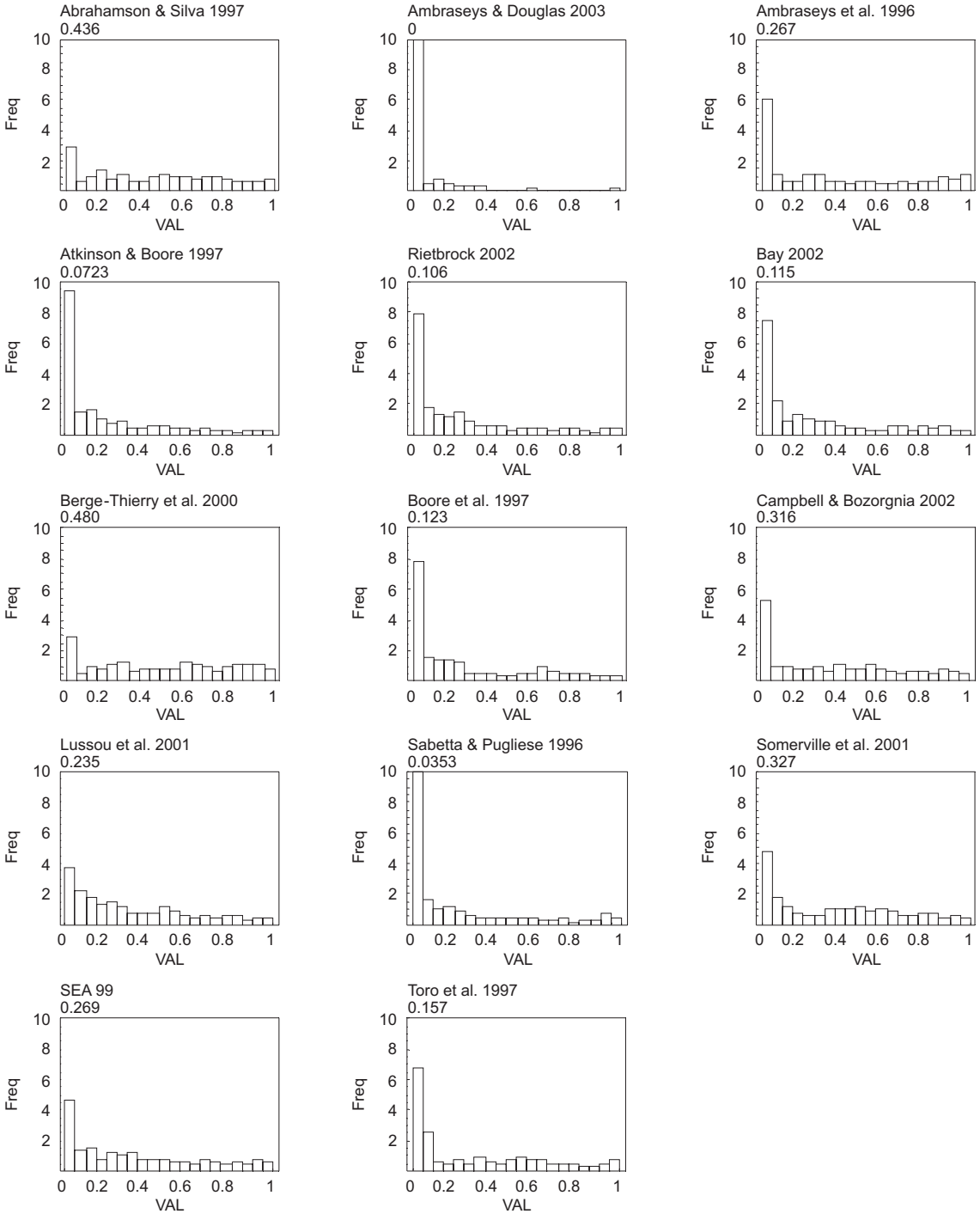

Fig. 16: Distribution of $LH(y)$ for the EZ2B reference data set with respect to different attenuation relations

All panels are scaled to the same maximum value.

Tab. 7: Comparison of different attenuation relations to model the EZ2B reference data set

The goodness-of-fit measures shown are: likelihood (LH), variance reduction (VARRED), and the median of the sigma scaled deviation (MSSDEV).

Model Name	Rating	LH	LH Ratio	VARRED	MSSDEV	MSSDEV Ratio	#
Berge-Thierry et al. 2000	GOOD	0.48	1.	0.997	0.217	0.207	20
Abrahamson & Silva 1997	FAIR	0.436	0.908	1.	0.0449	1.	20
Somerville et al. 2001	FAIR	0.327	0.68	0.989	0.309	0.145	20
Campbell & Bozorgnia 2002	FAIR	0.316	0.658	0.946	0.945	0.0475	20
SEA 99	POOR	0.269	0.56	0.991	0.103	0.437	20
Ambraseys et al. 1996	POOR	0.267	0.555	0.986	0.395	0.114	20
Lussou et al. 2001	POOR	0.235	0.49	0.95	0.98	0.0458	20
Toro et al. 1997	UA	0.157	0.327	0.913	1.25	0.0359	20
Boore et al. 1997	UA	0.123	0.255	0.897	1.53	0.0294	20
Bay 2002	UA	0.115	0.239	0.939	1.38	0.0326	20
Rietbrock 2002	UA	0.106	0.221	0.94	1.43	0.0314	20
Atkinson & Boore 1997	UA	0.0723	0.15	0.833	1.68	0.0268	20
Sabetta & Pugliese 1996	UA	0.0353	0.0734	0.917	2.09	0.0215	20
Ambraseys & Douglas 2003	UA	0	0	-1.04	9.26	0.00485	20

Based on the *LH values* and the criteria derived above, I have rated each ground motion model as GOOD (LH > .45), FAIR (.3 ≤ LH < .45), POOR (.2 ≤ LH < .3), or UNACCEPTABLE (UA; LH < .2). The rows of the unacceptable models are indicated in Table 7 by their dark shading. The low rating for the truly Swiss models (Bay 2002, Rietbrock 2002) is caused by the fact that the Swiss models produce too low spectral values in the complete frequency band. There are several potential reasons for this:

- Based on the assumption that most of the records were obtained on site class B stations, I assumed that the v_{s30} range between 750 to 1500 m/s captures the site situations for the reasonably well. What if the upper bound of these values is too low? This question has been raised by Philip Birkhäuser in his email to me dated 5/16/2003.
- The Swiss models are dominated by weak motion data from small earthquakes. What if they are simply not representative in terms e.g. stress drop, geometrical spreading etc.? This issue has been the topic of discussion within the seismological community for quite some time without having been resolved yet.

In order to shed some light on this problem, I have performed a grid search for modifications of the model parameters of the Bay model (Bay 2002) which would cause the response spectra obtained for the St. Dié earthquake to be matched. Since the problem is under determined, a full inversion for all model parameters is not possible and in order to obtain unique solutions, a sub-set of the parameters needs to be constrained. Below I have considered three different scenarios:

- Scenario A: Bay model (Bay 2002) with magnitude dependent stress drop (A_{inc}). The coefficient for the power law $\Delta\sigma \sim M_0^{0.25}$ were determined by fitting a polynomial through the stress drop values of her preferred model given in table on page 65 as shown in Figure 20. For $M_w = 4.8$ this resulted in a stress drop of 13 bar. For the site response filter a v_{s30} of 1100 m/s. (site class B) was assumed. The corresponding spectra are shown in Figure 17. The variance reduction (Cotton & Campillo 1995) obtained for this model was 0.63226.

- Scenario B: The stress drop was allowed to vary between 50 and 125 bars in steps of 5 bars, and the v_{s30} values from 500 to 1500 m/s in steps of 50 m/s. The corresponding spectra are shown in Figure 18. The best variance reduction of 0.98385 was obtained for a stress drop of 90 bars and a v_{s30} of 650 m/s.
- Scenario C: In order to find out how these values would potentially trade off with other model parameters the following model parameter variations were allowed simultaneously: the exponent of the last segment of the geometrical spreading term (> 100 km) which in (Bay, 2002) was obtained as *-0.5*, was allowed to vary between *-0.2* and *-0.7*. *kappa* was allowed to vary on the following set *(0.005, 0.00629463, 0.00792447, 0.00997631, 0.0125594, 0.0158114, 0.0199054, 0.0250594, 0.0315479, 0.0397164, 0.05)* (obtained by equal log spacing between *0.005* and *0.05*). Furthermore, the stress drop was allowed to vary between 60 and 130 bars in steps of 10 bars again and v_{s30} between 500 and 1300 m/s. This range was obtained by trial and error on a larger range with a coarser step size in order to keep the computer time in feasible limits. The corresponding spectra are shown in Figure 19. The best variance reduction of 0.98343 (essentially the same as for scenario B) and was obtained for a stress drop of 80 bars, a v_{s30} of 1000 m/s, a kappa value of *0.00629463* and a geometrical spreading exponent of *-0.2*.

These results indicate that the most likely explanation for the under prediction of the St. Dié earthquake records is the *high stress drop* of this event. In both scenarios this value is at least 80 bars which puts it in a range far above even the increasing stress drop model of Bay (Bay 2002) (Figure 20).

I judge the visual spectral fit for both scenarios B and C as fairly good considering the simplicity of the model. Since for a particular distance range both under- and over prediction of the recorded spectra can be observed (cf. spectra at 190 – 195 km distances in Figure 19), I speculate that the fit could possible be improved by taking the radiation pattern into account.

The fact that scenario C cannot improve the fit in comparison to scenario B, gives some support to the Bay model in terms of having already captured the medium properties as good as possible, at least in a descriptive sense. From the comparison with the study of Rietbrock (Rietbrock 2002) one could still argue that there is an alternative interpretation of the Q model, but even the geometrical spreading terms in his interpretation are not very different from the study of Bay (Bay 2002). Therefore, I believe that the main limitation of the Bay model is the lack of data from high stress drop events but that it seems to fairly well capture the other regional parameters necessary for stochastic simulation at least up to $M_w = 5$.

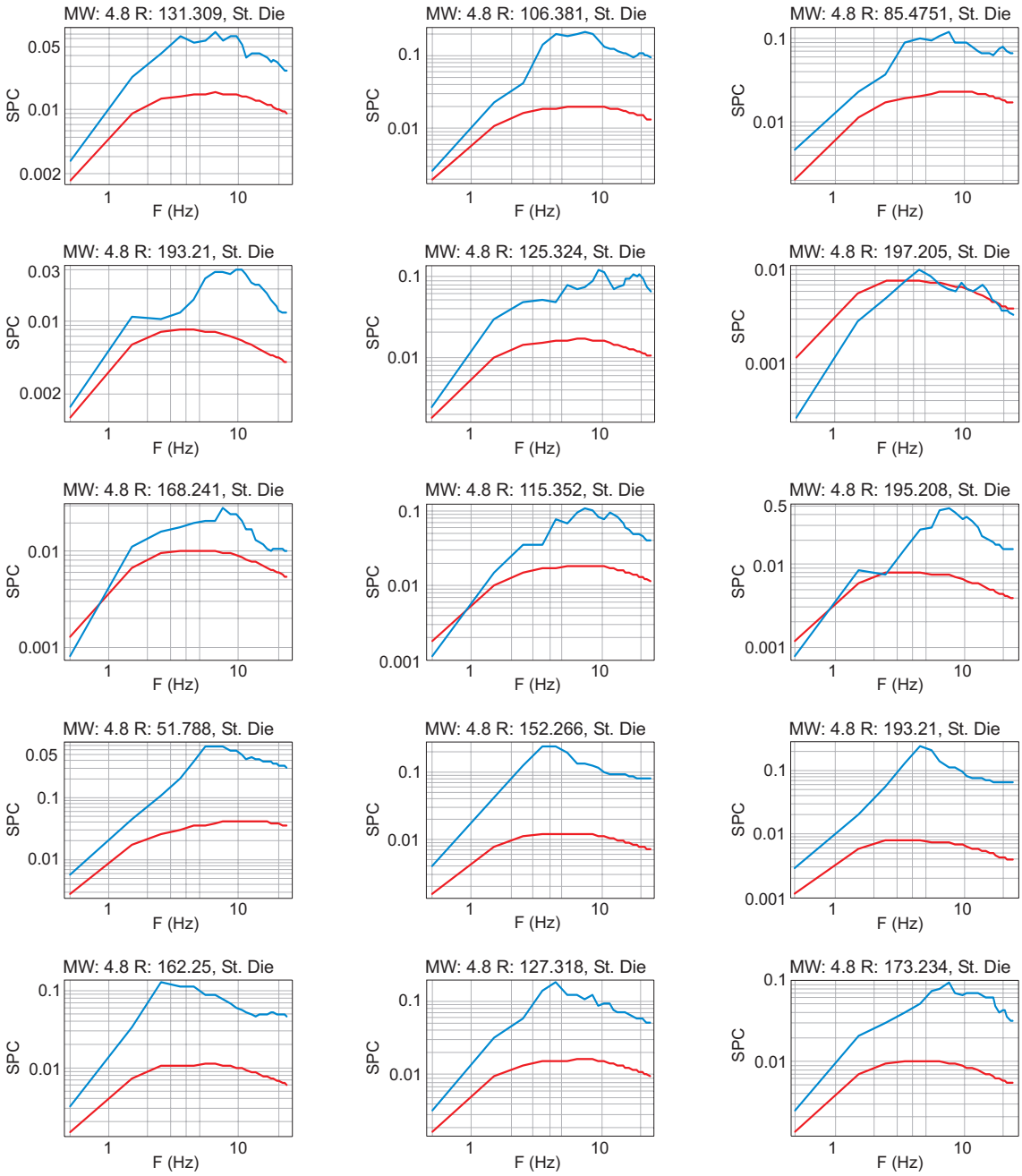

Fig. 17: Comparison of observed response spectra for the St. Dié earthquake of 22.2.2003 (M_w = 4.8) with model of Bay (Bay 2002) using a v_{s30} of 1100 m/s (scenario A)

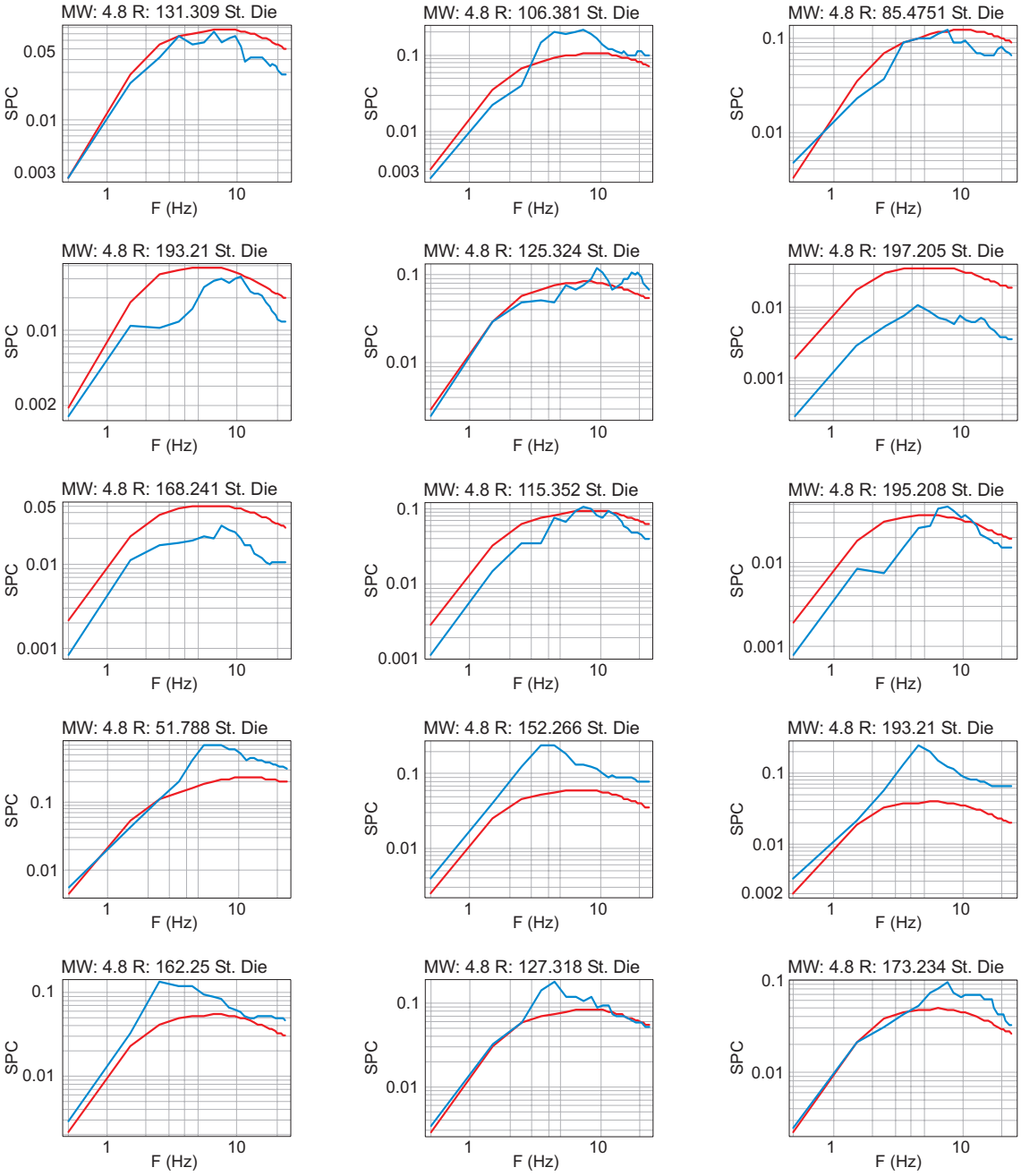

Fig. 18: Comparison of observed response spectra for the St. Dié earthquake of 22.2.2003 ($M_w = 4.8$) with the modified model of Bay (Bay 2002) according to scenario B

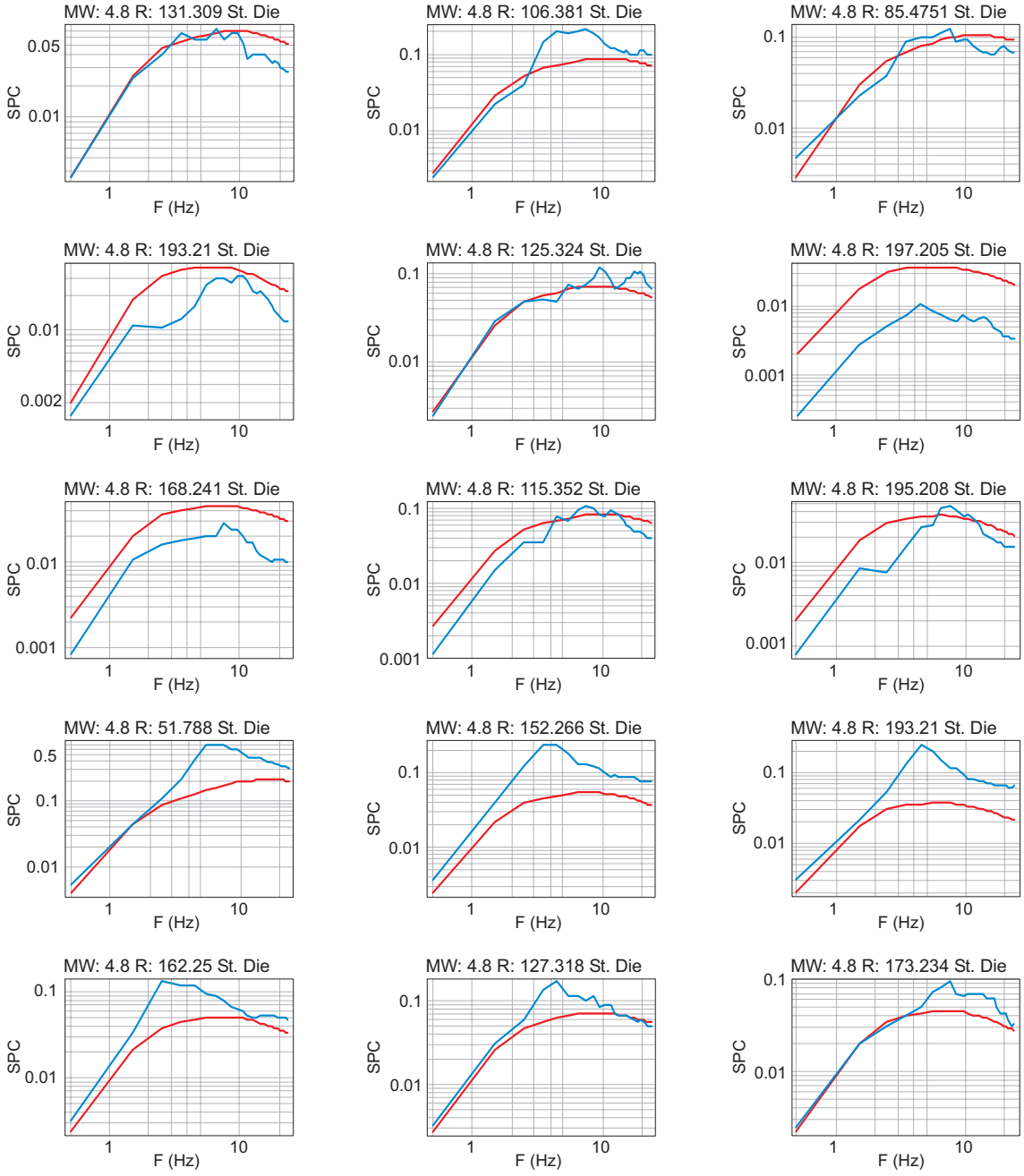

Fig. 19: Comparison of observed response spectra for the St. Dié earthquake of 22.2.2003 (M_w = 4.8) with the modified model of Bay (Bay 2002) according to scenario C

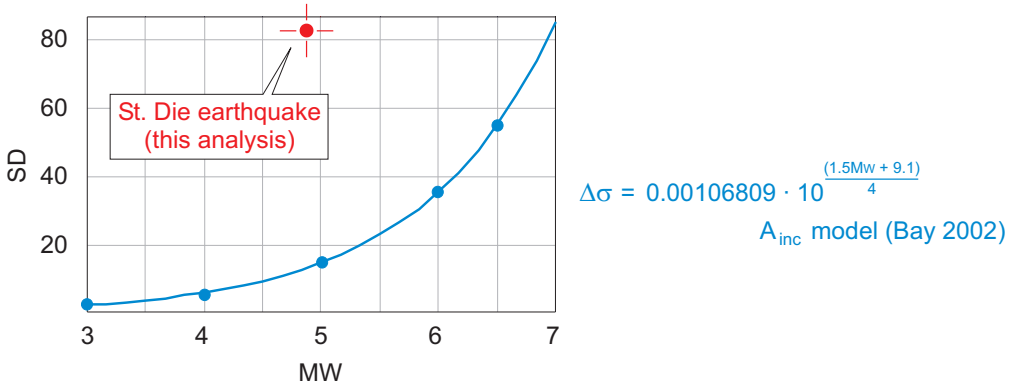

Fig. 20: Determination of magnitude dependent stress drop relation for the Bay model (Bay 2002) and comparison with the results of the analysis of the St. Dié earthquake

3 MEDIAN HORIZONTAL MOTION

3.1 Logic Tree Structure

Appendix C and the files logictree1.pdf contain the logic tree for the median spectral acceleration of the horizontal component. It contains a total number of 8 sections, of which 5 consist only of single branches. Section 1 (attenuation model) contains one branch for each of the 14 candidate ground motion models. Section 2 (magnitude conversion) treats the adjustment for the different magnitude definitions as described in chapter 3.5. Section 3 (distance conversion) is accounting for the conversion of the individual distance metric in use. For the actual hazard calculations this section is actually implemented outside of the SP2 experts model. Section 4 (missing frequencies) takes care of the conversion for missing frequencies by linear interpolation in log10-lin space. Section 5 (horizontal component conversion) accounts for the different definitions of horizontal components which are employed by the different candidate models. For each of the models that require conversion, this section contains 3 branches described in chapter 3.6. Section 6 (site condition conversions) accounts for the differences in the shallow subsurface velocity models and of kappa between the host region of each ground motion model and the target region Switzerland. To capture the comparatively large epistemic uncertainty involved in these conversions, both of these quantities are described by 3 branches, resulting in a total of 9 subbranches in this section. These are described in chapters 3.3 – 3.4. Section 7 (host-to-target-region conversion) consists in the application of the relative ground motion model adjustment factors given in Table 11. Finally, section 8 (style-of-faulting adjustment) accounts for difference in focal mechanisms as described in chapter 3.8.

3.2 Selected proponent models and weights

The list of selected proponent models together with the prior weighting factors calculated according to the method described in chapter 1.2 is given in appendices E and F and in the text files: priorwfH.txt and priorwfH_PGA.txt for SA and PGA, respectively.

3.3 Reference Rock velocity profiles

Due to the lack of specific information about the velocity profiles at sites representative for individual ground motion models, I am proposing to use a set of generic rock models with v_{s30} as single free parameter. The purpose of these models is to correct for the differences between the reference rock site for Switzerland and the sites which are assumed to be representative for the ground motion models under consideration. In this context I have mainly drawn on a study by Boore (Boore & Joyner 1997). I have generated the model set such that for v_{s30} = 620 m/s, the model matches the Californian rock model (table 1 in Boore & Joyner 1997) while for v_{s30} = 2800 m/s it matches the hard rock model for ENA (table 2 in Boore & Joyner 1997). My way of constructing this model is at follows.

First, I interpolated both rock models from (Boore & Joyner 1997) by piece wise power law models ($v \sim z^{\alpha}$) which are anchored at depths of 30, 190, 4000, and 8000 ms. An advantage of using power law models is that the average velocity to a certain depth can analytically be determined.

Next, I generated new velocity-depths models in which the velocity differences between neighboring models at the anchoring depths were equally spaced in log scale. For each of them, was subsequently determined together with its interpolation fraction (in log scale) with respect to the two end member models. The interpolation fraction between 0 and 1 corresponds to v_{s30} = 620 m/s and 2800 m/s, respectively. The interpolation fraction was finally fit by a second

order polynomial in v_{s30} to obtain an analytical way to construct the single parameter rock site model. The resulting function is:

$$if = - 3.533955 + 0.4562687 \log (v_{s30}) + 0.01454608 \log (v_{s30})^2 \quad (3\text{-}1)$$

with v_{s30} in m/s. Regarding the implementation, the following procedure has been used. Once the interpolation fraction for a particular has been determined, the model parameters at the anchoring depths are estimated from linear interpolation in log scale between the two end member models of (Boore & Joyner 1997). Finally, all model parameters (velocities, density, Q) are represented by piece wise power law models between the anchoring depths. Figures 21 and 22 show the complete range of velocity-depth models and corresponding site amplification functions, respectively, captured by this model.

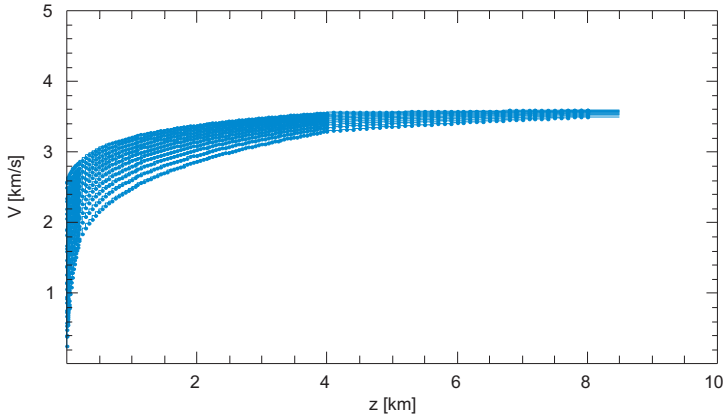

Fig. 21: Generic single parameter (v_{s30}) rock site models to be used for site condition conversion

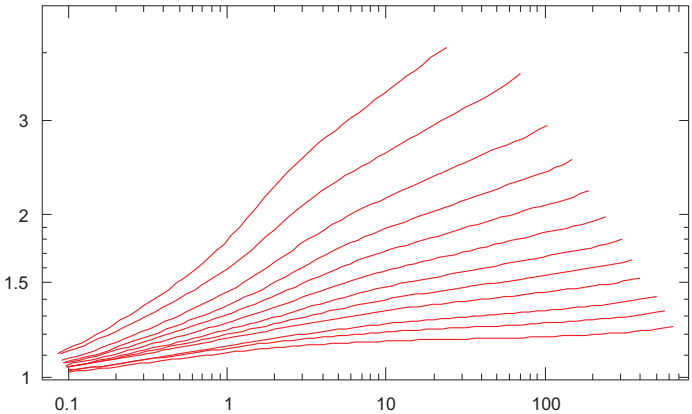

Fig. 22: Site amplification functions (Fourier spectra) for the generic rock models shown in Figure 21 calculated by the quarter wavelength approach.

For each of the ground motion models, representative v_{s30} values were determined based on the information given in the corresponding papers and augmented with lower and upper bounds which seemed to reasonably cover their epistemic uncertainties (Table 8). The corresponding velocity models are given as text files VS30_XXXX.vmod. For the Swiss reference rocksite, a central value of v_{s30} of 1100 m/s was chosen.

Tab. 8: Reference rock site surface rock velocity values for site conditions conversion
For the Swiss reference velocity, a value of 1100 m/s was chosen (shaded cell).

Reference region or model name	Central value (lit.) v_{s30} [m/s]	Lower value v_{s30} [m/s]	Upper value v_{s30} [m/s]
Abrahamson & Silva 1997	600	450	900
Ambraseys & Douglas 2000	800	450	1100
Ambraseys & Simpson 1996	800	550	1200
Ambraseys et al. 1996	800	550	1200
Atkinson & Boore 1997	2800	2800	2800
Bay 2002	1100	750	1500
Rietbrock 2002	1100	750	1500
Berge-Thierry et al. 2000	800	550	2000
Boore et al. 1997	600	500	750
Campbell & Bozorgnia 2002	600	450	900
Lussou et al. 2001	500	350	900
Sabetta & Pugliese 1996	1000	700	1300
SEA 99	800	550	1100
Somerville et al. 2001	2800	2800	2800
Toro et al. 1997	2800	2800	2800

I am aware of the fact that the generic rock model is not capturing all the complexity of the true rock site velocity-depth distributions in Europe as can be seen for example from the comparison with the mean Italian rock sites (TP2-TN-350) shown in Figure 23.

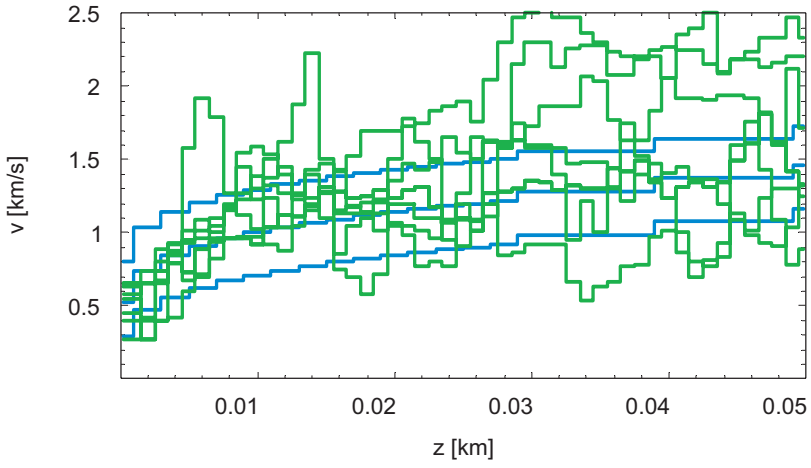

Fig. 23: Comparison of selected Italian rock site models (green curves, cf. TP2-TN-350) with generic rock models for v_{s30} of 700, 1000, and 1300 m/s (blue curves)

Therefore, I am assigning the following rather broad distribution of weights on the three branches of the rocksite conversion section of my logic tree:

central value: 0.5
lower bound: 0.3
upper bound: 0.2

A smaller weight is given to the upper bound because I am assuming that (due to an unknown amount of weathering) the bulk of the surface rock velocities for the host-region sites is located between the central value and the lower bound.

The amplification functions for the lower, central value, and upper bound assumed to be representative for Switzerland are shown in Figure 24.

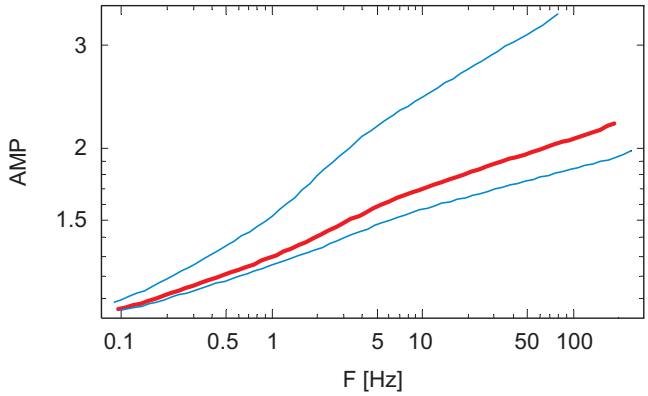

Fig. 24: Fourier spectrum amplification function for the Swiss reference velocity-depth profiles (lower, central value (red), upper bound) based on the model of Bay (2002)

3.4 Adjustment of proponent models to Swiss conditions

Empirical ground motion models even if they are based on good data sets in terms of magnitudes, distances, and frequency coverage may only perform poorly for a particular region if strong systematic differences between target region and host region of the GMM regarding the properties of wave propagation- and/or source properties exist. If these differences can be quantified, one can attempt to correct for them and thus improve the performance of the ground motion model. One way to do this in the hazard calculation is based on the idea of the hybrid approach of Campbell (Campbell 2001). Random vibration theory (Boore 1983, Boore & Joyner 1984, Herrmann 1985) can be used to generate response-spectral "correction filters" for each ground motion model to account for differences in source, medium and site parameters between host and target regions. For this purpose, reference models in terms of attenuation, site response, average stress drop, kappa, geometrical spreading, etc. – transformation parameters – have to be specified for each GMM as well as for the target region (Switzerland).

Since there was no time to set up and run a full inversion which could sufficiently explore the parameter space and detect trade-offs and ambiguities, I used a combination of trial and error and partial grid search to derive equivalent stochastic models for all the candidate empirical ground motion models. In the last step of each run, I ran a grid search on the optimum kappa values (Table 9) which in connection with the v_{s30} value in Table 8 (central values) would provide the best fit for SA response spectra of the empirical models for $5 < M_w < 7$ and distances below 150 km. This attempt was successful in the sense that the median empirical spectra for essentially all attenuation relations could be fairly well represented by stochastic models. A comparison of the resulting stochastic model spectra with the empirical spectra is shown below for three selected examples (Figures 25 – 27).

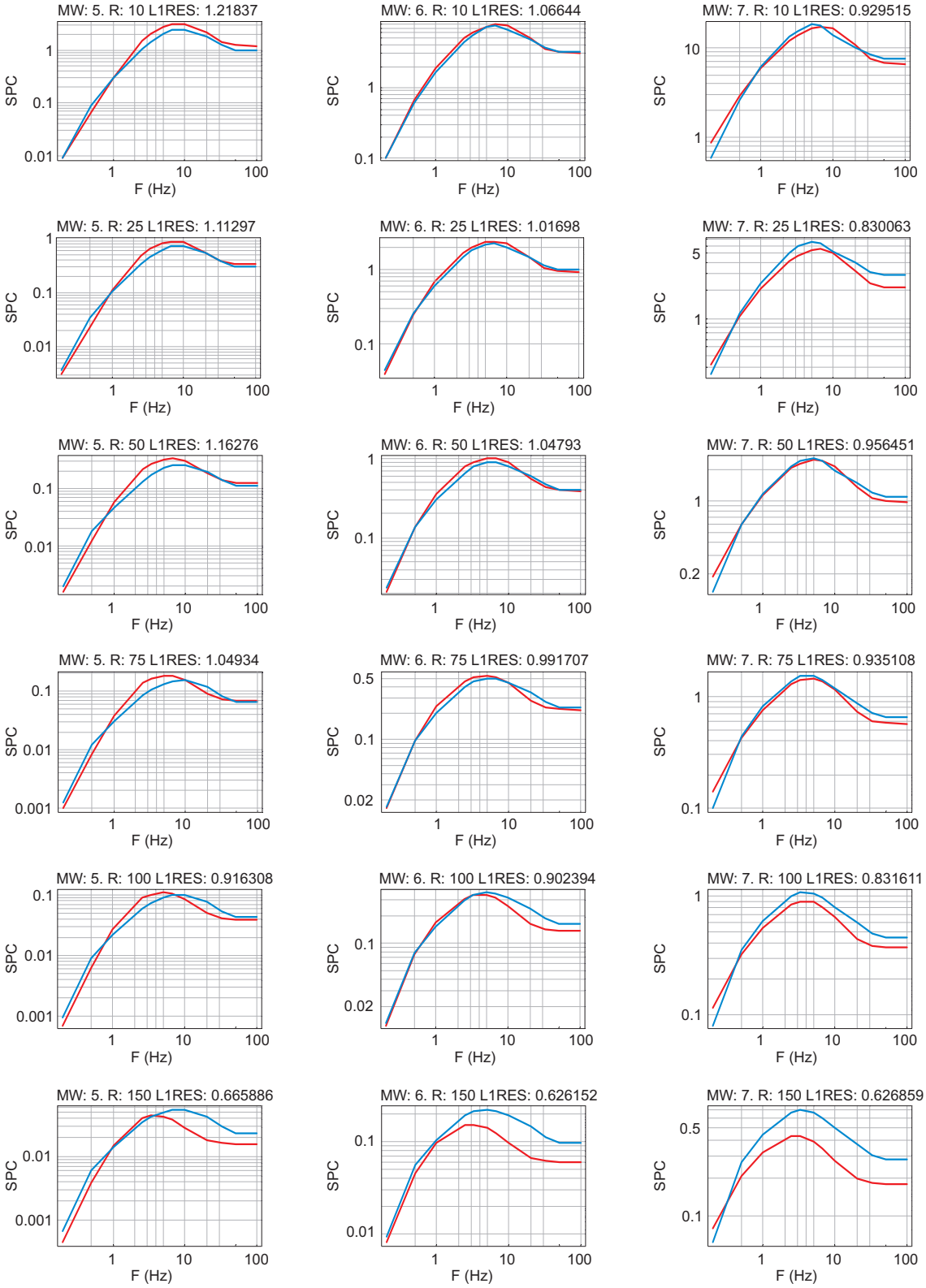

Fig. 25: Determination of an equivalent stochastic model for the Abrahamson & Silva (1997) ground motion model

The blue lines show the empirical model spectra while the red lines show stochastic models derived from the combination of trial and error and grid search on the stochastic parameters.

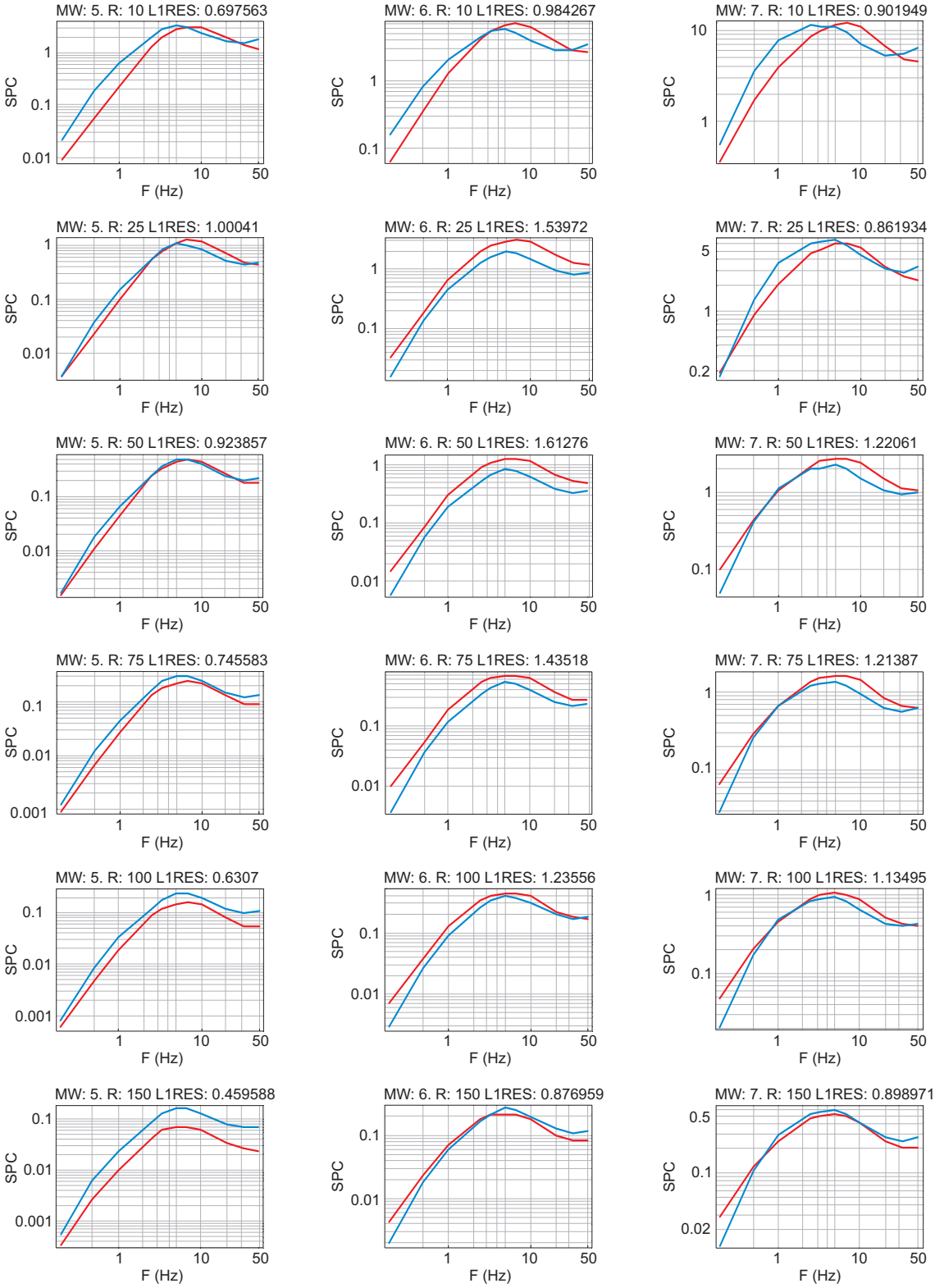

Fig. 26: Determination of an equivalent stochastic model for the Lussou et al. (2001) ground motion model

The blue lines show the empirical model spectra while the red lines show stochastic models derived from the combination of trial and error and grid search on the stochastic parameters.

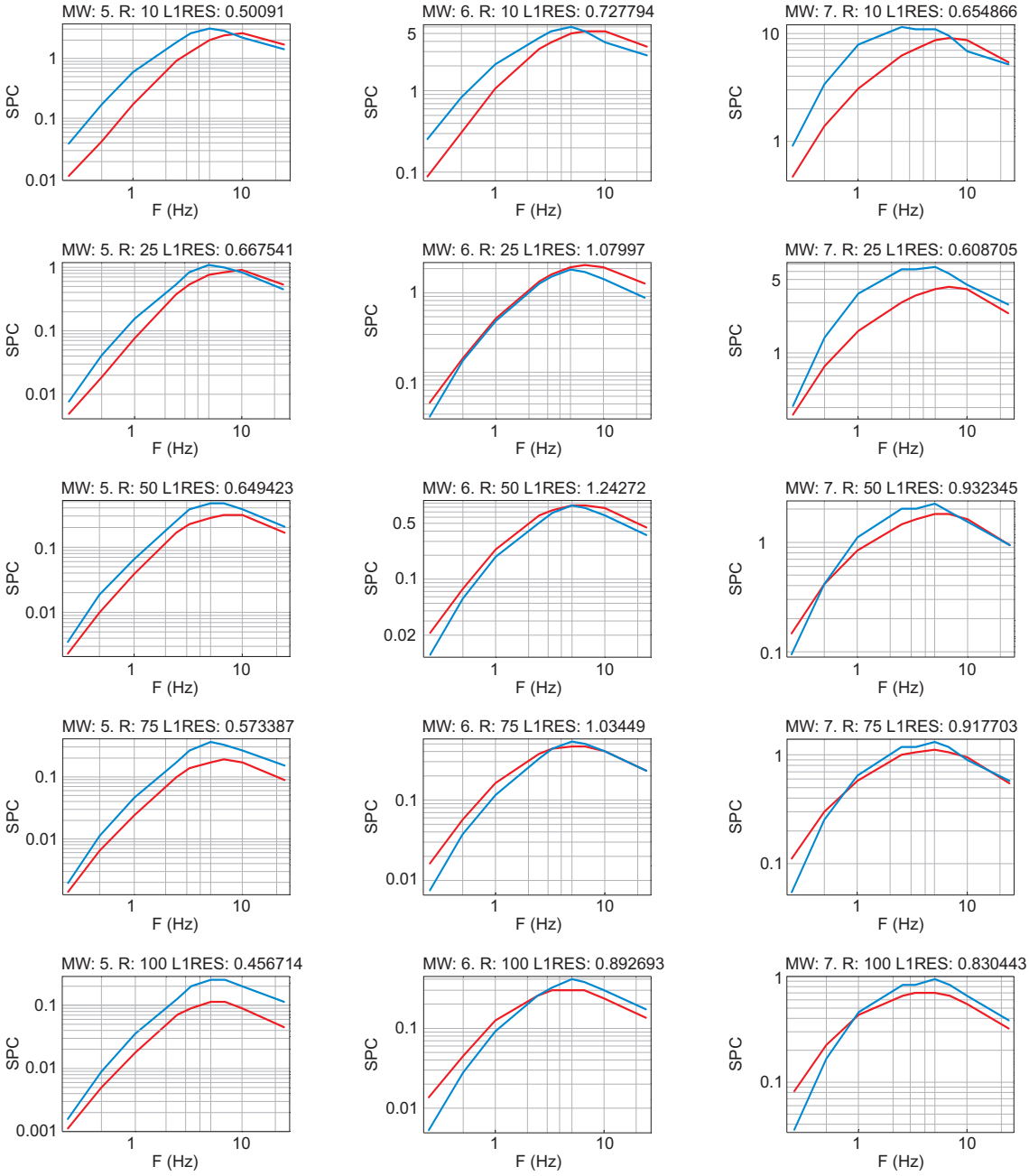

Fig. 27: Determination of an equivalent stochastic model for the Sabetta & Pugliese (1996) ground motion model

The blue lines show the empirical model spectra while the red lines show stochastic models derived from the combination of trial and error and grid search on the stochastic parameters.

The parameter values obtained from this approach seem reasonable at first glance and e.g. the resulting kappa values match well with the study of Silva et al. (1998), but sometimes the stochastic models show considerable differences to values proposed by other authors for what seems regionally close. E.g., I was unable to even closely reproduce the Sabetta & Pugliese model with the model parameters of the Appennines model of Malagnini et al. (2000). Starting with the Abrahamson & Silva model and modifying stress drop, kappa, and geometrical spreading I obtained a much better fit. This was done by first performing a grid search on the geometrical spreading resulting in the following two segment ((1, -0.9),(40, -0.5)). Finally,

stress drop and kappa were searched for, resulting in 60 bars for the stress drop and a value of appr. 0.03 for kappa (cf. Figure 27). Based on this and similar experiences with some of the other ground motion models I came to the conclusion that my confidence in the uniqueness of the obtained set of stochastic parameters is not yet strong enough to allow the application of the *full* hybrid model in all its beauty. However, since the kappa values in Table 9 match well with the study of Silva et al. (1998) and seem to reasonably well allow the modeling the spectral shapes for all the proponent models in the magnitude range 5 – 7 in conjunction with the rocksite models based on the values in Table 8, I consider them robust enough to be used for a mild form of the hybrid model (consisting only of the conversion for the local rock site conditions and for differences in kappa). The corresponding kappa correction filter for the Fourier amplitude which has to be applied is given by the expression

$$kcorr(f) = e^{-(\kappa_0^{REF} + \kappa_0^{GMM}) \cdot \pi \cdot f} = e^{-\Delta\kappa \cdot \pi \cdot f} \qquad (3\text{-}2)$$

with κ_0^{REF} corresponding to the chosen reference value for Switzerland and κ_0^{GMM} corresponding to the kappa value representative for the ground motion model under consideration (Table 9). The kappa values in Table 9 are resulting from my attempt to optimally parametrize each candidate model by a stochastic model and are therefore consistent with the adjusted v_{s30} values in Table 8.

Tab. 9: Kappa values to be used for site conditions conversion

Model name	κ_0 (s)	method used
Abrahamson & Silva 1997	0.0375	grid search
Ambraseys & Douglas 2000	0.0119	grid search
Ambraseys et al. 1996	0.0179	grid search
Ambraseys & Simpson 1996	0.0179	Since the data set is essentially the same as Ambraseys et al. (1996), the same value was assumed.
Atkinson & Boore 1997	0.0011	grid search
Bay 2002	0.0125	from Bay's thesis (Bay 2002)
Rietbrock 2002	0.0125	A large range of kappa values is given in his study. Therefore the value was set to the same value as Bay (2002).
Berge-Thierry et al. 2000	0.0225	grid search
Boore et al. 1997	0.05	The grid search was inconclusive. Therefore, the kappa value was manually adjusted so that the peaks of response spectra would match.
Campbell & Bozorgnia 2002	0.05	same procedure as for Boore et al. (1997)
Lussou et al. 2001	0.0353	grid search
Sabetta & Pugliese 1996	0.02978	grid search
SEA 99	0.03341	grid search
Somerville et al. 2001	0.00665	grid search
Toro et al. 1997	0.0021	grid search

The complete modification of the proponent models to Swiss conditions should combine the v_{s30} rock-site filter and the kappa filter.

The distribution of kappa versus v_{s30} values obtained here for the proponent models shows a clear correlation similar to the results reported by Silva (Silva et al. 1998) (cf. Figure 28).

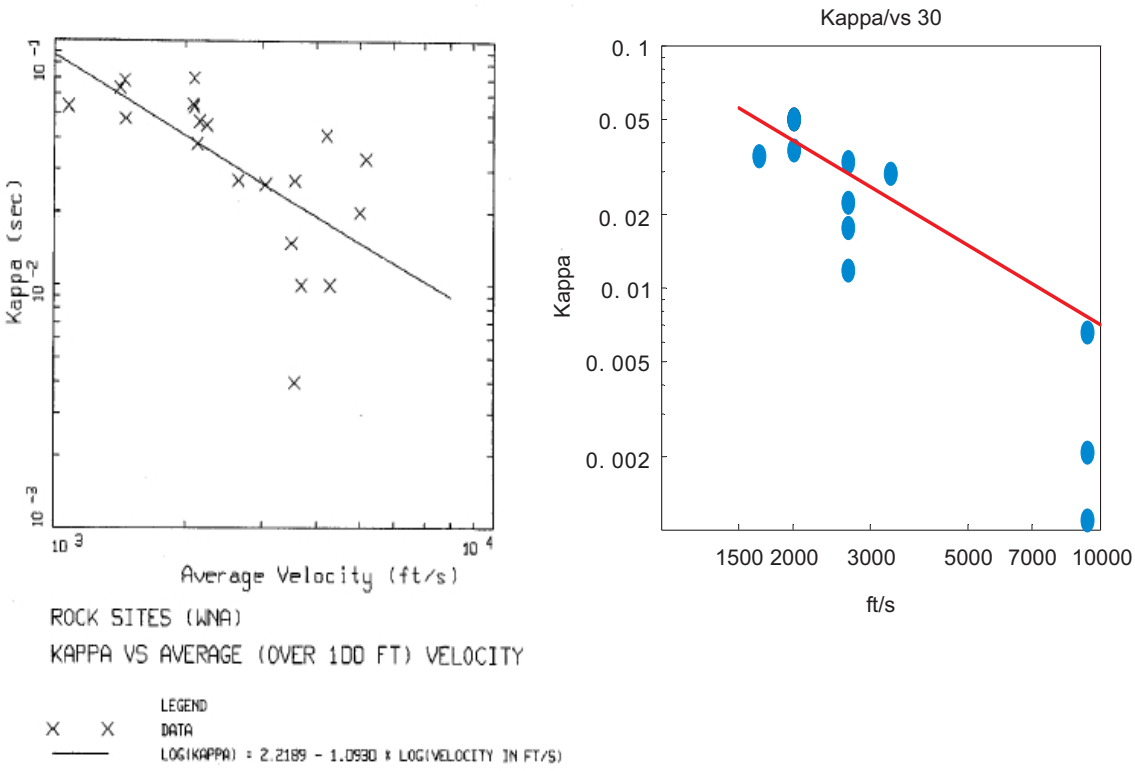

Fig. 28: Comparison of the kappa versus average v_{s30} values from Silva et al. (1998) (left panel) and the values obtained here (right panel: red line shows regression line from left panel)

This indicates that at least for the host regions of the proponent models the "shallow site effects" may not really be decoupled from "deeper site effects" which are partially captured by the kappa value. *In this case*, since the effects of the conversion for rock site conditions and kappa counteract each other (Figures 29 – 31), a *decoupling* of the uncertainties on the v_{s30} values from the epistemic uncertainties on kappa could lead to a *possible overestimation* of the total epistemic uncertainties in the adjustment of the proponent models for Swiss conditions. On the other hand, a correlation between v_{s30} and kappa may not exist in general, e.g. if the physical parameters of the different crustal levels are decoupled as could be argued in regions which have been severely affected by ice erosion. (This is an argument, which I believe has been brought up by Donat Fäh in discussions at some PEGASOS workshops). *In such a situation*, a *coupling* of the uncertainties on the v_{s30} values from the epistemic uncertainties on kappa could lead to a *possible underestimation* of the total epistemic uncertainties in the adjustment of the proponent models for Swiss conditions. The effects can be rather large for certain frequencies as Figures 29 – 31 and Figures 33 – 34 demonstrate. At present, I have no physical basis to decide on either hypothesis. Without further information on a potential coupling of v_{s30} and kappa values for Switzerland I assume them to be uncoupled.

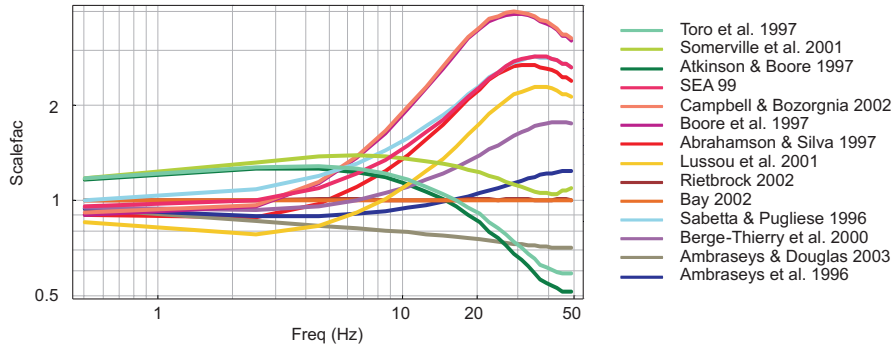

Fig. 29: Conversion for the combined effect of local rock site conditions and for differences in kappa with respect to Swiss conditions (v_{s30} = 1100 m/s; reference kappa = 0.0125 s)

Shown are the scale factors for the response spectra.

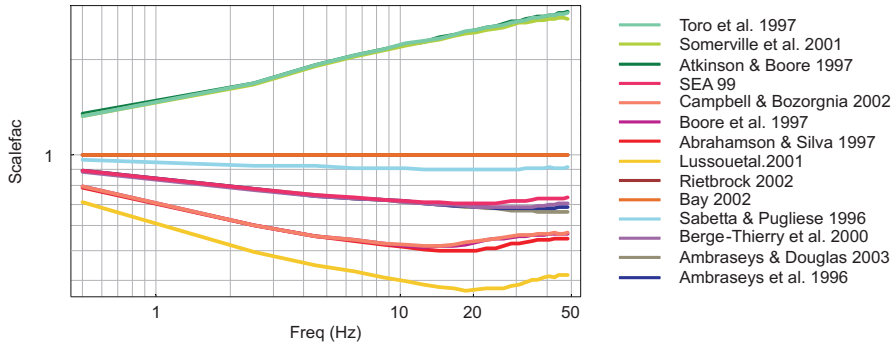

Fig. 30: Conversion for the effect of local rock site conditions to Swiss conditions (central value of v_{s30} = 1100 m/s)

Shown are the scale factors for the response spectra.

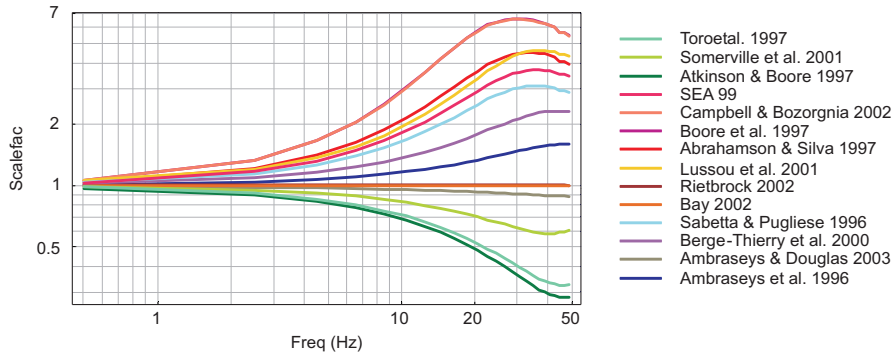

Fig. 31: Conversion for the effect of differences in kappa with respect to Swiss conditions (average kappa = 0.0125 s)

Shown are the scale factors for the response spectra.

As for the v_{s30} values, three different branches should account for the epistemic uncertainties in the kappa values. Due to the lack of a physical model for a correlation between v_{s30} and kappa, I treat the uncertainties in the kappa values as independent from the uncertainties in v_{s30}.

For the host regions of the proponent models, the values given in Table 9 should be applied with a weighting factor of 0.4, while two additional branches with lower (20 %) and higher (20 %) κ^{GMM} values should be applied with weights of 0.3 each. The reason for assigning a broad distribution (03, 0.4, 0.3) is that I consider the kappa values to have a "broad" uncertainty.

For the target region, however, I believe that the situation is more complicated. As the study of Rietbrock demonstrates (Rietbrock 2002), kappa values for Switzerland range from 0 for his reference site and appr. 0.04 s (cf. Figure 32 and his table 3).

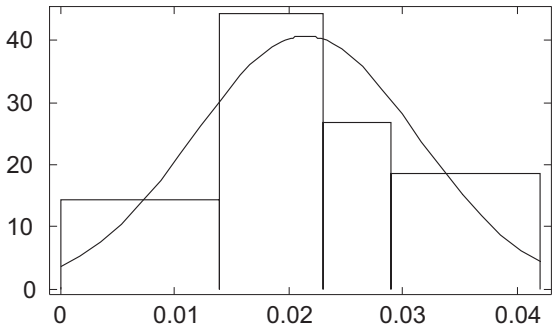

Fig. 32: Distribution of kappa values obtained for Switzerland (Rietbrock 2002)

Mean value: 0.02155, standard deviation: 0.0098.

The value of 0.0125 s is from the study of Bay (2002) and I assume as reference value that it may be considerably off for other sites in Switzerland. Using the mean value from the Rietbrock analysis (Rietbrock 2002) for example, would result in considerably adjustments for the effects of differences in kappa as Figure 33 demonstrates. As a consequence, the overall adjustment for the combined effect of differences in kappa and rocksite conditions would be considerably different as well (Figure 34).

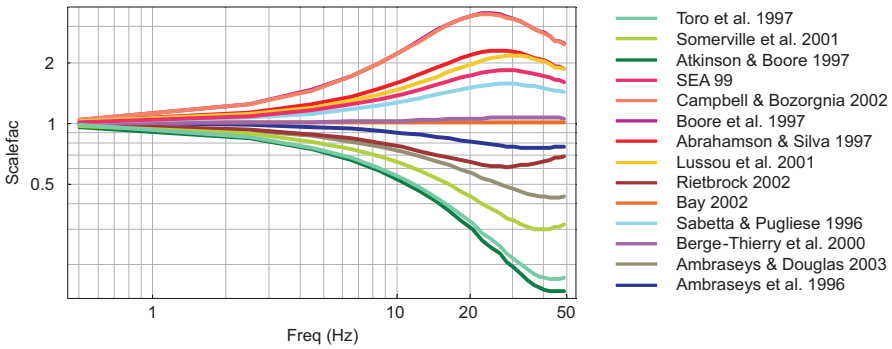

Fig. 33: Conversion for the effect of kappa differences for a reference kappa of 0.02155 s

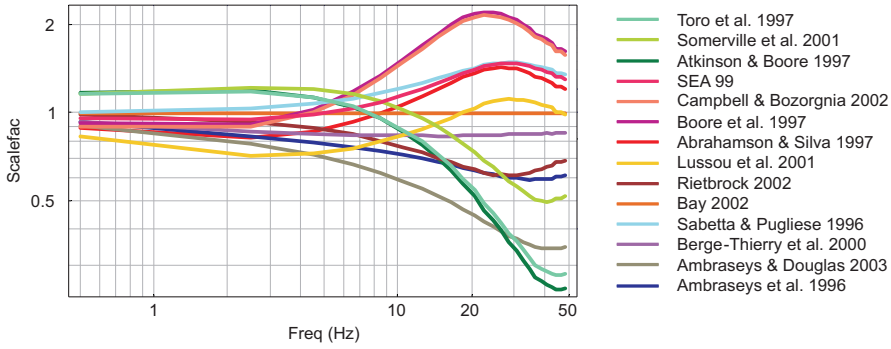

Fig. 34: Conversion for the combined effect of local rock site conditions and for differences in kappa with respect to v_{s30} = 1100 m/s and a reference kappa of 0.0125 s

In order to be consistent with the Bay analysis (Bay 2002) I have chosen a kappa of 0.0125s as central reference value for this part of the logic tree. In order to capture the epistemic uncertainties, on the median kappa for Switzerland I am assuming two side branches, a lower one with kappa of 0.00625 s and an upper one with kappa of 0.025 s (both with weights of 0.3). Again, I am considering this parameter to have a "broad" uncertainty.

3.4.1 Relative adjustment factors for Swiss conditions

As discussed at length in chapter 2, my approach to the adjustment of proponent models to Swiss conditions consists of two parts. After the first part, the host-to-target-region conversion (consisting of adjustments for differences in site conditions and kappa) is applied to all candidate models, the performance of the modified models is tested by using a goodness-of-fit measure on a reference data set of observed response spectra. Based on the outcome of this second part, all the models are categorized into different quality bins describing the applicability to the target region, in other words to match the reference data set. In the final step, relative adjustment factors to are defined to reduce the weights on those models performing poorly.

The strategy to obtain data driven relative adjustment factors for Swiss conditions as described in chapter 2.1.1 is based on the interpretations of *LH values* for the reference data for Switzerland (all records from the PEGASOS database which fall into the EZ2B-region and which have distances less than 200 km and moment magnitudes larger than 4.5).

Setting temporarily aside all considerations of validity range in terms of magnitude, distance and frequency coverage of the individual models, I have compared the resulting spectra to all proponent models. The results are shown in Figure 35. The corresponding residual and *LH* value distributions are shown in Figures 36 and 37. Table 10 lists the corresponding goodness-of-fit values.

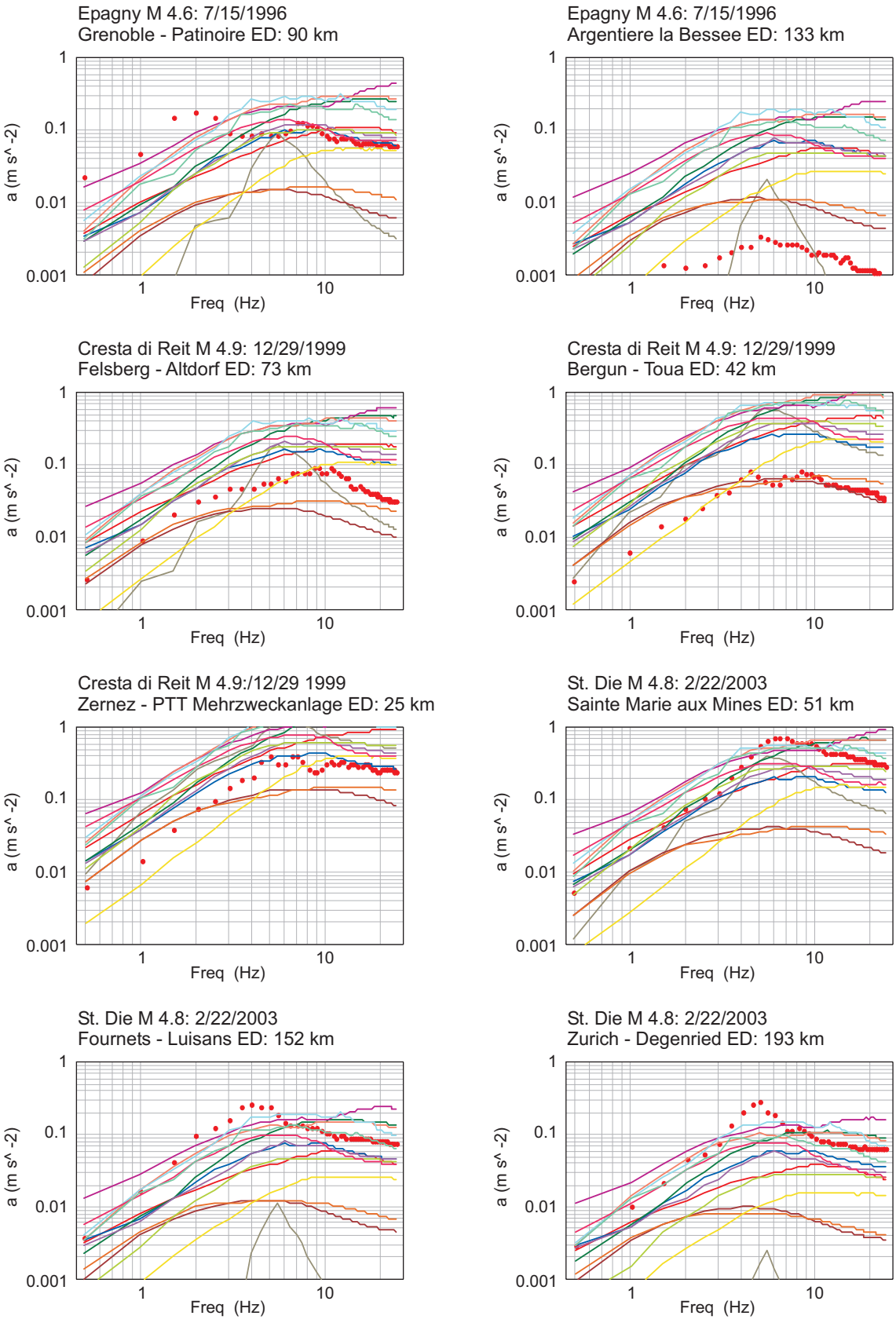

Fig. 35: Comparison of the original proponent models (with modifications for site and kappa differences) to the reference data set (EZ2B region, r < 200 km, M_w > 4.5)

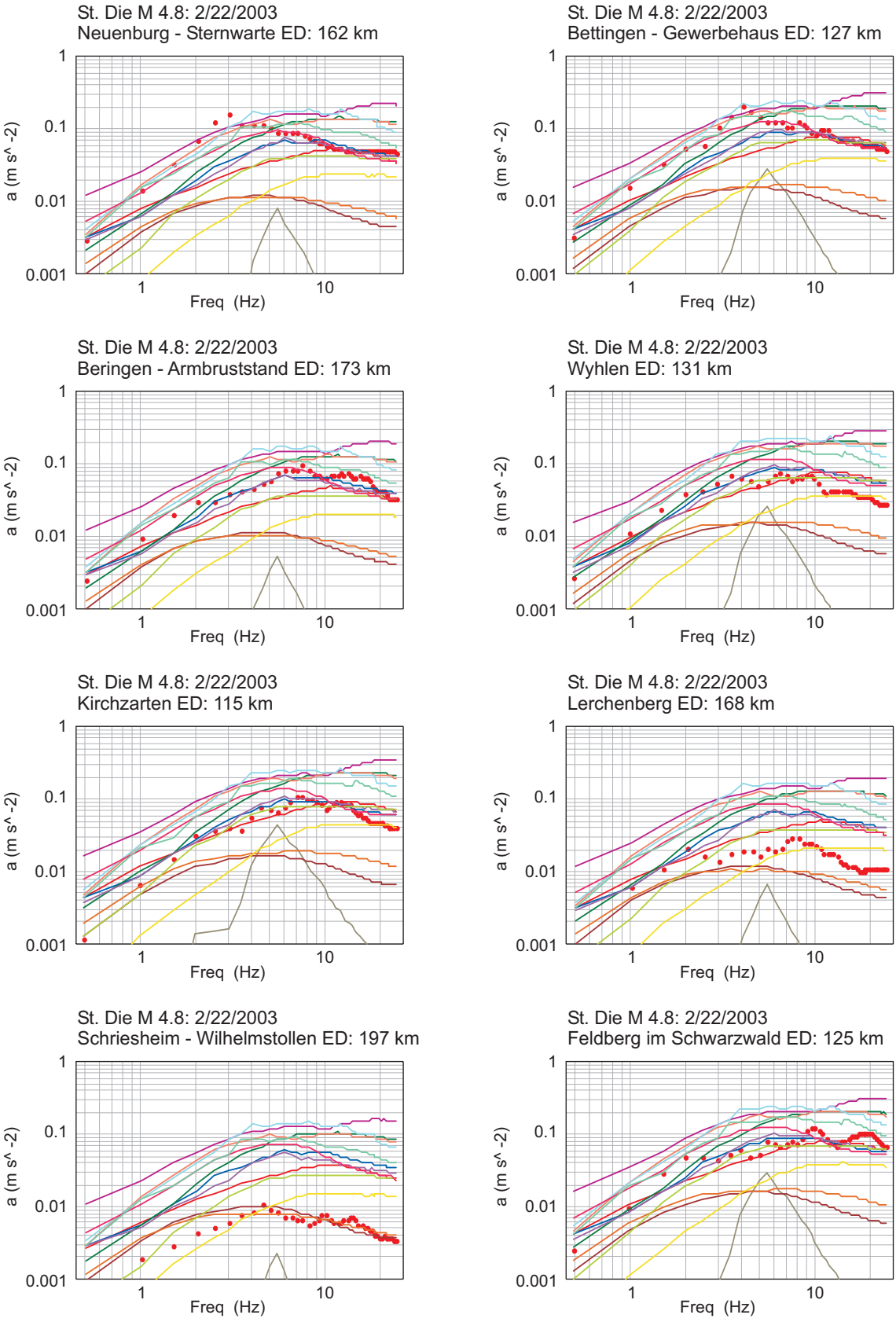

Fig. 35: (Cont.) Comparison of the original proponent models (with modifications for site and kappa differences) to the reference data set (EZ2B region, $r < 200$ km, $M_w > 4.5$)

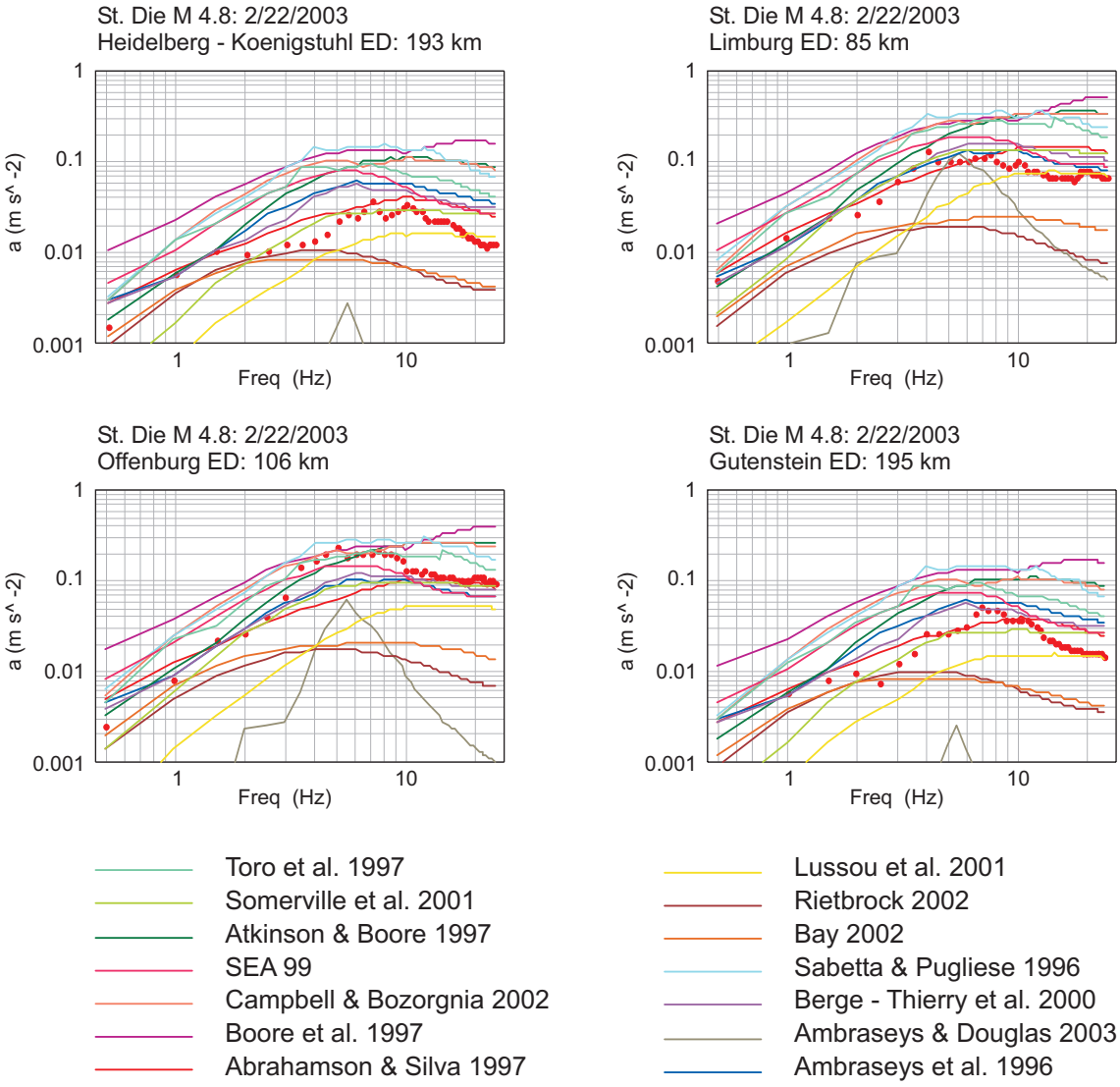

Fig. 35: (Cont.) Comparison of the original proponent models (with modifications for site and kappa differences) to the reference data set (EZ2B region, $r < 200$ km, $M_w > 4.5$)

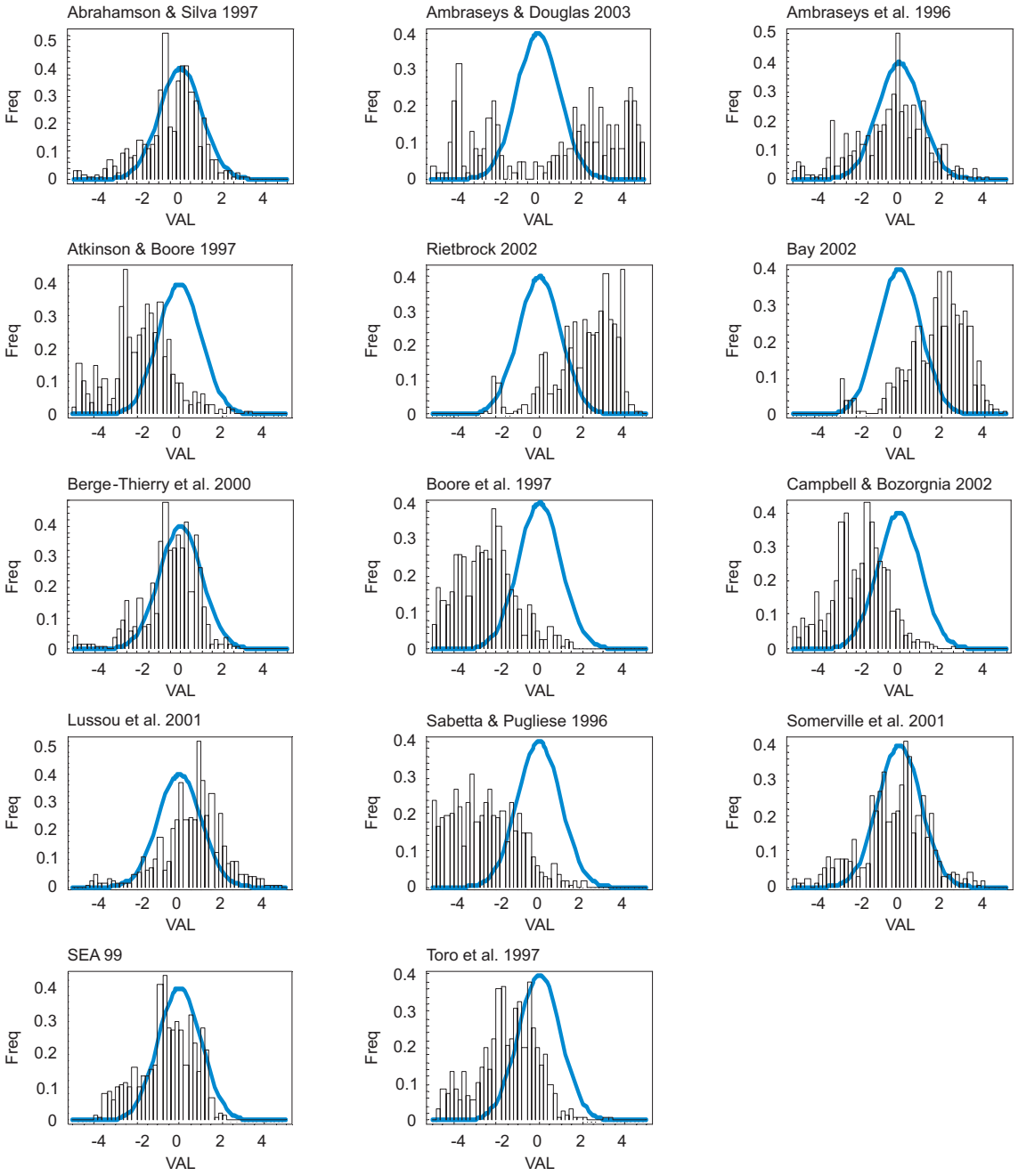

Fig. 36: Residual distribution (scaled by model mean and model variance) for the EZ2B reference data set with respect to different attenuation relations (with modifications for site and kappa differences)

The blue curve shows the expected distribution function for a unit variance normally distributed random variable.

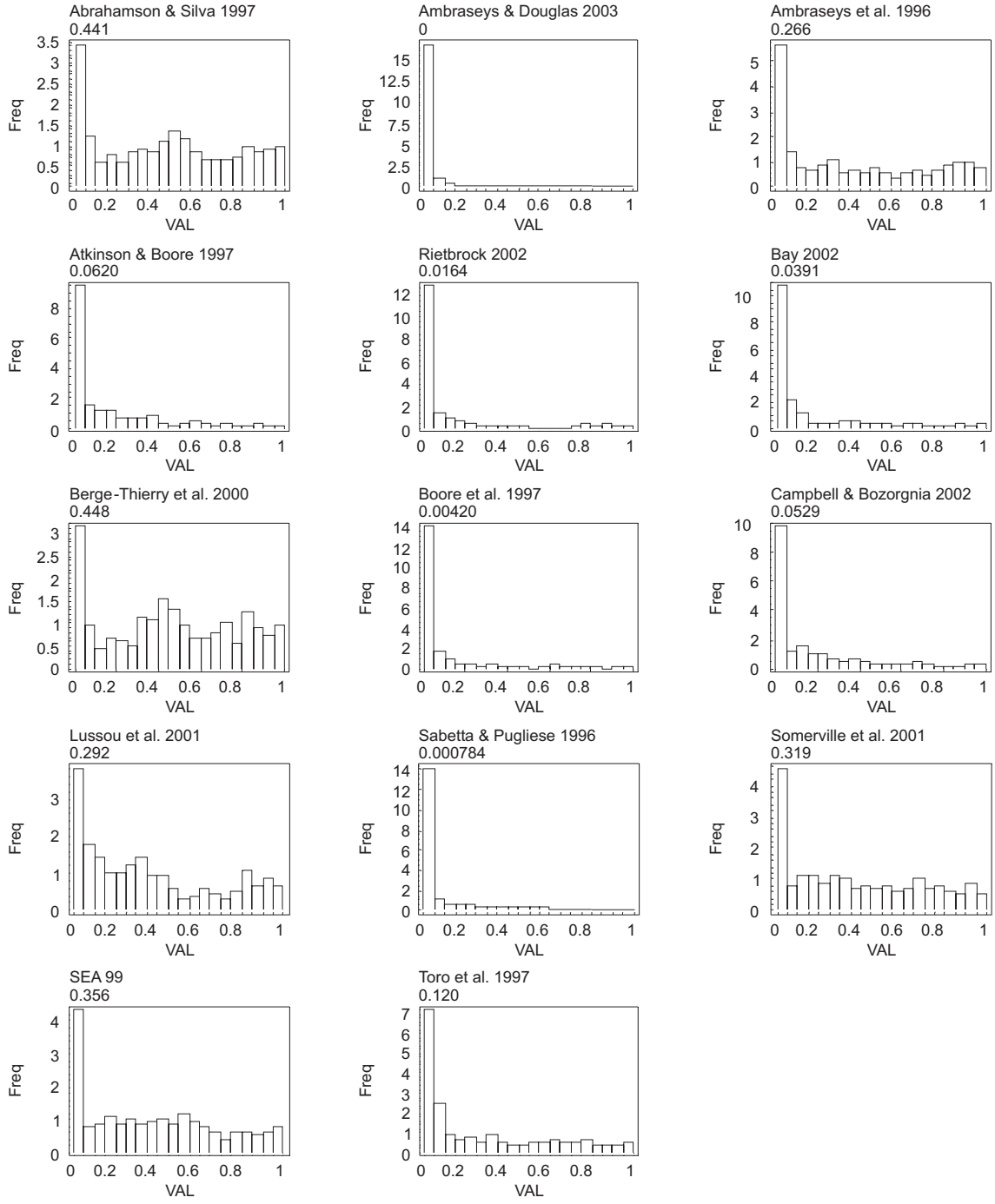

Fig. 37: Distribution of for the EZ2B reference data set with respect to different attenuation relations (with modifications for site and kappa differences)

All panels are scaled to the same maximum value.

Tab. 10: Comparison of different attenuation relations (with modifications for site and kappa differences) to model the EZ2B reference data set

The goodness-of-fit measures shown are: likelihood (LH), variance reduction (VARRED), and the median of the sigma scaled deviation (MSSDEV).

Model Name	Rating	LH	LH Ratio	VARRED	MSSDEV	MSSDEV-Ratio	# records
Berge-Thierry et al. 2000	GOOD	0.448	1.	0.997	0.38	0.309	20
Abrahamson & Silva 1997	GOOD	0.441	0.986	0.99	0.227	0.518	20
SEA 99	FAIR	0.356	0.794	0.989	0.613	0.192	20
Somerville et al. 2001	FAIR	0.319	0.712	0.996	0.118	1.	20
Lussou et al. 2001	POOR	0.292	0.651	0.955	0.805	0.146	20
Ambraseys et al. 1996	POOR	0.266	0.593	1.	0.282	0.417	20
Toro et al. 1997	UA	0.12	0.267	0.91	1.53	0.077	20
Atkinson & Boore 1997	UA	0.062	0.138	0.845	1.79	0.0659	20
Campbell & Bozorgnia 02	UA	0.0529	0.118	0.827	1.93	0.0609	20
Bay 2002	UA	0.0391	0.0872	0.876	1.92	0.0612	20
Rietbrock 2002	UA	0.0164	0.0366	0.801	2.38	0.0495	20
Boore et al. 1997	UA	0.0042	0.00937	0.746	2.86	0.0411	20
Sabetta & Pugliese 1996	UA	0.000784	0.00175	0.836	3.36	0.035	20
Ambraseys & Douglas 2003	UA	0	0	-1.21	9.8	0.012	20

Based on the *LH values* and the criteria derived above, I have rated each ground motion model as GOOD (LH > .45), FAIR (.3 ≤ LH < .45), POOR (.2 ≤ LH < .3), or UNACCEPTABLE (UA; LH < .2). The rows of the unacceptable models are indicated in Table 10 by their dark shading. The comparison with Figure 36 shows that this leads to a quality ranking consistent with the residual distribution.

For the assignment of relative GMM adjustment factors, the same set of conversion rules is used as the one used in the context of assigning prior GMM weighting factors for the conversion of the verbose quality assignment in terms of magnitude, distance, and frequency coverage (cf. chapter 1.2):

NA → 0
GOOD → 1
FAIR → 0.66
POOR → 0.33

The relative ground motion model adjustment factors for the modified ground motion models are given in Table 11.

Tab. 11: Relative ground motion model adjustment factors for the modified ground motion models

Model name	Rating	Relative GMM adjustment factor
Berge-Thierry et al. 2000	GOOD	1
Abrahamson & Silva 1997	GOOD	1
SEA 99	FAIR	0.66
Somerville et al. 2001	FAIR	0.66
Lussou et al. 2001	POOR	0.33
Ambraseys et al. 1996	POOR	0.33
Toro et al. 1997	UA	0
Atkinson & Boore 1997	UA	0
Campbell & Bozorgnia 2002	UA	0
Bay 2002	UA	0
Rietbrock 2002	UA	0
Boore et al. 1997	UA	0
Sabetta & Pugliese 1996	UA	0
Ambraseys & Douglas 2003	UA	0

3.5 Magnitude conversions

Essentially two magnitude scales have to be converted (M_S and M_{JMA}). While there is a wealth of experience and literature on M_S to M_w conversion (Ambraseys 1990, Ambraseys et al. 1996, Ambraseys & Free 1997, Atkinson 1995, Bungum et al. 2002, Ekström & Dziewonski 1988, Hanks & Kanamori 1979, Hanks & Boore 1984, Kanamori 1983), very little is found in the western literature on the conversion of M_{JMA} to M_w (Heaton et al., 1986). Since all the ground motion models which require a conversion from moment magnitude to surface wave magnitudes are "European", I decided to use the Ambraseys & Free relation (without depth dependence) (Ambraseys & Free 1997) for these events. For the conversion of JMA magnitude, I have not found any relationship different from (Heaton et al. 1986) which is stating that M_w and M_{JMA} are equal, Therefore, this is a 1 to 1 conversion. The same is true for the local magnitudes for (Sabetta & Pugliese 1996) which according to Sabetta (pers. comm., 2002) does not require any conversion.

3.6 Component conversions

Horizontal ground motion models are either defined for the largest horizontal component or the average (commonly the geometric mean; average of the logarithms). Both definitions are present in the ground motion model under consideration (Table 12).

Tab. 12: Type of horizontal ground motion in PEGAOSOS GMMs

LARGERH(ENV) uses the envelope of the two horizontal components spectra while LARGERH(PGA) uses the horizontal component with the larger PGA and takes the spectral ordinate at all periods from that component.

Abrahamson & Silva 1997	AVH
Ambraseys & Douglas 2000	LARGERH(ENV)
Ambraseys et al. 1996	LARGERH(ENV)
Atkinson & Boore 1997	AVH
Rietbrock 2002	AVH
Bay 2002	AVH
Berge-Thierry et al. 2000	AVH
Boore et al. 1997	AVH
Campbell & Bozorgnia 2002	AVH
Lussou et al. 2001	AVH
Sabetta & Pugliese 1996	LARGERH (PGA)
Somerville et al. 2001	AVH
SEA 99	AVH
Toro et al. 1997	AVH

Regarding PGA the largest component is roughly 10 – 20 % larger than the average (Ansary et al. 1995, Campbell 1981, Campbell 1997, Campbell 2002). Therefore, for PGA I suggest to use three branches with equal weight which decrease the values of PGA for those relations based on the larger component (LARGERH in Table 12) by 20, 15, and 10 % respectively. Regarding SA, I am basing my judgment on the analysis performed by Proseis (PEGASOS TP2-TN-0269). For the Sabetta & Pugliese (1996) model, I suggest to use three branches. In two of them the values of SA should be reduced by constant 10% (weight 0.2), and 5% (weight.0.2), respectively. In the third branch (weight 0.6), the SA should be reduced by the linear approximation to the frequency dependent result for the Larger PGA/geom. mean ratio from TP2-TN-0269. A similar approach is chosen for the Ambraseys et al. (1996) and the Ambraseys & Douglas (2000) models. Here, in two of the three branches the values of SA should be reduced by constant 15 % (weight 0.2), and 20 % (weight.0.2), respectively. In the third branch (weight 0.6), the SA should be reduced by the linear approximation to the frequency dependent result for the Larger Envelope/geom. mean ratio from TP2-TN-0269.

3.7 Missing frequencies

For the missing frequencies I propose to follow the procedure described in PEGASOS TP2-TN-0270 and to interpolate the coefficients linearly in log10-lin space. Since in a number of ground motion models the coefficient show very abrupt changes as a function of frequency higher order interpolation (of the coefficients) should not be used.

3.8 Style-of-faulting adjustments

Of all the proponent models considered, only three distinguish different style-of-faulting mechanisms (Abrahamson & Silva 1997, Boore et al. 1997, Campbell & Bozorgnia 2002). As of today, I have only become convinced of clear observational evidence for systematic ground motion amplitude differences between reverse + thrust versus normal + strike slip mechanisms. It has been suggested that differences in predicted response spectra between strike-slip, reverse and thrust faulting appear to be consistent with differences in dynamic stress drop (Campbell & Bozorgnia 2002). For the differences between normal faulting events and strike slip mechanisms, however, this hypothesis can not explain the observed lack of differences for the vertical component in the Yucca Mt. evaluation of this issue (Abrahamson 2003). The currently available strong motion data sets for normal faulting events do not contain sufficient unambiguous evidence to allow the distinction of potential style-of-faulting effects from effects caused by different regimes. Therefore, I am only considering an adjustment of reverse + thrust versus normal + strike-slip mechanisms.

Based on the presentation of scale factors from different studies (Abrahamson 2003), I am suggesting to use a set of frequency dependent scale factors (Table 13) to represent the higher ground motion of reverse+thrust mechanism. They essentially – ignoring the high frequency bump- follow the values derived from the study of Campbell & Bozorgnia (2002). This seemed to be justified based on the information provided at the London workshop, that

1. the corresponding data set is more or less a super set of the older studies (Abrahamson & Silva 1997, Boore et al. 1997, Campbell & Bozorgnia 2002) and
2. that the (Abrahamson 2003) subset for $M \leq 5.8$ was dominated by the Coalinga data and therefore not taken into account.

Tab. 13: Reference scaling factors to account for the differences between reverse + thrust versus normal + strike-slip mechanisms

F (Hz)	Horizontal	Vertical
0.5	1.05	1.1
1.0	1.4	1.35
100	1.4	1.25

Based on the percentage of reverse + thrust (plus half of the undefined mechanisms) in the generating data sets of the proponent models, I suggest to adjust those models not containing mechanism scale factors to either reverse + thrust or normal + strike-slip mechanisms by the following procedure:

a) For a given frequency determine $R_{RVT}(f)$ the reference scale factor for reverse + thrust mechanism with respect to normal + strike slip by linear interpolation in Log frequency – Lin scale factor space.

b) Determine $ACTPERC_{EVT}$, the actual percentage of reverse + thrust + half of the undefined mechanisms for the proponent model considered from Table 14.

c) Determine the apparent "amplification" at that frequency $AAGMM(f)$ with respect to normal + strike slip mechanisms as:

$$AAGMM(f) = 1. + \frac{ACTPERC_{RVT} \cdot (R_{RVT}(f) - 1)}{100}$$

d) Divide the SA at the considered frequency by $AAGMM(f)$ to obtain apparent normal + strike slip SA. Correspondingly, multiply the SA by $R_{RVT}(f)/AAGMM(f)$ to obtain apparent reverse + thrust mechanisms SA.

Tab. 14: Percentage of reverse + thrust + half of the undefined mechanisms in the proponent model generating data sets

Model name	% Reverse + Thrust + 1/2 Undefined
Abrahamson & Silva 1997	Scale factors available
Ambraseys & Douglas 2000	52.7
Ambraseys et al. 1996	50.3
Atkinson & Boore 1997	100
Rietbrock 2002	12.0
Bay 2002	12.0
Berge-Thierry et al. 2000	32.0
Boore et al. 1997	Scale factors available
Campbell & Bozorgnia 2002	Scale factors available
Lussou et al. 2001	32.5
Sabetta & Pugliese 1996	47.5
Somerville et al. 2001	100
SEA 99	0.0
Toro et al. 1997	81.0

In order to capture the epistemic uncertainty in these scale factors, two alternative branches with 10 % increased and 10 % decreased reference scale factors should be used. The weighting factors should be 0.5 for the central branch and 0.25 for either side branch.

4 MEDIAN V/H RATIOS

4.1 Approaches for V/H ratios

There are two different strategies to approach the determination of V/H ratios a) direct regression or b) dividing predicted vertical spectral accelerations by predicted horizontal accelerations. Advantages and draw-backs of either method are still a matter of discussion (Ambraseys & Douglas 2000, Campbell & Bozorgnia 2002). The majority of studies follows the second method, which is also the strategy suggested here. Below, I will discuss the logic tree structure and the weights for the candidate models for vertical components with the understanding that in order to obtain the V/H ratios, they should be combined with their companion equations for the corresponding horizontal components. In this context, the vertical components from (Ambraseys & Simpson 1996) should be combined with the companion equation contained in (Ambraseys et al. 1996). In all other cases considered, horizontal and vertical components are treated within the same study.

4.2 Logic tree structure

Appendix D and the file logictree2.pdf contain the logic tree for the median spectral acceleration of the vertical component. Appendix B contains the complete documentation of the knowledge base for the vertical ground motion models.

4.3 Selected proponent models and weights

The list of selected proponent models together with the prior weighting factors calculated according to the method described in chapter 1.2 is given in appendices G and H and in the text files: priorwfV.txt and priorwfV_PGA.txt for SA and PGA, respectively.

The strategy to obtain data driven relative adjustment factors for Swiss conditions is the same as for the horizontal components described above. It is based on the interpretations of *LH values* for the same reference data set as for the horizontal components. The comparison of the observed spectra with the modified ground motion models is shown in Figure 38. The corresponding residual and *LH*- value distributions are given in Figures 39 and 40. Table 15 lists the corresponding goodness-of-fit values. One problematic aspect of this approach is the fact, that the same modifications for site and kappa differences are used as for the horizontal components. Therefore, I consider these modifications less reliable as the ones for the horizontal components.

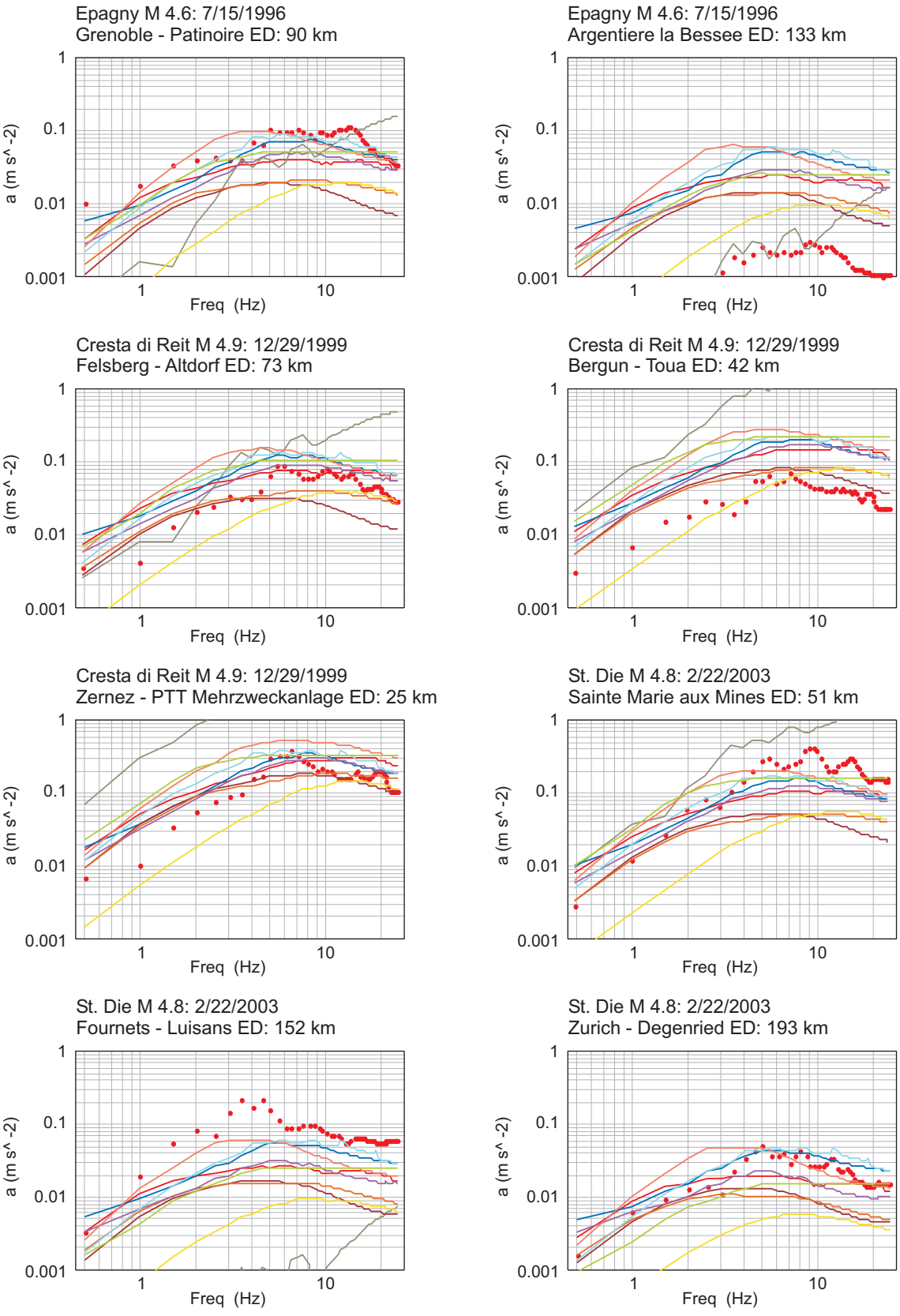

Fig. 38: Comparison of the original proponent models (with modifications for site and kappa differences) to the vertical components of the reference data set (EZ2B region, r < 200 km, M_w > 4.5)

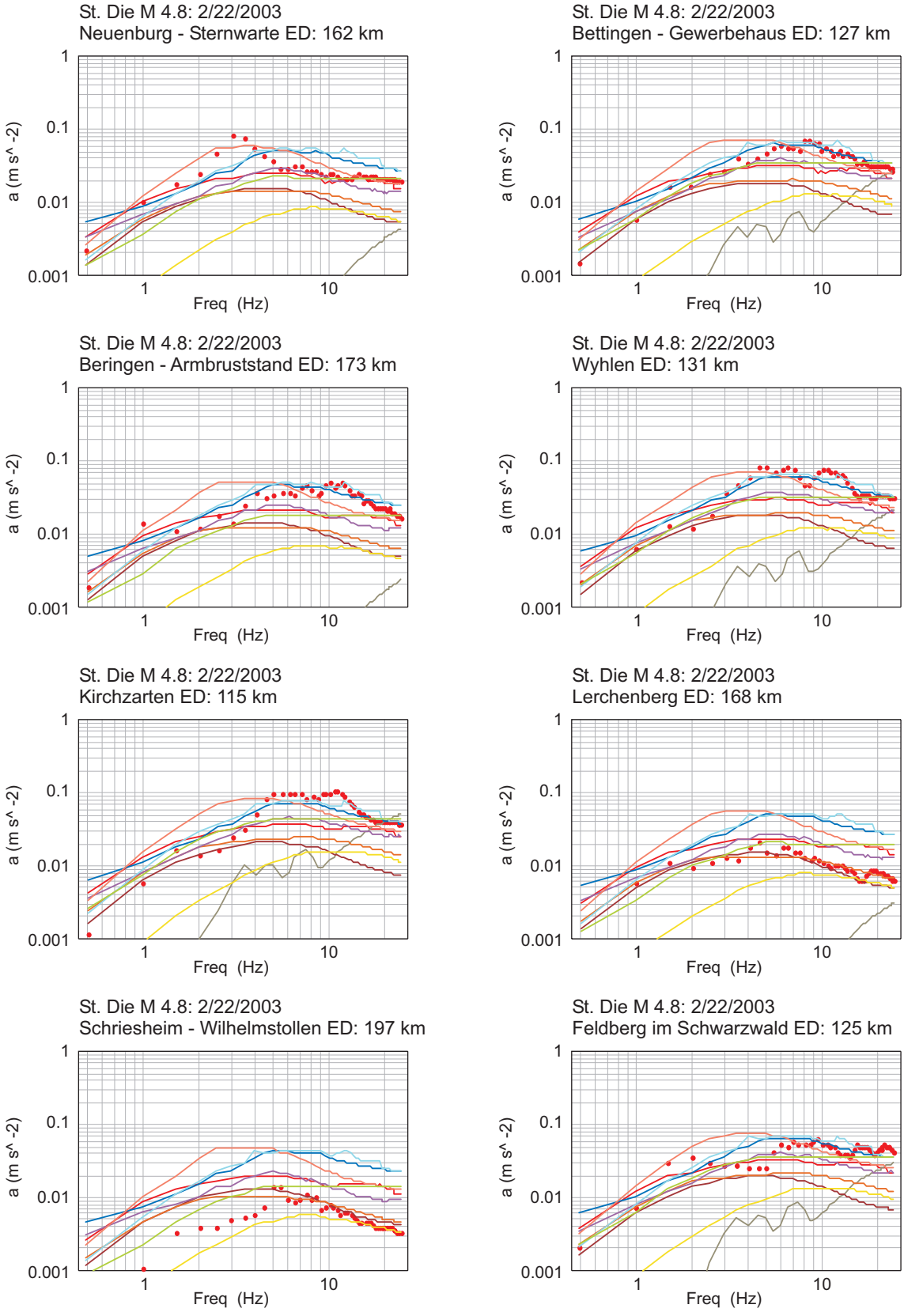

Fig. 38: (Cont.) Comparison of the original proponent models (with modifications for site and kappa differences) to the vertical components of the reference data set (EZ2B region, r < 200 km, M_w > 4.5)

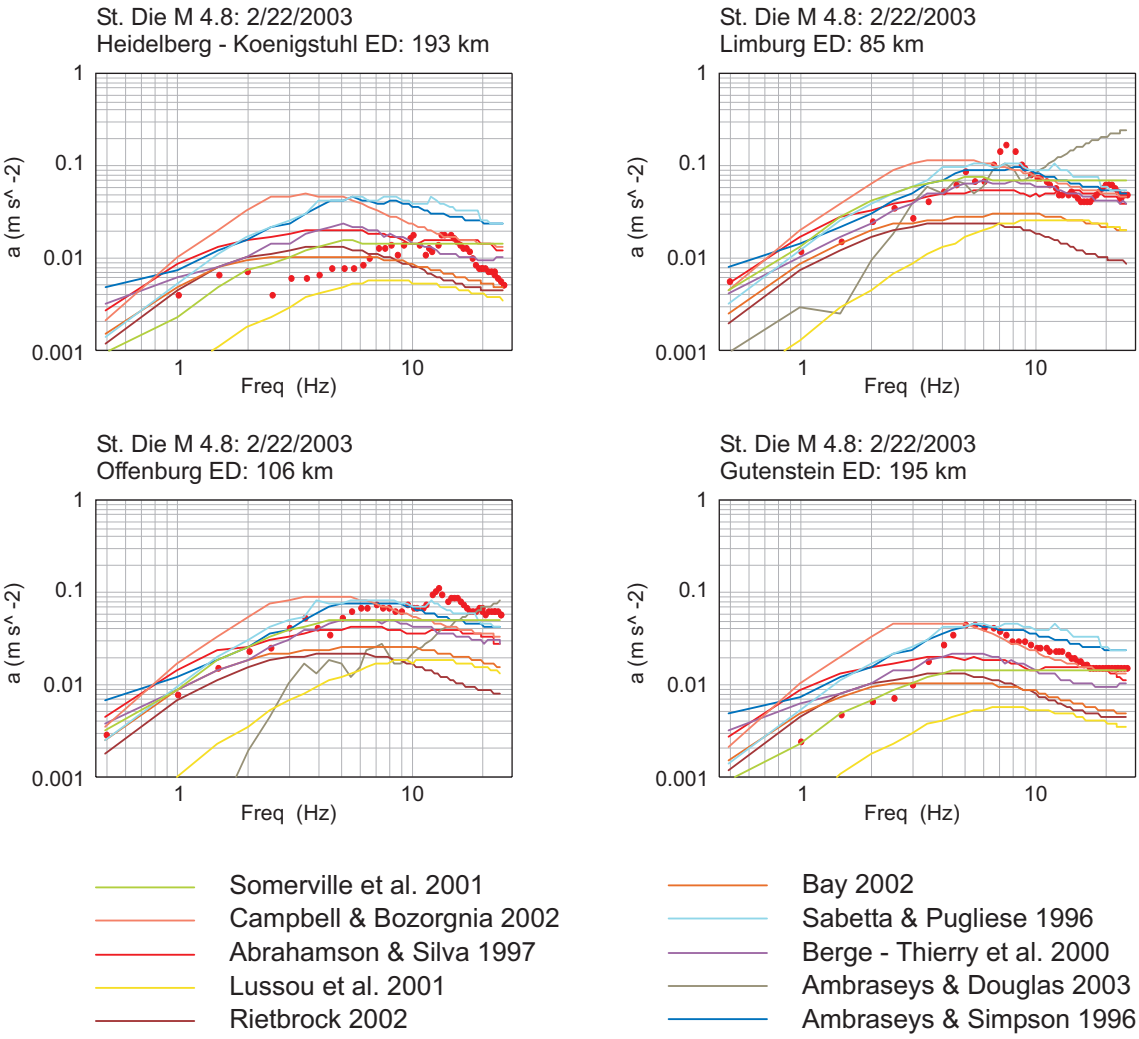

Fig. 38: (Cont.) Comparison of the original proponent models (with modifications for site and kappa differences) to the vertical components of the reference data set (EZ2B region, r < 200 km, M_w > 4.5)

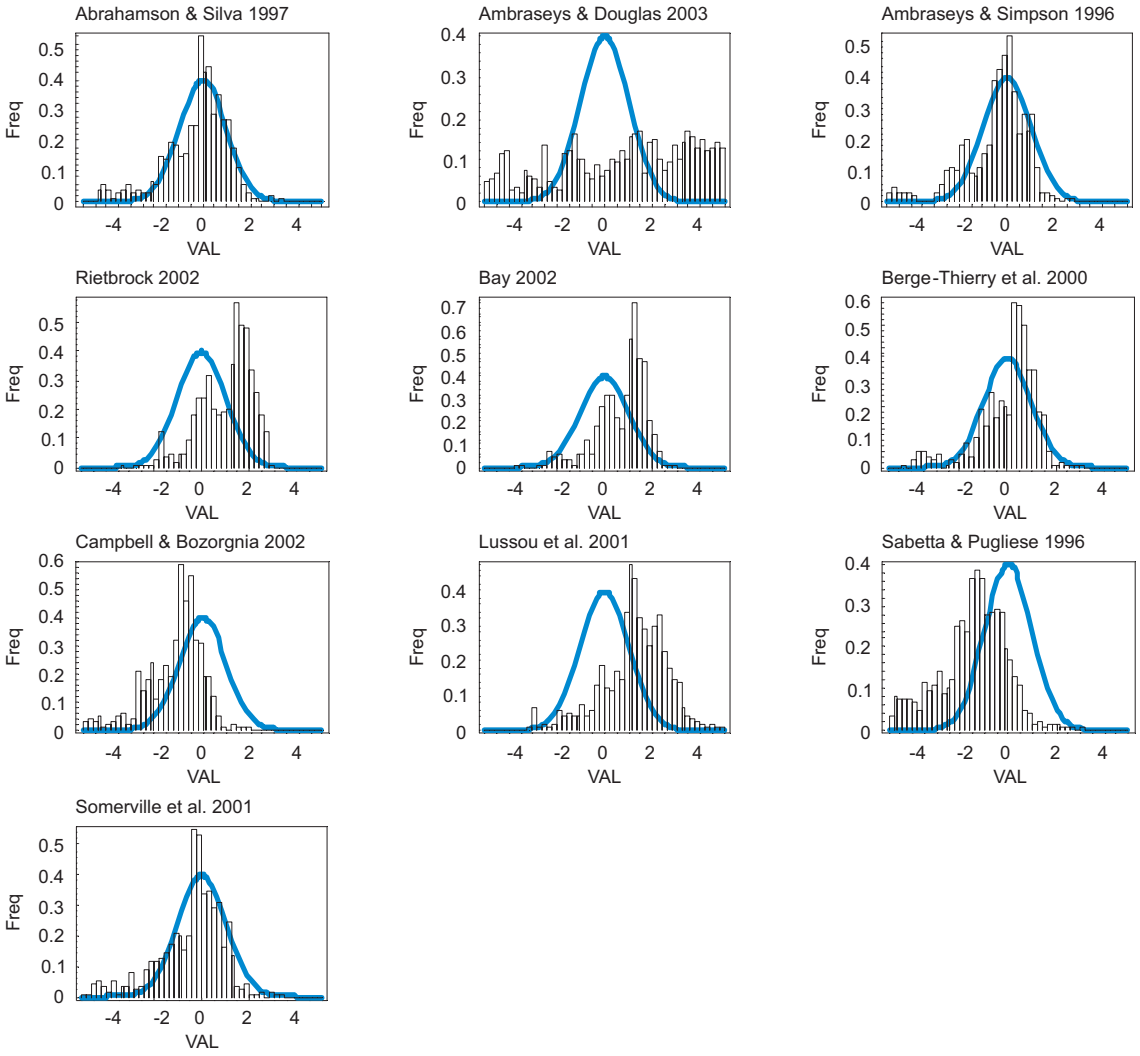

Fig. 39: Residual distribution (scaled by model mean and model variance) for the vertical components of the EZ2B reference data set with respect to different attenuation relations (with modifications for site and kappa differences)

The blue curve shows the expected distribution function for a unit variance normally distributed random variable.

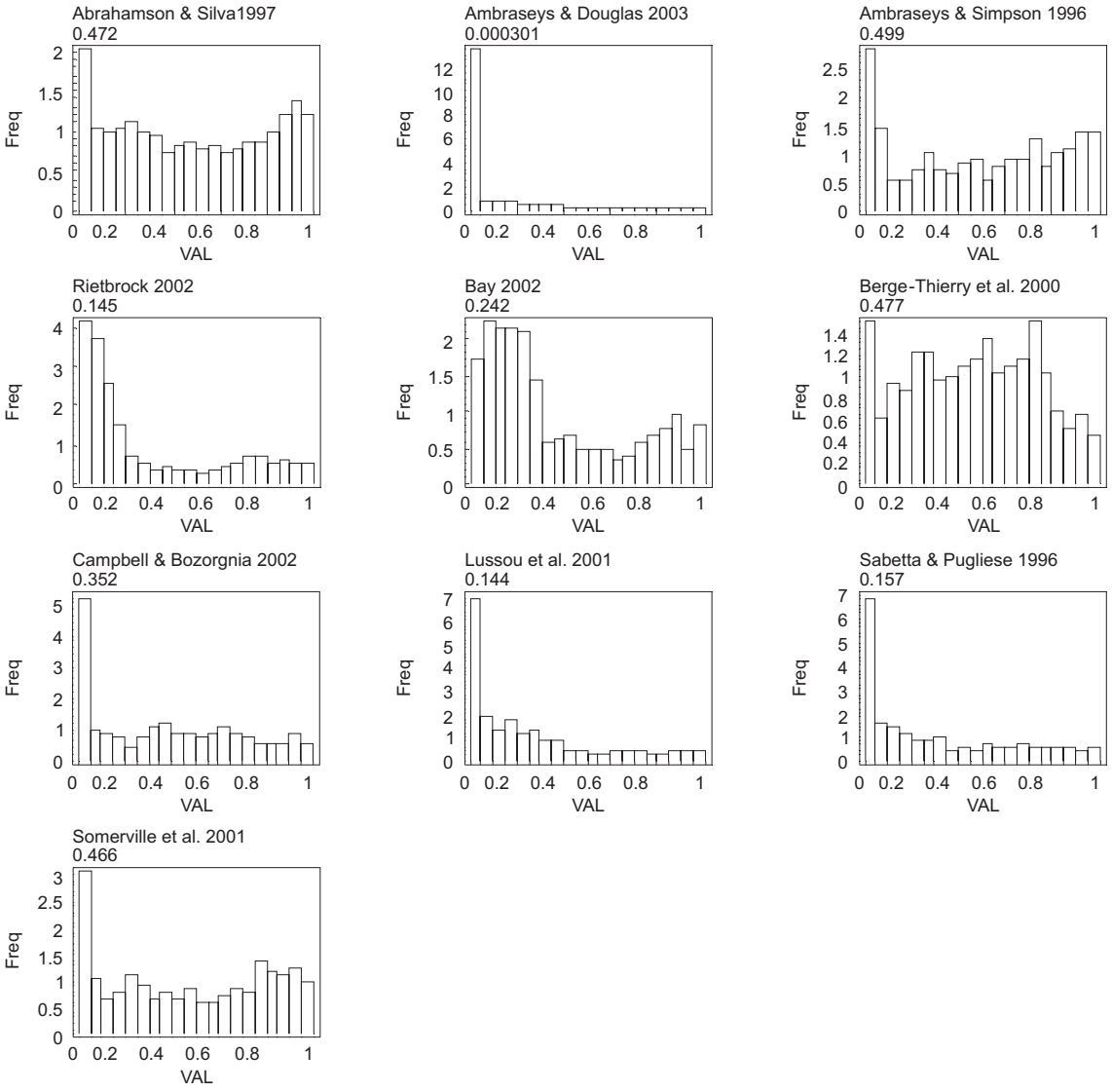

Fig. 40: Distribution of *LH(y)* for the EZ2B reference data set with respect to different attenuation relations (with modifications for site and kappa differences)

All panels are scaled to the same maximum value.

Tab. 15: Comparison of different attenuation relations (with modifications for site and kappa differences) to model the EZ2B reference data set

The goodness-of-fit measures shown are: likelihood (LH), variance reduction (VARRED), and the median of the sigma scaled deviation (MSSDEV).

Model Name	Rating	LH	LH Ratio	VARRED	MSSDEV	MSSDEV Ratio	#
Ambraseys & Simpson 1996	GOOD	0.499	1.	0.991	0.172	0.0613	20
Berge-Thierry et al. 2000	GOOD	0.477	0.956	1.	0.357	0.0296	20
Abrahamson & Silva 1997	GOOD	0.472	0.947	0.991	0.0106	1.	20
Somerville et al. 2001	GOOD	0.466	0.934	0.988	0.216	0.049	20
Campbell & Bozorgnia 2002	FAIR	0.352	0.706	0.937	0.909	0.0116	20
Bay 2002	POOR	0.242	0.484	0.963	1.1	0.00958	20
Sabetta & Pugliese 1996	UA	0.157	0.314	0.941	1.38	0.00767	20
Rietbrock 2002	UA	0.145	0.29	0.922	1.38	0.00768	20
Lussou et al. 2001	UA	0.144	0.288	0.902	1.36	0.00776	20
Ambraseys & Douglas 2003	UA	3.01e-4	0.000602	0.198	2.68	0.00395	20

Based on the *LH values* and the criteria derived above, I have rated each ground motion model as GOOD (LH > .45), FAIR (.3 ≤ LH < .45), POOR (.2 ≤ LH < .3), or UNACCEPTABLE (UA; LH < .2). The rows of the unacceptable models are indicated in Table 15 by their dark shading. The relative ground motion model adjustment factors for the modified ground motion models obtained with the same set of conversion rules as for the horizontal components are shown in Table 16.

Tab. 16: Relative ground motion model adjustment factors for the vertical components of the modified ground motion models

Model Name	Rating	Relative GMM adjustment factor
Ambraseys & Simpson 1996	GOOD	1
Berge-Thierry et al. 2000	GOOD	1
Abrahamson & Silva 1997	GOOD	1
Somerville et al. 2001	GOOD	1
Campbell & Bozorgnia 2002	FAIR	.66
Bay 2002	POOR	.33
Sabetta & Pugliese 1996	UA	0
Rietbrock 2002	UA	0
Lussou et al. 2001	UA	0
Ambraseys & Douglas 2003	UA	0

For the V/H ratio I suggest to use the quality rating from the horizontal components resulting in the final adjustment factors shown in Table 17. One reason for that is that I consider the site corrections for the horizontal components more reliable.

Tab. 17: Relative ground motion model adjustment factors for the V/H components of the modified ground motion models

Model Name	Rating H/V	Relative GMM adjustment factor
Berge-Thierry et al. 2000	GOOD / GOOD	1
Abrahamson & Silva 1997	GOOD / GOOD	1
Somerville et al. 2001	FAIR / GOOD	0.66
Ambraseys et al. 1996 / Ambraseys & Simpson 1996	POOR / GOOD	0.33

5 ALEATORY VARIABILITY FOR HORIZONTAL GROUND MOTION

5.1 Logic tree structure

The logic tree for the aleatory uncertainties has only two sections. For the first section, the attenuation model section, I suggest to use the same weighting factors as for the spectral acceleration. As second section, I suggest to account for the magnitude conversion effects as a potentially relevant source of additional variability.

5.2 Weights for proponent models

Same as for the spectral values.

5.3 Horizontal component conversion effects

Not considered relevant.

5.4 Magnitude conversion effects

Here, I suggest to calculate the modified as

$$\delta\sigma = \sqrt{\sigma^2 + \left(\frac{\partial Y}{\partial m}\delta m\right)^2} \tag{5-1}$$

I suggest to treat the uncertainty coming from the magnitude conversion in two different branches with equal weight and assuming $\partial m = 0.2$ and 0.3, respectively.

5.5 Distance conversion effect

Regarding the distance conversions, I believe that it should be accounted for by additional variability in those models that are subject to this conversion. An example is shown in Figure 41 for the Berge-Thierry model (Berge-Thierry et al. 2000) for two different magnitudes using the conversion relations described in (Scherbaum 2002). Since the distance conversion issue has been taken out of the expert models, this issue cannot be addressed in my logic tree.

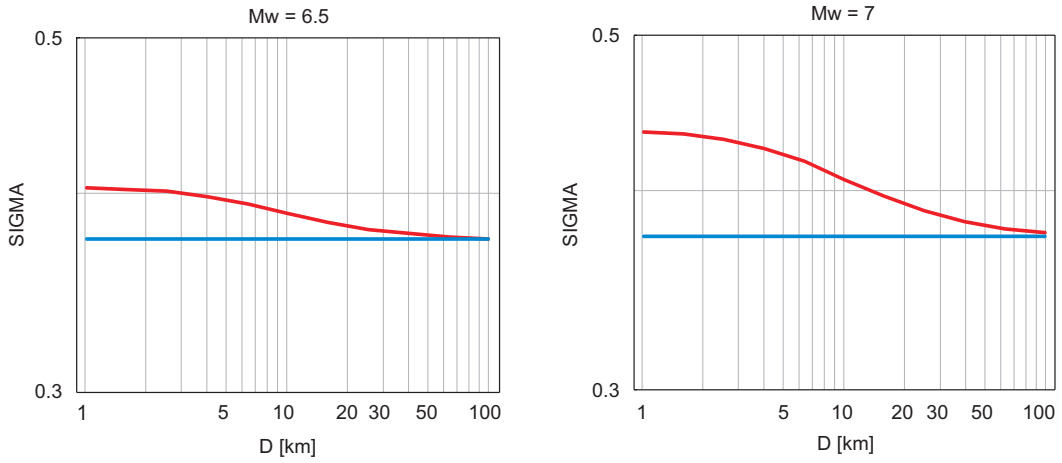

Fig. 41: Effect of distance conversion from Joyner-Boore distance to hypocentral distance on the ground motion model variability for the Berge-Thierry ground motion model (Berge-Thierry et al. 2000)

6 MAXIMUM GROUND MOTIONS FOR THE HORIZONTAL COMPONENT

To know what you don't know, is the best part of what you know. (Lao-tse, Tao-te-king, 71)

Considering the still very limited observational constraints on near source strong ground motion and the still very limited capabilities to perform fully dynamic simulations of the earthquake rupture process, any estimate of upper bounds of strong ground motion must be considered extremely speculative. All considerations below fall into this category but in the PEGASOS spirit I'll try to document my speculations in a consistent way.

The upper bound of ground motion is controlled by a multitude of factors which are not fully understood yet. I see three different classes of information which in principle could help to determine maximum amplitudes:

- observed data,
- simulations,
- statistical considerations.

I'll discuss my opinion regarding each of them one by one.

6.1 Evaluation of empirical data

Observed ground motion does carry information about maximum observable ground motion. This sounds trivial, but one could also take the completely pessimistic view and argue that we don't know anything about maximum ground motion because the current observations haven't really sampled the distribution of large motion well enough. I interpret the data set of largest observed ground motion as an estimate of the lower bounds of the maximum ground motion. Of course, there is also the chance that we have already observed the maximum possible ground motion ever (this would be the completely optimistic view), but I consider this chance very small (so small that I ignore it). The reason is that the observation of maximum ground motion requires very special geometrical conditions to be met, which are very unlikely to have been sampled with the existing data set. Therefore, I consider the data set of the largest ground motion recordings on rock as an estimate of the *lowest bound on maximum ground motion.* However, since none of the observations is actually obtained at the source, it is unknown to what degree local and regional propagation characteristics are captured by the existing observations. For that reason, I put all the weight on the numerical simulations discussed below.

6.2 Evaluation of numerical simulations

I believe that most of the factors controlling the maximum ground motion are deterministic in the sense that they can be modelled by deterministic source models, provided the modelling is physically appropriate. For that reason I believe that the *numerical simulations* that have been performed by Priolo and Pitarka – except those that have to be considered as unrealistic/ unphysical – can be considered as realizations of earthquakes that have not been observed yet and can help to identify scenarios to observe possible maximum ground motion. I believe that the scenarios covered in the (undoubtedly) physically acceptable range of input parameters of the models of Priolo and Pitarka (the subshear rupture speed range) sample the distribution of maximum ground motion scenarios for Switzerland.

Since both models are purely kinematic, and since I am not an expert in rupture dynamics, I trust the assessment of Madariaga regarding the physical realizability of the scenarios covered. I consider the subshear models of both Priolo and Pitarka as sampling the distribution of maximum ground motion scenarios somewhere close to the center of the distribution. I consider Priolo's model to be on the upper side for the reason that Madariaga considered the instantaneous slip front which is used by Priolo as not very likely. On the other hand, he has not dismissed it as unphysical. If one believes the argument of the authors of the k^{-2} model (Herrero & Bernard 1994), on which the Priolo source model is based, it can be seen as an approximation to some non-classical models of rise-time (e.g. self-healing rupture models). This is discussed in Herrero & Bernard (1994), I cite: "Paradoxically, a first-order approximation of the effect of such a non classical rise time function is provided by a propagating rupture front at which the slip instantaneously reaches its final value, i.e. a very classical dislocation model, associated with a heterogeneous final slip distribution" (p. 1222 in Herrero & Bernard 1994). Since, the instantaneous slip function is a very effective source of high frequency radiation, this in my opinion puts the results of Priolo on the upper side of what I feel could be the center of the distribution of possible maximum ground motion scenarios for Switzerland.

On the other hand, I do not share the concerns of Madariaga concerning the high *fmax* (which was put at the Nyquist frequency of 20 Hz), since taking the value of Bay ($\kappa = 0.0125$) would result in an even higher value of $fmax = (0.0125\pi)^{-1} = 25$ Hz. Since the Pitarka model is based on a rather low frequency model instead, it would naturally puts its results on the lower side of those of Priolo.

As Madariaga pointed out, both simulations satisfy the k^{-2} models for the final slip distribution either explicitly (Priolo) or implicitly (Pitarka). A a consequence, the resulting far-field spectra should both satisfy the omega-square model and it should be possible to match them by "driving the control parameters of the Swiss models into some unusual range". Out of curiosity and ignoring all my doubts that it may not be possible to extrapolate the information from the analysis of the small magnitude earthquakes to larger ones, I have used the model of (Bay 2002) to simulate a $M_w = 5.5$ and a $M_w = 7$ event at a distance of 5 km using stochastic simulation. One can come up with many arguments against doing that, starting from the argument that one should model finite-fault effects for the higher magnitude (Beresnev & Atkinson 1997, 1998a, b and c) to geometrical problems of scaling in this magnitude range (Douglas 2002, Romanowicz & Rundle 1993, Romanowicz 1994, Romanowicz & Rundle 1994, Scholz 1994a, b and 1997, Sornette & Sornette 1994, Stock & Smith 2000). If I ignore the finite size problem based on the observation that the stochastic method still shows reasonable agreement with observations up to magnitude 7.5 (Boore 2002), I am essentially left with the scaling problem for the stress drop. With respect to maximum amplitude problem, the question is if the control parameter which despite criticism is still called stress drop (Atkinson & Beresnev 1997) can be treated as constant with magnitude or not. As the discussion in the recent literature and during the special session on that topic at the last AGU meeting demonstrates, this is still an unresolved issue (Abercrombie 2002, Beroza et al. 2002, Bilek et al. 2002, Chen & Atkinson 2002, Favreau & Archuleta 2002, Kanamori 2002, Mai & Beroza 2000, Mayeda & Walter 1996, McGarr & Fletcher 2002, Mori & Tanaka 2002, Nadeau & Johnson 2002, Prejean & Ellsworth 2001, Richardson & Jordan 2002, Walter et al. 2002).

Based on the positive experience with fitting the records of the St. Dié earthquake, I have used the model of Bay (Bay 2002) as background model to capture "Swiss propagation conditions" but ignored her stress drop estimate. Instead, I have used various stress drop estimates up to 250 bar.

Figures 42 and 43 show the resulting acceleration response spectra based on these considerations in comparison to the results of Pitarka and Priolo (Pitarka 2002 and Priolo 2002).

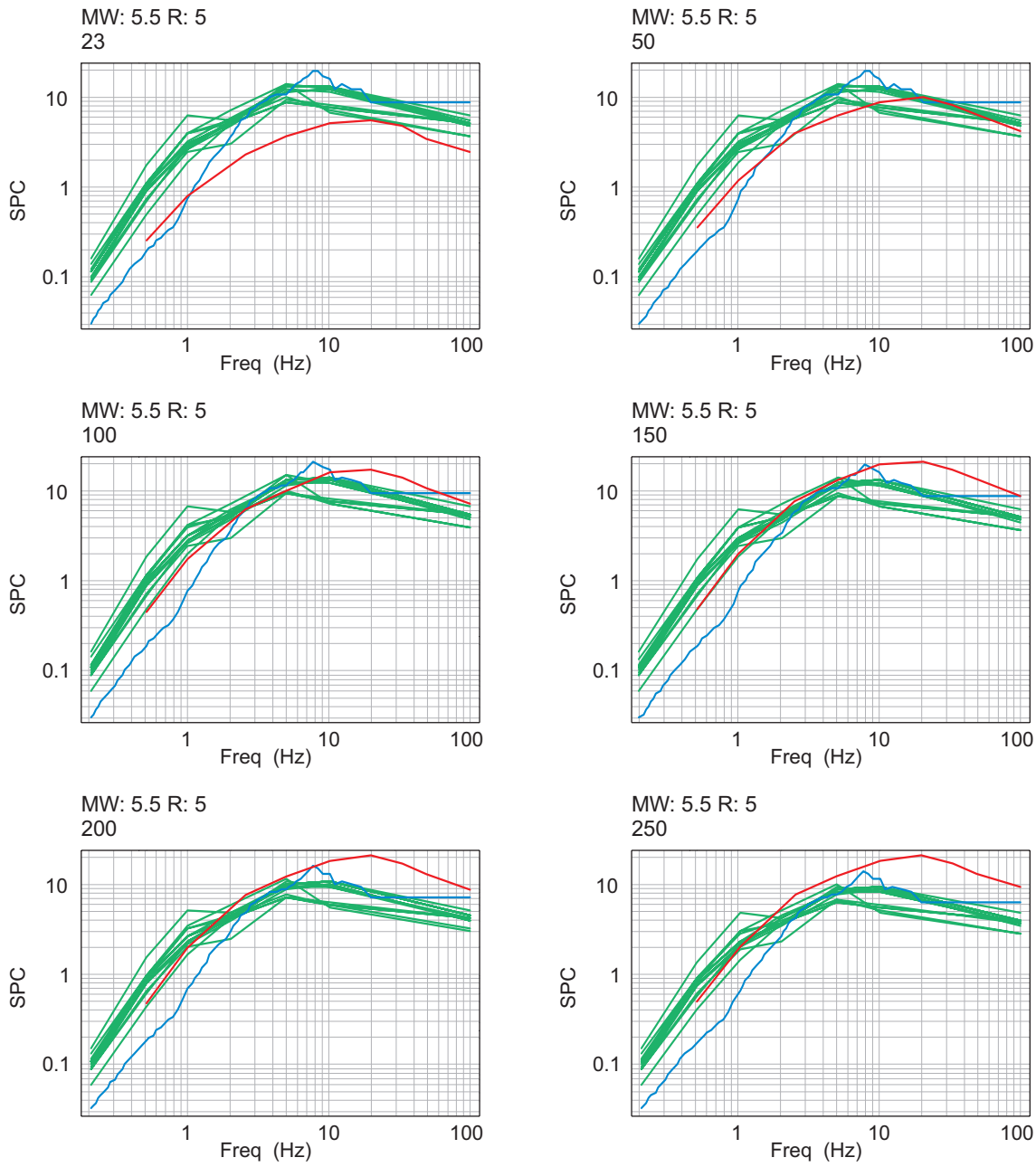

Fig. 42: Extrapolation of the model of Bay to model a magnitude M_w = 5.5 earthquake in 5 km distance using 6 different stress drops (red lines) in comparison to the Pitarka (green lines) and Priolo results (blue lines) as described in Pitarka (2002) and Priolo (2002), respectively

If one believes that the propagation properties for Switzerland are fairly well captured in the Bay analysis, the comparison of the resulting spectra with the simulations by Priolo and Pitarka – which were designed to give maximum amplitudes – can be used to "calibrate" the stress drop parameter to adapt the original median Swiss models to put out numbers that should be closer to the maximum values of ground motion. Again, a number of arguments can be brought up against this procedure, but doing so allows me to describe at least the magnitude – frequency – distance behavior of the maximum amplitude in a justifiable way, even if the absolute value of the stress drop (which simply acts as a tuning parameter) carries very large uncertainties and cannot really be interpreted physically. In order to approximately match the average ground motion for the simulations in Figures 42 and 43 for frequencies between 1 and 10 Hz, a stress drop of at least 150 bars is required for the spectra extrapolated from the Bay model.

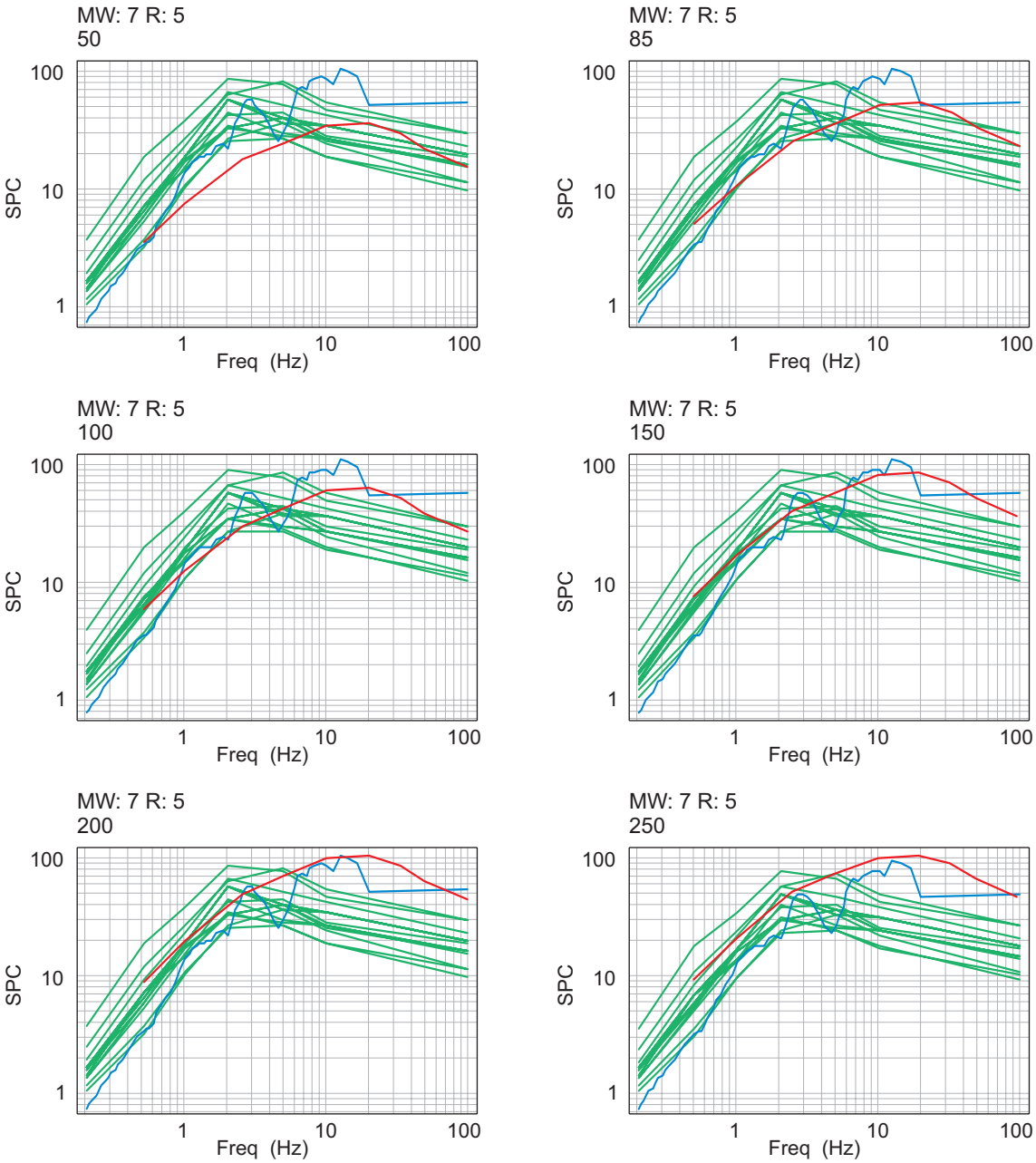

Fig. 43: Extrapolation of the model of Bay to model a magnitude M_w = 7.0 earthquake in 5 km distance using 6 different stress drops (red lines) in comparison to the Pitarka (green lines) and Priolo results (blue lines) as described in Pitarka (2002) and Priolo (2002), respectively

Using the hypocentral distance as equivalent point source distance for the stochastic simulation of an extended source could lead to ground motion amplitudes which are strongly biased for small Joyner-Boore distances. Based on the experience of fitting stochastic models to observed ground motion in California (Abrahamson pers. comm 2003), I therefore suggest to use SQRT(RJB^2 + 64) as equivalent point source distance for the simulation of the maximim ground motion.

6.3 Logic Tree structure

In order to capture the epistemic uncertainties corresponding to the numerous assumptions along the way, I assume a logic tree with three branches:

150 bar (weight 0.7)
200 bar (weight 0.2)
250 bar (weight 0.1)

6.4 Weights for maximum ground motion

The summary tables with the values for each frequency, magnitude and distance are documented in Appendix K and delivered in files UPPERBOUNDSD150.txt, UPPERBOUNDSD200.txt, and UPPERBOUNDSD250.txt (Appendix 10).

6.5 A final general remark concerning the prediction of maximum amplitudes.

Although the PEGASOS PMT has provided SP2 with all the supporting computations which were considered necessary and possible within the resources of the project, I think the prediction of maximum amplitudes remains an unresolved issue. Recently proposed hybrid approaches (Guatteri et al. 2002, Mai & Beroza 2002, Mai & Beroza 2002) possibly offer computationally feasible solutions for the near future, but at present the best I felt I could do, was trying to be consistent in my reasoning and to follow my own rule not to look at the results before I had decided about how I wanted to approach the problem. By using the Bay model (Bay 2002) to describe the regional characteristics I have tried to accommodate Swiss conditions, but I am aware of the fact that it is a very questionable if for example the geometrical spreading relations can be extrapolated to those events considered here. Therefore, I consider the epistemic uncertainties on my results huge, without even being able to quantify them.

7 MAXIMUM GROUND MOTIONS FOR THE VERTICAL COMPONENT

The extrapolation of the Bay model (Bay 2002) to match the horizontal components of the numerical simulations of Pitarka and Priolo (Pitarka 2002 and Priolo 2002) has resulted in a very speculative and highly uncertain estimate for the maximum horizontal ground motion. The same exercise with the vertical component records would result in an equally speculative and uncertain estimate. The corresponding V/H ratio would essentially be undetermined and most probably be inconsistent with the median V/H ratios. Since I am not convinced that the numerical simulations justify the conclusion that the maximum ground motion V/H ratio is different from the median V/H ratios, I suggest to turn the argument around and actually assume that they are equal. As a consequence, the results of chapter 4 can directly be used to scale the estimates for the maximum horizontal ground motion to vertical components.

7.1 Evaluation of empirical data

Same comments apply as for the horizontal ground motions.

7.2 Evaluation of numerical simulations

See comments above.

7.3 Logic tree structure

Same as for median V/H ratios in chapter 4.2.

7.4 Weights for maximum ground motions

Same as for median V/H in chapter 4.3.

8 UPPER TAIL OF THE GROUND MOTION DISTRIBUTION FOR THE HORIZONTAL COMPONENT

The problem of modeling the upper tail of the ground motion distribution is closely linked to the problem of predicting maximum ground motion. I consider "maximum ground motion" and "upper tail" as two aspects of the same problem, concerning the "how" and "where" of ground motion truncation. Since I have already speculated on the "where", I continue in the same spirit.

Although I believe that observations put a lowest limit on the upper bounds, due to the limited sampling of large amplitudes, they can not really help to constrain the shape of the upper tail (yet). On the other hand, there is no observational support for systematic deviations of the distribution of ground motion from a lognormal distribution below 2 σ (Abrahamson 2000, #4002). This is also demonstrated by the data example from the WAF database (Figure 44). Above 2 σ, the situation is less clear. If I "mentally average" the plots in Figure 44 for all the frequency bands displayed, lognormal behavior may even continue up to 3 σ. Based on this interpretation, I put the *lowest* limit of where I believe modification of the lognormal model should be allowed to start at a value of 3 σ.

As a consequence, my upper tail model is constrained by two arguments:

1. at 3 σ above the median still lognormal
2. zero probability at the maximum ground motion amplitudes defined in chapters 6 and 7. Since I see the problem of maximum ground motion as a physical not a statistical one, I don't see any theoretical basis to define the maximum ground motion amplitude in terms of standard deviations.

Regarding the shape of the distribution between these two anchoring points, I express my epistemic uncertainty by two models:

Branch 1 (weight 0.4): *linear interpolation from the 3 σ point to the point of maximum ground motion amplitudes defined in chapters 6 and* 7. In favor of this branch I would argue that the linear interpolation could be seen as a approximation which would best express my lack of knowledge in a pragmatic sense.

Branch 2 (weight 0.6): *lognormal behavior up to the maximum ground motion amplitudes defined in chapters 6 and* 7. Here, I base my reasoning on the fact, that the problem to define a shape for the upper tail is similar to the problem of defining a shape for the truncation of the magnitude frequency distribution. There, it has been shown that the least biased distribution in the face of missing information turns out to be the truncated exponential (Berill & Davis 1980, Main & Burton 1984). This corresponds to the model that the Gutenberg-Richter distribution would continue unmodified up to the maximum magnitude. Although I haven't done it, it is my gut feeling that a similar exercise would yield the simple truncated lognormal distribution as the least bias distribution in the face of the lack of information about the true shape. Therefore, I assign a slightly higher weight to this branch.

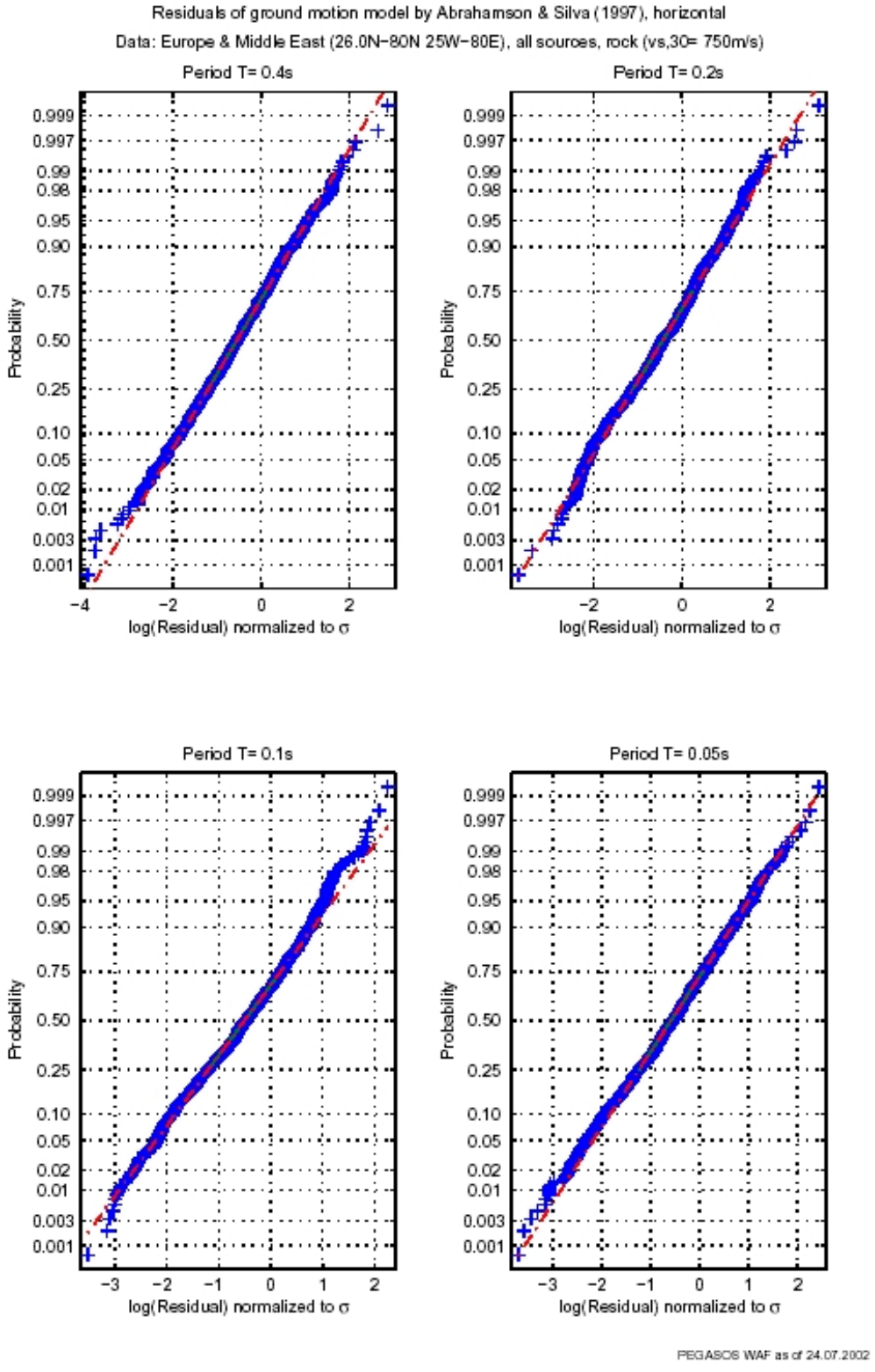

Fig. 44: Example of ground motion residuals from the WAF database

9 REFERENCES

Abercrombie, R.E. 2002: How Good are our Source Parameter Estimates for Small Earthquakes? EOS Trans. AGU 83/47. Fall Meet. Suppl. Abstr. S71E-03.

Abrahamson, N.A. & Silva, W.J. 1997: Empirical response spectral attenuation relations for shallow crustal earthquakes. Seismological Research Letters 68/1, 94 -127.

Abrahamson, N.A. 2003: Style of faulting factors (PEGASOS TP2-RF-0391).

Ambraseys, N.N. 1990: Uniform magnitude re-evaluation for European earthqakes associated with strong-motion records. Earthq. Eng. Struct. Dyn. 19, 1-20.

Ambraseys, N.N. & Simpson, K.A. 1996: Prediction of vertical response spectra in Europe. Earthq. Eng. Struct. Dyn. 25, 401-412.

Ambraseys, N.N., Simpson, K.A. & Bommer, J.J. 1996: Prediction of horizontal response spectra in Europe. Earthq. Eng. Struct. Dyn. 25, 371-400.

Ambraseys, N.N. & Free, M.W. 1997: Surface-wave magnitude calibration for european region earthquakes. Journal of Earthquake Engineering 1/1, 1-22.

Ambraseys, N.N. & Douglas, A. 2000: ….Imperial College of Science, Technology and Medicine Civil Engineering Department.

Ambraseys, N.N. & Douglas, A. 2003: Near-field horizontal and vertical ground motions. Soil Dynamics and Earthquake Engineering 23, 1-18.

Ansary, M.A., Yamazaki, F. & Katayama, T. 1995: Statistical analysis of peaks and directivity of earthquake ground motion. Earthq. Eng. Struct. Dyn. 24, 1527-1539.

Atkinson, G.M. 1995: Optimal choice of magnitude scales for seismic hazard estimates in Eastern North America. Seismological Research Letters 66/1, 51-55.

Atkinson, G.M. & Beresnev, I.A. 1997: Don't call it stress drop. Seismological Research Letters 68/1, 3-4.

Atkinson, G.M. & Boore, D.M. 1997: Some comparisons between recent ground-motion relations. Seismological Research Letters 68/1, 24-40.

Bay, F. 2002: Ground motion scaling in Switzerland: Implications for hazard assessment….

Beresnev, I.A. & Atkinson, G.M. 1997: Modeling finite-fault radiaton from the omega^n spectrum. Bull. Seism. Soc. Am. 87, 67-84.

Beresnev, I.A. & Atkinson, G.M. 1998a: FINSIM – a Fortran program simulating stochastic acceleration time histories from finite faults. Seismological Research Letters 69, 27-32.

Beresnev, I.A. & Atkinson, G.M. 1998b: Stochastic finite-fault modeling of ground motions from the 1994 Northridge, California earthquake. I: Validation on rock sites. Bull. Seism. Soc. Am. 88, 1392-1401.

Beresnev, I.A. & Atkinson, G.M. 1998c: Generic finite-fault model for ground-motion prediction in eastern North America. Bull. Seism. Soc. Am. 89, 608-625.

Berge-Thierry, C., Cotton, F., Cushing, M., Griot-Pommera, D.A. & Joly, J. 2000: Méthode de determination des spectres horizontaux et verticaux adaptés au site dans le cadre de la RFS 1.2.c.

Berill, J.B. & Davis, R.O. 1980: Maximum entropy and the magnitude distribution. Bull. Seism. Soc. Am. 70, 1823-1831.

Beroza, G.C., Perez-Campos, X., Venkatarman, A., Singh, S.K., Prejean, S. & Ide, S. 2002: Progress Towards More Reliable Seismic Energy Estimates. EOS Trans. AGU 83/47, S71E-04, Fall Meet. Suppl. Abstr.

Bilek, S.L., Lay, T. & Ruff, L.J. 2002: Estimates of radiated energy from global shallow subduction zone earthquake. EOS Trans. AGU 83/47, Fall Meet. Suppl. Abstr. S71E-05.

Boore, D.M. 1983: Stochastic simulation of high-frequency ground motions based on seismological models of the radiated spectra. Bull. Seism. Soc. Am. 73/6, 1865-1894.

Boore, D.M. 2000: SMSIM – Fortran programs for simulating ground motions from earthquakes: version 2.0 – a revision of OFR 96-80-A, U.S. Geological Survey OFR 00-509.

Boore, D.M. 2002: Simulation of ground motion using the stochastic method. Pure and Applied Geophysics, in press.

Boore, D.M. & Joyner, W.B. 1984: A note on the use of random vibration theory to predict peak amplitudes of transient signals. Bull. Seism. Soc. Am. 74/5, 2035-2039.

Boore, D.M., Joyner, W.B. & Fumal, T.E. 1993: Estimation of response spectra and peak accelerations from western North American earthquakes: an interim report.

Boore, D.M. & Joyner, W.B. 1997: Site amplifications for generic rock sites. Bull. Seism. Soc. Am. 87/2, 327-341.

Boore, D.M., Joyner, W.B. & Fumal, T.E. 1997: Equations for estimating horizontal response spectra and peak acceleration from western North American earthquakes; a summary of recent work. Seismological Research Letters 68/1, 128-153.

Bungum, H., Lindholm, C.D. & Dahle, A. 2002: Long-period ground-motions for large European earthquakes, 1905-1992, and comparisons with stochastic predictions. J. Seism., in press.

Campbell, K.W. 1981: Near-source attenuation of peak horizontal acceleration. Bull. Seism. Soc. Am. 71, 2039-2070.

Campbell, K.W. 1997: Empirical near-source attenuation relationships for horizontal and vertical components of peak ground acceleration, peak ground velocity, and pseudo-absolute acceleration response spectra. Seismological Research Letters 68/1, 154-179.

Campbell, K.W. 2001: Prediction of strong ground motion using the hybrid empirical method: Example application to eastern North America. Bull. Seism. Soc. Am., submitted.

Campbell, K.W. 2002: A contemporary guide to strong-motion attenuation relations.

Campbell, K.W. & Bozorgnia, Y. 2002: Updated near-source ground motion relations for the horizontal and vertical components of peak ground acceleration and acceleration response spectra. Bull. Seism. Soc. Am. ……..

Chen, S.-Z. & Atkinson, G.M. 2002: Global comparisons of earthquake source spectra. Bull. Seism. Soc. Am. 92/3, 885-895.

Cotton, F. & Campillo, M. 1995: Frequency domain inversion of strong motions: Application to the 1992 Landers earthquake. Journal of Geophysical Research 100/B3, 3961-3975.

Douglas, J. 2002: Note on scaling of peak ground acceleration and peak ground velocity with magnitude. Geophysical Journal International 148, 336-339.

Edwards, A.W.F. 1992: Likelihood. Expanded edition ed. The Johns Hopkins University Press.

Ekström, G. & Dziewonski, A.M. 1988: Evidence of bias in estimations of earthquake size. Nature 332, 319-323.

Favreau, P.P. & Archuleta, R.J. 2002: Direct Seismic Energy Modeling and Application to the 1979 Imperial Valley Earthquake. EOS Trans. AGU 83/47. Fall Meet. Suppl. Abstr. S71E-07.

Guatteri, M., Mai, P.M., Beroza, G.C. & Boatwright, J. 2002: Strong ground motion prediction from stochastic-dynamic source models. Bull. Seism. Soc. Am., in press.

Hanks, T.C. & Kanamori, H. 1979: A moment magnitude scale. Journal of Geophysical Research 84/B5, 2348-2350.

Hanks, T.C. & Boore, D.M. 1984: Moment- magnitude relations in theory and practice. Journal of Geophysical Research 89/B7, 6229-6235.

Heaton, T., Tajima, F. & Wildenstein Mori, A. 1986: Estimating ground motions using recorded accelerograms. Surveys in Geophysics, 8, 25-83.

Herrero, A. & Bernard, P. 1994: A kinematic self-similar rupture process for earthquakes, BSSA, 84, 4, 1216-1228. Herrmann, R.B. (1985). An extension of random vibration theory estimates of strong ground motion to large distances. Bull. Seism. Soc. Am. 75/5, 1447-1453.

Kanamori, H. 1983: Magnitude scale and quantification of earthquakes. Tectonophysics 93, 185-199.

Kanamori, H. 2002: Are Large and Small Earthquakes Dynamically Different? EOS Trans. AGU 83/47, Fall Meet. Suppl. Abstr. S71E-02.

Mai, M. & Beroza, G.C. 2000: Source scaling properties from finite-fault-rupture models. Bull. Seism. Soc. Am. 90/3, 604-615.

Mai, P.M. & Beroza, G.C. 2002: A spatial random field model to characterize complexity in earthquake slip. Journal of Geophysical Research 107/B11, 2308, doi:2310.1029/ 2001JB000588.

Mai, P.M. & Beroza, G.C. 2002: A hybrid method for calculating near-source, broadband seismograms: Application to strong motion prediction. PAGEOPH, in press.

Main, I.G. & Burton, P.W. 1984: Information theory and the earthquake frequency-magnitude distribution. Bull. Seism. Soc. Am. 74/4, 1409-1426.

Malagnini, L., Herrmann, R.B. & Di, B.M. 2000: Ground-motion scaling in the Apennines (Italy). Bull. Seism. Soc. Am. 90/4, 1062-1081.

Mayeda, K. & Walter, W.R. 1996: Moment, energy, stress drop, and source spectra of western United States earthquakes from regional coda envelopes. Journal of Geophysical Research 101/B5, 11195-11208.

McGarr, A. & Fletcher, J.B. 2002: Observations that Constrain the Scaling of Apparent Stress. EOS Trans. AGU 83/47, Fall Meet. Suppl.. Abstr. S71E-11.

Mori, J. & Tanaka, H. 2002: Energy Budget of the 1999 Chichi, Taiwan Earthquake. EOS Trans. AGU 83/47, Fall Meet. Suppl. Abstr. S71E-09.

Nadeau, R.M. & Johnson, L.R. 2002: Energy Released by an Asperity Model of an Earthquake. EOS Trans. AGU 83/47, Fall Meet. Suppl. Abstr. S71E-12.

PEGASOS EG2-EXM-0024: Scherbaum, F.: Final model F. Scherbaum.

PEGASOS EG2-ES-0038: Scherbaum, F.: Assoc. EXM. EG2-EXM-0024 – Draft of final model F. Scherbaum.

PEGASOS TP2-TN-0269: Roth, Ph.: Note on the statistical analysis of the ratios between different definitions of the horizontal component.

PEGASOS TP2-TN-0270: Hölker, A. 2002: Note on the estimation of coefficients of ground motion models at missing frequencies.

PEGASOS TP2-TN-350: Lacave, C. 2003: Computation of scaling factors for three 'realistic' rock profiles.

PEGASOS TP2-TN-0363: Lacave, C., Koller, M. & Birkhäuser, Ph. 2003: Final report on the computation of scaling factors for 20 generic "rock" profiles.

Pitarka, A. 2002: Numerical Simulations for Evaluation of Median and Upper Limit Ground Motions in Switzerland (PEGASOS EXT-TN-0277).

Prejean, S.G. & Ellsworth, W.L. 2001: Observations of earthquake source parameters at 2 km depth in the Long Valley Caldera, Eastern California. Bull. Seism. Soc. Am. 91/2, 165-177.

Press, W.H., Teukolsky, S.A., Vetterling, W.T. & Flannery, B.P. 2001: Numerical Recipes in Fortran 77. The art of scientific computing. 2 ed.

Priolo, E. 2002: Estimation of the Ground Motion Upper Limit in Switzerland: EXWIM Numerical Simulations (PEGASOS EXT-TN-0278).

Restrepo-Velez, L.F., Bommer, J.J. & Sabetta, F. 2002: An exploration of the nature of the scatter in ground-motion prediction equations and the implications for seismic hazard assessment. Journal of Earthquake Engineering, 1-33.

Richardson, E. & Jordan, T.H. 2002: Apparent Stress Scaling Relations for Mining-Induced Seismicity. EOS Trans. AGU 83/47, Fall Meet. Suppl. Abstr. S71E-10.

Rietbrock, A. 2002: Determination of input parameters for the stochastic simulation of strong ground motion for Switzerland (PEGASOS EXT-TN-0306).

Romanowicz, B. & Rundle, J. 1993: On scaling relations for large earthquakes. Bull. Seism. Soc. Am. 83, 1294-1297.

Romanowicz, B. 1994: Comment on "A rappraisal of large earthquake scaling" by C. Scholz. Bull. Seism. Soc. Am. 84/5, 1675-1676.

Romanowicz, B. & Rundle, J. 1994: Reply to Comment on "On scaling relations for large earthquakes" by B. Romanowicz and J. Rundle, from the perspective of a recent nonlinear diffusion equation linking short-time deformation to long-time tectonics. Bull. Seism. Soc. Am. 84/5, 1684.

Sabetta, F. & Pugliese, A. 1996: Estimation of response spectra and simulation of nonstationary earthquake ground motion. Bull. Seism. Soc. Am. 86/2, 337-352.

Scherbaum, F., Schmedes, J. & Cotton, F. 2002: On the conversion of source-to-site distance measures for extended earthquake source models. Submitted to Bull. Seism. Soc. Am.

Scholz, C.H. 1994a: A rappraisal of large earthquake scaling. Bull. Seism. Soc. Am. 84/1, 215-218.

Scholz, C.H. 1994b: Reply to Comments on "A reappraisal of large earthquake scaling" by C. Scholz. Bull. Seism. Soc. Am. 84/5, 1677-1678.

Scholz, C.H. 1997: Size distributions for large and small earthquakes. Bull. Seism. Soc. Am. 87/4, 1074-1077.

Silva, W., Darragh, R.B. & Gregor, N. 1998: Reassessment of site coefficients and near-fault factors for building code provisions (PEGASOS EXT-RF-0394).

Somerville, P., Collins, N., Abrahamson, N.A., Graves, M.R. & Saikia, C. 2001: Ground motion attenuation relations for the central and eastern United States…..

Sornette, D. & Sornette, A. 1994: Comment on "On scaling relations for large earthquakes" by B. Romanowicz and J. Rundle, from the perspective of a recent nonlinear diffusion equation linking short-time deformation to long-time tectonics. Bull. Seism. Soc. Am. 84/5, 1679-1683.

Stock, C. & Smith, E.G.C. 2000: Evidence for different scaling of earthquake source parameters for large earthquakes depending on faulting mechanism. Geophysical Journal International 143/1, 157-162.

Walter, W.R., Mayeda, K. & Ruppert, S. 2002: Earthquake Apparent Stress Scaling. EOS Trans. AGU 83/47, Fall Meet. Suppl., Abstr. S71E-01.

APPENDIX 1: HORIZONTAL GROUND MOTION MODELS

File: AppendixA.txt

A 1-1 Abrahamson & Silva 1997

General remarks: POTENTIALOVERPREDICTION
According to the discussion in the paper, the model is biased to larger motions for 2 reasons: a) Since the usable bandwidth was evaluated separately for each record, larger ground motion will be more likely to be observed in the frequency range not equally covered (0.5 – 20 Hz). b) No distance cutoff for the first non-triggered instrument was used. Regarding swiss conditions, an additional potential bias towards overprediction comes from from the fact that only 1 normal faulting event is present in the data set. Therefore I rate the ground motion model as POTENTIALOVERPREDICTION.

Magnitude coverage: Range < 4.4: 4.4 - 5.: 5. - 7.: 7. - 7.4: > 7.4:
Quality: NA POOR GOOD POOR NA
Reasons: The total magnitude range is 4.4 – 7.4. Since only 6 events with M < 5 and 4 events with M > 7 are present in the dataset, I judge the range 5 – 7 as GOOD, the ranges 4.4 – 5.0 and 7 – 7.4 as POOR. The rest as NA.

Frequency coverage: Range [Hz]: < 0.2: 0.2 - 0.5: 0.5 - 20.: 20. - 30.: 30. - 100.: > 100:
Quality: NA FAIR GOOD FAIR POOR NA
Reasons: The total magnitude range is 4.4 – 7.4. Since only 6 events with M < 5 and 4 events with M > 7 are present in the dataset, I judge the range 5 – 7 as GOOD, the ranges 4.4 – 5.0 and 7 – 7.4 as POOR. The rest as NA.

Distance coverage: Range [km]: < 3: 3 - 150: > 150:
Quality: NA GOOD NA
Reasons: Judging from the figures 2 and 3, the distance range covered well is 3 – 150 km and was rated GOOD. The rest as NA.

A 1-2 Ambraseys & Douglas 2000

General remarks: NOOBJECTION
No obvious reason seen to reduce the rating of this model for Switzerland.

Magnitude coverage: Range: < 4.8: 4.8 - 5.8: 5.8 - 7.8: > 7.8
Quality: NA POOR GOOD NA
Reasons: More than 40 EQs in the magnitude range of 2 units is considered good coverage (GOOD). Fair agreement was found by the authors with the results of a study for spectral acceleration using smaller magnitude events [Ambraseys 1996 #3769, Ambraseys 1996 #3770]. For this reason, one magnitude unit below the actual magnitude range covered in this study was still considered useable, although with a rating of POOR. No data exist for magnitudes above M = 7.8 and therefore the model was assumed not applicable (NA) in this range.

Frequency coverage: Range [Hz]: < 0.2: 0.2 - 0.5: 0.5 - 10.: 10. - 25.: > 25
Quality: NA POOR GOOD POOR NA
Reasons: More than 40 EQs in the magnitude range of 2 units is considered good coverage (GOOD). Fair agreement was found by the authors with the results of a study for spectral acceleration using smaller magnitude events [Ambraseys 1996 #3769, Ambraseys 1996 #3770]. For this reason, one magnitude unit below the actual magnitude range covered in this study was still considered useable, although with a rating of POOR. No data exist for magnitudes above M = 7.8 and therefore the model was assumed not applicable (NA) in this range.

Distance coverage: Range [km]: < 0: 0 - 15: > 15:
Quality: NA GOOD NA
Reasons: The range < 15 km is covered well (fig. 4.7) and is considered reliable (GOOD). Since amplitude decay is treated only as large 'strain anelastic decay', the model is not considered extrapolateable beyond 15 km (NA).

A 1-3 Ambraseys et al. 1996

General remarks: NOOBJECTION
I don't see any obvious reason to reduce the rating of this model for Switzerland.

Magnitude coverage: Range: < 4.: 4. - 7.3: 7.3 - 7.9: > 7.9:
Quality: NA GOOD POOR NA
Reasons: The magnitude range covered by the data is 4.0 – 7.9 and the recommended magnitude range given is 4.0 – 7.5 (p. 375). However, since there is only 1 event with magnitude larger than 7.3, I judge the magnitude range 7.3 – 7.9 as POOR, the range from 4.0 – 7.3 as GOOD.

Frequency coverage: Range [Hz]: < 0.5: 0.5 - 10.: > 10.:
Quality: NA GOOD NA
Reasons: The magnitude range covered by the data is 4.0 – 7.9 and the recommended magnitude range given is 4.0 – 7.5 (p. 375). However, since there is only 1 event with magnitude larger than 7.3, I judge the magnitude range 7.3 – 7.9 as POOR, the range from 4.0 – 7.3 as GOOD.

Distance coverage: Range [km]: < 0: 0 - 100: 100 - 200: > 200:
Quality: NA GOOD POOR NA
Reasons: The total distance range covered by the data set is 0-260 km. Since only two events were recorded beyond 200 km, the distance range larger than 200 km was not considered useable at all and judged NA. This corresponds to the useable distance range as judged by the authors (p. 375). The majority of the data comes from distances between 0 and 100 km. Therefore, this was considered the distance range which could be judged as GOOD. The distance range between 100 and 150 km is covered only by 12 rock records and is therefore judged as POOR.

A 1-4 Atkinson & Boore 1997

General remarks: POTENTIALOVERPREDICTION-ENA
The faulting mechanism is not specified, but the regional faulting style is mostly thrust. Therefore, I assume this model to potentially overpredict Swiss conditions (POTENTIALOVERPREDICTION-ENA)

Magnitude coverage: Range: < 4.: 4. - 5.5: 5.5 - 7.25: > 7.25:
Quality: NA POOR GOOD NA
Reasons: The total magnitude range as stated by the authors is 4 – 7.25 (p. 26). The approximate attenuation relation was obtained from the simulation by fitting with a simple quadratic equation. This, however, grossly overpredicts ground motion for small-tomoderate events at distances greater 30 km. Therefore, I rank the magnitude range below M = 5.5 as POOR.

Frequency coverage: Range [Hz]: < 0.5: 0.5 - 20.: > 20:
Quality: NA GOOD NA
Reasons: The total magnitude range as stated by the authors is 4 – 7.25 (p. 26). The approximate attenuation relation was obtained from the simulation by fitting with a simple quadratic equation. This, however, grossly overpredicts ground motion for small-tomoderate events at distances greater 30 km. Therefore I rank the magnitude range below M = 5.5 as POOR.

Distance coverage: Range [km]: < 10: 10 - 500: > 500:
Quality: NA GOOD NA
Reasons: Distance range as stated by the authors (p. 26). I didn't see a reason to downrate it.

A 1-5 Rietbrock 2002

General remarks: SMALLMAGNITUDEDOMINANCE
The dataset is dominated by small events observed mostly at large distances. As a consequence, the observed spectrum is dominated by the attenuation and site filters. E.g. for a magnitude 3 event, differences in stress drop between 10 and 30 bars don't show up in the accessible distance and spectral range. I mark this issue by the label SMALLMAGNITUDEDOMINANCE.

Magnitude coverage: Range: < 2.: 2. - 3.: 3. - 5.: 5. - 6.5: > 6.5:
Quality: NA FAIR GOOD POOR NA
Reasons: The magnitude range of the complete dataset covers 2.0 ≤ Ml ≤ 5.2 (1.8 ≤ Mw ≤ 5.0 according to the ETH conversion formula). The data analysis was performed only on events with Mw > 3.0, which makes up roughly 20 % of the complete data set. Since it was not included in the calculation of the model, the magnitude range between 2.0 – 3.0 is consequently considered less reliable, although still useable (FAIR). Ground motion predictions are made for larger magnitudes than covered by the data (Mw = 5.0 largest event in dataset). I have strong doubts, that the source parameters determined in this study for the small events are reliable estimators of source parameters for larger events. Therefore, the range 5.0 – 6.5 is rated as POOR.

Frequency coverage: Range [Hz]: < 0.5: 0.5 - 1.: 1. - 15.: 15. - 20.: > 20:
Quality: NA POOR GOOD POOR NA
Reasons: The magnitude range of the complete dataset covers 2.0 ≤ Ml ≤ 5.2 (1.8 ≤ Mw ≤ 5.0 according to the ETH conversion formula). The data analysis was performed only on events with Mw > 3.0, which makes up roughly 20 % of the complete data set. Since it was not included in the calculation of the model, the magnitude range between 2.0 – 3.0 is consequently considered less reliable, although still useable (FAIR). Ground motion predictions are made for larger magnitudes than covered by the data (Mw = 5.0 largest event in dataset). I have strong doubts, that the source parameters determined in this study for the small events are reliable estimators of source parameters for larger events. Therefore, the range 5.0 – 6.5 is rated as POOR.

Distance coverage: Range [km]: < 10: 10 - 40: 40 - 180: 180 - 300: > 300:
Quality: NA POOR GOOD POOR NA
Reasons: Roughly 75 % of the data were recorded in the distance range from 40 – 180 km (p. 14 of [Bay 2002 #3756]) Therefore, this is considered the most reliable distance range and rated GOOD. An additonal reason to downweight the closer distance range is that for events with Mw > 2.7 (Ml > 2.9) most records are clipped at close distances (p. 15 of [Bay 2002 #3756]).

A 1-6 Bay 2002

General remarks: SMALLMAGNITUDEDOMINANCE
The dataset is dominated by small events observed mostly at large distances. As a consequence, the observed spectrum is dominated by the attenuation and site filters. E.g. for a magnitude 3 event, differences in stress drop between 10 and 30 bars don't show up in the accessible distance and spectral range. I mark this issue by the label SMALLMAGNITUDEDOMINANCE.

Magnitude coverage: Range: < 2.: 2. - 3.: 3. - 5.: 5. - 6.5: > 6.5:
Quality: NA FAIR GOOD POOR NA
Reasons: The magnitude range of the complete dataset covers 2.0 ≤ Ml ≤ 5.2 (1.8 ≤ Mw ≤ 5.0 according to the ETH conversion formula). The data analysis was performed only on events with Mw > 3.0, which makes up roughly 20 % of the complete data set. Since it was not included in the calculation of the model, the magnitude range between 2.0 – 3.0 is consequently considered less reliable, although still useable (FAIR). Ground motion predictions are made for larger magnitudes than covered by the data (Mw = 5.0 largest event in dataset). I have strong

doubts, that the source parameters determined in this study for the small events are reliable estimators of source parameters for larger events. Therefore, the range 5.0 – 6.5 is rated as POOR.

Frequency coverage: Range [Hz]: < 0.5: 0.5 - 1.: 1. - 15.: 15. - 20.: > 20:
Quality: NA POOR GOOD POOR NA
Reasons: The magnitude range of the complete dataset covers 2.0 ≤ Ml ≤ 5.2 (1.8 ≤ Mw ≤ 5.0 according to the ETH conversion formula). The data analysis was performed only on events with Mw > 3.0, which makes up roughly 20 % of the complete data set. Since it was not included in the calculation of the model, the magnitude range between 2.0 – 3.0 is consequently considered less reliable, although still useable (FAIR). Ground motion predictions are made for larger magnitudes than covered by the data (Mw = 5.0 largest event in dataset). I have strong doubts, that the source parameters determined in this study for the small events are reliable estimators of source parameters for larger events. Therefore, the range 5.0 – 6.5 is rated as POOR.

Distance coverage: Range [km]: < 10: 10 - 40: 40 - 180: 180 - 300: > 300:
Quality: NA POOR GOOD POOR NA
Reasons: Roughly 75 % of the data were recorded in the distance range from 40 – 180 km (p. 14 of [Bay 2002 #3756]) Therefore, this is considered the most reliable distance range and rated GOOD. An additonal reason to downweight the closer distance range is that for events with Mw > 2.7 (Ml > 2.9) most records are clipped at close distances (p. 15 of [Bay 2002 #3756]).

A 1-7 Berge-Thierry et al. 2000

General remarks: NOOBJECTION
No obvious reason to downrate the model was seen.

Magnitude coverage: Range: < 4.: 4. - 7.3: > 7.3:
Quality: NA GOOD NA
Reasons: The magnitude distribution in the data set is reported as 4 – 7.3 (p. 4 of paper). This defines the overall useable range which was rated as GOOD.

Frequency coverage: Range [Hz]: < 0.1: 0.1 - 0.25: 0.25 - 25.: 25. - 34.: > 34:
Quality: NA POOR GOOD POOR NA
Reasons: The magnitude distribution in the data set is reported as 4 – 7.3 (p. 4 of paper). This defines the overall useable range which was rated as GOOD.

Distance coverage: Range [km]: < 5: 5 - 15: 15 - 100: > 100:
Quality: NA POOR GOOD NA
Reasons: The validity range as stated by the authors (p. 7 of paper) is 5 – 100 km. However, since no near field saturation term is included, there is a tendency to overprediction at very close distances (< 10 – 15 km) → Therefore, below 10 km the distances were rated as POOR.

A 1-8 Boore et al. 1997

General remarks: NOOBJECTION
No obvious reason seen to give lower rating.

Magnitude coverage: Range: < 5.5: 5.5 - 6.: 6. - 7.5: > 7.5:
Quality: NA POOR GOOD NA
Reasons: The valid magnitude range as stated by the authors is 5.5 – 7.5 (p. 148). However, since events with magnitude < 6 are poorly represented in the data set (p. 150), the corresponding range is rated POOR, the range 6 – 7.5 as GOOD.

Frequency coverage: Range [Hz]: < 0.5: 0.5 - 10.: > 10:
Quality: NA GOOD NA

Reasons: The valid magnitude range as stated by the authors is 5.5 – 7.5 (p. 148). However, since events with magnitude < 6 are poorly represented in the data set (p. 150), the corresponding range is rated POOR, the range 6 – 7.5 as GOOD.

Distance coverage: Range [km]: < 1: 1 - 80: > 80:
Quality: NA GOOD NA
Reasons: As stated by the authors (p. 148). No reason seen to give lower rating.

A 1-9 Campbell & Bozorgnia 2002

General remarks: NOOBJECTION
No obvious reason seen to rate lower.

Magnitude coverage: Range: < 4.7: 4.7 - 5.: 5. - 7.7: > 7.7:
Quality: NA POOR GOOD NA
Reasons: The data cover a range between 4.7 – 7.7. Since the recommended range by the authors is > 5, I judge the range 4.7 – 5.0 as
POOR, the range 5.0-7.7 as GOOD:

Frequency coverage: Range [Hz]: < 0.25: 0.25 - 20.: > 20:
Quality: NA GOOD NA
Reasons: The data cover a range between 4.7 – 7.7. Since the recommended range by the authors is > 5, I judge the range 4.7 – 5.0 as POOR, the range 5.0 – 7.7 as GOOD:

Distance coverage: Range [km]: < 3: 3 - 60: 60 - 100: > 100:
Quality: NA GOOD POOR NA
Reasons: The recommended distance range by the authors is < 60 km. Since 3 km was the smallest distance in the figures, the range 3 – 60 km is rated GOOD. Since the authors assume that the relation can be extrapolated to 100 km (p. 19), I include this range into the valid range, but rate it as POOR.

A 1-10 Lussou et al. 2001

General remarks: POTENTIALREGIONANDSITEMISMATCH
The site classification in this study is completely based on borehole investigations from Japan. This generates a potential mismatch with respect to the other models.

Magnitude coverage: Range: < 3.5: 3.5 - 3.7: 3.7 - 6.3: > 6.3:
Quality: NA POOR GOOD NA
Reasons: The validity range stated by the authors is 3.5 – 6.3. The lowest magnitude in the data set is 3.7 (fig. 1). The range above this value is covered well and therefore judged as GOOD. The range 3.5 – 3.7 is judged as POOR since no data are present in this range but it is still recommended as useable by the authors.

Frequency coverage: Range [Hz]: < 0.1: 0.1 - 50.: > 50:
Quality: NA GOOD NA
Reasons: The validity range stated by the authors is 3.5 – 6.3. The lowest magnitude in the data set is 3.7 (fig. 1). The range above this value is covered well and therefore judged as GOOD. The range 3.5 – 3.7 is judged as POOR since no data are present in this range but it is still recommended as useable by the authors.

Distance coverage: Range [km]: < 10: 10 - 200: > 200:
Quality: NA GOOD NA
Reasons: The total distance range (10 – 200 km) as recommended by the authors (p. 18) was judged as GOOD.

A 1-11 Sabetta & Pugliese 1996

General remarks: POTENTIALREGIONMISMATCH
Due to the small number of events (17) just from Italy with its potentially different stress regime, I define the label POTENTIALREGIONMISMATCH to rate the applicability to Switzerland.

Magnitude coverage: Range: < 4.6: 4.6 - 6.8: > 6.8:
Quality: NA GOOD NA
Reasons: Judging from fig. 1, the magnitude coverage seems to be good for the complete recommended range 4.6 – 6.8 (GOOD).

Frequency coverage: Range [Hz]: < 0.25: 0.25 - 25.: > 25:
Quality: NA GOOD NA
Reasons: Judging from fig. 1, the magnitude coverage seems to be good for the complete recommended range 4.6 – 6.8 (GOOD).

Distance coverage: Range [km]: < 0: 0 - 10: 10 - 100: > 100:
Quality: NA POOR GOOD NA
Reasons: The overall recommended distance range is 0 – 100 km (p. 338). For distances less than 10 km, however, the results should be very sensitive to the actual source depth distribution because of the small number of events (17). Therefore, I judged the distance range up to 10 km as POOR, 10 – 100 km as GOOD.

A 1-12 Somerville et al. 2001

General remarks: POTENTIALOVERPREDICTION-ENA
events are purely reverse type mechanisms, I judge the applicability to Switzerland as POTENTIALOVERPREDICTIONENA. Since the calibration

Magnitude coverage: Range: < 6.: 6. - 7.5: > 7.5:
Quality: NA GOOD NA
Reasons: Since the models are based on synthetic seismograms, the full range for which they are developed (6 < Mw ≤ 7.5) is rated GOOD.

Frequency coverage: Range [Hz]: < 0.25: 0.25 - 100.: > 100:
Quality: NA GOOD NA
Reasons: Since the models are based on synthetic seismograms, the full range for which they are developed (6 < Mw ≤ 7.5) is rated GOOD.

Distance coverage: Range [km]: < 1: 1 - 500: > 500:
Quality: NA GOOD NA
Reasons: Since the models are based on synthetic seismograms, the full range for which they are developed (0 - 500 km) is rated GOOD.

A 1-13 SEA 99

General remarks: POTENTIALROCKVSMISMATCH
as POTENTIALROCKVSMISMATCH. For rock sites, SEA99 overestimates the data from which it was created on the average by 20 %. The reason as discussed on p. 1164-1165 is that the difference between rock and soil motion was forced to match the difference between rock and soil motion in (Boore et al. 1997). The fit is better for soil data. The authors conclude (p. 1164/65) that their assumption of vs-rock = 620 m/s for the average rock in their data set might be too low. Therefore, I judge the applicability for Swiss rock sites

Magnitude coverage: Range: < 5.: 5. - 6.5: 6.5 - 7.: > 7.:
Quality: NA GOOD POOR NA

Reasons: The recommended range of applicability is 5.0 < Mw < 7.7 (p. 1162). The authors report a magnitude dependence of the SEA99 residuals. The magnitude coefficients were used from a different, larger data set by (Boore et al. 1997). SEA99 underpredicts observed motions at large magnitudes more than at small ones (fig. 6) and the magnitude dependence is stronger for rock. This is interpreted by the authors (p. 1165/66) as sampling problem since all M > 6.7 records are from Irpinia. Vice versa, at high frequencies, the magnitude dependence is strongly affected by few high residuals at small magnitudes. As a consequence, I judged the M range for rock sites above 6.5 as POOR. Furthermore, since there are no rock records in the data set with magnitudes larger than 7, I limit the range of applicability to M = 7.

Frequency coverage: Range [Hz]: < 0.5: 0.5 - 10.: > 10:
Quality: NA GOOD NA
Reasons: The recommended range of applicability is 5.0 < Mw < 7.7 (p. 1162). The authors report a magnitude dependence of the SEA99 residuals. The magnitude coefficients were used from a different, larger data set by (Boore et al. 1997). SEA99 underpredicts observed motions at large magnitudes more than at small ones (fig. 6) and the magnitude dependence is stronger for rock. This is interpreted by the authors (p. 1165/66) as sampling problem since all M > 6.7 records are from Irpinia. Vice versa, at high frequencies, the magnitude dependence is strongly affected by few high residuals at small magnitudes. As a consequence, I judged the M range for rock sites above 6.5 as POOR. Furthermore, since there are no rock records in the data set with magnitudes larger than 7, I limit the range of applicability to M = 7.

Distance coverage: Range [km]: < 0: 0 - 10: 10 - 100: > 100:
Quality: NA POOR GOOD NA
Reasons: The recommended range of applicability is < 100 km (p. 1162). Since rock sites are only well represented above 10 km (fig. 2), the range 10 – 100 km is rated as GOOD, the range 0 – 10 km as POOR.

A 1-14 Toro et al. 1997

General remarks: POTENTIALOVERPREDICTION-ENA
Point source model may lead to overprediction at sites near large ruptures (roughly less than 2 × rupture size). Together with the fact that the predominant faulting type in ENA is reverse faulting, this let's me judge the applicability to Switzerland as POTENTIALOVERPREDICTION-ENA.

Magnitude coverage: Range: < 5: 5. - 8.: > 8.:
Quality: NA GOOD NA
Reasons: I didn't see a reason to reduce weighting for any particular magnitude band. Therefore, I rate the whole range 5.0 < Mw < 8.0 as GOOD.

Frequency coverage: Range [Hz]: < 1.: 1. - 35.: > 35:
Quality: NA GOOD NA
Reasons: I didn't see a reason to reduce weighting for any particular magnitude band. Therefore, I rate the whole range 5.0 < Mw < 8.0 as GOOD.

Distance coverage: Range [km]: < 1: 1 - 100: 100 - 500: > 500:
Quality: NA GOOD FAIR NA
Reasons: The range of validity as stated by the authors is 1-500 km (emphasis on 1 – 100 km). Therefore, I rated the range 1 – 100 km as GOOD, the range 100 – 500 km as FAIR.

APPENDIX 2: VERTICAL GROUND MOTION MODELS

(partially identical with Appendix A where the same GMMs are concerned)
File: AppendixB.txt

A 2-1 Abrahamson & Silva 1997

General remarks: POTENTIALOVERPREDICTION
According to the discussion in the paper, the model is biased to larger motions for 2 reasons: a) Since the usable bandwidth was evaluated separately for each record, larger ground motion will be more likely to be observed in the frequency range not equally covered (0.5 – 20 Hz). b) No distance cutoff for the first non-triggered instrument was used. Regarding swiss conditions, an additional potential bias towards overprediction comes from from the fact that only 1 normal faulting event is present in the data set. Therefore I rate the ground motion model as POTENTIALOVERPREDICTION.

Magnitude coverage: Range: < 4.4: 4.4 - 5.: 5. - 7.: 7. - 7.4: > 7.4:
Quality: NA POOR GOOD POOR NA
Reasons: The total magnitude range is 4.4 – 7.4. Since only 6 events with M < 5 and 4 events with M > 7 are present in the dataset, I judge the range 5 – 7 as GOOD, the ranges 4.4 – 5.0 and 7 – 7.4 as POOR. The rest as NA.

Frequency coverage: Range [Hz]: < 0.2: 0.2 - 0.5: 0.5 - 20.: 20. - 30.: 30. - 100.: > 100:
Quality: NA FAIR GOOD FAIR POOR NA
Reasons: The total magnitude range is 4.4 – 7.4. Since only 6 events with M < 5 and 4 events with M > 7 are present in the dataset, I judge the range 5 – 7 as GOOD, the ranges 4.4 – 5.0 and 7 – 7.4 as POOR. The rest as NA.

Distance coverage: Range [km]: < 3: 3 - 150: > 150:
Quality: NA GOOD NA
Reasons: Judging from the figures 2 and 3, the distance range covered well is 3 – 150 km and was rated GOOD. The rest as NA.

A 2-2 Ambraseys & Douglas 2000

General remarks: NOOBJECTION
No obvious reason seen to reduce the rating of this model for Switzerland.

Magnitude coverage: Range: < 4.8: 4.8 - 5.8: 5.8 - 7.8: > 7.8:
Quality: NA POOR GOOD NA
Reasons: More than 40 EQs in the magnitude range of 2 units is considered good coverage (GOOD). Fair agreement was found by the authors with the results of a study for spectral acceleration using smaller magnitude events [Ambraseys 1996 #3769, Ambraseys 1996 #3770]. For this reason, one magnitude unit below the actual magnitude range covered in this study was still considered useable, although with a rating of POOR. No data exist for magnitudes above M = 7.8 and therefore the model was assumed not applicable (NA) in this range.

Frequency coverage: Range [Hz]: < 0.2: 0.2 - 0.5: 0.5 - 10.: 10. - 25.: > 25:
Quality: NA POOR GOOD POOR NA
Reasons: More than 40 EQs in the magnitude range of 2 units is considered good coverage (GOOD). Fair agreement was found by the authors with the results of a study for spectral acceleration using smaller magnitude events [Ambraseys 1996 #3769, Ambraseys 1996 #3770]. For this reason, one magnitude unit below the actual magnitude range covered in this study was

still considered useable, although with a rating of POOR. No data exist for magnitudes above M = 7.8 and therefore the model was assumed not applicable (NA)in this range.

Distance coverage: Range [km]: < 0: 0 - 15: > 15:
Quality: NA GOOD NA
Reasons: The range < 15 km is covered well (fig. 4.7) and is considered reliable (GOOD). Since amplitude decay is treated only as large 'strain anelastic decay', the model is not considered extrapolateable beyond 15 km (NA).

A 2-3 Ambraseys & Simpson 1996

General remarks: NOOBJECTION
No obvious reason seen to reduce the rating of this model for Switzerland.

Magnitude coverage: Range: < 4.: 4. - 7.3: 7.3 - 7.9: > 7.9:
Quality: NA GOOD POOR NA
Reasons: This study uses the same dataset as the companion paper [Ambraseys 1996 #3769]. Therefore, the same discussion applies. The magnitude range covered by the data is 4.0 – 7.9 and the recommended magnitude range given is 4.0 – 7.5 (p. 375 in [Ambraseys 1996 #3769]). However, since there is only 1 event with magnitude larger than 7.3, I judge the magnitude range 7.3 – 7.9 as POOR, the range from 4.0 – 7.3 as GOOD.

Frequency coverage: Range [Hz]: < 0.5: 0.5 - 10.: > 10.:
Quality: NA GOOD NA
Reasons: This study uses the same dataset as the companion paper [Ambraseys 1996 #3769]. Therefore, the same discussion applies. The magnitude range covered by the data is 4.0 – 7.9 and the recommended magnitude range given is 4.0 – 7.5 (p. 375 in [Ambraseys 1996 #3769]). However, since there is only 1 event with magnitude larger than 7.3, I judge the magnitude range 7.3 – 7.9 as POOR, the range from 4.0 – 7.3 as GOOD.

Distance coverage: Range [km]: < 0: 0 - 100: 100 - 200: > 200:
Quality: NA GOOD POOR NA
Reasons: The total distance range covered by the data set is 0 – 260 km. Since only two events were recorded beyond 200 km, the distance range larger than 200 km was not considered useable at all and judged NA. This corresponds to the useable distance range as judged by the authors (p. 375 in [Ambraseys 1996 #3769]). The majority of the data comes from distances between 0 and 100 km. Therefore, this was considered the distance range which could be judged as GOOD. The distance range between 100 and 150 km is covered only by 12 rock records and is therefore judged as POOR.

A 2-4 Rietbrock 2002

General remarks: SMALLMAGNITUDEDOMINANCE
The dataset is dominated by small events observed mostly at large distances. As a consequence, the observed spectrum is dominated by the attenuation and site filters. E.g. for a magnitude 3 event, differences in stress drop between 10 and 30 bars don't show up in the accessible distance and spectral range. I mark this issue by the label
SMALLMAGNITUDEDOMINANCE.

Magnitude coverage: Range: < 2.: 2. - 3.: 3. - 5.: 5. - 6.5: > 6.5:
Quality: NA FAIR GOOD POOR NA
Reasons: The magnitude range of the complete dataset covers $2.0 \leq Ml \leq 5.2$ ($1.8 \leq Mw \leq 5.0$ according to the ETH conversion formula). The data analysis was performed only on events with $Mw > 3.0$, which makes up roughly 20 % of the complete data set. Since it was not included in the calculation of the model, the magnitude range between 2.0 – 3.0 is consequently considered less reliable, although still useable (FAIR). Ground motion predictions are made for

larger magnitudes than covered by the data (Mw = 5.0 largest event in dataset). I have strong doubts, that the source parameters determined in this study for the small events are reliable estimators of source parameters for larger events. Therefore, the range 5.0 – 6.5 is rated as POOR.

Frequency coverage: Range [Hz]: < 0.5: 0.5 - 1.: 1. - 15.: 15. - 20.: > 20:
Quality: NA POOR GOOD POOR NA
Reasons: The magnitude range of the complete dataset covers 2.0 ≤ Ml ≤ 5.2 (1.8 ≤ Mw ≤ 5.0 according to the ETH conversion formula). The data analysis was performed only on events with Mw > 3.0, which makes up roughly 20 % of the complete data set. Since it was not included in the calculation of the model, the magnitude range between 2.0 – 3.0 is consequently considered less reliable, although still useable (FAIR). Ground motion predictions are made for larger magnitudes than covered by the data (Mw = 5.0 largest event in dataset). I have strong doubts, that the source parameters determined in this study for the small events are reliable estimators of source parameters for larger events. Therefore, the range 5.0 – 6.5 is rated as POOR.

Distance coverage
Range [km]: < 10: 10 - 40: 40 - 180: 180 - 300: > 300:
Quality: NA POOR GOOD POOR NA
Reasons:
Roughly 75 % of the data were recorded in the distance range from 40 – 180 km (p. 14 of [Bay 2002 #3756]) Therefore, this is considered the most reliable distance range and rated GOOD. An additional reason to downweight the closer distance range is that for events with Mw > 2.7 (Ml > 2.9) most records are clipped at close distances (p. 15 of [Bay 2002 #3756]).

A 2-5 Bay 2002

General remarks: SMALLMAGNITUDEDOMINANCE
The dataset is dominated by small events observed mostly at large distances. As a consequence, the observed spectrum is dominated by the attenuation and site filters. E.g. for a magnitude 3 event, differences in stress drop between 10 and 30 bars don't show up in the accessible distance and spectral range. I mark this issue by the label
SMALLMAGNITUDEDOMINANCE.

Magnitude coverage: Range: < 2.: 2. - 3.: 3. - 5.: 5. - 6.5: > 6.5:
Quality: NA FAIR GOOD POOR NA
Reasons: The magnitude range of the complete dataset covers 2.0 ≤ Ml ≤ 5.2 (1.8 ≤ Mw ≤ 5.0 according to the ETH conversion formula). The data analysis was performed only on events with Mw > 3.0, which makes up roughly 20 % of the complete data set. Since it was not included in the calculation of the model, the magnitude range between 2.0 – 3.0 is consequently considered less reliable, although still useable (FAIR). Ground motion predictions are made for larger magnitudes than covered by the data (Mw = 5.0 largest event in dataset). I have strong doubts, that the source parameters determined in this study for the small events are reliable estimators of source parameters for larger events. Therefore, the range 5.0 – 6.5 is rated as POOR.

Frequency coverage: Range [Hz]: < 0.5: 0.5 - 1.: 1. - 15.: 15. - 20.: > 20:
Quality: NA POOR GOOD POOR NA
Reasons: The magnitude range of the complete dataset covers 2.0 ≤ Ml ≤ 5.2 (1.8 ≤ Mw ≤ 5.0 according to the ETH conversion formula). The data analysis was performed only on events with Mw > 3.0, which makes up roughly 20 % of the complete data set. Since it was not included in the calculation of the model, the magnitude range between 2.0 – 3.0 is consequently considered less reliable, although still useable (FAIR). Ground motion predictions are made for larger magnitudes than covered by the data (Mw = 5.0 largest event in dataset). I have strong doubts, that the source parameters determined in this study for the small events are reliable

estimators of source parameters for larger events. Therefore, the range 5.0 – 6.5 is rated as POOR.

Distance coverage: Range [km]: < 10: 10 - 40: 40 - 180: 180 - 300: > 300:
Quality: NA POOR GOOD POOR NA
Reasons: Roughly 75 % of the data were recorded in the distance range from 40 – 180 km (p. 14 of [Bay 2002 #3756]) Therefore, this is considered the most reliable distance range and rated GOOD. An additonal reason to downweight the closer distance range is that for events with Mw > 2.7 (Ml > 2.9) most records are clipped at close distances (p. 15 of [Bay 2002 #3756]).

A 2-6 Berge-Thierry et al. 2000

General remarks: NOOBJECTION
No obvious reason to downrate the model was seen.

Magnitude coverage: Range: < 4.: 4. - 7.3: > 7.3:
Quality: NA GOOD NA
Reasons: The magnitude distribution in the data set is reported as 4 – 7.3 (p. 4 of paper). This defines the overall useable range which was rated as GOOD.

Frequency coverage: Range [Hz]: < 0.1: 0.1 - 0.25: 0.25 - 25.: 25. - 34.: > 34:
Quality: NA POOR GOOD POOR NA
Reasons: The magnitude distribution in the data set is reported as 4 – 7.3 (p. 4 of paper). This defines the overall useable range which was rated as GOOD.

Distance coverage: Range [km]: < 5: 5 - 15: 15 - 100: > 100:
Quality: NA POOR GOOD NA
Reasons:The validity range as stated by the authors (p. 7 of paper) is 5 – 100 km. However, since no near field saturation term is included, there is a tendency to overprediction at very close distances (< 10 – 15 km) → Therefore, below 10 km the distances were rated as POOR.

A 2-7 Campbell & Bozorgnia 2002

General remarks: NOOBJECTION
No obvious reason seen to rate lower.

Magnitude coverage: Range: < 4.7: 4.7 - 5.: 5. - 7.7: > 7.7:
Quality: NA POOR GOOD NA
Reasons: The data cover a range between 4.7 – 7.7. Since the recommended range by the authors is > 5, I judge the range 4.7 – 5.0 as POOR, the range 5.0 – 7.7 as GOOD:

Frequency coverage: Range [Hz]: < 0.25: 0.25 - 20.: > 20:
Quality: NA GOOD NA
Reasons: The data cover a range between 4.7 – 7.7. Since the recommended range by the authors is > 5, I judge the range 4.7 – 5.0 as POOR, the range 5.0 – 7.7 as GOOD:

Distance coverage: Range [km]: < 3: 3 - 60: 60 - 100: > 100:
Quality: NA GOOD POOR NA
Reasons: The recommended distance range by the authors is < 60 km. Since 3 km was the smallest distance in the figures, the range 3 – 60 km is rated GOOD. Since the authors assume that the relation can be extrapolated to 100 km (p. 19), I include this range into the valid range, but rate it as POOR.

A 2-8 Lussou et al. 2001

General remarks: POTENTIALREGIONANDSITEMISMATCH
The site classification in this study is completely based on borehole investigations from Japan. This generates a potential mismatch with respect to the other models.

Magnitude coverage: Range: < 3.5: 3.5 - 3.7: 3.7 - 6.3: > 6.3:
Quality: NA POOR GOOD NA
Reasons: The validity range stated by the authors is 3.5 – 6.3. The lowest magnitude in the data set is 3.7 (fig. 1). The range above this value is covered well and therefore judged as GOOD. The range 3.5 – 3.7 is judged as POOR since no data are present in this range but it is still recommended as useable by the authors.

Frequency coverage: Range [Hz]: < 0.1: 0.1 - 50.: > 50:
Quality: NA GOOD NA
Reasons: The validity range stated by the authors is 3.5 – 6.3. The lowest magnitude in the data set is 3.7 (fig. 1). The range above this value is covered well and therefore judged as GOOD. The range 3.5 – 3.7 is judged as POOR since no data are present in this range but it is still recommended as useable by the authors.

Distance coverage: Range [km]: < 10: 10 - 200: > 200:
Quality: NA GOOD NA
Reasons: The total distance range (10 – 200 km) as recommended by the authors (p. 18) was judged as GOOD.

A 2-9 Sabetta & Pugliese 1996

General remarks: POTENTIALREGIONMISMATCH
Due to the small number of events (17) just from Italy with its potentially different stress regime, I define the label POTENTIALREGIONMISMATCH to rate the applicability to Switzerland.

Magnitude coverage: Range: < 4.6: 4.6 - 6.8: > 6.8:
Quality: NA GOOD NA
Reasons: Judging from fig. 1, the magnitude coverage seems to be good for the complete recommended range 4.6 – 6.8 (GOOD).

Frequency coverage: Range [Hz]: < 0.25: 0.25 - 25.: > 25:
Quality: NA GOOD NA
Reasons: Judging from fig. 1, the magnitude coverage seems to be good for the complete recommended range 4.6 - 6.8 (GOOD).

Distance coverage: Range [km]: < 0: 0 - 10: 10 - 100: > 100:
Quality: NA POOR GOOD NA
Reasons: The overall recommended distance range is 0 – 100 km (p. 338). For distances less than 10 km, however, the results should be very sensitive to the actual source depth distribution because of the small number of events (17). Therefore, I judged the distance range up to 10 km as POOR, 10 – 100 km as GOOD.

A 2-10 Somerville et al. 2001

General remarks: POTENTIALOVERPREDICTION-ENA
events are purely reverse type mechanisms, I judge the applicability to Switzerland as POTENTIALOVERPREDICTIONENA. Since the calibration

Magnitude coverage: Range: < 6.: 6. - 7.5: > 7.5:
Quality: NA GOOD NA

Reasons: Since the models are based on synthetic seismograms, the full range for which they are developed ($6 < Mw \leq 7.5$) is rated GOOD.

Frequency coverage: Range [Hz]: < 0.25: 0.25 - 100.: > 100:
Quality: NA GOOD NA
Reasons: Since the models are based on synthetic seismograms, the full range for which they are developed ($6 < Mw \leq 7.5$) is rated GOOD.

Distance coverage: Range [km]: < 1: 1 - 500: > 500:
Quality: NA GOOD NA
Reasons: Since the models are based on synthetic seismograms, the full range for which they are developed (0 – 500 km) is rated GOOD.

APPENDIX 3: LOGIC TREE FOR HORIZONTAL COMPONENT GROUND MOTION MODELS

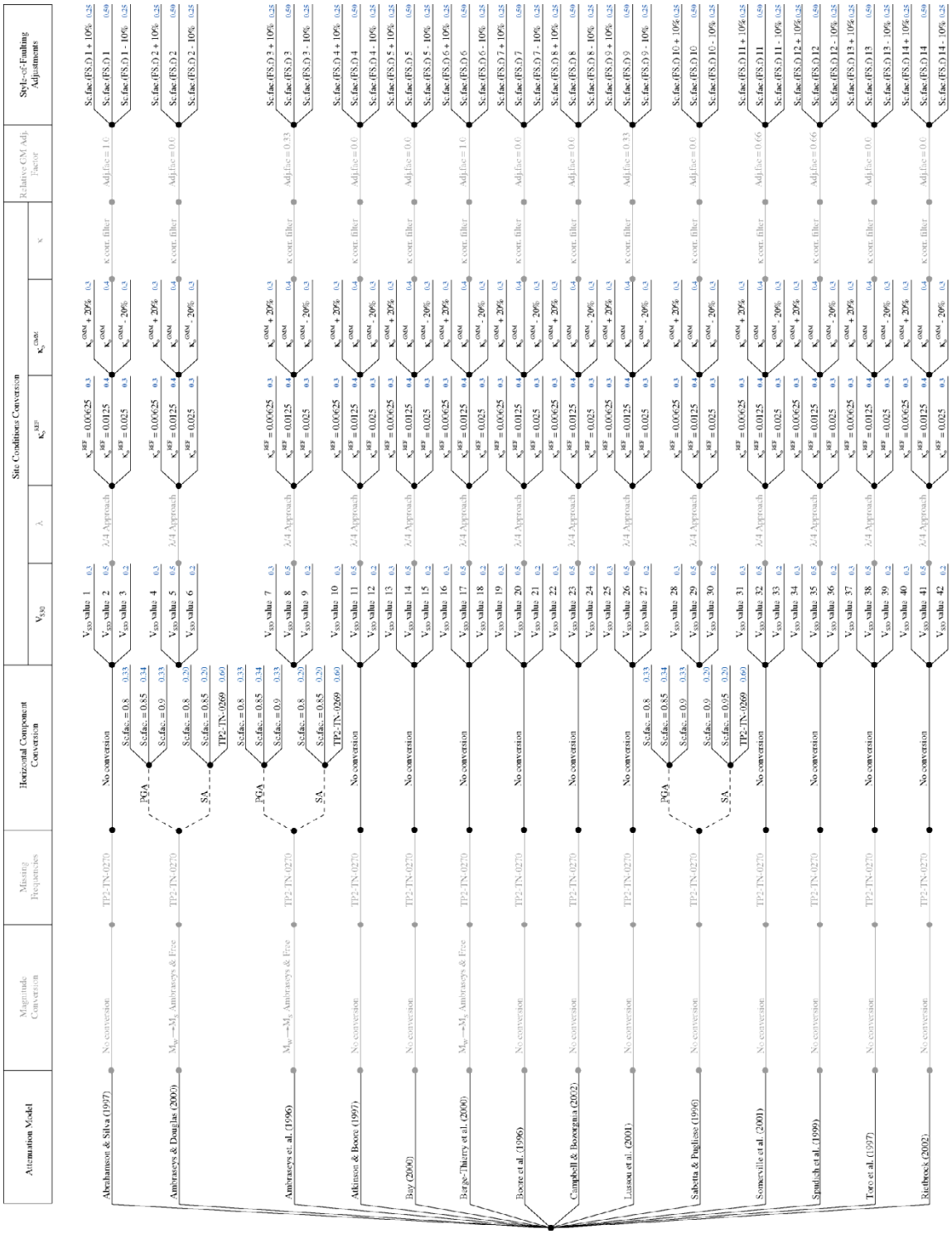

APPENDIX 4: LOGIC TREE FOR VERTICAL COMPONENT GROUND MOTION MODELS (V/H RATIO)

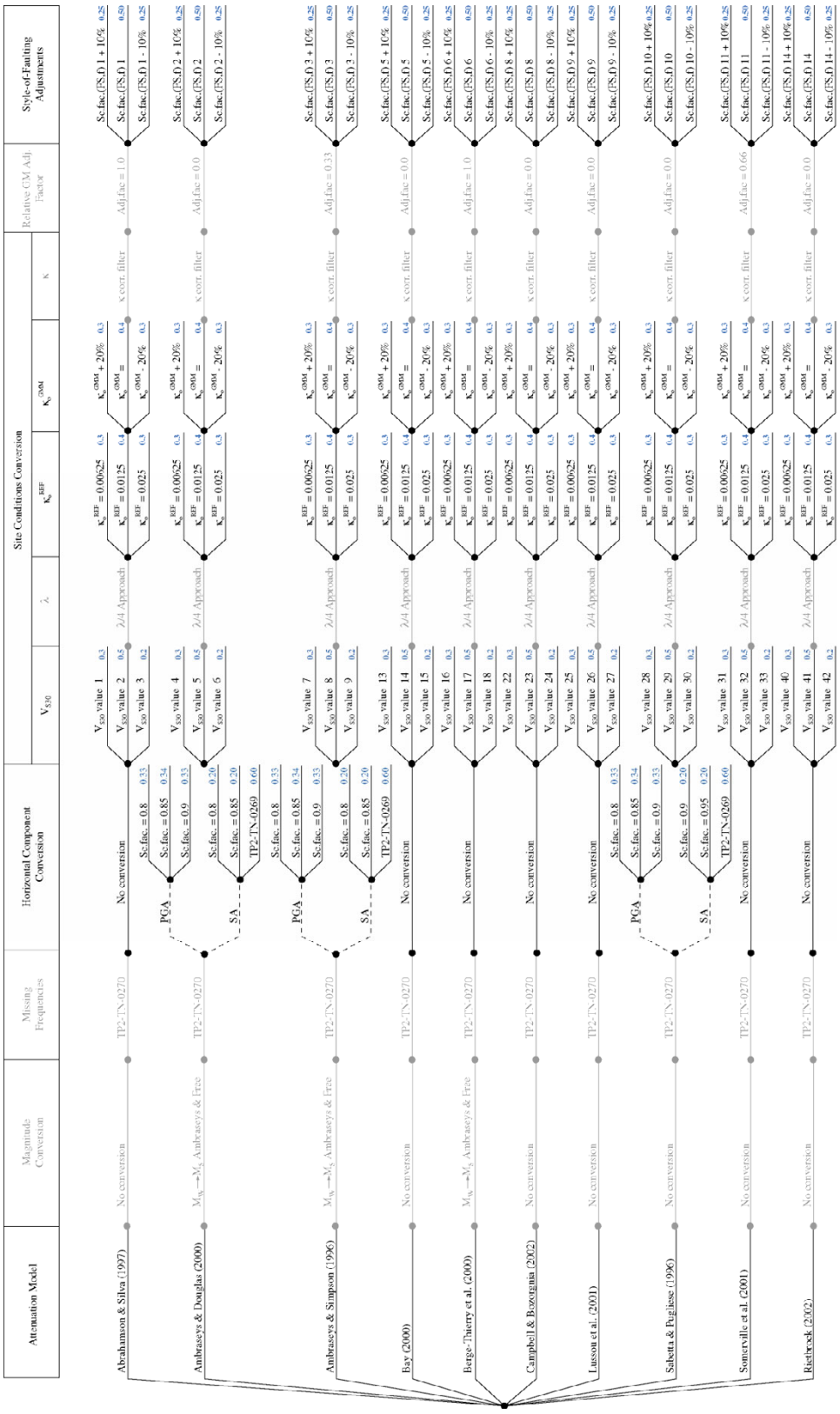

APPENDIX 5: LOGIC TREE FOR THE ALEATORY UNCERTAINTY

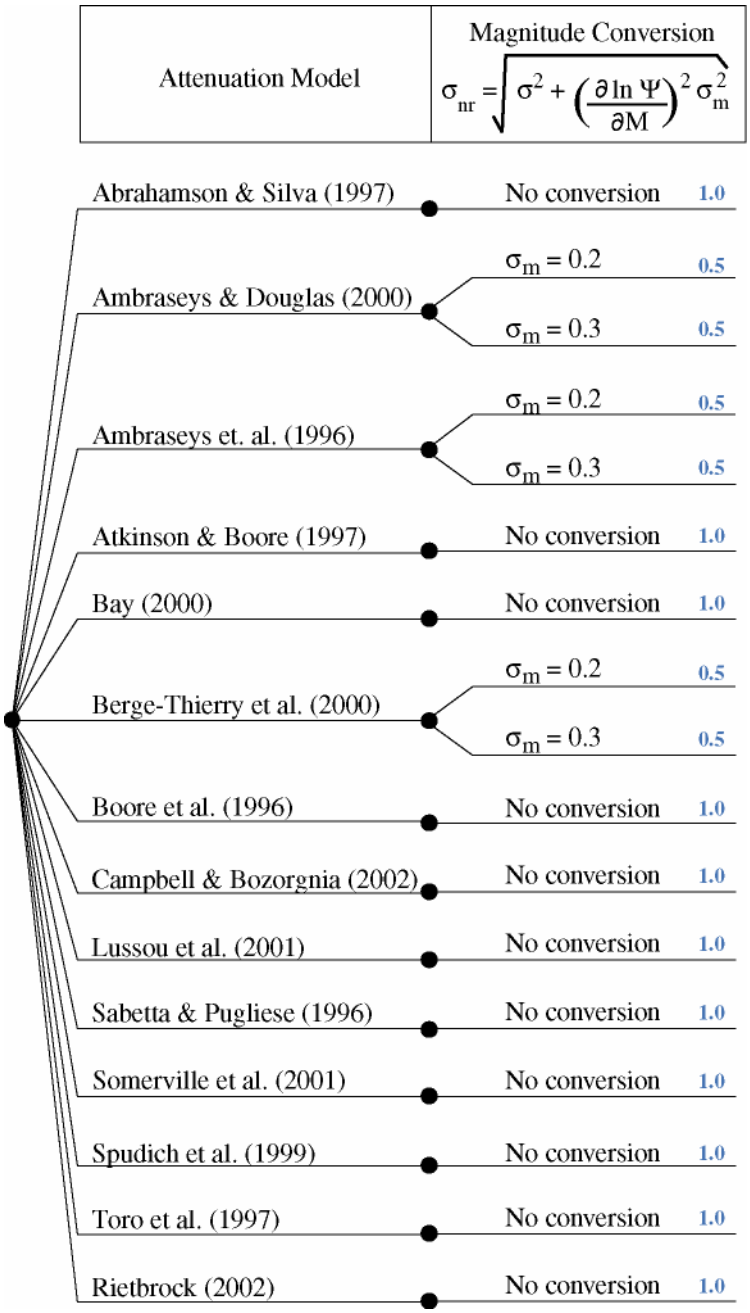

APPENDIX 6: PRIOR WEIGHTING FACTORS FOR HORIZONTAL COMPONENT GMMs

File: priorwfH.txt

	M: 5-6 R: 0-15 km	M: 5-6 R: 15-50 km	M: 5-6 R: 50-70 km	M: 5-6 R: 70-100 km	M: 5-6 R: 100-200 km	M: 6-7 R: 0-15 km	M: 6-7 R: 15-50 km	M: 6-7 R: 50-70 km	M: 6-7 R: 70-100 km	M: 6-7 R: 100-200 km	M: 7-7.5 R: 0-15 km	M: 7-7.5 R: 15-50 km	M: 7-7.5 R: 50-70 km	M: 7-7.5 R: 70-100 km	M: 7-7.5 R: 100-200 km
F: 0.5 Hz															
Abrahamson & Silva 1997	0.169	0.13	0.136	0.145	0.202	0.126	0.12	0.126	0.141	0.167	0.047	0.055	0.06	0.074	0.073
Ambraseys & Douglas 2003	0.082	0	0	0	0	0.133	0	0	0	0	0.188	0	0	0	0
Ambraseys et al. 1996	0.144	0.089	0.093	0.099	0.091	0.107	0.082	0.086	0.096	0.075	0.112	0.104	0.113	0.139	0.091
Atkinson & Boore 1997	0.032	0.059	0.062	0.066	0.184	0.036	0.082	0.086	0.096	0.229	0.025	0.071	0.077	0.095	0.189
Bay 2002	0.002	0.005	0.01	0.011	0.026	0.001	0.002	0.005	0.005	0.011	0	0	0	0	0
Rietbrock 2002	0.002	0.005	0.01	0.011	0.026	0.001	0.002	0.005	0.005	0.011	0	0	0	0	0
Berge-Thierry et al. 2000	0.054	0.152	0.158	0.169	0	0.04	0.14	0.146	0.164	0	0.034	0.145	0.158	0.195	0
Boore et al. 1997	0.022	0.015	0.015	0.005	0	0.1	0.082	0.086	0.032	0	0.142	0.142	0.154	0.063	0
Campbell & Bozorgnia 2002	0.197	0.152	0.105	0.056	0	0.147	0.14	0.097	0.054	0	0.208	0.242	0.175	0.107	0
Lussou et al. 2001	0.081	0.152	0.158	0.169	0.471	0.018	0.042	0.044	0.049	0.117	0	0	0	0	0
Sabetta & Pugliese 1996	0.136	0.152	0.158	0.169	0	0.081	0.112	0.117	0.131	0	0	0	0	0	0
Somerville et al. 2001	0	0	0	0	0	0.171	0.14	0.146	0.164	0.39	0.243	0.242	0.263	0.325	0.646
SEA 99	0.079	0.089	0.093	0.099	0	0.039	0.054	0.057	0.064	0	0	0	0	0	0
Toro et al. 1997	0	0	0	0	0	0	0	0	0	0	0	0	0	0	0
F: 1. Hz															
Abrahamson & Silva 1997	0.141	0.115	0.117	0.123	0.152	0.107	0.106	0.108	0.121	0.134	0.039	0.046	0.049	0.061	0.058
Ambraseys & Douglas 2003	0.082	0	0	0	0	0.133	0	0	0	0	0.183	0	0	0	0
Ambraseys et al. 1996	0.176	0.115	0.117	0.123	0.1	0.133	0.106	0.108	0.121	0.089	0.134	0.129	0.137	0.168	0.107
Atkinson & Boore 1997	0.039	0.077	0.078	0.082	0.202	0.044	0.106	0.108	0.121	0.269	0.03	0.088	0.094	0.115	0.221
Bay 2002	0.005	0.014	0.028	0.029	0.063	0.002	0.007	0.013	0.014	0.028	0	0	0	0	0
Rietbrock 2002	0.005	0.014	0.028	0.029	0.063	0.002	0.007	0.013	0.014	0.028	0	0	0	0	0
Berge-Thierry et al. 2000	0.039	0.115	0.117	0.123	0	0.029	0.106	0.108	0.121	0	0.024	0.106	0.112	0.138	0
Boore et al. 1997	0.027	0.019	0.019	0.007	0	0.124	0.106	0.108	0.04	0	0.171	0.176	0.187	0.077	0
Campbell & Bozorgnia 2002	0.141	0.115	0.078	0.041	0	0.107	0.106	0.072	0.04	0	0.147	0.176	0.124	0.076	0
Lussou et al. 2001	0.058	0.115	0.117	0.123	0.303	0.013	0.032	0.032	0.036	0.08	0	0	0	0	0
Sabetta & Pugliese 1996	0.097	0.115	0.117	0.123	0	0.059	0.084	0.086	0.097	0	0	0	0	0	0
Somerville et al. 2001	0	0	0	0	0	0.124	0.106	0.108	0.121	0.269	0.171	0.176	0.187	0.23	0.443
SEA 99	0.097	0.115	0.117	0.123	0	0.049	0.07	0.072	0.08	0	0	0	0	0	0
Toro et al. 1997	0.096	0.068	0.068	0.072	0.117	0.073	0.062	0.063	0.071	0.104	0.1	0.103	0.109	0.135	0.171
F: 2.5 Hz															
Abrahamson & Silva 1997	0.131	0.109	0.109	0.115	0.134	0.101	0.101	0.102	0.114	0.122	0.036	0.043	0.046	0.056	0.052
Ambraseys & Douglas 2003	0.076	0	0	0	0	0.127	0	0	0	0	0.171	0	0	0	0
Ambraseys et al. 1996	0.164	0.109	0.109	0.115	0.089	0.127	0.101	0.103	0.114	0.081	0.125	0.12	0.127	0.154	0.095
Atkinson & Boore 1997	0.036	0.073	0.073	0.076	0.179	0.042	0.101	0.103	0.114	0.246	0.028	0.082	0.087	0.105	0.197
Bay 2002	0.006	0.019	0.036	0.038	0.077	0.002	0.009	0.017	0.019	0.035	0	0	0	0	0
Rietbrock 2002	0.006	0.019	0.036	0.038	0.077	0.002	0.009	0.017	0.019	0.035	0	0	0	0	0
Berge-Thierry et al. 2000	0.036	0.109	0.109	0.115	0	0.028	0.101	0.103	0.114	0	0.023	0.098	0.104	0.126	0
Boore et al. 1997	0.025	0.018	0.018	0.006	0	0.118	0.101	0.103	0.038	0	0.16	0.164	0.174	0.07	0
Campbell & Bozorgnia 2002	0.131	0.109	0.073	0.038	0	0.101	0.101	0.068	0.038	0	0.137	0.164	0.115	0.069	0
Lussou et al. 2001	0.054	0.109	0.109	0.115	0.268	0.013	0.03	0.031	0.034	0.073	0	0	0	0	0
Sabetta & Pugliese 1996	0.09	0.109	0.109	0.115	0	0.056	0.08	0.082	0.091	0	0	0	0	0	0
Somerville et al. 2001	0	0	0	0	0	0.118	0.101	0.103	0.114	0.246	0.16	0.164	0.174	0.21	0.395
SEA 99	0.09	0.109	0.109	0.115	0	0.046	0.067	0.068	0.076	0	0	0	0	0	0
Toro et al. 1997	0.153	0.109	0.109	0.115	0.177	0.118	0.101	0.103	0.114	0.162	0.16	0.164	0.174	0.21	0.261
F: 5. Hz															
Abrahamson & Silva 1997	0.131	0.109	0.109	0.115	0.134	0.101	0.101	0.102	0.114	0.122	0.036	0.043	0.046	0.056	0.052
Ambraseys & Douglas 2003	0.076	0	0	0	0	0.127	0	0	0	0	0.171	0	0	0	0
Ambraseys et al. 1996	0.164	0.109	0.109	0.115	0.089	0.127	0.101	0.103	0.114	0.081	0.125	0.12	0.127	0.154	0.095
Atkinson & Boore 1997	0.036	0.073	0.073	0.076	0.179	0.042	0.101	0.103	0.114	0.246	0.028	0.082	0.087	0.105	0.197
Bay 2002	0.006	0.019	0.036	0.038	0.077	0.002	0.009	0.017	0.019	0.035	0	0	0	0	0
Rietbrock 2002	0.006	0.019	0.036	0.038	0.077	0.002	0.009	0.017	0.019	0.035	0	0	0	0	0
Berge-Thierry et al. 2000	0.036	0.109	0.109	0.115	0	0.028	0.101	0.103	0.114	0	0.023	0.098	0.104	0.126	0
Boore et al. 1997	0.025	0.018	0.018	0.006	0	0.118	0.101	0.103	0.038	0	0.16	0.164	0.174	0.07	0
Campbell & Bozorgnia 2002	0.131	0.109	0.073	0.038	0	0.101	0.101	0.068	0.038	0	0.137	0.164	0.115	0.069	0
Lussou et al. 2001	0.054	0.109	0.109	0.115	0.268	0.013	0.03	0.031	0.034	0.073	0	0	0	0	0
Sabetta & Pugliese 1996	0.09	0.109	0.109	0.115	0	0.056	0.08	0.082	0.091	0	0	0	0	0	0
Somerville et al. 2001	0	0	0	0	0	0.118	0.101	0.103	0.114	0.246	0.16	0.164	0.174	0.21	0.395
SEA 99	0.09	0.109	0.109	0.115	0	0.046	0.067	0.068	0.076	0	0	0	0	0	0
Toro et al. 1997	0.153	0.109	0.109	0.115	0.177	0.118	0.101	0.103	0.114	0.162	0.16	0.164	0.174	0.21	0.261
F: 10. Hz															
Abrahamson & Silva 1997	0.163	0.126	0.127	0.133	0.141	0.13	0.119	0.122	0.132	0.129	0.047	0.052	0.056	0.064	0.055
Ambraseys & Douglas 2003	0.057	0	0	0	0	0.099	0	0	0	0	0.136	0	0	0	0
Ambraseys et al. 1996	0.084	0.052	0.053	0.055	0.039	0.067	0.05	0.051	0.055	0.035	0.068	0.06	0.064	0.073	0.042
Atkinson & Boore 1997	0.045	0.084	0.084	0.089	0.188	0.054	0.119	0.122	0.132	0.258	0.037	0.098	0.105	0.121	0.209
Bay 2002	0.007	0.022	0.042	0.044	0.081	0.003	0.01	0.02	0.022	0.037	0	0	0	0	0
Rietbrock 2002	0.007	0.022	0.042	0.044	0.081	0.003	0.01	0.02	0.022	0.037	0	0	0	0	0
Berge-Thierry et al. 2000	0.045	0.126	0.127	0.133	0	0.036	0.119	0.122	0.132	0	0.029	0.118	0.126	0.145	0
Boore et al. 1997	0.013	0.009	0.009	0.003	0	0.063	0.05	0.051	0.018	0	0.087	0.082	0.087	0.033	0
Campbell & Bozorgnia 2002	0.163	0.126	0.084	0.044	0	0.13	0.119	0.081	0.043	0	0.179	0.197	0.14	0.08	0
Lussou et al. 2001	0.067	0.126	0.127	0.133	0.283	0.016	0.036	0.036	0.039	0.077	0	0	0	0	0
Sabetta & Pugliese 1996	0.112	0.126	0.127	0.133	0	0.072	0.095	0.097	0.105	0	0	0	0	0	0
Somerville et al. 2001	0	0	0	0	0	0.152	0.119	0.122	0.132	0.258	0.208	0.197	0.211	0.242	0.418

	M: 5-6 R: 0-15 km	M: 5-6 R: 15-50 km	M: 5-6 R: 50-70 km	M: 5-6 R: 70-100 km	M: 5-6 R: 100-200 km	M: 6-7 R: 0-15 km	M: 6-7 R: 15-50 km	M: 6-7 R: 50-70 km	M: 6-7 R: 70-100 km	M: 6-7 R: 100-200 km	M: 7-7.5 R: 0-15 km	M: 7-7.5 R: 15-50 km	M: 7-7.5 R: 50-70 km	M: 7-7.5 R: 70-100 km	M: 7-7.5 R: 100-200 km
F: 20. Hz															
Abrahamson & Silva 1997	0.209	0.155	0.158	0.162	0.164	0.166	0.148	0.151	0.155	0.141	0.06	0.063	0.066	0.069	0.054
Ambraseys & Douglas 2003	0.038	0	0	0	0	0.066	0	0	0	0	0.09	0	0	0	0
Ambraseys et al. 1996	0	0	0	0	0	0	0	0	0	0	0	0	0	0	0
Atkinson & Boore 1997	0.03	0.053	0.054	0.056	0.113	0.036	0.077	0.078	0.08	0.147	0.025	0.062	0.065	0.068	0.105
Bay 2002	0.002	0.006	0.012	0.012	0.021	0.001	0.003	0.006	0.006	0.009	0	0	0	0	0
Rietbrock 2002	0.002	0.006	0.012	0.012	0.021	0.001	0.003	0.006	0.006	0.009	0	0	0	0	0
Berge-Thierry et al. 2000	0.06	0.163	0.166	0.171	0	0.048	0.156	0.159	0.163	0	0.04	0.152	0.158	0.165	0
Boore et al. 1997	0	0	0	0	0	0	0	0	0	0	0	0	0	0	0
Campbell & Bozorgnia 2002	0.108	0.08	0.054	0.028	0	0.086	0.077	0.052	0.026	0	0.119	0.124	0.086	0.045	0
Lussou et al. 2001	0.108	0.194	0.197	0.202	0.41	0.026	0.055	0.056	0.058	0.106	0	0	0	0	0
Sabetta & Pugliese 1996	0.138	0.148	0.151	0.155	0	0.088	0.113	0.115	0.119	0	0	0	0	0	0
Somerville et al. 2001	0	0	0	0	0	0.242	0.185	0.188	0.194	0.354	0.333	0.299	0.312	0.327	0.507
SEA 99	0	0	0	0	0	0	0	0	0	0	0	0	0	0	0
Toro et al. 1997	0.304	0.194	0.197	0.202	0.271	0.242	0.185	0.188	0.194	0.234	0.333	0.299	0.312	0.327	0.334
F: 33. Hz															
Abrahamson & Silva 1997	0.276	0.193	0.193	0.193	0.137	0.175	0.171	0.171	0.171	0.115	0.058	0.065	0.065	0.065	0.04
Ambraseys & Douglas 2003	0.009	0	0	0	0	0.012	0	0	0	0	0.015	0	0	0	0
Ambraseys et al. 1996	0	0	0	0	0	0	0	0	0	0	0	0	0	0	0
Atkinson & Boore 1997	0	0	0	0	0	0	0	0	0	0	0	0	0	0	0
Bay 2002	0	0	0	0	0	0	0	0	0	0	0	0	0	0	0
Rietbrock 2002	0	0	0	0	0	0	0	0	0	0	0	0	0	0	0
Berge-Thierry et al. 2000	0.035	0.09	0.09	0.09	0	0.023	0.08	0.08	0.08	0	0.017	0.069	0.069	0.069	0
Boore et al. 1997	0	0	0	0	0	0	0	0	0	0	0	0	0	0	0
Campbell & Bozorgnia 2002	0	0	0	0	0	0	0	0	0	0	0	0	0	0	0
Lussou et al. 2001	0.269	0.456	0.456	0.456	0.649	0.051	0.121	0.121	0.121	0.162	0	0	0	0	0
Sabetta & Pugliese 1996	0.032	0.032	0.032	0.032	0	0.016	0.023	0.023	0.023	0	0	0	0	0	0
Somerville et al. 2001	0.001	0	0	0	0	0.482	0.404	0.404	0.404	0.544	0.607	0.578	0.578	0.578	0.722
SEA 99	0	0	0	0	0	0	0	0	0	0	0	0	0	0	0
Toro et al. 1997	0.378	0.228	0.228	0.228	0.214	0.241	0.201	0.201	0.201	0.179	0.303	0.288	0.288	0.288	0.238
F: 50. Hz															
Abrahamson & Silva 1997	0.656	0.443	0.443	0.443	0.284	0.213	0.227	0.227	0.227	0.128	0.07	0.08	0.08	0.08	0.042
Ambraseys & Douglas 2003	0	0	0	0	0	0	0	0	0	0	0	0	0	0	0
Ambraseys et al. 1996	0	0	0	0	0	0	0	0	0	0	0	0	0	0	0
Atkinson & Boore 1997	0	0	0	0	0	0	0	0	0	0	0	0	0	0	0
Bay 2002	0	0	0	0	0	0	0	0	0	0	0	0	0	0	0
Rietbrock 2002	0	0	0	0	0	0	0	0	0	0	0	0	0	0	0
Berge-Thierry et al. 2000	0	0	0	0	0	0	0	0	0	0	0	0	0	0	0
Boore et al. 1997	0	0	0	0	0	0	0	0	0	0	0	0	0	0	0
Campbell & Bozorgnia 2002	0	0	0	0	0	0	0	0	0	0	0	0	0	0	0
Lussou et al. 2001	0.342	0.557	0.557	0.557	0.715	0.033	0.085	0.085	0.085	0.096	0	0	0	0	0
Sabetta & Pugliese 1996	0	0	0	0	0	0	0	0	0	0	0	0	0	0	0
Somerville et al. 2001	0.002	0.001	0.001	0.001	0.001	0.753	0.688	0.688	0.688	0.776	0.93	0.92	0.92	0.92	0.958
SEA 99	0	0	0	0	0	0	0	0	0	0	0	0	0	0	0
Toro et al. 1997	0	0	0	0	0	0	0	0	0	0	0	0	0	0	0

APPENDIX 7: PRIOR WEIGHTING FACTORS FOR THE PGA OF THE HORIZONTAL COMPONENT GMMs

File: priorwfH_PGA.txt

	M: 5-6 R: 0-15 km	M: 5-6 R: 15-50 km	M: 5-6 R: 50-70 km	M: 5-6 R: 70-100 km	M: 5-6 R: 100-200 km	M: 6-7 R: 0-15 km	M: 6-7 R: 15-50 km	M: 6-7 R: 50-70 km	M: 6-7 R: 70-100 km	M: 6-7 R: 100-200 km	M: 7-7.5 R: 0-15 km	M: 7-7.5 R: 15-50 km	M: 7-7.5 R: 50-70 km	M: 7-7.5 R: 70-100 km	M: 7-7.5 R: 100-200 km
PGA															
Abrahamson & Silva 1997	0.131	0.109	0.109	0.115	0.134	0.101	0.101	0.102	0.114	0.122	0.036	0.043	0.046	0.056	0.052
Ambraseys & Douglas 2003	0.076	0	0	0	0	0.127	0	0	0	0	0.171	0	0	0	0
Ambraseys et al. 1996	0.164	0.109	0.109	0.115	0.089	0.127	0.101	0.103	0.114	0.081	0.125	0.12	0.127	0.154	0.095
Atkinson & Boore 1997	0.036	0.073	0.073	0.076	0.179	0.042	0.101	0.103	0.114	0.246	0.028	0.082	0.087	0.105	0.197
Bay 2002	0.006	0.019	0.036	0.038	0.077	0.002	0.009	0.017	0.019	0.035	0	0	0	0	0
Rietbrock 2002	0.006	0.019	0.036	0.038	0.077	0.002	0.009	0.017	0.019	0.035	0	0	0	0	0
Berge-Thierry et al. 2000	0.036	0.109	0.109	0.115	0	0.028	0.101	0.103	0.114	0	0.023	0.098	0.104	0.126	0
Boore et al. 1997	0.025	0.018	0.018	0.006	0	0.118	0.101	0.103	0.038	0	0.16	0.164	0.174	0.07	0
Campbell & Bozorgnia 2002	0.131	0.109	0.073	0.038	0	0.101	0.101	0.068	0.038	0	0.137	0.164	0.115	0.069	0
Lussou et al. 2001	0.054	0.109	0.109	0.115	0.268	0.013	0.03	0.031	0.034	0.073	0	0	0	0	0
Sabetta & Pugliese 1996	0.09	0.109	0.109	0.115	0	0.056	0.08	0.082	0.091	0	0	0	0	0	0
Somerville et al. 2001	0	0	0	0	0	0.118	0.101	0.103	0.114	0.246	0.16	0.164	0.174	0.21	0.395
SEA 99	0.09	0.109	0.109	0.115	0	0.046	0.067	0.068	0.076	0	0	0	0	0	0
Toro et al. 1997	0.153	0.109	0.109	0.115	0.177	0.118	0.101	0.103	0.114	0.162	0.16	0.164	0.174	0.21	0.261

APPENDIX 8: PRIOR WEIGHTING FACTORS FOR VERTICAL COMPONENT GMMs

File: priorwfV.txt

	M: 5-6 R: 0-15 km	M: 5-6 R: 15-50 km	M: 5-6 R: 50-70 km	M: 5-6 R: 70-100 km	M: 5-6 R: 100-200 km	M: 6-7 R: 0-15 km	M: 6-7 R: 15-50 km	M: 6-7 R: 50-70 km	M: 6-7 R: 70-100 km	M: 6-7 R: 100-200 km	M: 7-7.5 R: 0-15 km	M: 7-7.5 R: 15-50 km	M: 7-7.5 R: 50-70 km	M: 7-7.5 R: 70-100 km	M: 7-7.5 R: 100-200 km
F: 0.5 Hz															
Abrahamson & Silva 1997	0.196	0.158	0.168	0.18	0.264	0.153	0.155	0.165	0.176	0.223	0.057	0.07	0.078	0.088	0.09
Ambraseys & Douglas 2003	0.096	0	0	0	0	0.161	0	0	0	0	0.226	0	0	0	0
Ambraseys & Simpson 1996	0.167	0.108	0.115	0.123	0.119	0.13	0.106	0.112	0.12	0.101	0.134	0.132	0.147	0.166	0.113
Berge-Thierry et al. 2000	0.063	0.184	0.196	0.209	0	0.049	0.18	0.192	0.205	0	0.041	0.184	0.205	0.232	0
Campbell & Bozorgnia 2002	0.228	0.184	0.13	0.069	0	0.178	0.18	0.128	0.068	0	0.25	0.307	0.228	0.128	0
Lussou et al. 2001	0.094	0.184	0.196	0.209	0.616	0.022	0.054	0.057	0.061	0.156	0	0	0	0	0
Sabetta & Pugliese 1996	0.157	0.184	0.196	0.209	0	0.098	0.144	0.153	0.164	0	0	0	0	0	0
Somerville et al. 2001	0	0	0	0	0	0.208	0.18	0.192	0.205	0.521	0.292	0.307	0.342	0.387	0.797
F: 1. Hz															
Abrahamson & Silva 1997	0.192	0.167	0.177	0.188	0.273	0.151	0.164	0.173	0.184	0.234	0.056	0.073	0.081	0.09	0.096
Ambraseys & Douglas 2003	0.111	0	0	0	0	0.189	0	0	0	0	0.263	0	0	0	0
Ambraseys & Simpson 1996	0.24	0.167	0.177	0.188	0.18	0.189	0.164	0.174	0.184	0.155	0.192	0.204	0.224	0.25	0.176
Berge-Thierry et al. 2000	0.053	0.167	0.177	0.188	0	0.042	0.164	0.174	0.184	0	0.035	0.167	0.184	0.205	0
Campbell & Bozorgnia 2002	0.192	0.167	0.117	0.062	0	0.151	0.164	0.115	0.061	0	0.21	0.278	0.204	0.113	0
Lussou et al. 2001	0.08	0.167	0.177	0.188	0.546	0.019	0.049	0.052	0.055	0.14	0	0	0	0	0
Sabetta & Pugliese 1996	0.132	0.167	0.177	0.188	0	0.083	0.131	0.139	0.147	0	0	0	0	0	0
Somerville et al. 2001	0	0	0	0	0	0.176	0.164	0.174	0.184	0.47	0.245	0.278	0.307	0.342	0.728
F: 2.5 Hz															
Abrahamson & Silva 1997	0.192	0.167	0.177	0.188	0.273	0.151	0.164	0.173	0.184	0.234	0.056	0.073	0.081	0.09	0.096
Ambraseys & Douglas 2003	0.111	0	0	0	0	0.189	0	0	0	0	0.263	0	0	0	0
Ambraseys & Simpson 1996	0.24	0.167	0.177	0.188	0.18	0.189	0.164	0.174	0.184	0.155	0.192	0.204	0.224	0.25	0.176
Berge-Thierry et al. 2000	0.053	0.167	0.177	0.188	0	0.042	0.164	0.174	0.184	0	0.035	0.167	0.184	0.205	0
Campbell & Bozorgnia 2002	0.192	0.167	0.117	0.062	0	0.151	0.164	0.115	0.061	0	0.21	0.278	0.204	0.113	0
Lussou et al. 2001	0.08	0.167	0.177	0.188	0.546	0.019	0.049	0.052	0.055	0.14	0	0	0	0	0
Sabetta & Pugliese 1996	0.132	0.167	0.177	0.188	0	0.083	0.131	0.139	0.147	0	0	0	0	0	0
Somerville et al. 2001	0	0	0	0	0	0.176	0.164	0.174	0.184	0.47	0.245	0.278	0.307	0.342	0.728
F: 5. Hz															
Abrahamson & Silva 1997	0.192	0.167	0.177	0.188	0.273	0.151	0.164	0.173	0.184	0.234	0.056	0.073	0.081	0.09	0.096
Ambraseys & Douglas 2003	0.111	0	0	0	0	0.189	0	0	0	0	0.263	0	0	0	0
Ambraseys & Simpson 1996	0.24	0.167	0.177	0.188	0.18	0.189	0.164	0.174	0.184	0.155	0.192	0.204	0.224	0.25	0.176
Berge-Thierry et al. 2000	0.053	0.167	0.177	0.188	0	0.042	0.164	0.174	0.184	0	0.035	0.167	0.184	0.205	0
Campbell & Bozorgnia 2002	0.192	0.167	0.117	0.062	0	0.151	0.164	0.115	0.061	0	0.21	0.278	0.204	0.113	0
Lussou et al. 2001	0.08	0.167	0.177	0.188	0.546	0.019	0.049	0.052	0.055	0.14	0	0	0	0	0
Sabetta & Pugliese 1996	0.132	0.167	0.177	0.188	0	0.083	0.131	0.139	0.147	0	0	0	0	0	0
Somerville et al. 2001	0	0	0	0	0	0.176	0.164	0.174	0.184	0.47	0.245	0.278	0.307	0.342	0.728
F: 10. Hz															
Abrahamson & Silva 1997	0.235	0.185	0.197	0.211	0.305	0.185	0.181	0.193	0.206	0.258	0.071	0.083	0.093	0.106	0.107
Ambraseys & Douglas 2003	0.083	0	0	0	0	0.141	0	0	0	0	0.203	0	0	0	0
Ambraseys & Simpson 1996	0.122	0.077	0.082	0.087	0.084	0.096	0.075	0.08	0.086	0.071	0.102	0.096	0.107	0.122	0.081
Berge-Thierry et al. 2000	0.065	0.185	0.197	0.211	0	0.051	0.181	0.193	0.206	0	0.044	0.189	0.212	0.24	0
Campbell & Bozorgnia 2002	0.235	0.185	0.131	0.07	0	0.185	0.181	0.128	0.068	0	0.268	0.316	0.235	0.132	0
Lussou et al. 2001	0.097	0.185	0.197	0.211	0.611	0.023	0.054	0.058	0.062	0.154	0	0	0	0	0
Sabetta & Pugliese 1996	0.162	0.185	0.197	0.211	0	0.102	0.145	0.154	0.165	0	0	0	0	0	0
Somerville et al. 2001	0	0	0	0	0	0.216	0.181	0.193	0.207	0.517	0.312	0.316	0.353	0.4	0.812
F: 20. Hz															
Abrahamson & Silva 1997	0.316	0.209	0.217	0.226	0.286	0.23	0.202	0.209	0.217	0.235	0.094	0.099	0.106	0.114	0.096
Ambraseys & Douglas 2003	0.058	0	0	0	0	0.091	0	0	0	0	0.141	0	0	0	0
Ambraseys & Simpson 1996	0	0	0	0	0	0	0	0	0	0	0	0	0	0	0
Berge-Thierry et al. 2000	0.091	0.22	0.229	0.238	0	0.067	0.212	0.22	0.228	0	0.062	0.237	0.254	0.273	0
Campbell & Bozorgnia 2002	0.163	0.108	0.075	0.039	0	0.119	0.104	0.072	0.037	0	0.185	0.195	0.138	0.074	0
Lussou et al. 2001	0.163	0.261	0.271	0.282	0.714	0.036	0.075	0.078	0.081	0.176	0	0	0	0	0
Sabetta & Pugliese 1996	0.208	0.2	0.208	0.216	0	0.122	0.154	0.16	0.166	0	0	0	0	0	0
Somerville et al. 2001	0	0	0	0	0	0.335	0.252	0.261	0.271	0.589	0.519	0.469	0.501	0.539	0.904
F: 33. Hz															
Abrahamson & Silva 1997	0.444	0.25	0.25	0.25	0.175	0.231	0.214	0.214	0.214	0.14	0.084	0.091	0.091	0.091	0.053
Ambraseys & Douglas 2003	0.014	0	0	0	0	0.016	0	0	0	0	0.022	0	0	0	0
Ambraseys & Simpson 1996	0	0	0	0	0	0	0	0	0	0	0	0	0	0	0
Berge-Thierry et al. 2000	0.057	0.117	0.117	0.117	0	0.03	0.1	0.1	0.1	0	0.024	0.097	0.097	0.097	0
Campbell & Bozorgnia 2002	0	0	0	0	0	0	0	0	0	0	0	0	0	0	0
Lussou et al. 2001	0.433	0.59	0.59	0.59	0.825	0.067	0.151	0.151	0.151	0.198	0	0	0	0	0
Sabetta & Pugliese 1996	0.051	0.042	0.042	0.042	0	0.021	0.029	0.029	0.029	0	0	0	0	0	0
Somerville et al. 2001	0.001	0	0	0	0.001	0.635	0.506	0.506	0.506	0.662	0.87	0.812	0.812	0.812	0.947
F: 50. Hz															
Abrahamson & Silva 1997	0.656	0.443	0.443	0.443	0.284	0.213	0.227	0.227	0.227	0.128	0.07	0.08	0.08	0.08	0.042
Ambraseys & Douglas 2003	0	0	0	0	0	0	0	0	0	0	0	0	0	0	0
Ambraseys & Simpson 1996	0	0	0	0	0	0	0	0	0	0	0	0	0	0	0
Berge-Thierry et al. 2000	0	0	0	0	0	0	0	0	0	0	0	0	0	0	0
Campbell & Bozorgnia 2002	0	0	0	0	0	0	0	0	0	0	0	0	0	0	0
Lussou et al. 2001	0.342	0.557	0.557	0.557	0.715	0.033	0.085	0.085	0.085	0.096	0	0	0	0	0
Sabetta & Pugliese 1996	0	0	0	0	0	0	0	0	0	0	0	0	0	0	0
Somerville et al. 2001	0.002	0.001	0.001	0.001	0.001	0.753	0.688	0.688	0.688	0.776	0.93	0.92	0.92	0.92	0.958

APPENDIX 9: PRIOR WEIGHTING FACTORS FOR THE PGA OF THE VERTICAL COMPONENT GMMs

File: priorwfV_PGA.txt

	M: 5-6 R: 0-15 km	M: 5-6 R: 15-50 km	M: 5-6 R: 50-70 km	M: 5-6 R: 70-100 km	M: 5-6 R: 100-200 km	M: 6-7 R: 0-15 km	M: 6-7 R: 15-50 km	M: 6-7 R: 50-70 km	M: 6-7 R: 70-100 km	M: 6-7 R: 100-200 km	M: 7-7.5 R: 0-15 km	M: 7-7.5 R: 15-50 km	M: 7-7.5 R: 50-70 km	M: 7-7.5 R: 70-100 km	M: 7-7.5 R: 100-200 km
PGA															
Abrahamson & Silva 1997	0.192	0.167	0.177	0.188	0.273	0.151	0.164	0.173	0.184	0.234	0.056	0.073	0.081	0.09	0.096
Ambraseys & Douglas 2003	0.111	0	0	0	0	0.189	0	0	0	0	0.263	0	0	0	0
Ambraseys & Simpson 1996	0.24	0.167	0.177	0.188	0.18	0.189	0.164	0.174	0.184	0.155	0.192	0.204	0.224	0.25	0.176
Berge-Thierry et al. 2000	0.053	0.167	0.177	0.188	0	0.042	0.164	0.174	0.184	0	0.035	0.167	0.184	0.205	0
Campbell & Bozorgnia 2002	0.192	0.167	0.117	0.062	0	0.151	0.164	0.115	0.061	0	0.21	0.278	0.204	0.113	0
Lussou et al. 2001	0.08	0.167	0.177	0.188	0.546	0.019	0.049	0.052	0.055	0.14	0	0	0	0	0
Sabetta & Pugliese 1996	0.132	0.167	0.177	0.188	0	0.083	0.131	0.139	0.147	0	0	0	0	0	0
Somerville et al. 2001	0	0	0	0	0	0.176	0.164	0.174	0.184	0.47	0.245	0.278	0.307	0.342	0.728

APPENDIX 10: UPPER BOUNDS

File: UPPERBOUNDS150.txt

STRESS DROP: 150 [bar]

SA(f) in (m/s^2) / MW: 5.

f [Hz]	0.5	1	2.5	5	10	20	33	50	100
RHYP 5 [km]	0.149	0.711	3.89	7.31	11.6	12.9	10.8	8.03	5.41
RHYP 30 [km]	0.0149	0.0761	0.334	0.523	0.705	0.677	0.517	0.378	0.282
RHYP 70 [km]	0.00568	0.027	0.105	0.148	0.176	0.146	0.103	0.0792	0.067
RHYP 100 [km]	0.00556	0.0258	0.0946	0.125	0.137	0.104	0.0725	0.0587	0.0526
RHYP 150 [km]	0.00416	0.0188	0.0637	0.0768	0.0737	0.0497	0.0361	0.0317	0.03
RHYP 200 [km]	0.00314	0.0136	0.0422	0.0462	0.0392	0.0248	0.0194	0.018	0.0175

SA(f) in (m/s^2) / MW: 6.

f [Hz]	0.5	1	2.5	5	10	20	33	50	100
RHYP 5 [km]	1.51	4.79	14.4	22.3	32.6	35.2	29.2	21.8	15.1
RHYP 30 [km]	0.188	0.522	1.27	1.7	2.18	2.07	1.59	1.18	0.906
RHYP 70 [km]	0.0726	0.185	0.398	0.482	0.546	0.451	0.327	0.258	0.223
RHYP 100 [km]	0.072	0.178	0.362	0.412	0.43	0.328	0.238	0.199	0.181
RHYP 150 [km]	0.0543	0.13	0.243	0.253	0.233	0.162	0.125	0.113	0.108
RHYP 200 [km]	0.0414	0.0945	0.162	0.154	0.127	0.0863	0.0718	0.0677	0.0662

SA(f) in (m/s^2) / MW: 7.

f [Hz]	0.5	1	2.5	5	10	20	33	50	100
RHYP 5 [km]	7.33	16.5	39.8	56.8	79.5	83.6	68.6	51.1	35.6
RHYP 30 [km]	0.888	1.78	3.75	4.88	6.18	5.84	4.49	3.36	2.6
RHYP 70 [km]	0.347	0.644	1.22	1.44	1.62	1.34	0.979	0.78	0.678
RHYP 100 [km]	0.345	0.621	1.11	1.24	1.28	0.98	0.72	0.608	0.557
RHYP 150 [km]	0.258	0.448	0.737	0.749	0.688	0.486	0.381	0.347	0.332
RHYP 200 [km]	0.199	0.331	0.498	0.463	0.383	0.268	0.228	0.216	0.212

SA(f) in (m/s^2) / MW: 7.5

f [Hz]	0.5	1	2.5	5	10	20	33	50	100
RHYP 5 [km]	13.3	27.4	61.9	86	118	123	100	74.7	52.1
RHYP 30 [km]	1.6	3.03	6.19	7.97	10	9.45	7.26	5.44	4.21
RHYP 70 [km]	0.625	1.11	2.05	2.41	2.7	2.23	1.63	1.3	1.13
RHYP 100 [km]	0.622	1.07	1.87	2.07	2.14	1.64	1.21	1.02	0.938
RHYP 150 [km]	0.47	0.777	1.25	1.26	1.16	0.82	0.646	0.59	0.566
RHYP 200 [km]	0.359	0.567	0.835	0.771	0.639	0.45	0.384	0.365	0.358

File: UPPERBOUNDS200.txt

STRESS DROP: 200 [bar]

SA(f) in (m/s^2) / MW: 5.

f [Hz]	0.5	1	2.5	5	10	20	33	50	100
RHYP 5 [km]	0.16	0.767	4.5	8.71	14	15.7	13.1	9.72	6.52
RHYP 30 [km]	0.0156	0.0823	0.388	0.626	0.854	0.822	0.627	0.457	0.34
RHYP 70 [km]	0.00589	0.029	0.121	0.176	0.211	0.175	0.124	0.0948	0.0799
RHYP 100 [km]	0.00578	0.0278	0.11	0.15	0.165	0.125	0.0873	0.0703	0.0629
RHYP 150 [km]	0.00425	0.0199	0.0729	0.0905	0.0875	0.0589	0.0424	0.0372	0.0351
RHYP 200 [km]	0.00327	0.0147	0.0493	0.0554	0.0473	0.0298	0.0231	0.0214	0.0208

SA(f) in (m/s^2) / MW: 6.

f [Hz]	0.5	1	2.5	5	10	20	33	50	100
RHYP 5 [km]	1.73	5.71	17.7	27.6	40.6	44	36.5	27.3	18.8
RHYP 30 [km]	0.212	0.618	1.54	2.07	2.66	2.53	1.94	1.45	1.11
RHYP 70 [km]	0.0814	0.218	0.481	0.585	0.663	0.548	0.397	0.313	0.27
RHYP 100 [km]	0.0808	0.209	0.437	0.5	0.522	0.398	0.288	0.24	0.219
RHYP 150 [km]	0.0603	0.151	0.291	0.304	0.281	0.195	0.149	0.135	0.129
RHYP 200 [km]	0.0469	0.112	0.198	0.188	0.156	0.105	0.0872	0.0822	0.0803

SA(f) in (m/s^2) / MW: 7.

f [Hz]	0.5	1	2.5	5	10	20	33	50	100
RHYP 5 [km]	8.83	20.2	49.4	71	99.5	105	86.2	64.3	44.7
RHYP 30 [km]	1.07	2.17	4.59	5.98	7.58	7.17	5.51	4.12	3.18
RHYP 70 [km]	0.419	0.788	1.5	1.77	1.99	1.65	1.2	0.958	0.833
RHYP 100 [km]	0.413	0.754	1.35	1.51	1.56	1.2	0.878	0.742	0.679
RHYP 150 [km]	0.313	0.551	0.911	0.927	0.852	0.601	0.471	0.429	0.411
RHYP 200 [km]	0.239	0.401	0.607	0.564	0.468	0.326	0.277	0.263	0.257

SA(f) in (m/s^2) / MW: 7.5

f [Hz]	0.5	1	2.5	5	10	20	33	50	100
RHYP 5 [km]	16.1	33.7	76.9	107	148	154	126	93.7	65.3
RHYP 30 [km]	1.95	3.73	7.66	9.87	12.4	11.7	9.01	6.75	5.23
RHYP 70 [km]	0.758	1.35	2.52	2.96	3.31	2.74	2	1.6	1.39
RHYP 100 [km]	0.755	1.31	2.29	2.54	2.63	2.01	1.48	1.25	1.15
RHYP 150 [km]	0.569	0.948	1.53	1.55	1.42	1	0.791	0.722	0.692
RHYP 200 [km]	0.436	0.693	1.02	0.946	0.784	0.552	0.471	0.447	0.438

File: UPPERBOUNDS250.txt

STRESS DROP: 250 [bar]

SA(f) in (m/s^2) / MW: 5.

f [Hz]	0.5	1	2.5	5	10	20	33	50	100
RHYP 5 [km]	0.17	0.818	5.05	10	16.3	18.3	15.3	11.4	7.59
RHYP 30 [km]	0.0162	0.0869	0.434	0.719	0.989	0.955	0.728	0.53	0.392
RHYP 70 [km]	0.00607	0.0307	0.136	0.202	0.245	0.204	0.144	0.109	0.0919
RHYP 100 [km]	0.00599	0.0295	0.124	0.173	0.193	0.146	0.101	0.0813	0.0726
RHYP 150 [km]	0.00437	0.021	0.0815	0.104	0.101	0.068	0.0486	0.0425	0.0401
RHYP 200 [km]	0.00332	0.0154	0.0545	0.0629	0.0541	0.0338	0.0261	0.0241	0.0234

SA(f) in (m/s^2) / MW: 6.

f [Hz]	0.5	1	2.5	5	10	20	33	50	100
RHYP 5 [km]	1.87	6.38	20.3	31.8	47	51	42.4	31.7	21.8
RHYP 30 [km]	0.229	0.695	1.77	2.39	3.08	2.92	2.24	1.67	1.28
RHYP 70 [km]	0.0886	0.246	0.556	0.679	0.77	0.637	0.461	0.363	0.313
RHYP 100 [km]	0.0879	0.237	0.505	0.58	0.607	0.462	0.334	0.278	0.253
RHYP 150 [km]	0.0658	0.172	0.338	0.354	0.327	0.227	0.174	0.156	0.149
RHYP 200 [km]	0.0505	0.126	0.226	0.216	0.179	0.12	0.0996	0.0938	0.0917

SA(f) in (m/s^2) / MW: 7.

f [Hz]	0.5	1	2.5	5	10	20	33	50	100
RHYP 5 [km]	10.2	23.6	58.5	84.3	119	125	103	76.8	53.3
RHYP 30 [km]	1.23	2.52	5.37	7	8.87	8.39	6.45	4.83	3.73
RHYP 70 [km]	0.485	0.921	1.76	2.08	2.34	1.94	1.42	1.13	0.978
RHYP 100 [km]	0.475	0.875	1.58	1.76	1.83	1.4	1.02	0.865	0.791
RHYP 150 [km]	0.359	0.638	1.06	1.08	0.991	0.7	0.548	0.498	0.477
RHYP 200 [km]	0.275	0.466	0.708	0.658	0.546	0.38	0.323	0.306	0.299

SA(f) in (m/s^2) / MW: 7.5

f [Hz]	0.5	1	2.5	5	10	20	33	50	100
RHYP 5 [km]	19	40	92.1	129	178	186	152	113	78.8
RHYP 30 [km]	2.25	4.32	8.92	11.5	14.5	13.7	10.5	7.88	6.1
RHYP 70 [km]	0.888	1.59	2.97	3.49	3.91	3.23	2.37	1.89	1.64
RHYP 100 [km]	0.876	1.52	2.68	2.98	3.08	2.35	1.73	1.47	1.34
RHYP 150 [km]	0.655	1.1	1.77	1.79	1.65	1.17	0.917	0.836	0.802
RHYP 200 [km]	0.512	0.817	1.21	1.12	0.929	0.653	0.557	0.528	0.518

APPENDIX 11: EG2-HID-0041 HAZARD INPUT DOCUMENT FINAL MODEL F. SCHERBAUM

A 11-1 Introduction

This document describes the implementation and parameterization of Frank Scherbaum's expert model EG2-EXM-0024, as described in the Elicitation Summary EG2-ES-0038 and delivered on 30.05.2003. The purpose of this document is to translate the expert's evaluation of ground motion into an input useable by the hazard software.

A 11-2 Model Implementation

Based on F. Scherbaum's Elicitation Summary EG2-ES-0038 and on subsequent discussions between the expert and the TFI team, the logic trees for the median horizontal ground motion, the vertical/horizontal ratio and the aleatory variability of the horizontal component were implemented in FORTRAN and the results displayed graphically.

Key elements in F. Scherbaum's model include:

Median horizontal ground motion

- 14 out of the 15 candidate models were included based on these prior weights.
- A two step approach is discussed, which initially rates the frequency-, magnitude-, and distance coverage of the original candidate models, leading to the so-called "prior weights", while in a second step the applicability of the adapted models to Switzerland is estimated based upon a comparison with actual data or on expert's judgment. The second step leads to the derivation of "relative adjustment factors". These two approaches lead to different weights assigned to the attenuation models. The weights from these two approaches were then combined to give a total weight for each attenuation relation. Finally, the total weights are renormalized so that they all sum up to 1. Only 6 models were given non-zero relative GMM adjustment factors.
- For the prior weighting of the ground motion models, the magnitude – distance - frequency (M-R-f) space is sub-divided into $3 \times 5 \times 9 = 135$ bins with the following limits: M1 = 6.0, M2 = 7.0, R1 = 15 km, R2 = 50 km, R3 = 70 km, R4 = 100 km. f1 = 0.5 Hz, f2 = 1Hz, f3 = 2.5 Hz, f4 = 5 Hz, f5 = 10 Hz, f6 = 20 Hz, f7 = 33 Hz, f8 = 50 Hz, f9 = PGA-frequency are the centers of the frequency bins.
- Representative average values for the shear wave velocity v_{s30} have been assigned to each individual ground motion model. Epistemic uncertainty is captured through the introduction of two additional branches with lower and higher velocities. The adjustment to a reference rock site with a v_{s30} value of 1100 m/s is made via the application of scaling factors derived from site amplification functions calculated using the quarter wavelength approach. In a second correction step, ground motion is scaled from 1100 m/s to the SP3 reference velocity of 2000 m/s using factors provided by TP2-TN-0363 (Lacave et al. 2003).
- To account for specific Swiss conditions ground motion is corrected according to the differences in κ of the host regions (proponent models) and the Swiss target region. For this reason, representative average values for κ have been assigned to each individual ground motion model. Epistemic uncertainty in these host region values is captured through the introduction of two additional +20 % and -20 % branches. For the target region a mean κ is used as the central branch along with two side branches containing the lower and upper values. The kappa correction is performed by applying scale factors derived using RVT for

different kappa values and the source and path parameters from the particular host region parameterization. The scaling factors are computed for a combination of five distances and three magnitudes. They are listed in Tables A11-4 to A11-9 at the end of this document.

- The only magnitude conversions used are M_w to M_s and M_w to M_{JMA}. The M_w to M_s uses the Ambraseys & Free (1997) relation without depth dependence. The M_w to M_{JMA} assumes that the scales are equal. No epistemic uncertainty is considered in this conversion.
- The conversion of the different types of larger horizontal components to the geometric mean definition is based on TP2-TN-0269 for spectral acceleration. Epistemic uncertainty is introduced by the addition of a second and a third branch at this level, (constant 20 % and 15 % reductions for Ambraseys & Douglas 2000 and Ambraseys et al. 1996, and constant 10 % and 5 % reductions for Sabetta & Pugliese 1996, respectively). For PGA the largest component is reduced by 20, 15, and 10 %, with equal weights assigned to these three alternatives.
- Missing coefficients in the ground motion models considered have to be derived according to the procedure described in TP2-TN-0270.
- Style-of-faulting adjustments are to be made for those equations that do not account for faulting mechanisms. The correction is based on frequency dependent reference scaling factors and the distributions of faulting mechanisms underlying the proponent models. The epistemic uncertainty is captured by two alternative branches with ± 10 % variations of the reference scale factors.

V/H Ratio

- V/H ratios are obtained by using models that predict both horizontal and vertical components.
- A similar procedure as described above for horizontal ground motion has been applied to combine the "prior weights" with the "relative adjustment factors" which results in a total number of 4 models with non-zero weights.
- For the vertical component, the same adjustment with respect to site conditions is applied as described above for the horizontal component.
- Magnitude conversion is considered for both horizontal and vertical components.
- The conversion of components to the geometric mean is based on TP2-TN-0269 and only applied to the horizontal components.
- Missing coefficients in the ground motion models predicting vertical components have been derived according to the procedure described in TP2-TN-0270.
- Style-of-faulting adjustment for the vertical component are applied in the same way as described for horizontal ground motion above, except that the vertical reference scale factors are also incorporated into these adjustments.

Aleatory variability for the horizontal component

- The logic tree computations for the aleatory uncertainties are based on the same set of models and weights as those used to model horizontal ground motion.
- The effect of propagating the aleatory uncertainty in the magnitude conversion is considered by two branches with equal weights and alternative values of σ_m.
- Figures A11-1, A11-2 and A11-3 show the logic trees for the horizontal component, the V/H ratio and the aleatory variability, resp., as they have been implemented in the code.

Maximum Ground Motion and upper tail truncation

The maximum ground motion for the Scherbaum model was computed using the Stochastic model (Boore 2000) with the Bay (2002) source path, and site parameters except for the stress-drop. In order to capture the epistemic uncertainty, three values of stress-drop are used: 150 bars, 200 bars, and 250 bars.

The stochastic ground motion parameters are listed in Table A11-1. The Bay model has a frequency dependent duration but the Boore (2000) program only allows for a frequency independent duration. To account for the frequency dependence, the program was run for four separate frequency bands: 0.5 – 1.0 Hz, 2.5 Hz, 5 Hz, 10 – 50 Hz. The frequency dependent path duration parameters are listed in Table A11-2. The crustal amplification factors (Table A11-3) were taken from the Scherbaum factors for a v_{s30} value of 1100 m/s.

In the implementation of the model, the point source distance is computed using a minimum effective depth of 8 km. That is:

$$Dist_{Point\,Source} = \sqrt{Dist_{JB}^2 + 8^2}$$

For each frequency, the maximum ground motions were computed for the three alternative stress-drops at each of the JB distances used in the SP2 ground motion tables.

The ground motion distribution is considered to be lognormal until 3σ or until the maximum ground motion (as defined above) is reached, whichever value is smaller. If maximum ground motion is larger than 3σ two alternatives are considered. In the first one a linear scaling function (a linear taper) is applied to the lognormal distribution, with a scaling value of 1 at 3σ and a scaling value of 0 at the point of maximum ground motion. In the second alternative the ground motion distribution has a lognormal shape up to the point of maximum ground motion.

A 11-3 Model Parameterization

The ground motion is parameterized for the final Rock Hazard Computations at the following spectral frequencies: 0.5 Hz, 1 Hz, 2.5 Hz, 5 Hz, 10 Hz, 20 Hz, 33 Hz, 50 Hz and at peak acceleration. The implementation of the logic trees results in: (a) a set of alternative estimates of the median horizontal ground motion, aleatory variability of the horizontal ground motion and V/H ratios at each spectral frequency, earthquake magnitude, fault style, and distance, and (b) the weight associated to each individual branch of the logic tree.

Ground motions have been modeled for seven magnitudes [5.0 : 0.5 : 8.0] and 14 distances (1.0, 1.6, 2.5, 4.0, 6.3, 10, 16, 25, 40, 63, 85, 100, 160, 250 kilometers).

The ground motion from the implementation of the SP2 logic trees has been parameterized using a composite model approach. At each distance, magnitude and spectral frequency and for each fault style, the alternative estimates of the median ground motion are sorted in ascending spectral acceleration. The weights associated with the sorted median amplification factors are summed, resulting in a cumulative distribution of the amplification factors. No smoothing of the cumulative distribution has been applied. The values of the ground motion are selected for cumulative distributions corresponding to the following fractiles: 0.13 %, 2.28 %, 16 %, 50 %, 84 %, 97.72 %, and 99.87 %. The seven fractiles correspond to median, ± 1 σ, ± 2 σ, and ± 3 σ levels. By using the discrete fractiles, no assumption regarding the symmetry of the epistemic uncertainty is made.

For the aleatory variability, the same process is repeated but with the sorting on the amplitude of the aleatory variability.

Tab. A11-1: Parameterization of the Bay model used in computing the maximum ground motions for Scherbaum

Parameter	
rho	2.8
beta	3.5
Prtitn	0.707
Radpat	0.55
fs	2.0
Spectral shape Source number	1 (single corner)
pf	2.0
pd	1.0
Stress-drop	150, 200, 250 bars
Geometrical spreading	dist range a_s 1-50 km -1.1 50-70 km 70- -0.6 100 km 0.2 >100 km -0.5
Q	270 $f^{0.5}$
Source duration weights	1/fa = 0.5 1/fb = 0.0
Path duration	See Table A11-2
Site Amp	See Table A11-3
kappa	0.0125 s
fm	1000 Hz

Tab. A11-2: Path Duration Model Parameters

Distance [km]	0.5 – 1.0 Hz	2.5 Hz	5 Hz	10 – 50 Hz and PGA
0	0.0	0.0	0.0	0.0
10	2.4	2.3	2.1	1.8
30	7.5	7.1	6.0	4.1
75	14.3	13.5	11.1	7.2
90	15.0	14.1	11.4	6.9
120	12.0	11.4	9.5	6.4
150	11.9	11.3	9.6	6.8
Slope for > 150 km	0.05	0.05	0.05	0.05

Tab. A11-3: Crustal Amplification Factor

Freq [Hz]	Amp factor
0.01	1
0.1	1.06
0.3	1.38
1	1.88
2	2.38
3	2.29
4	2.22
5	2.21
6	2.34
7	2.41
8	2.46
9	2.51
10	2.53
15	2.55
30	2.76
100	3.12

A conversion for the different distance measures was conducted using the Scherbaum conversion factors. Two sets of conversions were done. The first converted the distances to JB distances and the second converted the distances to rupture distance. The main differences between the JB distance and the rupture distance occur for small magnitudes at short distances. However, to avoid potential jumps in the models at bin boundaries, the conversions were applied to all the bins (unlike what had been done for the sensitivity computations, where the conversion was not applied to the smallest magnitude and shortest distance bin ($M < 5.5$, $D < 10$)).

The values of ground motion resulting from this procedure are directly input into the rock hazard software without further parameterization or fitting.

The Maximum Ground Motion estimates are also parameterized in a similar manner. Tables of the maximum ground motion are developed for the same magnitude and distance bins for each style of faulting and for the seven fractiles.

Figures A11-4 to A11-6 on the next pages of this document show one example (for PGA, the Joyner-Boore distance and strike-slip) of the ground motion for the horizontal component, for the V/H ratio and for the aleatory variability for the horizontal component, respectively. The figures display four subplots. The upper plot shows the median as a distance and magnitude dependent surface. The central plot shows the median ground motion as a distance and fractile dependent surface for magnitude 6.5. The lower left plot shows the median for the 7 magnitudes (magnitude 5.0 to 8.0 in 0.5 magnitude steps) while the lower right subplot shows the 7 fractiles (corresponding to median, $\pm$ 1 σ, $\pm$ 2 σs, and $\pm$ 3 σs) for magnitude 6.5.

Figures 4 to 129 of the associated PDF file (EG2-HID-0041_Scherbaum_figures_rev2.pdf) show the full set of figures.

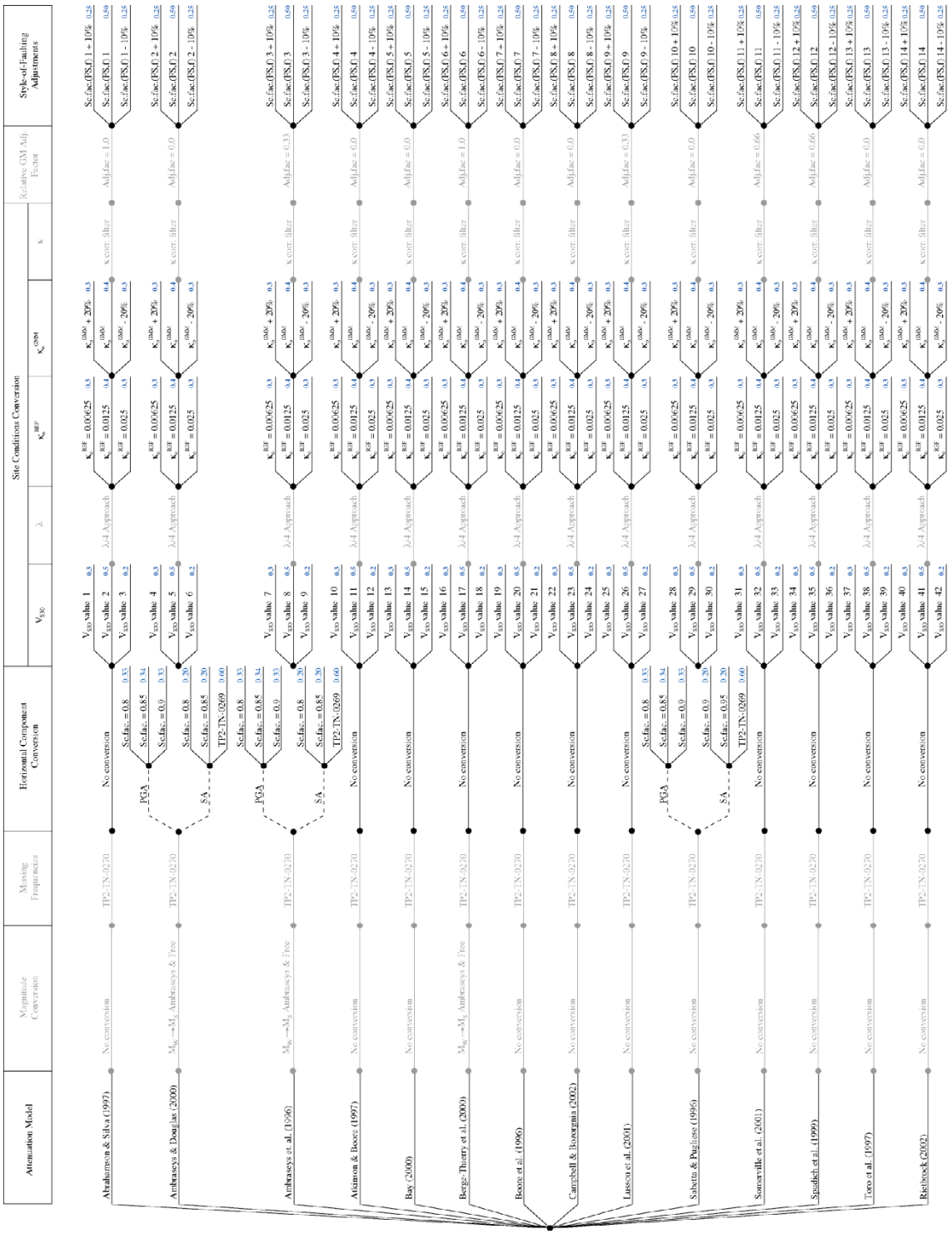

Fig. A11-1: Logic tree for the horizontal ground motion

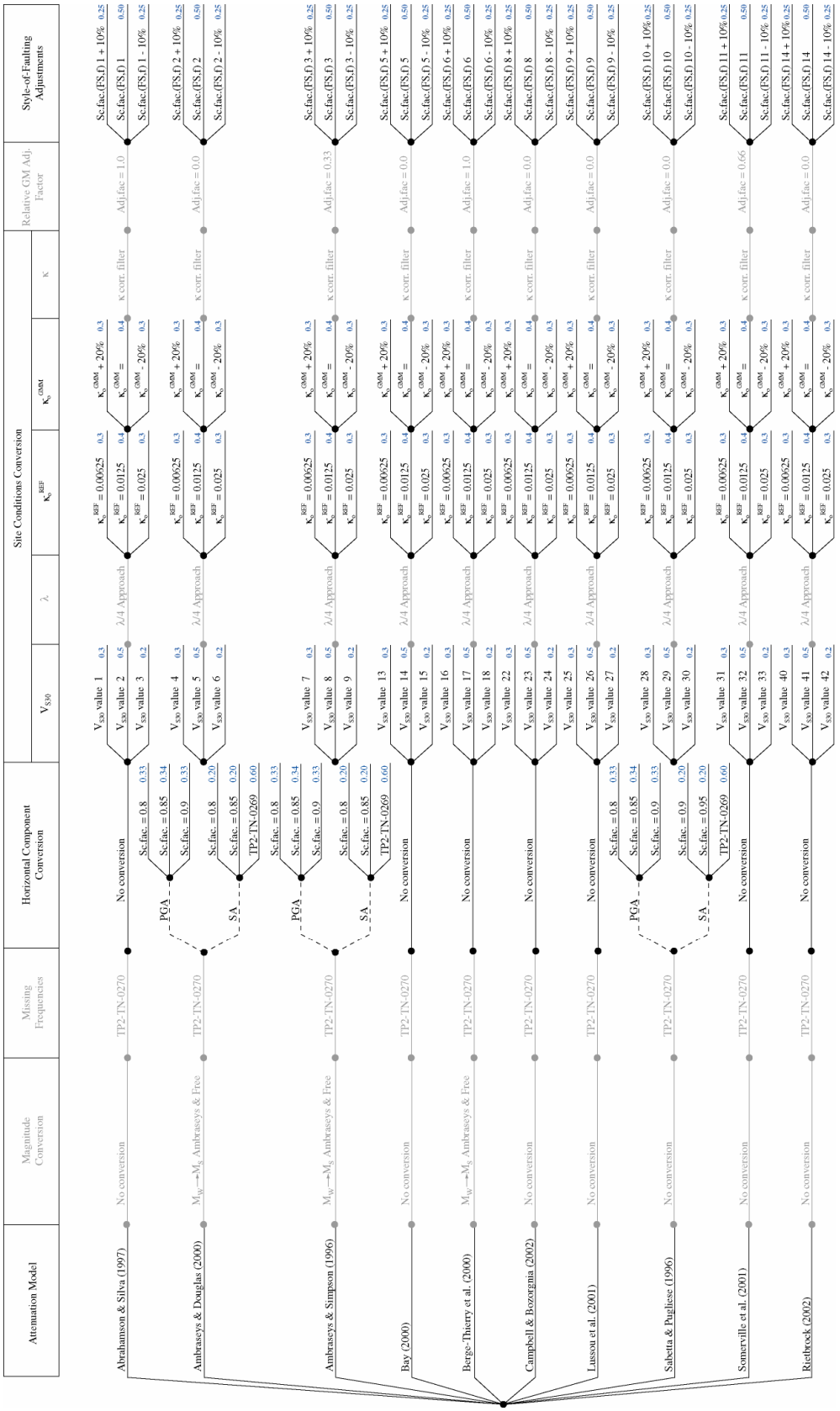

Fig. A11-2: Logic tree for the V/H ratio

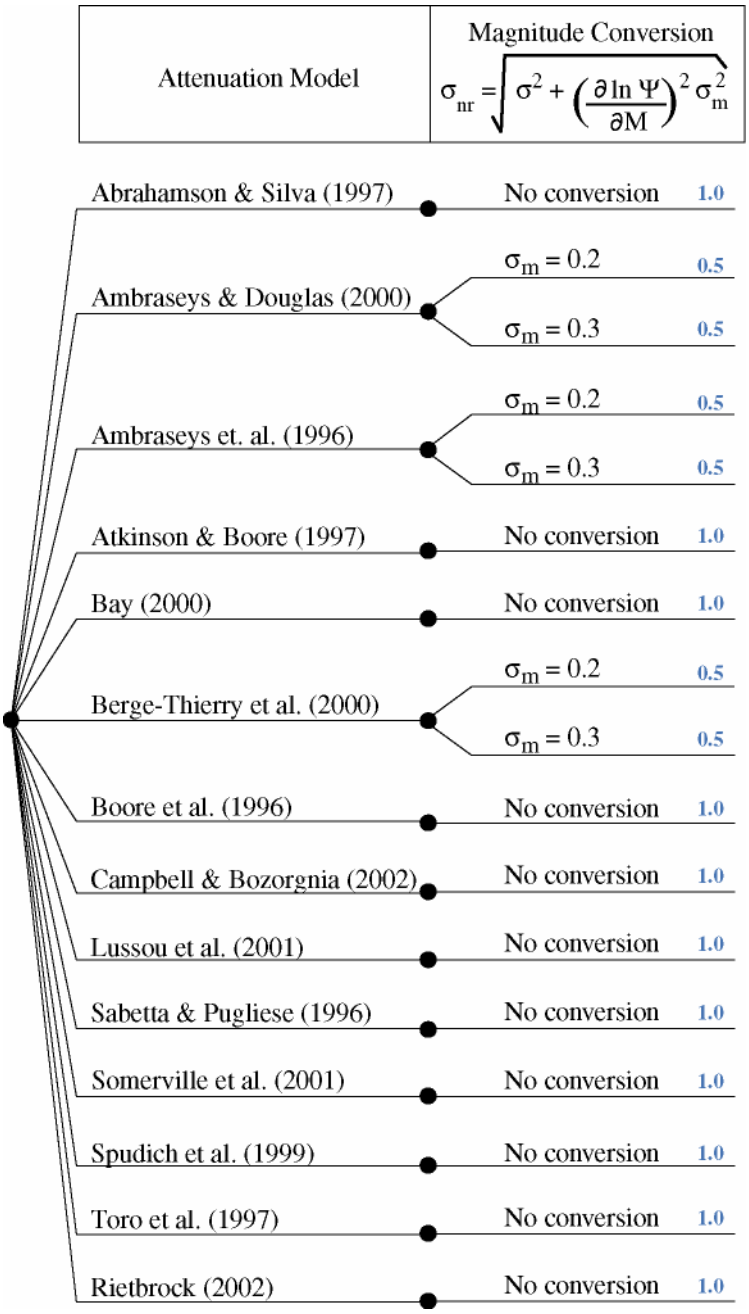

Fig. A11-3: Logic tree for the aleatory uncertainty

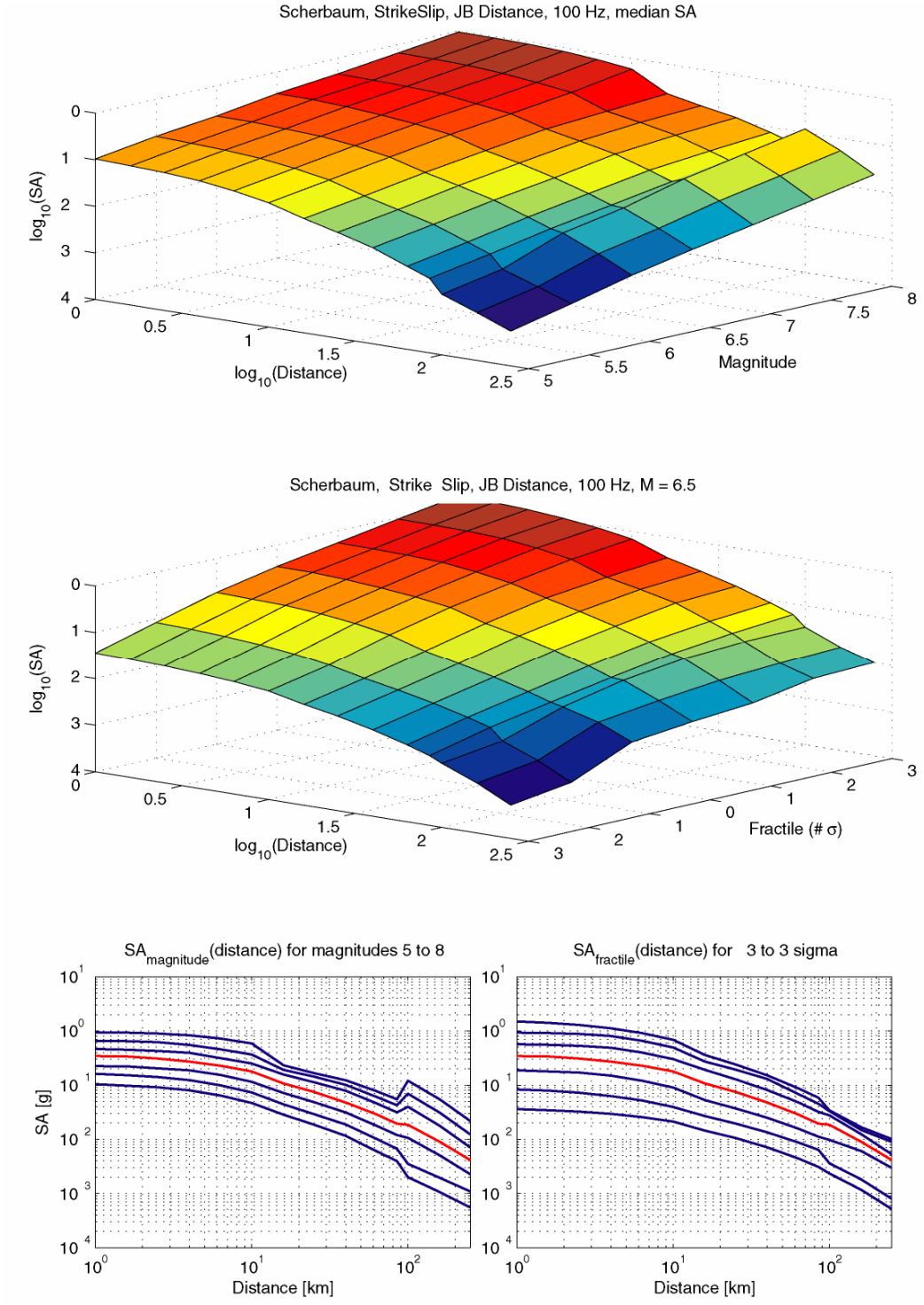

Fig. A11-4: Spectral acceleration (SA) for PGA (100 Hz), assuming strike-slip mechanism and Joyner-Boore distances

The upper plot shows SA (distance, magnitude) for the median. The middle plot shows SA (distance, fractile) for magnitude 6.5. The lower left-hand plot shows the median SA (distance) for different magnitudes. The lower right-hand plot shows SA (distance) for different fractiles and magnitude 6.5.

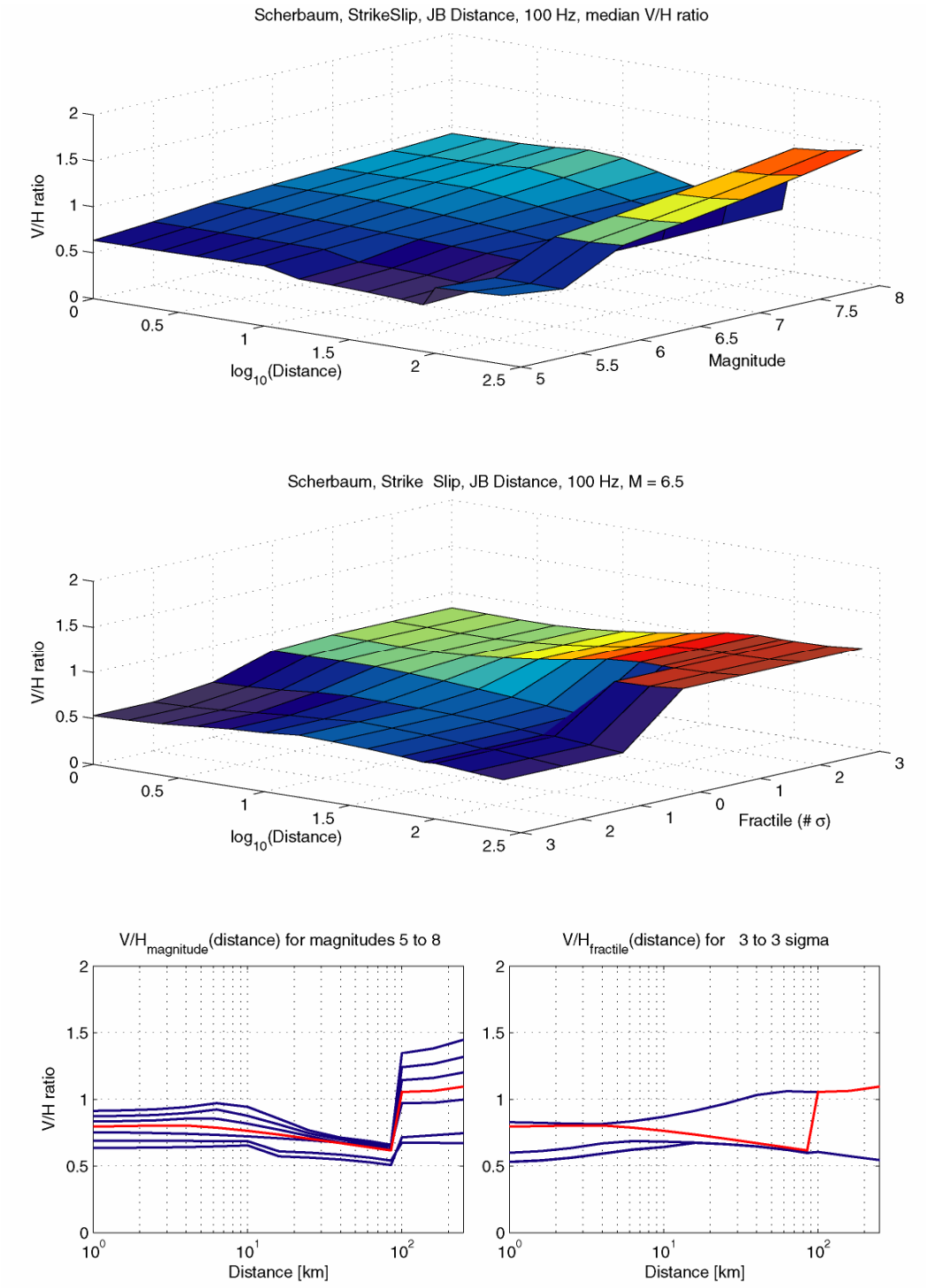

Fig. A11-5: V/H ratio (V/H) for PGA (100 Hz), assuming strike-slip mechanism and Joyner-Boore distances

The upper plot shows V/H (distance, magnitude) for the median. The middle plot shows V/H (distance, fractile) for magnitude 6.5. The lower left-hand plot shows the median V/H (distance) for different magnitudes. The lower right-hand plot shows V/H (distance) for different fractiles and magnitude 6.5

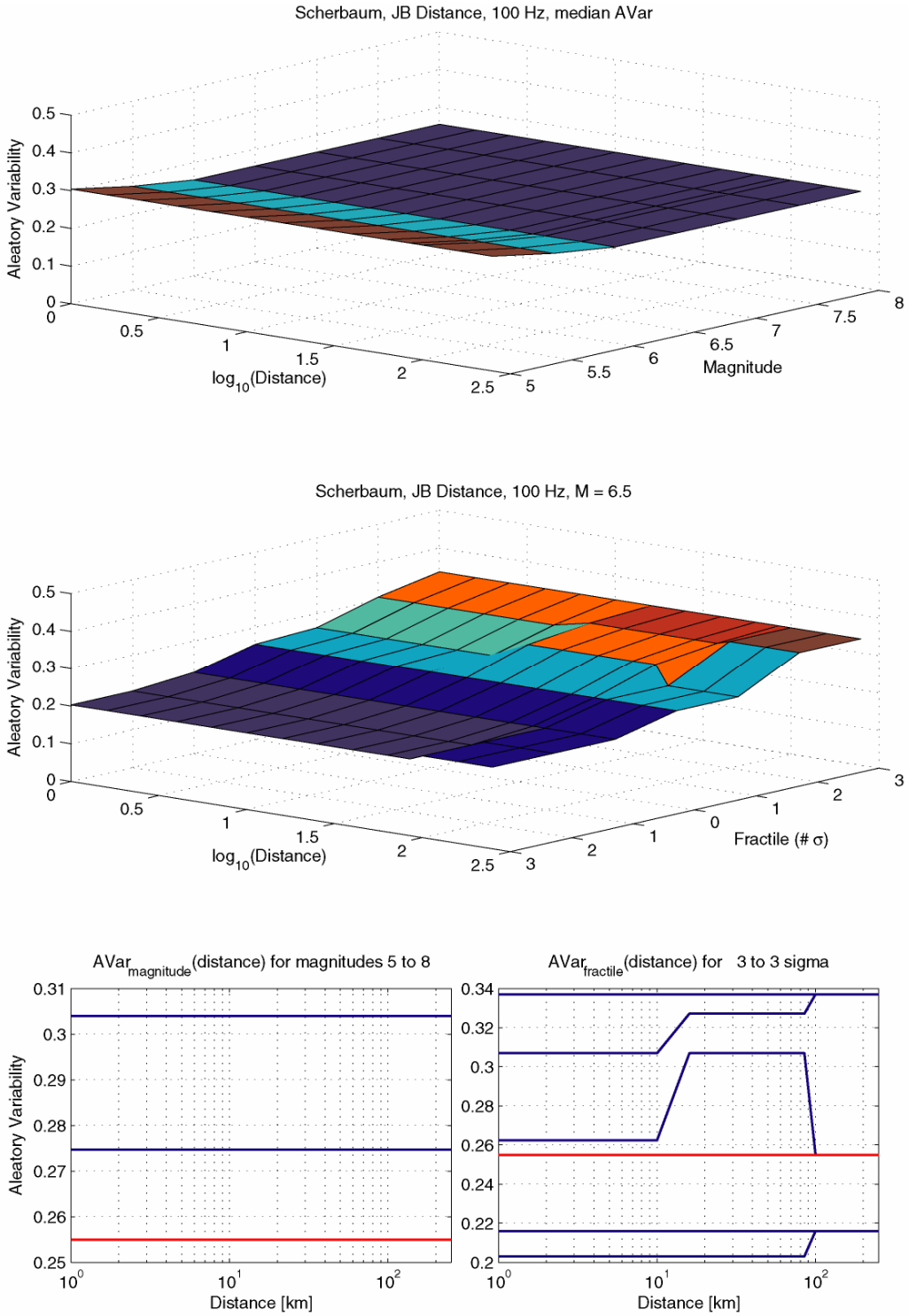

Fig. A11-6: Aleatory variability (AVar) for PGA (100 Hz), assuming strike-slip mechanism and Joyner-Boore distances

The upper plot shows AVar (distance, magnitude) for the median. The middle plot shows AVar (distance, fractile) for magnitude 6.5. The lower left-hand plot shows the median AVar (distance) for different magnitudes. The lower right-hand plot shows AVar (distance) for different fractiles and magnitude 6.5

Tab. A11-4: Scaling factors derived for kappa correction – Abrahamson & Silva (1997) model

Abrahamson & Silva (1997) RVT GM for							Resulting scale factors (GM target / GM host) for target (above) and host (below) κ values								
	κ target			κ host			0.00625			0.0125			0.025		
freq	0.00625	0.0125	0.025	0.03	0.0375	0.045	0.03	0.0375	0.045	0.03	0.0375	0.045	0.03	0.0375	0.045
M / dist: 5.5 / 7.5															
0.5	28.9	28.62	28.1	27.9	27.61	27.32	1.036	1.047	1.058	1.026	1.037	1.048	1.007	1.018	1.029
1	123.8	121.8	117.5	115.7	113.1	110.5	1.070	1.095	1.120	1.053	1.077	1.102	1.016	1.039	1.063
2.5	502.5	478.4	433.3	416.6	392.7	370.3	1.206	1.280	1.357	1.148	1.218	1.292	1.040	1.103	1.170
5	1026	930.5	766.6	709.9	633.2	565.2	1.445	1.620	1.815	1.311	1.470	1.646	1.080	1.211	1.356
10	1753	1447	993.9	858	690.8	559.2	2.043	2.538	3.135	1.686	2.095	2.588	1.158	1.439	1.777
20	2536	1748	868	671.3	472.1	348.1	3.778	5.372	7.285	2.604	3.703	5.022	1.293	1.839	2.494
33	2900	1604	600.3	450.5	325.7	257.2	6.437	8.904	11.275	3.560	4.925	6.236	1.333	1.843	2.334
50	2866	1268	457.4	366.7	287.9	239.4	7.816	9.955	11.972	3.458	4.404	5.297	1.247	1.589	1.911
100	1139	682.9	393	337	277.7	235.8	3.380	4.102	4.830	2.026	2.459	2.896	1.166	1.415	1.667
M / dist: 5.5 / 30															
0.5	6.711	6.645	6.512	6.46	6.383	6.306	1.039	1.051	1.064	1.029	1.041	1.054	1.008	1.020	1.033
1	27.42	26.9	25.85	25.44	24.84	24.24	1.078	1.104	1.131	1.057	1.083	1.110	1.016	1.041	1.066
2.5	96.38	91.73	83.11	79.91	75.36	71.07	1.206	1.279	1.356	1.148	1.217	1.291	1.040	1.103	1.169
5	175.6	159.4	131.5	121.9	108.8	97.24	1.441	1.614	1.806	1.308	1.465	1.639	1.079	1.209	1.352
10	265.2	219.5	151.6	131.3	106.2	86.46	2.020	2.497	3.067	1.672	2.067	2.539	1.155	1.427	1.753
20	332.9	231.6	118.6	93.37	67.87	51.92	3.565	4.905	6.412	2.480	3.412	4.461	1.270	1.747	2.284
33	337.5	192.6	81.03	64.09	49.27	40.53	5.266	6.850	8.327	3.005	3.909	4.752	1.264	1.645	1.999
50	301.7	146.2	65.54	55.01	45.07	38.5	5.484	6.694	7.836	2.658	3.244	3.797	1.191	1.454	1.702
100	137.4	93.22	59.19	51.9	43.86	37.97	2.647	3.133	3.619	1.796	2.125	2.455	1.140	1.350	1.559
M / dist: 5.5 / 60															
0.5	4.107	4.064	3.98	3.946	3.896	3.847	1.041	1.054	1.068	1.030	1.043	1.056	1.009	1.022	1.035
1	15.34	15.03	14.44	14.21	13.87	13.53	1.080	1.106	1.134	1.058	1.084	1.111	1.016	1.041	1.067
2.5	46.63	44.39	40.25	38.71	36.52	34.46	1.205	1.277	1.353	1.147	1.215	1.288	1.040	1.102	1.168
5	75.26	68.38	56.57	52.47	46.92	41.99	1.434	1.604	1.792	1.303	1.457	1.628	1.078	1.206	1.347
10	98.76	82.05	57.22	49.76	40.57	33.33	1.985	2.434	2.963	1.649	2.022	2.462	1.150	1.410	1.717
20	104.8	74.16	40.09	32.52	24.84	19.95	3.223	4.219	5.253	2.280	2.986	3.717	1.233	1.614	2.010
33	92.55	56.22	28.29	23.75	19.43	16.63	3.897	4.763	5.565	2.367	2.893	3.381	1.191	1.456	1.701
50	75.38	43.08	24.56	21.51	18.35	16.09	3.504	4.108	4.685	2.003	2.348	2.677	1.142	1.338	1.526
100	43.55	33.03	23.13	20.75	18.01	15.92	2.099	2.418	2.736	1.592	1.834	2.075	1.115	1.284	1.453
M / dist: 5.5 / 85															
0.5	3.043	3.011	2.947	2.923	2.885	2.849	1.041	1.055	1.068	1.030	1.044	1.057	1.008	1.021	1.034
1	10.64	10.42	10.01	9.851	9.615	9.386	1.080	1.107	1.134	1.058	1.084	1.110	1.016	1.041	1.066
2.5	29.21	27.82	25.24	24.28	22.92	21.63	1.203	1.274	1.350	1.146	1.214	1.286	1.040	1.101	1.167
5	43.12	39.22	32.51	30.18	27.02	24.21	1.429	1.596	1.781	1.300	1.452	1.620	1.077	1.203	1.343
10	50.82	42.39	29.84	26.06	21.42	17.77	1.950	2.373	2.860	1.627	1.979	2.385	1.145	1.393	1.679
20	47.5	34.3	19.67	16.42	13.08	10.9	2.893	3.631	4.358	2.089	2.622	3.147	1.198	1.504	1.805
33	38.43	25.1	14.63	12.74	10.82	9.494	3.016	3.552	4.048	1.970	2.320	2.644	1.148	1.352	1.541
50	30.48	20.19	13.26	11.9	10.4	9.277	2.561	2.931	3.286	1.697	1.941	2.176	1.114	1.275	1.429
100	21.24	17.15	12.75	11.62	10.26	9.199	1.828	2.070	2.309	1.476	1.672	1.864	1.097	1.243	1.386
M / dist: 5.5 / 140															
0.5	1.784	1.765	1.728	1.714	1.692	1.671	1.041	1.054	1.068	1.030	1.043	1.056	1.008	1.021	1.034
1	5.507	5.398	5.186	5.103	4.982	4.864	1.079	1.105	1.132	1.058	1.084	1.110	1.016	1.041	1.066
2.5	12.45	11.86	10.78	10.37	9.796	9.253	1.201	1.271	1.346	1.144	1.211	1.282	1.040	1.100	1.165
5	15.36	14	11.67	10.85	9.75	8.771	1.416	1.575	1.751	1.290	1.436	1.596	1.076	1.197	1.331
10	14.6	12.32	8.926	7.907	6.655	5.669	1.846	2.194	2.575	1.558	1.851	2.173	1.129	1.341	1.575
20	10.97	8.475	5.701	5.056	4.353	3.847	2.170	2.520	2.852	1.676	1.947	2.203	1.128	1.310	1.482
33	8.334	6.521	4.793	4.391	3.931	3.577	1.898	2.120	2.330	1.485	1.659	1.823	1.092	1.219	1.340
50	7.159	5.879	4.59	4.262	3.862	3.536	1.680	1.854	2.025	1.379	1.522	1.663	1.077	1.189	1.298
100	6.342	5.554	4.519	4.216	3.835	3.519	1.504	1.654	1.802	1.317	1.448	1.578	1.072	1.178	1.284
M / dist: 6.5 / 7.5															
0.5	214.1	212.4	208.9	207.4	205.1	202.8	1.032	1.044	1.056	1.024	1.036	1.047	1.007	1.019	1.030
1	520.4	510.5	490.9	483.2	471.9	460.9	1.077	1.103	1.129	1.056	1.082	1.108	1.016	1.040	1.065
2.5	1393	1326	1202	1156	1091	1029	1.205	1.277	1.354	1.147	1.215	1.289	1.040	1.102	1.168
5	2485	2255	1861	1724	1540	1376	1.441	1.614	1.806	1.308	1.464	1.639	1.079	1.208	1.352
10	3951	3264	2248	1944	1570	1275	2.032	2.517	3.099	1.679	2.079	2.560	1.156	1.432	1.763
20	5490	3790	1899	1472	1047	783.8	3.730	5.244	7.004	2.575	3.620	4.835	1.290	1.814	2.423
33	6160	3417	1302	990.3	731.9	590.6	6.220	8.416	10.430	3.450	4.669	5.786	1.315	1.779	2.205
50	6024	2682	1001	815.5	653.7	553.4	7.387	9.215	10.885	3.289	4.103	4.846	1.227	1.531	1.809
100	2389	1459	865.9	750.8	628.5	541.8	3.182	3.801	4.409	1.943	2.321	2.693	1.153	1.378	1.598
M / dist: 6.5 / 30															
0.5	48.68	48.27	47.41	47.05	46.51	45.98	1.035	1.047	1.059	1.026	1.038	1.050	1.008	1.019	1.031
1	111.4	109.2	105	103.4	100.9	98.58	1.077	1.104	1.130	1.056	1.082	1.108	1.015	1.041	1.065
2.5	272.6	259.5	235.5	226.5	213.8	201.8	1.204	1.275	1.351	1.146	1.214	1.286	1.040	1.101	1.167
5	449	407.8	337.2	312.8	279.6	250.2	1.435	1.606	1.795	1.304	1.459	1.630	1.078	1.206	1.348
10	646.6	535.8	371.4	322.2	261.6	214	2.007	2.472	3.021	1.663	2.048	2.504	1.153	1.420	1.736
20	791.8	552.2	285.5	226.4	166.9	130	3.497	4.744	6.091	2.439	3.309	4.248	1.261	1.711	2.196
33	794	455.3	196.6	157.7	123.9	103.9	5.035	6.408	7.642	2.887	3.675	4.382	1.247	1.587	1.892
50	706	345.7	161.4	137	114.3	99.17	5.153	6.177	7.119	2.523	3.024	3.486	1.178	1.412	1.628
100	324.7	223.9	146.3	129.6	111.1	97.6	2.505	2.923	3.327	1.728	2.015	2.294	1.129	1.317	1.499
M / dist: 6.5 / 60															
0.5	29.05	28.78	28.24	28.02	27.69	27.37	1.037	1.049	1.061	1.027	1.039	1.052	1.008	1.020	1.032
1	61.82	60.62	58.28	57.37	56.04	54.74	1.078	1.103	1.129	1.057	1.082	1.107	1.016	1.040	1.065
2.5	135.7	129.3	117.4	113	106.7	100.8	1.201	1.272	1.346	1.144	1.212	1.283	1.039	1.100	1.165
5	202.1	183.8	152.4	141.5	126.8	113.7	1.428	1.594	1.777	1.299	1.450	1.617	1.077	1.202	1.340
10	256.4	213.4	149.6	130.5	107	88.5	1.965	2.396	2.897	1.635	1.994	2.411	1.146	1.398	1.690
20	267.8	190.4	104.7	85.86	66.85	54.82	3.119	4.006	4.885	2.218	2.848	3.473	1.219	1.566	1.910
33	235.5	144.5	75.43	64.28	53.64	46.74	3.664	4.390	5.039	2.248	2.694	3.092	1.173	1.406	1.614
50	191.8	111.8	66.3	58.78	50.97	45.37	3.263	3.763	4.227	1.902	2.193	2.464	1.128	1.301	1.461
100	113	87.11	62.7	56.84	50.06	44.87	1.988	2.257	2.518	1.533	1.740	1.941	1.103	1.252	1.397

Abrahamson & Silva (1997) RVT GM for							Resulting scale factors (GM target / GM host) for target (above) and host (below) κ values								
	κ target			κ host			0.00625			0.0125			0.025		
freq	0.00625	0.0125	0.025	0.03	0.0375	0.045	0.03	0.0375	0.045	0.03	0.0375	0.045	0.03	0.0375	0.045
M / dist: 6.5 / 85															
0.5	21.34	21.14	20.73	20.57	20.33	20.09	1.037	1.050	1.062	1.028	1.040	1.052	1.008	1.020	1.032
1	43.01	42.17	40.55	39.92	39	38.09	1.077	1.103	1.129	1.056	1.081	1.107	1.016	1.040	1.065
2.5	86.7	82.63	75.1	72.29	68.3	64.54	1.199	1.269	1.343	1.143	1.210	1.280	1.039	1.100	1.164
5	119.2	108.5	90.21	83.86	75.25	67.62	1.421	1.584	1.763	1.294	1.442	1.605	1.076	1.199	1.334
10	136.7	114.3	81.04	71.09	58.89	49.32	1.923	2.321	2.772	1.608	1.941	2.318	1.140	1.376	1.643
20	126.5	92.01	54.14	45.82	37.32	31.77	2.761	3.390	3.982	2.008	2.465	2.896	1.182	1.451	1.704
33	102.4	68.07	41.37	36.57	31.64	28.22	2.800	3.236	3.629	1.861	2.151	2.412	1.131	1.308	1.466
50	81.82	55.58	37.88	34.4	30.55	27.65	2.378	2.678	2.959	1.616	1.819	2.010	1.101	1.240	1.370
100	58.25	47.8	36.56	33.64	30.17	27.43	1.732	1.931	2.124	1.421	1.584	1.743	1.087	1.212	1.333
M / dist: 6.5 / 140															
0.5	12.49	12.37	12.12	12.03	11.89	11.75	1.038	1.050	1.063	1.028	1.040	1.053	1.007	1.019	1.031
1	22.57	22.14	21.3	20.97	20.49	20.02	1.076	1.102	1.127	1.056	1.081	1.106	1.016	1.040	1.064
2.5	38.19	36.43	33.16	31.95	30.22	28.59	1.195	1.264	1.336	1.140	1.205	1.274	1.038	1.097	1.160
5	44.38	40.54	33.94	31.65	28.55	25.79	1.402	1.554	1.721	1.281	1.420	1.572	1.072	1.189	1.316
10	41.51	35.23	25.94	23.17	19.79	17.15	1.792	2.098	2.420	1.521	1.780	2.054	1.120	1.311	1.513
20	31.45	24.76	17.4	15.73	13.82	12.46	1.999	2.276	2.524	1.574	1.792	1.987	1.106	1.259	1.396
33	24.46	19.65	15.03	13.94	12.69	11.72	1.755	1.928	2.087	1.410	1.548	1.677	1.078	1.184	1.282
50	21.39	17.96	14.47	13.59	12.5	11.61	1.574	1.711	1.842	1.322	1.437	1.547	1.065	1.158	1.246
100	19.18	17.07	14.28	13.46	12.42	11.57	1.425	1.544	1.658	1.268	1.374	1.475	1.061	1.150	1.234
M / dist: 7.25 / 7.5															
0.5	547.5	542.4	532	527.9	521.8	515.7	1.037	1.049	1.062	1.027	1.039	1.052	1.008	1.020	1.032
1	1093	1072	1030	1014	990.2	967.1	1.078	1.104	1.130	1.057	1.083	1.108	1.016	1.040	1.065
2.5	2587	2462	2233	2148	2027	1914	1.204	1.276	1.352	1.146	1.215	1.286	1.040	1.102	1.167
5	4406	3998	3302	3061	2734	2445	1.439	1.612	1.802	1.306	1.462	1.635	1.079	1.208	1.351
10	6817	5634	3884	3359	2715	2208	2.029	2.511	3.087	1.677	2.075	2.552	1.156	1.431	1.759
20	9314	6433	3223	2509	1790	1347	3.712	5.203	6.915	2.564	3.594	4.776	1.285	1.801	2.393
33	10360	5755	2207	1685	1255	1021	6.148	8.255	10.147	3.415	4.586	5.637	1.310	1.759	2.162
50	10080	4499	1701	1394	1127	960	7.231	8.944	10.500	3.227	3.992	4.686	1.220	1.509	1.772
100	3994	2460	1477	1286	1085	938.5	3.106	3.681	4.256	1.913	2.267	2.621	1.149	1.361	1.574
M / dist: 7.25 / 30															
0.5	123	121.8	119.5	118.6	117.2	115.8	1.037	1.049	1.062	1.027	1.039	1.052	1.008	1.020	1.032
1	235.2	230.6	221.7	218.3	213.2	208.3	1.077	1.103	1.129	1.056	1.082	1.107	1.016	1.040	1.064
2.5	518.4	493.7	448.1	431.2	407	384.4	1.202	1.274	1.349	1.145	1.213	1.284	1.039	1.101	1.166
5	822.3	747	618.1	573.4	513	459.4	1.434	1.603	1.790	1.303	1.456	1.626	1.078	1.205	1.345
10	1159	960.4	666.6	578.5	470.3	385.4	2.003	2.464	3.007	1.660	2.042	2.492	1.152	1.417	1.730
20	1400	977.1	506.9	402.8	298.4	233.9	3.476	4.692	5.985	2.426	3.274	4.177	1.258	1.699	2.167
33	1395	801.1	348.8	281.4	222.8	188.3	4.957	6.261	7.408	2.847	3.596	4.254	1.240	1.566	1.852
50	1236	607.2	287	245.7	206.3	180.1	5.031	5.991	6.863	2.471	2.943	3.371	1.168	1.391	1.594
100	569.7	395.9	261.5	232.6	200.6	177.1	2.449	2.840	3.217	1.702	1.974	2.235	1.124	1.304	1.477
M / dist: 7.25 / 60															
0.5	72.86	72.17	70.78	70.23	69.41	68.6	1.037	1.050	1.062	1.028	1.040	1.052	1.008	1.020	1.032
1	131.8	129.3	124.3	122.4	119.6	116.8	1.077	1.102	1.128	1.056	1.081	1.107	1.016	1.039	1.064
2.5	264.8	252.4	229.3	220.7	208.5	197	1.200	1.270	1.344	1.144	1.211	1.281	1.039	1.100	1.164
5	382.8	348.2	289	268.5	240.6	216	1.426	1.591	1.772	1.297	1.447	1.612	1.076	1.201	1.338
10	477.5	397.6	279.2	243.7	200.2	166.1	1.959	2.385	2.875	1.632	1.986	2.394	1.146	1.395	1.681
20	493.7	351.4	194.4	160	125.4	103.6	3.086	3.937	4.765	2.196	2.802	3.392	1.215	1.550	1.876
33	432	266.1	140.7	120.6	101.4	88.97	3.582	4.260	4.856	2.206	2.624	2.991	1.167	1.388	1.581
50	351.4	206.1	124.2	110.7	96.62	86.5	3.174	3.637	4.062	1.862	2.133	2.383	1.122	1.285	1.436
100	208.3	161.7	117.7	107.1	94.87	85.48	1.945	2.196	2.437	1.510	1.704	1.892	1.099	1.241	1.377
M / dist: 7.25 / 85															
0.5	53.45	52.94	51.92	51.51	50.91	50.32	1.038	1.050	1.062	1.028	1.040	1.052	1.008	1.020	1.032
1	92.5	90.72	87.27	85.93	83.96	82.04	1.076	1.102	1.127	1.056	1.081	1.106	1.016	1.039	1.064
2.5	172.3	164.2	149.4	143.8	135.9	128.5	1.198	1.268	1.341	1.142	1.208	1.278	1.039	1.099	1.163
5	230.8	210.2	175	162.7	146.1	131.5	1.419	1.580	1.755	1.292	1.439	1.598	1.076	1.198	1.331
10	261	218.4	155.3	136.4	113.3	95.24	1.913	2.304	2.740	1.601	1.928	2.293	1.139	1.371	1.631
20	239.6	174.8	103.7	88.21	72.41	62.13	2.716	3.309	3.856	1.982	2.414	2.813	1.176	1.432	1.669
33	193.6	129.4	79.87	70.99	61.89	55.57	2.727	3.128	3.484	1.823	2.091	2.329	1.125	1.291	1.437
50	154.8	106.1	73.46	67.02	59.89	54.5	2.310	2.585	2.840	1.583	1.772	1.947	1.096	1.227	1.348
100	111.1	91.78	70.97	65.56	59.12	54.03	1.695	1.879	2.056	1.400	1.552	1.699	1.083	1.200	1.314
M / dist: 7.25 / 140															
0.5	31.36	31.06	30.46	30.23	29.88	29.53	1.037	1.050	1.062	1.027	1.039	1.052	1.008	1.019	1.031
1	49.42	48.48	46.66	45.95	44.91	43.9	1.076	1.100	1.126	1.055	1.079	1.104	1.015	1.039	1.063
2.5	78.28	74.7	68.08	65.6	62.09	58.78	1.193	1.261	1.332	1.139	1.203	1.271	1.038	1.096	1.158
5	89.26	81.61	68.46	63.9	57.73	52.26	1.397	1.546	1.708	1.277	1.414	1.562	1.071	1.186	1.310
10	82.78	70.4	52.17	46.76	40.16	35.02	1.770	2.061	2.364	1.506	1.753	2.010	1.116	1.299	1.490
20	62.7	49.71	35.48	32.19	28.59	25.97	1.948	2.193	2.414	1.544	1.739	1.914	1.102	1.241	1.366
33	49.06	39.81	30.93	28.83	26.41	24.55	1.702	1.858	1.998	1.381	1.507	1.622	1.073	1.171	1.260
50	43.15	36.56	29.85	28.14	26.04	24.33	1.533	1.657	1.774	1.299	1.404	1.503	1.061	1.146	1.227
100	38.9	34.83	29.45	27.87	25.88	24.22	1.396	1.503	1.606	1.250	1.346	1.438	1.057	1.138	1.216

Tab. A11-5: Scaling factors derived for the kappa correction – Ambraseys et al. (1996) model

Ambraseys et al. (1996) RVT GM for							Resulting scale factors (GM target / GM host) for target (above) and host (below) κ values								
	κ target			κ host			0.00625			0.0125			0.025		
freq	0.00625	0.0125	0.025	0.03	0.0375	0.045	0.03	0.0375	0.045	0.03	0.0375	0.045	0.03	0.0375	0.045
M / dist: 5.5 / 7.5															
0.5	22.4	22.29	22.01	22.25	22.18	22.09	1.007	1.010	1.014	1.002	1.005	1.009	0.989	0.992	0.996
1	85.16	83.81	80.81	83.39	82.54	81.67	1.021	1.032	1.043	1.005	1.015	1.026	0.969	0.979	0.989
2.5	293.5	279.5	253.3	275.6	267.9	260.4	1.065	1.096	1.127	1.014	1.043	1.073	0.919	0.946	0.973
5	564	511.6	421.9	497.6	470.6	445.2	1.133	1.198	1.267	1.028	1.087	1.149	0.848	0.897	0.948
10	930.2	768.3	528.8	727.5	652.8	586.4	1.279	1.425	1.586	1.056	1.177	1.310	0.727	0.810	0.902
20	1319	910.4	454.7	820.2	668.5	548	1.608	1.973	2.407	1.110	1.362	1.661	0.554	0.680	0.830
33	1496	829.7	315.7	707.3	523.3	398.6	2.115	2.859	3.753	1.173	1.586	2.082	0.446	0.603	0.792
50	1475	656.4	243.3	538.3	384	295.7	2.740	3.841	4.988	1.219	1.709	2.220	0.452	0.634	0.823
100	591.5	358.6	210.4	324.2	273.3	237.1	1.824	2.164	2.495	1.106	1.312	1.512	0.649	0.770	0.887
M / dist: 5.5 / 30															
0.5	5.307	5.266	5.177	5.254	5.228	5.202	1.010	1.015	1.020	1.002	1.007	1.012	0.985	0.990	0.995
1	18.95	18.6	17.89	18.5	18.29	18.09	1.024	1.036	1.048	1.005	1.017	1.028	0.967	0.978	0.989
2.5	57.99	55.21	50.05	54.43	52.91	51.44	1.065	1.096	1.127	1.014	1.043	1.073	0.920	0.946	0.973
5	102	92.56	76.44	90.02	85.18	80.62	1.133	1.197	1.265	1.028	1.087	1.148	0.849	0.897	0.948
10	153.4	127	87.79	120.3	108.1	97.24	1.275	1.419	1.578	1.056	1.175	1.306	0.730	0.812	0.903
20	196.7	136.7	69.85	123.5	101.2	83.52	1.593	1.944	2.355	1.107	1.351	1.637	0.566	0.690	0.836
33	205.4	116.4	48.16	100.1	75.68	59.15	2.052	2.714	3.473	1.163	1.538	1.968	0.481	0.636	0.814
50	189.1	89.49	38.73	75.23	56.5	45.53	2.514	3.347	4.153	1.190	1.584	1.966	0.515	0.685	0.851
100	83.03	55.04	34.7	50.53	43.63	38.54	1.643	1.903	2.154	1.089	1.262	1.428	0.687	0.795	0.900
M / dist: 5.5 / 60															
0.5	2.402	2.38	2.334	2.374	2.36	2.347	1.012	1.018	1.023	1.003	1.008	1.014	0.983	0.989	0.994
1	7.892	7.739	7.436	7.695	7.607	7.52	1.026	1.037	1.049	1.006	1.017	1.029	0.966	0.978	0.989
2.5	21.42	20.39	18.5	20.11	19.55	19.01	1.065	1.096	1.127	1.014	1.043	1.073	0.920	0.946	0.973
5	34.27	31.13	25.76	30.29	28.68	27.16	1.131	1.195	1.262	1.028	1.085	1.146	0.850	0.898	0.948
10	46.45	38.56	26.85	36.57	32.92	29.67	1.270	1.411	1.566	1.054	1.171	1.300	0.734	0.816	0.905
20	52.78	37.11	19.68	33.65	27.84	23.23	1.568	1.896	2.272	1.103	1.333	1.598	0.585	0.707	0.847
33	49.92	29.42	13.81	25.69	20.11	16.34	1.943	2.482	3.055	1.145	1.463	1.800	0.538	0.687	0.845
50	42.72	22.47	11.71	19.58	15.7	13.3	2.182	2.721	3.212	1.148	1.431	1.689	0.598	0.746	0.880
100	21.93	15.94	10.86	14.87	13.18	11.88	1.475	1.664	1.846	1.072	1.209	1.342	0.730	0.824	0.914
M / dist: 5.5 / 85															
0.5	2.016	1.997	1.957	1.991	1.979	1.968	1.013	1.019	1.024	1.003	1.009	1.015	0.983	0.989	0.994
1	6.246	6.123	5.883	6.088	6.018	5.949	1.026	1.038	1.050	1.006	1.017	1.029	0.966	0.978	0.989
2.5	15.59	14.85	13.48	14.65	14.24	13.85	1.064	1.095	1.126	1.014	1.043	1.072	0.920	0.947	0.973
5	23.28	21.17	17.54	20.6	19.51	18.48	1.130	1.193	1.260	1.028	1.085	1.146	0.851	0.899	0.949
10	29.14	24.25	17	23.02	20.76	18.75	1.266	1.404	1.554	1.053	1.168	1.293	0.738	0.819	0.907
20	30.16	21.47	11.86	19.55	16.34	13.79	1.543	1.846	2.187	1.098	1.314	1.557	0.607	0.726	0.860
33	26.56	16.35	8.564	14.5	11.73	9.851	1.832	2.264	2.696	1.128	1.394	1.660	0.591	0.730	0.869
50	21.81	12.73	7.54	11.41	9.579	8.376	1.911	2.277	2.604	1.116	1.329	1.520	0.661	0.787	0.900
100	12.9	9.935	7.134	9.37	8.447	7.717	1.377	1.527	1.672	1.060	1.176	1.287	0.761	0.845	0.924
M / dist: 5.5 / 140															
0.5	1.367	1.353	1.325	1.349	1.341	1.333	1.013	1.019	1.026	1.003	1.009	1.015	0.982	0.988	0.994
1	3.801	3.726	3.58	3.704	3.662	3.62	1.026	1.038	1.050	1.006	1.017	1.029	0.967	0.978	0.989
2.5	8.101	7.719	7.014	7.613	7.406	7.204	1.064	1.094	1.125	1.014	1.042	1.071	0.921	0.947	0.974
5	10.53	9.596	7.983	9.343	8.859	8.402	1.127	1.189	1.253	1.027	1.083	1.142	0.854	0.901	0.950
10	11.21	9.402	6.717	8.945	8.108	7.363	1.253	1.383	1.522	1.051	1.160	1.277	0.751	0.828	0.912
20	9.689	7.171	4.406	6.619	5.696	4.968	1.464	1.701	1.950	1.083	1.259	1.443	0.666	0.774	0.887
33	7.668	5.357	3.492	4.936	4.293	3.831	1.553	1.786	2.002	1.085	1.248	1.398	0.707	0.813	0.912
50	6.243	4.539	3.252	4.255	3.829	3.497	1.467	1.630	1.785	1.067	1.185	1.298	0.764	0.849	0.930
100	4.807	4.04	3.163	3.876	3.594	3.359	1.240	1.338	1.431	1.042	1.124	1.203	0.816	0.880	0.942
M / dist: 6.5 / 7.5															
0.5	142.8	141.7	139.3	141.4	140.7	140	1.010	1.015	1.020	1.002	1.007	1.012	0.985	0.990	0.995
1	319.2	313.1	301.1	311.4	307.9	304.4	1.025	1.037	1.049	1.005	1.017	1.029	0.967	0.978	0.989
2.5	776.1	738.9	670.3	728.6	708.4	688.8	1.065	1.096	1.127	1.014	1.043	1.073	0.920	0.946	0.973
5	1328	1205	995.6	1172	1109	1050	1.133	1.197	1.265	1.028	1.087	1.148	0.849	0.898	0.948
10	2056	1699	1173	1610	1445	1299	1.277	1.423	1.583	1.055	1.176	1.308	0.729	0.812	0.903
20	2811	1943	977	1752	1430	1174	1.604	1.966	2.394	1.109	1.359	1.655	0.558	0.683	0.832
33	3133	1743	675.1	1488	1105	846.4	2.106	2.835	3.702	1.171	1.577	2.059	0.454	0.611	0.798
50	3059	1370	524.7	1127	810.8	631	2.714	3.773	4.848	1.216	1.690	2.171	0.466	0.647	0.832
100	1225	756.3	457	687.1	584.3	511	1.783	2.097	2.397	1.101	1.294	1.480	0.665	0.782	0.894
M / dist: 6.5 / 30															
0.5	32.56	32.28	31.7	32.2	32.03	31.86	1.011	1.017	1.022	1.002	1.008	1.013	0.984	0.990	0.995
1	69.28	67.95	65.34	67.57	66.81	66.06	1.025	1.037	1.049	1.006	1.017	1.029	0.967	0.978	0.989
2.5	157.2	149.7	135.9	147.6	143.6	139.6	1.065	1.095	1.126	1.014	1.042	1.072	0.921	0.946	0.973
5	253.5	230.2	190.5	224	212.1	200.8	1.132	1.195	1.262	1.028	1.085	1.146	0.850	0.898	0.949
10	365.3	302.7	209.9	286.9	258	232.2	1.273	1.416	1.573	1.055	1.173	1.304	0.732	0.814	0.904
20	457.4	318.5	164.2	287.9	236.4	195.7	1.589	1.935	2.337	1.106	1.347	1.627	0.570	0.695	0.839
33	472.5	268.9	113.8	231.7	176.1	138.6	2.039	2.683	3.409	1.161	1.527	1.940	0.491	0.646	0.821
50	432.6	206.5	92.58	174.3	132.2	107.7	2.482	3.272	4.017	1.185	1.562	1.917	0.531	0.700	0.860
100	191.2	128.9	83.47	118.8	103.4	92.05	1.609	1.849	2.077	1.085	1.247	1.400	0.703	0.807	0.907
M / dist: 6.5 / 60															
0.5	14.32	14.19	13.92	14.15	14.07	14	1.012	1.018	1.023	1.003	1.009	1.014	0.984	0.989	0.994
1	28.73	28.17	27.09	28.01	27.7	27.39	1.026	1.037	1.049	1.006	1.017	1.028	0.967	0.978	0.989
2.5	59.87	57.04	51.81	56.26	54.72	53.22	1.064	1.094	1.125	1.014	1.042	1.072	0.921	0.947	0.974
5	89.5	81.39	67.48	79.21	75.03	71.09	1.130	1.193	1.259	1.028	1.085	1.145	0.852	0.899	0.949
10	117.7	97.81	68.39	92.81	83.63	75.47	1.268	1.407	1.560	1.054	1.170	1.296	0.737	0.818	0.906
20	131.6	92.83	49.9	84.29	69.95	58.62	1.561	1.881	2.245	1.101	1.327	1.584	0.592	0.713	0.851
33	123.7	73.46	35.53	64.35	50.77	41.64	1.922	2.436	2.971	1.142	1.447	1.764	0.552	0.700	0.853
50	105.7	56.39	30.52	49.4	40.07	34.32	2.140	2.638	3.080	1.141	1.407	1.643	0.618	0.762	0.889
100	55.05	40.65	28.44	38.09	34.01	30.88	1.445	1.619	1.783	1.067	1.195	1.316	0.747	0.836	0.921

Ambraseys et al. (1996) RVT GM for							Resulting scale factors (GM target / GM host) for target (above) and host (below) κ values								
	κ target			κ host			0.00625			0.0125			0.025		
freq	0.00625	0.0125	0.025	0.03	0.0375	0.045	0.03	0.0375	0.045	0.03	0.0375	0.045	0.03	0.0375	0.045
M / dist: 6.5 / 85															
0.5	11.9	11.79	11.56	11.75	11.69	11.62	1.013	1.018	1.024	1.003	1.009	1.015	0.984	0.989	0.995
1	22.82	22.38	21.53	22.26	22.01	21.76	1.025	1.037	1.049	1.005	1.017	1.028	0.967	0.978	0.989
2.5	44.5	42.42	38.55	41.83	40.7	39.59	1.064	1.093	1.124	1.014	1.042	1.071	0.922	0.947	0.974
5	62.61	56.99	47.35	55.48	52.59	49.85	1.129	1.191	1.256	1.027	1.084	1.143	0.853	0.900	0.950
10	76.44	63.75	45.05	60.55	54.68	49.46	1.262	1.398	1.545	1.053	1.166	1.289	0.744	0.824	0.911
20	78.22	55.94	31.43	51.05	42.85	36.38	1.532	1.825	2.150	1.096	1.305	1.538	0.616	0.733	0.864
33	68.67	42.74	23.23	38.09	31.14	26.43	1.803	2.205	2.598	1.122	1.373	1.617	0.610	0.746	0.879
50	56.46	33.63	20.69	30.33	25.77	22.78	1.862	2.191	2.478	1.109	1.305	1.476	0.682	0.803	0.908
100	34.05	26.66	19.66	25.24	22.94	21.11	1.349	1.484	1.613	1.056	1.162	1.263	0.779	0.857	0.931
M / dist: 6.5 / 140															
0.5	8.03	7.953	7.799	7.93	7.886	7.842	1.013	1.018	1.024	1.003	1.008	1.014	0.983	0.989	0.995
1	14.09	13.82	13.29	13.74	13.59	13.44	1.025	1.037	1.048	1.006	1.017	1.028	0.967	0.978	0.989
2.5	23.93	22.82	20.77	22.51	21.91	21.33	1.063	1.092	1.122	1.014	1.042	1.070	0.923	0.948	0.974
5	29.63	27.04	22.58	26.34	25	23.73	1.125	1.185	1.249	1.027	1.082	1.139	0.857	0.903	0.952
10	31	26.1	18.85	24.86	22.6	20.59	1.247	1.372	1.506	1.050	1.155	1.268	0.758	0.834	0.915
20	26.73	20	12.71	18.54	16.1	14.18	1.442	1.660	1.885	1.079	1.242	1.410	0.686	0.789	0.896
33	21.31	15.23	10.36	14.13	12.45	11.25	1.508	1.712	1.894	1.078	1.223	1.354	0.733	0.832	0.921
50	17.57	13.11	9.727	12.37	11.22	10.37	1.420	1.566	1.694	1.060	1.168	1.264	0.786	0.867	0.938
100	13.81	11.79	9.483	11.36	10.62	9.999	1.216	1.300	1.381	1.038	1.110	1.179	0.835	0.893	0.948
M / dist: 7.25 / 7.5															
0.5	341.7	338.5	332.1	337.6	335.7	333.9	1.012	1.018	1.023	1.003	1.008	1.014	0.984	0.989	0.995
1	647.8	635.2	610.7	631.6	624.5	617.5	1.026	1.037	1.049	1.006	1.017	1.029	0.967	0.978	0.989
2.5	1417	1350	1225	1331	1294	1258	1.065	1.095	1.126	1.014	1.043	1.073	0.920	0.947	0.974
5	2329	2114	1747	2056	1946	1842	1.133	1.197	1.264	1.028	1.086	1.148	0.850	0.898	0.948
10	3518	2910	2010	2756	2476	2226	1.276	1.421	1.580	1.056	1.175	1.307	0.729	0.812	0.903
20	4738	3277	1652	2955	2413	1984	1.603	1.964	2.388	1.109	1.358	1.652	0.559	0.685	0.833
33	5243	2920	1138	2494	1854	1423	2.102	2.828	3.684	1.171	1.575	2.052	0.456	0.614	0.800
50	5095	2286	886.8	1883	1359	1062	2.706	3.749	4.798	1.214	1.682	2.153	0.471	0.653	0.835
100	2040	1269	775.6	1155	985.5	864.6	1.766	2.070	2.359	1.099	1.288	1.468	0.672	0.787	0.897
M / dist: 7.25 / 30															
0.5	77.36	76.63	75.17	76.42	76	75.58	1.012	1.018	1.024	1.003	1.008	1.014	0.984	0.989	0.995
1	141.7	139	133.7	138.2	136.7	135.1	1.025	1.037	1.049	1.006	1.017	1.029	0.967	0.978	0.990
2.5	293.7	279.7	254	275.8	268.3	260.9	1.065	1.095	1.126	1.014	1.042	1.072	0.921	0.947	0.974
5	457.6	415.8	344.2	404.6	383.1	362.8	1.131	1.194	1.261	1.028	1.085	1.146	0.851	0.898	0.949
10	646.5	535.8	372.1	508	456.9	411.5	1.273	1.415	1.571	1.055	1.173	1.302	0.732	0.814	0.904
20	799.5	557.1	288	503.7	413.9	342.8	1.587	1.932	2.332	1.106	1.346	1.625	0.572	0.696	0.840
33	820.5	467.8	199.5	403.3	307.1	242.3	2.034	2.672	3.386	1.160	1.523	1.931	0.495	0.650	0.823
50	748.7	358.5	163	303.1	230.8	188.8	2.470	3.244	3.966	1.183	1.553	1.899	0.538	0.706	0.863
100	331.6	225.1	147.4	207.9	181.6	162.1	1.595	1.826	2.046	1.083	1.240	1.389	0.709	0.812	0.909
M / dist: 7.25 / 60															
0.5	33.9	33.58	32.94	33.49	33.3	33.12	1.012	1.018	1.024	1.003	1.008	1.014	0.984	0.989	0.995
1	59.45	58.3	56.08	57.97	57.33	56.69	1.026	1.037	1.049	1.006	1.017	1.028	0.967	0.978	0.989
2.5	114.7	109.3	99.3	107.8	104.8	102	1.064	1.094	1.125	1.014	1.043	1.072	0.921	0.948	0.974
5	166.7	151.7	125.8	147.6	139.8	132.5	1.129	1.192	1.258	1.028	1.085	1.145	0.852	0.900	0.949
10	215.7	179.4	125.6	170.2	153.4	138.5	1.267	1.406	1.557	1.054	1.169	1.295	0.738	0.819	0.907
20	238.9	168.6	91.07	153.2	127.3	106.8	1.559	1.877	2.237	1.101	1.324	1.579	0.594	0.715	0.853
33	223.5	133	65.03	116.6	92.28	75.92	1.917	2.422	2.944	1.141	1.441	1.752	0.558	0.705	0.857
50	190.4	102.1	56.12	89.65	73.05	62.84	2.124	2.606	3.030	1.139	1.398	1.625	0.626	0.768	0.893
100	99.69	74.14	52.44	69.59	62.35	56.78	1.433	1.599	1.756	1.065	1.189	1.306	0.754	0.841	0.924
M / dist: 7.25 / 85															
0.5	28.18	27.91	27.37	27.83	27.67	27.52	1.013	1.018	1.024	1.003	1.009	1.014	0.983	0.989	0.995
1	47.67	46.76	44.98	46.5	45.98	45.47	1.025	1.037	1.048	1.006	1.017	1.028	0.967	0.978	0.989
2.5	86.73	82.68	75.19	81.55	79.35	77.21	1.064	1.093	1.123	1.014	1.042	1.071	0.922	0.948	0.974
5	119.1	108.5	90.2	105.6	100.1	94.95	1.128	1.190	1.254	1.027	1.084	1.143	0.854	0.901	0.950
10	143.4	119.7	84.55	113.7	102.7	92.99	1.261	1.396	1.542	1.053	1.166	1.287	0.744	0.823	0.909
20	145.6	104.3	58.96	95.22	80.04	68.11	1.529	1.819	2.138	1.095	1.303	1.531	0.619	0.737	0.866
33	127.3	79.58	43.82	71.01	58.28	49.67	1.793	2.184	2.563	1.121	1.365	1.602	0.617	0.752	0.882
50	104.6	62.74	39.21	56.73	48.43	43	1.844	2.160	2.433	1.106	1.295	1.459	0.691	0.810	0.912
100	63.52	50.08	37.33	47.51	43.31	39.98	1.337	1.467	1.589	1.054	1.156	1.253	0.786	0.862	0.934
M / dist: 7.25 / 140															
0.5	19.11	18.92	18.56	18.87	18.77	18.66	1.013	1.018	1.024	1.003	1.008	1.014	0.984	0.989	0.995
1	29.97	29.4	28.3	29.24	28.92	28.6	1.025	1.036	1.048	1.005	1.017	1.028	0.968	0.979	0.990
2.5	48.08	45.87	41.79	45.26	44.06	42.89	1.062	1.091	1.121	1.013	1.041	1.069	0.923	0.948	0.974
5	58.46	53.38	44.64	52.01	49.38	46.91	1.124	1.184	1.246	1.026	1.081	1.138	0.858	0.904	0.952
10	60.58	51.06	37.03	48.67	44.28	40.39	1.245	1.368	1.500	1.049	1.153	1.264	0.761	0.836	0.917
20	51.99	39.07	25.14	36.26	31.59	27.93	1.434	1.646	1.861	1.077	1.237	1.399	0.693	0.796	0.900
33	41.48	29.89	20.67	27.8	24.63	22.34	1.492	1.684	1.857	1.075	1.214	1.338	0.744	0.839	0.925
50	34.3	25.87	19.47	24.46	22.3	20.7	1.402	1.538	1.657	1.058	1.160	1.250	0.796	0.873	0.941
100	27.19	23.38	19	22.56	21.15	19.98	1.205	1.286	1.361	1.036	1.105	1.170	0.842	0.898	0.951

Tab. A11-6: Scaling factors derived for the kappa correction – Berge-Thierry et al. (2000) model

Berge-Thierry et al. (2000) RVT GM for							Resulting scale factors (GM target / GM host) for target (above) and host (below) κ values								
	κ target			κ host			0.00625			0.0125			0.025		
freq	0.00625	0.0125	0.025	0.03	0.0375	0.045	0.03	0.0375	0.045	0.03	0.0375	0.045	0.03	0.0375	0.045
M / dist: 5.5 / 7.5															
0.5	22.59	22.47	22.19	22.35	22.25	22.14	1.011	1.015	1.020	1.005	1.010	1.015	0.993	0.997	1.002
1	86.05	84.69	81.66	83.38	82.28	81.17	1.032	1.046	1.060	1.016	1.029	1.043	0.979	0.992	1.006
2.5	298	283.8	257.2	271.7	262.3	253.2	1.097	1.136	1.177	1.045	1.082	1.121	0.947	0.981	1.016
5	575.3	521.9	430.3	479.2	447.1	417.3	1.201	1.287	1.379	1.089	1.167	1.251	0.898	0.962	1.031
10	954.7	788.3	542.4	667.8	583.9	511.4	1.430	1.635	1.867	1.180	1.350	1.541	0.812	0.929	1.061
20	1365	941.2	469.3	686.8	536.1	423.1	1.987	2.546	3.226	1.370	1.756	2.225	0.683	0.875	1.109
33	1559	863	326	538.7	384.5	289.2	2.894	4.055	5.391	1.602	2.244	2.984	0.605	0.848	1.127
50	1546	684.8	250.3	394.7	286.9	227.9	3.917	5.389	6.784	1.735	2.387	3.005	0.634	0.872	1.098
100	615.6	369.9	215.7	279.7	234.6	202.6	2.201	2.624	3.038	1.322	1.577	1.826	0.771	0.919	1.065
M / dist: 5.5 / 30															
0.5	5.483	5.44	5.346	5.4	5.365	5.331	1.015	1.022	1.029	1.007	1.014	1.020	0.990	0.996	1.003
1	19.77	19.4	18.66	19.07	18.81	18.54	1.037	1.051	1.066	1.017	1.031	1.046	0.979	0.992	1.006
2.5	61.6	58.64	53.15	56.15	54.2	52.33	1.097	1.137	1.177	1.044	1.082	1.121	0.947	0.981	1.016
5	110.3	100.1	82.66	92.01	85.88	80.18	1.199	1.284	1.376	1.088	1.166	1.248	0.898	0.963	1.031
10	170.2	140.7	97.14	119.4	104.5	91.66	1.425	1.629	1.857	1.178	1.346	1.535	0.814	0.930	1.060
20	225.1	156	79.03	114.5	89.91	71.5	1.966	2.504	3.148	1.362	1.735	2.182	0.690	0.879	1.105
33	241.5	135.8	54.4	86.57	63.25	48.81	2.790	3.818	4.948	1.569	2.147	2.782	0.628	0.860	1.115
50	227.6	105.1	43.06	64.04	48.49	39.67	3.554	4.694	5.737	1.641	2.167	2.649	0.672	0.888	1.085
100	96.17	61.89	38.12	48.24	41.16	36.01	1.994	2.336	2.671	1.283	1.504	1.719	0.790	0.926	1.059
M / dist: 5.5 / 60															
0.5	2.564	2.54	2.491	2.518	2.501	2.483	1.018	1.025	1.033	1.009	1.016	1.023	0.989	0.996	1.003
1	8.586	8.42	8.09	8.274	8.155	8.038	1.038	1.053	1.068	1.018	1.032	1.048	0.978	0.992	1.006
2.5	24.16	23	20.86	22.03	21.27	20.54	1.097	1.136	1.176	1.044	1.081	1.120	0.947	0.981	1.016
5	40.11	36.43	30.11	33.49	31.27	29.21	1.198	1.283	1.373	1.088	1.165	1.247	0.899	0.963	1.031
10	57.06	47.29	32.8	40.19	35.25	30.97	1.420	1.619	1.842	1.177	1.342	1.527	0.816	0.930	1.059
20	68.9	48.23	24.97	35.62	28.24	22.71	1.934	2.440	3.034	1.354	1.708	2.124	0.701	0.884	1.100
33	68.57	39.49	17.3	26.04	19.69	15.72	2.633	3.482	4.362	1.517	2.006	2.512	0.664	0.879	1.101
50	60.89	30.11	14.23	19.79	15.72	13.28	3.077	3.873	4.585	1.521	1.915	2.267	0.719	0.905	1.072
100	28.52	19.79	12.97	15.96	13.88	12.33	1.787	2.055	2.313	1.240	1.426	1.605	0.813	0.934	1.052
M / dist: 5.5 / 85															
0.5	2.211	2.189	2.145	2.17	2.154	2.138	1.019	1.026	1.034	1.009	1.016	1.024	0.988	0.996	1.003
1	7.038	6.9	6.629	6.779	6.682	6.586	1.038	1.053	1.069	1.018	1.033	1.048	0.978	0.992	1.007
2.5	18.49	17.61	15.97	16.87	16.28	15.73	1.096	1.136	1.175	1.044	1.082	1.120	0.947	0.981	1.015
5	29.08	26.42	21.87	24.3	22.7	21.22	1.197	1.281	1.370	1.087	1.164	1.245	0.900	0.963	1.031
10	38.93	32.32	22.51	27.52	24.17	21.28	1.415	1.611	1.829	1.174	1.337	1.519	0.818	0.931	1.058
20	43.79	30.81	16.38	23.01	18.41	14.97	1.903	2.379	2.925	1.339	1.674	2.058	0.712	0.890	1.094
33	41.16	24.31	11.49	16.56	12.89	10.58	2.486	3.193	3.890	1.468	1.886	2.298	0.694	0.891	1.086
50	35.08	18.56	9.769	12.96	10.65	9.192	2.707	3.294	3.816	1.432	1.743	2.019	0.754	0.917	1.063
100	18.14	13.28	9.07	10.94	9.65	8.659	1.658	1.880	2.095	1.214	1.376	1.534	0.829	0.940	1.047
M / dist: 5.5 / 140															
0.5	1.59	1.574	1.542	1.56	1.548	1.536	1.019	1.027	1.035	1.009	1.017	1.025	0.988	0.996	1.004
1	4.625	4.533	4.355	4.454	4.39	4.328	1.038	1.054	1.069	1.018	1.033	1.047	0.978	0.992	1.006
2.5	10.71	10.2	9.263	9.778	9.444	9.122	1.095	1.134	1.174	1.043	1.080	1.118	0.947	0.981	1.015
5	15.15	13.79	11.44	12.7	11.87	11.1	1.193	1.276	1.365	1.086	1.162	1.242	0.901	0.964	1.031
10	17.93	14.96	10.54	12.79	11.28	9.98	1.402	1.590	1.797	1.170	1.326	1.499	0.824	0.934	1.056
20	17.48	12.56	7.125	9.616	7.887	6.599	1.818	2.216	2.649	1.306	1.592	1.903	0.741	0.903	1.080
33	14.77	9.396	5.281	6.941	5.754	4.968	2.128	2.567	2.973	1.354	1.633	1.891	0.761	0.918	1.063
50	11.94	7.468	4.745	5.834	5.063	4.529	2.047	2.358	2.636	1.280	1.475	1.649	0.813	0.937	1.048
100	7.704	6.126	4.535	5.28	4.771	4.365	1.459	1.615	1.765	1.160	1.284	1.403	0.859	0.951	1.039
M / dist: 6.5 / 7.5															
0.5	144	142.8	140.4	141.8	140.9	140	1.016	1.022	1.029	1.007	1.013	1.020	0.990	0.996	1.003
1	322.5	316.4	304.3	311	306.7	302.4	1.037	1.052	1.066	1.017	1.032	1.046	0.978	0.992	1.006
2.5	787.8	750.1	680.4	718.5	693.7	669.9	1.096	1.136	1.176	1.044	1.081	1.120	0.947	0.981	1.016
5	1354	1229	1015	1130	1055	984.9	1.198	1.283	1.375	1.088	1.165	1.248	0.898	0.962	1.031
10	2110	1744	1203	1478	1294	1135	1.428	1.631	1.859	1.180	1.348	1.537	0.814	0.930	1.060
20	2907	2009	1008	1469	1149	910.3	1.979	2.530	3.193	1.368	1.748	2.207	0.686	0.877	1.107
33	3265	1813	696.8	1137	817.6	620.9	2.872	3.993	5.258	1.595	2.217	2.920	0.613	0.852	1.122
50	3207	1429	539.4	833	613.4	494.2	3.850	5.228	6.489	1.715	2.330	2.892	0.648	0.879	1.091
100	1275	779.8	468	597.6	506.4	441.6	2.134	2.518	2.887	1.305	1.540	1.766	0.783	0.924	1.060
M / dist: 6.5 / 30															
0.5	33.6	33.32	32.72	33.06	32.84	32.62	1.016	1.023	1.030	1.008	1.015	1.021	0.990	0.996	1.003
1	72.23	70.85	68.12	69.64	68.66	67.7	1.037	1.052	1.067	1.017	1.032	1.047	0.978	0.992	1.006
2.5	166.9	159	144.3	152.3	147.1	142	1.096	1.135	1.175	1.044	1.081	1.120	0.947	0.981	1.016
5	274.2	249	205.9	229	213.8	199.8	1.197	1.283	1.372	1.087	1.165	1.246	0.899	0.963	1.031
10	405	335.3	232.1	284.7	249.5	219.1	1.423	1.623	1.848	1.178	1.344	1.530	0.815	0.930	1.059
20	523.2	363.3	185.5	267.3	210.5	168.1	1.957	2.486	3.112	1.359	1.726	2.161	0.694	0.881	1.104
33	555.5	313.3	128.1	201	148.1	115.5	2.764	3.751	4.810	1.559	2.115	2.713	0.637	0.865	1.109
50	520.3	242	102.5	149.4	114.6	94.93	3.483	4.540	5.481	1.620	2.112	2.549	0.686	0.894	1.080
100	220.9	144.4	91.34	114	98.14	86.62	1.938	2.251	2.550	1.267	1.471	1.667	0.801	0.931	1.054
M / dist: 6.5 / 60															
0.5	15.25	15.11	14.83	14.99	14.89	14.79	1.017	1.024	1.031	1.008	1.015	1.022	0.989	0.996	1.003
1	31.23	30.62	29.45	30.1	29.68	29.26	1.038	1.052	1.067	1.017	1.032	1.046	0.978	0.992	1.006
2.5	67.47	64.28	58.37	61.6	59.5	57.48	1.095	1.134	1.174	1.044	1.080	1.118	0.948	0.981	1.015
5	104.7	95.15	78.79	87.54	81.8	76.47	1.196	1.280	1.369	1.087	1.163	1.244	0.900	0.963	1.030
10	144.4	119.8	83.4	102	89.56	78.82	1.416	1.612	1.832	1.175	1.338	1.520	0.818	0.931	1.058
20	171.6	120.2	63.01	89.26	71.04	57.47	1.922	2.416	2.986	1.347	1.692	2.092	0.706	0.887	1.096
33	169.7	98.23	44.04	65.35	49.9	40.32	2.597	3.401	4.209	1.503	1.969	2.436	0.674	0.883	1.092
50	150.2	75.06	36.75	50.1	40.32	34.46	2.998	3.725	4.359	1.498	1.862	2.178	0.734	0.911	1.066
100	71.15	50.12	33.68	40.9	35.89	32.14	1.740	1.982	2.214	1.225	1.396	1.559	0.823	0.938	1.048

Berge-Thierry et al. (2000) RVT GM for							Resulting scale factors (GM target / GM host) for target (above) and host (below) κ values								
	κ target			κ host			0.00625			0.0125			0.025		
freq	0.00625	0.0125	0.025	0.03	0.0375	0.045	0.03	0.0375	0.045	0.03	0.0375	0.045	0.03	0.0375	0.045
M / dist: 6.5 / 85															
0.5	13.01	12.89	12.65	12.78	12.7	12.61	1.018	1.024	1.032	1.009	1.015	1.022	0.990	0.996	1.003
1	25.69	25.19	24.22	24.76	24.41	24.07	1.038	1.052	1.067	1.017	1.032	1.047	0.978	0.992	1.006
2.5	52.71	50.22	45.62	48.13	46.5	44.92	1.095	1.134	1.173	1.043	1.080	1.118	0.948	0.981	1.016
5	78.12	71.05	58.91	65.4	61.15	57.19	1.194	1.278	1.366	1.086	1.162	1.242	0.901	0.963	1.030
10	102	84.8	59.32	72.31	63.62	56.11	1.411	1.603	1.818	1.173	1.333	1.511	0.820	0.932	1.057
20	113.3	79.99	43.09	60.01	48.26	39.52	1.888	2.348	2.867	1.333	1.657	2.024	0.718	0.893	1.090
33	106	63.09	30.72	43.47	34.24	28.45	2.438	3.096	3.726	1.451	1.843	2.218	0.707	0.897	1.080
50	90.29	48.45	26.44	34.42	28.65	25	2.623	3.151	3.612	1.408	1.691	1.938	0.768	0.923	1.058
100	47.39	35.14	24.68	29.37	26.19	23.65	1.614	1.809	2.004	1.196	1.342	1.486	0.840	0.942	1.044
M / dist: 6.5 / 140															
0.5	9.309	9.22	9.041	9.141	9.077	9.013	1.018	1.026	1.033	1.009	1.016	1.023	0.989	0.996	1.003
1	17.1	16.77	16.13	16.48	16.26	16.03	1.038	1.052	1.067	1.018	1.031	1.046	0.979	0.992	1.006
2.5	31.56	30.09	27.36	28.85	27.88	26.95	1.094	1.132	1.171	1.043	1.079	1.117	0.948	0.981	1.015
5	42.51	38.72	32.21	35.69	33.41	31.29	1.191	1.272	1.359	1.085	1.159	1.237	0.902	0.964	1.029
10	49.39	41.28	29.28	35.39	31.31	27.77	1.396	1.577	1.779	1.166	1.318	1.486	0.827	0.935	1.054
20	47.8	34.55	20.05	26.68	22.07	18.66	1.792	2.166	2.562	1.295	1.565	1.852	0.751	0.908	1.074
33	40.4	26.08	15.24	19.59	16.47	14.41	2.062	2.453	2.804	1.331	1.583	1.810	0.778	0.925	1.058
50	32.81	21	13.83	16.7	14.67	13.26	1.965	2.237	2.474	1.257	1.431	1.584	0.828	0.943	1.043
100	21.63	17.46	13.27	15.23	13.89	12.82	1.420	1.557	1.687	1.146	1.257	1.362	0.871	0.955	1.035
M / dist: 7.25 / 7.5															
0.5	344.4	341.2	334.7	338.3	336	333.7	1.018	1.025	1.032	1.009	1.015	1.022	0.989	0.996	1.003
1	654.6	641.8	617.1	630.8	622	613.2	1.038	1.052	1.068	1.017	1.032	1.047	0.978	0.992	1.006
2.5	1439	1370	1243	1313	1268	1224	1.096	1.135	1.176	1.043	1.080	1.119	0.947	0.980	1.016
5	2375	2156	1782	1982	1850	1729	1.198	1.284	1.374	1.088	1.165	1.247	0.899	0.963	1.031
10	3611	2985	2061	2532	2217	1945	1.426	1.629	1.857	1.179	1.346	1.535	0.814	0.930	1.060
20	4902	3388	1704	2479	1941	1540	1.977	2.526	3.183	1.367	1.745	2.200	0.687	0.878	1.106
33	5462	3036	1174	1908	1375	1048	2.863	3.972	5.212	1.591	2.208	2.897	0.615	0.854	1.120
50	5341	2384	911	1396	1033	836.8	3.826	5.170	6.383	1.708	2.308	2.849	0.653	0.882	1.089
100	2121	1308	793.9	1008	857.4	750.3	2.104	2.474	2.827	1.298	1.526	1.743	0.788	0.926	1.058
M / dist: 7.25 / 30															
0.5	79.84	79.09	77.58	78.43	77.88	77.34	1.018	1.025	1.032	1.008	1.016	1.023	0.989	0.996	1.003
1	147.8	144.9	139.3	142.4	140.4	138.5	1.038	1.053	1.067	1.018	1.032	1.046	0.978	0.992	1.006
2.5	311.8	296.9	269.6	284.5	274.8	265.5	1.096	1.135	1.174	1.044	1.080	1.118	0.948	0.981	1.015
5	495	449.7	372	413.5	386.3	361	1.197	1.281	1.371	1.088	1.164	1.246	0.900	0.963	1.030
10	716.7	593.5	411.3	504.2	442	388.4	1.421	1.621	1.845	1.177	1.343	1.528	0.816	0.931	1.059
20	914.4	635.3	325.1	467.8	368.8	295	1.955	2.479	3.100	1.358	1.723	2.154	0.695	0.882	1.102
33	964.6	544.7	224.3	350.3	258.8	202.6	2.754	3.727	4.761	1.555	2.105	2.689	0.640	0.867	1.107
50	900.2	419.9	180.1	260.4	200.8	167.2	3.457	4.483	5.384	1.613	2.091	2.511	0.692	0.897	1.077
100	382.7	252	161.1	199.9	172.8	153	1.914	2.215	2.501	1.261	1.458	1.647	0.806	0.932	1.053
M / dist: 7.25 / 60															
0.5	36.11	35.77	35.09	35.47	35.22	34.98	1.018	1.025	1.032	1.008	1.016	1.023	0.989	0.996	1.003
1	64.6	63.35	60.93	62.27	61.4	60.55	1.037	1.052	1.067	1.017	1.032	1.046	0.978	0.992	1.006
2.5	129.2	123.1	111.8	118	114	110.1	1.095	1.133	1.173	1.043	1.080	1.118	0.947	0.981	1.015
5	195	177.2	146.9	163.1	152.4	142.6	1.196	1.280	1.367	1.086	1.163	1.243	0.901	0.964	1.030
10	264.6	219.6	153.1	187	164.3	144.7	1.415	1.610	1.829	1.174	1.337	1.518	0.819	0.932	1.058
20	311.4	218.1	114.8	162.2	129.3	104.8	1.920	2.408	2.971	1.345	1.687	2.081	0.708	0.888	1.095
33	306.3	177.6	80.34	118.5	90.82	73.7	2.585	3.373	4.156	1.499	1.956	2.410	0.678	0.885	1.090
50	270.4	135.6	67.33	91.05	73.66	63.26	2.970	3.671	4.274	1.489	1.841	2.144	0.739	0.914	1.064
100	128.5	91.14	61.89	74.74	65.82	59.14	1.719	1.952	2.173	1.219	1.385	1.541	0.828	0.940	1.046
M / dist: 7.25 / 85															
0.5	30.81	30.52	29.93	30.26	30.05	29.84	1.018	1.025	1.033	1.009	1.016	1.023	0.989	0.996	1.003
1	53.62	52.59	50.58	51.69	50.97	50.27	1.037	1.052	1.067	1.017	1.032	1.046	0.979	0.992	1.006
2.5	102.7	97.83	88.91	93.79	90.62	87.56	1.095	1.133	1.173	1.043	1.080	1.117	0.948	0.981	1.015
5	148.6	135.1	112.1	124.4	116.4	108.9	1.195	1.277	1.365	1.086	1.161	1.241	0.901	0.963	1.029
10	191.3	159.1	111.5	135.7	119.5	105.5	1.410	1.601	1.813	1.172	1.331	1.508	0.822	0.933	1.057
20	210.8	148.9	80.58	111.9	90.14	73.99	1.884	2.339	2.849	1.331	1.652	2.012	0.720	0.894	1.089
33	196.4	117.1	57.61	81.01	64.08	53.5	2.424	3.065	3.671	1.446	1.827	2.189	0.711	0.899	1.077
50	166.9	90	49.84	64.34	53.84	47.22	2.594	3.100	3.535	1.399	1.672	1.906	0.775	0.926	1.055
100	88.04	65.71	46.63	55.2	49.28	44.75	1.595	1.787	1.967	1.190	1.333	1.468	0.845	0.946	1.042
M / dist: 7.25 / 140															
0.5	22.12	21.92	21.49	21.73	21.58	21.43	1.018	1.025	1.032	1.009	1.016	1.023	0.989	0.996	1.003
1	36.34	35.64	34.3	35.04	34.56	34.08	1.037	1.052	1.066	1.017	1.031	1.046	0.979	0.992	1.006
2.5	63.35	60.41	54.96	57.94	56.01	54.14	1.093	1.131	1.170	1.043	1.079	1.116	0.949	0.981	1.015
5	83.76	76.33	63.56	70.39	65.91	61.75	1.190	1.271	1.356	1.084	1.158	1.236	0.903	0.964	1.029
10	96.32	80.58	57.29	69.15	61.22	54.37	1.393	1.573	1.772	1.165	1.316	1.482	0.828	0.936	1.054
20	92.67	67.14	39.27	51.98	43.14	36.61	1.783	2.148	2.531	1.292	1.556	1.834	0.755	0.910	1.073
33	78.19	50.7	30.04	38.32	32.39	28.48	2.040	2.414	2.745	1.323	1.565	1.780	0.784	0.927	1.055
50	63.51	40.98	27.39	32.82	28.98	26.31	1.935	2.192	2.414	1.249	1.414	1.558	0.835	0.945	1.041
100	42.19	34.29	26.32	30.05	27.5	25.46	1.404	1.534	1.657	1.141	1.247	1.347	0.876	0.957	1.034

Tab. A11-7: Scaling factors derived for the kappa correction – Lussou et al. (2001) model

Lussou et al. (2001) RVT GM for							Resulting scale factors (GM target / GM host) for target (above) and host (below) κ values								
	κ target			κ host			0.00625			0.0125			0.025		
freq	0.00625	0.0125	0.025	0.03	0.0375	0.045	0.03	0.0375	0.045	0.03	0.0375	0.045	0.03	0.0375	0.045
M / dist: 5.5 / 7.5															
0.5	8.902	8.703	8.398	8.33	8.192	8.064	1.069	1.087	1.104	1.045	1.062	1.079	1.008	1.025	1.041
1	39.15	38.26	36.62	36.22	35.36	34.52	1.081	1.107	1.134	1.056	1.082	1.108	1.011	1.036	1.061
2.5	215.9	205.2	185.5	180.8	170.8	161.4	1.194	1.264	1.338	1.135	1.201	1.271	1.026	1.086	1.149
5	500.8	453.6	372.9	354.8	317.9	285	1.411	1.575	1.757	1.278	1.427	1.592	1.051	1.173	1.308
10	904	744.9	509.6	463.1	375.5	305.6	1.952	2.407	2.958	1.609	1.984	2.438	1.100	1.357	1.668
20	1354	929.8	455.8	383.9	267.9	193.7	3.527	5.054	6.990	2.422	3.471	4.800	1.187	1.701	2.353
33	1589	871.3	312.4	253.9	174.9	132.8	6.258	9.085	11.965	3.432	4.982	6.561	1.230	1.786	2.352
100	614.7	352	192.6	172.3	139.3	116.3	3.568	4.413	5.285	2.043	2.527	3.027	1.118	1.383	1.656
M / dist: 5.5 / 30															
0.5	2.146	2.105	2.038	2.023	1.991	1.961	1.061	1.078	1.094	1.041	1.057	1.073	1.007	1.024	1.039
1	9.162	8.953	8.565	8.47	8.265	8.067	1.082	1.109	1.136	1.057	1.083	1.110	1.011	1.036	1.062
2.5	46.41	44.11	39.88	38.87	36.72	34.7	1.194	1.264	1.337	1.135	1.201	1.271	1.026	1.086	1.149
5	101.4	91.9	75.59	71.94	64.47	57.82	1.410	1.573	1.754	1.277	1.425	1.589	1.051	1.172	1.307
10	173.2	142.8	97.88	89	72.25	58.88	1.946	2.397	2.942	1.604	1.976	2.425	1.100	1.355	1.662
20	245.2	168.8	83.43	70.47	49.58	36.2	3.479	4.946	6.773	2.395	3.405	4.663	1.184	1.683	2.305
33	275.3	152.1	56.34	46.3	32.65	25.24	5.946	8.432	10.907	3.285	4.658	6.026	1.217	1.726	2.232
50	268.2	118.7	42.3	36.32	28.02	23.01	7.384	9.572	11.656	3.268	4.236	5.159	1.165	1.510	1.838
100	105.7	63.5	36.11	32.51	26.55	22.35	3.251	3.981	4.729	1.953	2.392	2.841	1.111	1.360	1.616
M / dist: 5.5 / 60															
0.5	1.027	1.01	0.981	0.974	0.959	0.945	1.054	1.071	1.087	1.037	1.053	1.069	1.007	1.023	1.038
1	4.152	4.059	3.884	3.841	3.748	3.659	1.081	1.108	1.135	1.057	1.083	1.109	1.011	1.036	1.061
2.5	19.3	18.35	16.59	16.17	15.28	14.45	1.194	1.263	1.336	1.135	1.201	1.270	1.026	1.086	1.148
5	39.66	35.94	29.59	28.16	25.25	22.66	1.408	1.571	1.750	1.276	1.423	1.586	1.051	1.172	1.306
10	63.59	52.5	36.07	32.82	26.69	21.79	1.938	2.383	2.918	1.600	1.967	2.409	1.099	1.351	1.655
20	84.03	58.09	29.06	24.65	17.55	13.01	3.409	4.788	6.459	2.357	3.310	4.465	1.179	1.656	2.234
33	89.13	49.87	19.4	16.2	11.78	9.317	5.502	7.566	9.566	3.078	4.233	5.353	1.198	1.647	2.082
50	82.82	38.01	14.99	13.08	10.33	8.608	6.332	8.017	9.621	2.906	3.680	4.416	1.146	1.451	1.741
100	34.53	22.02	13.14	11.91	9.855	8.377	2.899	3.504	4.122	1.849	2.234	2.629	1.103	1.333	1.569
M / dist: 5.5 / 85															
0.5	0.684	0.674	0.655	0.651	0.641	0.632	1.051	1.067	1.082	1.035	1.051	1.066	1.006	1.022	1.036
1	2.659	2.6	2.489	2.462	2.403	2.345	1.080	1.107	1.134	1.056	1.082	1.109	1.011	1.036	1.061
2.5	11.69	11.11	10.05	9.798	9.26	8.753	1.193	1.262	1.336	1.134	1.200	1.269	1.026	1.085	1.148
5	23	20.86	17.18	16.36	14.67	13.17	1.406	1.568	1.746	1.275	1.422	1.584	1.050	1.171	1.304
10	35.21	29.1	20.04	18.24	14.86	12.15	1.930	2.369	2.898	1.595	1.958	2.395	1.099	1.349	1.649
20	44.11	30.6	15.48	13.19	9.492	7.124	3.344	4.647	6.192	2.320	3.224	4.295	1.174	1.631	2.173
33	44.74	25.34	10.31	8.717	6.498	5.224	5.132	6.885	8.564	2.907	3.900	4.851	1.183	1.587	1.974
50	40.1	19.07	8.159	7.2	5.786	4.873	5.569	6.931	8.229	2.649	3.296	3.913	1.133	1.410	1.674
100	17.7	11.78	7.285	6.642	5.549	4.752	2.665	3.190	3.725	1.774	2.123	2.479	1.097	1.313	1.533
M / dist: 5.5 / 140															
0.5	0.359	0.354	0.345	0.343	0.338	0.334	1.047	1.062	1.075	1.032	1.047	1.060	1.006	1.021	1.033
1	1.3	1.272	1.219	1.205	1.177	1.149	1.079	1.105	1.131	1.056	1.081	1.107	1.012	1.036	1.061
2.5	5.169	4.916	4.45	4.339	4.102	3.878	1.191	1.260	1.333	1.133	1.198	1.268	1.026	1.085	1.147
5	9.378	8.509	7.02	6.684	6	5.389	1.403	1.563	1.740	1.273	1.418	1.579	1.050	1.170	1.303
10	13.07	10.83	7.493	6.832	5.584	4.587	1.913	2.341	2.849	1.585	1.939	2.361	1.097	1.342	1.634
20	14.66	10.26	5.345	4.6	3.4	2.627	3.187	4.312	5.581	2.230	3.018	3.906	1.162	1.572	2.035
33	13.57	7.944	3.597	3.126	2.444	2.028	4.341	5.552	6.691	2.541	3.250	3.917	1.151	1.472	1.774
50	11.37	5.939	2.998	2.701	2.239	1.924	4.210	5.078	5.910	2.199	2.653	3.087	1.110	1.339	1.558
100	5.802	4.178	2.764	2.547	2.168	1.884	2.278	2.676	3.080	1.640	1.927	2.218	1.085	1.275	1.467
M / dist: 6.5 / 7.5															
0.5	49.98	49.43	48.38	48.12	47.56	47	1.039	1.051	1.063	1.027	1.039	1.052	1.005	1.017	1.029
1	156.2	153	146.9	145.4	142.1	138.9	1.074	1.099	1.125	1.052	1.077	1.102	1.010	1.034	1.058
2.5	488.8	465	421.1	410.6	388.3	367.4	1.190	1.259	1.330	1.132	1.198	1.266	1.026	1.084	1.146
5	908.4	823.6	678.8	646.3	579.9	520.8	1.406	1.566	1.744	1.274	1.420	1.581	1.050	1.171	1.303
10	1484	1224	841.1	765.4	622.7	508.9	1.939	2.383	2.916	1.599	1.966	2.405	1.099	1.351	1.653
20	2117	1457	721.6	610.4	431.7	318	3.468	4.904	6.657	2.387	3.375	4.582	1.182	1.672	2.269
33	2431	1339	493.9	406.4	288.9	226.2	5.982	8.415	10.747	3.295	4.635	5.920	1.215	1.710	2.183
50	2426	1060	371.2	319.3	249	207	7.598	9.743	11.720	3.320	4.257	5.121	1.163	1.491	1.793
100	933.9	550.5	315.3	285.2	235.6	200.9	3.275	3.964	4.649	1.930	2.337	2.740	1.106	1.338	1.569
M / dist: 6.5 / 30															
0.5	14.18	14.02	13.73	13.65	13.49	13.33	1.039	1.051	1.064	1.027	1.039	1.052	1.006	1.018	1.030
1	42.97	42.1	40.42	40	39.09	38.2	1.074	1.099	1.125	1.053	1.077	1.102	1.011	1.034	1.058
2.5	129.2	122.9	111.3	108.6	102.7	97.16	1.190	1.258	1.330	1.132	1.197	1.265	1.025	1.084	1.146
5	232.7	211.1	174.1	165.7	148.8	133.7	1.404	1.564	1.740	1.274	1.419	1.579	1.051	1.170	1.302
10	367	303.1	208.6	189.9	154.7	126.6	1.933	2.372	2.899	1.596	1.959	2.394	1.098	1.348	1.648
20	501.9	346.5	173	146.8	104.8	78.02	3.419	4.789	6.433	2.360	3.306	4.441	1.178	1.651	2.217
33	555.7	308.6	117.7	97.93	71.17	56.6	5.674	7.808	9.818	3.151	4.336	5.452	1.202	1.654	2.080
50	537.3	240.3	90.25	78.56	62.24	52.28	6.839	8.633	10.277	3.059	3.861	4.596	1.149	1.450	1.726
100	214.1	131.9	78.17	71.06	59.23	50.84	3.013	3.615	4.211	1.856	2.227	2.594	1.100	1.320	1.538
M / dist: 6.5 / 60															
0.5	6.767	6.694	6.553	6.518	6.441	6.365	1.038	1.051	1.063	1.027	1.039	1.052	1.005	1.017	1.030
1	19.71	19.31	18.54	18.35	17.93	17.53	1.074	1.099	1.124	1.052	1.077	1.102	1.010	1.034	1.058
2.5	56.2	53.48	48.46	47.26	44.71	42.31	1.189	1.257	1.328	1.132	1.196	1.264	1.025	1.084	1.145
5	96.96	87.99	72.62	69.17	62.12	55.84	1.402	1.561	1.736	1.272	1.416	1.576	1.050	1.169	1.301
10	145.5	120.3	83.01	75.63	61.75	50.68	1.924	2.356	2.871	1.591	1.948	2.374	1.098	1.344	1.638
20	187.2	129.8	65.75	56.09	40.59	30.74	3.337	4.612	6.090	2.314	3.198	4.223	1.172	1.620	2.139
33	196.7	110.7	44.58	37.71	28.27	22.96	5.216	6.958	8.567	2.936	3.916	4.821	1.182	1.577	1.942
50	182	84.65	35.24	31.14	25.21	21.46	5.845	7.219	8.481	2.718	3.358	3.945	1.132	1.398	1.642
100	77.18	50.38	31.29	28.64	24.17	20.94	2.695	3.193	3.686	1.759	2.084	2.406	1.093	1.295	1.494

Lussou et al. (2001) RVT GM for							Resulting scale factors (GM target / GM host) for target (above) and host (below) κ values								
	κ target			κ host			0.00625			0.0125			0.025		
freq	0.00625	0.0125	0.025	0.03	0.0375	0.045	0.03	0.0375	0.045	0.03	0.0375	0.045	0.03	0.0375	0.045
M / dist: 6.5 / 85															
0.5	4.498	4.45	4.357	4.334	4.283	4.232	1.038	1.050	1.063	1.027	1.039	1.052	1.005	1.017	1.030
1	12.72	12.46	11.97	11.84	11.57	11.31	1.074	1.099	1.125	1.052	1.077	1.102	1.011	1.035	1.058
2.5	34.81	33.13	30.03	29.29	27.71	26.23	1.188	1.256	1.327	1.131	1.196	1.263	1.025	1.084	1.145
5	58.03	52.68	43.51	41.45	37.24	33.49	1.400	1.558	1.733	1.271	1.415	1.573	1.050	1.168	1.299
10	83.57	69.19	47.87	43.65	35.79	29.37	1.915	2.335	2.845	1.585	1.933	2.356	1.097	1.338	1.630
20	102.3	71.25	36.58	31.36	22.98	17.66	3.262	4.452	5.793	2.272	3.101	4.035	1.166	1.592	2.071
33	103	58.8	24.87	21.33	16.38	13.52	4.829	6.288	7.618	2.757	3.590	4.349	1.166	1.518	1.839
50	92.12	44.53	20.16	18.01	14.82	12.75	5.115	6.216	7.225	2.473	3.005	3.493	1.119	1.360	1.581
100	41.54	28.31	18.22	16.77	14.28	12.47	2.477	2.909	3.331	1.688	1.982	2.270	1.086	1.276	1.461
M / dist: 6.5 / 140															
0.5	2.369	2.344	2.295	2.283	2.256	2.23	1.038	1.050	1.062	1.027	1.039	1.051	1.005	1.017	1.029
1	6.319	6.193	5.948	5.887	5.754	5.624	1.073	1.098	1.124	1.052	1.076	1.101	1.010	1.034	1.058
2.5	15.93	15.17	13.76	13.42	12.7	12.03	1.187	1.254	1.324	1.130	1.194	1.261	1.025	1.083	1.144
5	24.72	22.46	18.58	17.71	15.93	14.34	1.396	1.552	1.724	1.268	1.410	1.566	1.049	1.166	1.296
10	32.63	27.09	18.86	17.23	14.16	11.72	1.894	2.304	2.784	1.572	1.913	2.311	1.095	1.332	1.609
20	35.93	25.29	13.45	11.67	8.829	7.01	3.079	4.070	5.126	2.167	2.864	3.608	1.153	1.523	1.919
33	33.13	19.64	9.351	8.247	6.639	5.646	4.017	4.990	5.868	2.381	2.958	3.479	1.134	1.408	1.656
50	27.8	14.89	7.973	7.269	6.164	5.403	3.824	4.510	5.145	2.048	2.416	2.756	1.097	1.293	1.476
100	14.62	10.78	7.423	6.905	5.996	5.309	2.117	2.438	2.754	1.561	1.798	2.031	1.075	1.238	1.398
M / dist: 7.25 / 7.5															
0.5	120.9	119.6	117.2	116.6	115.3	113.9	1.037	1.049	1.061	1.026	1.037	1.050	1.005	1.016	1.029
1	274.9	269.3	258.7	256.1	250.3	244.7	1.073	1.098	1.123	1.052	1.076	1.101	1.010	1.034	1.057
2.5	695.6	661.9	599.9	585.1	553.6	523.9	1.189	1.257	1.328	1.131	1.196	1.263	1.025	1.084	1.145
5	1214	1101	908.2	864.9	776.7	698	1.404	1.563	1.739	1.273	1.418	1.577	1.050	1.169	1.301
10	1919	1585	1090	992.4	808.5	662	1.934	2.374	2.899	1.597	1.960	2.394	1.098	1.348	1.647
20	2682	1849	919.1	779	553.9	411.3	3.443	4.842	6.521	2.374	3.338	4.496	1.180	1.659	2.235
33	3046	1681	627.8	519.3	373.9	296.5	5.866	8.147	10.273	3.237	4.496	5.669	1.209	1.679	2.117
50	3016	1325	475.4	411.8	325.1	273.2	7.324	9.277	11.040	3.218	4.076	4.850	1.154	1.462	1.740
100	1166	697	407.2	369.9	308.3	265.1	3.152	3.782	4.398	1.884	2.261	2.629	1.101	1.321	1.536
M / dist: 7.25 / 30															
0.5	40.5	40.08	39.28	39.07	38.63	38.19	1.037	1.048	1.060	1.026	1.038	1.049	1.005	1.017	1.029
1	90.51	88.7	85.21	84.34	82.45	80.61	1.073	1.098	1.123	1.052	1.076	1.100	1.010	1.033	1.057
2.5	223.2	212.4	192.6	187.8	177.7	168.2	1.188	1.256	1.327	1.131	1.195	1.263	1.026	1.084	1.145
5	380.4	345.1	284.9	271.3	243.7	219.1	1.402	1.561	1.736	1.272	1.416	1.575	1.050	1.169	1.300
10	583.8	482.5	332.5	302.9	247.1	202.7	1.927	2.363	2.880	1.593	1.953	2.380	1.098	1.346	1.640
20	786.2	543.2	272.4	231.6	166.1	124.7	3.395	4.733	6.305	2.345	3.270	4.356	1.176	1.640	2.184
33	863.5	480.5	185.3	155	113.9	91.66	5.571	7.581	9.421	3.100	4.219	5.242	1.195	1.627	2.022
50	830.8	373.1	143.1	125.3	100.4	85.12	6.630	8.275	9.760	2.978	3.716	4.383	1.142	1.425	1.681
100	332.3	207	124.8	113.9	95.73	82.81	2.917	3.471	4.013	1.817	2.162	2.500	1.096	1.304	1.507
M / dist: 7.25 / 60															
0.5	19.65	19.45	19.06	18.96	18.74	18.53	1.036	1.049	1.060	1.026	1.038	1.050	1.005	1.017	1.029
1	42.78	41.93	40.28	39.87	38.98	38.12	1.073	1.097	1.122	1.052	1.076	1.100	1.010	1.033	1.057
2.5	101.4	96.57	87.58	85.43	80.85	76.54	1.187	1.254	1.325	1.130	1.194	1.262	1.025	1.083	1.144
5	166.7	151.3	125	119.1	107.1	96.29	1.400	1.556	1.731	1.270	1.413	1.571	1.050	1.167	1.298
10	244.5	202.3	139.8	127.5	104.3	85.75	1.918	2.344	2.851	1.587	1.940	2.359	1.096	1.340	1.630
20	310.9	215.8	109.8	93.86	68.34	52.18	3.312	4.549	5.958	2.299	3.158	4.136	1.170	1.607	2.104
33	324.6	183.2	74.69	63.5	48.15	39.54	5.112	6.741	8.209	2.885	3.805	4.633	1.176	1.551	1.889
50	299.3	139.9	59.49	52.84	43.23	37.12	5.664	6.923	8.063	2.648	3.236	3.769	1.126	1.376	1.603
100	127.6	84.16	53.11	48.8	41.51	36.24	2.615	3.074	3.521	1.725	2.027	2.322	1.088	1.279	1.466
M / dist: 7.25 / 85															
0.5	13.11	12.98	12.72	12.65	12.51	12.37	1.036	1.048	1.060	1.026	1.038	1.049	1.006	1.017	1.028
1	27.95	27.4	26.32	26.06	25.48	24.91	1.073	1.097	1.122	1.051	1.075	1.100	1.010	1.033	1.057
2.5	64.16	61.08	55.41	54.06	51.17	48.45	1.187	1.254	1.324	1.130	1.194	1.261	1.025	1.083	1.144
5	102.3	92.88	76.79	73.18	65.8	59.22	1.398	1.555	1.727	1.269	1.412	1.568	1.049	1.167	1.297
10	144.4	119.6	82.9	75.65	61.99	51.11	1.909	2.329	2.825	1.581	1.929	2.340	1.096	1.337	1.622
20	174.9	121.9	62.94	54.09	39.92	30.95	3.233	4.381	5.651	2.254	3.054	3.939	1.164	1.577	2.034
33	175.2	100.3	43.03	37.1	28.82	24.04	4.722	6.079	7.288	2.704	3.480	4.172	1.160	1.493	1.790
50	156.3	76	35.16	31.57	26.24	22.75	4.951	5.957	6.870	2.407	2.896	3.341	1.114	1.340	1.545
100	70.96	48.84	31.92	29.49	25.32	22.27	2.406	2.803	3.186	1.656	1.929	2.193	1.082	1.261	1.433
M / dist: 7.25 / 140															
0.5	6.953	6.884	6.746	6.712	6.636	6.56	1.036	1.048	1.060	1.026	1.037	1.049	1.005	1.017	1.028
1	14.17	13.89	13.35	13.22	12.92	12.64	1.072	1.097	1.121	1.051	1.075	1.099	1.010	1.033	1.056
2.5	30.33	28.89	26.22	25.58	24.23	22.95	1.186	1.252	1.322	1.129	1.192	1.259	1.025	1.082	1.142
5	45.25	41.13	34.07	32.48	29.24	26.35	1.393	1.548	1.717	1.266	1.407	1.561	1.049	1.165	1.293
10	58.76	48.82	34.07	31.16	25.68	21.31	1.886	2.288	2.757	1.567	1.901	2.291	1.093	1.327	1.599
20	64.2	45.27	24.27	21.13	16.12	12.94	3.038	3.983	4.961	2.142	2.808	3.498	1.149	1.506	1.876
33	59.01	35.14	17.04	15.11	12.31	10.57	3.905	4.794	5.583	2.326	2.855	3.325	1.128	1.384	1.612
50	49.47	26.74	14.65	13.42	11.48	10.15	3.686	4.309	4.874	1.993	2.329	2.634	1.092	1.276	1.443
100	26.28	19.57	13.69	12.78	11.18	9.978	2.056	2.351	2.634	1.531	1.750	1.961	1.071	1.225	1.372

Tab. A11-8: Scaling factors derived for the kappa correction – Somerville et al. (2001) model

Somerville et al. (2001) RVT GM for							Resulting scale factors (GM target / GM host) for target (above) and host (below) κ values								
	κ target			κ host			0.00625			0.0125			0.025		
freq	0.00625	0.0125	0.025	0.03	0.0375	0.045	0.03	0.0375	0.045	0.03	0.0375	0.045	0.03	0.0375	0.045
M / dist: 5.5 / 7.5															
0.5	9.204	9.113	8.938	9.217	9.198	9.179	0.999	1.001	1.003	0.989	0.991	0.993	0.970	0.972	0.974
1	37.32	36.68	35.32	37.41	37.28	37.15	0.998	1.001	1.005	0.980	0.984	0.987	0.944	0.947	0.951
2.5	165.4	157.4	142.6	166.6	164.9	163.2	0.993	1.003	1.013	0.945	0.955	0.964	0.856	0.865	0.874
5	333.6	302.6	249.4	338.5	331.5	324.7	0.986	1.006	1.027	0.894	0.913	0.932	0.737	0.752	0.768
10	527.4	436.1	300.6	542.7	521	500.2	0.972	1.012	1.054	0.804	0.837	0.872	0.554	0.577	0.601
20	689.8	478.6	242.7	729.2	673.6	622.6	0.946	1.024	1.108	0.656	0.711	0.769	0.333	0.360	0.390
33	730.7	412.5	167.1	799.2	703.3	620.3	0.914	1.039	1.178	0.516	0.587	0.665	0.209	0.238	0.269
50	682.8	319.4	133.1	775.7	646.9	543.1	0.880	1.055	1.257	0.412	0.494	0.588	0.172	0.206	0.245
100	297.9	193.3	118.6	327.3	287.1	257.1	0.910	1.038	1.159	0.591	0.673	0.752	0.362	0.413	0.461
M / dist: 5.5 / 30															
0.5	2.823	2.798	2.747	2.827	2.822	2.817	0.999	1.000	1.002	0.990	0.991	0.993	0.972	0.973	0.975
1	11.35	11.16	10.74	11.38	11.34	11.3	0.997	1.001	1.004	0.981	0.984	0.988	0.944	0.947	0.950
2.5	49.45	47.06	42.63	49.81	49.29	48.78	0.993	1.003	1.014	0.945	0.955	0.965	0.856	0.865	0.874
5	97.39	88.37	72.89	98.81	96.78	94.8	0.986	1.006	1.027	0.894	0.913	0.932	0.738	0.753	0.769
10	148.1	122.6	84.74	152.4	146.3	140.5	0.972	1.012	1.054	0.804	0.838	0.873	0.556	0.579	0.603
20	182.4	127.2	65.54	192.7	178.2	164.8	0.947	1.024	1.107	0.660	0.714	0.772	0.340	0.368	0.398
33	181.7	104.6	45.12	198.3	175.1	155	0.916	1.038	1.172	0.527	0.597	0.675	0.228	0.258	0.291
50	160.7	79.71	36.98	181.5	152.7	129.5	0.885	1.052	1.241	0.439	0.522	0.616	0.204	0.242	0.286
100	76.55	52.72	33.74	82.69	74.23	67.64	0.926	1.031	1.132	0.638	0.710	0.779	0.408	0.455	0.499
M / dist: 5.5 / 60															
0.5	1.394	1.383	1.359	1.395	1.393	1.391	0.999	1.001	1.002	0.991	0.993	0.994	0.974	0.976	0.977
1	5.526	5.431	5.229	5.54	5.52	5.501	0.997	1.001	1.005	0.980	0.984	0.987	0.944	0.947	0.951
2.5	23.51	22.38	20.27	23.68	23.43	23.19	0.993	1.003	1.014	0.945	0.955	0.965	0.856	0.865	0.874
5	44.82	40.69	33.59	45.48	44.55	43.64	0.985	1.006	1.027	0.895	0.913	0.932	0.739	0.754	0.770
10	64.61	53.58	37.17	66.46	63.84	61.33	0.972	1.012	1.053	0.806	0.839	0.874	0.559	0.582	0.606
20	73.25	51.51	27.23	77.3	71.58	66.33	0.948	1.023	1.104	0.666	0.720	0.777	0.352	0.380	0.411
33	67.35	40.07	18.97	73.23	65	57.87	0.920	1.036	1.164	0.547	0.616	0.692	0.259	0.292	0.328
50	55.92	30.48	16.12	62.46	53.41	46.13	0.895	1.047	1.212	0.488	0.571	0.661	0.258	0.302	0.349
100	30.59	22.45	15.1	32.49	29.85	27.69	0.942	1.025	1.105	0.691	0.752	0.811	0.465	0.506	0.545
M / dist: 5.5 / 85															
0.5	0.965	0.957	0.942	0.966	0.964	0.963	0.999	1.001	1.002	0.991	0.993	0.994	0.975	0.977	0.978
1	3.785	3.718	3.579	3.794	3.781	3.767	0.998	1.001	1.005	0.980	0.983	0.987	0.943	0.947	0.950
2.5	15.69	14.93	13.53	15.81	15.64	15.48	0.992	1.003	1.014	0.944	0.955	0.964	0.856	0.865	0.874
5	29.01	26.34	21.76	29.43	28.83	28.24	0.986	1.006	1.027	0.895	0.914	0.933	0.739	0.755	0.771
10	39.88	33.12	23.06	41.01	39.41	37.87	0.972	1.012	1.053	0.808	0.840	0.875	0.562	0.585	0.609
20	42.2	29.92	16.21	44.48	41.26	38.29	0.949	1.023	1.102	0.673	0.725	0.781	0.364	0.393	0.423
33	36.49	22.45	11.49	39.52	35.28	31.61	0.923	1.034	1.154	0.568	0.636	0.710	0.291	0.326	0.363
50	29.22	17.32	10.03	32.26	28.05	24.66	0.906	1.042	1.185	0.537	0.617	0.702	0.311	0.358	0.407
100	17.93	13.71	9.544	18.86	17.57	16.47	0.951	1.020	1.089	0.727	0.780	0.832	0.506	0.543	0.579
M / dist: 5.5 / 140															
0.5	0.562	0.558	0.548	0.563	0.562	0.561	0.998	1.000	1.002	0.991	0.993	0.995	0.973	0.975	0.977
1	2.157	2.115	2.033	2.163	2.155	2.146	0.997	1.001	1.005	0.978	0.981	0.986	0.940	0.943	0.947
2.5	8.074	7.686	6.967	8.134	8.049	7.965	0.993	1.003	1.014	0.945	0.955	0.965	0.857	0.866	0.875
5	13.53	12.3	10.18	13.73	13.45	13.18	0.985	1.006	1.027	0.896	0.914	0.933	0.741	0.757	0.772
10	16.43	13.7	9.624	16.89	16.24	15.62	0.973	1.012	1.052	0.811	0.844	0.877	0.570	0.593	0.616
20	14.87	10.79	6.238	15.63	14.56	13.57	0.951	1.021	1.096	0.690	0.741	0.795	0.399	0.428	0.460
33	11.52	7.753	4.657	12.33	11.19	10.21	0.934	1.029	1.128	0.629	0.693	0.759	0.378	0.416	0.456
50	9.034	6.338	4.253	9.687	8.78	8.041	0.933	1.029	1.123	0.654	0.722	0.788	0.439	0.484	0.529
100	6.834	5.575	4.136	7.084	6.733	6.422	0.965	1.015	1.064	0.787	0.828	0.868	0.584	0.614	0.644
M / dist: 6.5 / 7.5															
0.5	56.99	56.51	55.47	57.05	56.96	56.86	0.999	1.001	1.002	0.991	0.992	0.994	0.972	0.974	0.976
1	159.6	156.5	150.4	160	159.4	158.7	0.998	1.001	1.006	0.978	0.982	0.986	0.940	0.944	0.948
2.5	389.7	371.1	336.8	392.5	388.4	384.4	0.993	1.003	1.014	0.945	0.955	0.965	0.858	0.867	0.876
5	620.3	563.6	466.3	629.3	616.5	604	0.986	1.006	1.027	0.896	0.914	0.933	0.741	0.756	0.772
10	878.2	728.1	505.6	903.4	867.7	833.6	0.972	1.012	1.054	0.806	0.839	0.873	0.560	0.583	0.607
20	1086	757.4	392.5	1147	1061	981.1	0.947	1.024	1.107	0.660	0.714	0.772	0.342	0.370	0.400
33	1120	640	274.6	1224	1079	953.4	0.915	1.038	1.175	0.523	0.593	0.671	0.224	0.254	0.288
50	1031	495.2	225.3	1169	978.1	824.4	0.882	1.054	1.251	0.424	0.506	0.601	0.193	0.230	0.273
100	461.9	312.4	203.7	503.6	446.6	403.9	0.917	1.034	1.144	0.620	0.700	0.773	0.404	0.456	0.504
M / dist: 6.5 / 30															
0.5	20.28	20.1	19.73	20.3	20.27	20.23	0.999	1.000	1.002	0.990	0.992	0.994	0.972	0.973	0.975
1	56.32	55.24	53.1	56.48	56.25	56.02	0.997	1.001	1.005	0.978	0.982	0.986	0.940	0.944	0.948
2.5	134.9	128.5	116.6	135.9	134.5	133.1	0.993	1.003	1.014	0.946	0.955	0.965	0.858	0.867	0.876
5	209.6	190.5	157.7	212.6	208.3	204.1	0.986	1.006	1.027	0.896	0.915	0.933	0.742	0.757	0.773
10	285.6	237.1	165.2	293.7	282.2	271.1	0.972	1.012	1.053	0.807	0.840	0.875	0.562	0.585	0.609
20	333.2	233.8	123.8	351.8	325.6	301.5	0.947	1.023	1.105	0.665	0.718	0.775	0.352	0.380	0.411
33	324.7	189.5	87.04	353.8	313	277.6	0.918	1.037	1.170	0.536	0.605	0.683	0.246	0.278	0.314
50	284.2	145.2	73.34	320.1	270.4	230.5	0.888	1.051	1.233	0.454	0.537	0.630	0.229	0.271	0.318
100	139.5	99.69	67.59	149.7	135.6	124.6	0.932	1.029	1.120	0.666	0.735	0.800	0.452	0.498	0.542
M / dist: 6.5 / 60															
0.5	10.18	10.09	9.9	10.19	10.17	10.15	0.999	1.001	1.003	0.990	0.992	0.994	0.972	0.973	0.975
1	27.93	27.39	26.33	28.01	27.9	27.78	0.997	1.001	1.005	0.978	0.982	0.986	0.940	0.944	0.948
2.5	65.05	61.97	56.26	65.52	64.85	64.18	0.993	1.003	1.014	0.946	0.956	0.966	0.859	0.868	0.877
5	97.44	88.61	73.46	98.82	96.85	94.91	0.986	1.006	1.027	0.897	0.915	0.934	0.743	0.758	0.774
10	125.5	104.4	73.14	129.1	124.1	119.3	0.972	1.011	1.052	0.809	0.841	0.875	0.567	0.589	0.613
20	134.8	95.6	52.18	142.1	131.8	122.3	0.949	1.023	1.102	0.673	0.725	0.782	0.367	0.396	0.427
33	121.5	73.76	37.53	131.8	117.4	104.8	0.922	1.035	1.159	0.560	0.628	0.704	0.285	0.320	0.358
50	100.3	56.89	32.73	111.6	96	83.51	0.899	1.045	1.201	0.510	0.593	0.681	0.293	0.341	0.392
100	56.96	43.33	30.82	60.13	55.73	52.12	0.947	1.022	1.093	0.721	0.777	0.831	0.513	0.553	0.591

Somerville et al. (2001) RVT GM for							Resulting scale factors (GM target / GM host) for target (above) and host (below) κ values								
	κ target			κ host			0.00625			0.0125			0.025		
freq	0.00625	0.0125	0.025	0.03	0.0375	0.045	0.03	0.0375	0.045	0.03	0.0375	0.045	0.03	0.0375	0.045
M / dist: 6.5 / 85															
0.5	7.07	7.007	6.875	7.08	7.067	7.053	0.999	1.000	1.002	0.990	0.992	0.993	0.971	0.973	0.975
1	19.18	18.81	18.08	19.23	19.15	19.07	0.997	1.002	1.006	0.978	0.982	0.986	0.940	0.944	0.948
2.5	43.56	41.5	37.69	43.87	43.42	42.98	0.993	1.003	1.013	0.946	0.956	0.966	0.859	0.868	0.877
5	63.25	57.55	47.75	64.15	62.87	61.61	0.986	1.006	1.027	0.897	0.915	0.934	0.744	0.760	0.775
10	77.75	64.81	45.61	79.91	76.84	73.9	0.973	1.012	1.052	0.811	0.843	0.877	0.571	0.594	0.617
20	78.05	55.92	31.48	82.18	76.35	71	0.950	1.022	1.099	0.680	0.732	0.788	0.383	0.412	0.443
33	66.39	41.93	23.2	71.7	64.26	57.84	0.926	1.033	1.148	0.585	0.653	0.725	0.324	0.361	0.401
50	53.19	33.02	20.72	58.4	51.18	45.42	0.911	1.039	1.171	0.565	0.645	0.727	0.355	0.405	0.456
100	33.99	26.9	19.78	35.54	33.38	31.55	0.956	1.018	1.077	0.757	0.806	0.853	0.557	0.593	0.627
M / dist: 6.5 / 140															
0.5	4.1	4.062	3.983	4.106	4.098	4.09	0.999	1.000	1.002	0.989	0.991	0.993	0.970	0.972	0.974
1	10.7	10.49	10.08	10.73	10.69	10.64	0.997	1.001	1.006	0.978	0.981	0.986	0.939	0.943	0.947
2.5	22.71	21.64	19.66	22.87	22.64	22.4	0.993	1.003	1.014	0.946	0.956	0.966	0.860	0.868	0.878
5	30.62	27.89	23.2	31.05	30.44	29.84	0.986	1.006	1.026	0.898	0.916	0.935	0.747	0.762	0.777
10	33.89	28.39	20.23	34.81	33.5	32.25	0.974	1.012	1.051	0.816	0.847	0.880	0.581	0.604	0.627
20	29.61	21.85	13.31	31.06	29.01	27.13	0.953	1.021	1.091	0.703	0.753	0.805	0.429	0.459	0.491
33	22.98	16.07	10.44	24.48	22.38	20.56	0.939	1.027	1.118	0.656	0.718	0.782	0.426	0.466	0.508
50	18.38	13.52	9.699	19.56	17.92	16.59	0.940	1.026	1.108	0.691	0.754	0.815	0.496	0.541	0.585
100	14.41	12.11	9.444	14.86	14.23	13.66	0.970	1.013	1.055	0.815	0.851	0.887	0.636	0.664	0.691
M / dist: 7.25 / 7.5															
0.5	144.6	143.2	140.5	144.8	144.5	144.2	0.999	1.001	1.003	0.989	0.991	0.993	0.970	0.972	0.974
1	291.9	286.3	275.2	292.8	291.5	290.3	0.997	1.001	1.006	0.978	0.982	0.986	0.940	0.944	0.948
2.5	572.4	545.4	495.4	576.6	570.6	564.8	0.993	1.003	1.013	0.946	0.956	0.966	0.859	0.868	0.877
5	852.1	774.7	642.1	864.3	846.9	829.9	0.986	1.006	1.027	0.896	0.915	0.933	0.743	0.758	0.774
10	1164	966.1	673.2	1197	1150	1105	0.972	1.012	1.053	0.807	0.840	0.874	0.562	0.585	0.609
20	1406	983	515	1485	1373	1271	0.947	1.024	1.106	0.662	0.716	0.773	0.347	0.375	0.405
33	1430	822.2	362.9	1562	1378	1219	0.915	1.038	1.173	0.526	0.597	0.674	0.232	0.263	0.298
50	1304	635.3	301.6	1477	1238	1045	0.883	1.053	1.248	0.430	0.513	0.608	0.204	0.244	0.289
100	594	410.3	275.1	644.7	575.4	523.1	0.921	1.032	1.136	0.636	0.713	0.784	0.427	0.478	0.526
M / dist: 7.25 / 30															
0.5	59.05	58.49	57.35	59.13	59.01	58.89	0.999	1.001	1.003	0.989	0.991	0.993	0.970	0.972	0.974
1	118.2	115.9	111.5	118.6	118.1	117.6	0.997	1.001	1.005	0.977	0.981	0.986	0.940	0.944	0.948
2.5	227.5	216.8	197	229.2	226.8	224.5	0.993	1.003	1.013	0.946	0.956	0.966	0.860	0.869	0.878
5	330.8	300.9	249.6	335.5	328.8	322.2	0.986	1.006	1.027	0.897	0.915	0.934	0.744	0.759	0.775
10	435.8	362.2	253.3	448.1	430.6	413.9	0.973	1.012	1.053	0.808	0.841	0.875	0.565	0.588	0.612
20	498.5	350.8	187.5	526.1	487.1	451.4	0.948	1.023	1.104	0.667	0.720	0.777	0.356	0.385	0.415
33	480.9	282.5	133.4	523.8	463.7	411.8	0.918	1.037	1.168	0.539	0.609	0.686	0.255	0.288	0.324
50	418.6	216.9	113.7	471	398.5	340.4	0.889	1.050	1.230	0.461	0.544	0.637	0.241	0.285	0.334
100	208.6	151.6	105.4	223.1	203.1	187.4	0.935	1.027	1.113	0.680	0.746	0.809	0.472	0.519	0.562
M / dist: 7.25 / 60															
0.5	30.19	29.9	29.32	30.24	30.17	30.11	0.998	1.001	1.003	0.989	0.991	0.993	0.970	0.972	0.974
1	59.67	58.52	56.27	59.85	59.6	59.35	0.997	1.001	1.005	0.978	0.982	0.986	0.940	0.944	0.948
2.5	111.5	106.3	96.64	112.4	111.2	110.1	0.992	1.003	1.013	0.946	0.956	0.965	0.860	0.869	0.878
5	156.4	142.3	118.2	158.6	155.4	152.4	0.986	1.006	1.026	0.897	0.916	0.934	0.745	0.761	0.776
10	194.9	162.4	114.2	200.3	192.6	185.2	0.973	1.012	1.052	0.811	0.843	0.877	0.570	0.593	0.617
20	205.4	146.2	80.93	216.5	200.9	186.5	0.949	1.022	1.101	0.675	0.728	0.784	0.374	0.403	0.434
33	183.6	112.5	59	199.1	177.5	158.8	0.922	1.034	1.156	0.565	0.634	0.708	0.296	0.332	0.372
50	151.3	87.24	52.02	168	144.9	126.4	0.901	1.044	1.197	0.519	0.602	0.690	0.310	0.359	0.412
100	87.39	67.51	49.19	92	85.6	80.34	0.950	1.021	1.088	0.734	0.789	0.840	0.535	0.575	0.612
M / dist: 7.25 / 85															
0.5	21.04	20.84	20.44	21.07	21.03	20.99	0.999	1.000	1.002	0.989	0.991	0.993	0.970	0.972	0.974
1	41.12	40.32	38.78	41.24	41.07	40.9	0.997	1.001	1.005	0.978	0.982	0.986	0.940	0.944	0.948
2.5	74.95	71.46	64.98	75.5	74.73	73.97	0.993	1.003	1.013	0.946	0.956	0.966	0.861	0.870	0.878
5	101.9	92.8	77.16	103.3	101.3	99.29	0.986	1.006	1.026	0.898	0.916	0.935	0.747	0.762	0.777
10	121.2	101.2	71.59	124.6	119.8	115.3	0.973	1.012	1.051	0.812	0.845	0.878	0.575	0.598	0.621
20	119.5	86.06	49.28	125.8	117	108.9	0.950	1.021	1.097	0.684	0.736	0.790	0.392	0.421	0.453
33	101	64.53	36.9	109	97.86	88.26	0.927	1.032	1.144	0.592	0.659	0.731	0.339	0.377	0.418
50	80.96	51.25	33.29	88.69	78	69.48	0.913	1.038	1.165	0.578	0.657	0.738	0.375	0.427	0.479
100	52.72	42.33	31.88	54.98	51.82	49.15	0.959	1.017	1.073	0.770	0.817	0.861	0.580	0.615	0.649
M / dist: 7.25 / 140															
0.5	12.17	12.05	11.81	12.19	12.16	12.14	0.998	1.001	1.002	0.989	0.991	0.993	0.969	0.971	0.973
1	23.09	22.64	21.78	23.15	23.06	22.96	0.997	1.001	1.006	0.978	0.982	0.986	0.941	0.944	0.949
2.5	39.69	37.85	34.44	39.98	39.57	39.17	0.993	1.003	1.013	0.947	0.957	0.966	0.861	0.870	0.879
5	50.36	45.92	38.29	51.06	50.06	49.08	0.986	1.006	1.026	0.899	0.917	0.936	0.750	0.765	0.780
10	54.14	45.47	32.63	55.59	53.53	51.56	0.974	1.011	1.050	0.818	0.849	0.882	0.587	0.610	0.633
20	46.71	34.72	21.65	48.96	45.78	42.87	0.954	1.020	1.090	0.709	0.758	0.810	0.442	0.473	0.505
33	36.26	25.77	17.31	38.55	35.34	32.58	0.941	1.026	1.113	0.668	0.729	0.791	0.449	0.490	0.531
50	29.21	21.94	16.21	30.98	28.52	26.53	0.943	1.024	1.101	0.708	0.769	0.827	0.523	0.568	0.611
100	23.28	19.83	15.8	23.96	23.01	22.16	0.972	1.012	1.051	0.828	0.862	0.895	0.659	0.687	0.713

Tab. A11-9: Scaling factors derived for the kappa correction – Spudich et al. (1999) model

Spudich et al. (1999) RVT GM for							Resulting scale factors (GM target / GM host) for target (above) and host (below) κ values								
	κ target			κ host			0.00625			0.0125			0.025		
freq	0.00625	0.0125	0.025	0.03	0.0375	0.045	0.03	0.0375	0.045	0.03	0.0375	0.045	0.03	0.0375	0.045
M / dist: 5.5 / 7.5															
0.5	25.71	25.54	25.17	25.12	24.91	24.7	1.023	1.032	1.041	1.017	1.025	1.034	1.002	1.010	1.019
1	105.8	104.2	100.5	100	97.98	95.96	1.058	1.080	1.103	1.042	1.063	1.086	1.005	1.026	1.047
2.5	394.9	376	340.7	336.2	319	302.7	1.175	1.238	1.305	1.118	1.179	1.242	1.013	1.068	1.126
5	779.5	707	582.8	567.9	512.6	463.1	1.373	1.521	1.683	1.245	1.379	1.527	1.026	1.137	1.258
10	1306	1079	741.7	705.6	580.7	479.9	1.851	2.249	2.721	1.529	1.858	2.248	1.051	1.277	1.546
20	1874	1293	644	589.5	424.1	316.3	3.179	4.419	5.925	2.193	3.049	4.088	1.092	1.519	2.036
33	2141	1186	447.5	403.7	288.5	225.5	5.303	7.421	9.494	2.938	4.111	5.259	1.108	1.551	1.984
50	2123	940.8	343.3	316.6	246.1	204.3	6.706	8.627	10.392	2.972	3.823	4.605	1.084	1.395	1.680
100	847.5	509.2	295.9	280.4	232.8	199.1	3.022	3.640	4.257	1.816	2.187	2.558	1.055	1.271	1.486
M / dist: 5.5 / 30															
0.5	6.161	6.107	5.994	5.979	5.918	5.857	1.030	1.041	1.052	1.021	1.032	1.043	1.003	1.013	1.023
1	24.21	23.76	22.85	22.73	22.25	21.77	1.065	1.088	1.112	1.045	1.068	1.091	1.005	1.027	1.050
2.5	80.31	76.44	69.28	68.36	64.87	61.57	1.175	1.238	1.304	1.118	1.178	1.242	1.013	1.068	1.125
5	145.5	132.1	109	106.2	95.94	86.73	1.370	1.517	1.678	1.244	1.377	1.523	1.026	1.136	1.257
10	224.2	185.4	128	121.8	100.5	83.31	1.841	2.231	2.691	1.522	1.845	2.225	1.051	1.274	1.536
20	294.4	204.2	103.5	95.09	69.51	52.83	3.096	4.235	5.573	2.147	2.938	3.865	1.088	1.489	1.959
33	313.3	176.9	71.19	64.93	48.29	38.86	4.825	6.488	8.062	2.724	3.663	4.552	1.096	1.474	1.832
50	293	136.2	56.52	52.72	42.3	35.83	5.558	6.927	8.178	2.583	3.220	3.801	1.072	1.336	1.577
100	125.2	81.22	50.2	47.82	40.37	34.98	2.618	3.101	3.579	1.698	2.012	2.322	1.050	1.243	1.435
M / dist: 5.5 / 60															
0.5	3.9	3.861	3.782	3.772	3.73	3.689	1.034	1.046	1.057	1.024	1.035	1.047	1.003	1.014	1.025
1	14.19	13.91	13.36	13.29	13	12.73	1.068	1.092	1.115	1.047	1.070	1.093	1.005	1.028	1.049
2.5	42.02	40	36.27	35.79	33.97	32.25	1.174	1.237	1.303	1.118	1.178	1.240	1.013	1.068	1.125
5	69.92	63.5	52.48	51.15	46.24	41.84	1.367	1.512	1.671	1.241	1.373	1.518	1.026	1.135	1.254
10	98.34	81.52	56.57	53.89	44.62	37.14	1.825	2.204	2.648	1.513	1.827	2.195	1.050	1.268	1.523
20	116.5	81.48	42.5	39.24	29.36	22.92	2.969	3.968	5.083	2.076	2.775	3.555	1.083	1.448	1.854
33	113.9	66.03	29.42	27.21	21.2	17.62	4.186	5.373	6.464	2.427	3.115	3.747	1.081	1.388	1.670
50	99.79	50.26	24.44	23.07	19.14	16.56	4.326	5.214	6.026	2.179	2.626	3.035	1.059	1.277	1.476
100	48.1	33.86	22.39	21.46	18.46	16.23	2.241	2.606	2.964	1.578	1.834	2.086	1.043	1.213	1.380
M / dist: 5.5 / 85															
0.5	2.969	2.938	2.877	2.869	2.837	2.805	1.035	1.047	1.058	1.024	1.036	1.047	1.003	1.014	1.026
1	10.23	10.03	9.632	9.58	9.375	9.174	1.068	1.091	1.115	1.047	1.070	1.093	1.005	1.027	1.050
2.5	28.09	26.75	24.26	23.94	22.73	21.58	1.173	1.236	1.302	1.117	1.177	1.240	1.013	1.067	1.124
5	43.99	39.98	33.08	32.25	29.18	26.42	1.364	1.508	1.665	1.240	1.370	1.513	1.026	1.134	1.252
10	57.79	48.01	33.48	31.91	26.52	22.16	1.811	2.179	2.608	1.505	1.810	2.167	1.049	1.262	1.511
20	63.22	44.61	23.93	22.2	16.98	13.56	2.848	3.723	4.662	2.009	2.627	3.290	1.078	1.409	1.765
33	58.04	34.69	16.88	15.78	12.72	10.81	3.678	4.563	5.369	2.198	2.727	3.209	1.070	1.327	1.562
50	48.71	26.56	14.51	13.8	11.71	10.28	3.530	4.160	4.738	1.925	2.268	2.584	1.051	1.239	1.411
100	26.31	19.55	13.55	13.04	11.37	10.1	2.018	2.314	2.605	1.499	1.719	1.936	1.039	1.192	1.342
M / dist: 5.5 / 140															
0.5	1.846	1.826	1.788	1.783	1.763	1.743	1.035	1.047	1.059	1.024	1.036	1.048	1.003	1.014	1.026
1	5.77	5.656	5.433	5.403	5.288	5.176	1.068	1.091	1.115	1.047	1.070	1.093	1.006	1.027	1.050
2.5	13.78	13.13	11.92	11.76	11.17	10.61	1.172	1.234	1.299	1.116	1.175	1.238	1.014	1.067	1.123
5	19.17	17.45	14.48	14.12	12.8	11.61	1.358	1.498	1.651	1.236	1.363	1.503	1.025	1.131	1.247
10	21.94	18.32	12.94	12.37	10.37	8.762	1.774	2.116	2.504	1.481	1.767	2.091	1.046	1.248	1.477
20	20.47	14.82	8.592	8.074	6.496	5.441	2.535	3.151	3.762	1.836	2.281	2.724	1.064	1.323	1.579
33	16.81	11	6.482	6.176	5.264	4.642	2.722	3.193	3.621	1.781	2.090	2.370	1.050	1.231	1.396
50	13.51	8.905	5.897	5.68	5.002	4.499	2.379	2.701	3.003	1.568	1.780	1.979	1.038	1.179	1.311
100	9.301	7.555	5.671	5.496	4.91	4.446	1.692	1.894	2.092	1.375	1.539	1.699	1.032	1.155	1.276
M / dist: 6.5 / 7.5															
0.5	185	183.6	180.6	180.1	178.4	176.6	1.027	1.037	1.048	1.019	1.029	1.040	1.003	1.012	1.023
1	432.3	424.2	408	405.8	397.4	389.1	1.065	1.088	1.111	1.045	1.067	1.090	1.005	1.027	1.049
2.5	1082	1030	934.4	922.1	875.5	831.4	1.173	1.236	1.301	1.117	1.176	1.239	1.013	1.067	1.124
5	1875	1702	1405	1369	1238	1120	1.370	1.515	1.674	1.243	1.375	1.520	1.026	1.135	1.254
10	2930	2422	1670	1590	1312	1087	1.843	2.233	2.695	1.523	1.846	2.228	1.050	1.273	1.536
20	4041	2792	1401	1285	932.3	703.9	3.145	4.334	5.741	2.173	2.995	3.966	1.090	1.503	1.990
33	4533	2518	969.1	878.1	640.3	510.9	5.162	7.079	8.873	2.868	3.933	4.929	1.104	1.514	1.897
50	4447	1984	750.7	696.4	552.8	467.3	6.386	8.045	9.516	2.849	3.589	4.246	1.078	1.358	1.606
100	1773	1086	651.7	620.1	522.6	453.4	2.859	3.393	3.910	1.751	2.078	2.395	1.051	1.247	1.437
M / dist: 6.5 / 30															
0.5	42.97	42.63	41.87	41.76	41.34	40.92	1.029	1.039	1.050	1.021	1.031	1.042	1.003	1.013	1.023
1	95.76	93.93	90.32	89.84	87.97	86.14	1.066	1.089	1.112	1.046	1.068	1.090	1.005	1.027	1.049
2.5	224.7	214	194.2	191.7	182	172.9	1.172	1.235	1.300	1.116	1.176	1.238	1.013	1.067	1.123
5	369.5	335.6	277.5	270.5	244.6	221.4	1.366	1.511	1.669	1.241	1.372	1.516	1.026	1.135	1.253
10	543.4	449.9	311.6	296.8	245.5	204.2	1.831	2.213	2.661	1.516	1.833	2.203	1.050	1.269	1.526
20	696.1	483.8	247.6	227.8	168.2	129.7	3.056	4.139	5.367	2.124	2.876	3.730	1.087	1.472	1.909
33	732.7	414.4	171.2	156.9	119	97.62	4.670	6.157	7.506	2.641	3.482	4.245	1.091	1.439	1.754
50	681.3	319.5	137.6	129.3	105.4	90.72	5.269	6.464	7.510	2.471	3.031	3.522	1.064	1.306	1.517
100	293.2	193.5	123.1	117.7	100.8	88.47	2.491	2.909	3.314	1.644	1.920	2.187	1.046	1.221	1.391
M / dist: 6.5 / 60															
0.5	26.41	26.18	25.69	25.63	25.36	25.1	1.030	1.041	1.052	1.021	1.032	1.043	1.002	1.013	1.024
1	55.68	54.6	52.5	52.22	51.14	50.07	1.066	1.089	1.112	1.046	1.068	1.090	1.005	1.027	1.049
2.5	121	115.3	104.7	103.3	98.13	93.24	1.171	1.233	1.298	1.116	1.175	1.237	1.014	1.067	1.123
5	186.4	169.4	140.3	136.8	123.9	112.2	1.363	1.504	1.661	1.238	1.367	1.510	1.026	1.132	1.250
10	253.6	210.5	146.7	139.8	116.2	97.19	1.814	2.182	2.609	1.506	1.812	2.166	1.049	1.262	1.509
20	295.5	207.3	109.5	101.4	76.88	61	2.914	3.844	4.844	2.044	2.696	3.398	1.080	1.424	1.795
33	287.2	167.6	76.95	71.56	56.88	48.13	4.013	5.049	5.967	2.342	2.947	3.482	1.075	1.353	1.599
50	250.9	128.1	64.83	61.47	51.85	45.51	4.082	4.839	5.513	2.084	2.471	2.815	1.055	1.250	1.425
100	122.7	87.82	59.76	57.46	50.11	44.63	2.135	2.449	2.749	1.528	1.753	1.968	1.040	1.193	1.339

Spudich et al. (1999) RVT GM for							Resulting scale factors (GM target / GM host) for target (above) and host (below) κ values								
	κ target			κ host			0.00625			0.0125			0.025		
freq	0.00625	0.0125	0.025	0.03	0.0375	0.045	0.03	0.0375	0.045	0.03	0.0375	0.045	0.03	0.0375	0.045
M / dist: 6.5 / 85															
0.5	19.9	19.72	19.35	19.29	19.09	18.89	1.032	1.042	1.053	1.022	1.033	1.044	1.003	1.014	1.024
1	40.25	39.48	37.96	37.76	36.97	36.21	1.066	1.089	1.112	1.046	1.068	1.090	1.005	1.027	1.048
2.5	82.48	78.59	71.39	70.47	66.96	63.64	1.170	1.232	1.296	1.115	1.174	1.235	1.013	1.066	1.122
5	120.6	109.7	91.03	88.76	80.43	72.96	1.359	1.499	1.653	1.236	1.364	1.504	1.026	1.132	1.248
10	154.5	128.3	89.94	85.83	71.64	60.21	1.800	2.157	2.566	1.495	1.791	2.131	1.048	1.255	1.494
20	166.6	118.1	64.4	59.96	46.58	37.88	2.779	3.577	4.398	1.970	2.535	3.118	1.074	1.383	1.700
33	152.4	91.93	46.39	43.62	35.93	30.99	3.494	4.242	4.918	2.108	2.559	2.966	1.064	1.291	1.497
50	127.9	71.02	40.42	38.71	33.29	29.63	3.304	3.842	4.317	1.835	2.133	2.397	1.044	1.214	1.364
100	70.39	53.2	37.96	36.65	32.4	29.16	1.921	2.173	2.414	1.452	1.642	1.824	1.036	1.172	1.302
M / dist: 6.5 / 140															
0.5	12.32	12.2	11.96	11.93	11.81	11.68	1.033	1.043	1.055	1.023	1.033	1.045	1.003	1.013	1.024
1	22.98	22.54	21.67	21.56	21.12	20.68	1.066	1.088	1.111	1.045	1.067	1.090	1.005	1.026	1.048
2.5	41.77	39.82	36.22	35.76	34	32.33	1.168	1.229	1.292	1.114	1.171	1.232	1.013	1.065	1.120
5	54.81	49.95	41.6	40.59	36.86	33.52	1.350	1.487	1.635	1.231	1.355	1.490	1.025	1.129	1.241
10	61.46	51.47	36.69	35.11	29.66	25.28	1.750	2.072	2.431	1.466	1.735	2.036	1.045	1.237	1.451
20	57.02	41.64	24.85	23.47	19.29	16.5	2.429	2.956	3.456	1.774	2.159	2.524	1.059	1.288	1.506
33	46.97	31.32	19.32	18.51	16.07	14.4	2.538	2.923	3.262	1.692	1.949	2.175	1.044	1.202	1.342
50	38.07	25.8	17.77	17.19	15.37	14.01	2.215	2.477	2.717	1.501	1.679	1.842	1.034	1.156	1.268
100	26.85	22.14	17.15	16.69	15.11	13.87	1.609	1.777	1.936	1.327	1.465	1.596	1.028	1.135	1.236
M / dist: 7.75 / 7.5															
0.5	465.1	460.8	452.1	450.9	446.3	441.6	1.031	1.042	1.053	1.022	1.032	1.043	1.003	1.013	1.024
1	900.3	882.8	848.7	844.2	826.7	809.5	1.066	1.089	1.112	1.046	1.068	1.091	1.005	1.027	1.048
2.5	2002	1906	1729	1707	1621	1540	1.173	1.235	1.300	1.117	1.176	1.238	1.013	1.067	1.123
5	3315	3010	2487	2424	2191	1983	1.368	1.513	1.672	1.242	1.374	1.518	1.026	1.135	1.254
10	5045	4172	2880	2742	2263	1879	1.840	2.229	2.685	1.522	1.844	2.220	1.050	1.273	1.533
20	6844	4732	2380	2184	1589	1205	3.134	4.307	5.680	2.167	2.978	3.927	1.090	1.498	1.975
33	7615	4235	1641	1489	1093	879.2	5.114	6.967	8.661	2.844	3.875	4.817	1.102	1.501	1.866
50	7435	3324	1275	1185	948.7	807.6	6.274	7.837	9.206	2.805	3.504	4.116	1.076	1.344	1.579
100	2961	1830	1112	1059	897.8	783	2.796	3.298	3.782	1.728	2.038	2.337	1.050	1.239	1.420
M / dist: 7.75 / 30															
0.5	106.9	105.9	103.9	103.6	102.6	101.5	1.032	1.042	1.053	1.022	1.032	1.043	1.003	1.013	1.024
1	200.7	196.8	189.2	188.2	184.3	180.5	1.066	1.089	1.112	1.046	1.068	1.090	1.005	1.027	1.048
2.5	425.6	405.3	368	363.2	345	327.8	1.172	1.234	1.298	1.116	1.175	1.236	1.013	1.067	1.123
5	674.3	612.6	506.9	494.1	447.1	404.9	1.365	1.508	1.665	1.240	1.370	1.513	1.026	1.134	1.252
10	970.4	804	557.4	530.9	439.7	366.2	1.828	2.207	2.650	1.514	1.829	2.196	1.050	1.268	1.522
20	1227	853.3	438.1	403.4	298.9	231.5	3.042	4.105	5.300	2.115	2.855	3.686	1.086	1.466	1.892
33	1283	726.7	302.6	277.8	212.3	175.4	4.618	6.043	7.315	2.616	3.423	4.143	1.089	1.425	1.725
50	1188	559.1	244.3	229.5	189	163.7	5.176	6.286	7.257	2.436	2.958	3.415	1.064	1.293	1.492
100	512.3	340.7	219.4	210	180.8	159.5	2.440	2.834	3.212	1.622	1.884	2.136	1.045	1.213	1.376
M / dist: 7.75 / 60															
0.5	65.3	64.68	63.45	63.28	62.62	61.97	1.032	1.043	1.054	1.022	1.033	1.044	1.003	1.013	1.024
1	117.8	115.6	111.1	110.5	108.3	106	1.066	1.088	1.111	1.046	1.067	1.091	1.005	1.026	1.048
2.5	235	223.9	203.4	200.8	190.8	181.4	1.170	1.232	1.295	1.115	1.173	1.234	1.013	1.066	1.121
5	351.4	319.5	264.9	258.3	233.9	212.1	1.360	1.502	1.657	1.237	1.366	1.506	1.026	1.133	1.249
10	470.1	390.5	272.5	259.8	216.2	181.1	1.809	2.174	2.596	1.503	1.806	2.156	1.049	1.260	1.505
20	542.3	380.9	202.1	187.2	142.6	113.8	2.897	3.803	4.765	2.035	2.671	3.347	1.080	1.417	1.776
33	524.4	306.6	142.3	132.6	106.2	90.51	3.955	4.938	5.794	2.312	2.887	3.387	1.073	1.340	1.572
50	456.9	234.3	120.5	114.4	97.22	85.83	3.994	4.700	5.323	2.048	2.410	2.730	1.053	1.239	1.404
100	224.4	161.8	111.4	107.2	94.01	84.14	2.093	2.387	2.667	1.509	1.721	1.923	1.039	1.185	1.324
M / dist: 7.75 / 85															
0.5	49.13	48.67	47.73	47.61	47.11	46.62	1.032	1.043	1.054	1.022	1.033	1.044	1.003	1.013	1.024
1	85.92	84.26	81.05	80.62	78.97	77.35	1.066	1.088	1.111	1.045	1.067	1.089	1.005	1.026	1.048
2.5	163	155.4	141.3	139.4	132.5	126	1.169	1.230	1.294	1.115	1.173	1.233	1.014	1.066	1.121
5	232.4	211.5	175.6	171.3	155.3	141	1.357	1.496	1.648	1.235	1.362	1.500	1.025	1.131	1.245
10	292.9	243.9	171.3	163.5	136.7	115.1	1.791	2.143	2.545	1.492	1.784	2.119	1.048	1.253	1.488
20	313.8	222.7	122.2	113.9	88.93	72.8	2.755	3.529	4.310	1.955	2.504	3.059	1.073	1.374	1.679
33	285.9	173.1	88.44	83.32	69	60.06	3.431	4.143	4.760	2.078	2.509	2.882	1.061	1.282	1.473
50	239.6	133.9	77.43	74.12	64.32	57.71	3.233	3.725	4.152	1.807	2.082	2.320	1.045	1.204	1.342
100	132.7	101	72.9	70.49	62.63	56.64	1.883	2.119	2.343	1.433	1.613	1.783	1.034	1.164	1.287
M / dist: 7.75 / 140															
0.5	30.48	30.19	29.61	29.53	29.23	28.92	1.032	1.043	1.054	1.022	1.033	1.044	1.003	1.013	1.024
1	49.89	48.94	47.09	46.85	45.89	44.96	1.065	1.087	1.110	1.045	1.066	1.089	1.005	1.026	1.047
2.5	85.11	81.17	73.87	72.95	69.39	66.02	1.167	1.227	1.289	1.113	1.170	1.229	1.013	1.065	1.119
5	109.5	99.88	83.29	81.28	73.89	67.26	1.347	1.482	1.628	1.229	1.352	1.485	1.025	1.127	1.238
10	121.6	101.9	72.9	69.79	59.11	50.56	1.742	2.057	2.405	1.460	1.724	2.015	1.045	1.233	1.442
20	112.2	82.18	49.56	46.89	38.81	33.45	2.393	2.891	3.354	1.753	2.117	2.457	1.057	1.277	1.482
33	92.32	61.98	38.87	37.31	32.64	29.43	2.474	2.828	3.137	1.661	1.899	2.106	1.042	1.191	1.321
50	74.95	51.28	35.9	34.78	31.29	28.69	2.155	2.395	2.612	1.474	1.639	1.787	1.032	1.147	1.251
100	53.34	44.28	34.7	33.8	30.78	28.39	1.578	1.733	1.879	1.310	1.439	1.560	1.027	1.127	1.222